De la biogenèse des centres fer-soufre à la persulfuration des protéines : identification et caractérisation des acteurs moléculaires impliqués dans le transfert de soufre chez les plantes

Jérémy Couturier

Ecole Doctorale SIReNa
Sciences et Ingénierie des Ressources Naturelles

Mémoire

présenté et soutenu publiquement pour l'obtention de

l'Habilitation à Diriger des Recherches

Mention « Biologie et écologie des forêts et des agrosystèmes »

par **Jérémy COUTURIER**

De la biogenèse des centres fer-soufre à la persulfuration des protéines : identification et caractérisation des acteurs moléculaires impliqués dans le transfert de soufre chez les plantes

Soutenance le 11 décembre 2020

Membres du jury :

Rapporteurs :

Mme Sandrine OLLAGNIER de CHOUDENS	DR CNRS, CEA, Grenoble
M. Benoît D'AUTREAUX	CR INSERM, I2BC, Saclay
M. David WENDEHENNE	PR, Université de Bourgogne, Dijon

Examinateurs :

Mme Sandrine BOSCHI-MULLER	PR, Université de Lorraine, Nancy
Mme Sophie RAHUEL-CLERMONT	DR CNRS, Université de Lorraine, Nancy
M. Stéphane LEMAIRE	DR CNRS, Sorbonne Université, Paris

Parrain Scientifique :

M. Nicolas ROUHIER	PR, Université de Lorraine, Nancy

UMR1136 Université de Lorraine/INRAE Interactions Arbres / Micro-organismes, Faculté des Sciences et Technologies, Boulevard des aiguillettes, 54500 Vandoeuvre-lès-Nancy

REMERCIEMENTS

HDR, ces trois lettres m'ont longtemps laissé perplexe, me laissant l'impression d'un rituel, d'un passage intermédiaire vers de nouveaux horizons. Après m'être plié à l'exercice, cela a notamment été l'occasion de remettre en perspective toutes les activités relatives à notre métier. Bien qu'elle soit délivrée à titre individuel, l'habilitation à diriger des recherches est le fruit du travail collectif de toutes les personnes qui m'ont accompagné ces dernières années et sans qui ces fameuses trois lettres resteraient un sigle parmi tant d'autres.

Je souhaite en premier lieu remercier les membres du jury d'avoir accepté d'évaluer mon travail et pris de leur temps pour assumer cette lourde tâche à la vue du nombre de pages du mémoire. J'espère ne pas avoir été trop long….

Je tiens à exprimer ma plus profonde gratitude à Nicolas Rouhier et Jean-Pierre Jacquot qui m'ont ouvert les portes du monde de la recherche, puis soutenu et conseillé tout au long de ma carrière. J'ai énormément appris à vos côtés et je continue d'apprendre jour après jour, un immense merci à vous deux.

Je remercie également tous les collègues qui partagent mon quotidien depuis toutes ces années Eric, Mélanie, Tiphaine, Arnaud, Rodnay, Jean-Michel, Raphaël, Benjamin, Corinne et tous les autres membres du laboratoire. Tous ensemble, vous participez à la bonne ambiance de travail régnant au sein de notre équipe, ambiance propice au développement des activités de chacun et chacune.

Une bonne partie des résultats obtenus vous est dûe, merci à vous toutes et tous, Tiphaine qui a grandement contribué à mettre le projet soufre sur de bons rails, les anciens doctorants Jonathan, Flavien, Mélanie et les petits nouveaux Damien et Loïck, avec lesquels nous allons essayer de faire aussi bien. J'ai une pensée particulière pour les « soufrés », Anna, Benjamin, et Alexis avec qui j'ai eu la chance de développer mes nouvelles idées. Malgré leur grand nombre (trop certainement) vous avez toujours répondu présent. Je tiens également à remercier les différents étudiants/étudiantes que j'ai pu superviser, chacun et chacune ayant à sa manière apporté sa pierre à l'édifice.

Je n’oublie pas les nombreux collaborateurs et collaboratrices sans qui bien des idées n’auraient pu aboutir et seraient encore dans les cartons. J’ai une pensée particulière pour Claude Didierjean, Pascale Tsan, Thomas Roret pour la caractérisation structurale des protéines, Mike Johnson et son équipe pour la caractérisation spectroscopique des protéines fer-soufre, Frédéric Gaymard, Chrisitian Dubos et l’équipe FeROS pour la caractérisation fonctionnelle de mutants d’*Arabidospis thaliana*, Stéphane Lemaire, Christophe Marchand, Pascal Rey et Andreas Meyer pour la régulation redox des protéines. Les échanges relatifs à toutes ces collaborations ont été enrichissants tant sur le plan scientifique que personnel.

Pour finir, je souhaite exprimer ma profonde gratitude à ma famille qui m’a soutenu depuis le début et tout particulièrement les trois personnes qui partagent mon quotidien, me soutiennent, me supportent, notamment durant les moments où je reste connecté « travail » et pendant lesquels je ne peux pas être disponible pour eux à la hauteur qu’ils le méritent, un immense merci à vos trois, Aude, Nathéo et Lou.

TABLE DES MATIERES

CURRICULUM VITAE

COUTURIER Jérémy
Né le 6 juillet 1981 à Verdun

Maître de conférences, classe normale
Université de Lorraine, Faculté des Sciences et Technologies
UMR1136 Université de Lorraine/INRAE "Interactions Arbres/Micro-organismes"

1. Titres universitaires

2001 DEUG sciences de la vie mention biologie option aspects moléculaires du métabolisme cellulaire, mention AB, obtenu à l'Université Henri Poincaré NANCY I

2002 Licence de biologie, mention biologie cellulaire et physiologie, option diversité et adaptation des végétaux, mention AB, obtenue à l'Université Henri Poincaré NANCY I

2003 Maîtrise de biologie, mention biologie cellulaire et physiologie, option sciences et techniques du végétal, mention AB, obtenue à l'Université Henri Poincaré NANCY I

2004 DEA Biologie Forestière, mention B, obtenu à l'Université Henri Poincaré NANCY I. Stage effectué sous la direction du Professeur Michel Chalot au sein du laboratoire Interactions Arbres/Micro-organismes UMR 1136 INRA/UHP

2007 Doctorat de Biologie Forestière à l'Université Henri Poincaré NANCY I. Etude de quelques mécanismes de transport impliqués dans l'absorption et la remobilisation de l'azote chez le peuplier. Doctorat réalisé sous la direction du Pr. Michel Chalot

2. Parcours professionnel

Février 2008 - Janvier 2010
Post doctorat, Université de Nancy, UMR1136 UL/INRA

Février 2010 - Juin 2010
Séjour post-doctoral au sein du laboratoire « Biochemistry and Physiology of Plants » du Pr. Karl-Josef Dietz (Bielefeld, Allemagne)

Juillet 2010 - Septembre 2013
Post doctorat, Université de Lorraine, UMR1136 UL/INRA

Depuis septembre 2013
Nomination en tant que Maître de conférences en physiologie végétale à l'Université de Lorraine (UMR 1136 UL/INRAE Interactions Arbres/Micro-organismes, Equipe Réponse aux stress et Régulation Redox), section CNU66
Titularisation le 1er septembre 2014

3. Expertises, contrats, animation scientifique, travaux et publications

3.1. Expertises d'articles pour différentes revues scientifiques

BBA General Subjects, BBA Gene Regulatory Mechanisms, Physiologia Plantarum, Plant Molecular Biology Reporter, Plant Science, Plant Cell and Physiology, Planta, Computational

Biology and Chemistry, Frontiers in Bioengineering and Biotechnology, Journal of Experimental Botany, Heliyon, Journal of Advanced Research, Plants.

Membre du Topic Board de Antioxidants depuis avril 2020.

3.2 Expertises pour des agences de recherche

Fondation croate pour la science (HRZZ)

3.3. Expertises scientifiques

- Participation à des jurys de thèse : 1
- Participation à des comités de thèse : 1

3.4. Animation scientifique

Responsable pédagogique d'un module de formation doctorale (Expression de protéines recombinantes dans la bactérie *Escherichia coli* et purification, 20H Travaux Pratiques, Ecole SIReNa) depuis septembre 2017.

3.5 Responsabilités administratives

Représentant MCF au conseil de service de l'UMR et représentant collège B au conseil du pôle scientifique A2F.

3.6. Travaux et publications

Communications orales propres : 7
Communications par affiches : 31
Travaux et publications : 48
Articles de recherche dans des journaux avec comité de lecture : 36
Articles de revue dans des journaux avec comité de lecture : 12
Données bibliométriques clés au 08/10/2020 :
Facteur h: 25 (Google Scholar)
Nombre de citations: 5831

RESPONSABILITES SCIENTIFIQUES

Au travers de mes activités de recherche, j'ai participé et coordonné (PI) différents projets de recherche depuis ma nomination en septembre 2013.

2013-2017: Projet ANR Blanc Fe-S traffic (Rouhier N. PI). The cellular trafficking of iron-sulfur (Fe-S) clusters in plants

2015-2016: Projet Région SULTRANS (**Couturier J. PI**). Study of the molecular mechanisms involved in sulfur transfer in plants (10 000 euros)

2016: Projet LabEx ARBRE FERPAR (**Couturier J. PI**). Identification of plant ferredoxin protein partners (10 000 euros)

2016-2019: Projet LabEx ARBRE METOX (N. Rouhier PI). Unravelling new metal- or redox-dependent proteins and processes in plants

2017-2020: Projet ANR Jeune Chercheur SULTRAF (**Couturier J. PI**). Deciphering the molecular mechanisms of sulfur trafficking in plants (227 000 euros)

2017-2018: Projet Région SULPAR (**Couturier J. PI**). Identification et caractérisation des partenaires de sulfurtransférases de plantes (20 000 euros)

2018-2020: Projet LabEX ARBRE SULPRO (**Couturier J. PI**). Developing redox biosensors for sulfur compounds (88 400 euros)

2019-2022: Projet ANR PRCI MITOGLU (N. Rouhier PI). Dissecting the molecular interactions of mitochondrial glutaredoxin S15 in plants

2019-2022: Projet LUE (Lorraine University of Excellence) **SULSENSE** (**Couturier J. PI**). Developing new optogenetic redox biosensors for sulfur compounds (140 520 euros)

ACTIVITES D'ENSEIGNEMENT

Depuis ma nomination en septembre 2013, j'ai pleinement rempli mes obligations de service d'enseignement au cours de chaque année universitaire. Entre les années universitaires 2013-2014 et 2017-2018, je suis intervenu dans les différents niveaux (L1, L2, L3) de la **licence Sciences du Vivant et de l'Environnement (SVE)** mais également dans les trois masters de biologie présents à Nancy de septembre 2013 à septembre 2018. Il s'agit du **master FAGE** (Biologie et écologie pour la forêt, l'agronomie et l'environnement), du **master BioMANE** (Biotechnologies, Microbiologie, Aliment, Nutrition, Environnement) et du **master BSIS** (BioSciences et Ingénierie de la Santé). Je suis également intervenu dans un module de la **licence professionnelle LP BAE** (Biologie Analytique et Expérimentale) et dans un module scientifique pour les doctorants de l'**école doctorale RP2E** (Ressources Procédés Produits Environnement). Le détail de la répartition des différents enseignements assurés est indiqué dans le tableau ci-dessous.

Filière	**Matière**	**2013-2014**	**2014-2015**	**2015-2016**	**2016-2017**	**2017-2018**
L1 SVE	Biologie végétale	20 h	40 h	22 h	24 h	22 h
L2 SVE	Physiologie végétale	30 h	30 h	46 h	60 h	58 h
L3 SVE	Cycle cellulaire et mort cellulaire	32 h	24 h	24 h	32 h	32 h
	Différenciation, motilité	16 h	8 h	8 h	16 h	16 h
	Réponse et signalisation en conditions de stress	17 h	11 h	17 h	17 h	17 h
LP BAE	Extraction, purification et caractérisation de protéines	24 h	24 h	24 h	24 h	24 h
M1 FAGE	Expérimentation en biologie végétale	15 h	15 h	15 h	-	15 h
M1BioMANE	Modifications des protéines et signalisation	8 h	10 h	10 h	16 h	16 h
M2 BioMANE	Microbiologie et Ingénierie protéique	26 h	6 h	26 h	10 h	-
M2 BSIS	Projet intégré	24 h	24 h	-	-	24 h
Ecole doctorale	Module de Formation Scientifique Ciblé	20 h	-	-	-	20 h
Total Heures (Eq TD)		232 h	192 h	192 h	199 h	244 h

Depuis septembre 2018, du fait de la nouvelle maquette de formation, l'offre d'enseignement a quelque peu évolué, principalement au niveau des masters. Comme lors des années précédentes, je suis intervenu dans les différents niveaux (L1, L2, L3) de la **licence Sciences du Vivant et de l'Environnement (SVE)** et dans les trois masters de biologie, le **master AETPF** (Agrosciences, Environnement, Territoires, Paysage, Forêt), le **master Microbiologie** et le **master SV** (Sciences du vivant). Je suis également intervenu dans un module de la **licence professionnelle LP BB prot** (Bioindustries et Biotechnologies – protéines recombinantes). Le détail de la répartition des différents enseignements assurés est indiqué dans le tableau ci-après.

Filière	**Matière**	**2018-2019**	**2019-2020**
L1 SVE	Biologie végétale	30 h	2 h
L2 SVE	Physiologie végétale	66 h	62 h
L3 SVE	Stratégies expérimentales en biologie	37,5 h	49 h
	Réponse et signalisation en conditions de stress	17 h	17 h
LP BB	Extraction et purification de protéines	24 h	24 h
M1 AETPF	Expérimentation en biologie végétale	15 h	15 h
M1 Microbiologie	Génomique structurale et fonctionnelle	3 h	3 h
	Fonctions métaboliques : régulation et signalisation	16 h	13 h
M2 AETPF	Ingénierie protéique	6 h	22 h
M2 SV	Génie génétique et purification	24 h	24 h
	Interactomique: méthodes *in vivo* et *in vitro*	6 h	6 h
Ecole doctorale SIReNa	Module de Formation Scientifique Ciblé	-	-
Total Heures (Eq TD)		244,5 h	237 h

Depuis septembre 2017, je suis le responsable pédagogique d'un module de formation doctorale (Expression de protéines recombinantes dans la bactérie *Escherichia coli* et purification, 20H Travaux Pratiques, Ecole SIReNa). Depuis septembre 2018, je suis également responsable du l'unité d'enseignement « Expérimentation en biologie végétale » du master 1 AETPF. Parallèlement, je participe au jury de soutenance de recherche bibliographique du master AETPF (anciennement master FAGE) chaque année depuis janvier 2015. J'ai également participé à trois jurys de soutenance de mémoire de master 2 (master FAGE, BioMANE et BSIS) en septembre 2015, 2016 et juillet 2018 et deux jurys de soutenance de projet tuteuré master 1 AETPF en juillet 2019 et 2020. Pour finir, j'ai présidé un jury du Baccalauréat en juillet 2015.

ENCADREMENTS SCIENTIFIQUES

Depuis ma nomination, j'ai encadré plusieurs doctorants, étudiants en master 1 et 2 et des étudiants de licence. J'ai également supervisé trois chercheurs post-doctorants. Ci-dessous sont listées les périodes ainsi que le contexte scientifique et les objectifs propres à chacun de ces encadrements. Concernant les étudiants de master, chaque période de stage (M1 et M2) s'est conclue par la rédaction d'un rapport (15 pages pour le M1 et 25 pages pour le M2), rapport suivi d'une soutenance orale de 15 minutes.

1. Doctorants

Jonathan Przybyla-Toscano, doctorant (octobre 2013 – février 2017)
Etude des protéines NFU, ISCA et FDX, impliquées dans la maturation des centres fer-soufre dans les mitochondries d'*Arabidopsis thaliana*
Co-encadrement (50 %) avec Nicolas Rouhier

Mélanie Roland, doctorante (octobre 2016 – décembre 2019)
Etude fonctionnelle de facteurs de maturation tardifs des protéines fer-soufre chloroplastiques chez *Arabidopsis thaliana*
Co-encadrement (50 %) avec Nicolas Rouhier

Flavien Zannini, doctorant (octobre 2016 - décembre 2019)
Analyse fonctionnelle de protéines métal- ou redox dépendantes chez les plantes
Co-encadrement (50 %) avec Nicolas Rouhier

Actuellement je co-encadre, avec Nicolas Rouhier, deux étudiants en thèse qui ont débuté le 1er octobre 2019. Damien Caubrière travaille sur le développement de nouveaux biosenseurs redox pour les composés soufrés et Loïck Christ s'intéresse à la dissection des interactions moléculaires de la glutarédoxine S15 mitochondriale chez les plantes.

2. Etudiants de master

Flavien Zannini, stage master 1 (avril - juin 2014)
Caractérisation de l'activité endonucléase des protéines BolA seules ou en complexe avec les glutarédoxines.

Mélanie Roland, stage master 1 (avril – juin 2015)
Caractérisation de l'activité des sulfurtransférases d'*Arabidopsis thaliana*.

Flavien Zannini, stage master 2 (février– juillet 2015)
Caractérisation biochimique de la glutarédoxine S16 d'*Arabidopsis thaliana*.

Xavier Marbehan, stage master 1 (avril - mai 2019)
Caractérisation biochimique d'une protéine de la famille des sulfurtransférases chez *Arabidopsis thaliana*
Co-encadrement (50 %) avec Benjamin Selles

Karine Vincenot, stage master 1 (avril-juin 2020)
Caractérisation biochimique de la protéine fusion FTR-STR de *Sulfurovum*.

3. Etudiants de licence

Au cours de cette période j'ai encadré deux étudiantes, Léa Marson (février-mai 2018) et Morgane Ziesel (février-mai 2020) qui ont effectué un stage de fin d'études de 4 mois dans le cadre de leur licence professionnelle. Chacun de ces stages s'est conclu par la rédaction d'un rapport (25 pages), suivi d'une soutenance orale de 15 minutes.

Enfin, j'ai supervisé des étudiantes de L3, pour lesquelles la durée du stage oscillait entre 3 et 8 semaines : Anaïs Makos de juin à juillet 2017, Fanny Vautrin et Camille Becker en juin 2019. Ces stages prenaient place dans le cadre d'une UE optionnelle « Stage » proposée au semestre 6 de la licence SVE. Ils ont donné lieu à la préparation d'un poster présenté lors d'une soutenance de 10 minutes suivie de questions diverses.

4. Chercheurs post-doctorants

Elena Hego (septembre 2015 – août 2016)
Identification des partenaires des ferrédoxines mitochondriales mFDX1 et mFDX2 d'*Arabidopsis thaliana*.

Anna Moseler (janvier 2017-aujourd'hui)
Caractérisation biochimique des 3-mercaptopyruvate sulfurtransférases d'*Arabidopsis thaliana* et développement de biosenseurs redox spécifiques à certains composés soufrés.

Benjamin Selles (septembre 2018-août 2020)
Caractérisation de protéines impliquées dans le transfert de soufre chez *Arabidopsis thaliana*.

TRAVAUX ET PUBLICATIONS

1. Publications

P46 Roret T, Alloing G, Girardet JM, Perrot T, Dhalleine T, **Couturier J**, Frendo P, Didierjean C, Rouhier N (2020) *Sinorhizobium meliloti* YrbA binds divalent metal cations using two conserved histidines. Bioscience Reports, 40:BSR20202956. doi: 10.1042/BSR20202956. IF 2019 2,942.

P45 Berger N, Vignols F, Przybyla-Toscano J, Roland M, Rofidal V, Touraine B, Zienkiewicz K, **Couturier J**, Feussner I, Santoni V, Rouhier N, Gaymard F, Dubos C (2020) Identification of client iron-sulfur proteins of the chloroplastic NFU2 transfer protein in *Arabidopsis thaliana*. Journal of Experimental Botany 71:4171-4187. doi: 10.1093/jxb/eraa166. IF 2019 5,908.

P44 Roland M, Przybyla-Toscano J, Vignols F, Berger N, Azam T, Christ L, Santoni V, Wu HC, Dhalleine T, Johnson MK, Dubos C, **Couturier J**, Rouhier N (2020) The plastidial Arabidopsis thaliana NFU1 protein binds and delivers [4Fe-4S] clusters to specific client proteins. The Journal of Biological Chemistry 295:1727-1742. doi:10.1074/jbc.RA119.011034. IF 2019 4,106.

P43 Rey P, Taupin-Broggini M, **Couturier J**, Vignols F, Rouhier N (2019) Is there a role for glutaredoxins and BOLAs in the perception of the cellular iron status in plants? Frontiers in Plant Science 10:712. doi: 10.3389/fpls.2019.00712. IF 4,402.

P42 Selles B, Moseler A, Rouhier N, **Couturier J** (2019) Rhodanese domain-containing sulfurtransferases: multifaceted proteins involved in sulfur trafficking in plants. Journal of Experimental Botany 70:4139-4154. doi: 10.1093/jxb/erz213. IF 5,908.

P41 Moseler A, Selles B, Rouhier N, **Couturier J** (2020) Novel insights into the diversity of the sulfurtransferase family in photosynthetic organisms with emphasis on oak. New Phytologist 226:967-977. doi: 10.1111/nph.15870. IF 2019 8,512.

P40 Touraine B, Vignols F, Przybyla-Toscano J, Ischebeck T, Dhalleine T, Wu HC, Magno C, Berger N, **Couturier J**, Dubos C, Feussner I, Caffarri S, Havaux M, Rouhier N, Gaymard F (2019) The iron-sulfur protein NFU2 plays a predominant role in branched-chain amino acid synthesis in Arabidopsis roots. Journal of Experimental Botany 70:1875-1889. doi: 10.1093/jxb/erz050. IF 5,908.

P39 Zannini F, Moseler A, Bchini R, Dhalleine T, Meyer AM, Rouhier N, **Couturier J** (2019) The thioredoxin-mediated recycling of *Arabidopsis thaliana* GRXS16 relies on a conserved C-terminal cysteine. Biochimica and Biophysica Acta General Subjects 1863:426-436. doi: 10.1016/j.bbagen.2018.11.014. IF 3,422.

P38 Zannini F, Roret T, Przybyla-Toscano J, Dhalleine T, Rouhier N, **Couturier J** (2018) Mitochondrial *Arabidopsis thaliana* TRXo Isoforms Bind an Iron-Sulfur Cluster and Reduce NFU Proteins *In Vitro*. Antioxidants (Basel) 7 pii: E142. doi: 10.3390/antiox7100142. IF 4,520.

P37 Gao H, Azam T, Randeniya S, **Couturier J**, Rouhier N, Johnson MK (2018) Function and maturation of the Fe-S center in dihydroxyacid dehydratase from Arabidopsis. The Journal of Biological Chemistry 293:4422-4433. doi: 10.1074/jbc.RA117.001592. IF 4,106.

P36 Przybyla-Toscano J, Roland M, Gaymard F, **Couturier J**, Rouhier N (2018) Roles and maturation of iron-sulfur proteins in plastids. Journal of Biological Inorganic Chemistry 23: 545-566. doi: 10.1007/s00775-018-1532-1. IF 3,632.

P35 Zannini F, **Couturier J**, Keech O, Rouhier N (2017) *In Vitro* Alkylation Methods for Assessing the Protein Redox State. Methods in Molecular Biology 1653:51-64. doi: 10.1007/978-1-4939-7225-8_4.

P34 Przybyla-Toscano J, Roret T, **Couturier J**, Rouhier N (2017) FeS Cluster Assembly: Role of Monothiol Grxs and Nfu Proteins. Encyclopedia of Inorganic and Bioinorganic Chemistry, Metalloprotein Active Site Assembly. doi: 10.1002/9781119951438.eibc2470.

P33 Selles B, Zannini F, **Couturier J**, Jacquot JP, Rouhier N (2017) Atypical protein disulfide isomerases (PDI): Comparison of the molecular and catalytic properties of poplar PDI-A and PDI-M with PDI-L1A. PLoS One 12:e0174753. doi: 10.1371/journal.pone.0174753. IF 2,766.

P32 Ribeiro CW, Baldacci-Cresp F, Pierre O, Larousse M, Benyamina S, Lambert A, Hopkins J, Castella C, Cazareth J, Alloing G, Boncompagni E, **Couturier J**, Mergaert P, Gamas P, Rouhier N, Montrichard F, Frendo P (2017) Regulation of Differentiation of Nitrogen-Fixing Bacteria by Microsymbiont Targeting of Plant Thioredoxin s1. Current Biology 27:250-256. doi: 10.1016/j.cub.2016.11.013. IF 9,251.

P31 Gütle DD, Roret T, Müller SJ, **Couturier J**, Lemaire SD, Hecker A, Dhalleine T, Buchanan BB, Reski R, Einsle O, Jacquot JP (2016) Chloroplast FBPase and SBPase are thioredoxin-linked enzymes with similar architecture but different evolutionary histories. Proceedings of the National Academy of Sciences USA 113: 6779-6784. doi: 10.1073/pnas.1606241113. IF 9,661.

P30 Jacquot JP, **Couturier J**, Didierjean C, Gelhaye E, Morel-Rouhier M, Hecker A, Plomion C, Gütle DD, Rouhier N (2016) Structural and functional characterization of tree proteins involved in redox regulation: a new frontier in forest science. Annals of Forest Science 73:119-134. doi: 10.1007/s13595-014-0442-9. IF 2,431.

P29 Rouhier N, Cerveau D, **Couturier J**, Reichheld JP, Rey P (2015) Involvement of thiol-based mechanisms in plant development. Biochimica and Biophysica Acta 1850:1479-1496. doi: 10.1016/j.bbagen.2015.01.023. IF 5,083.

P28 **Couturier J**, Przybyla-Toscano J, Roret T, Didierjean C, Rouhier N (2015) The roles of glutaredoxins ligating Fe-S clusters: Sensing, transfer or repair functions? Biochimica and Biophysica Acta Molecular Cell Research 1853:1513-1527. doi: 10.1016/j.bbamcr.2014.09.018. IF 5,128.

P27 Roret T, Pégeot H, **Couturier J**, Mulliert G, Rouhier N, Didierjean C (2014) X-ray structures of Nfs2, the plastidial cysteine desulfurase from *Arabidopsis thaliana*. Acta Crystallographica section F Structural Biology Communications 70:1180-1185. doi: 10.1107/S2053230X14017026. IF 0,524.

P26 Roret T, Tsan P, **Couturier J**, Zhang B, Johnson MK, Rouhier N, Didierjean C (2014) Structural and Spectroscopic Insights into BolA-Glutaredoxin Complexes. The Journal of Biological Chemistry 289:24588-24598. doi: 10.1074/jbc.M114.572701. IF 4,573.

P25 Dhalleine T, Rouhier N, **Couturier J** (2014) Putative roles of glutaredoxin-BolA holo-heterodimers in plants. Plant Signaling and Behaviour 9:e28564. doi: 10.4161/psb.28564.

P24 **Couturier J**, Wu HC, Dhalleine T, Pégeot H, Sudre D, Gualberto JM, Jacquot JP, Gaymard F, Vignols F, Rouhier N (2014) Monothiol Glutaredoxin-BolA Interactions: Redox Control of *Arabidopsis thaliana* BolA2 and SufE1. Molecular Plant 7:187-205. doi: 10.1093/mp/sst156. IF 6,337.

P23 **Couturier J**, Jacquot JP, Rouhier N (2013) Toward a refined classification of class I dithiol glutaredoxins from poplar: biochemical basis for the definition of two subclasses. Frontiers in Plant Science 4:518. doi: 10.3389/fpls.2013.00518. IF 3,637.

P22 Gao H, Subramanian S, **Couturier J**, Naik SG, Kim SK, Leustek T, Knaff DB, Wu HC, Vignols F, Huynh BH, Rouhier N, Johnson MK (2013) *Arabidopsis thaliana* Nfu2 accommodates [2Fe-2S] or [4Fe-4S] clusters and is competent for in vitro maturation of chloroplast [2Fe-2S] and [4Fe-4S] cluster-containing proteins. Biochemistry 52:6633-6645. doi: 10.1021/bi4007622. IF 3,194.

P21 Zhang B, Bandyopadhyay S, Shakamuri P, Naik SG, Huynh BH, **Couturier J**, Rouhier N, Johnson MK (2013) Monothiol glutaredoxins can bind linear [Fe3S4]+ and [Fe4S4]2+ clusters in addition to [Fe2S2]2+ clusters: spectroscopic characterization and functional implications. J Am Chem Soc. 135:15153-15164. doi: 10.1021/ja407059n. IF 11,444.

P20 **Couturier J**, Touraine B, Briat JF, Gaymard F, Rouhier N (2013) The iron-sulfur cluster assembly machineries in plants: current knowledge and open questions. Frontiers in Plant Science 4:259. doi: 10.3389/fpls.2013.00259. IF 3,637.

P19 **Couturier J**, Chibani K, Jacquot JP, Rouhier N (2013) Cysteine-based redox regulation and signaling in plants. Frontiers in Plant Science 4:105. doi: 10.3389/fpls.2013.00105. IF 3,637.

P18 Mapolelo D, Zhang B, Randeniya S, Albetel AN, Li H, **Couturier J**, Rouhier N, Outten CE, Johnson MK (2013) Monothiol glutaredoxins and A-type proteins: Partners in Fe-S cluster trafficking. Dalton Transactions 42:3107-3115. doi: 10.1039/c2dt32263c. IF 4,097.

P17 **Couturier J**, Prosper P, Winger AM, Hecker A, Hirasawa M, Knaff D, Gans P, Jacquot JP, Navaza A, Haouz A, Rouhier N (2013) In the absence of thioredoxins, what are the reductants for peroxiredoxins in *Thermotoga maritima*? Antioxidants and Redox Signaling 18:1613-1622. doi: 10.1089/ars.2012.4739. IF 7,667.

P16 Benyamina SM, Baldacci-Cresp F, **Couturier J**, Chibani K, Hopkins J, Bekki A, de Lajudie P, Rouhier N, Jacquot JP, Alloing G, Puppo A, Frendo P (2013) Two *Sinorhizobium meliloti* glutaredoxins regulate iron metabolism and symbiotic bacteroid differentiation. Environmental Microbiology 15:795-810. doi: 10.1111/j.1462-2920.2012.02835.x. IF 6,240.

P15 **Couturier J**, Vignols F, Jacquot JP, Rouhier N (2012) Glutathione- and glutaredoxin-dependent reduction of methionine sulfoxide reductase A. FEBS Letters 586: 3894-3899. doi: 10.1016/j.febslet.2012.09.020. IF 3,582.

P14 Bedhomme M, Adamo M, Marchand CH, **Couturier J**, Rouhier N, Lemaire SD, Zaffagnini M, Trost P (2012) Glutathionylation of cytosolic glyceraldehyde-3-phosphate dehydrogenase from the model plant *Arabidopsis thaliana* is reversed by both glutaredoxins and thioredoxins *in vitro*. Biochemical Journal. 445: 337-347. doi: 10.1042/BJ20120505. doi: 10.1042/BJ20120505. IF 4,654.

P13 Zaffagnini M, Bedhomme M, Marchand CH, **Couturier J**, Gao XH, Rouhier N, Trost P, Lemaire SD (2012) Glutaredoxin S12: unique properties for redox signaling. Antioxidants and Redox Signaling 16: 17-32. doi: 10.1089/ars.2011.3933. IF 7,189.

P12 **Couturier J**, Ströher E, Albetel AN, Roret T, Muthuramalingam M, Tarrago L, Seidel T, Tsan P, Jacquot JP, Johnson MK, Dietz KJ, Didierjean C, Rouhier N (2011) Arabidopsis chloroplastic glutaredoxin C5 as a model to explore molecular determinants for iron-sulfur cluster binding into glutaredoxins. The Journal of Biological Chemistry 286: 27515-27527. doi: 10.1074/jbc.M111.228726. IF 4,773.

P11 **Couturier J**, Didierjean C, Jacquot JP, Rouhier N (2010) Engineered mutated glutaredoxins mimicking peculiar plant class III glutaredoxins bind iron-sulfur centers and possess reductase activity. Biochemical and Biophysical Research Communications 403: 435-441. doi: 10.1016/j.bbrc.2010.11.050. IF 2,595.

P10 **Couturier J**, Doidy J, Guinet F, Wipf D, Blaudez D, Chalot M (2010) Glutamine, arginine and the amino acid transporter Pt-CAT11 play important roles during senescence in poplar. Annals of Botany 105: 1159-1169. doi: 10.1093/aob/mcq047. IF 3,388.

P9 **Couturier J**, de Faÿ E, Fitz M, Wipf D, Blaudez D, Chalot M (2010) PtAAP11, a high affinity amino acid transporter specifically expressed in differentiating xylem cells of poplar. Journal of Experimental Botany 61: 1671-1682. doi: 10.1093/jxb/erq036. IF 4,818.

P8 Rouhier N, **Couturier J,** Johnson MK, Jacquot JP (2010) Glutaredoxins: roles in iron homeostasis**.** Trends in Biochemical Sciences 35: 43-52. doi: 10.1016/j.tibs.2009.08.005. IF 10,364.

P7 Chibani K, **Couturier J**, Selles B, Jacquot JP, Rouhier N (2010) The chloroplastic thiol reducing systems: dual functions in the regulation of carbohydrate metabolism and regeneration of antioxidant enzymes, emphasis on the poplar redoxin equipment. Photosynthesis Research 104: 75-99. doi: 10.1007/s11120-009-9501-8. IF 2,410.

P6 Selles B, Rouhier N, Chibani K, **Couturier J**, Gama F, Jacquot JP (2009) Glutaredoxin: The Missing Link Between Thiol-Disulfide Oxidoreductases and Iron Sulfur Enzymes. Advances in Botanical Research 52: 405-436. doi: 10.1016/S0065-2296(10)52013-5. IF 1,333.
P5 **Couturier J**, Jacquot JP, Rouhier N (2009) Evolution and diversity of glutaredoxins in photosynthetic organisms. Cellular and Molecular Life Sciences 66: 2539-2557. doi: 10.1007/s00018-009-0054-y. IF 6,090.

P4 **Couturier J**, Koh CS, Zaffagnini M, Winger A, Gualberto JM, Corbier C, Decottignies P, Jacquot JP, Lemaire SD, Didierjean C, Rouhier N (2009) Structure-function relationship of the chloroplastic GrxS12 with an atypical WCSYS active site. The Journal of Biological Chemistry 284: 9299-9310. doi: 10.1074/jbc.M807998200. IF 5,328.

P3 **Couturier J**, Montanini B, Martin F, Brun A, Blaudez D, Chalot M (2007) The expanded family of ammonium transporters in the perennial poplar plant. New Phytologist 174:137-150. doi: 10.1111/j.1469-8137.2007.01992.x. IF 5,249.

P2 Tuskan GA, Difazio S, Jansson S, Bohlmann J, Grigoriev I, Hellsten U, Putnam N, Ralph S, Rombauts S, Salamov A, Schein J, Sterck L, Aerts A, Bhalerao RR, Bhalerao RP, Blaudez D, Boerjan W, Brun A, Brunner A, Busov V, Campbell M, Carlson J, Chalot M, Chapman J, Chen GL, Cooper D, Coutinho PM, **Couturier J**, Covert S, Cronk Q, Cunningham R, Davis J, Degroeve S, Dejardin A, Depamphilis C, Detter J, Dirks B, Dubchak I, Duplessis S, Ehlting J, Ellis B, Gendler K, Goodstein D, Gribskov M, Grimwood J, Groover A, Gunter L, Hamberger B, Heinze B, Helariutta Y, Henrissat B, Holligan D, Holt R, Huang W, Islam-Faridi N, Jones S, Jones-Rhoades M, Jorgensen R, Joshi C, Kangasjarvi J, Karlsson J, Kelleher C, Kirkpatrick R, Kirst M, Kohler A, Kalluri U, Larimer F, Leebens-Mack J, Leple JC, Locascio P, Lou Y, Lucas S, Martin F, Montanini B, Napoli C, Nelson DR, Nelson C, Nieminen K, Nilsson O, Pereda V, Peter G, Philippe R, Pilate G, Poliakov A, Razumovskaya J, Richardson P, Rinaldi C, Ritland K, Rouze P, Ryaboy D, Schmutz J, Schrader J, Segerman B, Shin H, Siddiqui A, Sterky F, Terry A, Tsai CJ, Uberbacher E, Unneberg P, Vahala J, Wall K, Wessler S, Yang G, Yin T, Douglas C, Marra M, Sandberg G, Van de Peer Y, Rokhsar D (2006) The genome of black cottonwood, *Populus trichocarpa* (Torr. & Gray). Science 313: 596-604. doi: 10.1126/science.1128691. IF 30,028.

P1 Rouhier N, **Couturier J**, Jacquot JP (2006) Genome-wide analysis of plant glutaredoxin systems. Journal of Experimental Botany 57: 1685-96. doi: 10.1093/jxb/erl001. IF 3,630.

2. Conférences

C7 Dhalleine T, Moseler A, Marchand C, Lemaire S, Rouhier N, **Couturier J**. Sulfur trafficking and H_2S-mediated redox signaling in plants: roles of Arabidopsis 3-MP sulfurtransferases. SPP1710 Conference Thiol-based switches and redox regulation – from microbes to men (Sant Feliu de Guixols, Espagne, 15-20 Septembre 2019).

C6 Hériché M, Dhalleine T, Rouhier N, **Couturier J**. Deciphering the biochemical properties of bacterial rhodanese fusion proteins. Fourth meeting of the study group redox biology of the German Society for Biochemistry and Molecular Biology (Berlin, Allemagne, 26-28 Septembre 2018).

C5 Zannini F, Moseler A, Meyer A, Rouhier N, **Couturier J**. Arabidopsis thaliana GRXS16, a multifaceted glutaredoxin in chloroplasts. 3rd Redox Biology Symposium, Redox regulation: Historical background and future developments (Nancy, France, 29-31 Mars 2017).

C4 Dhalleine T, Tsan P, Marchand C, Lemaire S, Rouhier N, **Couturier J**. Deciphering the molecular mechanisms of sulfur trafficking in plants. Third meeting of the study group redox biology of the German Society for Biochemistry and Molecular Biology (Düsseldorf, Allemagne, 4-5 Juillet 2016).

C3 Roret T, **Couturier J**, Tsan P, Zhang B, Jacquot JP, Johnson MK, Rouhier N, Didierjean C. Biochemical, spectroscopic and structural insights into BolA-glutaredoxin complexes. IUBMB Symposium FeS 2015 - Iron Sulfur Cluster Biogenesis and Regulation (Bergamo, Italie, 23-26 Juin 2015).

C2 **Couturier J**, Wu HC, Roret T, Tsan P, Dhalleine T, Pégeot H, Jacquot JP, Didierjean C, Vignols F, Rouhier N. Monothiol glutaredoxin and BolA in plants: two proteins with multiple interaction modes. 9th International Workshop on Sulfur Metabolism in Plants: Molecular Physiology and Ecophysiology of Sulfur » (Freiburg, Allemagne, 14-17 Avril 2014).

C1 **Couturier J**, Blaudez D, Chalot M. L'ère post-génomique chez le peuplier : caractérisation de la famille des transporteurs d'ammonium (AMT). 9èmes Journées du Groupe de Biologie Moléculaire des Ligneux (Orléans, France, 21-23 Mars 2006).

3. Communications par affiches

Le nom des personnes ayant présenté les posters est souligné.

A31 Selles B, Dhalleine T, Rouhier N, **Couturier J**. Do the biochemical properties of Arabidopsis sulfurtransferase 18 support a role in sulfur trafficking? (Sant Feliu de Guixols, Espagne, 15-20 Septembre 2019).

A30 Moseler A, Morgan B, Rouhier N, **Couturier J**. Developing redox biosensors for sulfur compounds SPP1710 Conference Thiol-based switches and redox regulation – from microbes to men (Sant Feliu de Guixols, Espagne, 15-20 Septembre 2019).

A29 Hériché M, Dhalleine T, Rouhier N, **Couturier J**. Deciphering the biochemical properties of a bacterial ferredoxin-thioredoxin reductase-rhodanese fusion protein. Fourth meeting of the study group redox biology of the German Society for Biochemistry and Molecular Biology (Berlin, Allemagne, 26-28 Septembre 2018).

A28 Moseler A, Rouhier N, **Couturier J**. Deciphering the biochemical properties of plastidial GRXS14 and mitochondrial GRXS15 isoforms of *Arabidopsis thaliana*. Fourth meeting of the study group redox biology of the German Society for Biochemistry and Molecular Biology (Berlin, Allemagne, 26-28 Septembre 2018).

A27 Zannini F, **Couturier J**, Rouhier N. MIA40 of *Arabidopsis thaliana* is essential for the optimal *in vitro* oxidation of TIM and COX proteins. Fourth meeting of the study group redox biology of the German Society for Biochemistry and Molecular Biology (Berlin, Allemagne, 26-28 Septembre 2018).

A26 Dhalleine T, Marchand C, Lemaire S, Rouhier N, **Couturier J**. Sulfur trafficking and H_2S mediated-redox signalling in plants: Biochemical characterization of *Arabidopsis thaliana* 3-MP sulfurtransferases. 12th Congress of the International Plant Molecular Biology (IPMB) (Montpellier, France, 5-10 Août 2018).

A25 Roland M, Przybyla-Toscano J, Dhalleine T, **Couturier J**, Rouhier N. Seeking the role of the plastidial NFU1 transfer protein in *Arabidopsis thaliana*. Iron-Sulfur Proteins-Biogenesis, Regulation and Function 39th Steenbock Symposium (Madison, Wisconsin USA, 29 Mai-2 Juin 2018).

A24 Azam T, Przybyla-Toscano J, **Couturier J**, Rouhier N, Johnson MK. Mitochondrial Fe-S cluster assembly in *Arabidopsis thaliana*: *In vitro* characterization of the properties and role of GRX, ISCA and NFU proteins. Iron-Sulfur Proteins-Biogenesis, Regulation and Function 39th Steenbock Symposium (Madison, Wisconsin USA, 29 Mai-2 Juin 2018).

A23 Roland M, Przybyla-Toscano J, Dhalleine T, **Couturier J**, Rouhier N. The cellular maturation of iron-sulfur proteins in plants. 1st FrenchBIC summer school, Methods for studying metals in biology (Carry-le-Rouet, France, 17-21 Septembre 2017).

A22 Dhalleine T, Tsan P, Marchand C, Didierjean C, Lemaire S, Rouhier N, **Couturier J**. Deciphering the biochemical properties of plant sulfurtransferases to dissect cellular sulfur trafficking mechanisms. "Thiol oxidation in toxicity and signalling" Workshop (Sant Feliu de Guixols, Espagne, 17-21 Septembre 2017).

A21 Zannini F, Peleh V, **Couturier J**, Herrmann JM, Rouhier N. Comparison of the redox properties of plant and yeast MIA40/ERV1 couples. "Thiol oxidation in toxicity and signalling" Workshop (Sant Feliu de Guixols, Espagne, 17-21 Septembre 2017).

A20 Rey P, Zannini F, Becuwe N, Tourrette S, **Couturier J**, Rouhier N. Towards the roles of Arabidopsis plastidial CGFS glutaredoxins: involvement of GRXS14 in the maintenance of chlorophyll content under specific physiological situations. "Thiol oxidation in toxicity and signalling" Workshop (Sant Feliu de Guixols, Espagne, 17-21 Septembre 2017).

A19 Roland M, Przybyla-Toscano J, Dhalleine T, **Couturier J**, Rouhier N. The cellular maturation of iron-sulfur proteins in plants. 1st FeSBioNet Training School (Lisbonne, Portugal, 19-23 Juin 2017).

A18 Zannini F, Maria C, Belli G, Herrero E, **Couturier J**, Rouhier N. Towards the function of the chloroplastic *Arabidopsis thaliana* glutaredoxin S16. 3rd meeting of the study group redox biology of the German Society for Biochemistry and Molecular Biology (Düsseldorf, Allemagne, 4-5 Juillet 2016).

A17 Roret T, **Couturier J**, Girardet JM, Didierjean C, Rouhier N. Structural characterization of BolA-metal complexes through *Sinorhizobium meliloti* YrbA. Congrès de l'Association Française de Cristallographie (AFC) (Marseille, France, 4-7 Juillet 2016).

A16 Hego E, Przybyla-Toscano J, Roret T, **Couturier J**, Rouhier N. Identification of mitochondrial ferredoxin partners from *Arabidospis thaliana* leaves. 18th International Symposium on Iron Nutrition and Interaction in Plants (Madrid, Espagne, 30 Mai-3 Juin 2016).

A15 Przybyla-Toscano J, Uzarska M, Magno C, Touraine B, Mühlenhoff U, Vignols F, **Couturier J**, Keech O, Lill R, Gaymard F, Rouhier N. Mitochondrial *Arabidopsis thaliana* NFU transfer proteins: cooperation with ISCA proteins to deliver [4Fe-4S] cluster to specific apo-targets. 18th International Symposium on Iron Nutrition and Interaction in Plants (Madrid, Espagne, 30 Mai-3 Juin 2016).

A14 Przybyla-Toscano J, Roret T, **Couturier J**, Jacquot JP, Rouhier N. Deciphering the functions and partners of mitochondrial ferredoxins from *Arabidopsis thaliana.* Chemistry & Biology of Iron-Sulfur Clusters 6th International IMBG Meeting & Advanced Courses (Villard de Lans, France, 13-18 Septembre 2015).

A13 Przybyla-Toscano J, Dhalleine T, Mühlenhoff U, Magno C, Gaymard F, **Couturier J**, Vignols F, Lill R, Rouhier N. Exploring the functions and partners of mitochondrial ISCA transfer proteins from *A. thaliana.* IUBMB Symposium FeS 2015 - Iron Sulfur Cluster Biogenesis and Regulation (Bergamo, Italie, 23-26 Juin 2015).

A12 Roret T, Tsan P, **Couturier J**, Zhang B, Johnson MK, Didierjean C, Rouhier N. Diverse structural forms involving BolA proteins. Mosbacher Kolloquium - Metals in Biology: Cellular functions and diseases (Mosbach, Allemagne, 26-28 Mars 2015).

A11 Przybyla-Toscano J, Dhalleine T, Mühlenhoff U, Magno C, Gaymard F, **Couturier J**, Vignols F, Lill R, Rouhier N. Exploring the functions and partners of mitochondrial ISCA transfer proteins from *A. thaliana*. Mosbacher Kolloquium - Metals in Biology: Cellular functions and diseases (Mosbach, Allemagne, 26-28 Mars 2015).

A10 Touraine B, Gao H, Wu HC, **Couturier J**, Subramanian S, Naik S, Lamant T, Huynh BH, Briat JF, Vignols F, Gaymard F, Johnson MK, Rouhier N. Arabidopsis thaliana plastidial Nfu2 and Nfu3 are required for the maturation of [4Fe-4S] clusters into photosystem I. 7th International Conference on Iron-Sulfur Cluster Biogenesis and Regulation (South Carolina, Etats-Unis, 20-24 Mai 2013).

A9 **Couturier J**, Wu HC, Roret T, Lamant T, Didierjean C, Jacquot JP, Vignols F, Tsan P, Rouhier N. Roles of glutaredoxins in iron-sulfur cluster biogenesis and intracellular iron sensing in plants. 5th International Meeting and Second Advanced Courses of the IMBG: Metals Homeostasis (Autrans, France, 17-21 Septembre 2012).

A8 Roret T, Tsan P, **Couturier J**, Rouhier N, Didierjean C. NMR Study of *Arabidopsis thaliana* BolA2 : Structure, Dynamics and Interaction with Glutaredoxins. XXVth International Conference on Magnetic Resonance in Biological Systems (Lyon, France, 19-24 Août 2012).

A7 Jacquot JP, Selles B, **Couturier J**, Chibani K, Rouhier N. Peroxide detoxification systems in poplar. Plant Abiotic Stress tolerance II. Section Plant Response to Oxidative Stress (Vienna, Autriche, 22-25 Février 2012).

A6 **Couturier J**, Tsan P, Sudre D, Wu HC, Lamant T, Roret T, Riondet C, Didierjean C, Rey P, Gaymard F, Vignols F, Rouhier N. Structure/function analysis of plant BolAs, deciphering their interaction with glutaredoxins. Biogenesis of iron sulphur proteins and regulatory functions. (Cambridge, Angleterre, 22-25 Août 2011).

A5 **Couturier J**, Koh CS, Zaffagnini M, Winger A, Gualberto J, Tarrago L, Laugier E, Gama F, Lemaire S, Rey P, Jacquot JP, Rouhier N. Structural and functional characterization of a plastidial poplar glutaredoxin with an atypical WCSYS active site. 36ème Forum des Jeunes Chercheurs de la Société Française de Biochimie et de Biologie Moléculaire (Nancy, France, 25-27 Août 2009).

A4 **Couturier J**, Koh CS, Zaffagnini M, Winger A, Gualberto J, Tarrago L, Laugier E, Gama F, Lemaire S, Rey P, Jacquot JP, Rouhier N. Structural and functional characterization of a plastidial poplar glutaredoxin with an atypical WCSYS active site. Glutathione International Symposium: Glutathione and related thiols in microorganisms and plants (Nancy, France, 26-29 Août 2008).

A3 **Couturier J**, Koh CS, Zaffagnini M, Winger A, Gualberto J, Tarrago L, Laugier E, Gama F, Lemaire S, Rey P, Jacquot JP, Rouhier N. Structural and functional characterization of a plastidial poplar glutaredoxin with an atypical WCSYS active site. Gordon Research Conferences : Thio-Based Redox Regulation & Signalling (Barga, Italie, 25-30 Mai 2008).

A2 **Couturier J**, Guinet F, Migeon A, Blaudez D, Chalot M. Nitrogen autumnal remobilization in poplar : roles of arginine and cationic amino acid transporters (CAT) 10èmes Journées du Groupe de Biologie Moléculaire des Ligneux (Nancy, France, 5-7 Mai 2008).

A1 **Couturier J**, Montanini B, Martin F, Brun A, Blaudez D, Chalot M. The expanded family of ammonium transporters in the perennial poplar plant XIV International Workshop Plant Membrane Biology (Valencia, Espagne, 26 Juin-1er Juillet 2007).

ACTIVITES DE RECHERCHE DOCTORALE

Etude de quelques mécanismes de transport impliqués dans l'absorption et la remobilisation de l'azote chez le peuplier

Mon doctorat de biologie forestière a été réalisé au sein de l'équipe « Physiologie et génomique fonctionnelle du transport » du Professeur Michel Chalot (UMR1136 INRA/UHP, Université Henri Poincaré, Nancy). Les principaux thèmes de recherches abordés au cours ce travail de thèse concernaient le métabolisme azoté chez le peuplier et notamment l'absorption et la remobilisation de l'azote.

Bien qu'il se trouve en quantité importante dans les sols, l'azote est un des éléments principaux limitant la croissance des plantes, puisqu'il se trouve majoritairement sous des formes non directement assimilables par les plantes. Ainsi, l'ammonium et le nitrate constituent les principales sources d'azote pour la croissance des plantes même s'ils ne représentent qu'une très faible partie de l'azote du sol. Au niveau des sols forestiers, l'ammonium représente la principale source d'azote inorganique pour les plantes (Marschner & Dell, 1994). Toutefois, les plantes présentent généralement une croissance optimale lorsque le nitrate et l'ammonium sont présents. Un nombre important de transporteurs permettant d'importer efficacement ces deux composés azotés sur de larges gammes de concentrations a été mis en évidence chez différentes plantes. D'autre part, l'ammonium constitue également un intermédiaire central généré lors de différents processus comme la réduction du nitrate, la fixation de l'azote atmosphérique, la photorespiration et le catabolisme protéique (Joy, 1988). En situation extrême, les plantes sont également capables d'absorber les acides aminés (Persson et al., 2003), mais ceux-ci représentent surtout la principale forme de transport à longue distance de l'azote organique. Les acides aminés jouent par ailleurs des rôles fondamentaux dans une multitude de processus métaboliques incluant la synthèse protéique, la croissance cellulaire, la signalisation cellulaire, l'adaptation à certains changements environnementaux, la germination et la sénescence (Ortiz-Lopez et al., 2002). L'existence d'un nombre important de transporteurs d'acides aminés était suggérée par la complexité du métabolisme azoté intracellulaire et la multiplicité des types cellulaires impliqués dans le transport à longue distance.

L'absorption d'azote organique et inorganique, ainsi que le transport de l'azote organique synthétisé au niveau des organes « source » vers les organes « puits », constituent des mécanismes essentiels à la physiologie et au développement des plantes. Ceci est d'autant plus vrai chez les espèces pérennes qui présentent des variations saisonnières au niveau du

contenu en azote dans leurs tissus, notamment au cours de la sénescence automnale et de la remobilisation printanière. Les précédentes études avaient principalement porté sur la mise en réserve de l'azote sous forme de protéines de stockage au cours de l'hiver et sur la remobilisation sous forme d'acides aminés de cet azote stocké au cours de l'hiver. Ces deux périodes avaient été principalement étudiées en se focalisant sur les flux printaniers d'acides aminés et la synthèse puis la dégradation des protéines de réserves. En ce qui concerne les aspects moléculaires de ces phénomènes et notamment les mécanismes de transfert et de translocation au niveau des différents tissus de l'arbre, peu de données existaient.

Les principales études portant sur la caractérisation moléculaire des transporteurs d'ammonium et d'acides aminés chez les plantes s'étaient focalisées sur des espèces herbacées et plus particulièrement *Arabidopsis thaliana*, la première plante dont le génome a été entièrement séquencé. Le séquençage du génome du peuplier permet à présent de mieux appréhender les mécanismes de transport d'une espèce pérenne, et en particulier ceux de l'ammonium et des acides aminés.

L'azote est un des éléments limitant la croissance des arbres et par conséquent la productivité forestière. L'azote est essentiel pour l'utilisation du carbone, la croissance et le développement des racines, ainsi que pour le transport d'autres nutriments entre les différents organes des plantes. L'application de fertilisants azotés est une des approches utilisées pour augmenter la croissance et la production des plantations forestières. Toutefois, les phénomènes de remobilisation de l'azote chez les arbres constituent une stratégie efficace pour l'économie et une meilleure utilisation des ressources azotées. Ces phénomènes étant peu caractérisés, mes travaux avaient pour but d'obtenir une meilleure compréhension de ces différents mécanismes pouvant aider à mieux appréhender les mécanismes utilisés par le peuplier pour absorber mais également transférer les principaux éléments azotés nécessaires à sa croissance et son développement et à plus long terme augmenter la productivité d'une des essences les plus cultivées en France.

1. Analyses bio-informatiques et annotation du génome du peuplier

La première partie de mon travail a consisté à identifier les gènes putatifs codant pour des protéines impliquées dans le transport de composés azotés mais également dans l'assimilation de l'azote inorganique. Ces analyses entraient également dans le cadre de la participation de notre équipe à l'annotation du génome du peuplier. Celui-ci fût le premier arbre pour lequel le séquençage et l'assemblage du génome ont été réalisés (Tuskan et al., 2006, P2).

Ce travail a permis d'identifier environ 45 000 gènes putatifs répartis sur 19 groupes de liaison. L'analyse du génome assemblé a également mis en évidence un évènement de duplication entière du génome, à l'issu duquel environ 8 000 paires de gènes dupliqués ont été conservées dans le génome du peuplier. Un second évènement de duplication plus ancien, coïncide avec la divergence entre *Populus* et *Arabidopsis*. Le peuplier présente ainsi un nombre plus important de gènes codant des protéines qu'*Arabidopsis*, avec en moyenne 1,4 à 1,6 homologues putatifs présents chez le peuplier pour chaque gène chez *Arabidopsis*. Les gènes surreprésentés chez le peuplier incluent des gènes associés avec la biosynthèse de la paroi ligno-cellulosique, le développement du méristème, la résistance aux maladies ainsi que le transport des métabolites. Pour les gènes reliés aux mécanismes de transport, environ 1800 gènes ont été répertoriés dans le génome du peuplier. Cela représente un peu moins du double du nombre de gènes présents chez *A. thaliana*. Néanmoins, une étude détaillée des différentes familles révèle l'expansion de certaines d'entre elles chez le peuplier. Ainsi pour les familles de transporteurs de composés azotés, le peuplier possède plus du double de gènes pour la famille des transporteurs d'ammonium (AMT) mais également pour les deux superfamilles principales de transporteurs d'acides aminés (ATF et APC) (Figure 1).

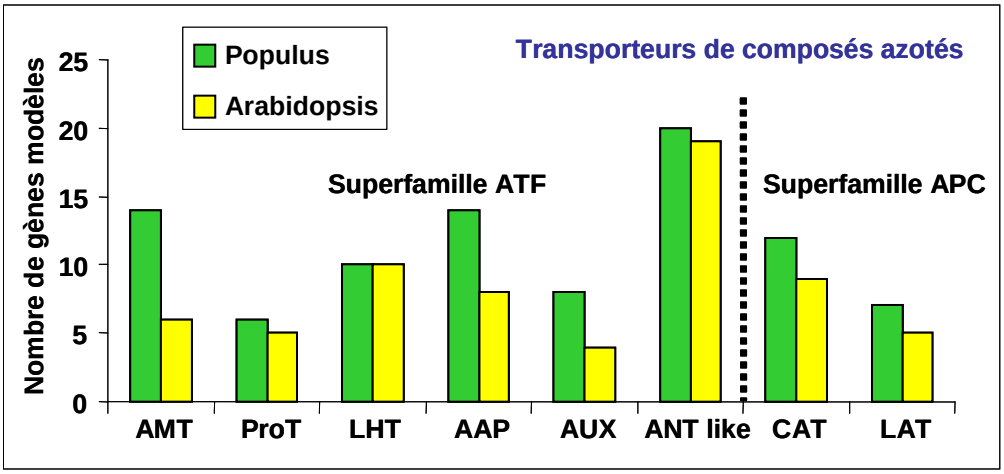

Figure 1. Comparaison de nombre de gènes modèles codant des transporteurs de certains composés azotés répertoriés chez le peuplier et *Arabidopsis thaliana*. Les abréviations utilisées sont : ATF, amino acid transporter superfamily ; APC, amino acid polyamine choline ; AMT, ammonium transporter ; ProT, proline transporter ; LHT, lysine histidine transporter ; AAP, amino acid permease ; AUX, auxin transporter; ANT like, aromatic and neutral amino acid transporter like ; CAT, cationic amino acid transporter ; LAT, L-type amino acid transporter.

Une fois les gènes répertoriés, un travail plus approfondi d'analyse *in silico* de l'expression des différents gènes d'intérêt via les banques d'ESTs disponibles a permis de mieux cerner les conditions expérimentales à utiliser pour la caractérisation de chacun de ces gènes. La mise en évidence d'une expansion du nombre de gènes codant des transporteurs d'ammonium et certains transporteurs d'acides aminés nous ont amené à nous focaliser sur ces familles de gènes et à entreprendre la caractérisation des membres de ces familles.

2. Caractérisation des membres de la famille des transporteurs d'ammonium

La seconde partie de mon travail a consisté à caractériser les membres de la famille des transporteurs d'ammonium impliqués dans l'absorption et le transport de l'ammonium chez le peuplier (Couturier et al., 2007, P3). La famille de transporteurs d'ammonium (AMT) est constituée de 14 gènes chez le peuplier, contre 6 chez *Arabidopsis* et 10 chez le riz. L'analyse par RT-PCR (reverse transcription-polymerase chain reaction) des profils d'expression de chaque membre *AMT* dans les différents organes de peuplier a révélé que certains transporteurs semblent spécifiquement ou préférentiellement exprimés dans des tissus particuliers (Figure 2).

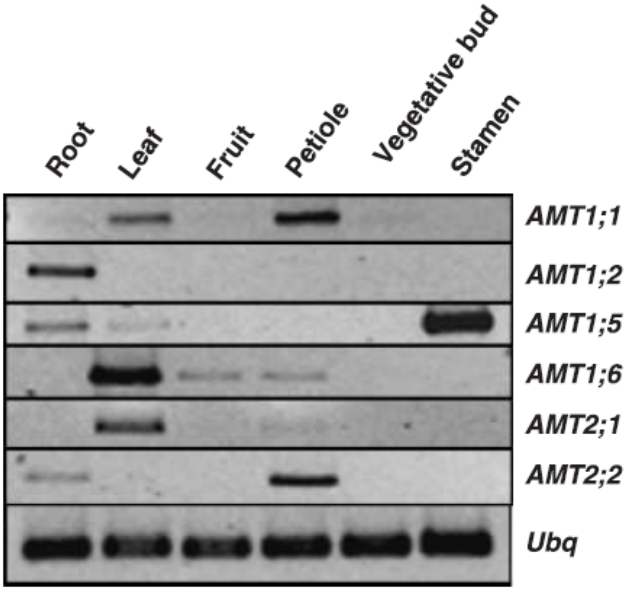

Figure 2. Etude de l'expression des *AMTs* dans différents organes de peuplier. L'expression des différents gènes a été évaluée par RT-PCR après extraction des ARN totaux de racine (root), feuille (leaf), fruit (fruit), pétiole (petiole, de bourgeon végétatif (vegetative bud) et d'étamines (stamen). Le gène ubiquitine (Ubq) a été amplifié et utilisé comme contrôle interne. Les expériences ont été répétées au moins trois fois, avec des résultats similaires (Couturier et al., 2007, P3).

Par exemple *AMT1;2* est uniquement exprimé au niveau des racines, *AMT1;5* est fortement exprimé dans les étamines et *AMT3;1* est uniquement exprimé dans les feuilles sénescentes. D'autre part, il a aussi été démontré qu'un évènement de duplication a abouti dans le cas de *AMT2;1* et *AMT2;2* à une spécialisation tissulaire, *AMT2;1* étant exprimé dans le limbe et *AMT2;2* plutôt dans le pétiole et les racines. Néanmoins, pris dans leur ensemble, les transporteurs d'ammonium du peuplier sont exprimés dans la majorité des tissus testés. Pour compléter ces résultats, des analyses complémentaires d'expression par RT-PCR couplées à des mesures par GC-MS (Gas Chromatography-Mass Spectrometry) des teneurs en acides aminés au niveau des feuilles et des racines de peuplier carencés en azote ont permis de mettre en évidence la régulation par l'azote de certains *AMTs*. Des analyses similaires visant à évaluer l'influence de la lumière et des composés carbonés sur l'expression des *AMTs* ont également été réalisées. L'expression hétérologue de AMT1;2 et AMT1;6 dans le mutant Δ*3mep* de levure a permis de déterminer l'affinité de ces transporteurs d'ammonium et de confirmer que ce sont bien des transporteurs d'ammonium à haute affinité. Pour conclure, les différents résultats obtenus permettent d'émettre l'hypothèse que de multiples gènes *AMT*, présentant des profils différents d'expression et de régulation, permettent à la plante de répondre efficacement à des conditions nutritionnelles environnementales variables. Finalement, cette étude a également mis en évidence des caractéristiques propres au style de vie pérenne du peuplier, comme la remobilisation de l'ammonium au cours de la sénescence (AMT3;1) et au sein de la symbiose ectomycorhizienne (AMT1;2), au travers de l'expression spécifique de certains gènes.

3. Etude de la remobilisation automnale de l'azote chez le peuplier

La troisième partie de mon travail consistait à étudier la sénescence automnale du peuplier en conditions naturelles, en se focalisant plus particulièrement sur les flux d'acides aminés entre les feuilles et les organes pérennes comme les tiges et les protéines potentiellement impliquées dans ces flux (Couturier et al., 2010, P10). L'analyse par GC-MS (Gas Chromatography- Mass Spectrometry) des teneurs en acides aminés dans le limbe, le pétiole et la tige au cours de la sénescence automnale a permis de montrer une remobilisation de l'azote des feuilles vers les organes pérennes du peuplier. Les acides aminés riches en azote, tels que la glutamine, sont transportés, via le phloème, des feuilles sénescentes vers les organes pérennes, tels que les tiges, où ils sont utilisés pour la synthèse de protéines de réserve. Cette étude montre une forte accumulation d'arginine au niveau des tiges au cours de l'automne et au début de l'hiver. Dans les mêmes conditions expérimentales, des analyses d'expression, par

RT-PCR semi-quantitative, des gènes codant des enzymes impliquées dans la synthèse de l'arginine laissent supposer que la synthèse d'arginine a préférentiellement lieu au niveau des tiges. D'autre part l'arginine serait également préférentiellement synthétisée à partir du carbamoyl-phosphate, dérivant lui-même de la glutamine issue de la remobilisation de l'azote au niveau des feuilles. Parallèlement, des analyses d'expression, par RT-PCR semi-quantitative, des gènes codant des transporteurs d'acides aminés cationiques (CAT) ont mis en évidence des motifs d'expression variables au cours de la sénescence et que certains pourraient être impliqués dans la remobilisation automnale de l'azote. Il s'agit notamment du transporteur CAT11 dont l'expression au niveau des tiges, est sujette à de fortes variations qui sont reliées aux teneurs en acides aminés et notamment la glutamine. De plus, la caractérisation fonctionnelle de ce transporteur via l'utilisation de deux mutants de levure a montré qu'il pouvait prendre en charge différents acides aminés et notamment la glutamine (Figure 3).

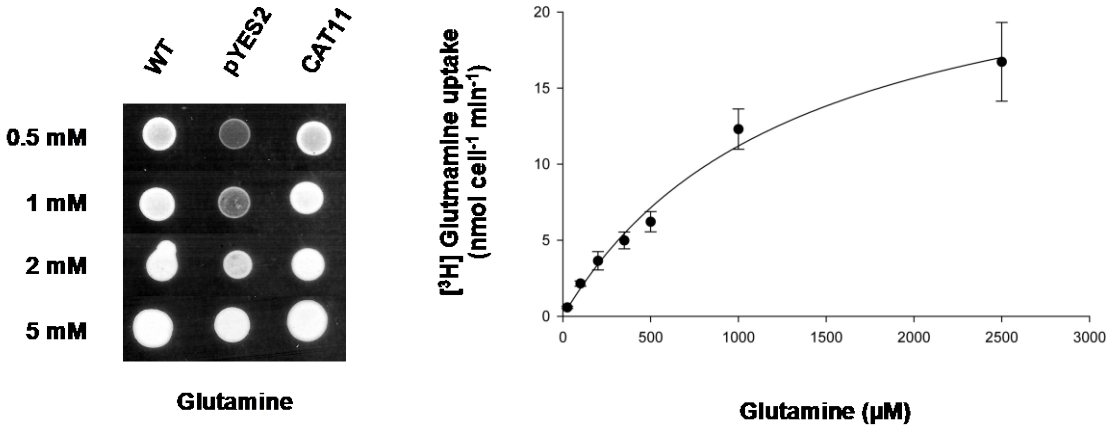

Figure 3. **Caractérisation fonctionnelle du transporteur PtCAT11 comme transporteur de glutamine.** (A) Complémentation du mutant JA248 de levure par expression hétérologue de PtCAT11 en présence de glutamine. La souche de levure JA248 a été transformée avec le vecteur d'expression pYES2 ou pYES2-PtCAT11. La croissance des différentes souches a été évaluée sur un milieu dépourvu d'azote N supplémenté par 0,5, 1, 2 ou 5 mM de L-glutamine comme seule source d'azote et 20 g/l de galactose comme source de carbone. Les photos ont été prises après 2 jours de croissance à 30°C et sont représentatives de trois répétitions. (B) Suivi cinétique du transport de glutamine [^{3}H] glutamine par la souche de levure JA248 exprimant PtCAT11 en présence de concentrations croissantes de glutamine (Couturier et al., 2007, P10).

PtCAT11 jouerait donc un rôle majeur lors de la remobilisation automnale de l'azote foliaire en favorisant l'export de la glutamine des feuilles vers les organes pérennes mais également en

facilitant le transfert de glutamine entre les tissus conducteurs et les cellules des organes pérennes, la glutamine servant de précurseur à la synthèse d'arginine notamment.

4. Etude de la remobilisation printanière de l'azote chez le peuplier

La dernière partie de mon travail, en relation avec la précédente, était d'étudier la remobilisation printanière de l'azote au travers d'un phénomène très visible, le débourrement des bourgeons. Ce travail s'est notamment attaché à caractériser un transporteur d'acides aminés principalement exprimé au niveau du bourgeon (Couturier et al., 2010, P9).

Des analyses phylogénétiques avaient révélé que le génome du peuplier contient 14 gènes codant pour des transporteurs d'acides aminés appartenant à la famille AAP (Amino Acid Permease). Des études d'expression par RT-PCR montrent qu'un membre de cette famille, *AAP11*, est uniquement exprimé au niveau du bourgeon végétatif. Des analyses complémentaires ont permis de montrer que ce gène est exprimé au cours de l'hiver, avant le débourrement printanier. Parallèlement, des études histologiques révèlent que le xylème est progressivement formé au cours de l'hiver au niveau des bourgeons. Après transformation de jeunes plants de peuplier, des analyses complémentaires d'expression par fusion promoteur - gène rapporteur *GUS* démontrent une expression spécifique du gène *AAP11* au niveau des cellules du xylème en différenciation de l'apex des tiges jeunes, des racines et des tiges âgées (Figure 4). La caractérisation fonctionnelle de ce transporteur à l'aide d'un mutant de levure a également été réalisée et a démontré que AAP11 était un transporteur d'acides aminés à haute affinité et plus particulièrement pour la proline. Ainsi, la caractérisation fonctionnelle du transporteur et les différentes études d'expression réalisées suggèrent que AAP11 tient un rôle majeur dans la xylogenèse (mise en place des vaisseaux du xylème) en facilitant la fourniture de proline pour la synthèse des protéines, riches en proline et en hydroxyproline, présentes au niveau des parois cellulaires des cellules du xylème.

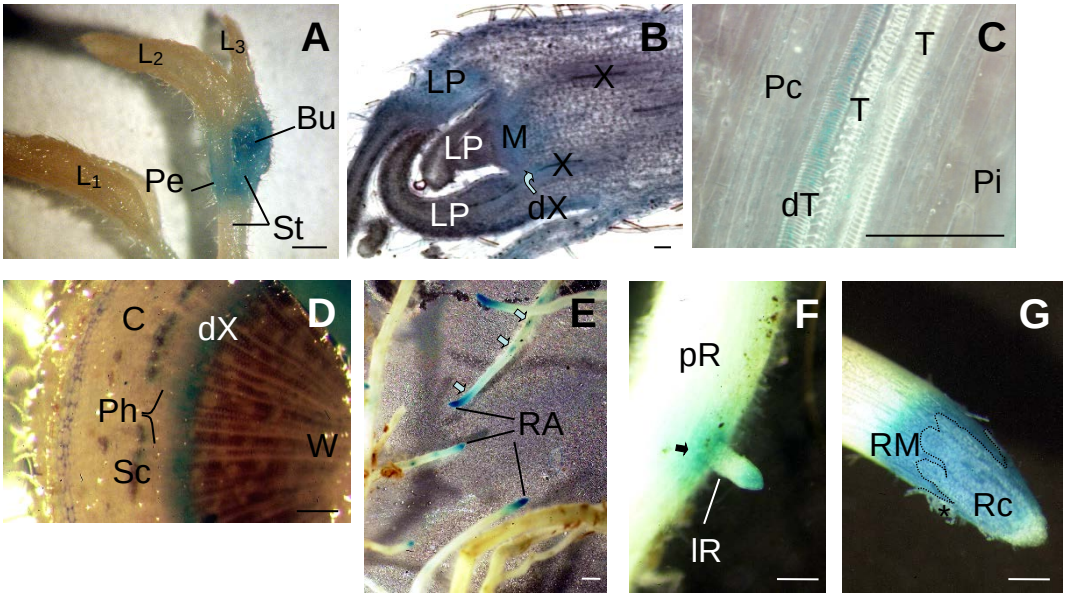

Figure 4. Analyses histo-chimiques de l'expression du transporteur AAP11 par fusion du promoteur du gène *AAP11* avec le gène rapporteur GUS. Ces analyses ont été réalisées à partir de plantes âgées de 3 semaines (A-C) et de 6 mois (D-G). (A) Dans la partie aérienne des plantes, l'expression de PtAAP11-GUS est limitée à l'extrémité de la pousse au niveau du bourgeon (Bu), de la jeune tige (St) et du pétiole (Pe). (B) Dans l'apex de la pousse (coupe longitudinale), l'expression PtAAP11-GUS est localisée au niveau du méristème apical de la pousse (M) et à la base du primordium de la feuille (LP), plus particulièrement dans les vaisseaux du xylème (X) et dans le xylème en différenciation (dX). (C) L'observation d'une coupe longitudinale du protoxylème situé à la base d'un primordium de feuille montre que l'expression de PtAAP11-GUS est limitée aux trachéides en différenciation (dT) proches du procambium (Pc). (D) Dans la partie basale des tiges, l'expression de PtAAP11-GUS est élevée dans le xylème secondaire en différenciation (dX) et faible au voisinage des cellules du sclérenchyme (Sc). (E) Dans les jeunes racines, l'expression de PtAAP11-GUS est très élevée à l'apex de la racine (PR) et plus faible et restreinte à certaines zones dans le cylindre vasculaire (flèches bleues). (F) PtAAP11-GUS est exprimé à la jonction racine parentale (pR) - racine latérale (lR) lors de l'émergence de cette dernière (flèche noire). (G) Une forte expression de PtAAP11-GUS est observée au niveau du méristème apical de la racine (RM), mais pas dans la partie la plus externe de la racine (Rc). Abréviations supplémentaires : C, cortex ; L1, L2, L3, feuilles numérotées par ordre d'apparition ; Ph, phloème ; Pi, moelle ; T, trachéide ; W, bois. Barres (A, D, F, G) 1 mm ; (E) 0,5 mm ; (B, C) 0,05 mm. Des résultats identiques ont été obtenus avec quatre lignées transgéniques indépendantes (Couturier et al., 2007, P9).

5. Principales conclusions et perspectives

L'azote est un des éléments limitant la croissance des arbres et par conséquent la productivité forestière. L'azote est essentiel pour l'utilisation du carbone, la croissance et le développement des racines, ainsi que pour le transport d'autres nutriments entre les différents

organes des plantes. L'application de fertilisants azotés est une des approches utilisées pour augmenter la croissance et la production des plantations forestières. Toutefois, les phénomènes de remobilisation de l'azote chez les arbres constituent une stratégie efficace pour l'économie et une meilleure utilisation des ressources azotées (Figure 5). Les différents travaux effectués au cours de mon travail de thèse s'inscrivaient dans des études plus globales visant à mieux comprendre les mécanismes utilisés par le peuplier pour absorber mais également transférer les principaux éléments azotés nécessaires à sa croissance et son développement. Ainsi, une meilleure compréhension de ces différents mécanismes pourrait aider à mieux appréhender les transferts d'azote de l'arbre et à plus long terme augmenter la productivité d'une des essences les plus cultivées en France.

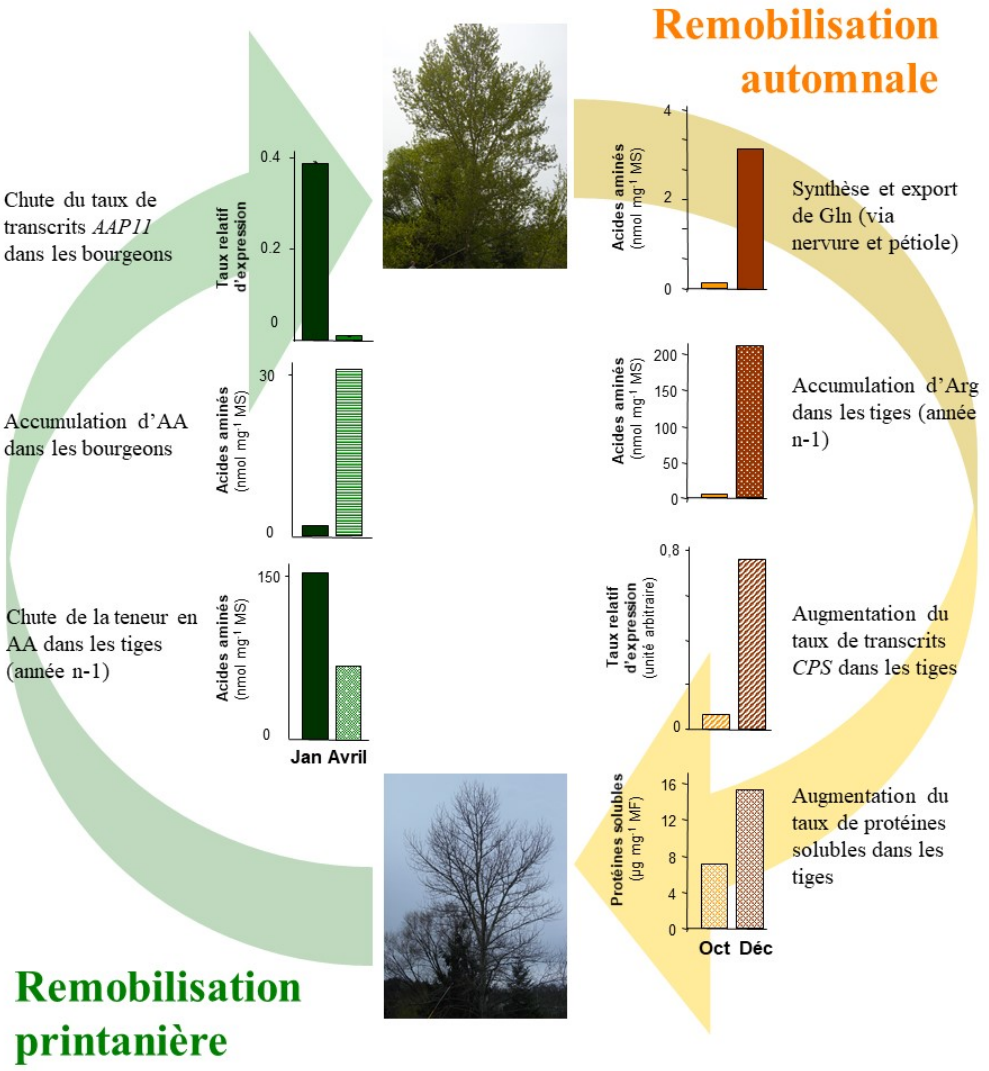

Figure 5. **Principaux mécanismes moléculaires de la remobilisation saisonnière de l'azote chez le peuplier.** Ces mécanismes identifiés au cours de mon doctorat portent à la fois sur la remobilisation printanière (partie gauche du schéma) que la remobilisation automnale (partie droite du schéma) et concernent les parties aériennes uniquement.

ACTIVITES DE RECHERCHE POST-DOCTORALE

Analyse biochimique, structurale et fonctionnelle des glutarédoxines de plantes

En février 2008, j'ai intégré l'équipe Réponse aux stress et Régulation Redox (UMR1136 IAM UL/INRA). Mes activités de recherche se sont alors articulées autour de deux grands thèmes principaux. Le premier thème portait sur la caractérisation biochimique et structurale des glutarédoxines de plantes (GRXs) tandis que le deuxième thème concernait l'implication de certaines GRXs dans la biogenèse des centres fer-soufre (Fe-S) et la régulation de l'homéostasie du fer chez les plantes. Les principaux modèles utilisés ont été le peuplier (*Populus trichocarpa*) et l'arabette (*Arabidopsis thaliana*). Au cours cette période post-doctorale, j'ai également effectué un séjour de quelques mois (février-juin 2010) au sein du laboratoire « Biochemistry and Physiology of Plants » dirigé par le Professeur Karl-Josef Dietz (Université de Bielefeld, Allemagne) afin d'y poursuivre la caractérisation d'une isoforme atypique de GRX. Ce séjour à Bielefeld m'a également permis d'initier l'étude d'une enzyme, la sédoheptulose bisphosphatase de peuplier, enzyme régulée du cycle de Calvin dont les propriétés étaient encore peu connues. Cette protéine est d'autant plus intéressante qu'elle est réduite par le système chloroplastique ferrédoxine/thiorédoxine. Ces travaux initiaux ont servi de base au projet de thèse de Désirée Gütle portant sur l'analyse comparative des propriétés biochimiques et structurales des protéines SBPase et FBPase de la mousse *Physcomitrella patens* (Gütle et al., 2016, P31).

En milieu aérobie, les organismes vivants sont inévitablement soumis à des conditions de stress oxydant caractérisées par la production d'espèces réactives de l'oxygène, de l'azote et du soufre. La génération de ces composés est souvent exacerbée chez les plantes faisant face à des contraintes biotiques et abiotiques. Chez les plantes, comme chez les autres organismes, la majorité de ces composés présente une double fonction, en pouvant endommager différentes macromolécules (ADN, lipides, protéines) mais en agissant également en tant que seconds messagers. Dûe à la réactivité de leur groupement thiol, certains résidus cystéine présents au sein des protéines sont particulièrement sensibles à l'oxydation par ces molécules. Les modifications post-traductionnelles induites et réversibles pour certaines d'entre elles, comme la formation de pont disulfure, la sulfénylation, la glutathionylation, la nitrosylation, et la persulfuration sont contrôlées par deux familles d'oxydoréductases, les glutarédoxines (GRXs) et les thiorédoxines (TRXs). Il est maintenant reconnu que les TRXs et les GRXs contrôlent l'état redox d'une myriade de protéines chez les organismes vivants et notamment les plantes.

Les GRXs et les TRXs ont été identifiées pour la première fois dans la bactérie *Escherichia coli* comme donneurs d'électrons pour la ribonucléotide réductase (RNR) (Laurent et al., 1964 ; Holmgren, 1976). Cependant, leur système de réduction est différent. Les TRXs dépendent généralement des NADPH- ou ferrédoxine-thiorédoxine réductases (NTR et FTR) alors que les GRXs dépendent du glutathion (GSH) et de la GSH réductase (GR) associée, dépendante du NADPH. Quelques études ont néanmoins démontré que certaines GRXs peuvent être réduites par les TRX réductases (Johansson et al., 2004 ; Fernandes et al., 2005 ; Zaffagnini et al., 2008) et quelques TRXs par le GSH et/ou GRX (Gelhaye et al., 2003 ; Koh et al., 2008 ; Zhang et al., 2014). Ces deux familles de protéines qui partagent une structure 3D similaire ont fait l'objet d'études approfondies tant chez les procaryotes que chez les eucaryotes afin de mieux comprendre et identifier leurs spécificités. Il apparaît ainsi que du fait de leur capacité à interagir et reconnaître le GSH, les GRXs sont plus particulièrement impliquées dans la réduction de protéines glutathionylées, alors que les TRXs sont plutôt impliquées dans la réduction des liaisons disulfure impliquant deux résidus cystéine protéiques. La glutathionylation correspond à la formation d'un pont disulfure spécifique entre la cystéine du GSH et un résidu cystéine d'une seule protéine. Cette modification représente un intermédiaire réactionnel de certains mécanismes catalytiques, mais elle est aussi considérée comme un mécanisme de régulation modulant la fonction des protéines pour la signalisation ou comme mécanisme de protection des résidus cystéine contre l'oxydation irréversible (Mieyal et al., 2008 ; Dalle-Donne et al., 2009 ; Zaffagnini et al., 2012). En principe, bien que la réduction des protéines glutathionylées ne nécessite qu'une seule cystéine catalytique, de nombreuses GRXs possèdent un site actif dithiol CxxC. Ce motif a initialement été utilisé pour différencier les GRXs dithiol avec un motif CPY/FC et les GRXs monothiol avec un site actif de type CGFS (Rodriguez-Manzaneque et al., 1999). Cependant, à partir d'analyses génomiques et phylogénétiques comparatives plus approfondies, la classification des GRXs a été affinée, notamment pour les organismes photosynthétiques (Alves et al., 2009 ; Couturier et al., 2009, P5). Ces analyses ont mis en lumière une variabilité dans les séquences des sites actifs avec par exemple de nombreuses GRXs ayant des sites actifs monothiol (CSYS ou CPYS) et formant un clade avec des isoformes ayant des sites actifs de type CPYC. Par conséquent, les GRXs ayant un site actif CPY/FC ou des sites actifs proches appartiennent à la classe I, alors que les GRXs avec un site actif CGFS appartiennent à la classe II (Couturier et al., 2009, P5). Les GRXs sont présentes chez la majorité des organismes procaryotes et eucaryotes, excepté certaines bactéries et archées avec au moins une isoforme de ces deux classes (Alves et al., 2009 ; Couturier et al., 2009, P5). Les plantes supérieures possèdent entre 25 et 40 isoformes GRX réparties principalement en quatre

sous-groupes distincts. La classe I regroupe les GRXs possédant un site actif de type C[P/G/S][Y/F][C/S], incluant donc les GRXs dithiol classiques. Les GRXs de la classe II ont un site actif strictement conservé de type CGFS. Cette classe inclut les homologues des GRXs 3, 4 et 5 de levure mais aussi de la GRX4 d'*E. coli*. Les plantes possèdent généralement 4 membres dans ce groupe (GRXS14, S15, S16 et S17). La classe III, spécifique aux plantes supérieures, regroupe les GRXs ayant un site actif de type CC[M/L][C/S] tandis que les isoformes de classe IV possèdent un domaine GRX fusionné à d'autres domaines protéiques (Couturier et al., 2009, P5).

Le mécanisme catalytique utilisé par les GRXs est notamment lié au nombre de cystéines du site actif et au type de liaison disulfure présente dans les protéines cibles (Rouhier et al., 2008) (Figure 6). Dans tous les cas, la cystéine du site actif en position N-terminale constitue le résidu catalytique et est indispensable à l'activité réductase. Les GRXs ayant au moins deux cystéines peuvent utiliser un mécanisme dithiol pour la réduction des ponts disulfure, de manière similaire au mécanisme utilisé par les TRXs. Ainsi, la réduction de la protéine cible conduit à la formation d'un pont disulfure intermoléculaire entre la protéine cible et la cystéine catalytique de la GRX. L'attaque de ce pont disulfure par une seconde cystéine de la GRX libère la protéine cible entièrement réduite et conduit à la formation d'un pont disulfure intramoléculaire au niveau de la GRX. Cette forme oxydée est réduite par l'action successive de deux molécules de GSH ou par une TRX réductase. Les GRXs ayant une seule cystéine au niveau de son site actif ou n'utilisant qu'une seule cystéine de son site actif pour catalyser la réaction de déglutathionylation des protéines emploie un mécanisme monothiol. Dans ce cas, la réduction ultérieure de l'intermédiaire glutathionylé de la GRX, formé après la première étape, nécessite une molécule de GSH libre. Néanmoins, pour les GRXs de classe I et II, ne possédant qu'une seule cystéine au niveau de leur site actif, la présence d'une cystéine additionnelle dans la région C-terminale, très souvent dans une séquence GGCD, et située à proximité au site actif peut mener à la formation d'un pont disulfure intramoléculaire et au suivi d'un mécanisme dithiol. Ainsi, toute GRX possédant au moins deux de ces cystéines peut en principe présenter une activité réductase par un mécanisme monothiol ou dithiol.

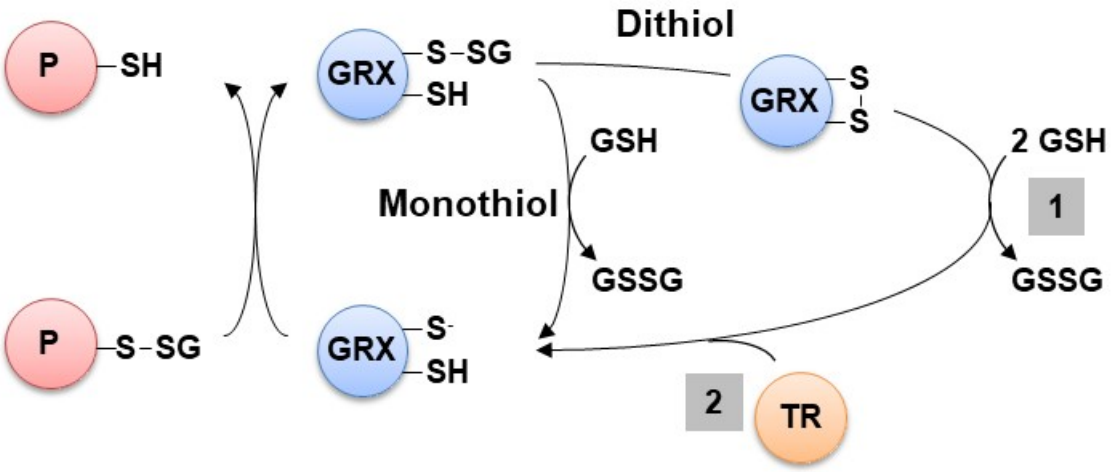

Figure 6. Description schématique des mécanismes catalytiques monothiol et dithiol employés par les GRXs pour la réduction de protéines cibles. Après réduction de l'adduit glutathion présent sur la protéine cible, la GRX devient elle-même glutathionylée. Dans le mécanisme monothiol, seule la cystéine catalytique est nécessaire, car la GRX est régénérée par une autre molécule de GSH. Dans le mécanisme dithiol, une seconde cystéine dite de recyclage, qui pourra être soit la deuxième cystéine du site actif, soit une autre cystéine, est responsable de la réduction de l'adduit de glutathion de la GRX conduisant à la formation d'un pont disulfure intramoléculaire. Celui-ci peut être réduit par deux molécules de GSH (1) ou par une TRX réductase (2)

Au début de mes travaux, la plupart des travaux biochimiques et structuraux menés sur les GRXs de plantes concernait certaines isoformes appartenant aux classes I et II. Mon travail s'insérait dans un projet plus global d'études des GRXs et de leurs rôles dans la physiologie des plantes. Les différents travaux menés ont principalement porté sur la caractérisation biochimique et structurale des GRXs de classe I, la caractérisation biochimique des GRXs de classe III pour lesquelles très peu de données biochimiques existaient et l'étude du rôle des GRXs de classe II dans la biogenèse des centres Fe-S et dans la régulation de l'homéostasie du fer.

1. Caractérisation biochimique et structurale des isoformes GRXS12 de peuplier et GRXC5 d'*A. thaliana*

Les analyses phylogénétiques conduites au début de mon post-doctorat (Couturier et al., 2009, P5) avaient mis en évidence l'existence chez les plantes, de GRXs de classe I présentant un site actif particulier différent du motif classique CPYC. La caractérisation biochimique et structurale de la GRXS12 de peuplier et de la GRXC5 d'*A. thaliana* présentant respectivement un site actif atypique WCSYS et WCSYC a donc été entreprise. Les différents travaux menés

ont ainsi démontré qu'en dépit d'une forte homologie de séquence (70% d'identité), GRXS12 et GRXC5 possèdent des propriétés biochimiques, structurales et spectroscopiques différentes (Couturier et al., 2009, P4 ; Couturier et al., 2011, P12 ; Zaffagnini et al., 2012, P13). Ces deux protéines sont localisées dans les chloroplastes et représentent un bel exemple d'évènement de duplication ayant abouti à une néo-fonctionnalisation.

La protéine recombinante PtGRXS12 est capable de réduire *in vitro* les substrats conventionnels des GRXs. Un travail de mutagenèse dirigée a permis de montrer que le mécanisme catalytique utilisé est de type monothiol c'est-à-dire qu'il n'implique que la cystéine du site actif, bien qu'une deuxième cystéine conservée (localisée dans la partie C-terminale de la protéine) soit très proche au niveau tridimensionnel. Couplée à des analyses de titration de groupements thiol, de fluorescence et de spectrométrie de masse, la résolution de la structure 3D de la protéine par cristallographie a permis d'identifier que la seule forme d'oxydation de la protéine observée consiste en la glutathionylation de la cystéine catalytique Cys29 (Figure 7). D'autre part, contrairement à d'autres isoformes de plantes, PtGRXS12 n'incorpore pas de centre Fe-S. Toutefois, des expériences de mutagenèse dirigée ont révélé que le simple remplacement du tryptophane W28 par une tyrosine permettait la fixation d'un centre Fe-S par PtGRXS12. Des expériences de modélisation structurale mimant les structures connues des formes holo de certaines isoformes GRX ont permis de formuler l'hypothèse que l'orientation de la chaîne latérale de ce résidu tryptophane empêche la fixation d'un centre Fe-S (Couturier et al., 2009, P4).

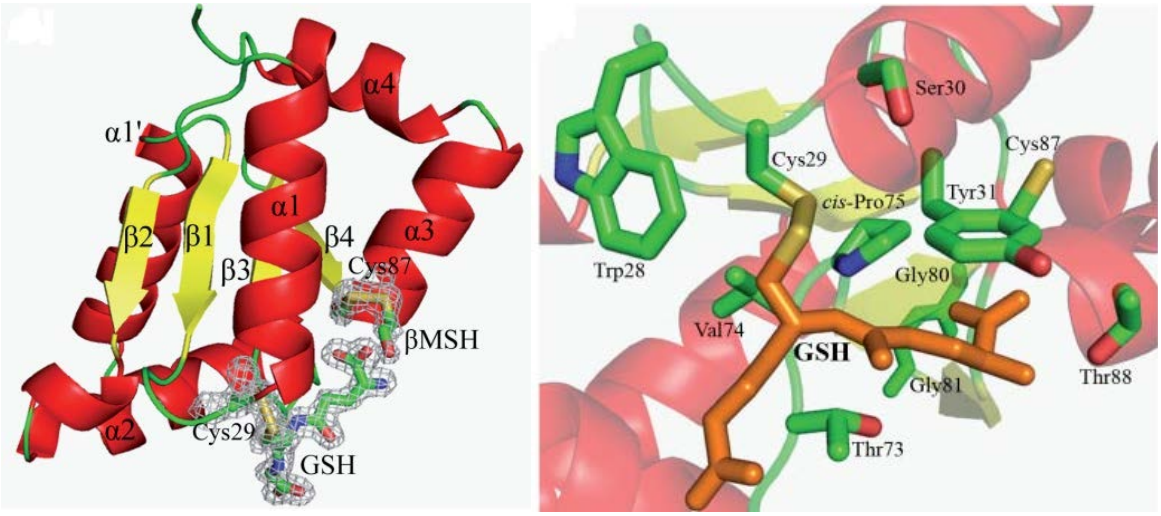

Figure 7. Structure cristallographique de la protéine PtGrxS12 sous forme glutathionylée. Les hélices α sont indiquées en rouge, les feuillets β en jaune et les boucles en vert. Les différentes structures secondaires sont également numérotées. Au niveau du site actif, une molécule de GSH (en orange) est liée de manière covalente à la cystéine catalytique Cys29 tandis que la présence du résidu Tyr31 empêche la formation d'un pont disufure intramoléculaire Cys29-Cys87 (Couturier et al., 2009, P4).

D’autre part, la caractérisation biochimique fine des mécanismes impliqués dans l’oxydation de cette protéine suggèrent que cette protéine jouerait un rôle de senseur du statut redox en relation avec le stress oxydant. En effet, lorsque cette protéine est glutathionylée, elle est temporairement inactivée jusqu’à sa réduction par le GSH. De plus, les propriétés biochimiques et thermodynamiques de PtGRXS12 suggèrent que la forme glutathionylée inactive de la protéine s’accumulerait en présence d’une oxydation modérée du pool de glutathion, phénomène observé lors d’un stress. Ainsi, PtGRXS12 agirait comme protéine senseur du statut redox en relation avec le stress et permettrait au GSH de jouer un rôle de signal de stress au travers de la glutathionylation des protéines cibles de la GRXS12 (Zaffagnini et al., 2012, P13).

Par la suite, dans la continuité de l’étude de l’isoforme GRXS12 de peuplier, j’ai entrepris la caractérisation biochimique et structurale de l’isoforme GRXC5 d’*A. thaliana*. Ce travail, débuté à Nancy, a été poursuivi au cours de mon séjour à Bielefeld (Allemagne) au sein du laboratoire dirigé par le Professeur Karl-Josef Dietz. Contrairement à l’isoforme GRXS12, GRXC5 est uniquement présente chez les Brassicacées suggérant un évènement de duplication propre à cette famille de plantes. AtGRXC5 possède un site actif atypique WCSYC, très proche de celui de GRXS12 et de la GRX2 humaine (SCSYC). Chez les mammifères, GRX2, qui peut fixer un centre Fe-S, serait impliquée dans la différentiation cellulaire et la progression tumorale (Lillig et al., 2005 ; Lönn et al., 2008 ; Bräutigam et al., 2011). La caractérisation biochimique et structurale de la protéine AtGRXC5 indique que contrairement à PtGRXS12 qui n’existe que sous forme apomonomérique, AtGRXC5 peut former un holodimère ayant la capacité de lier un centre [2Fe-2S] relativement stable et ayant des propriétés spectroscopiques très similaires à celles des autres GRXs de classe I, malgré la présence d’un résidu tryptophane en amont du site actif (Figure 8).

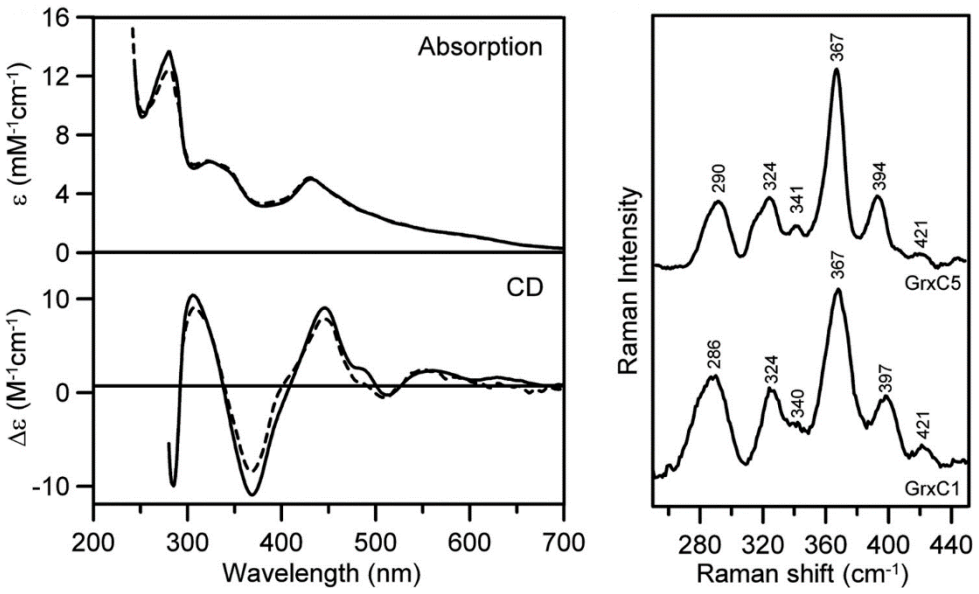

Figure 8. Comparaison des spectres d'absorption UV-visible, de dichroïsme circulaire et des spectres de résonance Raman des formes holoprotéines AtGRXC5 (trait plein) et PtGRXC1 (trait pointillé) (Couturier et al., 2011, P12).

D'autre part, comme PtGRXC1, AtGRXC5 ne peut pas transférer son centre Fe-S à une protéine acceptrice comme l'apoferrédoxine suggérant que cette GRX ne serait pas impliquée dans l'assemblage des centres Fe-S au niveau des chloroplastes. Des expériences de mutagenèse dirigée réalisées avec AtGRXC5 et PtGRXS12 et la résolution de la structure tridimensionnelle de la protéine sous forme holo, ont permis de démontrer que la présence d'une deuxième cystéine en position 32 au niveau du site actif était responsable de cette propriété, bien qu'elle ne constitue pas un ligand direct du centre Fe-S. De manière plus globale, la caractérisation des isoformes GRXC5 et GRXS12 a permis d'explorer certains déterminants moléculaires impliqués dans l'incorporation de centre Fe-S par les GRXs. Ainsi, il semble qu'en plus de la cystéine catalytique absolument nécessaire pour l'incorporation du centre [2Fe-2S], les résidus en position -1, +1 et +3 par rapport à la cystéine catalytique auraient des rôles cruciaux mais pas nécessairement avec le même poids. Enfin des mesures d'activité effectuées avec l'apoprotéine ont révélé que comparée à PtGRXS12, la présence d'une deuxième cystéine au niveau du site actif diminue l'efficacité catalytique de l'isoforme AtGRXC5 (Couturier et al., 2011, P12).

2. Analyse comparative des isoformes GRXC1, C2, C3 et C4 de peuplier

L'objectif de ce projet était d'apporter des éléments biochimiques permettant d'expliquer l'existence de plusieurs GRXs de classe I chez les plantes supérieures. Précédemment il avait été démontré que ces quatre isoformes présentent une plus ou moins grande spécificité d'expression tissulaire (Rouhier et al. 2006, P1). D'autre part, il a été mis en évidence la capacité de fixation d'un centre Fe-S par PtGRXC1 contrairement à PtGRXC2, PtGRXC3 et PtGRXC4 (Rouhier et al., 2007). Une analyse comparative approfondie des propriétés biochimiques et catalytiques des GRXs de la classe I dithiol du peuplier, à savoir PtGRXC1, PtGRXC2, PtGRXC3 et PtGRXC4 a donc été réalisée (Couturier et al., 2013, P23). L'évaluation de l'activité oxydoréductase *in vitro* de ces isoformes et de leurs mutants cystéiniques, couplée à la détermination du potentiel redox, des valeurs de pK_a de la cystéine catalytique, mais également des changements d'état redox en réponse à différents traitements oxydants, ont permis de distinguer deux sous-groupes. Les isoformes GRXC1 et GRXC2 présentent ainsi une plus faible efficacité catalytique que les isoformes GRXC3 et GRXC4. Ces différences d'efficacité catalytique sont en partie expliquées par les différences de réactivité de leur cystéine catalytique (pK_a) mais également par les différences d'affinité de chaque isoforme pour les substrats utilisés.

D'autre part, contrairement à GRXC3 et GRXC4, les isoformes GRXC1 et GRXC2 peuvent former des dimères covalents en raison de la présence d'une cystéine C-terminale additionnelle (CysC) absente chez les isoformes GRXC3 et GRXC4 (Figure 9). Bien que ces quatre isoformes possèdent toutes une seconde cystéine (CysB) au sein de leur site actif, la présence de ce résidu influence la réactivité de la cystéine catalytique (CysA) uniquement pour GRXC1 et GRXC2 (comme déjà observé précédemment pour AtGRXC5), mais pas pour GRXC3 et GRXC4. Cependant, toutes ces protéines peuvent former un pont disulfure intramoléculaire CysA-CysB impliquant les deux cystéines du site actif. Ceci pourrait représenter soit un mécanisme de protection contre la suroxydation de la cystéine catalytique, considérant que cette seconde cystéine n'est pas indispensable pour la réaction de déglutathionylation, soit un véritable intermédiaire catalytique se produisant lors de la réduction de substrats particuliers, ou dans des conditions ou des compartiments spécifiques où les niveaux de GSH sont insuffisants pour permettre la régénération de ces GRXs.

Dans l'ensemble, en plus de leur localisation subcellulaire et de leur spécificité d'expression tissulaire différentes, la duplication et le maintien au cours de l'évolution de

plusieurs GRXs de classe I chez plantes supérieures pourraient être expliqués par l'existence de propriétés biochimiques et catalytiques différentes.

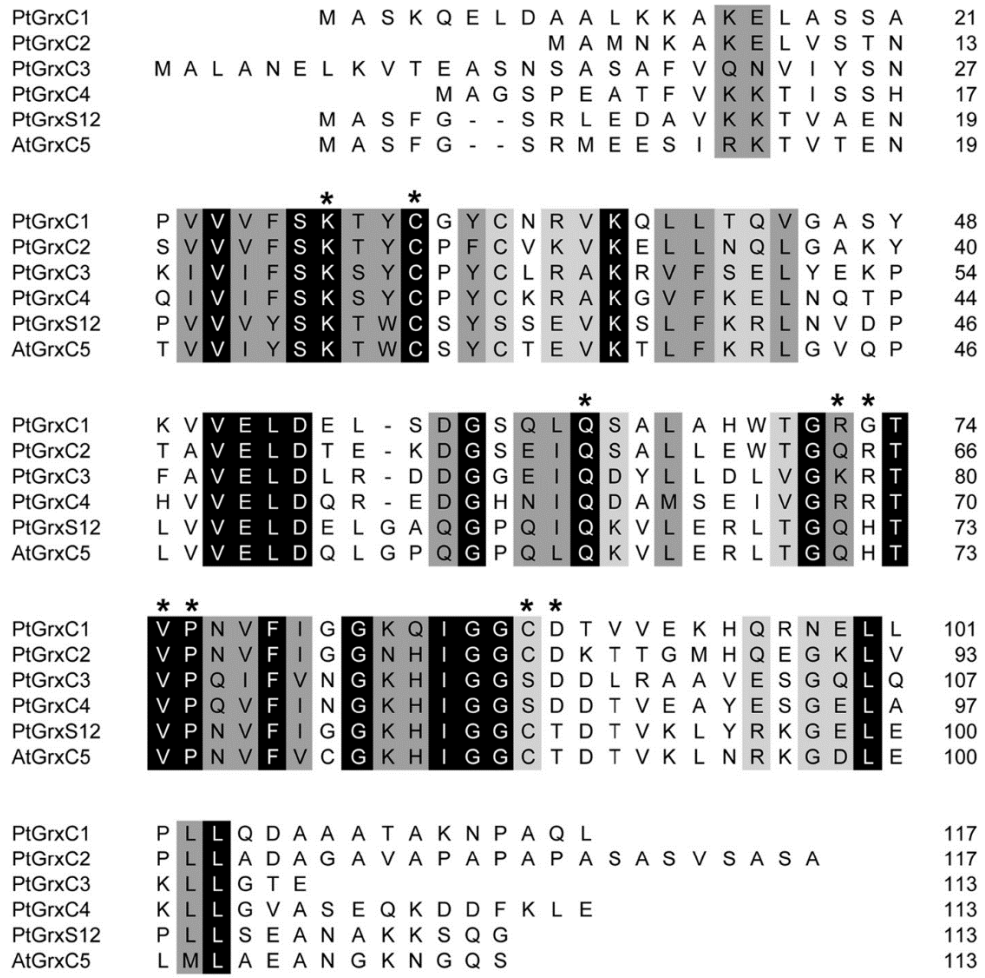

Figure 9. Alignement de séquences des GRXs de classe I. L'alignement a été réalisé à l'aide du logiciel ClustalW en utilisant les séquences primaires des protéines recombinantes dépourvues des séquences d'adressage potentielles. Les acides aminés strictement conservés sont représentés en blanc sur noir. Les acides aminés fortement conservés sont indiqués en noir sur gris. Enfin, les résidus impliqués dans la liaison du GSH, identifiés à partir des structures 3D de PtGRXC4, PtGRXS12 et AtGRXC5, sont marqués d'un astérisque (Couturier et al., 2013, P23).

3. Caractérisation biochimique des GRXs de classe III de peuplier

Les GRXs de classe III sont spécifiques aux plantes supérieures et possèdent un site actif de type CC[M/L][C/S] (Couturier et al., 2009, P5). Au début de ce projet, diverses études génétiques avaient mis en évidence le rôle particulier de certaines isoformes dans le développement floral et dans les mécanismes de défense contre les pathogènes au travers de l'interaction de ces GRXs avec des facteurs de transcription de type TGA. Il était suggéré que ces GRXs pourraient potentiellement réguler l'état redox de ces facteurs de transcription (Ndamukong et al., 2007 ; Xing & Zachgo, 2008, Li et al., 2009 ; Murmu et al. 2010, La Camera et al., 2011 ; Li et al., 2011). Néanmoins, aucune caractérisation biochimique de ces protéines n'avait été réalisée pour confirmer leur activité réductase. Cette absence de données était notamment liée à la difficulté de surexprimer ces protéines dans le système hétérologue bactérien *E. coli*. En effet, les différents essais de production de ces isoformes étaient infructueux, soit parce que les protéines n'étaient pas produites, soit parce qu'elles étaient insolubles et donc difficiles à purifier. Pour contourner ces différents obstacles et parvenir à étudier ces protéines d'un point de vue biochimique, j'ai donc entrepris un travail de génie génétique afin de transformer des GRXs de classe I en GRXs de classe III. Les sites actifs des isoformes PtGRXC1 et PtGRXC4 (respectivement YCGYC et YCPYC) ont été transformés en SCCMC et GCCMS par mutagenèse dirigée, mimant ainsi les sites les plus fréquemment observés dans les GRXs de classe III. Ainsi, j'ai pu produire et purifier des protéines solubles avec un site actif représentatif des GRXs de classe III. Un aspect remarquable de ce travail a été de montrer que toutes les protéines produites existaient sous une forme holoprotéine dimérique possédant un centre Fe-S et une forme apoprotéine monomérique n'incorporant pas de Fe-S, alors que seule PtGRXC1 pouvait naturellement incorporer un tel cluster. Ces résultats prometteurs ont été confirmés par l'obtention d'une véritable GRX de classe III, PtGRXS7.2 en remplaçant les cinq derniers acides aminés de cette protéine car ceux-ci semblent être liés à la non-expression et/ou l'insolubilité des protéines dans *E. coli*. La protéine ainsi purifiée présentait également la capacité de fixer un centre Fe-S. Concernant l'activité des apoformes, deux substrats classiquement utilisés dans le cas des GRXs, le DHA et le HED ont permis de mettre en évidence une faible activité réductase *in vitro* de ces protéines par rapport aux GRXs de classe I, PtGRXC1 et PtGRXC4.

4. Rôle des GRXs de classe II dans la biogenèse des centres Fe-S chez les plantes

Au début de ce projet, plusieurs travaux avaient mis en évidence que des versions recombinantes de GRXs de bactéries, de l'homme, de la levure et de plantes, produites dans *E. coli*, pouvaient assembler des centres Fe-S. Plusieurs isoformes GRX de classe I (GRXC1 de peuplier, GRXC5 d'*A. thaliana*, GRX2 humaine, Grx6 de levure et Grx1 de *Trypanosoma brucei*) fixent des centres de type [2Fe-2S] relativement stables (Lillig et al., 2005 ; Rouhier et al., 2007 ; Mesecke et al., 2008 ; Comini et al., 2008 ; Couturier et al., 2011, P12), tandis que les GRXs de classe II incorporent des centres [2Fe-2S] beaucoup plus labiles suggérant que ces GRXs auraient des fonctions bien différentes (Picciocchi et al., 2007 ; Bandyopadhyay et al., 2008, Iwema et al., 2009). Néanmoins, toutes les études spectroscopiques, structurales et de mutagenèse dirigée indiquent que les GRXs des classes I et II sont capables d'incorporer un centre [2Fe-2S] dans un homodimère, lié par la cystéine en position N-terminale du site actif de chaque monomère et par deux molécules externes de glutathion (Feng et al., 2006 ; Johansson et al., 2007 ; Rouhier et al., 2007 ; Iwema et al., 2009 ; Couturier et al., 2011, P12).

Initialement, un rôle pour la Grx5 de levure, une GRX de classe II, dans la biogenèse des centres Fe-S avait été suggéré à partir d'études du mutant de levure *grx5*. Les cellules de cette souche mutante présentent une déficience dans l'assemblage des centres Fe-S pour au moins deux protéines Fe-S (aconitase et succinate deshydrogénase) conduisant à des défauts de croissance et une augmentation de la sensibilité à un stress oxydant résultant probablement de l'accumulation de fer libre dans la cellule (Rodriguez-Manzaneque et al., 2002). Plus tard, il a été proposé que Grx5 faciliterait le transfert de centres pré-assemblés, de la protéine d'échafaudage Isu1 à des protéines acceptrices jouant ainsi le rôle de protéine de transfert (Mühlenhoff et al., 2003).

La conservation des mécanismes d'assemblage des centres Fe-S dans tout le règne vivant suggérait que les GRXs de classe II de plantes pourraient avoir des fonctions similaires. Des expériences de complémentation fonctionnelle du mutant de *S. cerevisiae* pour *grx5* avaient notamment démontré que la plupart des GRXs de classe II (notamment les isoformes de plantes, mais pas les GRXs de classe I, procaryotes ou eucaryotes peuvent fonctionnellement se substituer à Grx5, suggérant que ce rôle aurait été conservé au cours de l'évolution (Molina-Navarro et al., 2006 ; Bandyopadhyay et al., 2008 ; Cheng 2008). De plus, le rôle de protéine d'échafaudage ou de transfert pour les GRXs serait en accord avec la capacité des isoformes plastidiales de plantes, GRXS14 et GRXS16, de rapidement et quantitativement transférer leur centre [2Fe-2S] à une apoprotéine chloroplastique, la ferrédoxine, qui représente un potentiel

accepteur physiologique (Bandyopadhyay et al., 2008). Néanmoins, le rôle exact de ces protéines n'était pas déterminé et nécessitait d'être clarifié aussi bien chez les plantes que chez les eucaryotes non-photosynthétiques. En se basant sur la littérature existante, différentes protéines cibles potentielles ont été produites sous forme de protéines recombinantes dans le système hétérologue bactérien *E. coli* puis purifiées afin de réaliser des expériences de transfert *in vitro* et ainsi tester la possibilité de transfert de centres Fe-S entre ces protéines et les isoformes AtGRXS14 et AtGRXS16. Ces expériences réalisées en collaboration avec l'équipe du Professeur M.K. Johnson (Université de Géorgie, Athens, USA) ont notamment permis de mettre en évidence des transferts de centre Fe-S *in vitro* entre les GRXs, certaines protéines impliquées dans la biogenèse des centres Fe-S au niveau des chloroplastes. Par exemple la protéine de transfert AtNFU2 qui peut lier des centres de type [2Fe-2S] et [4Fe-4S] peut transférer spécifiquement un centre [2Fe-2S] à l'isoforme AtGRXS16 mais pas à l'isoforme AtGRXS14. Ce transfert est unidirectionnel puisque qu'aucun transfert de centre Fe-S n'a été observé entre AtGRXS14 et AtGRXS16 sous forme holoprotéine et AtNFU2 sous forme apoprotéine (Gao et al., 2013, P22). De plus, un transfert unidirectionnel de centre [2Fe-2S] a également été observé *in vitro* entre l'holoprotéine AtGRXS14 et l'apoprotéine AtSUFA1 qui est également une protéine de transfert chloroplastique (Mapolelo et al., 2013, P18).

Un transfert de centre [2Fe-2S] a également été caractérisé entre l'holoprotéine AtGRXS14 et l'apoprotéine AtSirB (sirohydrochlorine ferrochélatase) impliquée dans la voie de biosynthèse des sirohèmes au niveau des chloroplastes (Figure 10). Cette protéine qui possède un centre de type [2Fe-2S] (Raux-Deery et al., 2005) fût une cible de choix du fait que chez les vertébrés l'isoforme de classe II Grx5 est également requise pour la synthèse des hèmes chez les vertébrés sous-entendant que la biosynthèse de l'hème et du sirohème pourrait être affectée par des défauts dans l'insertion du centre [2Fe-2S] catalytiquement essentiel pour les ferrochélatases (Wingert et al., 2005). Néanmoins, ces résultats n'ont pas encore été publiés.

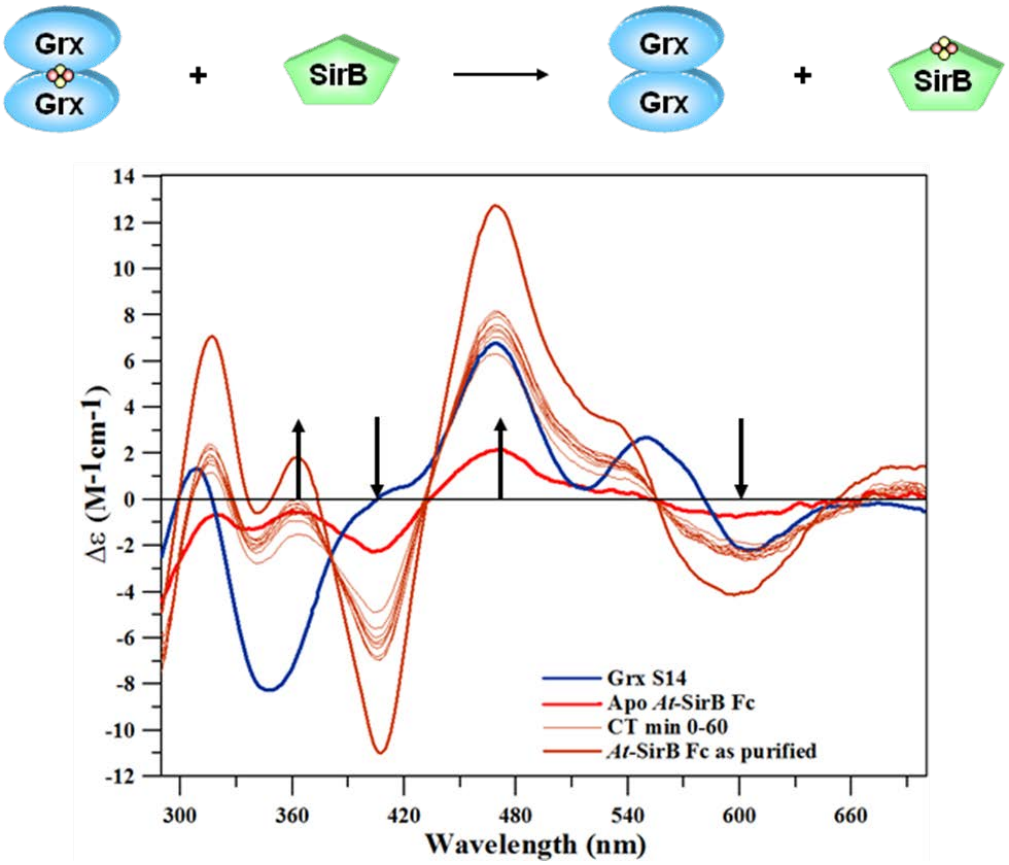

Figure 10. Suivi du transfert du centre [2Fe-2S] de l'holoprotéine GRXS14 vers l'apoprotéine SirB. Les flèches symbolisent le transfert de centre [2Fe-2S] en indiquant l'apparition au cours du temps du spectre caractéristique de l'holoprotéine SirB fixant un centre [2Fe-2S].

D'autres protéines ont également été produites et purifiées au cours de ce projet et les résultats obtenus ont pour certains servi de base à d'autres études postérieures comme la caractérisation fonctionnelle de la protéine AtNFU2 en collaboration avec l'équipe de Frédéric Gaymard (UMR Biochimie et Physiologie Moléculaire des Plantes, Montpellier) et le projet de thèse de Mélanie Roland (2016-2019) portant sur l'étude fonctionnelle de facteurs de maturation tardifs des protéines fer-soufre chloroplastiques chez *Arabidopsis thaliana*.

5. Rôle des GRXs de classe II dans le « sensing » et la régulation de l'homéostasie du fer chez les plantes : étude de l'interaction entre les GRX de classe II et les protéines BOLA

Chez la levure *Saccharomyces cerevisiae*, différentes études ont mis en évidence que les GRXs de classe II cytosoliques, Grx3 et Grx4, jouent un rôle dans la régulation de l'homéostasie du fer, dans la détection et le trafic de fer intracellulaire (Kumanovics et al., 2008 ; Mühlenhoff et al., 2010). De plus, la fonction de ces deux protéines dans le transfert

intracellulaire du fer est indépendante de leur rôle dans la régulation de l'homéostasie du fer et cette fonction centrale des GRXs de classe II dans le métabolisme du fer serait une explication à la conservation de cette famille de protéines chez les eucaryotes (Hoffmann et al., 2011). Grx3 et Grx4, forment un complexe cytosolique avec deux autres protéines nommées FRA1 et FRA2 (Fe repressor of activation-1 et 2) correspondant respectivement à une protéine aminopeptidase P-like et une protéine BolA-like (Kumanovics et al. 2008). Ce complexe protéique régule le facteur de transcription Aft1 qui est le facteur majeur de régulation de l'absorption du fer (Ojeda et al., 2006 ; Pujol Carrion et al., 2006 ; Kumanovics et al., 2008). La mutation d'un de ces quatre gènes ou un défaut dans le système mitochondrial de biogenèse des centres Fe-S provoque un phénotype similaire impliquant l'expression constitutive des gènes régulant l'homéostasie du fer. Des expériences génétiques et biochimiques réalisées chez la levure, montrent que l'homéostasie du fer dépend du complexe Grx3-Grx4-BolA-aminopeptidase qui agit comme un senseur du statut de la biogenèse mitochondriale des centres Fe-S. Ainsi, la formation de ce complexe avec Aft1 dans le cytosol inhibe la translocation au niveau du noyau de cette protéine et donc l'activation transcriptionnelle du régulon fer (Kumanovics et al., 2008). En outre, d'autres travaux suggèrent que la partie C-terminale des GRXs de classe II cytosoliques constitue le site de liaison de régulateurs transcriptionnels régulant la réponse au fer chez les champignons plus généralement (Hoffmann et al., 2011).

L'absence d'orthologues de Grx3 et Grx4 chez les bactéries, couplée à l'absence d'orthologues d'Aft1 chez les eucaryotes autres que la levure indique que ce mécanisme de perception du statut en fer dépendant d'Aft1 est restreint à quelques espèces de levure et pourrait faire intervenir d'autres acteurs chez les eucaryotes (Rouhier et al., 2010, P8). Néanmoins, ces organismes possèdent des protéines orthologues de Grx3, Grx4, de BolA et des études de génomique indiquaient que la capacité des GRXs à interagir avec des protéines de la famille BolA pourrait être étendue à la plupart des organismes. En effet, les deux gènes sont très souvent retrouvés côte à côte dans les génomes bactériens et il existe une très forte co-occurrence des gènes codant les GRXs monothiol et BolA (Couturier et al., 2009, P5). De plus, des études de l'interactome d'*E. coli* et de *S. cerevisiae* menées entre autres par des expériences de double hybride ont confirmé que ces protéines peuvent interagir (Butland et al., 2008 ; Yu et al., 2008 ; Braun et al., 2011).

L'étude des protéines BOLA de plantes a révélé l'existence de 4 protéines possédant un domaine BolA, appelée BOLA1, A2, A4 et SUFE1. SUFE1 est un composant essentiel de la machinerie d'assemblage des centres Fe-S au niveau des chloroplastes, qui présente un domaine BolA dans sa partie C-terminale (Xu & Møller 2006 ; Ye et al., 2006 ; Murphy et al., 2007).

Ces protéines étant prédites pour être localisées dans les mêmes compartiments subcellulaires que les GRXs de classe II, la question de leur interaction se posait également chez les plantes. Ainsi, en dépit de l'absence d'orthologue au facteur Aft1 chez les plantes, l'interaction entre les GRXs de classe II et les protéines BOLA pourrait représenter un des mécanismes essentiels de régulation de l'homéostasie du fer soit à travers la régulation des machineries d'assemblage des centres Fe-S, soit à travers le contrôle des voies de signalisation en réponse au statut en fer de la cellule (Rouhier et al., 2010, P8).

Afin de répondre à ces différentes questions et d'éclaircir le rôle des GRXs de classe II en relation avec les protéines BOLA dans l'homéostasie du fer chez les plantes, j'ai entrepris l'étude des interactions potentielles entre les différents membres de chacune des deux familles de protéines. Après avoir confirmé par des fusions co-traductionnelles avec la GFP la localisation subcellulaire des quatre isoformes BOLA d'*A. thaliana* (BOLA1, BOLA2, BOLA4 et SUFE1), nous avons en collaboration avec l'équipe de Frédéric Gaymard (UMR BPMP, Montpellier) tout d'abord validé l'interaction par double hybride en levure entre ces deux familles de protéines et confirmé par complémentation de fluorescence bimoléculaire *in planta* (BiFC) que ces interactions se produisaient dans les différents compartiments subcellulaires où s'expriment les isoformes de chaque famille protéique (Figure 11) (Couturier et al., 2014, P24). En outre, pour SUFE1 qui est une protéine à deux domaines, l'interaction avec les GRXS14 et S16 nécessite la présence du domaine BOLA de cette protéine. L'ensemble de ces résultats confirme que l'interaction entre les GRXs de classe II et les protéines BOLA est également un phénomène conservé chez les plantes.

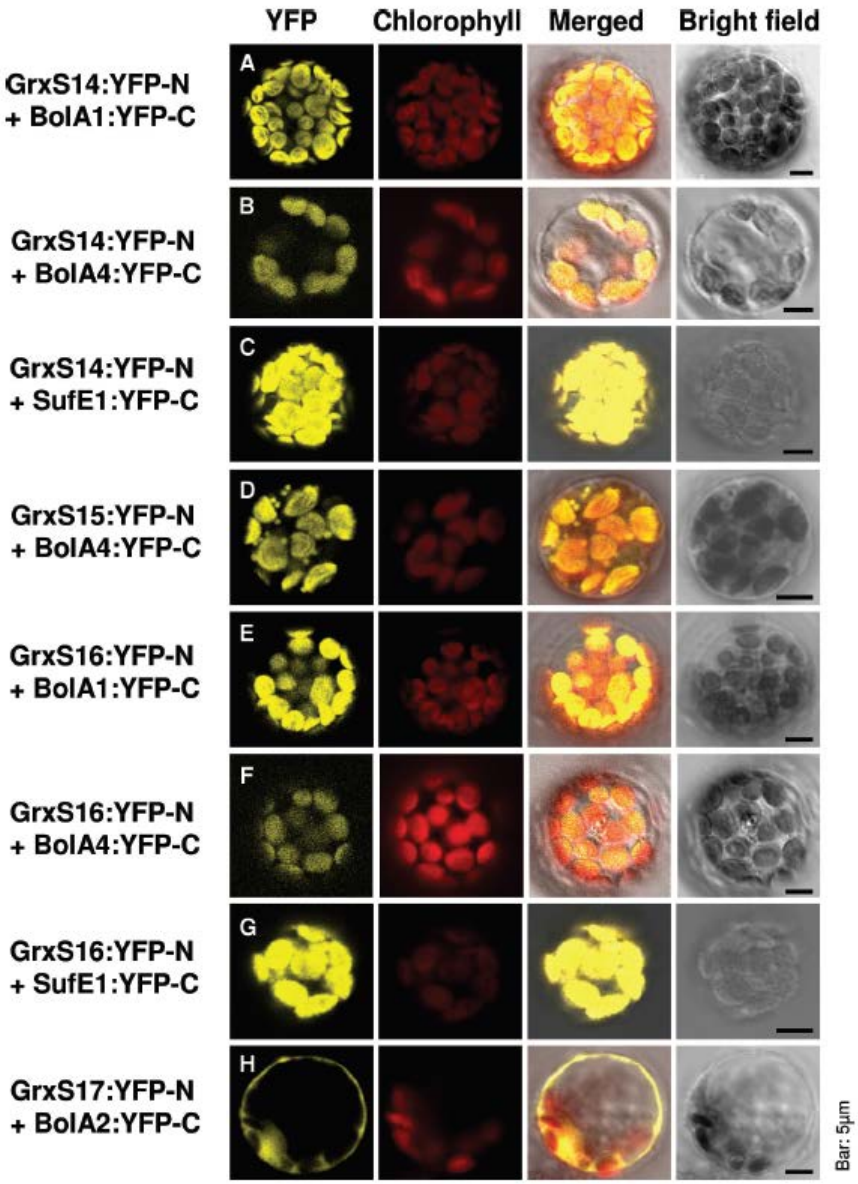

Figure 11. Etude des interactions entres les GRX de classe II et les protéines BOLA d'*A. thaliana*. Les séquences codantes des protéines étudiées ont été respectivement insérées dans les plasmides pUC-SPYNE et pUC-SPYNE en amont des séquences codantes pour la partie N-terminale (YFP-N) et C-terminale (YFP-C) de la protéine YFP. Ces plasmides ont ensuite été utilisés pour la co-transformation de protoplastes d'*A. thaliana* et après 16 à 24h d'incubation, le signal de fluorescence correspondant à la reconstitution de la protéine YFP (dûe à une interaction entre les protéines d'intérêt) a été évalué dans les protoplastes transformés. Les images présentées sont représentatives de trois expériences indépendantes. Les combinaisons impliquant des constructions GRX ou BOLA avec des vecteurs vides ne produisent pas de signal de fluorescence (Couturier et al., 2014, P24).

Au cours du développement de ce projet, des données issues de la littérature suggéraient notamment que les interactions entre les GRXs de classe II et les protéines BOLA pouvaient être multiples. En effet, il avait été démontré que l'interaction entre les protéines GRX et BOLA impliquait la formation d'hétérodimères liant un centre [2Fe-2S], cet hétérodimère GRX-BOLA étant plus stable que l'holodimère GRX-GRX fixant également un centre [2Fe-2S] (Li et al., 2009, 2011 ; Yeung et al., 2011). En outre, les données obtenues avec les orthologues d'*E. coli* n'excluaient pas que cette interaction GRX-BOLA puisse exister même lorsque la GRX ne liait pas de centre Fe-S (Yeung et al., 2011). Les mécanismes moléculaires sous-jacents à ces interactions ont été étudiés en collaboration avec Claude Didierjean et Pascale Tsan (UMR 7036 CRM2 Université de Lorraine-CNRS). Pour cela, les structures tridimensionnelles de l'isoforme AtBOLA1 et du domaine BOLA de la protéine AtSUFE1 ont été résolues par cristallographie et celle de la protéine AtBOLA2 par résonance magnétique nucléaire (RMN) (Figure 12).

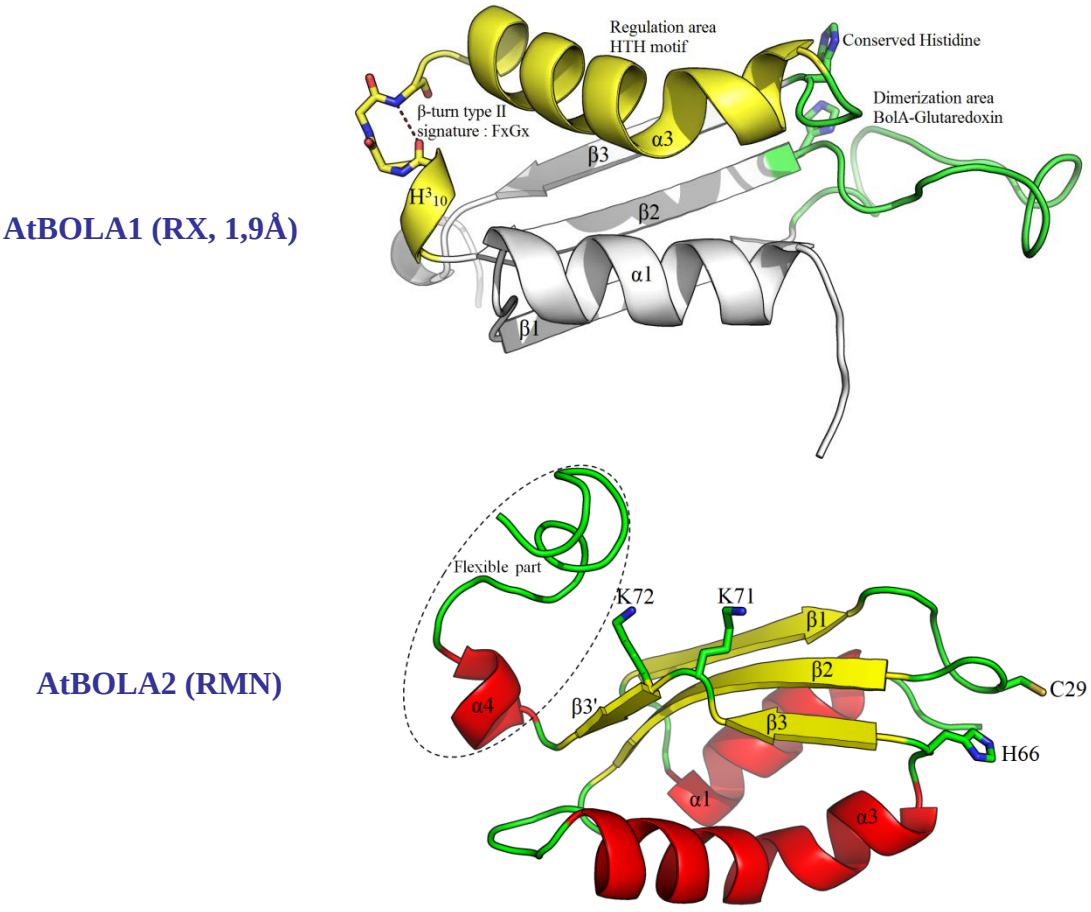

Figure 12. Structure tridimensionnelle des isoformes BOLA1 et BOLA2 d'Arabidopsis. Ces structures ont été résolues par cristallographie pour AtBOLA1 et par RMN pour AtBOLA2.

Les structures de ces protéines sont très semblables et diffèrent principalement par la taille d'une boucle variable nommée [H/C], qui contient soit une cystéine (BolA_C) soit une histidine conservée (groupe BolA_H) (Figure 13). De plus, elles présentent également en partie C-terminale un motif HTH (Helix-turn-helix) permettant la liaison à l'ADN, en accord avec l'observation que certaines isoformes BOLA_H bactériennes agissent en tant que facteurs de transcription en se liant au promoteur de gènes cibles (Freire et al., 2009 ; Cheng et al., 2011).

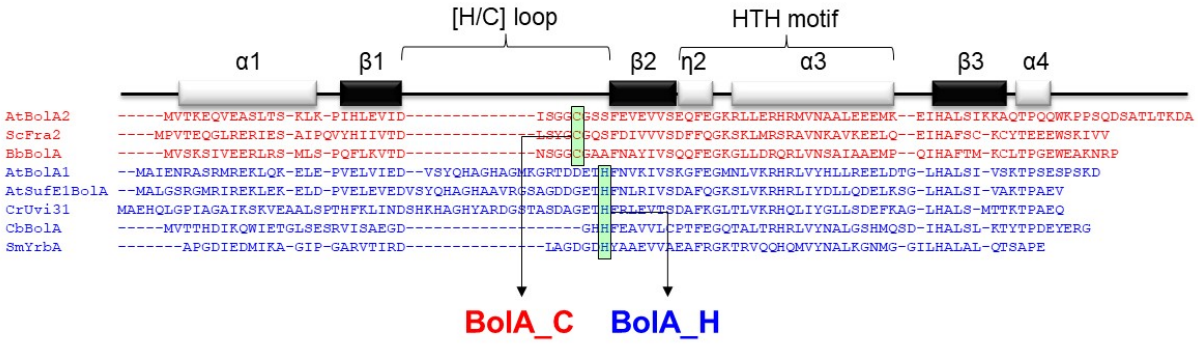

Figure 13. Analyse des éléments structuraux des protéines BOLA. L'alignement structural a été réalisé à l'aide des structures de protéines BOLA disponibles dans la base de données PDB. Les abréviations utilisées sont : At, *Arabidopsis thaliana* ; Bb, *Babesia bovis* ; Cb, *Coxiellia burnetii* ; Cr, *Chlamydomonas reinhardtii* ; Sc, *Saccharomyces cerevisiae* ; Sm, *Sinorhizobium meliloti*.

Des analyses de modélisation couplées à des analyses spectroscopiques de l'holo-hétérodimère formé par les protéines GRXS14 et BOLA1 (isoforme du groupe BOLA_H) d'*A. thaliana* suggèrent que la coordination du centre [2Fe-2S] est de type Rieseke, c'est-à-dire impliquant deux ligands cystéinyl et deux ligands histidinyl (Roret al., 2014, P26). Pour les isoformes BOLA_C, la cystéine conservée présente dans la boucle variable pourrait remplacer l'histidine conservée des isoformes BOLA_H en tant que ligand du centre Fe-S. En résumé, concernant l'holo-hétérodimère GRX-BOLA, l'interface du complexe protéique comprend le résidu conservé de la boucle [H/C], le résidu histidine invariant de BOLA (résidu conservé chez toutes les isoformes), la cystéine d'une molécule de GSH et la cystéine catalytique de la GRX.

Par des expériences de RMN, l'interaction impliquant la formation d'un apo-hétérodimère GRX-BOLA a été observée et les résidus protéiques impliqués identifiés. Dans le cas de l'apo-hétérodimère GRX-BOLA, la surface d'interaction entre les deux partenaires inclut étonnamment le motif de liaison à l'ADN de la protéine BOLA (zone chargée positivement) et la partie C-terminale de la GRX (zone chargée négativement) identifiée précédemment comme impliquée dans la liaison à des facteurs de transcription (Hoffmann et

al., 2011 ; Li et al., 2011). Tous ces résultats suggèrent que, la fonction/activité des GRXs de classe II et des protéines BOLA peut être ajustée par la formation d'apo et d'holo-hétérodimères. Un tel exemple où deux protéines interagissent avec deux régions distinctes est assez inhabituel (Roret al., 2014, P26).

La caractérisation biochimique des protéines BOLA d'*A. thaliana* a également mis en lumière la régulation redox de l'isoforme AtBOLA2 qui possède une cystéine conservée située dans la boucle [H/C] évoquée précédemment. AtBOLA2 est sensible à la présence de divers oxydants comme le peroxyde d'hydrogène (H_2O_2), le glutathion nitrosylé (GSNO) et le glutathion oxydé (GSSG) et cette protéine peut exister sous différents états d'oligomérisation dépendant de son niveau d'oxydation. Elle peut être sous forme monomérique réduite, monomérique glutathionylée et dimérique avec la présence d'un pont disulfure intermoléculaire (Figure 14) (Couturier et al., 2014, P24).

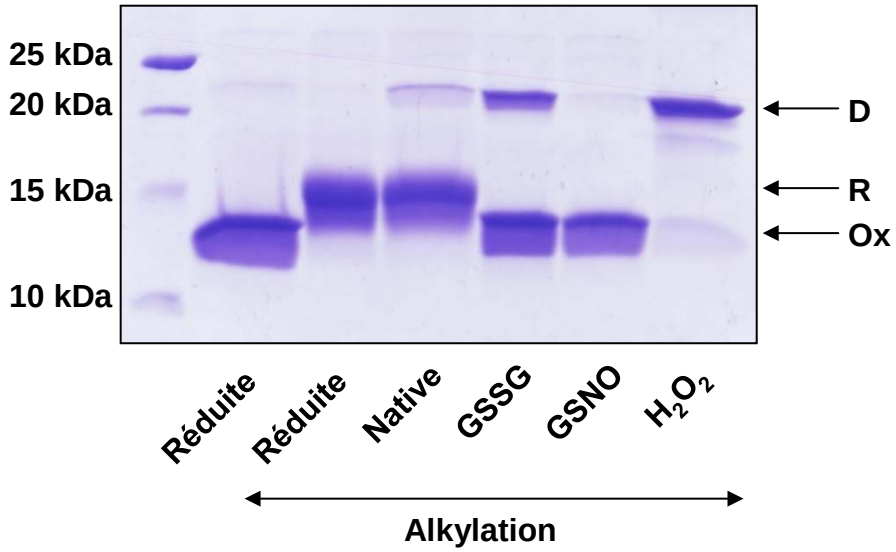

Figure 14. Analyse de la sensibilité de la protéine BOLA2 d'*A. thaliana* à l'oxydation. Le profil de migration de la protéine a été analysé en conditions non réductrices après traitement avec différents agents oxydants. Ainsi la protéine peut exister sous différents états, monomérique oxydé (Ox), monomérique réduit (R) et dimérique (D) (Couturier et al., 2014, P24).

Ces différents états d'oxydation sont réduits de manière préférentielle par les GRXs de classe II et notamment par la GRXS17 qui est le partenaire physiologique de BOLA2. Ces résultats suggèrent qu'un mécanisme de régulation redox, déconnecté de la capacité de ces protéines à former des hétérodimères liant ou non un centre fer-soufre, pourrait être physiologiquement pertinent pour BOLA2. Chez les bactéries, les gènes codant les protéines

BOLA sont notamment induits en cas de stress oxydant. Ainsi outre un rôle dans l'homéostasie du fer, les protéines BOLA, en relation avec les GRXs de classe II, pourraient également jouer un rôle dans la réponse au stress oxydant chez les plantes (Couturier et al., 2014, P24).

Pour finir, je me suis intéressé aux interactions GRXS14-SUFE1 et GRXS16-SUFE1 observées précédemment par double hybride en levure et par des expériences de BiFC *in planta* (Figure 11) qui suggéraient que ces GRXs pouvaient réguler la machinerie d'assemblage des centres Fe-S de type SUF présente au sein des chloroplastes. En effet, SUFE1 stimule l'activité de la cystéine désulfurase NFS2 qui est responsable de l'apport de soufre pour la biosynthèse des centres Fe-S au niveau des chloroplastes (Xu & Møller 2006 ; Ye et al., 2006). Les mutants perte de fonction pour ces gènes sont létaux au stade embryonnaire (Xu & Møller 2006 ; Van Hoewyk et al., 2007). Chez *E. coli*, des orthologues de SUFE1, SufE et de CsdE chez *E. coli* interagissent notamment avec les GRXs 3 et 4 (Bolstad & Wood, 2010 ; Bolstad et al., 2010). L'existence d'un pont disulfure intermoléculaire entre ces protéines suggérait une régulation redox des homologues SufE par les GRXs de classe II. A partir de ces différentes observations, j'ai initié des travaux portant sur la régulation redox des protéines impliquées dans la biogenèse des centres Fe-S au niveau des chloroplastes. En effet, au travers de la photosynthèse et des transferts d'électrons associés, les chloroplastes sont régulièrement soumis à des situations de stress oxydant pouvant aboutir entre autres à l'oxydation et à l'inactivation de certaines protéines possédant des cystéines. D'une manière globale, les protéines impliquées dans la mobilisation du soufre, NFS2 et SUFE1 mais également les protéines d'échafaudage et de transfert impliquées dans les différentes machineries d'assemblage des centres Fe-S possèdent des cystéines, généralement réactives, servant de ligands pour la fixation des centres Fe-S. Ainsi, dans des conditions de stress oxydant, ces protéines pourraient être oxydées et ainsi inactives pour la formation et le transfert des centres Fe-S. La réduction de ces différentes protéines par les GRXs et/ou les TRXs pourrait constituer un mode de régulation des machineries d'assemblage des centres Fe-S. Par exemple, chez *E. coli*, il a été démontré que la fixation du fer au niveau de IscA, un orthologue de la protéine de transfert SUFA1 de plante, était dépendante de la réduction préalable par le système TRX réductase (Ding et al., 2005). Il paraissait donc essentiel d'étudier plus en détail ces mécanismes pouvant réguler la fonction des différents composants de la machinerie chloroplastique des centres Fe-S. Je me suis focalisé sur la régulation de l'apport en soufre au travers de l'activité enzymatique du couple NFS2-SUFE1. Comme précédemment décrit, l'activité cystéine désulfurase de NFS2 est stimulée par la protéine SUFE1 qui est une protéine présentant deux domaines, un domaine SUFE contenant

une cystéine conservée et un domaine BOLA ne possédant pas de cystéine (Figure 12). Des essais *in vitro* ont permis de montrer que SUFE1 peut être glutathionylée en présence de glutathion nitrosylé (GSNO). De manière attendue, la glutathionylation de SUFE1 inhibe la stimulation de l'activité de NFS2 par SUFE1. Plusieurs GRXs chloroplastiques, partenaires physiologiques potentiels de SUFE1, sont capables de réduire la forme glutathionylée de SUFE1 et ainsi restaurer plus ou moins totalement la stimulation de l'activité de NFS2 par SUFE1. La restauration complète de l'activité est observée en présence des GRXs de classe I, GRXC5 et GRXS12, mais pas des GRXs de classe II, GRXS14 et GRXS16 (Figure 15).

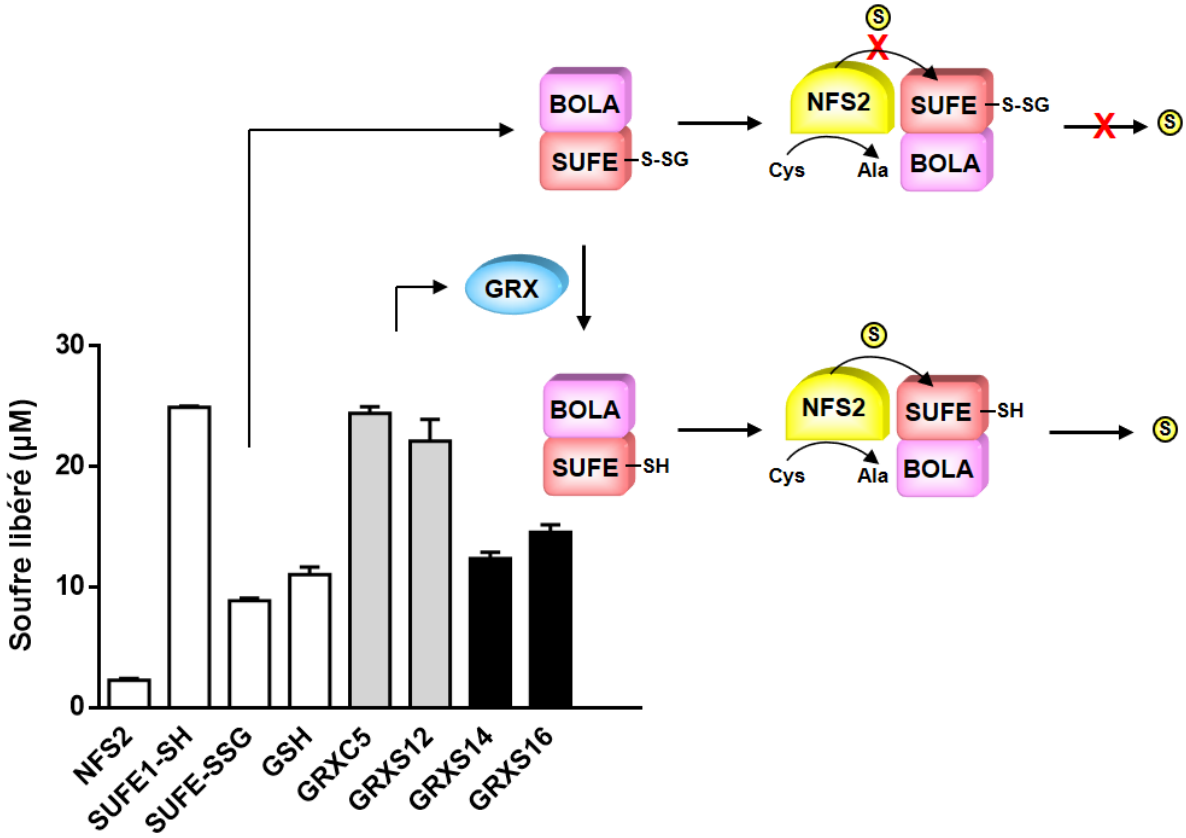

Figure 15. Influence de l'état d'oxydation de SUFE1 sur l'activité de NFS2 et régénération par les GRXs chloroplastiques. L'activité cystéine désufurase de NFS2 a été déterminée en mesurant la quantité de soufre libéré après 15 minutes d'incubation en absence ou en présence de SUFE1 réduite (SH) ou glutathionylée (SSG). Pour tester la régénération de SUFE1 glutathionylée, la protéine a été pré-incubée avec le système GSH seul ou en présence de différentes GRXs (C5, S12, S14 et S16).

Néanmoins, contrairement aux isoformes de classe II GRXS14 et GRXS16, les isoformes de classe I, GRXC5 et GRXS12 n'interagissent pas avec SUFE1 et une analyse plus approfondie démontre que l'interaction GRX-SUFE1 se fait au travers du domaine BOLA mais pas du domaine SUFE (Couturier et al., 2014, P24). Tous ces résultats suggèrent donc que les

GRXs de classe II ne seraient pas impliquées dans la régulation redox de SUFE1 mais pourraient réguler SUFE1 au travers d'une interaction avec son domaine BOLA (Figure 16).

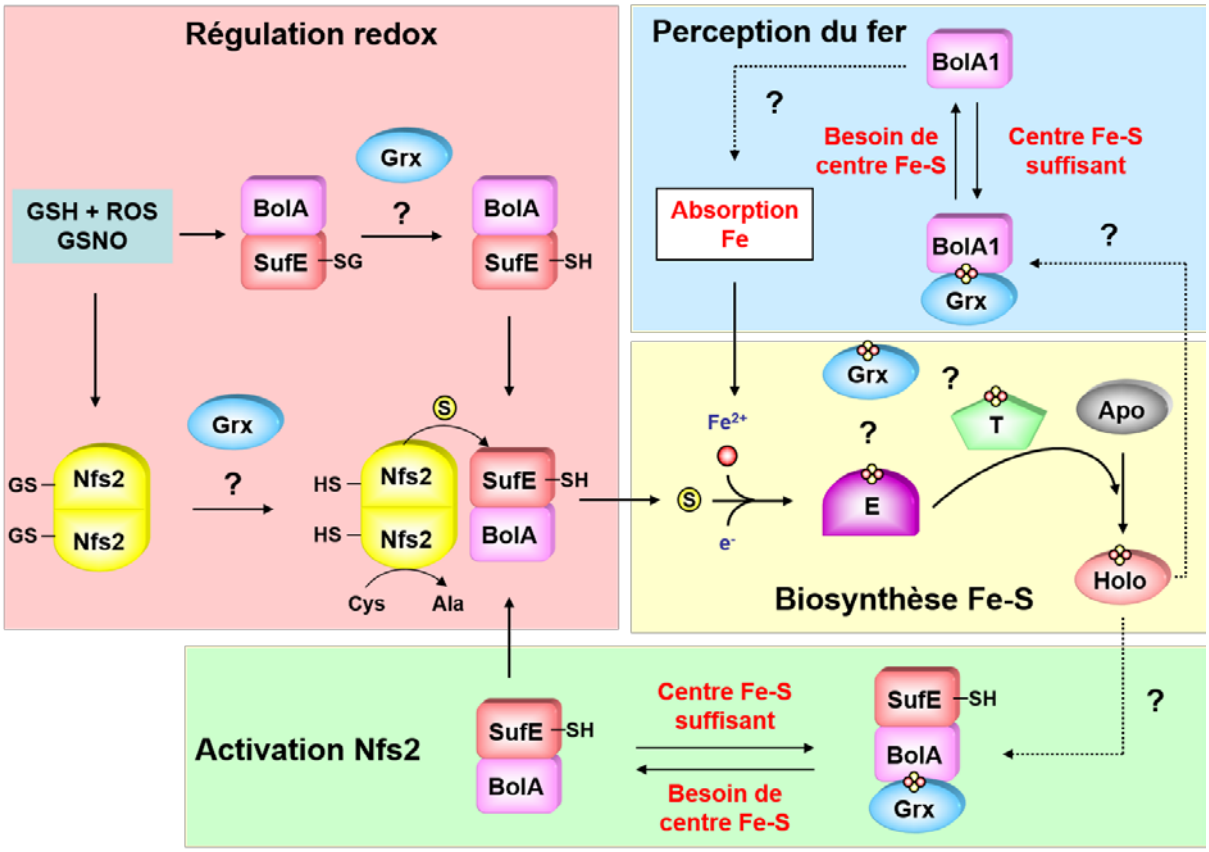

Figure 16. Modèle de régulation de la biosynthèse des centres Fe-S au niveau des chloroplastes par les GRXs de classe II. Dans des conditions de stress oxydant, NFS2 et SUFE1, du fait de leurs cystéines très réactives, pourraient être oxydées, et notamment glutathionylées, et donc inactives dans la fourniture de soufre, élément essentiel à la biosynthèse des centres Fe-S. (Cadre rouge). D'autre part, les GRXs de classe II sous forme holoprotéine (dimère fixant un centre Fe-S) pourraient également interagir avec SUFE1, en formant un hétérodimère liant un centre Fe-S et réguler ainsi l'activation de NFS2 par SUFE1 en cas d'excès de synthèse de centre Fe-S (Cadre vert). Enfin, les interactions entre l'isoforme BOLA1 et les GRXS14 et S16 pourraient jouer un rôle important dans la régulation de l'apport en fer pour la machinerie d'assemblage SUF plastidiale (Cadre bleu).

ACTIVITES DE RECHERCHE

Depuis ma nomination en tant que Maître de Conférences à l'Université de Lorraine en septembre 2013, mes activités de recherche se sont articulées autour de trois grands thèmes principaux. Dans la continuité de mon post-doctorat, le premier thème de recherche (axe redox) concerne la caractérisation de protéines de la superfamille des TRXs dont la fonction est reliée à la régulation redox. Le second thème de recherche (axe Fe-S) porte sur l'étude des mécanismes moléculaires impliqués dans la biogenèse des centres Fe-S au niveau des mitochondries et des chloroplastes. Le troisième thème de recherche est plus récent et concerne les mécanismes moléculaires impliqués dans la mobilisation et le transfert de soufre chez les plantes (axe soufre).

1. Etude des mécanismes moléculaires impliqués dans les étapes tardives de la biogenèse des centres Fe-S au sein des mitochondries et des chloroplastes

Les mitochondries et les chloroplastes ont un besoin important en fer afin d'assurer la fonctionnalité de nombreux processus vitaux tels que la photosynthèse, la respiration, l'assimilation de l'azote et du soufre et le catabolisme des chlorophylles. En effet, toutes ces voies métaboliques requièrent de nombreuses métalloprotéines incluant celles contenant des centres Fe-S, des hèmes et sirohèmes, et des centres à fer non hémique, mono- ou binucléaires. De manière analogue, d'autres processus tels que la réplication et la réparation de l'ADN et la biogenèse des ribosomes sont aussi dépendants de protéines ayant un centre Fe-S (Lill, 2009). Que ce soit chez les procaryotes ou les eucaryotes, les métalloprotéines sont tout d'abord synthétisées sous forme apoprotéine avant qu'un groupe prosthétique ne soit inséré dans le polypeptide grâce à des machineries d'assemblage spécifiques. Bien que les protéines Fe-S soient essentielles dans de nombreux processus cellulaires et voies métaboliques chez les plantes, le fonctionnement des machineries d'assemblage des centres Fe-S est loin d'être parfaitement connu. L'identification et la compréhension des mécanismes moléculaires impliqués dans ces processus ont été principalement obtenues à partir d'études menées chez *S. cerevisiae* et *E. coli* (Lill & Mühlenhoff, 2008 ; Roche et al., 2013) (Tableau 1). Des travaux plus récents menés pour d'autres organismes modèles ont confirmé que les principes de base et les acteurs impliqués dans la biogenèse des centres Fe-S sont conservés au sein du règne vivant (Couturier et al., 2013, P20 ; Beilschmidt & Puccio, 2014). Chez les plantes et les eucaryotes de manière plus générale, les composants impliqués dans l'assemblage des centres Fe-S,

appartiennent à trois systèmes dénommés, SUF (sulfur mobilization), ISC (iron-sulfur cluster) et CIA (cytosolic iron–sulfur cluster assembly) pour les protéines plastidiales, mitochondriales et cystosoliques/nucléaires respectivement (Lill & Mühlenhoff, 2006). De plus, un système d'export reliant les systèmes mitochondriaux et cytosoliques et impliquant le glutathion et le transporteur ABC ATM3 a été identifié chez *S. cerevisiae* et des protéines orthologues existent chez les plantes (Lill & Mühlenhoff, 2008) (Tableau 1).

Quel que soit le système d'assemblage considéré, le processus d'assemblage peut être décrit comme un processus en deux étapes principales (Figure 17). Tous les centres Fe-S sont assemblés *de novo* sur des protéines dites d'échafaudage servant de plate-forme moléculaire (première étape ou étape d'assemblage) avant leur transfert aux protéines acceptrices (deuxième étape ou étape de transfert).

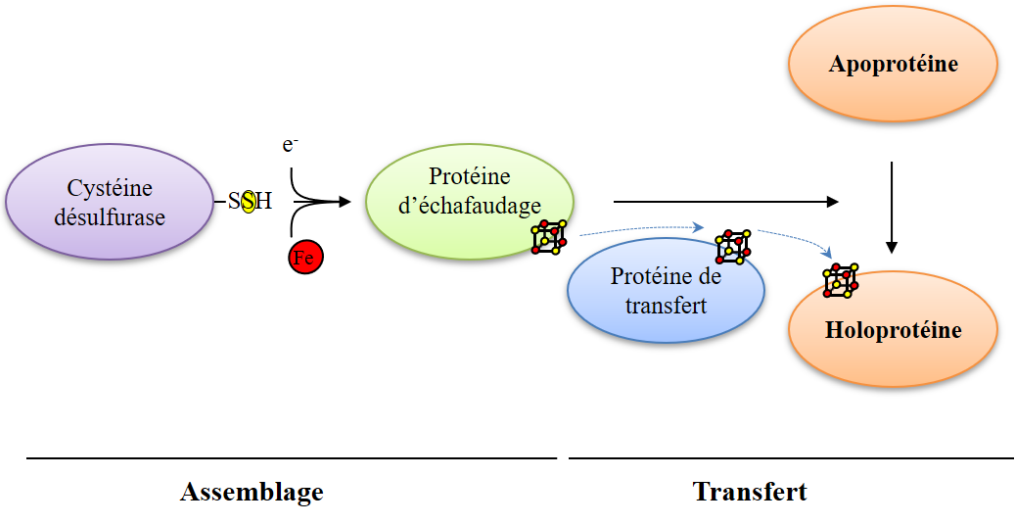

Figure 17. Représentation schématique des principales étapes de la biosynthèse des centres Fe-S et la maturation des protéines Fe-S. La biogenèse des groupes Fe-S peut être divisée en deux étapes principales : (i) la synthèse *de novo* du centre Fe-S sur une protéine d'échafaudage en utilisant des atomes de soufre fournis par une cystéine désulfurase sous la forme d'un groupement persulfure et des atomes de fer d'origine inconnue, (ii) le transfert vers les apoprotéines cibles par des protéines de transfert liant de façon transitoire les centres Fe-S en association avec des facteurs plus spécifiques impliquées dans le recrutement des protéines cibles (Przybyla-Toscano et al., 2017, P34).

Pour l'assemblage des centres Fe-S, les atomes de soufre nécessaires sont issus de la cystéine au travers de l'activité des cystéines désulfurases dont la cystéine catalytique se retrouve transitoirement persulfurée. L'incorporation du soufre implique la réduction de sulfane (S^0) en sulfure (S^{2-}). Les électrons nécessaires proviennent probablement du NADH ou du NADPH via les flavines pour le système SUF et la ferrédoxine réductase et la ferrédoxine (FDX) pour le système ISC. Bien que la frataxine et/ou IscX semblent fournir du fer ou

contrôler l'entrée du fer dans le complexe d’échafaudage de la machinerie ISC, la source du fer et son acheminement sont encore largement inconnus pour les systèmes SUF et CIA.

Après cette première étape, le centre Fe-S est libéré par la protéine d'échafaudage et inséré dans l’apoprotéine cible au cours de plusieurs étapes successives nécessitant différents types de protéines comme des chaperons, des co-chaperons, des facteurs d'échange nucléotidique, et des protéines de transfert liant de façon transitoire les centres Fe-S. Dans certains cas, le transfert final du centre Fe-S vers les apoprotéines cibles impliquent l’existence de facteurs de maturation qui assurent la spécificité de transfert du centre Fe-S vers l’apoprotéine acceptrice finale. Ce rôle serait important compte tenu de la grande variété de protéines Fe-S présentes dans les différents compartiments subcellulaires.

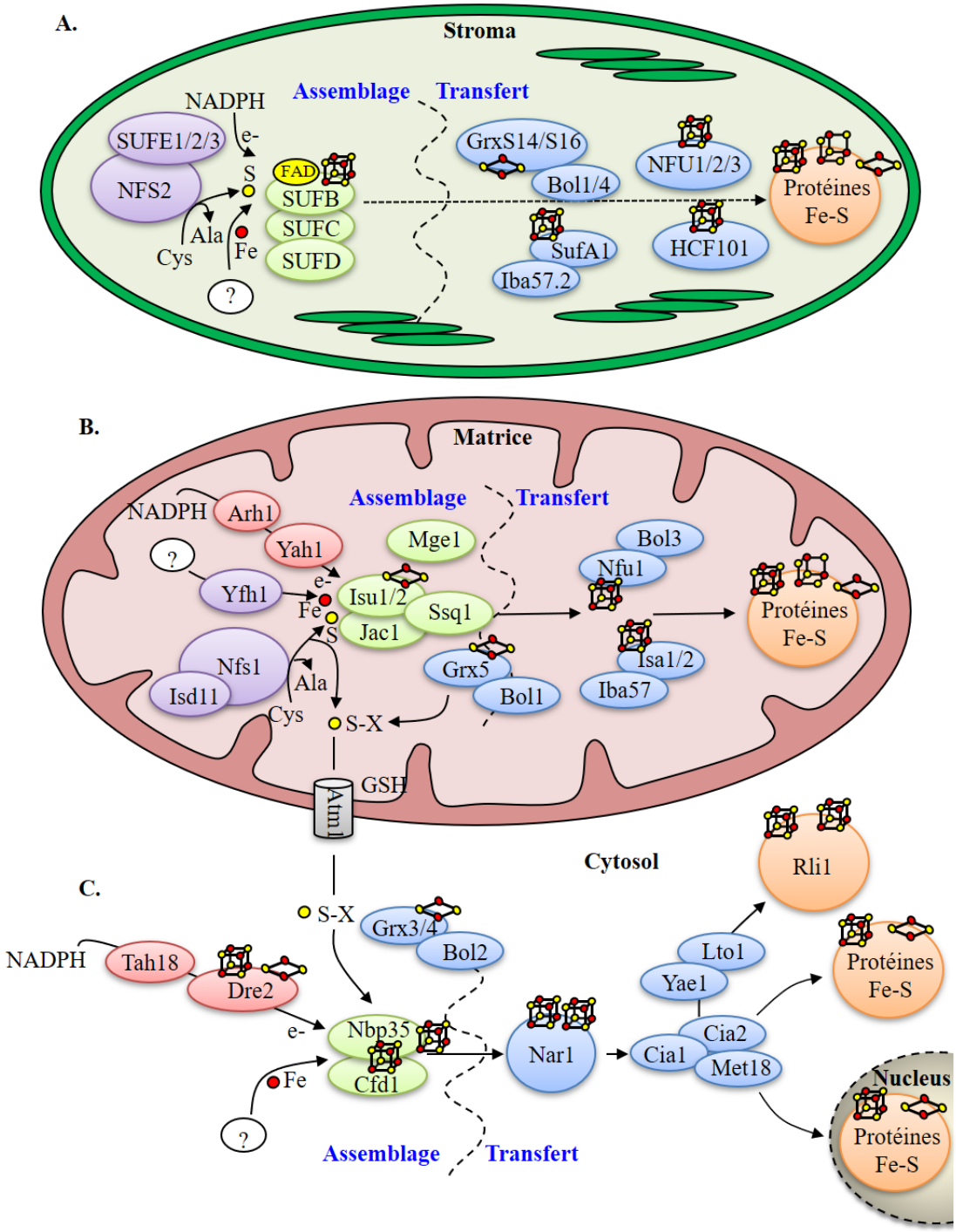

Figure 18. Modèles représentant les différents acteurs des machines d'assemblage des centres de Fe-S dans les cellules eucaryotes. Les machineries SUF (chloroplaste), ISC (mitochondie) et CIA (cytosol) sont représentées respecivement en A, B et C. Les nomenclatures des protéines d'Arabidopsis et de levure sont utilisées pour la machinerie SUF et et les machnieries ISC et CIA respectivement. Les protéines associées à l'étape de désulfuration de la cystéine sont représentées en violet, celles associées au transfert d'électrons en rouge, les protéines d'échafaudage en vert, les protéines de transfert et les facteurs de maturation en bleu et enfin, les protéines acceptrices finales en orange (Przybyla-Toscano et al., 2017, P34).

Fonctions	*E. coli*	*A. thaliana*	*H. sapiens*	*S. cerevisiae*
Machinerie SUF				
Cystéine désulfurase	SufS	NFS2		
Activateur Cystéine désulfurase	SufE	SUFE1/2/3		
Protéine d'échafaudage	SufB	SUFB		
Protéine d'échafaudage	SufC	SUFC		
Protéine d'échafaudage	SufD	SUFD		
Protéine de transfert	Grx4	GRXS14/S16		
Protéine de transfert	SufA, ErpA	SUFA1		
Protéine de transfert	NfuA	NFU1/2/3		
Protéine de transfert	Mrp	HCF101		
Facteur de maturation	BolA, YrbA	BOLA1/4		
Facteur de maturation	YgfZ	IBA57.2		
Machinerie ISC				
Cystéine désulfurase	IscS	NFS1	NFS1	Nfs1
Activateur Cystéine désulfurase	-	ISD11	ISD11	Isd11
Activateur Cystéine désulfurase /entrée Fe	CyaY	FH	FXN	Yfh1
Activateur Cystéine désulfurase /entrée Fe	IscX	-	-	-
Donneur d'électrons	Fdx	mFDX1/2	FDX2, FDX1L	Yah1
Donneur d'électrons	FNR	mFDR	FDXR	Arh1
Protéine d'échafaudage	IscU	ISU1/2/3	ISCU	Isu1/2
Protéine chaperon	HscA, Hsc66	HSCA1/2	GRP75, HSPA9	Ssq1
Protéine chaperon	HscB, Hsc20	HSCB	HSC20, HSCB	Jac1
Facteur d'échange nucléotidique	-	MGE1a/b	GRPEL1/2	Mge1
Protéine de transfert	Grx4	GRXS15	GLRX5	Grx5
Protéine de transfert	IscA, ErpA	ISCA1/2/3	ISCA1/2	Isa1/2
Protéine de transfert	NfuA	NFU4/5	NFU1	Nfu1
Facteur de maturation	Mrp	INDH	IND1, NUBPL	Ind1*
Facteur de maturation	YgfZ	IBA57.1	IBA57	Iba57
Facteur de maturation	BolA	BOLA4	BOLA3	Bol1, Bol3 (Aim1)
Système d'export ISC				
Transporteur ABC de composé soufré		ATM3	ABCB7	Atm1
Machinerie CIA				
Donneur d'électrons		TAH18	NDOR1	Tah18
Donneur d'électrons		DRE2	CIAPIN1	Dre2
Protéine d'échafaudage		NBP35	NBP35, NUBP1	Nbp35
Protéine d'échafaudage		-	CFD1 (NUBP2)	Cfd1
Protéine de transfert		NAR1	IOP1, NARFL	Nar1
Protéine de transfert		GRXS17	GLRX3	Grx3/4
Facteur de maturation		MET18	MMS19	Met18
Facteur de maturation		CIA1	CIA1, CIAO1	Cia1
Facteur de maturation		AE7, AEL1/2	CIA2A (FAM96A, MIP18)	Cia2
Facteur de maturation		-	CIA2B (FAM96B)	-
Facteur de maturation		BOLA2	BOLA2	Bol2 (Fra2)
Facteur de maturation		LTO1	ORAOV1	Lto1
Facteur de maturation		YAE1/2/3	YAE1D1	Yae1

Tableau 1. Nomenclature et fonction des acteurs moléculaires des machineries d'assemblage de quatre organismes modèles de référence, *E. coli*, *A. thaliana*, *H. sapiens* et *S. cerevisiae*. * cette protéine n'est pas présente chez *S. cerevisiae* mais présente chez d'autres champignons (Przybyla-Toscano et al., 2017, P34).

Concernant cette thématique, l'objectif principal des travaux réalisés au sein de notre équipe vise à comprendre le fonctionnement des machineries d'assemblage des centres Fe-S au niveau des mitochondries et des chloroplastes et plus précisément les mécanismes moléculaires impliqués dans les étapes tardives. Les travaux de thèse de Jonathan Przybyla-Toscano et

Mélanie Roland étaient associés à ce projet et ont combiné des approches moléculaires, biochimiques et génétiques, en collaboration avec l'équipe du Professeur M.K. Johnson (Université de Géorgie, Athens, USA) et l'équipe FeROS de Frédéric Gaymard et Christian Dubos (UMR Biochimie et Physiologie Moléculaire des Plantes, Montpellier). Ces deux projets de thèse étaient principalement focalisés sur l'étude de deux familles de protéines de transfert, les protéines NFU et les protéines de type A (SufA/IscA) pour lesquelles des travaux précédents suggéraient des fonctions dans le transfert de soufre au sein des machineries ISC et SUF. *A. thaliana* possède cinq isoformes NFU localisées dans les chloroplastes (NFU1, NFU2 et NFU3) et les mitochondries (NFU4 et NFU5), quatre protéines de type A, SUFA1 dans les chloroplastes et ISCA1a, ISCA1b et ISCA2 dans les mitochondries. Au début de ces différents travaux, mis à part NFU2, la fonction de ces protéines n'était pas fermement établie.

1.1. Etude des protéines NFU et ISCA impliquées dans la maturation des centres Fe-S dans les mitochondries d'*A. thaliana*

Lors de la maturation des protéines mitochondriales, un centre [2Fe-2S] est initialement assemblé sur la protéine d'échafaudage ISU puis transféré vers les apoprotéines cibles à l'aide de chaperons et de diverses protéines de transfert (Figure 17B). Des travaux précédents ont également montré que la GRXS15 est essentielle à la biogenèse mitochondriale des centres Fe-S et incorpore un centre [2Fe-2S] (Moseler et al., 2015 ; Ströher et al., 2016). Pour la maturation des protéines incorporant un centre [4Fe-4S], un couplage réductif de deux centres [2Fe-2S] est nécessaire, suggérant l'implication de protéines de transfert et un donneur d'électrons. Par double hybride en levure et des expériences BiFC, nous avons montré que la GRXS15 interagissait avec chacune des trois isoformes ISCA mitochondriales (1a, 1b et 2), celles-ci interagissant également entre-elles pour former des hétérodimères ISCA1a-ISCA2 et ISCA1b-ISCA2 (Azam et al., résultats non publiés). Après co-expression chez *E. coli*, ISCA1a et ISCA2, forment un hétérodimère liant un centre [2Fe-2S], cet hétérodimère pouvant fixer un centre [4Fe-4S] après reconstitution en présence d'une cystéine désulfurase. Des expériences de transfert *in vitro* ont confirmé la capacité de la GRXS15 à transférer un centre [2Fe-2S] à l'apoforme de la ferrédoxine 1 mitochondriale (mFDX1) et mis en évidence la formation d'un centre [4Fe-4S] dans un hétérodimère ISCA1a-ISCA2 en présence de GRXS15 liant un centre [2Fe-2S] et d'un excès de GSH. Ces résultats suggèrent que cet hétérodimère assemble un centre [4Fe-4S] via un couplage réductif de deux centres [2Fe-2S] et sont en accord avec ceux obtenus pour les protéines humaines GRX5, ISCA1 et ISCA2 (Brancaccio et al., 2014). Les

données présentes dans la littérature suggéraient que les protéines ISCA agissent en amont des protéines NFU. Les données obtenues ont confirmé l'interaction de ces deux familles de protéines chez *A. thaliana* (Azam et al., résultats non publiés). Bien qu'après expression hétérologue chez *E. coli* NFU4 et NFU5 étaient purifiées sous forme apoprotéine, elles sont capables de former des homodimères incorporant un centre [4Fe-4S] après reconstitution *in vitro*. Il a également été mis en évidence un transfert rapide et unidirectionnel d'un centre [4Fe-4S] depuis l'hétérodimère ISCA1a-ISCA2 vers NFU4 ou NFU5. Enfin, toutes ces protéines représentent des donneurs potentiels de centre [4Fe-4S] pour la maturation de protéines [4Fe-4S] comme l'aconitase 2 (ACO2) mitochondriale. Ces deux études ont permis de définir les interactions entre les protéines de transfert NFU, les protéines de type-A et la GRXS15 et ainsi proposer un modèle concernant la maturation des protéines [4Fe-4S] mitochondriales (Figure 18).

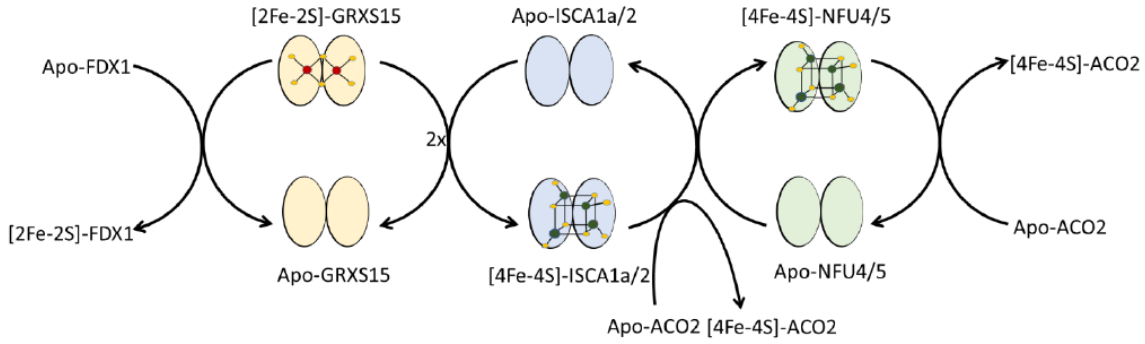

Figure 18. Schéma récapitulatif du transfert de centres Fe-S entre les protéines ISCA1a/2, NFU4, NFU5 et leurs protéines partenaires. Ce modèle a été construit à partir des données obtenues au cours des études Azam et al., résultats non publiés.

D'un point de vue fonctionnel, des expériences de complémentation en levure ont démontré que les protéines NFU et ISCA de plantes peuvent assurer les mêmes fonctions que leurs orthologues respectifs, suggérant que ces étapes tardives ont été conservées (Uzarska et al., 2018). Cependant, contrairement à la levure, la létalité du double mutant *nfu4 x nfu5* indique qu'elles sont essentielles pour le développement de l'embryon chez Arabidopsis. Ceci serait notamment dû au rôle des protéines NFU dans la maturation de la lipoate synthase, enzyme à centre [4Fe-4S] impliqué dans la synthèse de l'acide lipoïque dont dépend l'activité de plusieurs protéines centrales pour le métabolisme mitochondrial (Thèse Jonathan Przybyla-Toscano, résultats non publiés). Malgré la mise en évidence de son implication dans le couplage réductif

de centre [2Fe-2S] et la formation subséquente de centre [4Fe-4S] au sein d'un hétérodimère ISCA1a-ISCA2, le rôle exact de GRXS15 au sein de la machinerie d'assemblage des centres Fe-S mitochondriale chez les plantes, et son implication éventuelle dans le fonctionnement de la machinerie d'assemblage cytosolique CIA restent à déterminer. C'est dans ce cadre qu'a débuté la thèse de Loïck Christ portant sur la dissection des interactions moléculaires de la GRXS15 mitochondriale chez les plantes.

1.2. Etude fonctionnelle de facteurs de maturation tardifs des protéines Fe-S chloroplastiques chez *A. thaliana*

Les voies métaboliques présentes au sein du chloroplaste reposent sur de nombreuses protéines Fe-S, notamment celles appartenant à la chaîne de transfert d'électrons qui est essentielle à la plupart des autres processus métaboliques comme la fixation du carbone, l'assimilation de l'azote et du soufre, les voies de biosynthèse des pigments, des acides aminés et des vitamines (Przybyla-Toscano et al., 2017, P36). La maturation de ces protéines repose sur la machinerie d'assemblage SUF (Figure 18A). Tout d'abord un centre Fe-S est assemblé sur le complexe d'échafaudage $SUFBC_2D$, puis transféré *via* un ensemble de protéines de transfert vers les protéines cibles (Figure 18A) (Hu et al., 2017). Ces protéines de transfert appartiennent aux familles NFU, SUFA, GRX et HCF101. Les étapes tardives de la biogenèse des centres Fe-S au niveau des chloroplastes demeurent encore peu caractérisées bien que le rôle de certaines protéines comme NFU2, NFU3 et HCF101 notamment aient été étudiés de manière plus approfondie. Les plants mutants perte de fonction pour ces gènes présentent un phénotype nain associé à une chlorose des feuilles et ces protéines seraient impliquées dans la maturation de protéines [4Fe-4S], et notamment les sous-unités du photosystème I (Lezhneva et al., 2004 ; Touraine et al., 2004 ; Nath et al., 2016). Il a également été démontré que NFU2 et HCF101 peuvent incorporer des centres [4Fe-4S] (Schwenkert et al., 2009 ; Gao et al., 2013 P22). Plus récemment, une étude à laquelle notre équipe a participé a mis en évidence l'importance de NFU2 dans la maturation de la dihydroxyacide déshydratase (DHAD), protéine à centre [2Fe-2S] impliquée dans la synthèse d'acides aminés branchés (Touraine et al., 2019, P40). Le projet de thèse de Mélanie Roland s'inscrivait dans l'étude de plusieurs protéines, NFU1, SUFA1 et IBA57.2, supposées être impliquées dans les étapes tardives de l'assemblage des centres Fe-S (Figure 18A). Nous avons suivi la même approche globale que celle utilisée précédemment pour l'étude des isoformes mitochondriales NFU4 et NFU5 afin notamment d'identifier des éléments permettant d'expliquer la présence des trois isoformes NFU chez *A.*

thaliana. De manière attendue, même si NFU2 peut également lier des centres [2Fe-2S], NFU1 incorpore un centre [4Fe-4S] au sein d'un homodimère (Roland et al., 2020, P44). La spécificité de NFU1 vis-à-vis de NFU2 et NFU3 envers certaines protéines cibles potentielles a été testée au travers d'expériences de double hybride en levure et de BiFC. Des interactions spécifiques avec une protéine impliquée dans la biosynthèse des isoprénoïdes, la 1-hydroxy-2-méthyl-2-(E)-buténYl 4-diphosphate synthase (ISPG) et une autre impliquée dans la synthèse de la thiamine, la 4-amino-5-hydroxyméthyl-2-méthylpyrimidine phosphate synthase (THIC), ont également été détectées. Enfin, la mise en évidence d'une interaction entre NFU1 et la protéine d'échafaudage SUFD nous a conduit à proposer un modèle dans lequel NFU1 recevrait son centre Fe-S du complexe d'échafaudage SUFBC2D avant de le transférer à certaines protéines cibles comme ISPG et THIC et ainsi participer à leur maturation (Roland et al., 2020, P44). Les résultats obtenus ont permis de définir plus clairement le rôle de NFU1 dans la maturation des protéines clientes Fe-S dans les chloroplastes d'Arabidopsis parmi d'autres composants de la SUF. D'autres travaux réalisés en collaboration avec l'équipe FeROS (UMR BPMP, Montpellier) portant plus spécifiquement sur les isoformes NFU2 et NFU3 ont complété les données obtenues pour NFU1 et précisé les rôles respectifs de ces trois protéines dans la maturation de 24 protéines Fe-S chloroplastiques (Touraine et al., 2019, P40 ; Roland et al., 2020 P44 ; Berger et al., 2020, P45).

2. Caractérisation biochimique des isoformes GRXS16, TRXo1 et TRXo2 d'*A. thaliana*

Cette thématique de recherche a été notamment associée au travail de thèse de Flavien Zannini dont la thèse portait sur l'analyse fonctionnelle de protéines métal- ou redox-dépendantes chez les plantes (projet MetOx). L'objectif de ce projet était de caractériser des protéines possédant un ou plusieurs motifs CxxC conservés et dont la fonction est inconnue ou peu caractérisée chez les plantes. Dans ce cadre, nous avons réalisé la caractérisation biochimique de la GRX de classe II chloroplastique GRXS16 (Zannini et al., 2019, P39) et des isoformes mitochondriales TRXo1 et TRXo2 d'*A. thaliana* (Zannini et al., 2018, P38).

2.1. Caractérisation biochimique de l'isoforme GRXS16 d'*A. thaliana*

GRXS16 est une isoforme spécifique aux plantes qui possède un domaine endonucléase en position N-terminale et un domaine GRX en position C-terminale. Cette protéine possède une cystéine (Cys^{62}) conservée dans le domaine endonucléase et deux cystéines (Cys^{158} et

Cys^{215}) dans le domaine GRX, Cys^{158} étant le résidu catalytique du site actif CGFS. Les analyses biochimiques (activité redox, sensibilité à l'oxydation, pK_a des résidus cystéine, potentiel redox) de la protéine recombinante et de différents variants (simple et double mutants cystéiniques) ont révélé la plus forte sensibilité à l'oxydation d'AtGRXS16 en présence de GSSG et GSNO plutôt qu'en présence de H_2O_2. Cette oxydation entraîne la formation d'un pont disulfure entre les résidus Cys^{158} et Cys^{215} dont le potentiel redox (- 298 mV à pH 7,0) est cohérent avec un mode de réduction impliquant le système TRX chloroplastique et non le système GSH. Cette étude suggère donc que l'état redox de cette protéine pourrait être contrôlé par la lumière via la chaîne d'électrons photosynthétique et le système FTR/TRX (Figure 19).

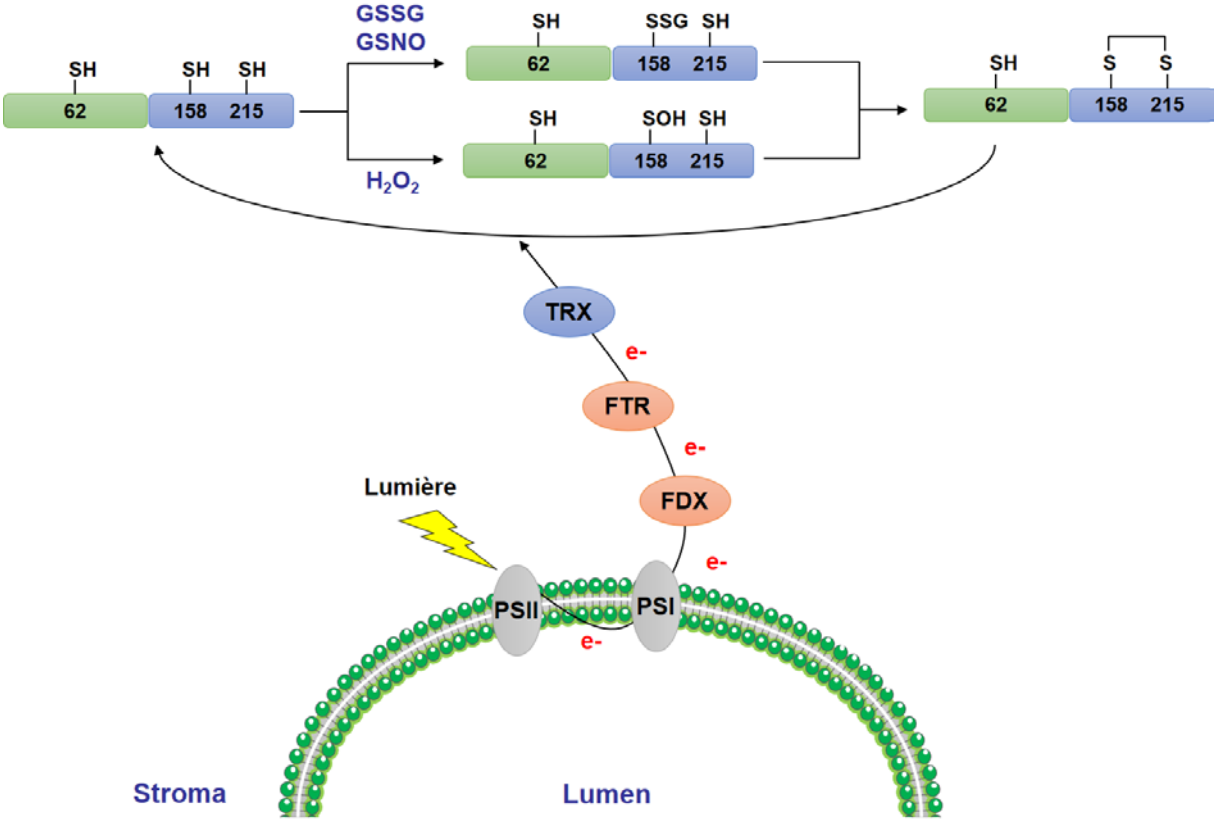

Figure 19. Régulation redox de l'isoforme GRXS16 d'*Arabidopsis thaliana*. La présence d'espèces oxydantes (H_2O_2, GSSG, GSNO) ou de substrats glutathionylés (non représentés sur le schéma) entraîne la formation d'un pont disulfure intramoléculaire au sein de la protéine. La réduction du pont disulfure par l'intermédiaire du système TRX/FTR/FDX chloroplastique suggère un contrôle redox de GRXS16 par la lumière via la chaîne de transfert d'électrons.

L'absence d'activité redox d'AtGRXS16 en présence des substrats classiquement utilisés *in vitro* (HED et DHA) nous a conduit à envisager des mesures d'activité utilisant la GFP sensible à l'oxydoréduction (roGFP2) comme protéine cible. Ces expériences n'ont pas révélé d'activité réductase dépendante du GSH alors qu'AtGRXS16 peut catalyser l'oxydation

de la roGFP2 en présence de GSSG bien que cette activité soit bien plus faible que celle observée avec l'isoforme de classe I, AtGRXC1 (Zannini et al., 2019, P39). AtGRXS16 serait ainsi plutôt reliée à la glutathionylation/l'oxydation de protéines cibles et non à leur réduction. D'un point de vue régulation, en favorisant la formation d'un pont disulfure intramoléculaire, le résidu Cys^{215} modulerait l'activité oxydoréductase de la protéine. Il est intéressant de noter que ce résidu cystéine est également conservée dans certains GRX de classe I (résidu CysC, section 2, page 33). Dans ce cas, cependant, la fonction semble être différente du rôle de ce même résidu chez AtGRXS16 car il n'est pas impliqué dans le mécanisme catalytique. En effet, dans le cas des isoformes PtGRXC1 et PtGRXC2, cette cystéine n'influence pas leur activité oxydoréductase mais est impliquée dans la formation d'un pont disulfure intermoléculaire qui est efficacement réduit par le GSH (Figure 20) (Couturier et al., 2013, P23).

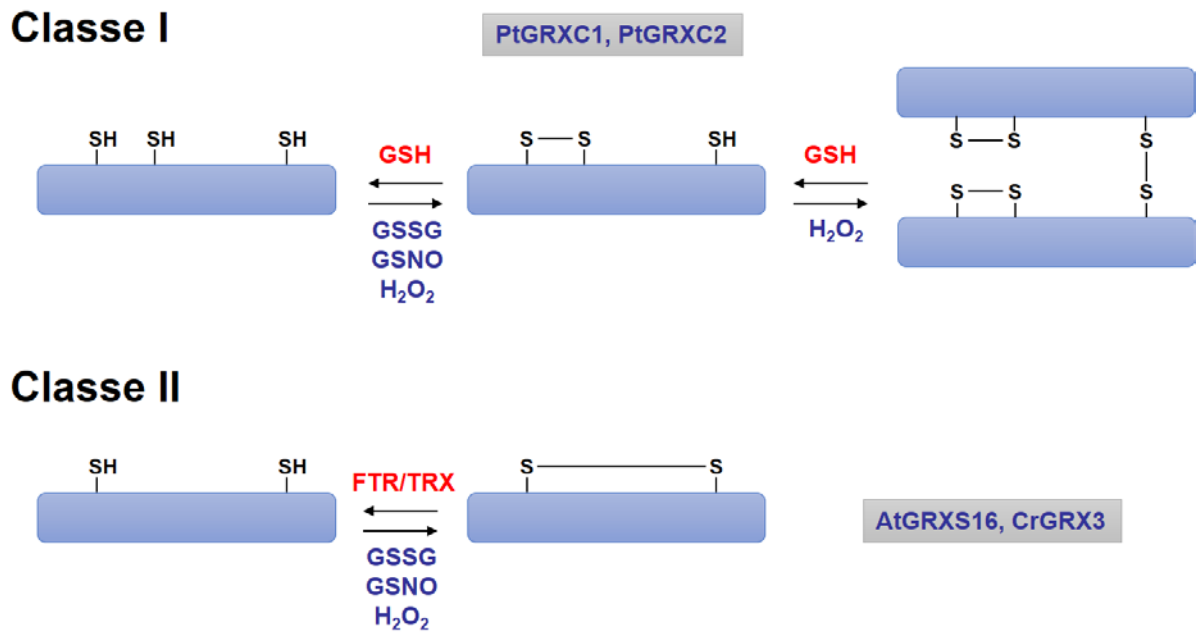

Figure 20. Schéma récapitulatif des processus impliqués dans l'oxydation des GRXs de classe I et II chez les organismes photosynthétiques. L'oxydation des GRXs réduites par différents composés oxydants comme H_2O_2, GSSG et GSNO conduit à la formation d'un pont disulfure intramoléculaire, entre les cystéines du site actif pour PtGRXC1 et PtGRXC2, et entre la cystéine catalytique et la cystéine conservée présente dans la partie C-terminale pour AtGRXS16 et *Chlamydomonas reinhardtii* GRX3. De manière intéressante, cette cystéine conservée également chez PtGRXC1 et PtGRXC2 est impliquée dans la formation d'un homodimère covalente de ces protéines en présence de H_2O_2. Les formes oxydées monomériques et dimériques des GRXs de classe I, PtGRXC1 et PtGRXC2, sont réduites par le GSH tandis que la réduction de la forme oxydée monomérique des GRXs de classe II, AtGRXS16 et CrGRX3, dépend du sytème TRX.

Pour conclure, la réduction d'AtGRXS16, nécessaire à son activité oxydoréductase et à la fixation de Fe-S clusters, dépend de la lumière au travers du système FTR/TRX chloroplastique. Par conséquent, la formation du pont disulfure intramoléculaire Cys^{158}-Cys^{215}, pourrait constituer un mécanisme de régulation redox contrôlant la fonction de la protéine GRXS16 en réponse à la transition jour/nuit ou à des conditions oxydantes.

2.2. Analyse comparative des isoformes TRXo1 et TRXo2 d'*A. thaliana*

Chez les organismes photosynthétiques, les TRXs forment une famille multigénique d'environ 40 membres mais seules les isoformes TRXh2 et TRXo sont retrouvées dans les mitochondries. En comparaison des TRXs chloroplastiques, les rôles moléculaires et physiologiques des TRXs mitochondriales sont encore peu caractérisés, bien que de nombreuses protéines mitochondriales soient supposées ou identifiées comme sensibles à des modifications post-traductionnelles réversibles redox et qu'une centaine de partenaires potentiels ont été identifiés pour l'isoforme TRXo1 d'*A. thaliana* (Yoshida et al., 2013). Contrairement à la plupart des autres espèces végétales, en plus de TRXh2, *A. thaliana* possède deux isoformes TRX de type o, TRXo1 et TRXo2, TRXo1 étant la principale isoforme (Yoshida & Hisabori, 2016). D'autre part, bien que les simples et double mutants perte de fonction n'aient pas de phénotype prononcé en conditions standard de croissance, une dérégulation de l'activité des enzymes du cycle de l'acide tricarboxylique (TCA), ou des enzymes associées, avait été rapporté pour le mutant perte de fonction *trxo1* d'*A. thaliana* (Daloso et al., 2015). Récemment AtTRXh2et AtTRXo1 ont été reliées à la régulation redox de la photorespiration (Reinholdt et al., 2019 ; Da Fonseca Pereira et al., 2020). En absence d'éléments pouvant expliquer leur redondance ou leur spécificité, nous avons entrepris une étude structure-fonction des protéines AtTRXo1 et AtTRXo2 (Zannini et al., 2018, P38).

Lorsqu'elles sont exprimées dans *E. coli*, ou après des expériences de reconstitution *in vitro*, les deux protéines recombinantes existent sous une forme apo-monomérique et une forme homodimérique liant un centre [4Fe-4S] (Figure 21). Cette observation était inattendue car ces deux TRXs possèdent un site actif classique WCGPC préalablement connu pour être défavorable à l'incorporation d'un centre Fe-S et que les travaux précédents réalisés avec AtTRXo1 ne mentionnaient pas la présence de ce cofacteur (Yoshida et al., 2013). Ces protéines ne possédant que deux résidus cystéine et l'absence de centre Fe-S dans les variants monocystéiniques suggèrent que ce sont bien les deux cystéines du site actif qui sont les ligands du centre Fe-S.

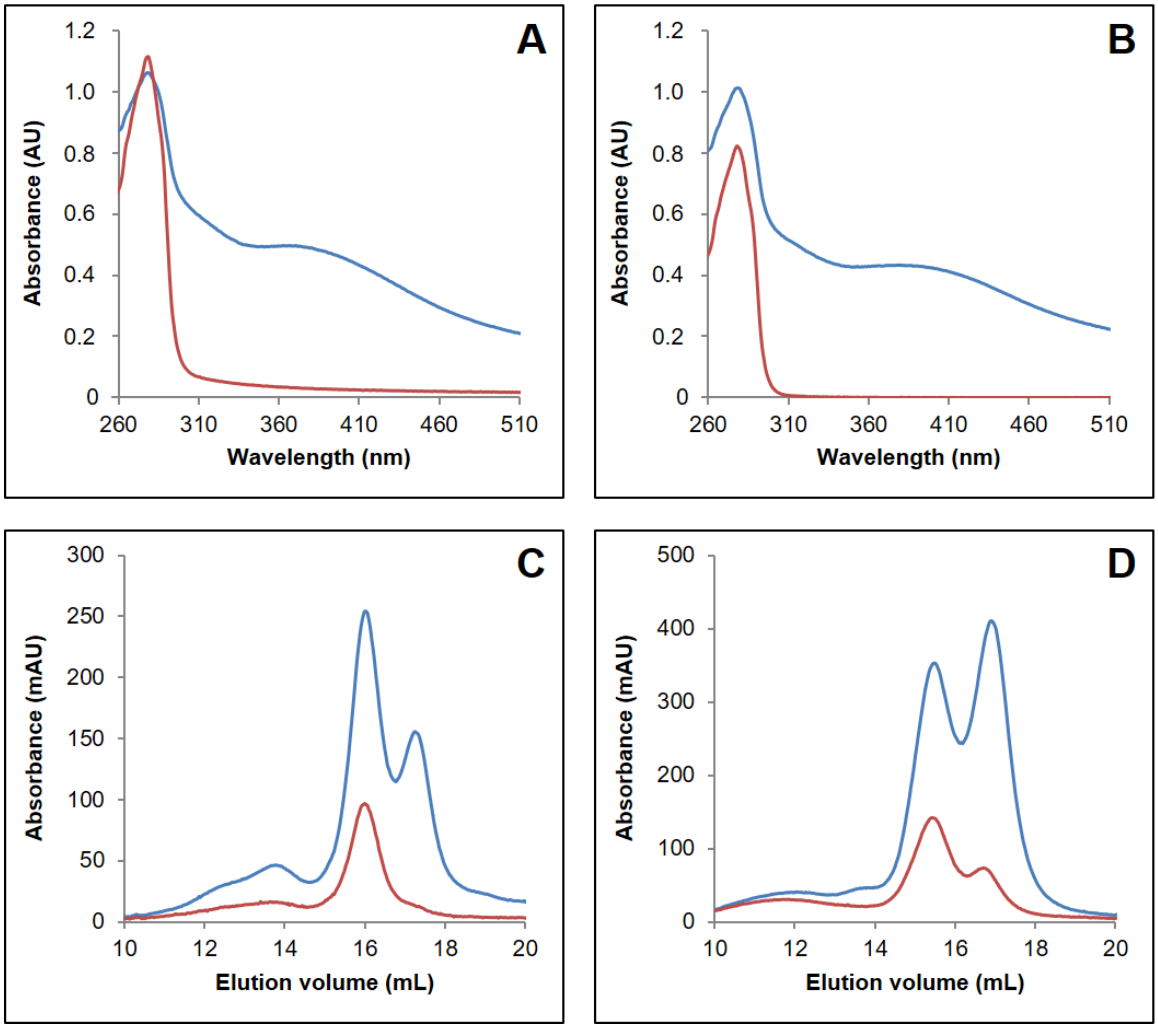

Figure 21. Reconstitution *in vitro* du centre Fe-S des isoformes TRXo d'*Arabidopsis thaliana*. Ces expériences ont été réalisées en utilisant la cystéine désulfurase IscS d'*E. coli*. Les spectres UV–visible des isoformes TRXo2 (A) et TRXo1 (B) ont été analysés avant (ligne rouge) et après (ligne bleue) reconstitution en condition anaérobie. L'état d'oligomérisation de TRXo2 (C) et TRXo1 (D) ainsi reconstituées a été analysé par gel filtration après dépôt de 100 à 300 µg sur une colonne Superdex S200 10/300. La présence respective du polypeptide et du centre Fe-S a été détectée en mesurant l'absorbance à 280 nm (ligne bleue) et à 420 nm (ligne rouge). Le pic d'élution à 16 ml correspond à la forme dimérique et le pic d'élution observé à 17 ml représente la forme monomérique des protéines TRXo.

Malgré plusieurs tentatives, la résolution de la structure 3D de la forme homodimérique des deux isoformes est restée infructueuse et n'a pas permis de confirmer et la nature des ligands de façon certaine. La résolution de la structure de la forme apo-monomérique n'a pas mis en évidence de différences fondamentales avec les autres TRXs pouvant expliquer la faculté de lier un centre Fe-S. Par contre, la comparaison de la structure des deux isoformes AtTRXo1 et AtTRXo2 a révélé des différences marquées dans la répartition des charges de surface, notamment dans certains domaines impliqués dans les interactions protéine-protéine avec des

protéines partenaires. Parmi les 101 partenaires présumés de TRXo1 identifiés lors d'une analyse protéomique (Yoshida et al., 2013), les protéines NFU4 et NFU5 ont retenu notre attention car elles étaient des protéines d'intérêt du projet de thèse de Jonathan Przybyla-Toscano (section 1.1 page 53). Ce sont des protéines de transfert de centre Fe-S impliquées dans les étapes tardives de la maturation des protéines Fe-S mitochondriales. Cette fonction est notamment associée au motif conservé CxxC permettant la fixation transitoire d'un centre Fe-S. Ainsi, ces protéines doivent être sous forme réduite afin de pouvoir recevoir ce cofacteur. Sous apoforme, TRXo1 et o2 réduisent les protéines NFU4/5 *in vitro* contrairement à GRXS15 une autre réductase potentielle au sein des mitochondries (Figure 22).

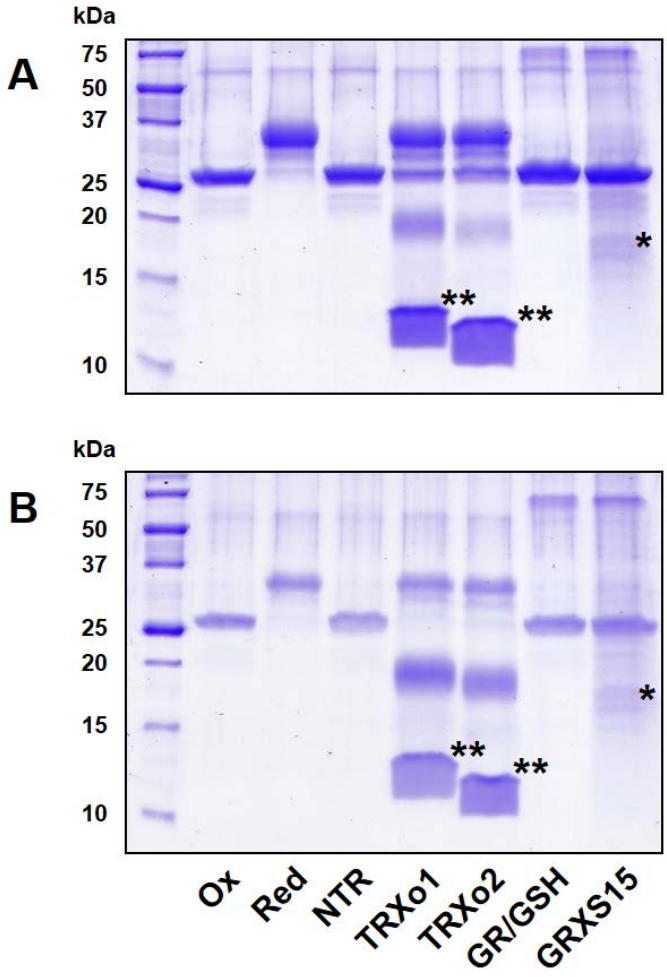

Figure 22. Le pont disulfure intramoléculaire des isoformes NUF4/5 est réduit par les TRXos mais pas par la GRXS15. La réduction des protéines NFU4 (A) et NFU5 (B) a été évaluée après 15 min d'incubation en présence de différents systèmes réducteurs : NTR (NADPH + NTR), TRXo1 (NADPH + NTR + TRXo1), TRXo2 (NADPH + NTR + TRXo2), GR/GSH (NADPH + GR + GSH) et GRXS15 (NADPH + GR + GSH + GRXS15). Les protéines ont ensuite été alkylées avec mPEG maleimide 2 kDa, puis séparées sur un gel SDS-PAGE 15%. Les formes réduite (Red) et oxydée (Ox) des protéines ont été utilisées comme contrôle. Les formes alkylées (*) et non alkylées (**) des différentes oxydoréductases utilisées sont également visibles dans certains cas (Zannini et al., 2018, P38).

De manière intéressante d'autres protéines (NFS1, ISCA4, ISU1) impliquées dans la maturation des protéines Fe-S mitochondriales ont été identifiées comme partenaires potentiels de TRXo1 (Yoshida et al., 2013). Ceci soulève la question de l'implication potentielle de TRXo1 et o2 dans la réduction de ces protéines dans des conditions où celles-ci seraient transitoirement oxydées. Cette observation n'est pas sans rapport avec l'étude précédente d'AtGRXS16 dans laquelle nous avons montré que cette protéine reliée à la biogenèse des centres Fe-S chloroplastique est réduite par le système FTR/TRX (Zannini et al., 2019, P39). De manière intéressante, une analyse protéomique des partenaires des TRXs chloroplastiques de *Chlamydomonas reinhardtii* a identifié plusieurs protéines (NFU1/2/3, SUFB/C/D, et SUFS) appartenant à cette machnierie d'assemblage (Pérez-Pérez et al., 2017). Ainsi, le contrôle de l'état redox des protéines impliquées dans la biogénèse des centres Fe-S par le système TRX pourrait être un mécanisme général au sein des organites mais également au sein des organismes.

3. Etude des mécanismes moléculaires impliqués dans la mobilisation et le transfert d'atomes de soufre chez les plantes

3.1 Analyse fonctionnelle des protéines impliquées dans la mobilisation et le transfert du soufre chez les plantes

Depuis septembre 2015, je développe un nouvel axe de recherche au sein de notre équipe. Il concerne l'identification des mécanismes moléculaires impliqués dans la mobilisation et le transfert d'atomes de soufre chez les plantes. Le projet SULTRAF a reçu le soutien de l'ANR dans le cadre de l'appel à projets ANR jeunes chercheurs-jeunes chercheuses (JCJC) 2016. Il est notamment centré sur deux familles protéiques : les cystéine désulfurases (CDs) et les sulfurtransférases (STRs). En effet, plusieurs exemples de l'implication des couples CD/STR dans les voies de synthèse de molécules contenant du soufre existent déjà chez les bactéries et l'homme (Lauhon & Kambampati, 2000 ; Dahl et al., 2011), alors que les études précédentes sur les CDs de plantes étaient principalement axées sur leur rôle dans la biogenèse des centres Fe-S et la sulfuration du cofacteur Moco (Heidenreich et al., 2005 ; Frazzon et al., 2007 ; Van Hoewyk et al., 2007).

Les études sur le métabolisme du soufre des plantes ne sont pas aussi avancées que celles relatives au métabolisme de l'azote et du phosphore, bien qu'une plus grande attention ait été accordée à cette voie depuis les observations des effets négatifs de la carence en soufre sur

le rendement des plantes cultivées (Schnug et al., 1995). Contrairement aux animaux qui ne peuvent pas assimiler le soufre inorganique et doivent donc absorber de la cystéine ou de la méthionine, les plantes sont capables de réduire du soufre inorganique sous forme sulfate au niveau des chloroplastes en soufre réduit utilisé ensuite pour la synthèse de cystéine dans le cytosol, les chloroplastes et les mitochondries (Takahashi et al., 2011). Donneur majeur de soufre, la cystéine est un métabolite clé pour la synthèse de méthionine et de GSH mais également pour la biosynthèse de nombreux composés soufrés. Bien que des expériences de synthèse enzymatique et non enzymatique *in vitro* de composés soufrés sont fréquemment réalisées avec du soufre libre (S^{2-}), sa toxicité et la nécessité d'une certaine spécificité suggèrent que des espèces chimiques non toxiques et plus stables doivent être utilisées pour l'apport de soufre dans diverses voies de biosynthèse. Ainsi, outre les exemples où le soufre est fourni par le sacrifice de centres Fe-S comme dans le cas de la biosynthèse des vitamines (biotine, thiamine, acide lipoïque) (Lanz & Booker, 2015) ou par une molécule de GSH comme dans le cas de la camaléxine (Su et al., 2011), les groupements persulfures représentent probablement une source majeure de soufre, en particulier pour la formation de centres Fe-S, de cofacteurs à molybdène (Moco) et de bases soufrées des ARNt (thionucléosides) (Mueller, 2006). Au niveau de ces voies de synthèse, les réactions de transfert de soufre reposent sur la formation de groupements persulfures sur les cystéines réactives, au travers de réactions de trans-persulfuration. Ces voies sont requises dans différents compartiments subcellulaires suggérant que plusieurs protéines/molécules spécifiques sont dédiées à la mobilisation et au transfert de soufre au sein et entre les compartiments subcellulaires.

Les cystéine désulfurases (CDs) constituent une famille d'enzymes responsables du transfert du soufre de la cystéine vers des molécules acceptrices (Mueller, 2006). Ce sont des enzymes pyridoxal 5'-phosphate (PLP) dépendantes qui catalysent la désulfuration de la cystéine en alanine (Zheng et al., 1993). Cette réaction globale peut être subdivisée en plusieurs étapes : liaison au substrat, clivage de la liaison C-S et activation du soufre par la formation d'une liaison persulfure. Dans la première étape, le substrat cystéine se lie au cofacteur PLP au niveau du site actif de l'enzyme, formant un intermédiaire aldimine externe PLP-Cys. Cet événement est suivi de l'attaque nucléophile par un groupement thiolate du site actif, qui conduit à la formation d'un intermédiaire persulfuré de l'enzyme et à la libération concomitante d'alanine (Belshad & Bollinger, 2009). Depuis la caractérisation de la protéine NifS d'*Azotobacter vinelandii* comme CD impliquée dans la maturation de la nitrogénase (Zheng et al., 1993), de nombreuses études ont permis de caractériser différentes isoformes procaryotes et eucaryotes et d'établir des fonctions dans la mobilisation du soufre et son transfert ultérieur vers diverses

voies métaboliques. Malgré un repliement global et un état d'oligomérisation (formation de dimère) conservés, les CDs présentent des différences structurales et de réactivité catalytique qui ont mené à la distinction de deux groupes (Mihara & Esaki, 2002). Les membres du groupe I contiennent une insertion de séquence de douze résidus comprenant la cystéine catalytique. En formant une boucle, cette extension est suffisamment souple pour permettre le transfert direct du soufre à de multiples partenaires biologiques, comme cela é été illustré pour l'isoforme IscS d'*E. coli* dont l'interaction avec différents accepteurs de soufre repose sur différences surfaces d'interaction (Shi et al., 2010). Pour les membres du groupe II, la boucle contenant la cystéine catalytique est plus courte (Roret et al., 2014, P27), ce qui explique que ces CDs nécessitent des activateurs spécifiques/accepteurs de soufre conduisant ainsi à la formation d'un système CD-activateur (Loiseau et al., 2003 ; Outten et al., 2003 ; Loiseau et al., 2005).

L'efficacité et la spécificité du transfert de soufre vers les molécules acceptrices varient selon la sous-classe de CD et le type d'accepteurs de soufre dont la nature et la fonction dictent la direction et le flux du transfert de soufre. Ainsi, bien que le glutathion persulfuré (GSSH) puisse représenter une forme de transport relativement stable et spécifique des atomes de soufre (Hildebrandt & Grieshaber, 2008 ; Ida et al., 2014), le transfert de soufre, au travers de réactions de trans-persulfuration, implique l'existence de protéines de transfert, notamment de la famille des STRs afin de garantir la spécificité du transfert de soufre aux accepteurs. Ces protéines possèdent un ou plusieurs domaines rhodanese (Rhd) présentant généralement une cystéine catalytique (Bordo & Bork, 2002 ; Cipollone et al., 2007). Ces protéines sont retrouvées quasiment dans l'ensemble du règne vivant, mais elles diffèrent considérablement en termes de séquences primaires, de nombre de domaine protéique et de structure/longueur de la boucle de leur site actif (Bordo & Bork, 2002). Néanmoins, trois groupes distincts ont été définis (Bordo & Bork, 2002 ; Cipollone et al., 2007). Le premier comprend les STRs n'ayant qu'un seul domaine Rhd. Ce groupe comprend les phosphatases CDC25 et les thiosulfate-sulfurtransférases (TSTs) nommées ainsi selon leur capacité à utiliser le thiosulfate comme donneur de soufre *in vitro*. La présence d'un résidu supplémentaire dans la boucle du site actif des phosphatases CDC25 (sept résidus contre six pour les TSTs) constitue une différence importante dans la capacité des protéines CDC25 à déphosphoryler les résidus tyrosine (Bordo & Bork, 2002). Le deuxième groupe est constitué des STRs possédant 2 domaines Rhd mais seul le domaine C-terminal possède la cystéine catalytique. Elles sont capables d'utiliser *in vitro* le 3-mercaptopyruvate (3-MP) comme substrat. Elles sont ainsi nommées 3-MP-STR ou mercaptopyruvate-sulfurtransférases (MST) et sont présentes dans la plupart des organismes (Nakamura et al., 2000 ; Papenbrock & Schmidt, 2000 ; Colnaghi et al., 2001 ; Yadav et al.,

2013). Les mammifères possèdent également d'autres isoformes STR à deux domaines Rhd qui possèdent une activité TST comme l'isoforme rhodanese bobine appelée Rhobov (Blumenthal & Heinrikson, 1971 ; Bordo & Bork, 2002 ; Nambi et al., 2015). Enfin, le troisième groupe est formé par les STRs contenant un domaine Rhd fusionné à un autre domaine qui dicte probablement la spécificité et le rôle de la protéine, bien que la cystéine catalytique du domaine Rhd soit nécessaire (Bordo & Bork, 2002 ; Cipollone et al., 2007).

Les isoformes ayant une cystéine catalytique sont impliquées dans des réactions de trans-persulfuration en catalysant le transfert d'un atome de soufre d'un donneur vers un accepteur nucléophile. Au cours de la réaction, les STRs passent elles-mêmes par un état intermédiaire où leur cystéine catalytique est persulfurée. Leur rôle dans les réactions de transfert de soufre est par exemple bien illustré par le rôle du domaine Rhd de l'isoforme CNX5 humaine dans la synthèse du cofacteur molybdène (Matthies et al., 2004) et l'implication de ces protéines dans le transfert de soufre chez les micro-organismes utilisant cet élément comme source d'énergie (Aussignargues et al., 2012 ; Stockdreher et al., 2014). Une analyse approfondie du génome de 25 organismes photosynthétiques nous a permis d'illustrer la diversité de la famille STR chez les plantes avec la présence d'une vingtaine d'isoformes chez les plantes supérieures, réparties en 9 sous-groupes (Moseler et al., 2020, P41). Les plantes possèdent des isoformes présentes chez les organismes non photosynthétiques telles que STR1/2 (MST) (groupe I), STR13/CNX5 (groupe VII) et les isoformes TSTs (groupes VIII et IX), qui remplissent très probablement des fonctions similaires à leurs orthologues non végétales. Les plantes possèdent des isoformes additionnelles qui pourraient être reliées à la complexité des processus moléculaires dans les cellules végétales, y compris de nouvelles voies moléculaires. D'autre part, la localisation chloroplastique avérée ou prédite de la moitié des isoformes STR représente une autre particularité intéressante, tout comme les fonctions énigmatiques de plusieurs isoformes spécifiques aux plantes (groupes IV, V et VI) (Moseler et al., 2020, P41). Au début de ce projet, seules quelques études avaient analysé les fonctions biologiques et les propriétés biochimiques de certaines isoformes STR chez les plantes (Papenbrock et al., 2011). Ces travaux concernaient certaines des 21 isoformes repertoriées pour *A. thaliana* (Tableau 2).

Nom	Numéro accession	Domaines	Site actif	Localisation subcellulaire	Fonction
STR1	At1g79230	Rhod Rhod	**C**GTGVT	Mitochondrie	Détoxication du soufre
STR2	At1g16460	Rhod Rhod	**C**GTGVT	Cytosol	Indéterminée
STR3	At5g23060	Rhod	DSYTDS	Chloroplaste	Régulation de la fermeture des stomates
STR4	At4g01050	Rhod	DKFDGN	Chloroplaste	Recrutement de la FNR dans les thylakoïdes
STR4a	At3g25480	Rhod	DNFDGN	Chloroplaste	Indéterminée
STR5	At5g03455	Rhod	**C**ALSQVR	Noyau	Tolérance à l'arsenic
STR6	At1g09280	Rhod FSH1	**C**TGGIR	Cytosol	Indéterminée
STR7	At2g40760	Rhod	**C**TGGIR	Mitochondrie	Indéterminée
STR8	At1g17850	Rhod	**C**TGGIR	Chloroplaste	Indéterminée
STR9	At2g42220	Rhod	**C**QEGLR	Chloroplaste	Indéterminée
STR10	At3g08920	Rhod	**C**GEGLR	Mitochondrie	Indéterminée
STR11	At4g24750	Rhod	**C**QKGLR	Chloroplaste	Indéterminée
STR12	At5g19370	Rota Rhod	CKVGGR	Chloroplaste	Indéterminée
STR13	At5g55130	MoeB Rhod	**C**RRGND	Cytosol	Synthèse du cofacteur Moco et thiolation des ARNt
STR14	At4g27700	Rhod	**C**SSAGT	Chloroplaste	Indéterminée
STR15	At4g35770	Rhod	**C**ESGQM	Chloroplaste	Indéterminée
STR16	At5g66040	Rhod	**C**QSGGR	Chloroplaste	Indéterminée
STR17	At2g17850	Rhod	**C**KSGVR	Réticulum endoplasmique	Indéterminée
STR17a	At2g21045	Rhod	**C**NAGGR	Cytosol/Noyau	Tolérance à l'arsenic
STR18	At5g66170	Rhod	**C**QSGAR	Cytosol	Indéterminée
STR19	At3g59780	Rhod	DADGTR	Chloroplaste	Indéterminée

Tableau 2. Principales caractéristiques des isoformes STR d'*Arabidopsis thaliana*. Les domaines Rhd colorés en bleu possèdent une cystéine catalytique, tandis que les domaines Rhd colorés en vert n'ont pas de cystéine catalytique. L'isoforme STR5 présente un site actif constitué de 7 acides aminés au lieu de 6. Les autres domaines représentés sont FSH1, sérine hydrolase, Rota, rotamase et MoeB, biosynthèse de la molybdoptérine. Lorsque les localisations subcellulaires ne sont basées que sur des prédictions, elles sont soulignées.

Les isoformes les mieux caractérisées, les isoformes MST, STR1 et STR2, jouent un rôle important dans le développement de la graine et de l'embryon chez *A. thaliana* (Mao et al., 2011). Un lien fonctionnel entre STR1 et la sulfure dioxygénase ETHE1 a en outre été suggéré dans la détoxication du soufre au niveau des mitochondries (Krüßel et al., 2014). L'isoforme STR13, également dénommée CNX5 est impliquée dans la voie de biosynthèse des molybdoptérines et dans la thio-modification des ARNt (Nakai et al., 2012 ; Kruse et al., 2018). Enfin d'autres travaux ont révélé que les isoformes STR5 et STR17 présentent une activité de réduction de l'arsenic et seraient ainsi impliquées dans la tolérance à cet élément toxique (Duan et al., 2007 ; Sánchez-Bermejo et al., 2014). Tous ces rôles mais également les caractéristiques biochimiques et structurales des isoformes d'*A. thaliana* ont été détaillées récemment (Selles et al., 2019, P42).

Le projet de recherche SULTRAF vise à élucider les mécanismes moléculaires impliqués dans la mobilisation et le transfert d'atomes de soufre chez les plantes. Pour cela, une approche intégrée combinant des méthodes *in vitro* et *in vivo* a été developpée afin de réaliser une analyse fonctionnelle des protéines impliquées dans la mobilisation (cystéine désulfurases) et le transfert (sulfurtransférases) du soufre chez *A. thaliana*. Ainsi, le rôle des STRs, notamment celles qui sont spécifiques des plantes ou qui n'ont pas encore été caractérisées jusqu'à présent, est étudié en définissant leurs propriétés biochimiques et structurales (premier objectif), en étudiant leur interaction avec les CDs (deuxième objectif), en identifiant des protéines partenaires, puis en validant et caractérisant ces interactions par des approches complémentaires *in vitro* et *in vivo* (troisième objectif). Ce projet a pour but de permettre de répondre à trois questions principales :

1. Les couples CD/STR remplissent-ils un rôle central dans la mobilisation et le transfert de soufre chez les plantes ?
2. Comment les STRs différencient-elles et interagissent-elles avec les donneurs et les accepteurs de soufre ?
3. Les STRs et leurs partenaires physiologiques sont-ils impliqués dans la biogenèse d'H_2S et les mécanismes de signalisation associés aux réactions de trans-persulfuration ?

3.1.1. Caractérisation de l'interaction entre ABA3 et STR18 chez *A. thaliana*

Un des objectifs du projet SULTRAF étant d'étudier les interactions CD-STR et d'identifier également des protéines cibles des STRs, nous nous sommes notamment focalisés

sur l'isoforme STR18, une isoforme TST cytosolique. Une approche de type « Pull-down » à partir d'extraits protéiques totaux de feuilles d'*A. thaliana*, a permis d'identifier environ 250 partenaires potentiels pour STR18. Parmi ceux-ci figuraient notamment la protéine ABA3 qui peut être considérée comme la troisième isoforme CD chez les plantes. Contrairement à NFS1 et NFS2 qui constituent les principaux systèmes de mobilisation du soufre pour la biogenèse des centres Fe-S dans les mitochondries, le cytosol et les chloroplates (Frazzon et al., 2007 ; Van Hoewyk et al., 2007), ABA3 qui est localisée dans le cytosol, est impliquée dans la sulfuration du cofacteur Moco et participe ainsi à l'activation de l'aldéhyde oxydase (AO) et de la xanthine déshydrogénase (XDH) dans le cytosol (Bittner et al., 2001 ; Heidenreich et al., 2005). Cette protéine se compose de deux domaines, un domaine N-terminal CD qui transfère un atome de soufre à un cofacteur Moco lié au domaine C-terminal, avant le transfert et l'insertion de ce Moco sulfuré aux protéines AO et XDH (Wollers et al., 2008). Ces deux enzymes sont impliquées respectivement dans la biosynthèse de l'acide abscissique et la dégradation des purines. Plusieurs mutants alléliques *aba3* avec des phénotypes légèrement différents ont été décrits (Xiong et al., 2001 ; Dai et al., 2005 ; Zhong et al., 2010 ; Bernard et al., 2013), ce qui suggère que différentes voies dépendent de l'activité de cette protéine. Les feuilles des plantes mutantes *los5-1* et *los5-2*, mais pas celles des plantes mutantes *aba3-1* et *aba3-2*, sont plus étroites et légèrement dentelées sur le bord par rapport aux feuilles plus rondes des plantes WT. Comme les mutations des mutants *los5-1* et *los5-2* affectent le domaine CD alors que celles des mutants *aba3-1* et *aba3-2* se situent dans la partie centrale de la protéine, les auteurs ont conclu que l'activité CD est nécessaire en particulier pour une morphologie foliaire correcte (Xiong et al., 2001). L'isolement d'ABA3 comme partenaire de STR18 prenait tout son sens vis-à-vis du projet mais également vis-à-vis de l'existence de protéines fusions CD-STR chez certaines bactéries. Nous avons donc entrepris de caractériser en parallèle les mécanismes moléculaires impliqués dans l'interaction ABA3-STR18 et les propriétés biochimiques de la protéine fusion CD-STR de la bactérie *Pseudorhodoferax sp.* (Selles et al., résultats non publiés).

La présence dans le spectre UV-visible d'une bande d'absorption à 418 nm, caractéristique de la présence d'un cofacteur PLP, et le fait que la protéine CD-STR existe majoritairement sous forme homodimérique, constituent des propriétés similaires aux autres CDs précédemment caractérisées (Figure 23) (Black & Dos Santos, 2015). Des mesures d'activité enzymatique *in vitro* en présence d'un des deux substrats potentiels, la cystéine pour le domaine CD et le thiosulfate pour le domaine STR, ont confirmé que cette protéine est bifonctionnelle et présente une double activité cystéine désulfurase et thiosulfate-

sulfurtransférase (Figure 23). Oure le fait que la présence d'un domaine STR n'empêche pas l'activité du domaine CD, il semble que celui-ci permet au contraire d'augmenter l'activité CD de la protéine. En effet, les données obtenues suggèrent que l'isoforme CD-STR de Pseudorhodoferax est la CD la plus efficace caractérisée à ce jour, avec une activité de 2800 nmol de soufre libéré par min par mg de protéine, qui est de 8 à 250 fois plus élevée que celle mesurée pour les autres CDs déjà caractérisées chez les bactéries et les eucaryotes (Selles et al., résultats non publiés).

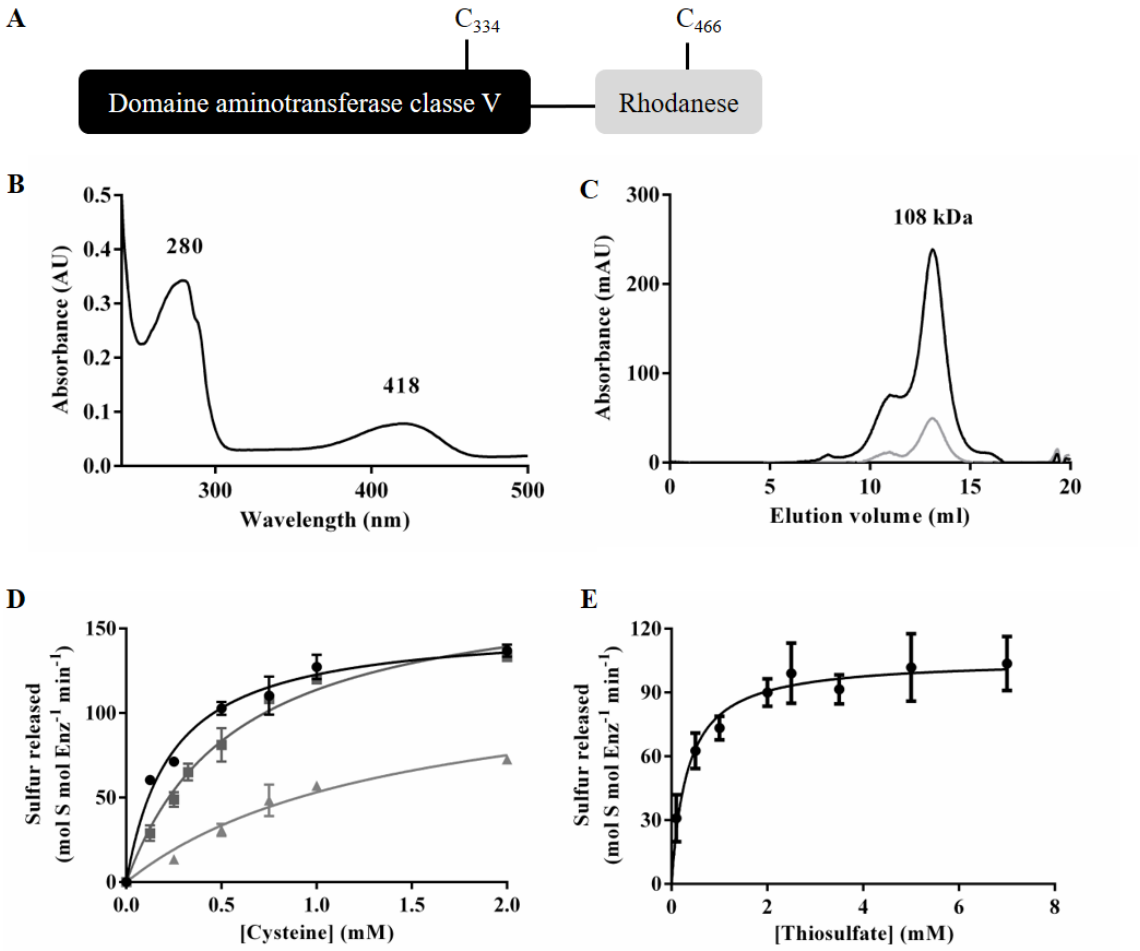

Figure 23. La protéine CD-STR de *Pseudorhodoferax* possède une double activité enzymatique. Organisation modulaire de l'isoforme CD-STR de Pseudorhodoferax (WP_056898193.1) (A). Les résidus C334 et C446 représentent la cystéine catalytique de chaque domaine protéique. Spectre d'absorption UV-visible de la protéine recombinante CD-STR possédant une étiquette polyhistidine dans sa partie N-terminale (B). Analyse de l'état d'oligomérisation par gel filtration sur une colonne Superdex S200 10/300 (C). La présence du polypeptide et du cofacteur PLP a été détectée en mesurant l'absorbance à 280 nm (ligne noire) et à 418 nm (ligne grise). Suivi de l'activité cystéine désulfurase de la protéine CD-STR en présence de concentrations croissantes de cystéine (D). Les mesures ont été effectuées en présence de 5 mM DTT (cercles noirs), 5 mM GSH (triangles gris) ou 5 mM β-mercaptoéthanol (carrés gris). Suivi de l'activité thiosulfate-sulfurtransférase de la protéine CD-STR en présence de 5 mM β-mercaptoethanol (Selles et al., résultats non publiés).

Concernant l'interaction ABA3-STR18, STR18 stimule l'efficacité catalytique de la protéine ABA3 d'un facteur 5, en agissant comme un accepteur de soufre et en augmentant l'affinité d'ABA3 pour la cystéine. Des analyses de spectrométrie de masse ont confirmé que la cystéine catalytique de STR18 devient persulfurée en présence d'ABA3 et de cystéine (Figure 24, adduit de 32 Da après traitement), cette persulfuration étant dépendante du domaine CD d'ABA3.

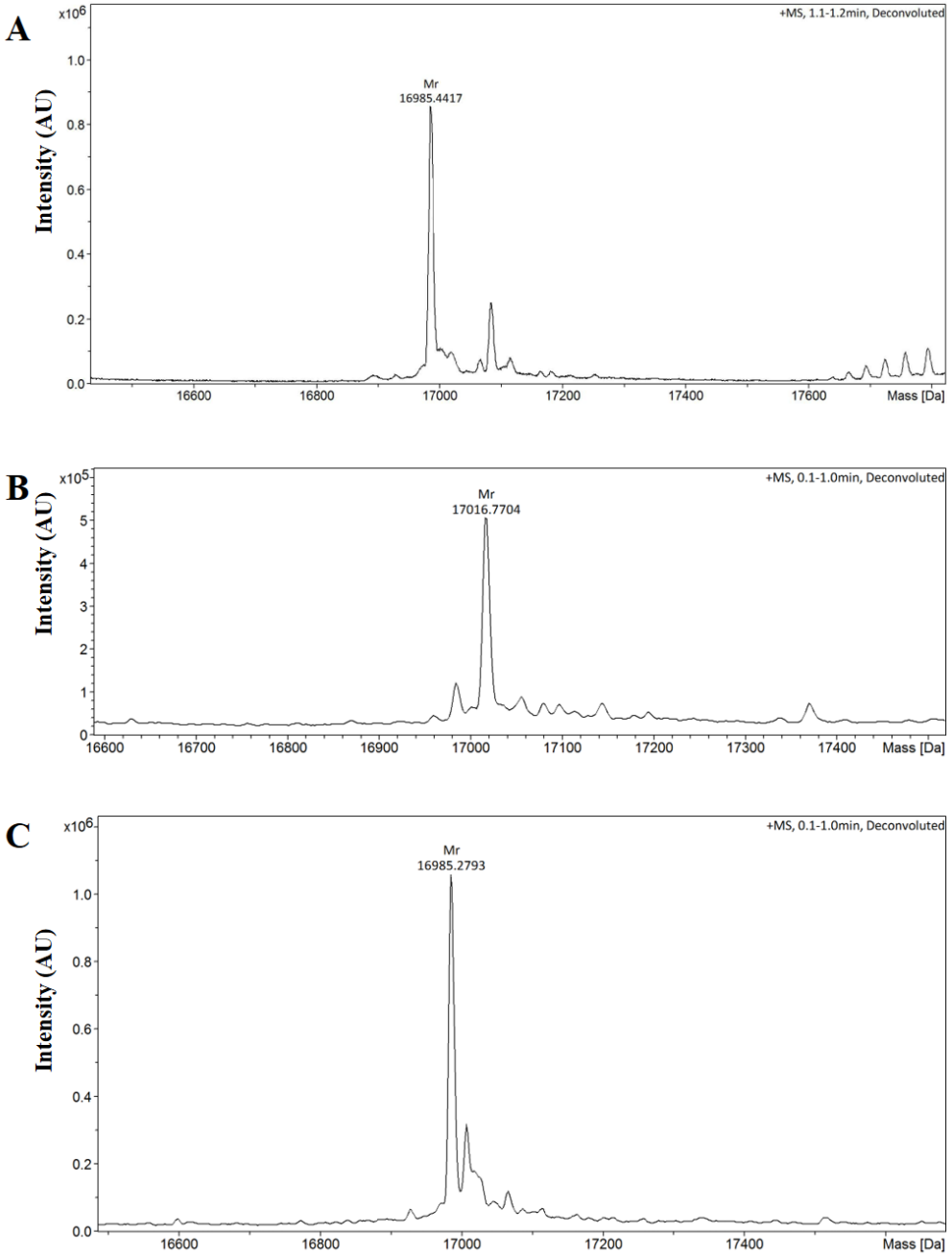

Figure 24. Analyse de l'état redox de STR18 par spectrométrie de masse (ESI-MS). Les spectres de masse ont déterminés pour la protéine réduite (A), la protéine réduite incubée avec de la L-cystéine et ABA3 avant (B) et après traitement en présence de DTT (C) (Selles et al., résultats non publiés).

Bien que l'interaction *in vivo* entre ces deux protéines reste encore à confirmer, plusieurs éléments sont en faveur d'une interaction pertinente d'un point de vue physiologique. Par exemple les valeurs apparentes de K_m de STR18 pour le thiosulfate (273 ± 38 µM) et d'ABA3 pour STR18 (1,1 ± 0,3 µM) (Figure 24B), mais aussi la capacité d'ABA3 à promouvoir la persulfuration de STR18 plus efficacement que le thiosulfate, suggèrent qu'ABA3 peut être considéré comme le donneur de soufre préférentiel pour STR18. D'autre part, la valeur apparente de K_m d'ABA3 pour STR18 est 8 fois plus faible que celle pour la cystéine. Enfin, nous avons démontré la capacité du couple ABA3-STR18 à catalyser des réactions de trans-persulfuration de protéines cibles en utilisant la roGFP2 comme cible *in vitro*. Ainsi, en plus d'illustrer pour la première fois une interaction CD-STR chez les plantes, ce travail a mis en évidence que l'interaction ABA3-STR18 pourrait représenter une nouvelle voie de transfert du soufre dans le cytosol, indépendante de la fonction d'ABA3 dans la maturation du cofacteur Moco.

3.1.2. Etude structure-fonction de l'isoforme STR18 d'*A. thaliana*

Dans la continuité de l'étude de l'interaction ABA3-STR18, nous avons entrepris une étude structure-fonction de STR18 (Selles et al., résultats non publiés). Bien que la résolution de la structure tridimensionnelle par RMN soit en cours de finalisation (collaboration avec Pascale Tsan, UMR 7036 CRM2 Université de Lorraine-CNRS), les données d'ores et déjà obtenues mettent en lumière une régulation redox de la protéine. En effet, STR18 qui possède deux résidus cystéine est sensible à l'oxydation par H_2O_2. La présence de faibles concentrations de H_2O_2 entraîne la formation d'un pont disulfure intramoléculaire inactivant l'activité enzymatique de la protéine et induisant également un changemenent conformationnel important de la protéine, confirmé par des analyses de dichroïsme circulaire et de chromatographie d'exclusion de taille couplée à la diffusion de lumière multi-angle (SEC-MALS). Par contre, la présence de fortes concentrations de H_2O_2 conduit à la formation d'un dimère covalent. Ces deux formes oxydées différentes de STR18 sont réduites par la systèmre NADPH/NTR/TRX, et notamment l'isoforme TRXh1 pour laquelle une interaction a été détéctée avec STR18 chez *A. thaliana* (Henne et al., 2015). Concernant son activité enzymatique, STR18 présente une activité TST beaucoup plus importante en présence du système GRX que du sytème TRX (environ 1000 fois) (Figure 25A). L'activité mesurée en présence de GSH ou de cystéine était également faible suggérant que ces deux molécules ne représenteraient pas des accepteurs de soufre physiologiques pour STR18 (Figure 25B).

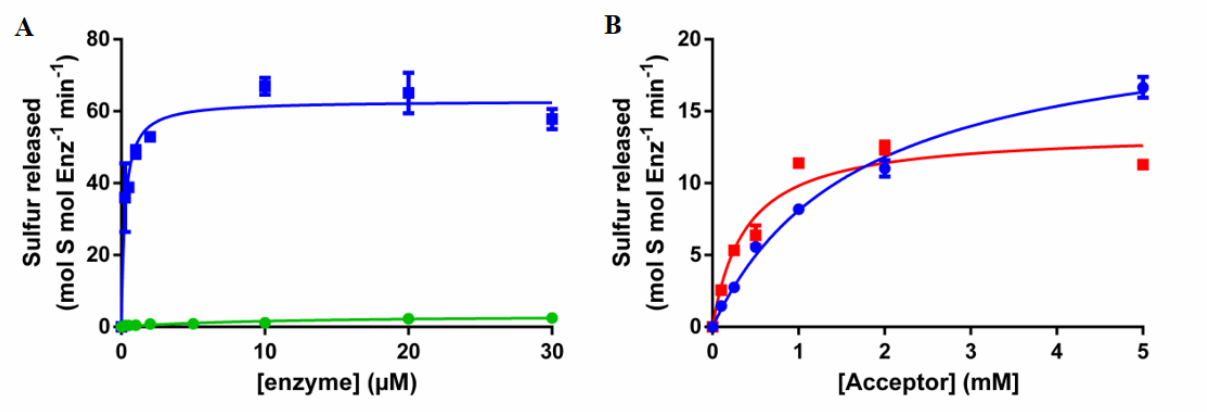

Figure 25. STR18 présente une faible activité thiosulfate-sulfurtransférase en présence de différents réducteurs physiologiques. Les mesures ont été effectuées avec 20 nM STR18 en présence de 250 µM thiosulfate. Le mélange réactionnel contenait 250 µM NADPH, 200 nM NTRB et 0 à 30 µM TRXh1 (ligne verte) ou 250 µM NADPH, 250 µM GSH, 0.5U GR et 0 à 30 µM GRXC4 (ligne bleue) (A). Le mélange réactionnel contenait 250 µM NADPH, 0.5U GR et 0 à 5 mM GSH ou de 0 à 5 mM cystéine (ligne rouge) (B) (Selles et al., résultats non publiés).

Le système TRX serait donc impliqué dans la régulation de l'état redox de STR18 plutôt que d'agir en tant qu'accepteur de soufre et ainsi participer à son activité enzymatique. Enfin, considérant la faible efficacité générale de la réaction entre STR18 et les réducteurs cellulaires testés (mis à part le système GRX), STR18 ne serait pas impliquée dans la formation de sulfure d'hydrogène mais plutôt dans le transfert de soufre en catalysant des réactions de trans-persufluration comme évoqué précédemment (section 3.1.1).

3.1.3. Caractérisation fonctionnelle des isoformes STR1 et 2 d'*A. thaliana*

D'un point de vue évolutif, la plupart des organismes vivants si ce n'est tous, possède au moins une isoforme MST caractérisée par la présence de deux domaines Rhd et utilisant le 3-MP, un produit de dégradation de la cystéine, comme substrat. Les plantes possèdent au moins une isoforme MST avec une signature CG[S/T]GVT caractéristique au niveau de leur site actif (Moseler et al., 2020, P41), *A. thaliana* contenant deux MSTs, nommées STR1 et STR2, situées respectivement dans la mitochondrie et le cytosol (Nakamura et al., 2000 ; Bauer et al., 2004). Chez les bactéries et les mammifères, la fonction des MSTs dans le métabolisme soufré est notamment reliée à la synthèse de H_2S (Shatalin et al., 2011 ; Kabil & Banerjee, 2014), tandis que chez les plantes, le rôle de ces protéines n'est pas encore clairement établi. Chez Arabidopsis, STR1 et STR2 seraient ainsi des enzymes multifonctionnelles impliquées dans le catabolisme de la cystéine et la détoxication du cyanure (Mao et al., 2011 ; Krüßel et

al., 2014 ; Höfler et al., 2016). Au niveau des mitochondries, une voie de dégradation de la cystéine repose sur une cystéine aminotransférase (encore non identifiée chez les plantes) qui convertit la cystéine en 3-MP. Ce dernier est ensuite transformé en pyruvate par STR1, qui en devenant persulfurée, synthétiserait du GSH persulfuré (GSSH) en interagissant avec le GSH réduit (Höfler et al., 2016). STR1 catalyserait également la production de thiosulfate à partir du sulfite produit par la protéine ETHE1 dont le substrat est le GSSH (Höfler et al., 2016). Ces rôles proposés pour STR1 dans la dégradation de la cystéine, sont notamment basés sur l'observation que le phénotype du double mutant *ethe1 x str1* n'est pas plus marqué que celui du simple mutant *str1* (Höfler et al., 2016). D'autre part, une interaction des deux isoformes STR1 et STR2 a été observée avec les TRXs par BiFC, mais aucune étude approfondie du rôle de ces deux systèmes et de leur interaction dans la biosynthèse de H_2S et la persulfuration des protéines n'a été réalisée (Henne et al., 2015).

Dans cette étude, nous avons étudié les relations entre les deux isoformes MST d'*A. thaliana* et différents réducteurs physiologiques non enzymatiques, la cystéine et le GSH, et enzymatiques, les systèmes GSH/GRX et NTR/TRX (Moseler et al., résultats non publiés). Comme attendu, STR1 et STR2 utilisent préférentiellement le 3-MP comme donneur de soufre et deviennent per-polysulfurées en absence de réducteur, suggérant que les formes réduites et per/polysulfurées de ces protéines sont toutes deux enzymatiquement actives. Ces deux formes sont sensibles à l'oxydation en présence de H_2O_2, ce qui conduit à l'inhibition de leur activité 3-MP sulfurtransférase. Néanmoins, cette inhibition est majoritairement irréversible pour la forme réduite alors, que les systèmes réducteurs GSH/GR et NTR/TRX sont capables de restaurer l'activité de la forme persuflurée suggérant que la persulfuration de STR1 et STR2 représente un mécanisme de protection contre la suroxydation en présence de H_2O_2. Cette observation rejoint celles précédemment réalisées concernant le rôle de protection de la persulfuration contre la suroxydation irréversible pour d'autres protéines (Millikin et al., 2016 ; Wedmann et al., 2016). Les mesures d'activité *in vitro* des deux isoformes confirment la capacité de ces protéines à générer H_2S en présence du système TRX, avec un niveau d'activité proche de celui observé pour les protéines humaines mais également en présence du système GSH/GRX pour lequel il n'y avait pas d'informations jusqu'à présent (Figure 26). D'autre part, la libération de H_2S en présence de GSH ou de cystéine, bien que plus faible qu'en présence des systèmes réducteurs enzymatiques, suggèrent la formation par STR1 et STR2, de molécules persulfurées de faible poids moléculaire comme le GSSH et la cystéine persulfurée (Cys-SSH) au moins comme intermédiaires réactionnels (Figure 26).

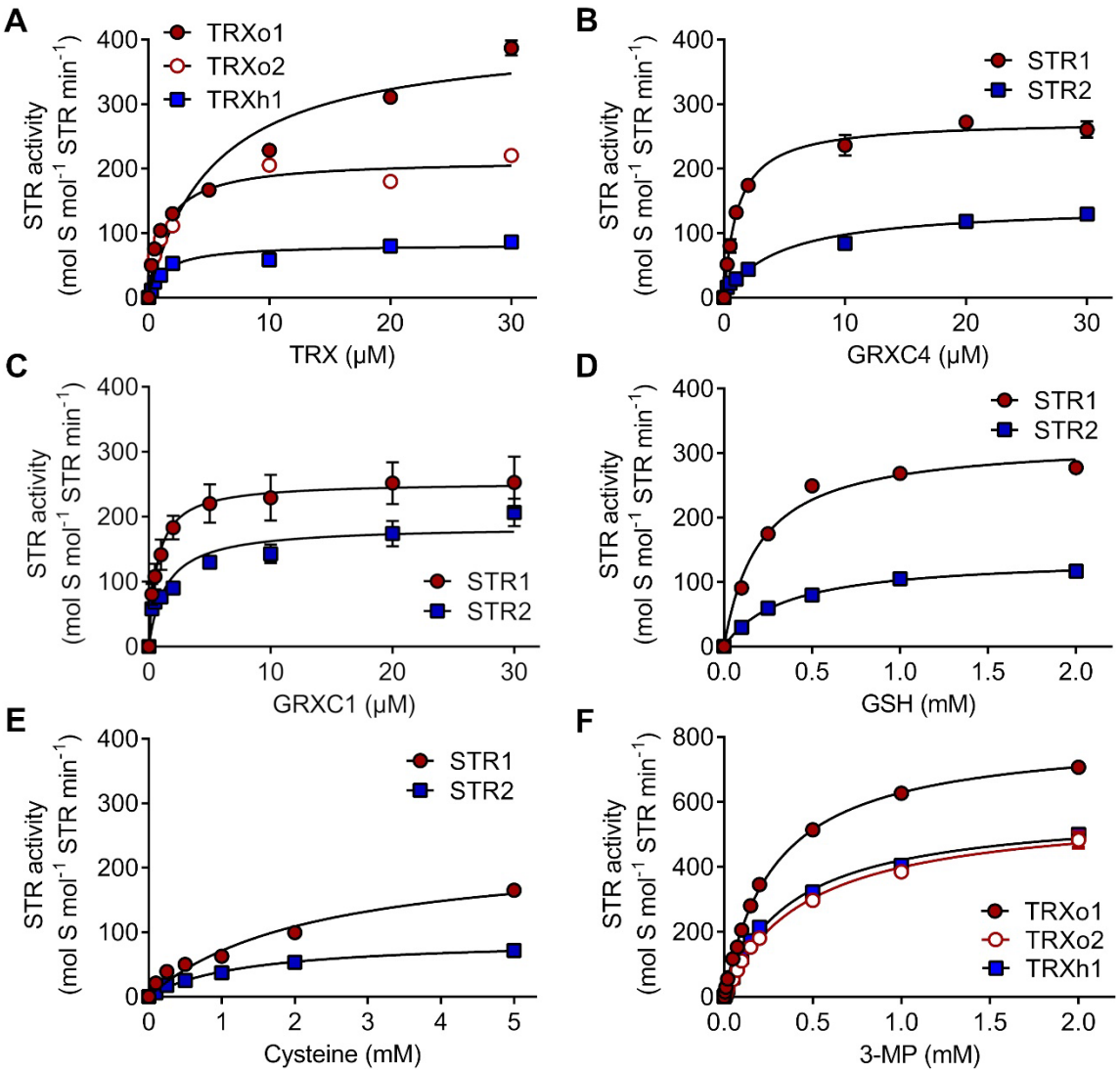

Figure 26. Analyse de l'activité 3-MP sulfurtransférase des isoforms STR1 et STR2 en présence de divers réducteurs physiologiques. L'activité des proteins a été mesurée avec 20 nM STR en présence de 250 µM 3-MP. Le mélange réactionnel contenait 250 µM NADPH, 200 nM NTRB, 0 à 30 µM TRX (A), 250 µM NADPH, 250 µM GSH, 0.5U GR, 0 à 30 µM GRXC4 (B) ou GRXC1 (C), 250 µM NADPH, 0.5U GR, 0 à 2 mM GSH (D) ou 0 à 5 mM cystéine (E). L'influence de la concentration en 3-MP a été évaluée en utilisant 20 nM STR en présence de 0 à 2 mM 3-MP, 200 µM NADPH, 200 nM NTRB, 30 µM TRXo1/o2 pour STR1 et 10 µM TRXh1 pour STR2 (Moseler et al., résultats non publiés).

Une étude récente a mis en évidence ce rôle pour l'isoforme MST d'*E.coli* (Li et al., 2019). Le GSSH et la Cys-SSH appartiennent à une forme particulière de soufre appelée « sulfane sulfur » qui regroupe les molécules/protéines contenant un atome de soufre lié de manière covalente à deux ou plusieurs atomes de soufre (R-S-S_n-S-R, Prot-S-S_n-S-Prot) ou à un atome de soufre et un hydrogène ionisable (R-S-S-H, Prot-S-S-H). Suite aux premières mesures d'activité *in vitro*, nous avons testé la capacité de STR1 et STR2 à produire du

« sulfane sulfur » à partir d'extraits foliaires d'*A. thaliana*. Les résultats obtenus confirment la capacité de ces deux protéines à synthétiser du « sulfane sulfur ». L'analyse et la comparaison des taux de « sulfane sulfur » total et lié aux protéines, présents dans les plantes sauvages et les simples mutants *str1* et *str2* ne mettent pas en évidence de différences significatives et ne permettent donc pas de confirmer un rôle de STR1 et STR2 dans la synthèse de « sulfane sulfur » *in vivo* (Moseler et al., résultats non publiés). Néanmoins, les deux plants mutants *str1* et *str2* présentent tous les deux une activité de 3MP-sulfurtransférase qui pourrait suffire à compenser l'absence de chaque isoforme et donc à maintenir un niveau de « sulfane sulfur » similaire à celui observé dans les plantes sauvages. D'autres expériences sont donc nécessaires pour valider ou exclure l'implication de STR1 et STR2 dans la production de H_2S et de « sulfane sulfur » chez les plantes.

3.2. Développement de biosenseurs redox spécifiques de composés soufrés

La caractérisation biochimique de certaines isoformes STR a mis en évidence une spécificité de ces protéines pour différents substrats soufrés (3-MP, thiosulfate) issus du catabolisme de la cystéine *in vivo*. Cette spécificité de substrat couplée à la capacité de STR1 et STR18 notamment à oxyder une version redox sensible de la GFP (roGFP2) nous a conduit à proposer un nouveau projet visant à utiliser les propriétés enzymatiques de certaines STRs pour développer de nouveaux biosenseurs redox fluorescents afin de pouvoir étudier les dynamiques du métabolisme de la cystéine et des processus associés de transfert du soufre en temps réel chez les plantes mais également les autres organismes vivants. Ce projet a reçu le soutien financier du Laboratoire d'Excellence ARBRE (projet SULPRO) et de l'initiative Lorraine Université d'Excellence (projet SULSENSE).

Une pléthore de biosenseurs fluorescents redox codés génétiquement a été mise au point ces dernières années, ce qui a ouvert de nouvelles voies dans les mesures dynamiques d'un large éventail de substances biologiques. La protéine roGFP2 (réduction-oxydation GFP) constitue l'un de ces biosenseurs qui permettent des études d'imagerie cellulaire non invasive, en temps réel et qui peuvent cibler des compartiments subcellulaires spécifiques. L'état redox de la protéine est couplé à la modification du rapport de la fluorescence émise après excitation à deux maxima compris entre 390 et 405 nm et entre 475 et 488 nm. La présence de deux maxima d'excitation avec des décalages d'intensité inverses permet des mesures ratiométriques, c'est-à-dire indépendantes du niveau d'expression. La roGFP2 est également insensible aux variations de pH, du moins dans la gamme des valeurs de pH physiologiques (Meyer & Dick, 2010). La

première sonde roGFP a été conçue en introduisant deux cystéines exposées en surface dans deux brins β adjacents, à proximité immédiate du chromophore, de manière à ce que ces deux cystéines puissent former un pont disulfure, entraînant de petites modifications structurelles influençant la fluorescence de la protéine (Ostergaard et al., 2001 ; Hanson et al., 2004). La réduction/oxydation de ce pont disulfure dépend du couple GSH/GSSG et l'équilibre entre les formes réduite et oxydée est rapidement atteint en présence de GRXs endogènes (Meyer et al., 2007). Par la suite, la protéine roGFP a été fusionnée à différentes oxydoréductases. Ainsi, un biosenseur permettant d'étudier les dynamiques du couple GSH/GSSH a été développé en fusionnant l'isoforme humaine Grx1 et la roGFP2 (Gutscher et al., 2008). En effet, bien que l'interaction entre la roGFP2 seule et le couple GSH/GSSG soit spécifique, la réaction redox reste néanmoins très lente. Coupler la roGFP2 à la Grx1 a permis d'améliorer la cinétique de la réaction (100 000 fois plus rapide) et de la rendre indépendante de la disponibilité des GRXs endogènes, permettant ainsi des mesures comparables du couple GSH/GSSG dans différents compartiments subcellulaires, types cellulaires et organismes (Meyer et al., 2007 ; Gutscher et al., 2008 ; Schwarzländer et al., 2016). Pour certains organismes ne possédant pas de glutathion et de GRX, la roGFP2 a ensuite été associée à des thiol peroxydases (TPXs) de levure, Orp1 et Tsa2 afin de développer des biosenseurs spécifiques de H_2O_2 (Gutscher et al., 2009 ; Morgan et al., 2016). Enfin, certains organismes ne possèdent pas de glutathion et de GRX, mais d'autres composés thiol à faible poids moléculaire, associé à des rédoxines spécifiques. Ainsi, le biosenseur associant la mycorédoxine Mrx1 à la roGFP2 permet d'étudier spécifiquement la dynamique du mycothiol (MSH/MSSM) pour les espèces du genre Mycobacterium (Bhaskar et al., 2014). Pour certaines espèces bactériennes ayant du bacillithiol (BSH/BSSB), un biosenseur bacillirédoxine (Brx)-roGFP2 a été développé (Loi et al., 2017). Ces différents exemples illustrent ainsi la capacité théorique de toute protéine possédant une cystéine catalytique oxydée lors de l'interaction avec le substrat à transmettre l'oxydation à la roGFP2 et ainsi servir de rapporteur fluorescent des niveaux du substrat (Figure 27).

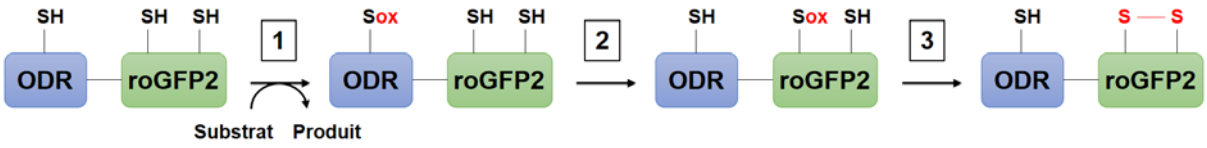

Figure 27. Répresentation schématique du mécanisme d'oxydation de la protéine roGFP2 dépendante de l'activité d'une oxydoréductase. En présence de son substrat spécifique, la cysteine catalytique de l'oxydoréductase passe sous un état oxydé (1). Cette forme d'oxydation est ensuite transférée à l'un des deux résidus cystéine présents au sein de la roGFP2 (2) conduisant de manière finale à la réduction de l'oxydoréductase et à l'oxydation de la roGFP2 au travers de la formation du pont disulfure intramoléculaire (3).

En lien avec le projet SULTRAF et l'étude du transfert du soufre chez les plantes, nous essayons de développer des biosenseurs redox spécifiques permettant une meilleure compréhension du métabolisme de la cystéine. Les concentrations intracellulaires de cystéine sont hautement contrôlées pour concilier son effet toxique potentiel (dû à la réactivité de son groupe thiol) et son rôle de donneur de soufre dans les cellules. Par exemple, la dégradation de la cystéine dans les mitochondries entraîne la production de 3-MP et de thiosulfate (Höfler et al., 2016). En se basant notamment sur nos différents résultats exposés précédemment, nous avons sélectionné plusieurs STRs d'Arabidopsis, STR1, STR16 et STR18, pour leurs spécificités respectives vis-à-vis du 3-MP et du thiosulfate (Moseler et al., résultats non publiés). Tout d'abord, la fusion de ces différentes isoformes STR à la roGFP2 n'influence les propriétés biochimiques de cette dernière. D'autre part, ces fusions sont fonctionnelles *in vitro* puisqu'une oxydation réversible de la roGFP2 est observée en présence des susbtrats soufrés, le 3-MP pour STR1-roGFP2 et le thiosulfate pour STR16-roGFP2 et STR18-roGFP2. Des mesures complémentaires ont néanmoins démontré que les systèmes TRX et GSH, tout particulièrement dans le cas de la fusion STR1-roGFP2, limitent l'oxydation de la roGFP2. Cette inhibition serait liée à la capacité de ces systèmes réducteurs à agir en trant qu'accepteur de soufre pour la STR, inhibant ainsi le transfert de soufre vers la roGFP2.

Bien que ces différents senseurs puissent être exprimés dans le cystosol de la levure, ils ne sont pas sensibles à l'application externe de leur substrat respectif (Moseler et al., résultats non publiés). Le développemet du biosenseur spécifique de la cystéine représente le projet de thèse de Damien Caubrière. Pour ce projet, plusieurs isoformes CD ont été retenues. Il s'agit de la protéine CD-STR de *Pseudorhodoferax*, des isoformes ABA3 d'Arabidopsis et IscS d'*E. coli*. La stratégie expérimentale consistera tout d'abord à valider *in vitro* la capacité des différents candidats retenus à oxyder spécifiquement la roGFP2 en présence de cystéine et des différents systèmes réducteurs physiologiques. La validation *in vivo* de la fonctionnalité des constructions sera effectuée chez la levure et Arabidopsis en collaboration avec l'équipe du Professeur Bruce Morgan (Université de la Sarre, Allemagne) et de celle du Professeur Andreas Meyer (Université de Cologne, Allemagne), qui sont des spécialistes reconnus des biosenseurs roGFP2.

PROJET DE RECHERCHE

Etude des mécanismes moléculaires impliqués dans la persulfuration des protéines chez les plantes

1. État de l'art

1.1. Sulfure d'hydrogène et persulfuration des protéines

Chez la majorité des organismes vivants, le sulfure d'hydrogène (H_2S) est à présent reconnu pour être impliqué dans une grande variété de processus physiologiques. Par exemple, il est impliqué dans la protection des bactéries contre les antibiotiques (Shatalin et al., 2011) et est lié à une variété de fonctions homéostatiques et de pathologies en biologie humaine (Filipovic et al., 2018). Chez les plantes, H_2S est associé à diverses fonctions physiologiques comme les réponses aux stress abiotiques et biotiques, le développement (germination des graines, développement des racines, sénescence des feuilles), la photosynthèse, l'autophagie et le mouvement des stomates (Gotor et al., 2019). Trois voies distinctes présentes dans différents compartiments subcellulaires produisent H_2S. Il est principalement produit dans les chloroplastes par la sulfite réductase lors de l'assimilation du sulfate. Le soufre est ensuite utilisé pour la biosynthèse de cystéine dans le cytosol, les plastes et les mitochondries (Takahashi et al., 2011). Dans les mitochondries, la β-cyanoalanine CAS-C1 catalyse la conversion du cyanure et de la cystéine en β-cyanoalanine et H_2S (Álvarez et al., 2012). Dans le cytosol, la L-cystéine désulfhydrase 1 (DES1) dégrade la cystéine en H_2S, ammoniaque et pyruvate (Álvarez et al., 2010).

H_2S peut modifier des protéines spécifiques et il a été suggéré que l'oxydation de résidus cystéine sous forme de persulfures est le principal moyen par lequel H_2S exerce ses fonctions biologiques (Filipovic, 2015). Par conséquent, les fonctions de signalisation liées à H_2S reposent probablement sur la persulfuration de protéines spécifiques. Il est important de mentionner que H_2S ne réagit qu'avec les cystéines oxydées, notamment sulfénylées, nitrosylées, glutathionylées ou formant une liaison disulfure. Il existe donc des interactions complexes entre toutes ces modifications post-traductionnelles (MPT) redox. Par ailleurs, la persulfuration des protéines par H_2S se produit également lorsque les polysulfures (RS(S)nH et RS(S)nSR) dérivés de H_2S réagissent avec les résidus cystéine (Greiner et al., 2013). Des quantités remarquables de ces polysulfures ont été détectées *in vivo* dans des cellules de

mammifères en plus de cystéine persulfurée (Cys-SSH) et de glutathion persulfuré (GSSH) (Ida et al., 2014). Toutes ces espèces de persulfures présentes dans les cellules, c'est-à-dire les polysulfures (notamment H_2S_2 et H_2S3), les molécules persulfurées de faible poids moléculaire (Cys-SSH et GSSH) et les cystéines persulfurées des protéines, ont été regroupées sous le terme de « sulfane sulfur ». Jusqu'à présent, les liens entre les protéines synthétisant H_2S et l'état de persulfuration cellulaire n'ont pas été clairement identifiés. Une analyse protéomique a identifié 2015 protéines persulfurées dans des feuilles d'*Arabidopsis thaliana* sauvage cultivées dans des conditions contrôlées (Aroca et al., 2017), suggérant qu'au moins 5% de l'ensemble du protéome d'Arabidopsis est persulfuré dans ces conditions. Malgré une réduction de 30% de la production de H_2S (Álvarez et al., 2010) et le fait que plusieurs voies physiologiques telles que la sénescence, l'autophagie, la fermeture stomatique et l'immunité soient affectées, le même nombre (2130 protéines persulfurées) et presque les mêmes protéines (85% de concordance) ont été identifiées chez le mutant perte de fonction *des1* (Aroca et al., 2017). Seules 47 protéines, comme des protéines kinases, des protéines phosphatases et des récepteurs de l'acide abscissique, sont moins persulfurées chez le mutant *des1*. La protéine DES1 aurait donc un rôle restreint dans la persulfuration des protéines et d'autres acteurs majeurs encore inconnus et nécessitant donc d'être identifiés, seraient impliqués dans la persulfuration des protéines chez les plantes.

Chez les mammifères, H_2S est produit par les réactions secondaires de deux enzymes de la voie de trans-sulfuration, la cystathionine β-synthase (CBS) et la cystathionine γ-lyase (CSE), qui transforment normalement la cystéine en homocystéine (Kabil & Banerjee, 2014). Dans les mitochondries, H_2S est libéré lors de la réduction de la forme persulfurée de la 3-mercaptopyruvate sulfurtransférase (MST) par un réducteur comme la thiorédoxine (TRX) ou l'acide dihydrolipoïque (DHLA) (Shibuya et al., 2009 ; Mikami et al., 2011 ; Yadav et al., 2013). Chez les mammifères, la cysteinyl-ARNt synthétase (CARS2) a été caractérisée comme la principale Cys-SSH synthase *in vivo*, jouant un rôle important dans la formation de polysulfures de faible poids moléculaire et de protéines persulfurées (Akaike et al., 2017). De plus, plusieurs voies non conventionnelles impliquant des protéines contenant des métaux comme la catalase (CAT), la superoxyde dismutase (SOD) et le cytochrome C (Cyt C) ont été récemment associées au métabolisme des polysulfures et de H_2S chez les mammifères (Olson et al., 2017, 2018 ; Vitvitsky et al., 2018).

La persulfuration des résidus cystéine représente un mécanisme de signalisation lié à H_2S. Les protéines persulfurées identifiées dans les plantes d'Arabidopsis sont localisées dans plusieurs compartiments subcellulaires et sont impliquées dans diverses voies suggérant que la

persulfuration des protéines représenterait un mécanisme de régulation redox similaire aux autres MPTs redox (Aroca et al., 2017). Par conséquent, sa régulation doit être également finement contrôlée. Dans les hépatocytes de souris dépourvus de TRX réductase (TR) et de glutathion réductase (GR), le taux de protéines persulfurées est nettement élevé (Dóka et al., 2016), soulignant l'importance de ces systèmes dans la régulation de la persulfuration des protéines, bien que leur contribution exacte reste incertaine. En dépit de l'importance de H_2S dans la physiologie des plantes et des relations entre H_2S et persulfuration des protéines, les mécanismes moléculaires impliqués dans ce processus et sa régulation demeurent peu étudiés. Leur élucidation devrait devenir une priorité et des études plus approfondies sont nécessaires pour comprendre l'effet de ces modifications sur la fonction des protéines. H_2S étant une molécule très répandue, certaines protéines/voies communes, comme les MSTs et les voies non conventionnelles récentes, pourraient être responsables de la persulfuration des protéines dans les organismes vivants.

1.2. Les 3-MP sulfurtransférases : protéines conservées du métabolisme de H_2S

Les sulfurtransférases (STRs) constituent une famille protéique large et complexe caractérisée par la présence d'un domaine rhodanese (Rhd). Elles catalysent le transfert de soufre et sont impliquées dans divers processus moléculaires et de signalisation notamment chez les plantes (Selles et al., 2019, P42). Les STRs contenant deux domaines Rhd mais dont seul le domaine C-terminal possède la cystéine catalytique sont appelées 3-MP-STRs ou MSTs de par leur capacité à utiliser le 3-mercaptopyruvate (3-MP) comme substrat *in vitro* (Yadav et al., 2013). Présentes dans la plupart des organismes, elles semblent avoir une fonction conservée dans le métabolisme de H_2S. Chez les mammifères, elles sont localisées dans le cytosol et les mitochondries, l'activité MST étant 3 fois plus élevée dans les mitochondries que dans le cytosol dans le foie du rat (Nagahara et al., 1998). Leur caractérisation biochimique a révélé que la TRX est le meilleur accepteur physiologique de soufre (Yadav et al., 2013). Par la réaction du persulfure lié à l'enzyme avec des réducteurs (TRX ou acide dihydrolipoïque), les MSTs mitochondriales participent à la production de H_2S (Shibuya et al., 2009 ; Mikami et al., 2011). De plus, en absence de réducteur, elles produisent les polysulfures H_2S_2 et H_2S_3 (Kimura et al., 2015) alors que la formation de Cys-SSH et GSSH a été observée en présence de concentrations physiologiques de cystéine et GSH (Kimura et al., 2017). En outre, dans le cerveau de mutants de souris MST-KO, les niveaux totaux des espèces persulfurées sont inférieurs à 50% de ceux du cerveau de souris sauvages, indiquant que la MST mitochondriale

est un acteur important (Kimura et al., 2015, 2017). Des observations similaires ont été réalisées chez *E. coli* où l'orthologue MST SseA participe à la production de « sulfane sulfur », notamment GSSH et GSSSH (Li et al., 2019).

La plupart des plantes supérieures possèdent deux isoformes MST, tandis que certaines espèces pourraient avoir perdu un de ces gènes dupliqués au cours de l'évolution (Moseler et al., 2020, P41). L'isoforme additionnelle plus courte dans sa partie N-terminale devrait être cytosolique alors que l'isoforme plus longue possède une séquence d'adressage mitochondriale. Pour les plantes ne possédant que la version longue, un site alternatif de traduction peut conduire à la synthèse d'une protéine plus courte suggérant que les protéines cytosolique et mitochondriale peuvent être codées par un gène unique (Moseler et al., 2020, P41). *A. thaliana* possède deux MSTs, STR1 et STR2, présentes dans les mitochondries et le cytosol, qui peuvent former H_2S en interagissant avec les TRXs (Henne et al., 2015). Comme observé dans le foie de rat, la plus grande partie de l'activité MST mesurée chez Arabidopsis dépend de l'isoforme mitochondriale STR1 (Mao et al., 2011). En effet, l'étude des mutants perte de fonction *str* indique que STR1 représente 50 à 80% de l'activité MST foliaire alors que les plants mutants *str2* possèdent la même activité qu'une plante sauvage (Mao et al., 2011 ; Höfler et al., 2016). Cependant, leurs rôles physiologiques et moléculaires in planta n'ont pas été élucidés car les mutants *str2* sont aphénotypiques et les mutants *str1* forment des graines de taille réduite. Environ 87,5% de ces graines présentent des embryons arrêtés à un stade précoce tandis que les autres graines peuvent germer et former des plantes ayant un développement normal du tissu végétatif (Mao et al, 2011). Il est important de noter que le double mutant *str1x str2* mutant est létal, indiquant que les deux STRs assurent une fonction essentielle au moins au développement embryonnaire (Mao et al., 2011). Il a été proposé que STR1 participerait à la dégradation de la cystéine en formant du GSSH qui serait ensuite oxydé en sulfite (SO_3^{2-}) (Krüßel et al., 2014). D'autre part, en plus de la formation de GSSH, STR1 pourrait produire H_2S en interagissant avec les TRXo1 et TRXo2 mitochondriales (Yoshida et al., 2013 ; Henne et al., 2015). Une interaction similaire observée dans le cytosol entre STR2 et TRXh1, suggère que STR2 pourrait représenter une voie de synthèse de H_2S dans le cytosol (Henne et al., 2015).

1.3. De nouveaux acteurs sont impliqués dans le métabolisme de H_2S

Ces deux dernières années, plusieurs nouveaux acteurs ont été reliés au métabolisme de H_2S et à la persulfuration des protéines. Chez les mammifères, des quantités appréciables de persulfures ont été détectées dans plusieurs cellules et tissus n'exprimant pas les enzymes CBS

et CSE générant H_2S mais aussi chez des souris CBS/CSE KO (Akaike et al., 2017). Ainsi, une étude visant à identifier les voies responsables de cette synthèse de H_2S indépendante des protéines CBS et CSE a révélé le rôle des cystéinyl-ARNt synthétases (CARS) dans le métabolisme des polysulfures (Akaike et al, 2017). La protéine CARS d'*E. coli* catalyse la synthèse de CysSSH et la polysulfuration co-traductionnelle des protéines. Elle possède une activité cystéine persulfurée synthase (CPERS) efficace en plus de ses fonctions indépendantes dans la biosynthèse de l'aminoacyl-ARNt (Akaike et al., 2017). Les mammifères possèdent deux isoformes CARS, CARS1 et CARS2, localisées respectivement dans le cytosol et les mitochondries. Toutes deux présentent une forte activité CPERS *in vitro* mais seule CARS2 semble jouer un rôle prédominant dans la production de persulfures *in vivo*. De plus, la Cys-SSH formée par l'activité CARS2 est métabolisée via la chaîne de transfert d'électrons (CTE) des mitochondries conduisant à la formation de H_2S sous forme SH^- (Akaike et al., 2017).

Un autre lien entre la CTE mitochondriale et le métabolisme de H_2S implique le cytochrome c (Cyt C) (Vitvitsky et al., 2018). Cette étude récente a démontré que la réduction du Cyt C par H_2S conduit à la formation de thiosulfate et stimule ensuite la persulfuration des protéines *in vitro*. De manière concordante, l'inactivation du Cyt C entraîne une légère diminution de la persulfuration des protéines dans les cellules HeLa cultivées dans des conditions normoxiques et diminue l'augmentation de la persulfuration des protéines, observée dans les cellules cultivées dans des conditions hypoxiques. En outre, la réduction du Cyt C par H_2S pourrait alimenter la CTE, et conduire à l'accumulation d'espèces réactives du soufre (ERS) (Vitvitsky et al., 2018).

Enfin, deux enzymes antioxydantes bien connues ont été récemment suggérées pour être impliqués dans le métabolisme de H_2S. Il s'agit de la catalase (CAT) qui catalyse la dismutation du superoxyde en oxygène et H_2O_2, et la superoxyde dismutase (SOD) qui catalyse la dismutation de H_2O_2 en oxygène et eau. Ces protéines existant avant l'apparition de l'O_2, elles remplissaient initialement des fonctions biochimiques sur des substrats autres que les espèces réactives de l'oxygène (ERO). A cette période, le métabolisme dépendait principalement du soufre et des ERS telles que H_2S, HS, H_2S_n (n = 2-7) et $H_2S^{\cdot-}$ qui sont chimiquement similaires à H_2O et aux ERO telles que HO, H_2O_2, $O2^{\cdot-}$. Ainsi, les protéines CAT et SOD pourraient métaboliser les ERS. Des expériences *in vitro* ont révélé que CAT catalyse la production de H_2S en hypoxie et l'oxydation de H_2S en polysulfures en présence d'O_2 (Olson et al., 2017). Ainsi, lorsque les niveaux d'O_2 chutent, l'activité CAT évolue de l'oxydation de H_2S vers sa synthèse, couplant ainsi la signalisation de H_2S à la formation d'oxygène (Olson et al., 2017). D'autre part, les protéines Cu/ZnSOD et MnSOD catalysent *in vitro* l'oxydation de H_2S en

polysulfures. *A contrario*, les SODs sont incapables de métaboliser les polysulfures (Olson et al., 2018). Tous ces résultats suggèrent que les protéines CAT et SOD auraient constitué un mécanisme ancien de détoxication du soufre ou de régulation des ERS. Ce mécanisme de protection pourrait perdurer dans les organismes vivants actuels (Olson et al., 2017, 2018). Les plantes possèdent des orthologues pour les différents nouveaux acteurs décrits ci-dessus. Jusqu'à présent, leur implication présumée dans le métabolisme de H_2S est inconnue et doit être clarifiée.

1.4. Double rôle des systèmes réducteurs dans la persulfuration des protéines

Le lien entre les systèmes réducteurs et la synthèse de H_2S a initialement été reporté pour les MSTs et les TRXs des mammifères qui fonctionnent de concert pour produire H_2S (Shibuya et al., 2009 ; Mikami et al., 2011 ; Yadav et al., 2013). Un lien identique entre STR1 et le système TRX semble également exister chez les plantes, STR1 ayant été isolée à plusieurs reprises comme partenaire des TRXs, incluant l'isoforme mitochondriale TRXo1 d'Arabidopsis (Yoshida et al., 2013). Chez cette espèce, les interactions STR1-TRXo1 dans les mitochondries et STR2-TRXh1 dans le cytosol ont été confirmées *in vivo* par des expériences de complémentation bimoléculaire de fluorescence (Henne et al., 2015). Contrairement aux TRXs, le glutathion réduit (GSH) ne semble pas représenter un accepteur physiologique des MSTs de mammifères (Mikami et al., 2011 ; Yadav et al., 2013). De plus, aucune interaction STR-GRX n'a été rapportée jusqu'à présent, bien que des protéines de fusion naturelles possédant les deux domaines protéiques existent chez certains procaryotes. Si une telle interaction est confirmée, il sera important de faire une distinction entre les systèmes de réduction TRX et GSH/GRX. En effet, la majorité des TRXs de plantes utilisent deux cystéines pour réduire leurs substrats alors que les GRXs utilisent principalement une seule cystéine. Par conséquent, la présence d'un groupe persulfure sur une cystéine catalytique d'une TRX devrait être de courte durée et entraîner la libération de H_2S. Au contraire, un groupe persulfure formé sur la cystéine catalytique d'une GRX peut être plus stable et permettre des réactions de trans-persulfuration avec certaines protéines partenaires (Mishanina et al., 2015). Sept isoformes GRX et seize isoformes TRX ont été identifiées comme persulfurées chez *A. thaliana* (Aroca et al., 2017). L'interaction avec les TRXs ou GRXs permettrait ainsi de modifier spécifiquement certaines protéines cibles.

Outre leur potentielle implication dans la persulfuration des protéines, les systèmes réducteurs sont impliqués dans leur réduction. Par exemple, les TRXs réduisent efficacement

la cystéine persulfurée de la protéine-tyrosine phosphatase 1B (PTP1B), des sérum albumine humaine et bovine (SAH et SAB) mais aussi la CysSSH libre (Krishnan et al, 2011 ; Dóka et al, 2016 ; Wedmann et al, 2016). Après traitement avec l'auranofine, un inhibiteur de la TRX réductase (TrxR), les cellules présentaient un taux de persulfuration intracellulaire accru (Wedmann et al., 2016). De même, le taux de protéines persulfurées augmente dans les cellules rénales embryonnaires humaines (HEK293) ayant une expression diminuée de TrxR1 (knock down) (Dóka et al., 2016). Le système GSH/GRX réduit efficacement les polysulfures et la SAB persulfurée *in vitro* (Dóka et al., 2016). Enfin, dans les hépatocytes de souris dépourvus de TRX réductase (TrxR) et de glutathion réductase (GR), le taux de protéines persulfurées est nettement élevé (Dóka et al., 2016). Le profil des protéines persulfurées étant distinct dans les cellules sauvages, simples (GR) et doubles (TrxR/GR) mutantes suggèrent des rôles spécifiques pour chacun des systèmes qui pourraient être potentiellement impliqués dans différentes voies de signalisation (Dóka et al., 2016). Toutes ces données soulignent l'importance des systèmes réducteurs dans la persulfuration des protéines, bien que leur contribution exacte reste incertaine.

1.5. Interactions entre H_2S, persulfuration des protéines et stress oxydant

Chez plusieurs bactéries, l'inactivation d'enzymes produisant H_2S impacte fortement sa production et les rend très sensibles aux antibiotiques et au stress oxydant (Shatalin et al., 2011). Chez *E. coli*, H_2S issu de l'activité MST protègerait les bactéries contre H_2O_2 en séquestrant le fer ferrique et en limitant les effets de la réaction de Fenton (Mironov et al., 2017). Récemment, il a été suggéré que ce soit le « sulfane sulfur » issu de l'activité MST qui contribuerait à la résistance à H_2O_2 (Li et al., 2019). Bien que H_2S puisse théoriquement piéger directement des oxydants, sa concentration relativement faible et la concurrence avec d'autres thiols empêcheraient cette fonction *in vivo* (Filipovic et al., 2018). Par conséquent, l'effet antioxydant de H_2S serait dû à un effet indirect sur les protéines. H_2S peut potentiellement réagir avec les ponts disulfures et les acides sulféniques (RSOH) et induire ainsi la persulfuration des protéines (Cuevasanta et al., 2015). Dans des cultures cellulaires traitées soit par H_2O_2, soit par du diamide, entraînant soit la formation d'acide sulfénique et de pont disulfure soit de pont disulfure seulement, une augmentation du taux de persulfuration intracellulaire n'a été observée que dans les cellules traitées avec H_2O_2, suggérant que les persulfures sont formés par réaction entre H_2S et l'acide sulfénique (Cuevasanta et al., 2015 ; Wedmann et al., 2016). H_2O_2 oxydant spécifiquement certaines cystéines des protéines cibles sous forme d'acide sulfénique, la

réaction subséquente avec H_2S permettrait la persulfuration spécifique des protéines cibles et représenterait un lien entre H_2O_2 et H_2S. De plus, en réduisant les acides sulféniques, H_2S pourrait empêcher leur suroxydation irréversible en acide sulfinique (RSO_2H) et sulfonique (RSO_3H). Les persulfures peuvent également réagir avec les oxydants et former des acides perthiosulféniques (RSSOH), perthiosulfiniques ($RSSO_2H$) et perthiosulfoniques ($RSSO_3H$). De telles formes oxydées ont déjà été identifiées dans plusieurs protéines comme la papaïne, l'albumine et la glutathion peroxydase (Cuevasanta et al., 2015 ; Pan & Carroll, 2013 ; Zhang et al., 2014). Ces formes peuvent être réduites par des réducteurs communs et plus particulièrement par des TRXs (Millikin et al., 2016 ; Wedmann et al., 2016). Toutes ces observations confirment que les groupements persulfures peuvent représenter un mécanisme de protection des groupements thiols des protéines contre l'oxydation irréversible. Cela suggère en outre un lien entre H_2O_2, H_2S et persulfuration des protéines et soulève la question des mécanismes moléculaires sous-jacents et de leur importance dans la physiologie des plantes.

2. Objectifs, originalité et nouveauté du projet

Ce projet de recherche vise à décrypter les mécanismes moléculaires de la persulfuration des protéines chez les plantes. À partir des résultats obtenus pour d'autres organismes non photosynthétiques et de nos résultats préliminaires, les protéines MST, CARS, CAT, SOD et Cyt C seraient impliquées dans la persulfuration des protéines au travers de la synthèse de H_2S, de polysulfures et/ou de « sulfane sulfur ». Les protéines persulfurées étant présentes dans de multiples compartiments subcellulaires, leur rôle potentiel est une question qui doit être abordée. De plus, le rôle des systèmes réducteurs TRX et GRX dans la régulation de la persulfuration et dans les réactions de trans-persulfuration des protéines doit également être pris en compte. Nous focaliserons notre étude sur *Arabidopsis thaliana* et développerons une approche intégrée combinant des approches *in vitro* et *in vivo* afin d'effectuer une analyse fonctionnelle des protéines impliquées dans la biogenèse de H_2S/polysulfures/sulfane suflur (premier objectif), dans la réduction des protéines persulfurées (deuxième objectif) et pour étudier les interactions entre H_2O_2 et H_2S (troisième objectif). Cela nous permettra de répondre à trois grandes questions :

1. Quelles voies enzymatiques sont responsables de la persulfuration des protéines chez les plantes ?

Bien que les protéines MST, CARS, CAT, SOD et Cyt C soient présentes dans la plupart sinon tous les organismes, leurs fonctions dans la synthèse de H_2S et/ou la persulfuration des protéines dans les plantes sont inconnues. En outre, malgré l'importance reconnue de la persulfuration des protéines chez d'autres organismes vivants, les mécanismes moléculaires sous-jacents de cette MPT redox chez les plantes restent non-identifiés bien qu'elle pourrait être aussi importante que les autres MPTs redox majeures.

2. Les systèmes réducteurs GRX et TRX et leurs partenaires physiologiques participent-ils à la régulation de la persulfuration des protéines et aux mécanismes de signalisation associés à la trans-persulfuration ?

L'idée associant la production de H_2S et les réactions de trans-persulfuration à des mécanismes de signalisation importants n'est apparue que récemment. Les mécanismes sous-jacents, et plus particulièrement leur spécificité et leur importance dans un certain contexte physiologique, doivent être explorés plus en détails.

3. Quels sont les liens entre la persulfuration des protéines et les mécanismes oxydatifs dépendant de H_2O_2 ?

Au niveau protéique, la persulfuration des résidus cystéine protège contre l'oxydation irréversible et l'inactivation concomitante des protéines. De plus, un mécanisme plausible de persulfuration des cystéines implique la réaction entre H_2S et les acides sulféniques ou les ponts disulfures des protéines. Les interactions entre persulfuration et stress oxydant ne sont pas encore clairement identifiées et doivent être analysées plus précisément.

Avancées majeures attendues

La production de H_2S et les rôles physiologiques et de signalisation qui lui sont associés chez plusieurs organismes modèles représentent un domaine de recherche récent. Néanmoins de nombreux aspects demeurent mystérieux, notamment chez les plantes (Mustafa et al., 2009 ; Paul & Snyder, 2012 ; Greiner et al., 2013 ; Longen et al., 2016 ; Aroca et al., 2017). Par rapport à d'autres MPTs redox comme que la glutathionylation et la nitrosylation, et les voies de signalisation associées, la persulfuration est une thématique de recherche récente présentant un intérêt grandissant. Ce projet devrait générer des quantités importantes de données et plusieurs percées majeures. Il étendra les connaissances sur les mécanismes moléculaires conduisant à la

persulfuration des protéines chez les plantes (i) en identifiant les acteurs majeurs générant H_2S, polysulfures et/ou « sulfane sulfur » menant à la persulfuration des protéines (ii) en identifiant les systèmes impliqués dans la réduction des protéines persulfurées, (iii) en apportant de nouvelles perspectives sur le mécanisme et la spécificité de la persulfuration des protéines et (iv) en fournissant des éléments sur les relations entre persulfuration des protéines et réponse au stress oxydant.

3. Programme scientifique et technique, organisation du projet

3.1. Programme scientifique et structure du projet

Ce projet a été élaboré pour une durée initiale de 60 mois et le plan de travail associé est divisé en quatre grandes tâches (Figure 28). Bien qu'il existe plusieurs liens entre la plupart des tâches, toutes sont indépendantes et seront initiées en parallèle au cours de la première année. Une série d'approches complémentaires *in vivo* et *in vitro* a été conçue pour les tâches 1 à 3 afin de caractériser de nouvelles enzymes productrices de H_2S/ « sulfane sulfur » et pour étudier leur rôle dans la persulfuration des protéines. La tâche 4, axée sur les relations entre H_2O_2, la persulfuration des protéines et le stress oxydant, combinera des approches *in vitro* et *in planta* basées sur des méthodes biochimiques, physiologiques et protéomiques.

La tâche 1 sera consacrée à la caractérisation biochimique et structurale des candidats sélectionnés (MST, CARS, CAT, SOD et Cyt C), produits sous forme de protéines recombinantes dans le système hétérologue *E. coli*. Des mesures d'activité *in vitro* par la quantification de H_2S libéré et de la formation de « sulfane sulfur » ont été développées pour déterminer les paramètres cinétiques des réactions et les propriétés catalytiques des protéines. La cristallographie aux rayons X et la résonance magnétique nucléaire (RMN) seront utilisées pour tenter de résoudre la structure 3D des candidats. **La tâche 2 visera à confirmer que les candidats sélectionnés sont des acteurs majeurs dans la persulfuration des protéines chez les plantes.** Les mesures d'activité en présence d'extraits de différents tissus de plantes révèleront la capacité des candidats à participer à la persulfuration des protéines. Des analyses protéomiques globales d'extraits de plantes incubés ou non avec les candidats (sauvages et mutants pour les candidats prometteurs) permettront d'identifier les protéines cibles persulfurées. Une approche complémentaire intéressante consistera à comparer les niveaux de protéines persulfurées entre les plantes sauvages et mutantes pour les candidats les plus prometteurs. **La tâche 3 décryptera les relations entre la persulfuration des protéines et les**

systèmes réducteurs TRX et GSH/GRX. Cette partie du projet commencera par l'utilisation d'approches *in vitro* et *in vivo* employées dans les tâches 1 et 2. Nous comparerons les niveaux de protéines persulfurées entre les plantes sauvages et mutantes déjà caractérisées et disponibles pour les deux systèmes réducteurs. **La tâche 4 sera consacrée à l'étude des liens entre la persulfuration des protéines et le métabolisme de H_2O_2.** Pour mieux comprendre la relation entre ces deux voies, nous mesurerons les niveaux de H_2O_2, de « sulfane sulfur » et le taux de protéines persulfurées dans des lignées déficientes en enzymes produisant et dégradant H_2O_2. Nous générerons notamment des lignées exprimant des biosenseurs fluorescents pour H_2O_2 (HyPer, roGFPs). Nous étudierons également l'évolution de la persulfuration des protéines chez les plantes soumises à diverses conditions de stress liées à H_2O_2 et la capacité des plantes dont le niveau de protéines persulfurées est élevé à faire face au stress oxydant.

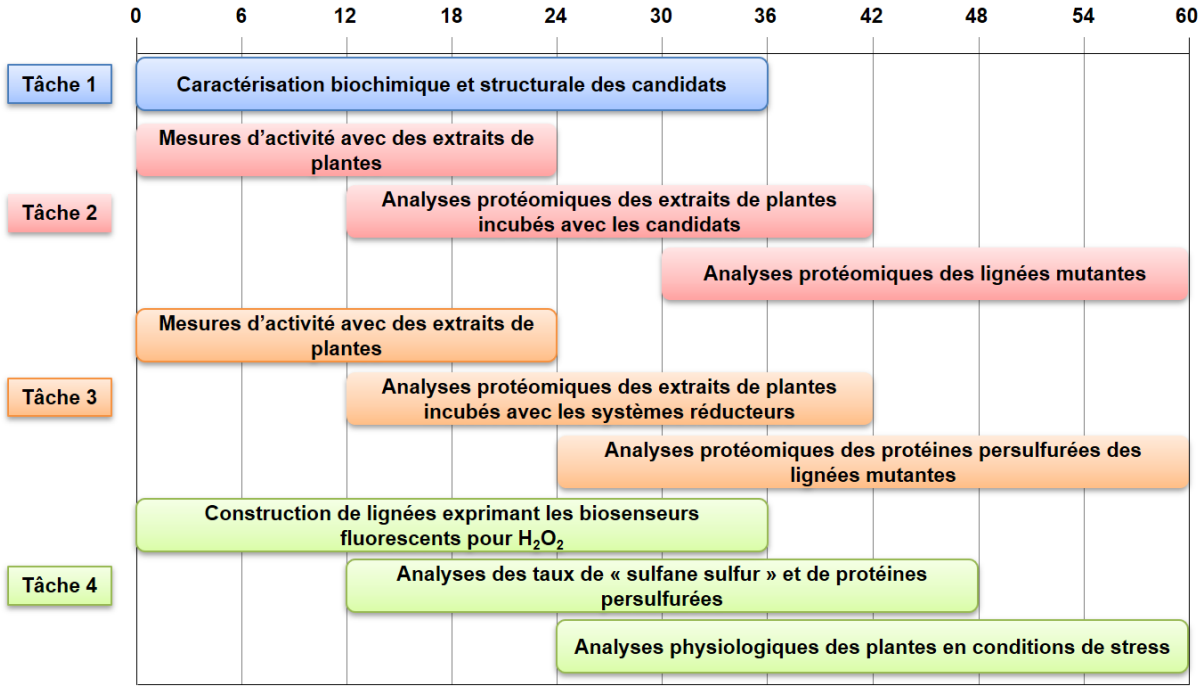

Figure 28. Programme prévisionnel et répartition des tâches pendant la durée du projet.

3.2. Description, pertinence du partenariat et équipements disponibles

Ce projet s'appuie sur une approche fonctionnelle et intégrative combinant plusieurs disciplines et compétences, de la biochimie, de la biologie structurale à la biologie cellulaire et à la génétique végétale, pour identifier les mécanismes moléculaires de la persulfuration des protéines chez les plantes.

Notre laboratoire possède une grande expérience dans la caractérisation biochimique et structurale des protéines régulées redox chez divers organismes, et notamment pour les deux

espèces modèles végétales *Populus trichocarpa* et *A. thaliana*. Le laboratoire est entièrement équipé pour exprimer et purifier les protéines recombinantes nécessaires aux analyses biochimiques et enzymatiques (purificateur Äkta, spectrophotomètres, spectrofluorimètres et HPLC reliés à différents détecteurs, SEC-MALS). Dans le cas où l'oxygène serait préjudiciable à la stabilité, à la réactivité et à l'activité des protéines, une boîte à gants permettant de travailler dans des conditions anaérobies (concentration en O2 < 1 ppm) est disponible. La modification des séquences protéiques (génie génétique, mutagenèse dirigée) et la construction de colonnes d'affinité sont couramment effectuées dans l'équipe. Pour la partie structurale, ce projet bénéficiera d'une collaboration longue et fructueuse avec le Dr Claude Didierjean et le Dr Pascale Tsan, de l'UMR 7036 CRM2 Université de Lorraine-CNRS qui ont respectivement une forte expertise en cristallographie par rayons X et spectroscopie RMN. Pour la partie protéomique, nous avons développé une collaboration avec le Dr Stéphane Lemaire et le Dr Christophe Marchand (Institut de Biologie Physico-Chimique, Paris), qui possèdent des installations de spectrométrie de masse de pointe et développent des méthodes pour étudier la persulfuration chez *Chlamydomonas reinhardtii* et *Saccharomyces cerevisiae*. Nous utiliserons les collaborations existantes avec le Dr Pascal Rey (CEA Cadarache) et le Dr Jean Philippe Reichheld (Laboratoire Génome et Développement des Plantes, Université Perpignan Via Domitia, Perpignan), qui possèdent l'expertise et les collections de mutants d'*A. thaliana,* notamment pour les systèmes GSH et TRX, pour réaliser ce projet. Nous collaborerons aussi avec le Pr Bruce Morgan (Université de la Sarre, Allemagne), le Pr Andreas Meyer (Université de Bonn, Allemagne) et le Pr Markus Schwartzländer (Université de Münster, Allemagne) qui ont développé des biosenseurs de H_2O_2 et du GSH et qui sont des experts reconnus en biologie redox.

REFERENCES BIBLIOGRAPHIQUES

Akaike T, Ida T, Wei FY, Nishida M, Kumagai Y, Alam MM, Ihara H, Sawa T, Matsunaga T, Kasamatsu S, Nishimura A, Morita M, Tomizawa K, Nishimura A, Watanabe S, Inaba K, Shima H, Tanuma N, Jung M, Fujii S, Watanabe Y, Ohmuraya M, Nagy P, Feelisch M, Fukuto JM, Motohashi H (2017) Cysteinyl-tRNA synthetase governs cysteine polysulfidation and mitochondrial bioenergetics. Nature Communications 8:1177.

Álvarez C, Calo L, Romero LC, García I, Gotor C (2010) An O-acetylserine(thiol)lyase homolog with L-cysteine desulfhydrase activity regulates cysteine homeostasis in Arabidopsis. Plant Physiology 152:656-669.

Álvarez C, García I, Romero LC, Gotor C (2012) Mitochondrial sulfide detoxification requires a functional isoform O-acetylserine(thiol)lyase C in *Arabidopsis thaliana*. Molecular Plant 5:1217-1226.

Alves R, Vilaprinyo E, Sorribas A, Herrero E (2009) Evolution based on domain combinations: the case of glutaredoxins. BMC Evolutionary Biology 9:66.

Aroca A, Benito JM, Gotor C, Romero LC (2017) Persulfidation proteome reveals the regulation of protein function by hydrogen sulfide in diverse biological processes in Arabidopsis. Journal of Experimental Botany 68:4915-4927.

Aussignargues C, Giuliani MC, Infossi P, Lojou E, Guiral M, Giudici-Orticoni MT, Ilbert M (2012) Rhodanese functions as sulfur supplier for key enzymes in sulfur energy metabolism. The Journal of Biological Chemistry 287:19936-19948.

Bandyopadhyay S, Gama F, Molina-Navarro MM, Gualberto JM, Claxton R, Naik SG, Huynh BH, Herrero E, Jacquot JP, Johnson MK, Rouhier N (2008) Chloroplast monothiol glutaredoxins as scaffold proteins for the assembly and delivery of [2Fe-2S] clusters. The EMBO Journal 27:1122-1133.

Bauer M, Dietrich C, Nowak K, Sierralta WD, Papenbrock J (2004) Intracellular localization of Arabidopsis sulfurtransferases. Plant Physiology 135:916-926.

Behshad E, Bollinger JM Jr (2009) Kinetic analysis of cysteine desulfurase CD0387 from *Synechocystis* sp. PCC 6803: formation of the persulfide intermediate. Biochemistry 48:12014-12023.

Beilschmidt LK, Puccio HM (2014) Mammalian Fe-S cluster biogenesis and its implication in disease. Biochimie 100:48-60.

Bernard DG, Netz DJ, Lagny TJ, Pierik AJ, Balk J (2013) Requirements of the cytosolic iron-sulfur cluster assembly pathway in Arabidopsis. Philosophical Transactions of the Royal Society of London Series B: Biological Sciences 368:20120259.

Bhaskar A, Chawla M, Mehta M, Parikh P, Chandra P, Bhave D, Kumar D, Carroll KS, Singh A (2014) Reengineering redox sensitive GFP to measure mycothiol redox potential of *Mycobacterium tuberculosis* during infection. PLoS Pathogens 10:e1003902.

Bittner F, Oreb M, Mendel RR (2001) ABA3 is a molybdenum cofactor sulfurase required for activation of aldehyde oxidase and xanthine dehydrogenase in *Arabidopsis thaliana*. The Journal of Biological Chemistry 276:40381-40384.

Black KA, Dos Santos PC (2015) Shared-intermediates in the biosynthesis of thio-cofactors: Mechanism and functions of cysteine desulfurases and sulfur acceptors. Biochimica et Biophysica Acta 1853:1470-1480.

Bolstad HM, Wood MJ (2010) An *in vivo* method for characterization of protein interactions within sulfur trafficking systems of *E. coli*. Journal of Proteome Research 9:6740-6751.

Bolstad HM, Botelho DJ, Wood MJ (2010) Proteomic analysis of protein-protein interactions within the Cysteine Sulfinate Desulfinase Fe-S cluster biogenesis system. Journal of Proteome Research 9:5358-5369.

Bordo D, Bork P (2002) The rhodanese/Cdc25 phosphatase superfamily. Sequence-structure-function relations. EMBO Reports 3:741-746.

Brancaccio D, Gallo A, Mikolajczyk M, Zovo K, Palumaa P, Novellino E, Piccioli M, Ciofi-Baffoni S, Banci L (2014) Formation of [4Fe-4S] clusters in the mitochondrial iron-sulfur cluster assembly machinery. Journal of the American Chemical Society 136:16240-16250.

Braun P, Carvunis AR, Charloteaux B, Dreze M, Ecker JR, Hill DE, Roth FP, Vidal M, Galli M, Balumuri P, Bautista V, Chesnut JD, Kim RC, de los Reyes C, Gilles P, Kim CJ, Matrubutham U, Mirchandani J, Olivares E, Patnaik S, Quan R, Ramaswamy G, Shinn P, Swamilingiah GM, Wu S, Ecker JR, Dreze M, Byrdsong D, Dricot A, Duarte M, Gebreab F, Gutierrez BJ, MacWilliams A, Monachello D, Mukhtar MS, Poulin MM, Reichert P, Romero V, Tam S, Waaijers S, Weiner EM, Vidal M, Hill DE, Braun P, Galli M, Carvunis AR, Cusick ME, Dreze M, Romero V, Roth FP, Tasan M, Yazaki J, Braun P, Ecker JR, Carvunis AR, Ahn YY, Barabási AL, Charloteaux B, Chen H, Cusick ME, Dangl JL, Dreze M, Ecker JR, Fan C, Gai L, Galli M, Ghoshal G, Hao T, Hill DE, Lurin C, Milenkovic T, Moore J, Mukhtar MS, Pevzner SJ, Przulj N, Rabello S, Rietman EA, Rolland T, Roth FP, Santhanam B, Schmitz RJ, Spooner W, Stein J, Tasan M, Vandenhaute J, Ware D, Braun P, Vidal M. Arabidopsis Interactome Mapping Consortium (2011) Evidence for network evolution in an Arabidopsis interactome map. Science 333:601-607.

Bräutigam L, Schütte LD, Godoy JR, Prozorovski T, Gellert M, Hauptmann G, Holmgren A, Lillig CH, Berndt C (2011) Vertebrate-specific glutaredoxin is essential for brain development. Proceedings of the National Academy of Sciences USA 110:20057-20062.

Butland G, Babu M, Díaz-Mejía JJ, Bohdana F, Phanse S, Gold B, Yang W, Li J, Gagarinova AG, Pogoutse O, Mori H, Wanner BL, Lo H, Wasniewski J, Christopolous C, Ali M, Venn P, Safavi-Naini A, Sourour N, Caron S, Choi JY, Laigle L, Nazarians-Armavil A, Deshpande A, Joe S, Datsenko KA, Yamamoto N, Andrews BJ, Boone C, Ding H, Sheikh B, Moreno-Hagelseib G, Greenblatt JF, Emili A (2008) eSGA: *E. coli* synthetic genetic array analysis. Nature Methods 5:789-795.

Cheng NH (2008) AtGRX4, an Arabidopsis chloroplastic monothiol glutaredoxin, is able to suppress yeast *grx5* mutant phenotypes and respond to oxidative stress. FEBS Letters 582:848-854.

Cheng Z, Miura K, Popov VL, Kumagai Y, Rikihisa Y (2011) Insights into the CtrA regulon in development of stress resistance in obligatory intracellular pathogen *Ehrlichia chaffeensis*. Molecular Microbiology 82:1217-1234.

Cipollone R, Ascenzi P, Visca P (2007) Common themes and variations in the rhodanese superfamily. IUBMB Life 59:51-59.

Colnaghi R, Cassinelli G, Drummond M, Forlani F, Pagani S (2001) Properties of the *Escherichia coli* rhodanese-like protein SseA: contribution of the active-site residue Ser240 to sulfur donor recognition. FEBS Letters 500:153-156.

Comini MA, Rettig J, Dirdjaja N, Hanschmann EM, Berndt C, Krauth-Siegel RL (2008) Monothiol glutaredoxin-1 is an essential iron-sulfur protein in the mitochondrion of African trypanosomes. The Journal of Biological Chemistry 283:27785-27798.

Cuevasanta E, Lange M, Bonanata J, Coitiño EL, Ferrer-Sueta G, Filipovic MR, Alvarez B (2015) Reaction of Hydrogen Sulfide with Disulfide and Sulfenic Acid to Form the Strongly Nucleophilic Persulfide. The Journal of Biological Chemistry 290:26866-26880.

Da Fonseca-Pereira P, Souza PVL, Hou LY, Schwab S, Geigenberger P, Nunes-Nesi A, Timm S, Fernie AR, Thormählen I, Araújo WL, Daloso DM (2020) Thioredoxin h2 contributes to the redox regulation of mitochondrial photorespiratory metabolism. Plant Cell and Environment 43:188-208.

Dahl JU, Urban A, Bolte A, Sriyabhaya P, Donahue JL, Nimtz M, Larson TJ, Leimkühler S (2011) The identification of a novel protein involved in molybdenum cofactor biosynthesis in *Escherichia coli*. The Journal of Biological Chemistry 286:35801-35812.

Dai X, Hayashi K, Nozaki H, Cheng Y, Zhao Y (2005) Genetic and chemical analyses of the action mechanisms of sirtinol in *Arabidopsis*. Proceedings of the National Academy of Sciences USA 102:3129-3134.

Dalle-Donne I, Rossi R, Colombo G, Giustarini D, Milzani A (2009) Protein S glutathionylation: a regulatory device from bacteria to humans. Trends in Biochemical Sciences 34:85-96.

Daloso DM, Müller K, Obata T, Florian A, Tohge T, Bottcher A, Riondet C, Bariat L, Carrari F, Nunes-Nesi A, Buchanan BB, Reichheld JP, Araújo WL, Fernie AR (2015) Thioredoxin, a master regulator of the tricarboxylic acid cycle in plant mitochondria. Proceedings of the National Academy of Sciences USA 112:1392-1400.

Ding B, Smith ES, Ding H (2005) Mobilization of the iron centre in IscA for the iron-sulphur cluster assembly in IscU. Biochemical Journal 389:797-802.

Dóka É, Pader I, Bíró A, Johansson K, Cheng Q, Ballagó K, Prigge JR, Pastor-Flores D, Dick TP, Schmidt EE, Arnér ES, Nagy P (2016) A novel persulfide detection method reveals protein persulfide- and polysulfide-reducing functions of thioredoxin and glutathione systems. Science Advances 2:e1500968.

Duan GL, Zhou Y, Tong YP, Mukhopadhyay R, Rosen BP, Zhu YG (2007) A CDC25 homologue from rice functions as an arsenate reductase. New Phytologist 174:311-321.

Feng Y, Zhong N, Rouhier N, Hase T, Kusunoki M, Jacquot JP, Jin C, Xia B (2006) Structural insight into poplar glutaredoxin C1 with a bridging iron-sulfur cluster at the active site. Biochemistry 45:7998-8008.

Fernandes AP, Fladvad M, Berndt C, Andresen C, Lillig CH, Neubauer P, Sunnerhagen M, Holmgren A, Vlamis-Gardikas A (2005) A novel monothiol glutaredoxin (Grx4) from *Escherichia coli* can serve as a substrate for thioredoxin reductase. The Journal of Biological Chemistry 280:24544-24552.

Filipovic MR (2015) Persulfidation (S-sulfhydration) and H2S. Handbook of Experimental Pharmacology 230:29-59.

Filipovic MR, Zivanovic J, Alvarez B, Banerjee R (2018) Chemical Biology of H2S Signaling through Persulfidation. Chemical Reviews 118:1253-1337.

Frazzon AP, Ramirez MV, Warek U, Balk J, Frazzon J, Dean DR, Winkel BS (2007) Functional analysis of Arabidopsis genes involved in mitochondrial iron-sulfur cluster assembly. Plant Molecular Biology 64:225-240.

Freire P, Moreira RN, Arraian, CM (2009) BolA inhibits cell elongation and regulates MreB expression levels. Journal of Molecular Biology 385:1345–1351.

Gelhaye E, Rouhier N, Jacquot JP (2003) Evidence for a subgroup of thioredoxin h that requires GSH/Grx for its reduction. FEBS Letters 555:443-448.

Gotor C, García I, Aroca Á, Laureano-Marín AM, Arenas-Alfonseca L, Jurado-Flores A, Moreno I, Romero LC (2019) Signaling by hydrogen sulfide and cyanide through post-translational modification. Journal of Experimental Botany 70:4251-4265.

Greiner R, Pálinkás Z, Bäsell K, Becher D, Antelmann H, Nagy P, Dick TP (2013) Polysulfides link H2S to protein thiol oxidation. Antioxidants and Redox Signaling 19:1749-1765.

Gutscher M, Pauleau AL, Marty L, Brach T, Wabnitz GH, Samstag Y, Meyer AJ, Dick TP (2008) Real-time imaging of the intracellular glutathione redox potential. Nature Methods 5:553-559.

Gutscher M, Sobotta MC, Wabnitz GH, Ballikaya S, Meyer AJ, Samstag Y, Dick TP (2009) Proximity-based protein thiol oxidation by H2O2-scavenging peroxidases. The Journal of Biological Chemistry 284:31532-31540.

Hanson GT, Aggeler R, Oglesbee D, Cannon M, Capaldi RA, Tsien RY, Remington SJ (2004) Investigating mitochondrial redox potential with redox-sensitive green fluorescent protein indicators. The Journal of Biological Chemistry 279:13044-13053.

Heidenreich T, Wollers S, Mendel RR, Bittner F (2005) Characterization of the NifS-like domain of ABA3 from *Arabidopsis thaliana* provides insight into the mechanism of molybdenum cofactor sulfuration. The Journal of Biological Chemistry 280:4213-4218.

Henne M, König N, Triulzi T, Baroni S, Forlani F, Scheibe R, Papenbrock J (2015) Sulfurtransferase and thioredoxin specifically interact as demonstrated by bimolecular fluorescence complementation analysis and biochemical tests. FEBS Open Bio 5:832-843.

Hildebrandt TM, Grieshaber MK (2008) Three enzymatic activities catalyze the oxidation of sulfide to thiosulfate in mammalian and invertebrate mitochondria. FEBS Journal 275:3352-3361.

Hoffmann B, Uzarska MA, Berndt C, Godoy JR, Haunhorst P, Lillig CH, Lill R, Mühlenhoff U (2011) The multidomain thioredoxin-monothiol glutaredoxins represent a distinct functional group. Antioxidants and Redox Signaling 15:19-30.

Höfler S, Lorenz C, Busch T, Brinkkötter M, Tohge T, Fernie AR, Braun HP, Hildebrandt TM (2016) Dealing with the sulfur part of cysteine: four enzymatic steps degrade l-cysteine to pyruvate and thiosulfate in Arabidopsis mitochondria. Physiologia Plantarum 157:352-366.

Holmgren A (1976) Hydrogen donor system for Escherichia coli ribonucleoside diphosphate reductase dependent upon glutathione. Proceedings of the National Academy of Sciences USA 73:2275-2279.

Hu X, Kato Y, Sumida A, Tanaka A, Tanaka R (2017) The SUFBC2D complex is required for the biogenesis of all major classes of plastid Fe–S proteins. The Plant Journal 90:235-248.

Ida T, Sawa T, Ihara H, Tsuchiya Y, Watanabe Y, Kumagai Y, Suematsu M, Motohashi H, Fujii S, Matsunaga T, Yamamoto M, Ono K, Devarie-Baez NO, Xian M, Fukuto JM, Akaike T (2014) Reactive cysteine persulfides and S-polythiolation regulate oxidative stress and redox signaling. Proceedings of the National Academy of Sciences USA 111:7606-7611.

Iwema T, Picciocchi A, Traore DA, Ferrer JL, Chauvat F, Jacquamet L (2009) Structural basis for delivery of the intact [Fe2S2] cluster by monothiol glutaredoxin. Biochemistry 48:6041-6043.

Johansson C, Kavanagh KL, Gileadi O, Oppermann U (2007) Reversible sequestration of active site cysteines in a 2Fe-2S-bridged dimer provides a mechanism for glutaredoxin 2 regulation in human mitochondria. The Journal of Biological Chemistry 282:3077-3082.

Johansson C, Lillig CH, Holmgren A (2004) Human mitochondrial glutaredoxin reduces S-glutathionylated proteins with high affinity accepting electrons from either glutathione or thioredoxin reductase. The Journal of Biological Chemistry 279:7537-7543.

Joy KW (1988) Ammonia, glutamine and asparagine: a carbon-nitrogen interface. Canadian Journal of Botany 66:2103-2109.

Kabil O, Banerjee R (2014) Enzymology of H2S biogenesis, decay and signaling. Antioxidants and Redox Signaling 20:770-782.

Kambampati R, Lauhon CT (2000) Evidence for the transfer of sulfane sulfur from IscS to ThiI during the in vitro biosynthesis of 4-thiouridine in *Escherichia coli* tRNA. The Journal of Biological Chemistry 275:10727-10730.

Kimura Y, Toyofuku Y, Koike S, Shibuya N, Nagahara N, Lefer D, Ogasawara Y, Kimura H (2015) Identification of H2S3 and H2S produced by 3-mercaptopyruvate sulfurtransferase in the brain. Scientific Reports 5:14774.

Kimura Y, Koike S, Shibuya N, Lefer D, Ogasawara Y, Kimura H (2017) 3-Mercaptopyruvate sulfurtransferase produces potential redox regulators cysteine- and glutathione-persulfide (Cys-SSH and GSSH) together with signaling molecules H2S2, H2S3 and H2S. Scientific Reports 7:10459.

Koh CS, Navrot N, Didierjean C, Rouhier N, Hirasawa M, Knaff DB, Wingsle G, Samian R, Jacquot JP, Corbier C, Gelhaye E (2008) An atypical catalytic mechanism involving three cysteines of thioredoxin. The Journal of Biological Chemistry 283:23062-23072.

Krishnan N, Fu C, Pappin DJ, Tonks NK (2011) H2S-Induced sulfhydration of the phosphatase PTP1B and its role in the endoplasmic reticulum stress response. Science Signaling 4:ra86.

Kruse I, Maclean AE, Hill L, Balk J (2018) Genetic dissection of cyclic pyranopterin monophosphate biosynthesis in plant mitochondria. Biochemical Journal 475:495-509.

Krüßel L, Junemann J, Wirtz M, Birke H, Thornton JD, Browning LW, Poschet G, Hell R, Balk J, Braun HP, Hildebrandt TM (2014) The mitochondrial sulfur dioxygenase ETHYLMALONIC ENCEPHALOPATHY PROTEIN1 is required for amino acid catabolism during carbohydrate starvation and embryo development in Arabidopsis. Plant Physiology 165:92-104.

Kumánovics A, Chen OS, Li L, Bagley D, Adkins EM, Lin H, Dingra NN, Outten CE, Keller G, Winge D, Ward DM, Kaplan J (2008) Identification of FRA1 and FRA2 as genes involved in regulating the yeast iron regulon in response to decreased mitochondrial iron-sulfur cluster synthesis. The Journal of Biological Chemistry 283:10276-10286.

La Camera S, L'haridon F, Astier J, Zander M, Abou-Mansour E, Page G, Thurow C, Wendehenne D, Gatz C, Métraux JP, Lamotte O (2011) The glutaredoxin ATGRXS13 is required to facilitate *Botrytis cinerea* infection of *Arabidopsis thaliana* plants. The Plant Journal 68:507-519.

Lanz ND, Booker SJ (2015) Auxiliary iron-sulfur cofactors in radical SAM enzymes. Biochimica et Biophysica Acta 1853:1316-1334.

Laurent TC, Moore EC, Reichard P (1964) Enzymatic synthesis of deoxyribonucleotides. IV. Isolation and characterization of thioredoxin, the hydrogen donor from *Escherichia coli* B. The Journal of Biological Chemistry 239:3436-3444.

Lezhneva L, Amann K, Meurer J (2004) The universally conserved HCF101 protein is involved in assembly of [4Fe–4S]-cluster-containing complexes in *Arabidopsis thaliana* chloroplasts. The Plant Journal 37:174-185.

Li H, Mapolelo DT, Dingra NN, Naik SG, Lees NS, Hoffman BM, Riggs-Gelasco PJ, Huynh BH, Johnson MK, Outten CE (2009) The yeast iron regulatory proteins Grx3/4 and Fra2 form heterodimeric complexes containing a [2Fe-2S] cluster with cysteinyl and histidyl ligation. Biochemistry 48:9569-9581.

Li H, Mapolelo DT, Dingra NN, Keller G, Riggs-Gelasco PJ, Winge DR, Johnson MK, Outten CE (2011) Histidine-103 in Fra2 is an iron-sulfur cluster ligand in the [2Fe-2S] Fra2-Grx3 complex and is required for in vivo iron signaling in yeast. The Journal of Biological Chemistry 286:867-876.

Li K, Xin Y, Xuan G, Zhao R, Liu H, Xia Y, Xun L (2019) *Escherichia coli* Uses Separate Enzymes to Produce H2S and Reactive Sulfane Sulfur From L-cysteine. Frontiers in Microbiology 10:298.

Li S, Lauri A, Ziemann M, Busch A, Bhave M, Zachgo S (2009) Nuclear activity of ROXY1, a glutaredoxin interacting with TGA factors, is required for petal development in *Arabidopsis thaliana*. The Plant Cell 21:429-441.

Li S, Gutsche N, Zachgo S (2011) The ROXY1 C-Terminal L**LL Motif Is Essential for the Interaction with TGA Transcription Factors. Plant Physiology 157:2056-2068.

Lill R, Mühlenhoff U (2006) Iron-sulfur protein biogenesis in eukaryotes: components and mechanisms. Annual Review of Cell and Developmental Biology 22:457-486.

Lill R, Mühlenhoff U (2008) Maturation of iron-sulfur proteins in eukaryotes: mechanisms, connected processes, and diseases. Annual Review of Biochemistry 77:669-700.

Lill R (2009) Function and biogenesis of iron-sulphur proteins. Nature 460:831-838.

Lillig CH, Berndt C, Vergnolle O, Lönn ME, Hudemann C, Bill E, Holmgren A (2005) Characterization of human glutaredoxin 2 as iron-sulfur protein: a possible role as redox sensor. Proceedings of the National Academy of Sciences USA 102:8168-8173.

Loi VV, Harms M, Müller M, Huyen NTT, Hamilton CJ, Hochgräfe F, Pané-Farré J, Antelmann H (2017) Real-Time Imaging of the Bacillithiol Redox Potential in the Human Pathogen *Staphylococcus aureu*s Using a Genetically Encoded Bacilliredoxin-Fused Redox Biosensor. Antioxidants and Redox Signaling 26:835-848.

Loiseau L, Ollagnier-de-Choudens S, Nachin L, Fontecave M, Barras F (2003) Biogenesis of Fe-S cluster by the bacterial Suf system: SufS and SufE form a new type of cysteine desulfurase. The Journal of Biological Chemistry 278:38352-38359.

Loiseau L, Ollagnier-de Choudens S, Lascoux D, Forest E, Fontecave M, Barras F (2005) Analysis of the heteromeric CsdA-CsdE cysteine desulfurase, assisting Fe-S cluster biogenesis in *Escherichia coli*. The Journal of Biological Chemistry 280:26760-26769.

Longen S, Richter F, Köhler Y, Wittig I, Beck KF, Pfeilschifter J (2016) Quantitative Persulfide Site Identification (qPerS-SID) Reveals Protein Targets of H2S Releasing Donors in Mammalian Cells. Scientific Reports 6:29808.

Lönn ME, Hudemann C, Berndt C, Cherkasov V, Capani F, Holmgren A, Lillig CH (2008) Expression pattern of human glutaredoxin 2 isoforms: identification and characterization of two testis/cancer cell-specific isoforms. Antioxidants and Redox Signaling 10:547-557.

Mao G, Wang R, Guan Y, Liu Y, Zhang S (2011) Sulfurtransferases 1 and 2 play essential roles in embryo and seed development in *Arabidopsis thaliana*. The Journal of Biological Chemistry 286:7548-7557.

Marschner H, Dell B (1994) Nutrient uptake in mycorrhizal symbiosis. Plant and Soil 159:89-102.

Matthies A, Rajagopalan KV, Mendel RR, Leimkühler S (2004) Evidence for the physiological role of a rhodanese-like protein for the biosynthesis of the molybdenum cofactor in humans. Proceedings of the National Academy of Sciences USA 101:5946-5951.

Mesecke N, Mittler S, Eckers E, Herrmann JM, Deponte M (2008) Two novel monothiol glutaredoxins from *Saccharomyces cerevisiae* provide further insight into iron-sulfur cluster binding, oligomerization, and enzymatic activity of glutaredoxins. Biochemistry 47:1452-1463.

Meyer AJ, Brach T, Marty L, Kreye S, Rouhier N, Jacquot JP, Hell R (2007) Redox-sensitive GFP in *Arabidopsis thaliana* is a quantitative biosensor for the redox potential of the cellular glutathione redox buffer. The Plant Journal 52:973-986.

Meyer AJ, Dick TP (2010) Fluorescent protein-based redox probes. Antioxidants and Redox Signaling 13:621-650.

Mieyal JJ, Gallogly MM, Qanungo S, Sabens EA, Shelton MD (2008) Molecular mechanisms and clinical implications of reversible protein S-glutathionylation. Antioxidants and Redox Signaling 10:1941-1988.

Mihara H, Esaki N (2002) Bacterial cysteine desulfurases: their function and mechanisms. Applied Microbiology and Biotechnology 60:12-23.

Mikami Y, Shibuya N, Kimura Y, Nagahara N, Ogasawara Y, Kimura H (2011) Thioredoxin and dihydrolipoic acid are required for 3-mercaptopyruvate sulfurtransferase to produce hydrogen sulfide. Biochemical Journal 439:479-485.

Millikin R, Bianco CL, White C, Saund SS, Henriquez S, Sosa V, Akaike T, Kumagai Y, Soeda S, Toscano JP, Lin J, Fukuto JM (2016) The chemical biology of protein hydropersulfides: Studies of a possible protective function of biological hydropersulfide generation. Free Radical Biology and Medicine 97:136-147.

Mironov A, Seregina T, Nagornykh M, Luhachack LG, Korolkova N, Lopes LE, Kotova V, Zavilgelsky G, Shakulov R, Shatalin K, Nudler E (2017) Mechanism of H2S-mediated protection against oxidative stress in *Escherichia coli*. Proceedings of the National Academy of Sciences USA 114:6022-6027.

Mishanina TV, Libiad M, Banerjee R (2015) Biogenesis of reactive sulfur species for signaling by hydrogen sulfide oxidation pathways. Nature Chemical Biology 11:457-464.

Molina-Navarro MM, Casas C, Piedrafita L, Bellí G, Herrero E (2006) Prokaryotic and eukaryotic monothiol glutaredoxins are able to perform the functions of Grx5 in the biogenesis of Fe/S clusters in yeast mitochondria. FEBS Letters 80:2273-2280.

Morgan B, Van Laer K, Owusu TN, Ezeriņa D, Pastor-Flores D, Amponsah PS, Tursch A, Dick TP (2016) Real-time monitoring of basal H2O2 levels with peroxiredoxin-based probes. Nature Chemical Biology 12:437-443.

Moseler A, Aller I, Wagner S, Nietzel T, Przybyla-Toscano J, Mühlenhoff U, Lill R, Berndt C, Rouhier N, Schwarzländer M, Meyer AJ (2015) The mitochondrial monothiol glutaredoxin S15 is essential for iron-sulfur protein maturation in *Arabidopsis thaliana*. Proceedings of the National Academy of Sciences USA 112:13735-13740.

Mueller EG (2006) Trafficking in persulfides: delivering sulfur in biosynthetic pathways. Nature Chemical Biology 2:185-194.

Mühlenhoff U, Gerber J, Richhardt N, Lill R (2003) Components involved in assembly and dislocation of iron-sulfur clusters on the scaffold protein Isu1p. The EMBO Journal 22:4815-4825.

Mühlenhoff U, Molik S, Godoy JR, Uzarska MA, Richter N, Seubert A, Zhang Y, Stubbe J, Pierrel F, Herrero E, Lillig CH, Lill R (2010) Cytosolic monothiol glutaredoxins function in intracellular iron sensing and trafficking via their bound iron-sulfur cluster. Cell Metabolism 12:373-385.

Murmu J, Bush MJ, DeLong C, Li S, Xu M, Khan M, Malcolmson C, Fobert PR, Zachgo S, Hepworth SR (2010) Arabidopsis basic leucine-zipper transcription factors TGA9 and TGA10 interact with floral glutaredoxins ROXY1 and ROXY2 and are redundantly required for anther development. Plant Physiology 154:1492-1504.

Murthy NUM, Ollagnier-de-Choudens S, Sanakis Y, Abdel-Ghany SE, Rousset C, Ye H, Fontecave M, Pilon-Smits EA, Pilon M (2007) Characterization of *Arabidopsis thaliana* SufE2 and SufE3: functions in chloroplast iron-sulfur cluster assembly and Nad synthesis. The Journal of Biological Chemistry 282:18254-18264.

Mustafa AK, Gadalla MM, Sen N, Kim S, Mu W, Gazi SK, Barrow RK, Yang G, Wang R, Snyder SH (2009) H2S signals through protein S-sulfhydration. Science Signaling 2:ra72.
Nagahara N, Ito T, Kitamura H, Nishino T (1998) Tissue and subcellular distribution of mercaptopyruvate sulfurtransferase in the rat: confocal laser fluorescence and immunoelectron microscopic studies combined with biochemical analysis. Histochemistry and Cell Biology 110:243-250.

Nakai Y, Harada A, Hashiguchi Y, Nakai M, Hayashi H (2012) Arabidopsis molybdopterin biosynthesis protein Cnx5 collaborates with the ubiquitin-like protein Urm11 in the thio-modification of tRNA. The Journal of Biological Chemistry 287:30874-30884.

Nakamura T, Yamaguchi Y, Sano H (2000) Plant mercaptopyruvate sulfurtransferases: molecular cloning, subcellular localization and enzymatic activities. European Journal of Biochemistry 267:5621-5630.

Nath K, Wessendorf RL, Lu Y (2016) A nitrogen-fixing subunit essential for accumulating 4Fe–4S-containing photosystem I core proteins. Plant Physiology 172:2459–2470.

Ndamukong I, Abdallat AA, Thurow C, Fode B, Zander M, Weigel R, Gatz C (2007) SA-inducible *Arabidopsis* glutaredoxin interacts with TGA factors and suppresses JA-responsive PDF1.2 transcription. The Plant Journal 50:128-139.

Ojeda L, Keller G, Mühlenhoff U, Rutherford JC, Lill R, Winge DR (2006) Role of glutaredoxin-3 and glutaredoxin-4 in the iron regulation of the Aft1 transcriptional activator in *Saccharomyces cerevisiae*. The Journal of Biological Chemistry 281:17661-17669.

Olson KR, Gao Y, Arif F, Arora K, Patel S, DeLeon ER, Sutton TR, Feelisch M, Cortese-Krott MM, Straub KD (2018) Metabolism of hydrogen sulfide (H2S) and Production of Reactive Sulfur Species (RSS) by superoxide dismutase. Redox Biology 15:74-85.

Olson KR, Gao Y, DeLeon ER, Arif M, Arif F, Arora N, Straub KD (2017) Catalase as a sulfide-sulfur oxido-reductase: An ancient (and modern?) regulator of reactive sulfur species (RSS). Redox Biology 12:325-339.

Ortiz-Lopez A, Chang H, Bush DR (2000) Amino acid transporters in plants. Biochimica et Biophysica Acta 1465:275-280.

Ostergaard H, Henriksen A, Hansen FG, Winther JR (2001) Shedding light on disulfide bond formation: engineering a redox switch in green fluorescent protein. The EMBO Journal 20:5853-5862.

Outten FW, Wood MJ, Munoz FM, Storz G (2003) The SufE protein and the SufBCD complex enhance SufS cysteine desulfurase activity as part of a sulfur transfer pathway for Fe-S cluster assembly in *Escherichia coli*. The Journal of Biological Chemistry 278:45713-45719.

Pan J, Carroll KS (2013) Persulfide reactivity in the detection of protein s-sulfhydration. ACS Chemical Biology 8:1110-1116.

Papenbrock J, Schmidt A (2000) Characterization of two sulfurtransferase isozymes from *Arabidopsis thaliana*. European Journal of Biochemistry 267:5571-5579.

Papenbrock J, Guretzki S, Henne M (2011) Latest news about the sulfurtransferase protein family of higher plants. Amino Acids 41:43-57.

Paul BD, Snyder SH (2012) H_2S signalling through protein sulfhydration and beyond. Nature Reviews Molecular Cell Biology 13:499-507.

Pérez-Pérez ME, Mauriès A, Maes A, Tourasse NJ, Hamon M, Lemaire SD, Marchand CH (2017) The Deep Thioredoxome in *Chlamydomonas reinhardtii*: New Insights into Redox Regulation. Molecular Plant 10:1107-1125.

Persson J, Högberg P, Ekblad A, Högberg MN, Nordgren A, Näsholm T (2003) Nitrogen acquisition from inorganic and organic sources by boreal forest plants in the field. Oecologia 137:252-257.

Pujol-Carrion N, Belli G, Herrero E, Nogues A, de la Torre-Ruiz MA (2006) Glutaredoxins Grx3 and Grx4 regulate nuclear localisation of Aft1 and the oxidative stress response in *Saccharomyces cerevisiae*. Journal of Cell Science 119:4554-4564.

Raux-Deery E, Leech HK, Nakrieko KA, McLean KJ, Munro AW, Heathcote P, Rigby SE, Smith AG, Warren MJ (2005) Identification and characterization of the terminal enzyme of siroheme biosynthesis from *Arabidopsis thaliana*: a plastid-located sirohydrochlorin ferrochelatase containing a 2FE-2S center. The Journal of Biological Chemistry 280:4713-4721.

Reinholdt O, Schwab S, Zhang Y, Reichheld JP, Fernie AR, Hagemann M, Timm S (2019) Redox-Regulation of Photorespiration through Mitochondrial Thioredoxin o1. Plant Physiology 181:442-457.

Roche B, Aussel L, Ezraty B, Mandin P, Py B, Barras F (2013) Iron/sulfur proteins biogenesis in prokaryotes: formation, regulation and diversity. Biochimica et Biophysica Acta 1827:923-937.

Rodriguez-Manzaneque MT, Ros J, Cabiscol E, Sorribas A, Herrero E (1999) Grx5 glutaredoxin plays a central role in protection against protein oxidative damage in *Saccharomyces cerevisiae*. Molecular and Cellular Biology 19:8180-8190.

Rodríguez-Manzaneque MT, Tamarit J, Bellí G, Ros J, Herrero E (2002) Grx5 is a mitochondrial glutaredoxin required for the activity of iron/sulfur enzymes. Molecular and Cellular Biology 13:1109-1121.

Rouhier N, Unno H, Bandyopadhyay S, Masip L, Kim SK, Hirasawa M, Gualberto JM, Lattard V, Kusunoki M, Knaff DB, Georgiou G, Hase T, Johnson MK, Jacquot JP (2007) Functional, structural, and spectroscopic characterization of a glutathione-ligated [2Fe-2S] cluster in poplar glutaredoxin C1. Proceedings of the National Academy of Sciences USA 104:7379-7384.

Rouhier N, Lemaire SD, Jacquot JP (2008) The role of glutathione in photosynthetic organisms: emerging functions for glutaredoxins and glutathionylation. Annual Review of Plant Biology 59:143-166.

Sánchez-Bermejo E, Castrillo G, del Llano B, Navarro C, Zarco-Fernández S, Martinez-Herrera DJ, Leo-del Puerto Y, Muñoz R, Cámara C, Paz-Ares J, Alonso-Blanco C, Leyva A (2014) Natural variation in arsenate tolerance identifies an arsenate reductase in *Arabidopsis thaliana*. Nature Communications 5:4617.

Schnug E, Booth E, Haneklaus S, Walker KC (1995) Sulphur supply and stress resistance in oilseed rape; proceeding of the 9th international Rapeseed Congress, Cambridge 229-231.

Schwarzländer M, Dick TP, Meyer AJ, Morgan B (2016) Dissecting Redox Biology Using Fluorescent Protein Sensors. Antioxidants and Redox Signaling 24:680-712.

Schwenkert S, Netz DJ, Frazzon J, Pierik AJ, Bill E, Gross J, Lill R, Meurer J (2009) Chloroplast HCF101 is a scaffold protein for [4Fe–4S] cluster assembly. Biochemical Journal 425:207-218.

Shatalin K, Shatalina E, Mironov A, Nudler E (2011) H2S: a universal defense against antibiotics in bacteria. Science 334:986-990.

Shi R, Proteau A, Villarroya M, Moukadiri I, Zhang L, Trempe JF, Matte A, Armengod ME, Cygler M. (2010) Structural basis for Fe-S cluster assembly and tRNA thiolation mediated by IscS protein-protein interactions. PLoS Biology 8:e1000354.

Shibuya N, Tanaka M, Yoshida M, Ogasawara Y, Togawa T, Ishii K, Kimura H (2009) 3-Mercaptopyruvate sulfurtransferase produces hydrogen sulfide and bound sulfane sulfur in the brain. Antioxidants and Redox Signaling 11:703-714.

Stockdreher Y, Sturm M, Josten M, Sahl HG, Dobler N, Zigann R, Dahl C (2014) New proteins involved in sulfur trafficking in the cytoplasm of *Allochromatium vinosum*. The Journal of Biological Chemistry 289:12390-12403.

Ströher E, Grassl J, Carrie C, Fenske R, Whelan J, Millar AH (2016) Glutaredoxin S15 Is Involved in Fe-S Cluster Transfer in Mitochondria Influencing Lipoic Acid-Dependent Enzymes, Plant Growth, and Arsenic Tolerance in Arabidopsis. Plant Physiology 170:1284-1299.

Su T, Xu J, Li Y, Lei L, Zhao L, Yang H, Feng J, Liu G, Ren D (2011) Glutathione-indole-3-acetonitrile is required for camalexin biosynthesis in *Arabidopsis thaliana*. The Plant Cell 23:364-80.

Takahashi H, Kopriva S, Giordano M, Saito K, Hell R (2011) Sulfur assimilation in photosynthetic organisms: molecular functions and regulations of transporters and assimilatory enzymes. Annual Review of Plant Biology 62:157-184.

Touraine B, Boutin JP, Marion-Poll A, Briat JF, Peltier G, Lobréaux S (2004) Nfu2: a scaffold protein required for [4Fe–4S] and ferredoxin iron-sulphur cluster assembly in Arabidopsis chloroplasts. The Plant Journal 40:101-111.

Uzarska MA, Przybyla-Toscano J, Spantgar F, Zannini F, Lill R, Mühlenhoff U, Rouhier N (2018) Conserved functions of Arabidopsis mitochondrial late-acting maturation factors in the trafficking of iron-sulfur clusters. Biochimica et Biophysica Acta Molecular Cell Research 1865:1250-1259.

Van Hoewyk D, Abdel-Ghany SE, Cohu CM, Herbert SK, Kugrens P, Pilon M, Pilon-Smits EA (2007) Chloroplast iron-sulfur cluster protein maturation requires the essential cysteine desulfurase CpNifS. Proceedings of the National Academy of Sciences USA 104:5686-5691.

Vitvitsky V, Miljkovic JL, Bostelaar T, Adhikari B, Yadav PK, Steiger AK, Torregrossa R, Pluth MD, Whiteman M, Banerjee R, Filipovic MR (2018) Cytochrome c Reduction by H2S Potentiates Sulfide Signaling. ACS Chemical Biology 13:2300-2307.

Wedmann R, Onderka C, Wei S, Szijártó IA, Miljkovic JL, Mitrovic A, Lange M, Savitsky S, Yadav PK, Torregrossa R, Harrer EG, Harrer T, Ishii I, Gollasch M, Wood ME, Galardon E, Xian M, Whiteman M, Banerjee R, Filipovic MR (2016) Improved tag-switch method reveals that thioredoxin acts as depersulfidase and controls the intracellular levels of protein persulfidation. Chemical Science 7:3414-3426.

Wingert RA, Galloway JL, Barut B, Foott H, Fraenkel P, Axe JL, Weber GJ, Dooley K, Davidson AJ, Schmid B, Paw BH, Shaw GC, Kingsley P, Palis J, Schubert H, Chen O, Kaplan J, Zon LI; Tübingen 2000 Screen Consortium (2005) Deficiency of glutaredoxin 5 reveals Fe-S clusters are required for vertebrate haem synthesis. Nature 436:1035-1039.

Wollers S, Heidenreich T, Zarepour M, Zachmann D, Kraft C, Zhao Y, Mendel RR, Bittner F (2008) Binding of sulfurated molybdenum cofactor to the C-terminal domain of ABA3 from *Arabidopsis thaliana* provides insight into the mechanism of molybdenum cofactor sulfuration. The Journal of Biological Chemistry 283:9642-9650.

Xing S, Zachgo S (2008) ROXY1 and ROXY2, two Arabidopsis glutaredoxin genes, are required for anther development. The Plant Journal 53:790-801.

Xiong L, Ishitani M, Lee H, Zhu JK (2001) The Arabidopsis LOS5/ABA3 locus encodes a molybdenum cofactor sulfurase and modulates cold stress- and osmotic stress-responsive gene expression. The Plant Cell 13:2063-2083.

Xu XM, Møller SG (2006) AtSufE is an essential activator of plastidic and mitochondrial desulfurases in Arabidopsis. The EMBO Journal 25:900-909.

Yadav PK, Yamada K, Chiku T, Koutmos M, Banerjee R (2013) Structure and kinetic analysis of H2S production by human mercaptopyruvate sulfurtransferase. The Journal of Biological Chemistry 288:20002-20013.

Ye H, Abdel-Ghany SE, Anderson TD, Pilon-Smits EA, Pilon M (2006b) CpSufE activates the cysteine desulfurase CpNifS for chloroplastic Fe-S cluster formation. The Journal of Biological Chemistry 281:8958-8969.

Yeung N, Gold B, Liu NL, Prathapam R, Sterling HJ, Willams ER, Butland G (2011) The *E. coli* monothiol glutaredoxin GrxD forms homodimeric and heterodimeric FeS cluster containing complexes. Biochemistry 50:8957-8969.

Yoshida K, Hisabori T (2016) Adenine nucleotide-dependent and redox-independent control of mitochondrial malate dehydrogenase activity in *Arabidopsis thaliana*. Biochimica et Biophysica Acta 1857:810-818.

Yoshida K, Noguchi K, Motohashi K, Hisabori T (2013) Systematic exploration of thioredoxin target proteins in plant mitochondria. Plant Cell Physiology 54:875-892.

Yu H, Braun P, Yildirim MA, Lemmens I, Venkatesan K, Sahalie J, Hirozane-Kishikawa T, Gebreab F, Li N, Simonis N, Hao T, Rual JF, Dricot A, Vazquez A, Murray RR, Simon C, Tardivo L, Tam S, Svrzikapa N, Fan C, de Smet AS, Motyl A, Hudson ME, Park J, Xin X, Cusick ME, Moore T, Boone C, Snyder M, Roth FP, Barabási AL, Tavernier J, Hill DE, Vidal M (2008) High-quality binary protein interaction map of the yeast interactome network. Science 322:104-110.

Zaffagnini M, Michelet L, Massot V, Trost P, Lemaire SD (2008) Biochemical characterization of glutaredoxins from *Chlamydomonas reinhardtii* reveals the unique properties of a chloroplastic CGFS-type glutaredoxin. The Journal of Biological Chemistry 283:8868-8876.

Zaffagnini M, Bedhomme M, Marchand CH, Morisse S, Trost P, Lemaire SD (2012) Redox regulation in photosynthetic organisms: focus on glutathionylation. Antioxidants and Redox Signaling 16:567-586.

Zhang D, Macinkovic I, Devarie-Baez NO, Pan J, Park CM, Carroll KS, Filipovic MR, Xian M (2014) Detection of protein S-sulfhydration by a tag-switch technique. Angewandte Chemie International Edition in English 53:575-581.

Zhang H, Du Y, Zhang X, Lu J, Holmgren A (2014) Glutaredoxin 2 reduces both thioredoxin 2 and thioredoxin 1 and protects cells from apoptosis induced by auranofin and 4-hydroxynonenal. Antioxidants and Redox Signaling 21:669-681.

Zheng L, White RH, Cash VL, Jack RF, Dean DR (1993) Cysteine desulfurase activity indicates a role for NIFS in metallocluster biosynthesis. Proceedings of the National Academy of Sciences USA 90:2754-2758.

Zhong R, Thompson J, Ottesen E, Lamppa GK (2010) A forward genetic screen to explore chloroplast protein import *in vivo* identifies Moco sulfurase, pivotal for ABA and IAA biosynthesis and purine turnover. The Plant Journal 63:44-59.

PUBLICATIONS SIGNIFICATIVES

Couturier J, Montanini B, Martin F, Brun A, Blaudez D, Chalot M (2007) The expanded family of ammonium transporters in the perennial poplar plant. New Phytologist 174:137-150.

Couturier J, Ströher E, Albetel AN, Roret T, Muthuramalingam M, Tarrago L, Seidel T, Tsan P, Jacquot JP, Johnson MK, Dietz KJ, Didierjean C, Rouhier N (2011) Arabidopsis chloroplastic glutaredoxin C5 as a model to explore molecular determinants for iron-sulfur cluster binding into glutaredoxins. The Journal of Biological Chemistry 286: 27515-27527.

Couturier J, Wu HC, Dhalleine T, Pégeot H, Sudre D, Gualberto JM, Jacquot JP, Gaymard F, Vignols F, Rouhier N (2014) Monothiol Glutaredoxin-BolA Interactions: Redox Control of *Arabidopsis thaliana* BolA2 and SufE1. Molecular Plant 7:187-205.

Couturier J, Przybyla-Toscano J, Roret T, Didierjean C, Rouhier N (2015) The roles of glutaredoxins ligating Fe-S clusters: Sensing, transfer or repair functions? Biochimica and Biophysica Acta Molecular Cell Research 1853:1513-1527.

Selles B, Moseler A, Rouhier N, **Couturier J** (2019) Rhodanese domain-containing sulfurtransferases: multifaceted proteins involved in sulfur trafficking in plants. Journal of Experimental Botany 70:4139-4154.

The expanded family of ammonium transporters in the perennial poplar plant

Jérémy Couturier, Barbara Montanini, Francis Martin, Annick Brun, Damien Blaudez and Michel Chalot

Research Unit INRA/UHP 1136 'Tree–microbe Interactions', Nancy-University, BP 239, F–54506 Vandoeuvre-les-Nancy Cedex, France

Author for correspondence:
Michel Chalot
Tel: +33 3 83684238
Fax: +33 3 83684292
Email: Michel.Chalot@scbiol.uhp-nancy.fr

Received: *4 October 2006*
Accepted: *24 November 2006*

Summary

• Ammonium and nitrate are the prevalent nitrogen sources for growth and development of higher plants. Here, we report on the characterization of the ammonium transporter (AMT) family in the perennial species *Populus trichocarpa*.

• *In silico* analysis and expression analysis of *AMT* genes from poplar was performed. In addition, AMT1;2 and AMT1;6 function was studied in detail by heterologous expression in yeast.

• The *P. trichocarpa* genome contains 14 putative AMTs, which is more than twice the number of *AMTs* in *Arabidopsis*. In roots, the high-affinity AMT1;2 strongly increased upon mycorrhiza formation and might be partly responsible for the high-affinity ammonium uptake component measured in poplar. Transcript level for the high-affinity AMT1;6 was strongly affected by the diurnal cycle. *AMT3;1* was exclusively expressed in senescing poplar leaves. Remarkably *AMT2;1* was highly expressed in leaves while *AMT2;2* was mostly expressed in petioles. Specific expression of *AMT1;5* in stamen and of *AMT1;6* in female flower indicate that they have key functions in reproductive organ development in poplar.

• The present study provides basic genomic and transcriptomic information for the poplar AMT family and will pave the way for deciphering the precise role of AMTs in poplar physiology.

Key words: ammonium transport, ectomycorrhiza, expression analysis, metabolite pools, *Populus trichocarpa*, yeast complementation.

New Phytologist (2007) **174**: 137–150

doi: 10.1111/j.1469-8137.2007.01992.x

Introduction

Ammonium is a primary source of nitrogen (N) for both perennial and annual species. It is taken up from the soil by ammonium transporters through the plasma membrane of root cells (Kaiser *et al.*, 2002) and incorporated into glutamine via glutamine synthetase (GS) present in the cytoplasm and plastids, the biochemistry of which has also been described in perennial species (Suarez *et al.*, 2002). Ammonium is also produced within plants either by reduction of nitrate and nitrite obtained from the soil, or by catabolism of endogenous amino compounds. For example, the photorespiratory nitrogen cycle generates a large amount of ammonium in leaf mitochondrias that is subsequently transported to chloroplasts for reassimilation by GS, although this statement has now to be interpreted with caution, given the recent finding that the nuclear encoded GS *GLN2* may also be addressed to the mitochondria (Taira *et al.*, 2004).

The biochemistry and molecular biology of ammonium transport in plants has been extensively studied and recent comprehensive reviews are available (Schjoerring *et al.*, 2002; Loque & von Wiren, 2004). Physiological studies on ammonium uptake by plant roots has provided evidence for the existence of a low affinity nonsaturable transport system (LATS), which operates in the millimolar concentration range and a high-affinity transport system (HATS), which operates in the submillimolar concentration range. The HATS exhibits saturation kinetics, energy dependence, and leads to depolarization of the plasma membrane electrical potential (Ludewig *et al.*, 2002).

The first ammonium transporter (AMT) genes were identified in yeast (Marini *et al.*, 1994) and *Arabidopsis* (Ninnemann *et al.*, 1994) by functional complementation of a yeast mutant deficient in high-affinity ammonium uptake. In plants, the AMT family can be subdivided into two subfamilies (Loque & von Wiren, 2004). Members of the AMT1 subfamily are intron-free, except LjAMT1;1 (Salvemini *et al.*, 2001); whereas members of AMT2 subfamily contain some introns in their gene sequences. The AMT2 family has been further divided into three subclades in rice (Suenaga *et al.*, 2003). Several plant AMT1 subfamily members, including homologs from *Arabidopsis thaliana* (AtAMT1;1, AtAMT1;2, AtAMT1;3: Ninnemann *et al.*, 1994; Gazzarrini *et al.*, 1999), *Brassica napus* (BnAMT1;2: Pearson *et al.*, 2002), *Lotus japonicus* (LjAMT1;1, LjAMT1;2, LjAMT1;3: Salvemini *et al.*, 2001; D'Apuzzo *et al.*, 2004), *Lycopersicon esculentum* (LeAMT1;1, LeAMT1;2 and LeAMT1;3: Lauter *et al.*, 1996; von Wiren *et al.*, 2000b; Becker *et al.*, 2002; Ludewig *et al.*, 2002) or *Oryza sativa* (OsAMT1;1, OsAMT1;2, OsAMT1;3; Sonoda *et al.*, 2003) have been characterized in yeast or in *Xenopus* oocytes. *AtAMT1;1* encodes a high-affinity transporter with a K_m value of < 0.5 μM and is expressed in roots and leaves, while *AtAMT1;2* and *AtAMT1;3* encode transporters of lower affinity (K_m values of 25–40 μM) and are mainly expressed in roots (Gazzarrini *et al.*, 1999). AtAMT1;2 expressed in yeast mutant displays biphasic kinetics (K_m values of 36 μM and 3.0 mM) for methylammonium uptake (Shelden *et al.*, 2001). *AMT* expression has been studied in detail in *Arabidopsis* and rice, and the data demonstrated the close relationship between AMT1;1 and AMT1;3 expression with glutamine (Rawat *et al.*, 1999) and sugar (Gazzarrini *et al.*, 1999; Rawat *et al.*, 1999) concentrations, respectively.

More recently, a second subfamily of ammonium transporters (AMT2) with distinct biochemical features, has been identified in several plants such as *A. thaliana* (Sohlenkamp *et al.*, 2002), *L. japonicus* (Simon-Rosin *et al.*, 2003) and *O. sativa* (Suenaga *et al.*, 2003). Plant AMT2 family members are more closely related to ammonium transporters from prokaryotes than they are to plant AMT1. While plant members of the AMT1 subfamily are preferentially expressed in roots (with the exception of *LeAMT1;3* (von Wiren *et al.*, 2000b), *LjAMT1;1* and *LjAMT1;2* (D'Apuzzo *et al.*, 2004), *AtAMT2* showed a higher level of gene expression in shoots compared with roots (Sohlenkamp *et al.*, 2002) and *OsAMT2;1* presented a constitutive expression in shoots and roots (Suenaga *et al.*, 2003). These distinct expression patterns may support the fact that individual members of the AMT family would function not only in ammonium uptake in roots, but also in ammonium recycling during leaf senescence or photorespiration (Howitt & Udvardi, 2000; von Wiren *et al.*, 2000a). Multiple forms of ammonium transporters in higher plants allow a greater regulatory flexibility and organelle-, cell-, tissue- or organ-specialization, and enable cells to take up ammonium over a wide range of concentrations (D'Apuzzo *et al.*, 2004).

As exemplified above, most studies have focused on a few annual species (*A. thaliana*, *L. esculentum*, *L. japonicus* and *O. sativa*), thus available information concerning N transport in perennial woody models is much more limited, particularly at the molecular level. The perennial life style of trees implies specific physiological traits that have been recently discussed (Suarez *et al.*, 2002; Bhalerao *et al.*, 2003; Andersson *et al.*, 2004; Sterky *et al.*, 2004). Related to N nutrition, one of these traits is the mobilization and storage in perennial tissues of the N present in leaves during autumn, which is remobilized at the beginning of the next growing season (Suarez *et al.*, 2002). Thus, transport mechanisms for nitrogenous compounds are likely to be different from those used by annual species, and probably rely on perennial-specific transport functions.

Taking advantage of the shotgun sequenced *Populus trichocarpa* (Nisqually 1) genome (Tuskan *et al.*, 2006), we present here the expression analysis of *AMT* members from the perennial tree species poplar and extend the analysis of five AMT members to include the functional characterization of three AMT1 and two AMT2 members by heterologous expression in yeast.

Materials and Methods

Plant growth and media composition

Populus tremula × *alba* (clone INRA 717 1B4) cuttings were cultivated as described by Kohler *et al.* (2003) in a growth chamber for 6 wk with a light intensity of 80 μmol m^{-2} s^{-1} and a day–night temperature regime of 16 h at 24°C at 80% relative humidity and 8 h at 18°C at 60% relative humidity. For further experiments (N regime, light regime), *P. tremula* × *alba* plants were grown hydroponically for 2 months in the following nutrient solution: 0.75 mM $CaCl_2{\cdot}2H_2O$, 4.7 mM KNO_3, 5.15 mM NH_4NO_3, 0.375 mM $MgSO_4{\cdot}7H_2O$, 0.3 mM KH_2PO_4, 100 μM H_3BO_3, 5 μM KI, 100 μM $MnSO_4$ H_2O, 30 μM $ZnSO_4$ H_2O, 1 μM $Na_2Mo_4{\cdot}2H_2O$, 0.1 μM $CuSO_4{\cdot}5H_2O$, 0.1 μM $CoCl_2$, 100 μM $FeSO_4{\cdot}7H_2O$. The pH was adjusted to 5.6–5.8 with KOH. The nutrient solution was renewed every week. When needed, plants were then transferred to a N-free nutrient solution. To maintain K^+ at a constant concentration KCl (2.36 mM) and K_2SO_4 (1.17 mM) were substituted for KNO_3.

All experiments were carried out using the *P. tremula* × *alba* poplar clone, except when specific tissues were examined. Thus, fruits (harvested 21 April 2004), buds, stamens and female flowers (harvested 29 March 2005) were collected on 25-yr-old trees (*Populus trichocarpa* species) grown outdoors under natural conditions at the University campus.

Mycorrhizal inoculation

Populus tremula × *alba* (clone INRA 717 1B4) cuttings were cultivated in a growth chamber for 2 wk as already described

and then transferred onto Petri dishes, coinoculated with the ectomycorrhizal fungus *Paxillus involutus* (Batsch) Fr, in a modified MS solution (Murashige & Skoog, 1962), supplemented with 0.1% glucose and 1.5% agar. *Paxillus involutus* was pregrown for 10 d on agar medium containing modified Melin-Norkrans medium, as described by Selle *et al.* (2005). Mycorrhizal and nonmycorrhizal control roots were harvested 1 month after contact.

Cloning of AMTs cDNAs, yeast transformation and [^{14}C]MA uptake

Predicting coding sequences corresponding to AMT1;1, AMT1;2, AMT1;3, AMT1;4, AMT1;5, AMT1;6, AMT2;1, AMT2;2, AMT3;1 and AMT4;5 were amplified by polymerase chain reaction (PCR) from cDNA generated from same tissues used for reverse transcriptase polymerase chain reaction (RT-PCR) studies. The fidelity of PCR amplifications was verified by sequencing. The amplification products were cloned into pGEM-T Easy vector (Promega, Madison, WI, USA) and, after *Not*I digestion, inserted into the yeast expression vector pFL61 (Minet *et al.*, 1992). The yeast strain 31019b (*MATa mep1Δ mep2Δ::LEU2 mep3Δ::KanMX2 ura3*; (Marini *et al.*, 1997)) was transformed with pFL61 harboring the cDNA sequences of AMTs. Yeast transformants were selected on N-free minimal medium supplemented with 1 mM glutamine and 3% glucose. Yeast complementation tests were performed as described previously (Javelle *et al.*, 2003). Methylammonium uptake assays were conducted under previously described experimental conditions (Gazzarrini *et al.*, 1999; Montanini *et al.*, 2002).

RT-PCR

Total RNA extraction was performed with the RNeasy Plant Mini kit (Qiagen, Darmstadt, Germany) from approximately 100 mg of frozen tissues of poplar. To remove contaminating genomic DNA, the samples were treated with DNAse I (Qiagen). To obtain cDNA, 1 μg of total RNA was annealed to oligo-dT primers (Promega) and reverse transcribed using Reverse Transcriptase (Qiagen) at 37°C for 1 h. Every reaction was set up in three replicates. For each *AMT*, the PCR program was as follows: 94°C for 3 min and 37 cycles of 94°C for 30 s, 58°C for 45 s, and 72°C for 1 min 45 s. AMT fragments were gel-purified and sequenced to ensure accuracy and specificity. The whole set of *AMT* genes (14 genes) was tested by RT-PCR in every experiment carried out but only AMTs detected are retained in figures for greater clarity. A cDNA fragment corresponding to the constitutively expressed ubiquitin gene was amplified simultaneously (28 cycles) and used as a control. Cysteine protease (*CP*) gene was amplified (35 cycles) and used as control of the senescing state of leaves. The sequences of the gene-specific oligonucleotides designed in the nonconserved 5′ and 3′ regions of the genes were used for RT-PCR and are listed in Table 1.

Table 1 Primers used for reverse transcriptase polymerase chain reaction analysis

Name	Sequence
AMT1;1 f	AGAGACTCTGACATCCTTCACTCC
AMT1;1 r	AATATGAGGTCCCTCTTAGACG
AMT1;2 f	ATGGCCTGCTCAGCCTCTGAC
AMT1;2 r	GCATCAAACTTGATCACACATTG
AMT1;3 f	CTGTGTGACAGTACCCTTCACTTC
AMT1;3 r	ACAAAATAGTCCCTCTTACGCA
AMT1;4 f	TTTACAATGGCAGCTCTAACTTGC
AMT1;4 r	CTAGGGATCCGCCTTTGTCATCATAAA
AMT1;5 f	ACCTTTCAATGGCATCATCGCCT
AMT1;5 r	TCAGACAACACCTAGCTGCTT
AMT1;6 f	ATGGAGGTCTCATGGGAACAAAGT
AMT1;6 r	TCATGAATGATTTCGACCTTGG
AMT2;1 f	ATGAATGCCTCAACAGCTTATG
AMT2;1 r	TTGTTTCTGCATTGCTTAC
AMT2;2 f	ATGGATGCCCCCGCATATGAACAA
AMT2;2 r	GTATGCAGGCATCTAGCTTA
AMT3;1 f	AAAACCATGGCTGCTCTTCCACCCAA
AMT3;1 r	CTACAACACTTGAGTTGATGAC
AMT4;1 f	ATGAAGCAAGTCCAGCATGA
AMT4;1 r	CCCTGTCACATTATCAGTGT
AMT4;2 f	AATGAGCAATGATACTGCCTTCCC
AMT4;2 r	CTATGTCTTCTCAGCTTGACGA
AMT4;3 f	CGGAGGCAAAAAAGCCGTAGTC
AMT4;3 r	CATTTTCAAATAAGCACAACC
AMT4;4 f	ATGAACAAGGGAGACAATGCAT
AMT4;4 r	TCATACCATTTGAACATCACCG
AMT4;5 f	CTCCCTATGAATTTCCCACAAGGA
AMT4;5 r	TCAGAAGCGTTGTCGGCAGAAGTA
UBQf	GCACCTCTGGCAGACTACAA
UBQr	TAACAGCCGCTCCAAACAGT
CPf	AGTCACTGAGAAAGGCTGTGG
CPr	CCAAATGGATTGTTCTTGCTC
ASN2f	CAGGCCTGATCTTGGAAGGATT
ASN2r	GCAACTGTTGCAGTTTTCTCCAGC

Amino acid extraction and analysis

Amino acids were extracted twice from 10 to 20 mg dried plant tissues with 300 μL 70% (v : v) cold ethanol. The samples were dried using a Reacti-Therm. Heating Module (Pierce, Rockford, IL, USA) and resuspended in 400 μl 0.1 N HCl. Amino acids and standards were then purified on a Dowex 50WX-8 cation ion exchange column (Sigma-Aldrich, St Louis, MO, USA) and aliquots of purified samples were transferred to microvials, dried in a Reacti-Therm Heating Module (Pierce) and derivatized according to Javelle *et al.* (2003). Gas chromatography and mass spectrometry (GC-MS) analysis was performed as described previously (Javelle *et al.*, 2003).

Soluble sugars extraction and analysis

Soluble sugars were extracted from approx. 100 mg of fresh plant tissues, with 1.1 ml 70% (v : v) cold methanol. The extracts

were centrifuged to get supernatant for assay of soluble sugars by the anthrone solution colorimetric method (Miller, 1959). The sugar content was determined by measuring the absorbance at 620 nm. These values were then regressed against readings from a set of standard solutions of glucose.

Phylogenetic analyses

Full-length amino acid sequences were aligned by CLUSTALW and imported into the Molecular Evolutionary Genetics Analysis (MEGA) package version 3.1 (Kumar *et al.*, 2004). Phylogenetic analyses were conducted using the neighbor-joining (NJ) method implemented in MEGA, with the pairwise deletion option for handling alignment gaps, and with the Poisson correction model for distance computation. Bootstrap tests were conducted using 1000 replicates. Branch lengths (drawn in the horizontal dimension only) are proportional to phylogenetic distances. The accession numbers or gene models of version 1.1 of the *P. trichocarpa* genome database used were: PtrAMT1;1 (Poptr1_1 : 804848), PtrAMT1;2 (Poptr1_1 : 665333), PtrAMT1;3 (Poptr1_1 : 565016), PtrAMT1;4 (Poptr1_1 : 799507), PtrAMT1;5 (Poptr1_1 : 645545), PtrAMT1;6 (Poptr1_1 : 804509), PtrAMT2;1 (Poptr1_1 : 802015), PtrAMT2;2 (Poptr1_1 : 808726), PtrAMT3;1 (Poptr1_1 : 175190), PtrAMT4;1 (Poptr1_1 : 754260), PtrAMT4;2 (Poptr1_1 : 260884), PtrAMT4;3 (Poptr1_1 : 205629), PtrAMT4;4 (Poptr1_1 : 806873), PtrAMT4;5 (Poptr1_1 : 424130). Other accession numbers were: AtAMT1;1 (At4g13510), AtAMT1;2 (At1g64780), AtAMT1;3 (At3g24300), AtAMT1;4 (At4g28700), AtAMT1;5 (At3g24290), AtAMT2;1 (At2g38290), LeAMT1;1 (P58905), LeAMT1;2 (O04161), LeAMT1;3 (Q9FVN0), LjAMT1;1 (Q9FSH3), LjAMT1;2 (Q7Y1B9), LjAMT1;3 (Q70KK9), LjAMT2;1 (Q93 × 02), OsAMT1;1 (Os04g43070), OsAMT1;2 (Os02g40710), OsAMT1;3 (Os02g40730), OsAMT2;1 (Os05g39240), OsAMT2;2 (Os01g61550), OsAMT2;3 (Os01g61510), OsAMT3;1 (Os01g65000), OsAMT3;2 (Os02g34580), OsAMT3;3 (Os03g62200), OsAMT4;1 (Os12g01420). BnAMT1;2 (AAG28780), PttAMT1;2 (AJ646889).

Results

Cloning and *in silico* analysis of the AMT family

The first whole-genome sequence and assembly for a tree species, namely that of *P. trichocarpa* was recently reported (Tuskan *et al.*, 2006). The JGI *P. trichocarpa* gene search mode revealed the existence of 14 *AMT* gene models. As suggested by a phylogenetic tree based on protein multiple sequence alignment, six sequences from *P. trichocarpa* genome fell in the subgroup AMT1 and eight in the subgroup AMT2. *Populus* thus possesses a higher number of *AMT* genes in both subfamilies than *Arabidopsis* or rice. *Populus* AMT2 as well as rice AMT2 members further divided into three clades (Fig. 1).

Genes encoding proteins from different sub-branches markedly differ in their exon–intron structure: for example, the intron size and location of splicing sites are roughly conserved in genes in each AMT2 subclade, while *AMT1* genes contain no intron with the exception of *LjAMT1;1* (Salvemini *et al.*, 2001).

Analysis of the assembled genome revealed relatively recent whole-genome duplication shared among all modern taxa in Salicaceae. A second, older duplication appears to be shared with the *Arabidopsis* lineage (Tuskan *et al.*, 2006). These duplicated genes originated through very recent small-scale gene duplications and one relatively recent large-scale gene duplication event (Sterck *et al.*, 2005). A detailed analysis of duplication events for the *AMT* members revealed that *AMT1;1* and *AMT1;4* derived from a common ancestor through an ancient duplication event, and that *AMT2;2* and *AMT2;1* derived from a common ancestor through a recent duplication event. Interestingly, *AMT2;1* and *AMT2;2* showed specific expression patterns, with *AMT2;1* mostly expressed in leaves and *AMT2;2* mostly expressed in petioles (Fig. 2).

Figure 1 presents tentative signature sequences for the proteins of the AMT1 and AMT2 plant subfamilies, based on the existing AMT signature (Saier, 1998). Logo representation of the AMT signature was constructed at the web interface program WEBLOGO (Crooks *et al.*, 2004) on the basis of the alignment of 39 plant AMT members. These sequences may serve as identification motifs specific for the two subfamilies, and when scanned against the GenBank database, retrieved only members of each subfamily. These sequences can be used to identify additional members of the two subfamilies in other plant species as they are being sequenced.

Analyses carried out with the transmembrane (TM) prediction program THMM (http://www.CBS.dk) suggest that the poplar AMT family proteins are likely to have 9–11 TM domains as do the other AMT plant members (Schwacke *et al.*, 2003). *In silico* analysis accompanied by experiments using fusion proteins, indicate that the majority of the Mep/Amt proteins contain 11 membrane-spanning helices, with the *N*-terminus on the exterior face of the membrane and the *C*-terminus on the interior (Marini & Andre, 2000; Thomas *et al.*, 2000).

Table 2 shows that the *AMT* gene and AMT protein sequences share a high degree of identity between *Populus* species, with nucleotide and protein identities of at least 97.7% and 96.9%, respectively. This facilitates *in silico* and RT-PCR analyses and comparisons across *Populus* species.

It is also worth noting that most *AMT* genes are sporadically distributed across the poplar genome, except *AMT1;4, AMT1;5* and *AMT4;1* which are located on linkage group (LG) II. The *AMT1;4* locus stretches from position 23601578 to 23603065 while the *AMT1;5* locus extends from position

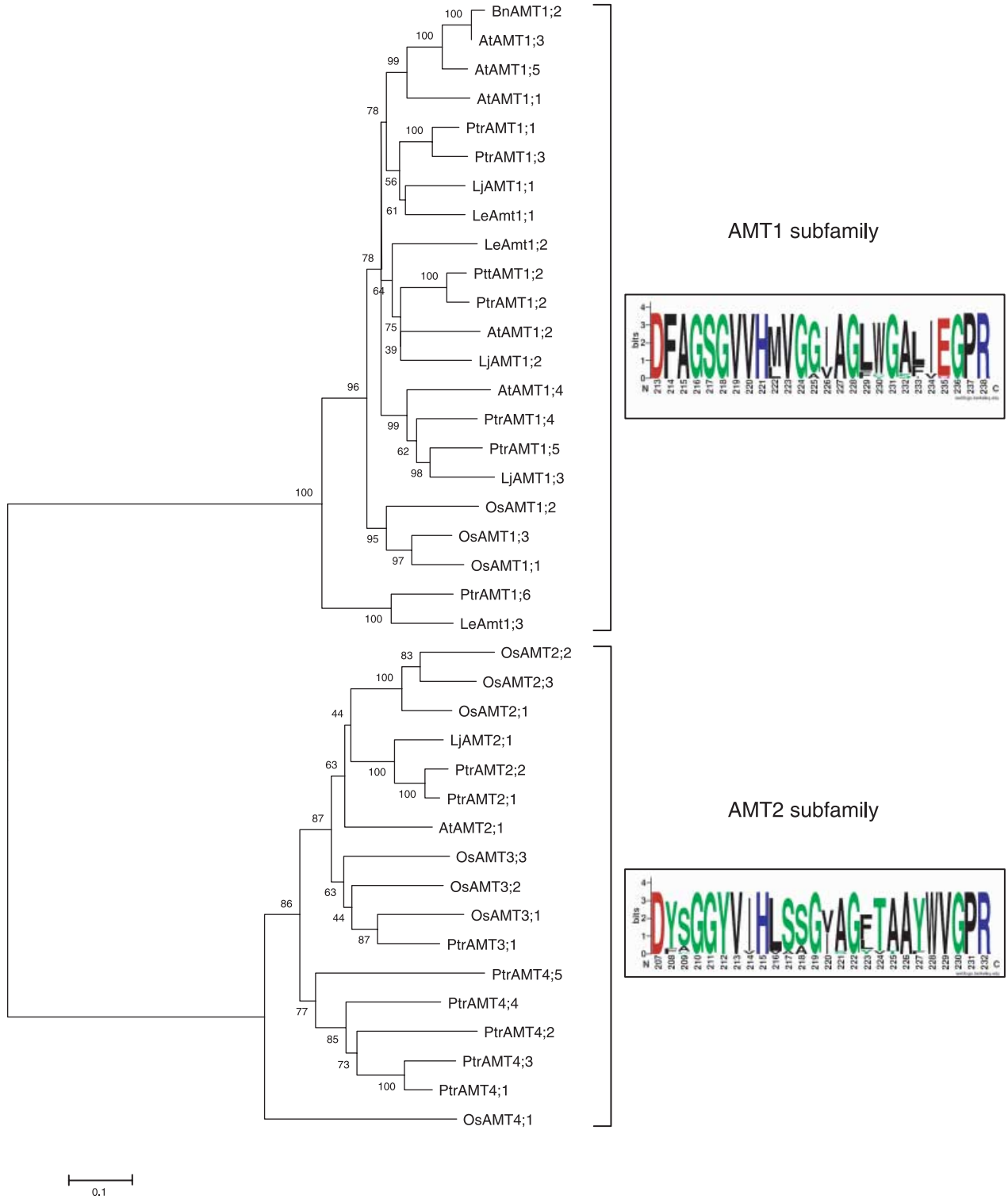

Fig. 1 An unrooted, neighbor-joining (NJ)-based tree of the ammonium transporter (AMT) family. The analysis was performed as described in the Material and Methods section. Branch lengths (drawn in the horizontal dimension only) are proportional to phylogenetic distances. Accession numbers are given in the Material and Methods section. Sequence logos of AMT1 and AMT2 subfamilies showed on the right were generated using WEBLOGO (http://weblogo.berkeley.edu/logo.cgi (Crooks *et al*., 2004)).

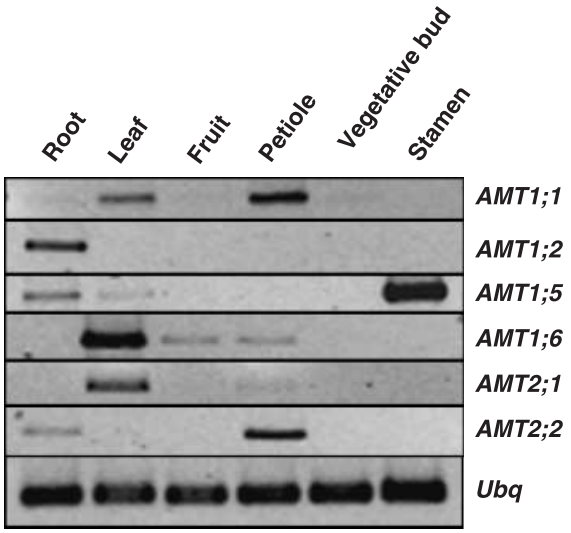

Fig. 2 Tissue-dependent expression of *AMTs* in poplar. Expression of *AMT1;1*, *AMT1;2 AMT1;5*, *AMT1;6 AMT2;1* and *AMT2;2* was analysed by reverse transcriptase polymerase chain reaction in tissues collected as described in the Material and Methods section. Aliquots of 1 μg total RNAs were reverse-transcribed into cDNA. The ubiquitin (Ubq) gene was amplified and used as an internal control. Experiments were repeated at least three times, with similar results.

Table 2 Identity between ammonium transporter (AMT) sequences cloned from *Populus tremula* × *alba* and sequences retrieved from the *Populus trichocarpa* database (http://genome.jgi-psf.org/Poptr1/Poptr1.home.html)

Gene name	% Identity (DNA sequence)	% Identity (protein sequence)
AMT1;1	99.6	99.2
AMT1;2	97.7	96.9
AMT1;3	99.9	99.6
AMT1;4	99.1	98.4
AMT1;5	99.3	99.2
AMT1;6	99.9	99.8
AMT2;1	99.9	99.8
AMT2;2	99.4	99.2
AMT3;1	99.4	99.4

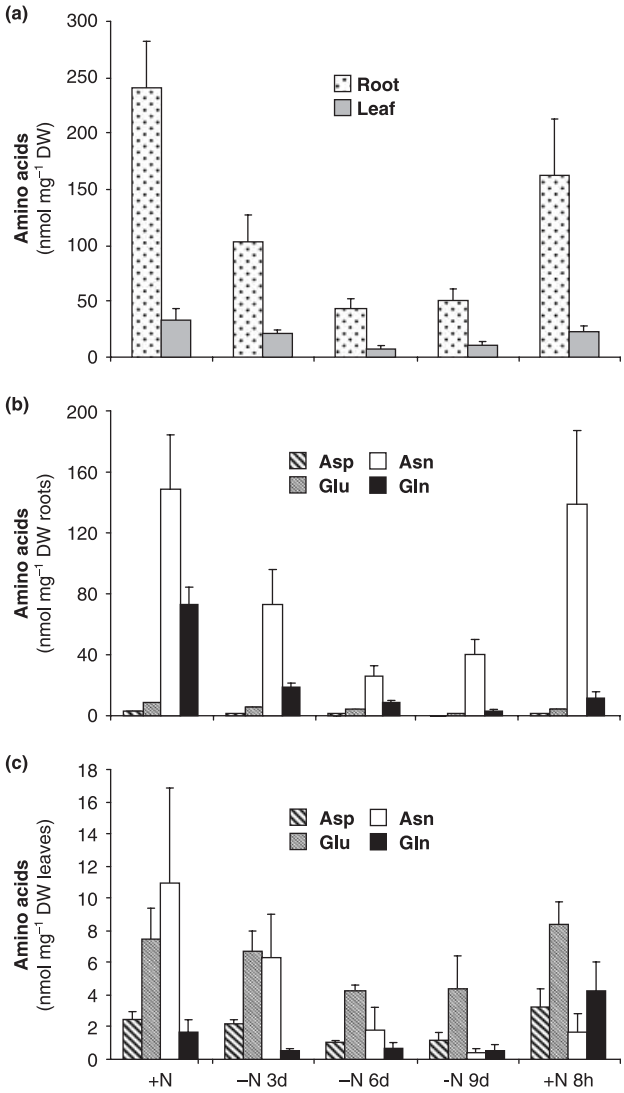

Fig. 3 Quantification of amino acids by gas chromatography–mass spectrometry in leaves and roots of poplar during nitrogen (N) deprivation and resupply. (a) Total free amino acid contents declined during N starvation in roots and leaves. (b) Asparagine and glutamine were the major amino acids in roots. (c) Asparagine and glutamate were the major amino acids in leaves. Values are expressed as means ± SE of four replicate experiments.

23599283–23600819 on poplar LG II, thus appearing as tandem repeats (see Supplementary Material, Fig. S1).

All transcript levels were measured in all experiments described later. Expression levels for *AMT1;3*, *AMT1;4*, *AMT4;1*, *AMT4;2*, *AMT4;3*, and *AMT4;4* were undetectable in any organs examined so far in poplar tissues. By contrast, the other *AMT* genes showed contrasting expression patterns as examined in the following text.

Effects of various N regimes

In order to investigate the impact of N regime on the regulation of *AMT* transcript levels, total RNAs and amino acids were extracted from roots and leaves of plants transferred in a N-free medium for various lengths of times, and further resupplied with N for 8 h. The concentration of total amino acids, measured by GC-MS, in roots and leaves decreased by five- and three-fold, respectively, during 9 d of N starvation (Fig. 3a). In N-fed poplar (grown for 2 months in N-supplied medium), asparagine was the predominant amino acid, accounting for 62% and 33% in roots and leaves, respectively, followed by glutamine in roots (Fig. 3b) and glutamate in leaves (Fig. 3c). The glutamine concentration decreased by 26-fold after 9 d of N-starvation in roots (Fig. 3b), whereas

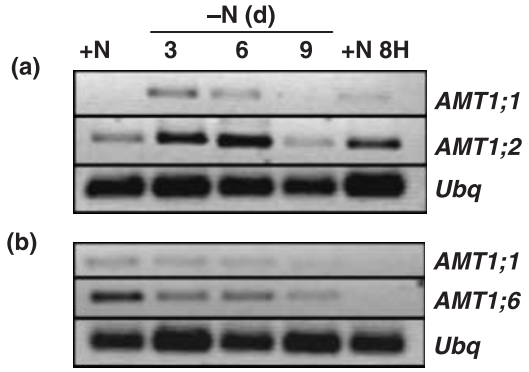

Fig. 4 Effect of the nitrogen (N) regime on *AMT* expression in leaves and roots of poplar. (a) Expression of the *AMT1;1* and *AMT1;2* transcripts in roots of poplar plants. (b) Expression of the *AMT1;1* and *AMT1;6* transcripts in leaves of poplar plants. RNA was extracted at different times of N starvation and 500 ng of total RNAs were reverse transcribed into cDNA. The ubiquitin (Ubq) gene was amplified and used as internal control. Analyses were performed by reverse transcriptase polymerase chain reaction in triplicate and without substantial variation of expression levels.

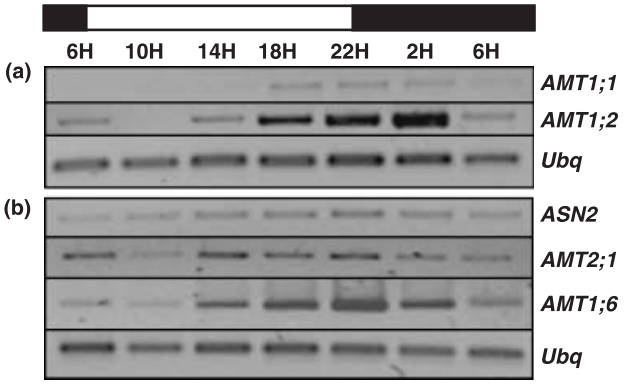

Fig. 5 Effect of the light–dark cycle on *AMT* expression in leaves and roots of poplar. (a) Expression of the *AMT1;1* and *AMT1;2* transcripts in roots of poplar plants. (b) Expression of the *AMT2;1*, *AMT1;6* and *ASN2* transcripts in leaves of poplar plants. RNA was extracted from tissues collected at 4-h intervals in poplar during a light–dark period. Aliquots of 500 ng total RNAs were reverse transcribed into cDNA. The ubiquitin (Ubq) gene was amplified and used as internal control. Analyses were performed by reverse transcriptase polymerase chain reaction in triplicate and without substantial variation of expression levels. ASN: asparagine synthetase gene.

asparagine decreased by 25-fold in leaves (Fig. 3c). The amino acid pools were rapidly reconstituted after 8 h of N resupply in roots, while in leaves the asparagine levels did not completely reached the +N level.

AMT1;2 transcripts strongly increased in roots under a short period of N starvation, but declined after 9 d of N starvation and increased again upon N resupply (Fig. 4a). It is worth noting that expression of *AMT1;2* was restricted to roots, whereas *AMT1;1* transcripts were detected in shoot and root tissues (Fig. 2). *AMT1;1* transcripts were undetectable under N-sufficient condition in roots, increased under N starvation, and remained weakly expressed during nitrogen resupply (Fig. 4a). In leaves, *AMT1;1* was weakly expressed and poorly affected by N starvation (Fig. 4b). Similarly, *AMT1;5* and *AMT2;1* were only weakly expressed under these experimental conditions (data not shown). *AMT1;6* transcripts declined under N starvation, compared with a N-sufficient growth condition, but remained low after N resupply (Fig. 4b), which might be linked to the poor increase in asparagine level at that time. All other *AMTs* were also analysed but were not detected under the conditions used in this experiment.

Effects of light regimes

Figure 5 shows diurnal variations in *AMT* expression levels in roots and leaves of plants collected at 4-h intervals in poplar. Our data indicate that *AMT1;1*, *AMT1;2*, *AMT1;6* and *AMT2;1* transcript levels exhibit diurnal rhythms, the largest diurnal changes in transcript levels being found for *AMT1;2* in root (Fig. 5a) and *AMT1;6* in leaf (Fig. 5b). *AMT1;1* and *AMT1;5* were only weakly expressed in leaves throughout the time course of the experiment (not shown). When light was switched off, the soluble sugar content in roots was at the highest level (98 mg equivalent glucose g^{-1} FW at 22 : 00 h) and decreased to 69 mg equivalent glucose g^{-1} FW after 8 h of dark regime. In leaves, the soluble sugar content was, respectively, 445 and 368 mg equivalent glucose g^{-1} FW at 22 : 00 h and 06 : 00 h. In addition, expression of a leaf asparagine synthetase gene (*ASN2*) was followed and showed a diurnal variation, similar to *AMT1;6* transcript level, although at a lesser extent.

AMT expression during senescence

The expression of the *AMTs* was studied in young, mature and senescing leaves. The senescing state of the leaves was confirmed by the parallel amplification of a cysteine protease gene (Bhalerao *et al.*, 2003; Andersson *et al.*, 2004), which was detected only at the latter stage (Fig. 6). *AMT1;5 and AMT1;6* showed increased expression levels in senescing leaves compared with young leaves. By contrast, *AMT3;1* was exclusively expressed in senescing leaves (Fig. 6).

AMT expression in reproductive organs

Stamens exhibited a strong expression level for *AMT1;5* transcripts, whereas female flowers showed expression for *AMT1;6* (Fig. 7a). Amino acid pools in these tissues also reached the highest levels ever measured in poplar tissues, especially in stamens (Fig. 7b). We might therefore conclude that *AMT1;5* and *AMT1;6* are not under the control of N catabolic repression in these poplar tissues. This also indicates that another as yet unidentified mechanism allowed for full

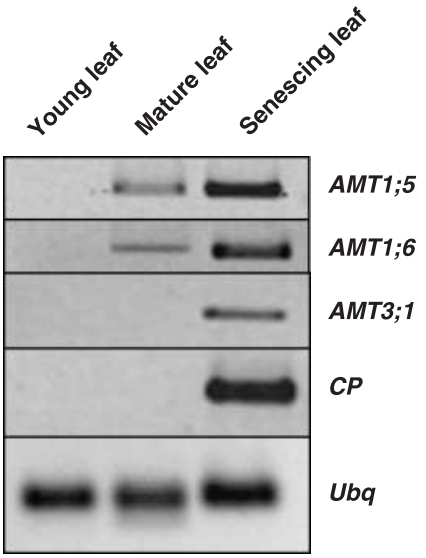

Fig. 6 Senescence-dependent expression of *AMT1;5*, *AMT1;6* and *AMT3;1* in leaves of poplar. Expression of *AMT1;5*, *AMT1;6* and *AMT3;1* was analysed by reverse transcriptase polymerase chain reaction in young, mature and senescing leaves. Aliquots of 300 ng total RNAs were reverse transcribed into cDNA. The ubiquitin (Ubq) gene was amplified and used as an internal control. Cystein protease (CP) was used as a marker of the senescing state (Bhalerao *et al*., 2003). Experiments were repeated for each member at least three times, with similar results.

derepression of *AMT1;5* and full repression of *AMT1;6* in stamens, and the reverse in female flowers.

Effects of mycorrhizal inoculation

Figure 8 shows variations in *AMT* expression levels of roots inoculated with the ectomycorrhizal fungus *Paxillus involutus*, collected after 1 month of growth after contact. Our data indicate a substantial increase of the root *AMT1;2* transcript level, whereas the other root expressed *AMTs* did not show any significant transcript variation (not shown).

In silico analysis of ESTs

An *in silico* analysis of poplar expressed sequence tags (ESTs) was carried out using the GenBank EST databases, from which 69 ESTs corresponding to *AMTs* from poplar could be retrieved. This analysis confirmed the broad distribution of *AMT1;1* and *AMT2;1* transcripts and the root distribution of *AMT1;2* transcripts. The lack of transcript for *AMT1;4* and for some *AMT4* subclade members is also confirmed. Expressed sequences tags corresponding to *AMT1;6* were mostly found in EST database from leaves (Table 3), which agreed with the fact that *AMT1;6* was mostly expressed in shoot tissues (Figs 2, 3, 4, 5 and 6).

Although detected by RT-PCR, no EST was retrieved for *AMT1;5* and *AMT2;2*, probably because there were no EST

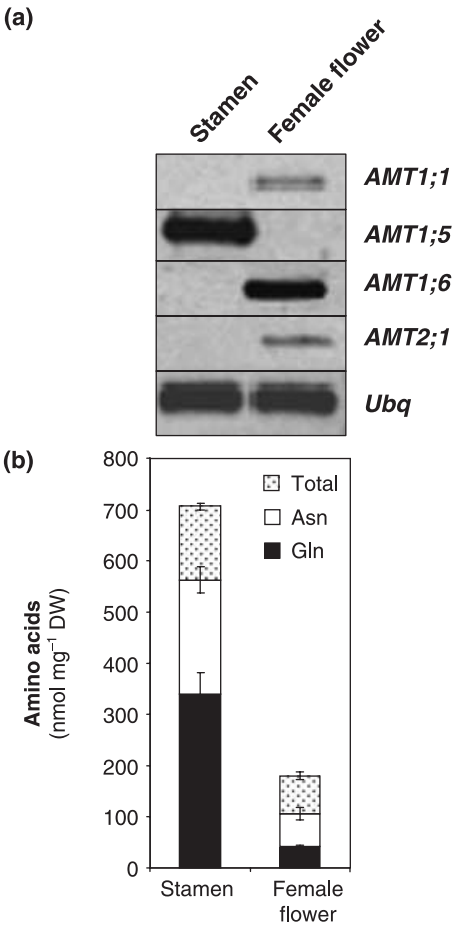

Fig. 7 Specific expression of *AMTs* in reproductive organs of poplar. (a) Expression of *AMT1;1*, *AMT1;5*, *AMT1;6* and *AMT2;1* genes in stamens and female flowers of poplar. Aliquots of 1 μg total RNAs were reverse-transcribed into cDNA. The ubiquitin (Ubq) gene was amplified and used as internal control. Analyses were performed by reverse transcriptase polymerase chain reaction in triplicate. (b) Quantification of free amino acids by gas chromatography-mass spectrometry in stamens and female flowers of poplar. Glutamine (Gln) was the major amino acid in stamens whereas asparagine (Asn) was the major amino acid in female flowers. Values are expressed as means ± SE of three replicate experiments.

databases for the specific tissues, i.e. stamens (*AMT1;5*). Conversely, ESTs were found for *AMT4;2* in floral bud databases, for *AMT3;1* in poplar bark database (Ralph *et al*., 2006) and for *AMT4;5* in poplar cultured cells. These are tissues that we have not investigated in the present study but this opens new perspectives for the search of *AMT4* subgroup transcripts. For *AMT3;1*, transcripts of which were detected specifically in senescing leaves (Fig. 6), four ESTs were retrieved from a leaf EST database, although the development state was not provided in the database. *AMT1;3* was not detected by RT-PCR, although we found five ESTs in leaf databases. However these studies were of *P. euphratica* (three ESTs (Brosche *et al*., 2005)) or systemically wound-induced leaf (two ESTs; Christopher *et al*., 2004) – specific conditions that were not tested in the present study.

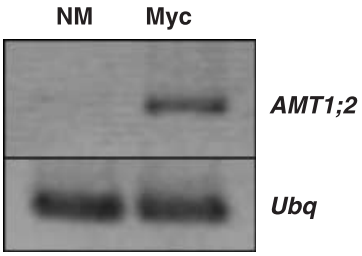

Fig. 8 Impact of ectomycorrhiza formation on *AMT1;2* expression in roots of poplar. Mycorrhizal (Myc) and nonmycorrhizal (NM) roots were collected on Petri dishes grown poplar, in association with *Paxillus involutus*. Aliquots of 200 ng and 100 ng total RNA from Myc and NM roots (to ensure equal amount of root material), respectively, were reverse transcribed into cDNA. The ubiquitin (Ubq) gene was amplified and used as internal control.

Table 3 *In silico* analyses of ammonium transporter (*AMT*) genes in poplars (*Populus*)

Gene name	Number of occurrences in EST database	EST tissue localization	RT-PCR product (present work)
AMT1;1	21	3C, 11L, 2SL, 2S, 1Ba, 1R, 1X	R, L, F, FF, P, B
AMT1;2	13	13R	R
AMT1;3	5	5L	
AMT1;4	0		
AMT1;5	0		R, L, St
AMT1;6	11	11L	L, F, FF, P
AMT2;1	9	1R, 2CC, 2FC, 1FB, 2SL, 1L	L, FF, P
AMT2;2	0		R, P
AMT3;1	7	4L, 1B, 2Ba	SL
AMT4;1	0		
AMT4;2	1	1FB	
AMT4;3	0		
AMT4;4	0		
AMT4;5	2	2CC	R, F

EST, expressed sequences tag; RT-PCR, reverse transcriptase polymerase chain reaction.
Number of occurrences and tissue localizations of *AMT* ESTs retrieved from the EST GenBank database (Altschul *et al*., 1997). Tissues were as follows: B, bud; Ba, bark; C, cambium; CC, cell culture; F, fruit; FB, floral bud; FC, female catkin; FF, female flower; L, leaf; P, petiole; R, root; S, stem; SL, senescing leaf; St, stamen; X, not determined.

Functional expression of AMTs in a yeast mutant defective in NH_4^+ uptake

Yeast has provided a genuine heterologous expression system for characterizing many plant nutrient and metabolite transporters. The yeast strain 31019b is defective in the three endogenous NH_4^+ transporters (*mep1*, *mep2* and *mep3*) and is unable to grow on medium containing 1 mM NH_4^+ as the sole N source (Marini *et al*., 1997). Transformation with the yeast expression vector pFL61 bearing the *AMT1;2*, *AMT1;5*, *AMT1;6*, *AMT2;1* or *AMT2;2* coding sequences under the control of the constitutive yeast phosphoglycerate kinase gene promoter (Minet *et al*., 1992), conferred the ability of 31019b to grow at 1 mM NH_4^+ as the sole N source (Fig. 9). Yeast transformed with empty plasmid (pFL61) was used as a negative control. Thus, all five genes encode functional NH_4^+ transporters. By contrast, the other three-expressed poplar *AMTs* (*AMT1;1*, *AMT3;1* and *AMT4;5*) were unable to complement the Mep deficiency in the yeast strain 31019b. This inability might result from poor targeting to the yeast plasma membrane. Two intron-free *AMTs*, for which transcripts were not detected (*AMT1;3* and *AMT1;4*), were cloned using their genomic sequence and used to transform the triple Mep mutant, but were unable to complement the growth deficiency on low ammonium (data not shown). Cells expressing AMT1; 5 grew less than the control strain on 10 mM ammonium (Fig. 9), suggesting that AMT1;5 expression was toxic to yeast cells.

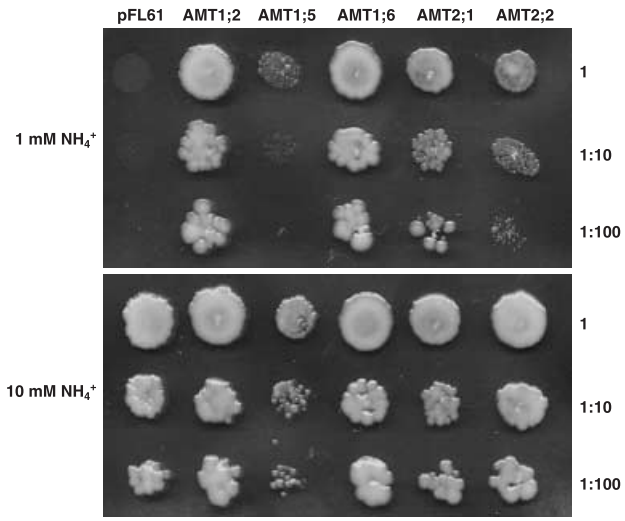

Fig. 9 Complementation of yeast mutant Δmep strain 31019b by poplar ammonium transporters (AMTs). Yeast strain 31019b was transformed with the yeast expression vector pFL61 or pFL61 harboring the coding sequences of *AMT1;2*, *AMT1;5*, *AMT1;6*, *AMT2;1*, or *AMT2;2*. Growth was assayed on minimal medium containing 1 mM or 10 mM NH_4^+ as sole nitrogen source. Pictures were taken after 2 d of growth at 30°C.

We further tested the sensitivity of yeast cells to increasing methylammonium concentrations (Fig. 10). Cells expressing AMT2;1, or AMT2;2 retained the ability to grow on methylammonium, therefore indicating that methylammonium was not taken up by these cells. As found for other AMT2 family members (Sohlenkamp *et al*., 2002), it seems that poplar AMT2;1, or AMT2;2 have a particularly low affinity for methylammonium, whereas AMT1 family members can readily take up methylammonium.

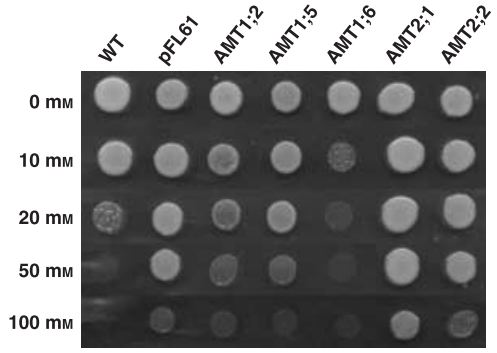

Fig. 10 Sensitivity of yeast cells to toxic concentrations of methylammonium. Yeast strain 31019b was transformed with the yeast expression vector pFL61 or pFL61 harboring the coding sequences of *AMT1;2*, *AMT1;5*, *AMT1;6*, *AMT2;1*, or *AMT2;2*. Growth was assayed on minimal medium containing 0.1% proline supplemented with 0–100 mM methylammonium. Pictures were taken after 3 d of growth at 30°C.

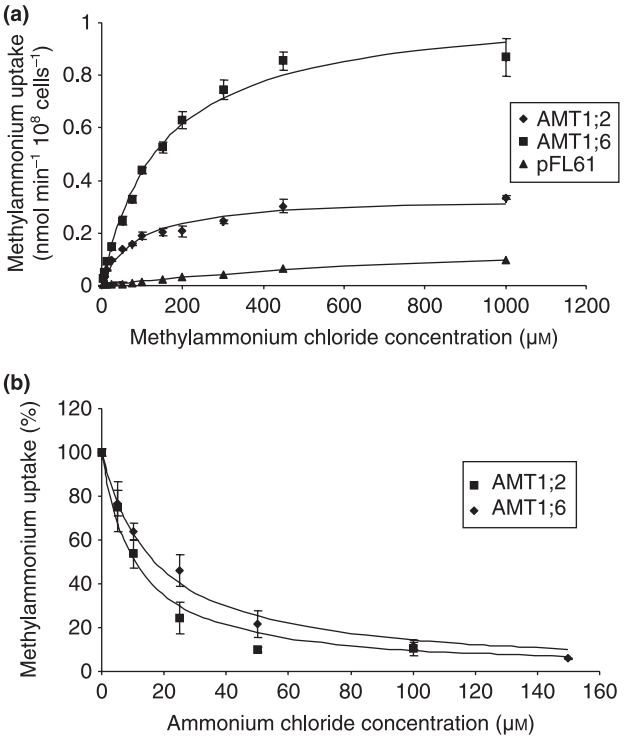

Fig. 11 Kinetic analysis of AMT1;2 and AMT1;6 in transformed yeast. (a) Concentration dependent kinetics of ^{14}C-methylammonium uptake by the yeast strain 31019b (Marini *et al*., 1997) transformed with pFL61 alone or pFL61 harboring *AMT1;2* and *AMT1;6*. (b) Influence of increasing NH_4^+ concentrations on ^{14}C-methylammonium uptake rates. The ^{14}C-methylammonium uptake was measured at the corresponding K_m of each AMT. Values are expressed as means ± SD of three replicate experiments.

Kinetics studies of AMT1;2 and AMT1;6 transporters expressed in yeast

To determine differences in substrate affinities between the AMT proteins, we used ^{14}C-labeled methylammonium as a substrate analog and measured short-term uptake in transformed yeast Δmep strain 31019b. Only members of the AMT1 subfamily showed methylamine uptake capacities (Sohlenkamp *et al*., 2002). Among the AMT1 members, expression of AMT1;2 and AMT1;6 conferred the ability to take up ^{14}C-labeled methylammonium in the range of 0.03–3 mM whereas 31019b transformed with the vector alone (Fig. 11a) did not take up significant amounts of ^{14}C-labeled methylammonium in the same concentration range. Kinetic parameters were calculated from Lineweaver–Burk plots. AMT1;2 displayed a higher affinity (K_m = 45 μM) and a lower capacity (V_m = 0.349 ± 0.007 nmol min^{-1} 10^8 cell^{-1}) for methylammonium than AMT1; 6 (K_m = 85 μM; V_m = 1.058 ± 0.024 nmol min^{-1} 10^8 cell^{-1}). Since the affinities for methylammonium do not necessarily reflect the affinity for ammonium, we performed inhibition studies with varying NH_4^+ concentrations. The K_i values were deduced from Dixon plots, and a 50% inhibition was observed at 11 and 16 μM for AMT1;2 and AMT1;6, respectively (Fig. 11b). Inhibition studies indicated that these two NH_4^+ transporters possess a much higher affinity for NH_4^+ than for methylammonium.

Discussion

An extended *AMT* family in the poplar genome

Analysis of genomes of *Arabidopsis* and rice revealed the presence of six and 10 *AMT* genes, respectively. In the poplar genome, 14 *AMT* genes were identified, and assigned to the AMT1 subfamily (six genes) or to the AMT2 subfamily (eight genes). Interestingly, poplar possesses a much greater number of *AMT2* genes than *Arabidopsis* and a greater number of *AMT1* genes than rice. Although a few poplar *AMT* transcripts were not detectable in any tissue tested in this work, the expression patterns of the expressed members strongly suggest specific features related to the peculiar physiology of a perennial and mycorrhizal tree. Trees differ fundamentally from annual plant species in that they are adapted to survive on a long time-scale. The most obvious manifestation of this is the development of wood, or secondary xylem, from the vascular cambium. This secondary meristem is essential for tree growth and development and in providing support for a tall structure. Taken with caution, a comparison of the number of *AMT* genes in different species might suggest that plant species from different environments or with different life style organize ammonium transport with a fairly unequal number of ammonium transporters.

The root specific *AMT1;2* is highly regulated by N availability and mycorrhization

AMT1;2 was specifically and highly expressed in roots (Figs 4 and 5). Determination of affinity constants for ^{14}C methylammonium uptake by AMT1;2 in yeast and transport inhibition by NH_4^+ revealed that this protein is a high-affinity ammonium transporter (K_m NH_4^+ = 11 μM), indicating that it might be partly responsible for the HATS ammonium uptake component measured in *Populus* species (Min *et al.*, 2000). The downregulation of *AMT* transcript in N-fed *P. tremula* × *alba* root is consistent with the downregulation of HATS ammonium influx measured in *P. tremuloides* (Min *et al.*, 2000). Indeed, *AMT1;2* transcript levels in poplar (Fig. 4a) negatively correlated with root glutamine concentrations (Fig. 3b), as already demonstrated for *AtAMT1;1* (Rawat *et al.*, 1999) and *LeAMT1;1* (von Wiren *et al.*, 2000b). *AMT1;2* seems to represent the functional ortholog of *AtAMT1;1* and *LeAMT1;1*. However, prolonged incubation in a N-deficient growth medium resulted in a decrease of the *AMT1;2* transcript level, probably owing to the appearance of proteolysis-derived ammonia. In addition, *AMT1;2* was overexpressed in *P. involutus* mycorrhizal roots. Indeed, expression of its closest ortholog *PttAMT1;2* from *Populus tremula* × *tremuloides* was increased fourfold in the ectomycorrhizal symbiosis between *P. tremula* × *tremuloides* and *Amanita muscaria*, suggesting an increased ammonium uptake capacity of mycorrhizal poplar roots (Selle *et al.*, 2005). Recent studies on the arbuscular mycorrhizal fungus *Glomus intraradices* demonstrated that ammonium is exported by intraradical hyphae in arbuscular mycorrhizal symbiosis (Govindarajulu *et al.*, 2005), suggesting that ammonium could be a major source of fungus-derived N in mycorrhizal symbiosis (Chalot *et al.*, 2006).

In roots, four other *AMT* genes, *AMT1;1* (Fig. 4), *AMT1;5* (Table 3), *AMT2;2* (Fig. 2) and *AMT4;5* (Table 3) were expressed, reflecting a potential role in covering the N demand through uptake of soil NH_4^+ in various N regime. Although the kinetic parameters were not determined for this subset of genes, we might hypothesize that some of them could be involved in the LATS component of ammonium influx (Min *et al.*, 2000), or in the retrieval of leaked ammonium (von Wiren *et al.*, 2000a). However, they were also expressed in other poplar tissues such as petiole (*AMT1;1* and *AMT2;2*) or stamen (*AMT1;5*) and therefore a specific function in root uptake can be ruled out.

The shoot-specific *AMT1;6* and *AMT3;1* are strongly upregulated during senescence

Several lines of evidence indicate that transport of NH_4^+, and hence leaf-expressed *AMTs*, might be of particular importance for N nutrition and metabolism in leaves. First, NH_4^+ can be imported from the atmosphere into leaf cells through stomata (Husted & Schjoerring, 1996). Second, significant concentrations of NH_4^+ have been measured in the xylem (Rawat *et al.*, 1999), indicating that a considerable amount of N is translocated to shoots in this form. Third, the photorespiratory N cycle generates a large amount of NH_4^+ in leaf mitochondria that is subsequently transported to chloroplasts for reassimilation by GS, implying that the expression of *AMT* genes can be important to ensure the recycling of NH_4^+ during photorespiration (D'Apuzzo *et al.*, 2004). Finally, the AMTs might also be recruited during the senescing process.

Expression of *AMT1;6, AMT2;1* and *AMT3;1* was exclusively detected in shoot tissues (Table 3). *AMT1;6* is the closest ortholog of *LeAMT1;3* in tomato (von Wiren *et al.*, 2000b) and both genes form a distant clade in the AMT1 subfamily (Fig. 1). AMT1;6 complemented the triple ΔMep yeast strain (Fig. 9) and had a high affinity constant (K_m NH_4^+ = 16 μM) comparable to that of AMT1;2 (Fig. 11b). It was suggested that LeAMT1;3 might be linked to the synthesis of asparagine as a N storage form in darkness or to the deamination of glutamate by glutamate dehydrogenase (von Wiren *et al.*, 2000b). Consistent with this observation, *AMT1;6* transcripts declined under N starvation in poplar (Fig. 4b), which was characterized by a decrease of the asparagine pool (Fig. 3c). In *Arabidopsis*, asparagine synthetase is encoded by a small gene family (*ASN1*, *ASN2* and *ASN3*) and it has been shown that *ASN2* expression correlates with ammonium metabolism (Wong *et al.*, 2004). Indeed, the light induction of *ASN2* is ammonium dependent and *ASN2* transcripts decreased after transfer to ammonium-free growth medium. It has been suggested that the physiological role of *ASN2* may be related, directly or indirectly to the recapture of lost N resources under stress conditions. However, the hypothesis that LeAMT1;3 is involved in the transport of photorespiratory NH_4^+ was not supported. *AMT1;6* expression was strongly affected by the diurnal cycle (Fig. 5b) and correlated well with the sugar content. This is in good agreement with a recent report, which indicated that sugars make a major contribution to the diurnal changes of gene expression, while light, N metabolites and water deficit may make smaller contributions (Blasing *et al.*, 2005).

Expression of *AMT1;5, AMT1;6* and *AMT3;1* increased with the state of maturation of leaves and highly correlated with the expression of the marker gene, cysteine protease whose implication in senescence has been revealed (Bhalerao *et al.*, 2003) (Fig. 6). However, in contrast to *AMT1;5* and *AMT1;6*, *AMT3;1* expression was only detected in senescing leaves. Ammonium release during senescence has been documented (Mattsson & Schjoerring, 2003) and the specific expression of the glutamine synthetase gene *NtGLN 1;3* was observed in senescing leaves of *Nicotiana tabacum* (Brugiere *et al.* 2000). In addition to the putative function of AMT2 members during leaf senescence (Howitt & Udvardi, 2000; von Wiren *et al.*, 2000a; van der Graaff *et al.*, 2006), our data suggest that AMT1 members might also be recruited

to ensure ammonium assimilation during the process of leaf senescence.

It is also worth noting the contrasting expression patterns of *AMT1;5* and *AMT1;6*: both were fully expressed in senescing leaves (Fig. 6), but the expression of *AMT1;5* in flowers was specific to stamens and that of *AMT1;6* specific to female flowers (Fig. 7a). The higher expression of *AMT1;5* in stamens (Fig. 7) is in good agreement with data on its closest ortholog *AtAMT1;4*. Indeed, to complement the poplar data, we extracted GENEVESTIGATOR (Zimmermann *et al.*, 2004) (www.genevestigator.ethz.ch) data for the *Arabidopsis* AMT gene family, which indicated that *AtAMT1;4* was solely expressed in male flower but not in female flower parts. *AMT1;5* and *AMT1;6*, might have important and specific roles in reproductive organ development in the dioecious plant, poplar. Further functional analysis is required to establish the precise role of AMTs and their correlation to plant reproduction mechanisms.

The two *AMT* genes *AMT2;1* and *AMT2;2* have been partly subfunctionalized during poplar evolution

AMT2;1 and AMT2;2 restored growth of the triple Mep mutant (Fig. 9) but were unable to take up methylamine, as demonstrated for other AMT2 members (Simon-Rosin *et al.*, 2003). The single members of the AMT2 subfamily in *Arabidopsis* and *L. japonicus*, as well as the closest ortholog in rice (*OsAMT2;1*) were expressed in all organs (Sohlenkamp *et al.*, 2002; Simon-Rosin *et al.*, 2003; Suenaga *et al.*, 2003). AtAMT2 was suggested to play a significant role in transferring ammonium between the apoplast and symplast of cells throughout the plant. Although expression of *AtAMT2* in shoots responded little to changes in root N status, transcript levels in leaves declined under high CO_2 conditions (Sohlenkamp *et al.*, 2002). The *LjAMT2;1* gene was found to be constitutively expressed throughout *Lotus* plants particularly in all major tissues of nodules. LjAMT2;1 would be implicated in the recovery of ammonium lost from nodule cells by efflux. A similar role may be fulfilled in other organs, especially leaves, which liberate ammonium during normal metabolism (Simon-Rosin *et al.*, 2003). Unlike other plant species, this set of *AMT* genes in poplar displayed specific expression pattern, *AMT2;2* being mostly expressed in petiole and *AMT2;1* being highly expressed in leaves (Fig. 2). *AMT2;2* and *AMT2;1* arose from a recent duplication event (Sterck *et al.*, 2005; Tuskan *et al.*, 2006), which, in addition, resulted in a functional specialization (this work). The release of duplicate copies from constraints enables the evolution of new functions (neofunctionalization) or the loss of function (formation of a pseudogene), as observed for MADS-box genes (Irish & Litt, 2005). Alternatively, duplicated gene copies can potentially diverge in their roles, retaining different subfunctions of the original gene. The distribution and tissue localization of this subset of *AMT2* genes in various plant species (*AtAMT2;1*, *LjAMT2;1*, *OsAMT2;1*, *AMT2;1* and *AMT2;2*) suggest that the two poplar genes have been partly subfunctionalized during poplar evolution.

The high expression of *AMT1;1* and *AMT2;2* in petiole tissues is intriguing (Fig. 2). Much controversy exists about whether or not NH_4^+ is translocated in the xylem from roots to shoots. It was demonstrated that NH_4^+ might indeed constitute a significant part of the N translocated from the roots to the shoot in the xylem. A fundamental requirement for ammonium translocation is the presence of transport systems capable of loading NH_4^+ into the xylem and of subsequently moving NH_4^+ from the leaf apoplast solution into the leaf cells (Schjoerring *et al.*, 2002). Furthermore, significant NH_4^+ contents were measured in the phloem sap of ammonium-fed tobacco plants, which was correlated with a higher glutamate dehydrogenase activity and polypeptide content in stems (Terce-Laforgue *et al.*, 2004). Considering the frequency of plasmodesmata along the palisade cell/bundle sheath cell/companion cell and paraveinal mesophyll cell/bundle sheath cell/companion cell routes, Russin & Evert (1985) concluded that *Populus deltoides* would rather behave as a symplastic loader, suggesting that N compounds may also use the symplastic route for loading. In that case, active transport would not be required during these transfer steps. The compartmentalization of the ammonia assimilatory pathway in the vascular tissue, especially in perennial plants (Paczek *et al.*, 2002), to better control carbon and N allocation at particular stages of plant development and/or under certain physiological conditions, needs to be better assessed.

Conclusion

The analysis of the *AMT* expression patterns in different organs of poplar show that expression of a given transporter can be very specific or can overlap with other genes, thus covering most tissues tested so far in poplar. The cell specificity of the individual members still remains to be demonstrated. The present data could show that multiple *AMT* genes with different spatial expression and transcriptional regulation allow the plant to respond differentially to varying nutritional conditions in the environment. Specific features of the perennial lifestyle plant, such as a high potential for ammonium remobilization during senescence or upon ectomycorrhization, together with subfunctionalization of AMT members, have been highlighted. The elucidation of the AMT gene family may present a comprehensive foundation for future studies on the ammonium nutrition of perennial plants.

Acknowledgements

B.M. was supported by a postdoctoral fellowship and J.C. by a PhD fellowship from the 'Ministère délégué à l'Enseignement supérieur et à la Recherche'. We thank Prof. Simone Ottonello

(University Parma, Italy) for providing facilities for yeast uptake experiments and Dr Pascal Frey and Veronica Pereda (INRA Nancy) for providing leaf material. Financial support from the IFR 110 (Génomiques, Ecophysiologie et Ecologie fonctionnelle) is gratefully acknowledged.

References

Altschul SF, Madden TL, Schaffer AA, Zhang JH, Zhang Z, Miller W, Lipman DJ. 1997. Gapped BLAST and PSI-BLAST – a new generation of protein database search programs. *Nucleic Acids Research* **25**: 3389–3402.

Andersson A, Keskitalo J, Sjodin A, *et al.* 2004. A transcriptional timetable of autumn senescence. *Genome Biology* **5**: R24.

Becker D, Stanke R, Fendrik I, Frommer WB, Vanderleyden J, Kaiser WM, Hedrich R. 2002. Expression of the NH_4^+-transporter gene LeAMT1; 2 is induced in tomato roots upon association with N_2-fixing bacteria. *Planta* **215**: 424–429.

Bhalerao R, Keskitalo J, Sterky F, Erlandsson R, Bjorkbacka H, Birve SJ, Karlsson J, Gardestrom P, Gustafsson P, Lundeberg J, Jansson S. 2003. Gene expression in autumn leaves. *Plant Physiology* **131**: 430–442.

Blasing OE, Gibon Y, Gunther M, Hohne M, Morcuende R, Osuna D, Thimm O, Usadel B, Scheible WR, Stitt M. 2005. Sugars and circadian regulation make major contributions to the global regulation of diurnal gene expression in *Arabidopsis*. *Plant Cell* **17**: 3257–3281.

Brosche M, Vinocur B, Alatalo ER, Lamminmaki A, Teichmann T, Ottow EA, Djilianov D, Afif D, Bogeat-Triboulot MB, Altman A, Polle A, Dreyer E, Rudd S, Paulin L, Auvinen P, Kangasjarvi J. 2005. Gene expression and metabolite profiling of *Populus euphratica* growing in the Negev desert. *Genome Biology* **6**: R101.

Brugiere N, Dubois F, Masclaux C, Sangwan RS, Hirel B. 2000. Immunolocalization of glutamine synthetase in senescing tobacco (*Nicotiana tabacum* L.) leaves suggests that ammonia assimilation is progressively shifted to the mesophyll cytosol. *Planta* **211**: 519–527.

Chalot M, Blaudez D, Brun A. 2006. Ammonia: a candidate for nitrogen transfer at the mycorrhizal interface. *Trends in Plant Sciences* **11**: 263–266.

Christopher ME, Miranda M, Major IT, Constabel CP. 2004. Gene expression profiling of systemically wound-induced defenses in hybrid poplar. *Planta* **219**: 936–947.

Crooks GE, Hon G, Chandonia JM, Brenner SE. 2004. WebLogo: a sequence logo generator. *Genome Research* **14**: 1188–1190.

D'Apuzzo E, Rogato A, Simon-Rosin U, El Alaoui H, Barbulova A, Betti M, Dimou M, Katinakis P, Marquez A, Marini AM, Udvardi MK, Chiurazzi M. 2004. Characterization of three functional high-affinity ammonium transporters in *Lotus japonicus* with differential transcriptional regulation and spatial expression. *Plant Physiology* **134**: 1763–1774.

Gazzarrini S, Lejay L, Gojon A, Ninnemann O, Frommer WB, von Wiren N. 1999. Three functional transporters for constitutive, diurnally regulated, and starvation-induced uptake of ammonium into *Arabidopsis* roots. *Plant Cell* **11**: 937–948.

Govindarajulu M, Pfeffer PE, Jin H, Abubaker J, Douds DD, Allen JW, Bucking H, Lammers PJ, Shachar-Hill Y. 2005. Nitrogen transfer in the arbuscular mycorrhizal symbiosis. *Nature* **435**: 819–823.

van der Graaff E, Schwacke R, Schneider A, Desimone M, Flugge U-I, Kunze R. 2006. Transcription analysis of *Arabidopsis* membrane transporters and hormone pathways during developmental and induced leaf senescence. *Plant Physiology* **141**: 776–792.

Howitt SM, Udvardi MK. 2000. Structure, function and regulation of ammonium transporters in plants. *Biochimica Biophysica Acta* **1465**: 152–170.

Husted S, Schjoerring JK. 1996. Ammonia flux between oilseed rape plants and the atmosphere in response to changes in leaf temperature, light intensity, and air humidity (interactions with leaf conductance and apoplastic NH_4^+ and H^+ concentrations). *Plant Physiology* **112**: 67–74.

Irish VF, Litt A. 2005. Flower development and evolution: gene duplication, diversification and redeployment. *Current Opinion in Genetic Development* **15**: 454–460.

Javelle A, Morel M, Rodriguez-Pastrana BR, Botton B, Andre B, Marini AM, Brun A, Chalot M. 2003. Molecular characterization, function and regulation of ammonium transporters (Amt) and ammonium-metabolizing enzymes (GS, NADP-GDH) in the ectomycorrhizal fungus *Hebeloma cylindrosporum*. *Molecular Microbiology* **47**: 411–430.

Kaiser BN, Rawat SR, Siddiqi MY, Masle J, Glass AD. 2002. Functional analysis of an *Arabidopsis* T-DNA 'knockout' of the high-affinity NH_4^+ transporter AtAMT1;1. *Plant Physiology* **130**: 1263–1275.

Kohler A, Delaruelle C, Martin D, Encelot N, Martin F. 2003. The poplar root transcriptome: analysis of 7000 expressed sequence tags. *FEBS Letters* **542**: 37–41.

Kumar S, Tamura K, Nei M. 2004. MEGA3: Integrated software for Molecular Evolutionary Genetics Analysis and sequence alignment. *Brief Bioinformatics* **5**: 150–163.

Lauter FR, Ninnemann O, Bucher M, Riesmeier JW, Frommer WB. 1996. Preferential expression of an ammonium transporter and of two putative nitrate transporters in root hairs of tomato. *Proceedings of the National Academy of Sciences, USA* **93**: 8139–8144.

Loque D, von Wiren N. 2004. Regulatory levels for the transport of ammonium in plant roots. *Journal of Experimental Botany* **55**: 1293–1305.

Ludewig U, von Wiren N, Frommer WB. 2002. Uniport of NH_4^+ by the root hair plasma membrane ammonium transporter LeAMT1; 1. *Journal of Biological Chemistry* **277**: 13548–13555.

Marini AM, Andre B. 2000. *In vivo* N-glycosylation of the mep2 high-affinity ammonium transporter of *Saccharomyces cerevisiae* reveals an extracytosolic N-terminus. *Molecular Microbiology* **38**: 552–564.

Marini AM, Vissers S, Urrestarazu A, Andre B. 1994. Cloning and expression of the MEP1 gene encoding an ammonium transporter in *Saccharomyces cerevisiae*. *EMBO Journal* **13**: 3456–3463.

Marini AM, Soussi-Boudekou S, Vissers S, Andre B. 1997. A family of ammonium transporters in *Saccharomyces cerevisiae*. *Molecular Cellular Biology* **17**: 4282–4293.

Mattsson M, Schjoerring JK. 2003. Senescence-induced changes in apoplastic and bulk tissue ammonia concentrations of ryegrass leaves. *New Phytologist* **160**: 489–499.

Miller GL. 1959. Use of dinitrosalicylic acid reagent for determination of reducing sugar. *Analytical Chemistry* **31**: 426–428.

Min X, Siddiqi MY, Guy RD, Glass ADM, Kronzucker HJ. 2000. A comparative kinetic analysis of nitrate and ammonium influx in two early-successional tree species of temperate and boreal forest ecosystems. *Plant, Cell & Environment* **23**: 321–328.

Minet M, Dufour ME, Lacroute F. 1992. Complementation of *Saccharomyces cerevisiae* auxotrophic mutants by *Arabidopsis thaliana* cDNAs. *Plant Journal* **2**: 417–422.

Montanini B, Moretto N, Soragni E, Percudani R, Ottonello S. 2002. A high-affinity ammonium transporter from the mycorrhizal ascomycete *Tuber borchii*. *Fungal Genetics and Biology* **36**: 22–34.

Murashige T, Skoog F. 1962. A revised medium for the growth and bioassay with tobacco tissue culture. *Physiologia Plantarum* **15**: 473–497.

Ninnemann O, Jauniaux JC, Frommer WB. 1994. Identification of a high affinity NH_4^+ transporter from plants. *EMBO Journal* **13**: 3464–3471.

Paczek V, Dubois F, Sangwan R, Morot-Gaudry JF, Roubelakis-Angelakis KA, Hirel B. 2002. Cellular and subcellular localisation of glutamine synthetase and glutamate dehydrogenase in grapes gives new insights on the regulation of carbon and nitrogen metabolism. *Planta* **216**: 245–254.

Pearson JN, Finnemann J, Schjoerring JK. 2002. Regulation of the high-affinity ammonium transporter (BnAMT1; 2) in the leaves of *Brassica napus* by nitrogen status. *Plant Molecular Biology* **49**: 483–490.

Ralph S, Oddy C, Cooper D, *et al.* 2006. Genomics of hybrid poplar (*Populus trichocarpa* × *deltoides*) interacting with forest tent caterpillars (*Malacosoma disstria*): normalized and full-length cDNA libraries, expressed sequence tags, and a cDNA microarray for the study of insect-induced defences in poplar. *Molecular Ecology* **15**: 1275–1297.

Rawat SR, Silim SN, Kronzucker HJ, Siddiqi MY, Glass AD. 1999. AtAMT1 gene expression and NH_4^+ uptake in roots of *Arabidopsis thaliana*: evidence for regulation by root glutamine levels. *Plant Journal* **19**: 143–152.

Russin WA, Evert RF. 1985. Studies on the leaf of *Populus deltoides* (Salicaceae): ultrastructure, plasmodesmatal frequency, and solute concentrations. *American Journal of Botany* **72**: 1256–1273.

Saier MH Jr. 1998. Molecular phylogeny as a basis for the classification of transport proteins from bacteria, archaea and eukarya. *Advances in Microbial Physiology* **40**: 81–136.

Salvemini F, Marini A, Riccio A, Patriarca EJ, Chiurazzi M. 2001. Functional characterization of an ammonium transporter gene from *Lotus japonicus*. *Gene* **270**: 237–243.

Schjoerring JK, Husted S, Mack G, Mattsson M. 2002. The regulation of ammonium translocation in plants. *Journal of Experimental Botany* **53**: 883–890.

Schwacke R, Schneider A, van der Graaff E, Fischer K, Catoni E, Desimone M, Frommer WB, Flugge UI, Kunze R. 2003. ARAMEMNON, a novel database for *Arabidopsis* integral membrane proteins. *Plant Physiology* **131**: 16–26.

Selle A, Willmann M, Grunze N, Gessler A, Weiss M, Nehls U. 2005. The high-affinity poplar ammonium importer PttAMT1.2 and its role in ectomycorrhizal symbiosis. *New Phytologist* **168**: 697–706.

Shelden MC, Dong B, De Bruxelles GL, Trevaskis B, Whelan J, Ryan PR, Howitt SM, Udvardi MK. 2001. *Arabidopsis* ammonium transporters, AtAMT1;1 and AtAMT1;2, have different biochemical properties and functional roles. *Plant and Soil* 231: 151–160.

Simon-Rosin U, Wood C, Udvardi MK. 2003. Molecular and cellular characterisation of LjAMT2; 1, an ammonium transporter from the model legume *Lotus japonicus*. *Plant Molecular Biology* **51**: 99–108.

Sohlenkamp C, Wood CC, Roeb GW, Udvardi MK. 2002. Characterization of *Arabidopsis* AtAMT2, a high-affinity ammonium transporter of the plasma membrane. *Plant Physiology* **130**: 1788–1796.

Sonoda Y, Ikeda A, Saiki S, von Wiren N, Yamaya T, Yamaguchi J. 2003. Distinct expression and function of three ammonium transporter genes (OsAMT1; 1–1; 3) in rice. *Plant and Cell Physiology* **44**: 726–734.

Sterck L, Rombauts S, Jansson S, Sterky F, Rouze P, van de Peer Y. 2005. EST data suggest that poplar is an ancient polyploid. *New Phytologist* **167**: 165–170.

Sterky F, Bhalerao RR, Unneberg P, Segerman B, Nilsson P, Brunner AM, Charbonnel-Campaa L, Lindvall JJ, Tandre K, Strauss SH, Sundberg B, Gustafsson P, Uhlen M, Bhalerao RP, Nilsson O, Sandberg G, Karlsson J, Lundeberg J, Jansson S. 2004. A Populus EST resource for plant functional genomics. *Proceedings of the National Academy of Sciences, USA* **101**: 13951–13956.

Suarez MF, Avila C, Gallardo F, Canton FR, Garcia-Gutierrez A, Claros MG, Canovas FM. 2002. Molecular and enzymatic analysis of ammonium assimilation in woody plants. *Journal of Experimental Botany* **53**: 891–904.

Suenaga A, Moriya K, Sonoda Y, Ikeda A, von Wiren N, Hayakawa T, Yamaguchi J, Yamaya T. 2003. Constitutive expression of a novel-type ammonium transporter OsAMT2 in rice plants. *Plant and Cell Physiology* **44**: 206–211.

Taira M, Valtersson U, Burkhardt B, Ludwig RA. 2004. *Arabidopsis thaliana* GLN2-encoded glutamine synthetase is dual targeted to leaf mitochondria and chloroplasts. *Plant Cell* **16**: 2048–2058.

Terce-Laforgue T, Dubois F, Ferrario-Mery S, de Crecenzo MA, Sangwan R, Hirel B. 2004. Glutamate dehydrogenase of tobacco is mainly induced in the cytosol of phloem companion cells when ammonia is provided either externally or released during photorespiration. *Plant Physiology* **136**: 4308–4317.

Thomas GH, Mullins JG, Merrick M. 2000. Membrane topology of the Mep/Amt family of ammonium transporters. *Molecular Microbiology* **37**: 331–344.

Tuskan GA, Difazio S, Jansson S, *et al.* 2006. The genome of black cottonwood, *Populus trichocarpa* (Torr. & Gray). *Science* **313**: 1596–1604.

von Wiren N, Gazzarrini S, Gojon A, Frommer WB. 2000a. The molecular physiology of ammonium uptake and retrieval. *Current Opinion in Plant Biology* **3**: 254–261.

von Wiren N, Lauter FR, Ninnemann O, Gillissen B, Walch-Liu P, Engels C, Jost W, Frommer WB. 2000b. Differential regulation of three functional ammonium transporter genes by nitrogen in root hairs and by light in leaves of tomato. *Plant Journal* **21**: 167–175.

Wong HK, Chan HK, Coruzzi GM, Lam HM. 2004. Correlation of ASN2 gene expression with ammonium metabolism in *Arabidopsis*. *Plant Physiology* **134**: 332–338.

Zimmermann P, Hirsch-Hoffmann M, Hennig L, Gruissem W. 2004. GENEVESTIGATOR. *Arabidopsis* microarray database and analysis toolbox. *Plant Physiology* **136**: 2621–2632.

Supplementary Material

The following supplementary material is available for this article online:

Fig. S1 Linkage map positions of ammonium transporter (AMT) poplar genes.

Table S1 Ratios (ammonium transporter (AMT) expression/ubiquitin (UBQ) expression) were calculated for each gene

This material is available as part of the online article from: http://www.blackwell-synergy.com/doi/abs/10.1111/j.1469-8137.2007.01992.x
(This link will take you to the article abstract).

Please note: Blackwell Publishing are not responsible for the content or functionality of any supplementary materials supplied by the authors. Any queries (other than missing material) should be directed to the corresponding author for the article.

THE JOURNAL OF BIOLOGICAL CHEMISTRY VOL. 286, NO. 31, pp. 27515–27527, August 5, 2011

Arabidopsis Chloroplastic Glutaredoxin C5 as a Model to Explore Molecular Determinants for Iron-Sulfur Cluster Binding into Glutaredoxins*[S]

Received for publication, February 7, 2011, and in revised form, May 17, 2011 Published, JBC Papers in Press, June 1, 2011, DOI 10.1074/jbc.M111.228726

Jérémy Couturier[‡§1], Elke Ströher[§1], Angela-Nadia Albetel[¶1], Thomas Roret[‖1], Meenakumari Muthuramalingam[§], Lionel Tarrago[‡], Thorsten Seidel[§], Pascale Tsan[‖], Jean-Pierre Jacquot[‡], Michael K. Johnson[¶], Karl-Josef Dietz[§], Claude Didierjean[‖2], and Nicolas Rouhier[‡3]

From the [‡]Unité Mixte de Recherches (UMR) 1136, Institut National de la Recherche Agronomique-Nancy Université, Interactions Arbres Microorganismes, Institut Fédératif de Recherche 110 Ecosystèmes Forestiers, Agroressources, Biomolécule et Alimentation, 54506 Vandoeuvre-lès-Nancy Cedex, France, [§]Faculty of Biology-W5-134, University of Bielefeld, D-33501 Bielefeld, Germany, [¶]Department of Chemistry and Center for Metalloenzyme Studies, University of Georgia, Athens, Georgia 30602, and [‖]Cristallographie, Résonance Magnétique et Modélisations, Equipe Biocristallographie, UMR 7036 CNRS-Université Henri Poincaré Faculté des Sciences et Technologies, Nancy Université, BP 239, 54506 Vandoeuvre-lès-Nancy Cedex, France

Unlike thioredoxins, glutaredoxins are involved in iron-sulfur cluster assembly and in reduction of specific disulfides (*i.e.* protein-glutathione adducts), and thus they are also important redox regulators of chloroplast metabolism. Using GFP fusion, AtGrxC5 isoform, present exclusively in Brassicaceae, was shown to be localized in chloroplasts. A comparison of the biochemical, structural, and spectroscopic properties of *Arabidopsis* GrxC5 (WCSYC active site) with poplar GrxS12 (WCSYS active site), a chloroplastic paralog, indicated that, contrary to the solely apomonomeric GrxS12 isoform, AtGrxC5 exists as two forms when expressed in *Escherichia coli*. The monomeric apoprotein possesses deglutathionylation activity mediating the recycling of plastidial methionine sulfoxide reductase B1 and peroxiredoxin IIE, whereas the dimeric holoprotein incorporates a [2Fe-2S] cluster. Site-directed mutagenesis experiments and resolution of the x-ray crystal structure of AtGrxC5 in its holoform revealed that, although not involved in its ligation, the presence of the second active site cysteine (Cys^{32}) is required for cluster formation. In addition, thiol titrations, fluorescence measurements, and mass spectrometry analyses showed that, despite the presence of a dithiol active site, AtGrxC5 does not form any inter- or intramolecular disulfide bond and that its activity exclusively relies on a monothiol mechanism.

Glutaredoxins (Grxs)[4] are thiol-disulfide oxidoreductases present in most prokaryotic and eukaryotic organisms and belonging to the thioredoxin (Trx) superfamily (1, 2). At the structural level, proteins of the Trx superfamily share the so-called Trx fold, which consists of four-stranded β-sheets surrounded by at least three α-helices (3). Using a C*XX*C or C*XX*S active site motif, Grxs are involved in the reduction of glutathionylated proteins. The regeneration of an active reduced form usually relies on glutathione (GSH), but some specific members such as human Grx2, *Escherichia coli* Grx4, and *Chlamydomonas reinhardtii* Grx3 are also or uniquely regenerated by thioredoxin reductases (4–6). This variation correlates with the type of Grx considered and depends on their redox potential and catalytic mechanism. Indeed, whereas classical Grxs have midpoint redox potentials between −170 and −230 mV (pH 7.0) (7, 8), *Chlamydomonas* Grx3 forms during its catalytic cycle an atypical intramolecular disulfide between the first active site cysteine and a second cysteine located in the C-terminal part of the protein (6). The more negative redox potential (−323 mV at pH 7.9) observed for this protein most likely explains its ability to receive electrons from ferredoxin:thioredoxin reductase but not from glutathione (6).

The initial Grx classification in non-plant organisms was first based on the active site sequences and resulted in defining two Grx types containing either a dithiol (CP(Y/F)C) or a monothiol (usually CGFS) active site motif (9). However, with the identification of new Grx sequences with more variable active site sequences, this classification has become insufficient. In particular, photosynthetic organisms possess a larger variety of Grxs with about 30 genes compared with two to seven in other prokaryotes or eukaryotes (10). An in-depth phylogenetic analysis of Grxs in photosynthetic organisms indicates that they are grouped into four classes (11). Class I includes "classical" Grxs with CPYC, CGYC, CPFC, or CSY(C/S) active sites and is sub-

* This work was supported, in whole or in part, by National Institutes of Health Grant GM62524 (to M. K. J.). This work was also supported by the Alexander von Humboldt Foundation (to J. P. J.), Agence Nationale de la Recherche Grant JC07_204825 (to J. C. and N. R.), and Deutsche Forschungsgemeinschaft Grant Di346-14 (to K. J. D.).

[S] The on-line version of this article (available at http://www.jbc.org) contains supplemental Tables 1–3 and Figs. 1–4.

The atomic coordinates and structure factors (codes 3RHB and 3RHC) have been deposited in the Protein Data Bank, Research Collaboratory for Structural Bioinformatics, Rutgers University, New Brunswick, NJ (http://www.rcsb.org/).

[1] These authors contributed equally to this work.
[2] To whom correspondence may be addressed. Tel.: 33383684879; E-mail: Claude.Didierjean@crm2.uhp-nancy.fr.
[3] To whom correspondence may be addressed. Tel.: 33383684225; E-mail: nrouhier@scbiol.uhp-nancy.fr.

[4] The abbreviations used are: Grx, glutaredoxin; GSH, reduced glutathione; Trx, thioredoxin; At, *A. thaliana*; Pt, poplar; HED, 2-hydroxyethyl disulfide; CFP, cyan fluorescent protein; DTT_{red}, reduced DTT; DTT_{ox}, oxidized DTT; GSSG, oxidized glutathione; DHA, dehydroascorbate; Prx, peroxiredoxin; Cr, *C. reinhardtii*.

divided into five subgroups called GrxC1, -C2, -C3, -C4 and -C5/S12. Class II contains Grxs with a conserved CGFS active site and is divided into four subgroups called GrxS14, -S15, -S16, and -S17. In addition, class III, which contains Grxs with a *CCXX* active site motif, is found in terrestrial plants, and class IV, which consists of multidomain proteins containing in their N-terminal part a Grx module, is present in eukaryotic photosynthetic organisms (11).

Through their disulfide reductase activity, class I Grxs are involved in the stress response, catalyzing the reduction of dehydroascorbate (12), and the regeneration of type II peroxiredoxins (13) and 1-Cys methionine sulfoxide reductase B1 (14, 15). These regeneration mechanisms likely occur via a glutathionylation step. Although Trxs have been reported to catalyze deglutathionylation in some organisms (16), this reaction is generally considered to be specifically catalyzed by Grxs (17). Protein deglutathionylation can proceed via a monothiol or a dithiol pathway depending on the involvement of one or two cysteines in the catalytic mechanism (6, 18, 19).

Besides its disulfide reductase activity, a novel function assigned to some bacterial, yeast, human, and plant class II Grxs is their involvement in the iron-sulfur (Fe-S) cluster assembly machinery most likely through their capacity to incorporate labile Fe-S clusters and transfer them to acceptor proteins (20–22). On the other hand, specific class I Grxs such as human Grx2 and plant GrxC1 also have the capacity to incorporate Fe-S clusters that are more stable than those found in class II Grxs (8, 23). Based on the observation that oxidized glutathione promotes cluster disassembly in human Grx2, it has been hypothesized that under defined redox conditions the release of Grxs in an active form might serve as a redox sensor in human cells (23).

The determination of the three-dimensional structure of poplar GrxC1 and human Grx2 indicated that the [2Fe-2S] cluster was ligated into a homodimer by the N-terminal active site cysteine of two monomers and two glutathione molecules (8, 24, 25). A similar ligation was observed for *E. coli* Grx4, a class II Grx, but the different orientation of the two monomers was proposed to be responsible for the differential cluster lability (26). The capacity of class I Grxs to bind an Fe-S cluster has been studied in detail by site-directed mutagenesis, and it was proposed that the nature of the residues adjacent to the first active site Cys determined this capacity (8, 27). In particular, for Grxs with a YCPFC or YCPYC active site, the replacement of the proline by a glycine, simulating GrxC1 (YCGYC), was sufficient to allow the incorporation of such a cluster (8) In addition, it has been hypothesized that the Trp residue adjacent to the catalytic cysteine residue in GrxS12 (WCSYS active site) prevented cluster incorporation because changing it into a Tyr allowed cluster incorporation (27).

A close paralog of GrxS12 having a WCSYC active site and named GrxC5 is present only in Brassicaceae. Here we have investigated the structure-function relationship of *Arabidopsis thaliana* GrxC5 (AtGrxC5) and compared it to poplar GrxS12 (PtGrxS12). The putative role of this Grx in plastids of Brassicaceae is discussed in the light of other functions identified so far for other Grx members.

EXPERIMENTAL PROCEDURES

Materials—G25 columns were purchased from GE Healthcare. 2-Hydroxyethyl disulfide (HED) and 5,5′-dithiobis-2-nitrobenzoic acid were from Acros Organics and Pierce, respectively. All other reagents were from Sigma.

Cloning and Construction of AtGrxC5 and PtGrxS12 Mutants by Site-directed Mutagenesis—The open reading frame sequence encoding *A. thaliana* GrxC5 (At4g28730) was amplified from leaf cDNA using AtGrxC5 forward and reverse primers (supplemental Table 1) and cloned into pET3d. The amplified sequence encodes a protein deprived of the first 63 amino acids corresponding to the putative targeting sequence and in which a methionine and an alanine have been added during cloning. The protein thus starts with the N-terminal sequence ^{1}MASFGSRM^{8} and ends with ^{98}GKNGQS^{113} at the C terminus. Using two complementary mutagenic primers, the four cysteines of AtGrxC5 were individually substituted into serines. The mutated proteins are called AtGrxC5 C29S, C32S, C80S, and C87S. Various combinations of cysteine substitutions by serine were also introduced in GrxC5 (C29S/C32S and C80S/C87S). In addition, to mimic the active site of AtGrxC5, a PtGrxS12 S32C variant was produced with the serine in position 32 modified into a cysteine. The primers are listed in supplemental Table 1.

Expression and Purification of Recombinant Proteins—For protein production, the *E. coli* BL21(DE3) strain, containing the pSBET plasmid, was co-transformed with the different recombinant plasmids (28). Cultures were successively amplified up to 2.4 liters in LB medium supplemented with ampicillin and kanamycin (50 $\mu g \cdot ml^{-1}$) at 37 °C. Protein expression was induced at exponential phase by adding 100 μM isopropyl β-D-thiogalactopyranoside for 4 h at 37 °C. The cultures were then centrifuged for 15 min at 4,400 × *g*. The pellets were resuspended in 30 ml of Tris-NaCl (30 mM Tris-HCl, pH 8.0, 200 mM NaCl) buffer with 1 mM GSH, and the cells were stored at −20 °C.

Cell lysis was performed by sonication (3 × 1 min with intervals of 1 min), and the soluble and insoluble fractions were separated by centrifugation for 30 min at 27,000 × *g*. The soluble part was then fractionated with ammonium sulfate in two steps, and the protein fraction precipitating between 40 and 80% saturation contained the recombinant protein as estimated by 15% SDS-PAGE. AtGrxC5 WT, C80S, and C87S and poplar GrxS12 S32C were purified by size exclusion chromatography after loading on an ACA44 (5 × 75-cm) column equilibrated in Tris-NaCl buffer usually supplemented with 100 μM GSH. However, some purifications were achieved without GSH. The fractions containing the protein were pooled, dialyzed by ultrafiltration to remove NaCl, and loaded onto a DEAE (diethylaminoethyl)-cellulose column (Sigma) equilibrated in a 30 mM Tris-HCl pH 8.0 buffer. The recombinant proteins passed through the DEAE column, were concentrated by ultrafiltration under nitrogen pressure (Amicon, YM10 membrane), and were stored in the same buffer at −20 °C.

Because they were mainly insoluble in the above described culture conditions, the culture and purification conditions of AtGrxC5 C29S and C32S were slightly modified following a

procedure described previously (29). Protein purity was checked by SDS-PAGE, and protein concentrations were determined spectrophotometrically using a molar extinction coefficient at 280 nm of 8,730 M^{-1} cm^{-1} for AtGrxC5 WT; 8,605 M^{-1} cm^{-1} for AtGrxC5 C29S, C32S, C80S, C87S, C29S/C32S, and C80S/C87S; and 10,095 M^{-1} cm^{-1} for PtGrxS12 S32C. PtGrxC1, PtGrxC3, PtGrxS12, PtTrxh1, AtMsrB1, and AtPrxIIE were purified as described previously (8, 14, 27, 30, 31).

Transcript Analysis—Four to 5-week-old plants were used for the analysis of transcript levels of the four plastidial Grxs (GrxC5, -S12, -S14, and -S16). *A. thaliana* ecotype Columbia was grown on soil under controlled conditions (10 h of light at 100 μmol quanta m^{-2} s^{-1} and 23 °C and 14 h of darkness at 18 °C; 50% relative humidity). Four hours after the onset of light, selected stress treatments were started. Cold stress was performed at 4 °C, and salt stress was applied by extensively watering the pots with 200 ml of 150 and 300 mM NaCl solution, respectively. A similar osmotic treatment was performed with 15% (w/v) PEG-5000 (same osmolarity as 150 mM NaCl). Complete rosettes of control and treated plants were harvested after 24 h, frozen immediately in liquid nitrogen, and stored at −80 °C. RNA isolation and the subsequent cDNA synthesis were performed according to Wormuth *et al.* (32). Supplemental Table 1 lists the combinations of primers used.

In Vivo Subcellular Localization by GFP Fusions—The putative targeting sequences of AtGrxC5, AtGrxC10 (At5g11930), AtGrxS12 (At2g20270), AtGrxS13 (At1g03850), AtGrxS14 (At3g54900), and AtGrxS16 (At2g38270) were cloned into the 35S-CFP-NosT or 35S-YFP-NosT vector between BamHI and AgeI restriction sites using primer combinations described in supplemental Table 1. The isolation, transfection of *A. thaliana* mesophyll protoplasts, and final fluorescence microscopy of protoplasts were performed according to Seidel *et al.* (33).

Electrospray Ionization-MS Analysis of Reduced and Oxidized Proteins—Three to 5 mg of proteins were reduced using 20 mM DTT_{red} for 15 min at 25 °C followed by desalting on G25 columns pre-equilibrated with 30 mM Tris-HCl, pH 8.0, 1 mM EDTA (TE) buffer. Oxidized Grxs were prepared by incubating prereduced Grxs with either 1 mM GSSG or 20 mM DTT_{ox} for a 15-min or longer period at 25 °C before desalting on G25 columns.

High resolution electrospray ionization-MS spectra of treated and untreated proteins were obtained on a Bruker microTOF-Q spectrometer (Bruker Daltonics, Bremen, Germany) equipped with an Apollo II electrospray ionization source with an ion funnel and operated in the negative ion mode. A concentrated sample (around 100 μl at 100 μM) in formic acid was injected at a flow rate of 10–20 μl min^{-1}. The potential between the spray needle and the orifice was set to 4.5 kV. Before each run, the instrument was calibrated externally with the Tunemix™ mixture (Agilent Technologies) in quadratic regression mode. Data were analyzed with DataAnalysis software (Bruker).

Fluorescence Properties of AtGrxC5—The intrinsic fluorescence of AtGrxC5 WT and mutants in the reduced and oxidized forms was recorded with a Cary Eclipse spectrofluorometer (Varian) with 10 μM samples in TE buffer and an excitation wavelength fixed at 270 nm. Control spectra were run with buffer only for each sample and subtracted from the spectra.

Thioltransferase Activity (HED and Dehydroascorbate (DHA) Assays)—The HED reduction was measured at 25 °C in steady-state conditions by following NADPH oxidation at 340 nm in the presence of a Grx reducing system. A 500-μl reaction mixture in 30 mM Tris-HCl, pH 8.0, 1 mM EDTA buffer contained 150 μM NADPH, 0.5 units of glutathione reductase from bakers' yeast, 2 mM GSH, 0.7 mM HED, and 400 nM Grx except for AtGrxC5 C32S (200 nM Grx). The dehydroascorbate reductase activity was measured using a similar method except that the test was performed in 100 mM phosphate pH 7.0 buffer with 1 mM DHA and 2 μM Grx (1 μM for AtGrxC5 C32S). The reaction was started by adding Grx after a 2-min preincubation. Grx activity was determined by subtracting the spontaneous reduction rate observed in the absence of Grx. The activity was expressed as nmol of NADPH oxidized/nmol of Grx/min using a molar extinction coefficient of 6,220 M^{-1} cm^{-1} at 340 nm for NADPH. Three independent experiments were performed at each substrate concentration, and the apparent k_{cat} and K_m values were calculated by non-linear regression using the program GraphPad Prism 4.

Insulin Reduction—Insulin reduction was monitored spectrophotometrically at 30 °C using 2 μM Trx or 10 μM Grx and a procedure described previously (29).

Glutaredoxin-dependent Peroxidase Activity of PrxIIE—Rates of peroxide reduction by PrxIIE were determined in an assay coupled with the glutaredoxin system by monitoring NADPH oxidation following absorbance at 340 nm. The assay typically contained 50 μM *t*-butyl hydroperoxide in 100 mM HEPES pH 8.0 buffer, 2 mM EDTA, 1 mM GSH, 150 μM NADPH, 2 μM PrxIIE, and from 0.1 to 6 μM Grx. The comparative mutant analysis was then performed with 1 μM Grx.

Methionine Sulfoxide Reductase Activity Assay—The MsrB1 activity was measured by following NADPH oxidation at 340 nm in the presence of a Grx reducing system at 25 °C. A 500-μl reaction mixture in 30 mM Tris-HCl, pH 8.0, contained 200 μM NADPH, 0.5 units of glutathione reductase from bakers' yeast, 10 mM GSH, 2 mM *N*-acetylmethionine sulfoxide, 2.5 μM MsrB1, and 25 μM AtGrxC5 corresponding to a saturating concentration. MsrB1 activity was calculated as described previously (14).

Analytical and Spectroscopic Methods—Analytical gel filtration analyses were performed with an ÄKTA Avant system (GE Healthcare). 150 μl at about 100 μM apo- and holoforms were separately loaded on a Superdex 75 HR 10/30 column (GE Healthcare) equilibrated with 50 mM Tris-HCl, pH 8.0, 150 mM NaCl and calibrated with gel filtration standards (Bio-Rad). Elution profiles were simultaneously recorded at 280 and 430 nm with a flow rate of 0.5 ml min^{-1}.

Protein concentrations were determined by using BSA as a standard using the Bio-Rad DC protein assay in conjunction with the microscale modified procedure of Brown *et al.* (34). Iron concentrations were determined colorimetrically by using bathophenanthroline under reducing conditions after digestion of the protein in 0.8% $KMnO_4$, 0.2 M HCl (35). Fe-S cluster reconstitution experiments in AtGrxC5 C32S were carried out under anaerobic conditions following a procedure described

previously (20). UV-visible absorption and CD spectra were recorded at room temperature using a Shimadzu UV-3101PC spectrophotometer and Jasco J-715 spectropolarimeter, respectively. Resonance Raman spectra were recorded as described previously (36) using an Instruments SA Ramanor U1000 spectrometer coupled with a Coherent Sabre argon ion laser with 20-μl frozen droplets of sample mounted on the cold finger of an Air Products Displex Model CSA-202E closed cycle refrigerator.

Crystallization, Data Collection, Structure Determination, and Crystallographic Refinement—Crystallization experiments were performed by the microbatch under oil (paraffin) method at 4 °C under aerobic conditions. Drops were prepared by mixing 1.5 μl of protein solution with an equal volume of crystallization solution. Solutions of apo- and holoproteins had concentrations of 8.9 and 16.7 mg·ml^{-1}, respectively. Suitable crystals for x-ray diffraction were obtained without optimization using crystallization screen kits. The apoform crystallized in 1.6 M ammonium sulfate and 500 mM lithium chloride (Jena Biosciences, JBS 5-B4), whereas brownish crystals were obtained for the holoform by using 0.1 M HEPES, pH 7.5 and 70% 2-methyl-2,4-pentanediol solution (Hampton Research crystal screen 2-35). X-ray diffraction experiments were performed at 100 K with holoform crystals flash cooled directly from the drop and apoform crystals and soaked briefly in crystallization solution supplemented with 20% (v/v) glycerol. Apo- and holoform data sets were collected on beamlines BM30A and ID23–1 at the European Synchrotron Radiation Facility (Grenoble, France), respectively. The data were indexed and processed using XDS (37) and scaled and merged with SCALA from the CCP4 program package (38, 39). Both structures were solved by molecular replacement with MOLREP (40) using the poplar GrxS12 coordinates (Protein Data Bank code 3FZ9). The models were refined using REFMAC version 5.4 (41) interspersed with manual inspection and corrections using COOT (42). In the final rounds of apoform refinement, anisotropic B-factors were included for selected atoms. The validation of both crystal structures was performed with MOLPROBITY (43). All figures were prepared with PyMOL. All statistics are available in Table 1.

TABLE 1
Statistics of x-ray diffraction data collection and model refinement

	Apoform	Holoform
Data collection		
Space group	$P2_12_12$	$R3$
Cell dimensions *a*, *b*, *c* (Å)	63.5, 39.0, 37.6	111.7, 111.7, 58.5
Resolution (Å)	33.25-1.2 (1.26-1.20)[a]	27.99-2.4 (2.53-2.4)[a]
R_{merge}	0.052 (0.221)	0.061 (0.33)
Mean $I/\sigma(I)$	21.9 (4.9)	15.5 (5.2)
Completeness (%)	94 (68)	99 (100)
n observations	211,463 (9,670)	60,442 (9,125)
Redundancy	7.5 (3.3)	5.7 (5.8)
Refinement		
Resolution (Å)	33.25-1.2 (1.23-1.2)	27.99-2.4 (2.46-2.4)
n reflections	26,715 (1288)	10,043 (740)
R_{all} (%)[b]	15.03 (18.6)	19.1 (24.3)
R_{free} (%)[b]	17.58 (24.1)	23.8 (28)
n residues		
Chain A	100 (6–105)	103 (3–105)
Chain B		103 (6–105)
n ligands	1 GSH, 3 SO_4	2 GSH, 1 [2Fe-2S]
n water molecules	108	29
n atoms	978	1,662
Isotropic	122	1,662
Anisotropic	857	0
Average B-factor (Å^2)	18.5	57.6
Ramachandran statistics (%)		
Residues in preferred regions	100	97
Residues in allowed regions	0	3
Outlier residues	0	0
r.m.s.[c] deviations		
Bond length (Å)	0.025	0.021
Bond angle (°)	2.209	1.999

[a] Values in parentheses are for highest resolution shell.
[b] R_{all} was determined from all the reflections (working set + test set), whereas R_{free} corresponds to a subset of 5% of reflections (test set).
[c] Root mean square.

RESULTS

AtGrxC5, the Fourth Plastidial Grx of A. thaliana—The *A. thaliana* Grx family is composed of 33 members, which are predicted to be distributed in different subcellular compartments (11). GrxS12, -S14, and -S16 in poplar as well as GrxS14 in *A. thaliana* (previously referred to as AtGRXcp) have already been confirmed as being located in plastids by GFP fusion (20, 27, 44). From localization prediction programs, only three additional *A. thaliana* Grxs exhibit a potential plastidial targeting sequence, namely AtGrxC5 (class I), AtGrxC10, and AtGrxS13 (class III) (10, 11). It is important to note that GrxC5 and GrxS12, which form a specific subgroup of class I Grxs, display about 70% identity when considering the mature form of the proteins. The phylogenetic analysis further indicated that whereas all plants analyzed possess a GrxS12 isoform only species of the Brassicaceae family possess both isoforms (supplemental Fig. 1).

The N-terminal targeting sequences of the six putative plastidial Grxs of *A. thaliana* were fused in-frame to the green fluorescent protein variants CFP and YFP. The constructs were used to transform *A. thaliana* mesophyll protoplasts. Similarly to poplar isoforms, AtGrxS12, -S14 and -S16 are clearly located in plastids as indicated by the superimposition of the YFP or CFP signal with the chlorophyll autofluorescence in the merged images (Fig. 1). Concerning AtGrxC5, the reporter protein is also directed to the chloroplast with some dots of stronger signal within the organelle. Although the fluorescence signal for AtGrxS13 is more diffuse than for AtGrxC10, both proteins likely have a cytosolic localization at least under these experimental conditions. Therefore, these two Grxs were excluded from further analysis.

Transcript Analysis of Plastidial Grxs under Environmental Constraints—The transcript expression of AtGrxC5, -S12, -S14, and -S16 was measured using semiquantitative RT-PCR in leaves of plants grown under control and stress conditions, namely cold treatment at 4 °C, salt stress administered by watering with 150 and 300 mM NaCl solutions, and osmotic stress induced by 15% (w/v) PEG-5000 for 24 h, respectively. Under these stress conditions, the plants developed a pronounced stress phenotype (45). The signals were detected after 34 PCR cycles for GrxC5 and GrxS12, 32 cycles for GrxS14, and 30 cycles for GrxS16 (Fig. 2*A*), indicating that, in these growth conditions, GrxS16 transcripts are the most abundant within the plastidial Grx group in rosettes. Regarding environmental constraints, a significant response of the *grx* transcript level could not be observed except for a slight down-regulation under extreme salinity for AtGrxS14 and an up-regulation of AtGrxC5 in plants subjected to a cold treatment (Fig. 2*B*). Likewise only moderate

responses to diverse environmental stress conditions were found when analyzing the Affymetrix GeneChip data available via the Genevestigator tool (supplemental Table 2).

AtGrxC5 Exists in Two Forms upon Expression in E. coli—To characterize the structure-function relationship of AtGrxC5, the mature form of the protein was produced in *E. coli* as a recombinant protein by removing the N-terminal 63 residues that constitute the putative targeting sequence. The final product comprises 113 amino acids with a predicted molecular mass of 12,482 Da. As observed for PtGrxC1, lysed bacterial cells had a slight but visible brownish color (8). Similarly, following gel filtration, the protein separated into two peaks, an apoform with an apparent size corresponding to a monomer and a holoform most likely containing an Fe-S center and with an apparent exclusion volume corresponding to a dimer (supplemental Fig. 2). This result was unexpected as AtGrxC5 possesses the active site Trp residue, which was thought previously to prevent the incorporation of an Fe-S cluster in the close paralog PtGrxS12 (27).

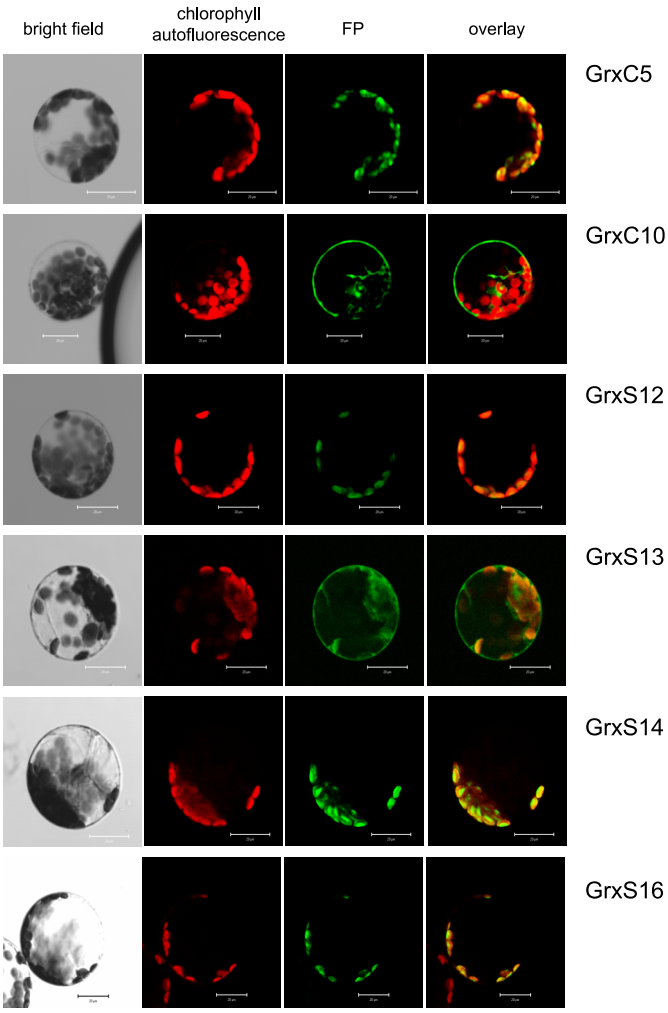

FIGURE 1. **YFP/CFP localization of putative plastidial Grxs in *A. thaliana* mesophyll protoplasts.** The sequences coding for the N-terminal extensions of AtGrxC5, AtGrxC10, AtGrxS12, AtGrxS14, AtGrxS15, and AtGrxS16 were fused in-frame with the CFP/YFP coding sequence, mesophyll protoplasts were transfected, and accumulation of the fluorescent reporter was monitored as described under "Experimental Procedures." The *scale bars* correspond to 20 μm.

The nature of the Fe-S center in holoGrxC5 was initially assessed using a combination of analytical and spectroscopic techniques. Iron and protein analyses of the holoform indicated 1.0 ± 0.2 iron/protein monomer consistent with one [2Fe-2S] cluster per dimer. This conclusion was unambiguously confirmed by the nearly identical UV-visible absorption/CD and resonance Raman spectra compared with those established for the structurally characterized PtGrxC1 (Fig. 3). Moreover, the close similarity of the spectroscopic properties of the $[2Fe\text{-}2S]^{2+}$ centers in AtGrxC5 and PtGrxC1 indicates analogous cluster coordination involving cysteinyl sulfur ligands from two GSHs and two Grxs. We have shown earlier by analyzing UV-visible absorption/CD and resonance Raman spectra that the Grx conformations are clearly distinct in class I and II Grxs, which both bind [2Fe-2S] clusters (8, 20, 26).

To determine how similar the ligation of the [2Fe-2S] cluster is to the one in PtGrxC1, the four cysteine residues of AtGrxC5 in positions 29, 32, 80, and 87 were substituted by serine residues. The substitution of either Cys^{80} or Cys^{87} did not prevent the incorporation of the Fe-S cluster. In contrast, the single substitution of Cys^{29} or Cys^{32} produced proteins that were devoid of the cluster, raising the question of the role of the second active site cysteine for cluster ligation or stability. Interestingly, a S32C variant of PtGrxS12, mimicking AtGrxC5 active site sequence, incorporated an Fe-S cluster with a UV-visible absorption spectrum similar to AtGrxC5 (supplemental Fig. 3). However, both the spectroscopic signature and the three-dimensional structure of holoGrxC5 (see below) showed that Cys^{32} is not a direct ligand for the Fe-S cluster. Next we wanted to determine whether the second cysteine is essential for cluster integration or only for its stability as observed previously for PtGrxC1. A PtGrxC1 C34S variant, although still

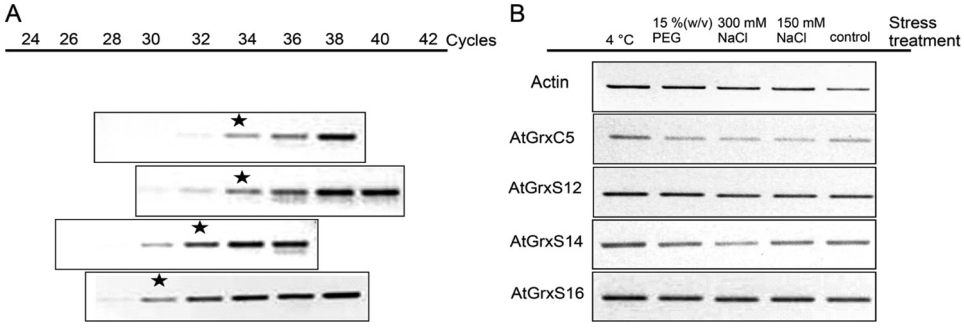

FIGURE 2. **Transcript analysis of plastidial Grxs in rosettes of *A. thaliana* wild type plants.** *A*, the abundance of Grx transcripts was semiquantified by RT-PCR. *Stars* indicate the number of cycles selected for the analysis of transcript abundance in response to the indicated stress conditions depicted in *B*. The pictures are from two independent experiments with two to three replicates with similar results.

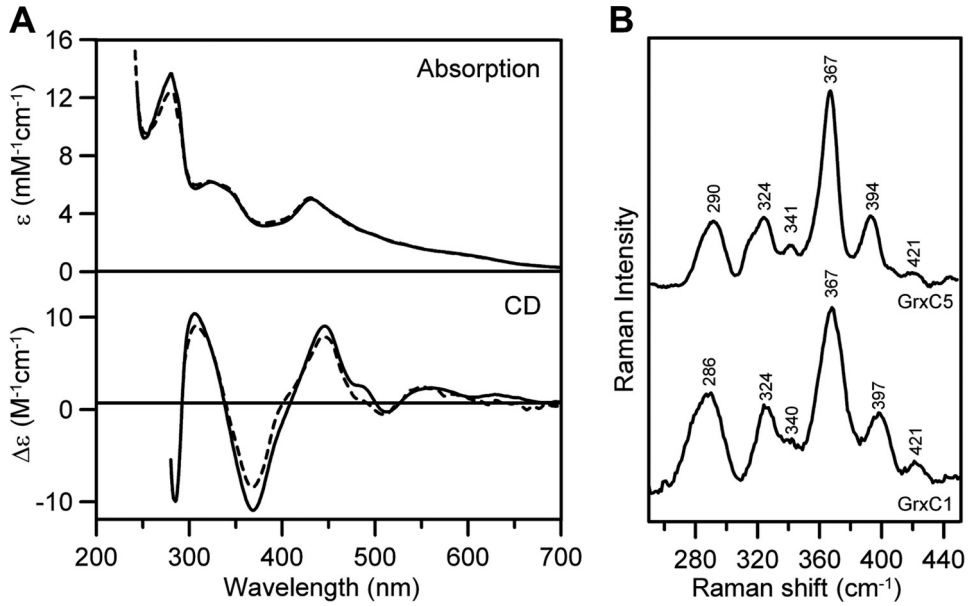

FIGURE 3. **Spectroscopic properties of AtGrxC5 holoform.** *A*, comparison of the UV-visible absorption and CD spectra of AtGrxC5 (*solid line*) and PtGrxC1 (*broken line*). ϵ and Δϵ values are expressed per Grx monomer. *B*, comparison of the resonance Raman spectra of AtGrxC5 (*solid line*) and PtGrxC1 (*broken line*) obtained at 17 K with 457.9-nm laser excitation at 7 cm^{-1} spectral bandwidth. Bands due to lattice modes of ice were subtracted from the spectra shown.

able to bind an Fe-S cluster, contained a far less stable Fe-S cluster with only 0.19 ± 0.04 iron/monomer (8). However, no Fe-S cluster could be reconstituted in AtGrxC5 C32S under anaerobic conditions following a standard procedure using glutathione and catalytic amounts of *E. coli* IscS, indicating that, in this case, the cysteine is indispensable (data not shown).

Determination of AtGrxC5 Redox State—The presence of four cysteine residues led us to investigate the redox state of the protein to better understand the catalytic mechanism utilized by the apoform of GrxC5. Whereas Cys^{29}, Cys^{32}, and Cys^{87} are conserved in many class I Grxs, Cys^{80} is not conserved even in other plant GrxC5 isoforms. Analysis by mass spectrometry of AtGrxC5 WT (purified or not in the presence of GSH) revealed the presence of three protein peaks with molecular masses of 12,348.2, 12,654.4, and 12,961.2 ± 2 Da (data not shown). Although the intensity of the different peaks varied slightly, similar results were obtained by treating prereduced AtGrxC5 with GSSG. The peak at 12,654.4 Da was generally predominant. The first peak is consistent with a protein where the methionine is cleaved. The other peaks, corresponding to mass increments of 306.2 and 613 Da, are consistent with proteins also deprived of the methionine but containing one or two glutathione adducts. After reduction with DTT, a single protein peak with a molecular mass of 12,350 Da was observed, further supporting that the protein is glutathionylated. The same three protein peaks were obtained for AtGrxC5 C80S, indicating that Cys^{80} is not a glutathionylation site. Concerning the AtGrxC5 C87S mutant, we detected two protein peaks corresponding to a reduced protein and to an oxidized protein with only one glutathione adduct, indicating that Cys^{87} is most likely one of the glutathionylation sites; the other site is either Cys^{29} or Cys^{32}. In the case of the AtGrxC5 C32S mutant, only two protein peaks corresponding to oxidized proteins with one or two glutathione adducts were detected, a result consistent with Cys^{29} and Cys^{87} being the two modified cysteines. For AtGrxC5 C29S, the protein is so unstable that we were not able to obtain reliable results confirming the loss of one glutathione adduct.

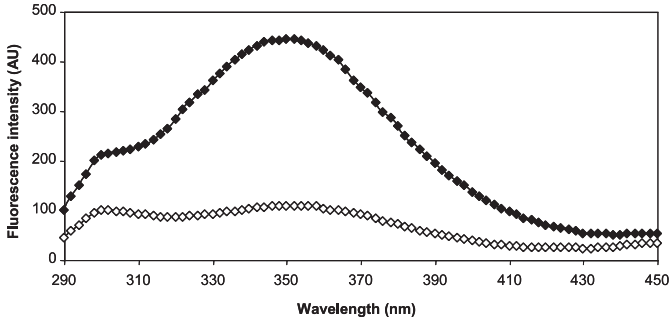

FIGURE 4. **Fluorescence spectra of AtGrxC5 under different redox states.** Emission spectra of reduced (*black squares*) and oxidized (*white squares*) apoforms of AtGrxC5 (excitation at 270 nm) were recorded with 10 μM protein at 25 °C in TE buffer. The reduced AtGrxC5 was obtained by treating the protein with 20 mM DTT before desalting on G25 columns. The prereduced AtGrxC5 was oxidized using 1 mM GSSG. *AU*, arbitrary units.

As AtGrxC5 possesses a single Trp residue as well as two Tyr residues very close to the active site at least in the primary sequence (IYSKTWCSYCT), the redox state of the apoform was also assessed by measuring its intrinsic fluorescence properties under reducing (GSH or DTT_{red}) or oxidizing (GSSG or DTT_{ox}) conditions. Reduced AtGrxC5 displayed an emission spectrum with two peaks at approximately 300 and 350 nm characteristic of a signal originating from Tyr and Trp residues, respectively (Fig. 4) (11). Addition of 1 mM GSSG but not DTT_{ox} led to the quenching of the fluorescence signal, whereas the subsequent addition of DTT_{red} restored the initial spectrum (Fig. 4 and data not shown). Because similar results were obtained for all monocysteinic mutants except AtGrxC5 C29S and because DTT_{ox} had no effect on the AtGrxC5 redox state, the fluorescence quenching can be attributed to the glutathionylation of Cys^{29}.

Reductase Activity and Catalytic Mechanism of AtGrxC5—To clarify the catalytic mechanism used by AtGrxC5 and to

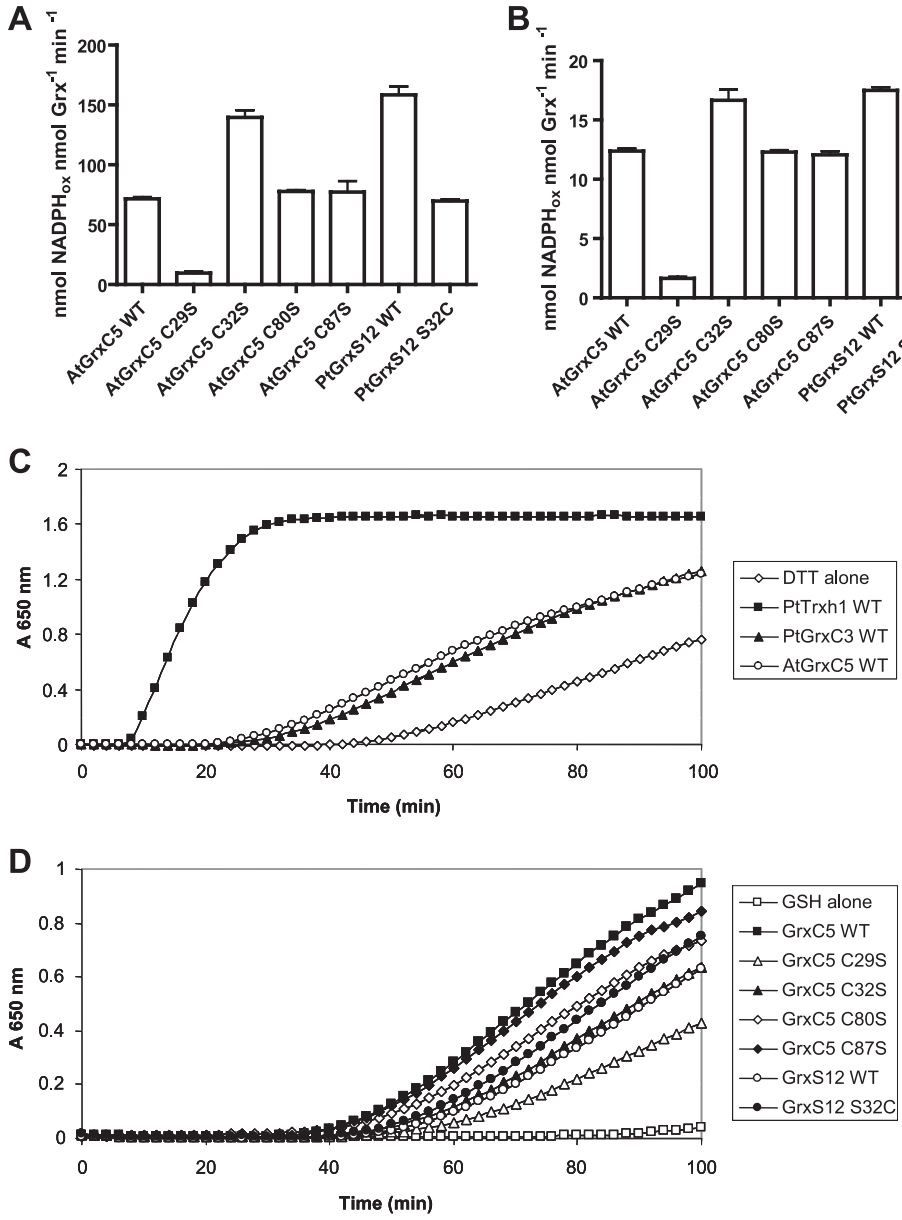

FIGURE 5. **Comparison of reductase activity between AtGrxC5 and PtGrxS12 mutants.** HED (*A*) and DHA (*B*) reduction was achieved, respectively, using 400 nM or 1 μM Grx in the presence of 2 mM GSH and either 0.7 mM HED or 1 mM DHA. The data are represented as mean ± S.D. of three separate experiments. Insulin reduction was measured either using a DTT-based assay (*C*) in the presence of 2 μM poplar Trxh1 or 10 μM Grxs or using a GSH-based assay (*D*) containing a complete GSH regeneration system (NADPH/glutathione reductase/GSH) and WT or mutated versions of AtGrxC5 and PtGrxS12.

compare its efficiency with that of PtGrxS12, we first measured the activity of all protein variants using the conventional DHA and HED assays at a fixed enzyme concentration by following NADPH oxidation in the presence of a glutathione recycling system. In both assays, we obtained very similar results: AtGrxC5 C29S was inactive, whereas AtGrxC5 C80S and AtGrxC5 C87S appeared to be as efficient as the WT protein, and AtGrxC5 C32S was nearly 2 times more efficient (Fig. 5, *A* and *B*). Strikingly, the AtGrxC5 C32S mutant, mimicking the GrxS12 active site, was as efficient as PtGrxS12, and PtGrxS12 S32C, a protein variant mimicking the GrxC5 active site, had a lower efficiency comparable with AtGrxC5 WT (Fig. 5, *A* and *B*). These results indicate that Cys^{32} is not essential for the reaction mechanism but that it influences protein reactivity.

Following these experiments, we determined the catalytic parameters of AtGrxC5 WT and all monocysteinic mutants in steady-state conditions (Table 2). During the initial preincubation time of the reaction mixture, HED and GSH give rise to a glutathionylated β-mercaptoethanol mixed disulfide (46). The kinetic analysis revealed an apparent K_m value of 0.20 ± 0.02 mM for glutathionylated β-mercaptoethanol and a k_{cat} of 1.21 ± 0.03 s^{-1}. These values are similar to those reported for human Grx2, which contains an SCSYC active site, but are lower by a factor 10–20 when compared with other class I Grxs including plant GrxC1 and -C4 (5).[5] Concerning DHA reductase activity, the results provided an apparent K_m value of 0.21 ± 0.03 mM for

[5] J. Couturier and N. Rouhier, unpublished data.

TABLE 2

Catalytic parameters for thioltransferase activity of AtGrxC5

The catalytic efficiency of AtGrxC5 WT and mutants was estimated using the HED and DHA activity assays under steady-state conditions following the procedures described under "Experimental Procedures." β-ME-SG, glutathionylated β-mercaptoethanol; ND, not determined.

Proteins	β-ME-SG			DHA			GSH		
	K_m	k_{cat}	k_{cat}/K_m	K_m	k_{cat}	k_{cat}/K_m	K_m	k_{cat}	k_{cat}/K_m
	mM	s^{-1}	M^{-1}/s^{-1}	mM	s^{-1}	M^{-1}/s^{-1}	mM	s^{-1}	M^{-1}/s^{-1}
GrxC5 WT	0.20 ± 0.02	1.21 ± 0.03	6.05×10^3	0.21 ± 0.03	0.23 ± 0.01	1.10×10^3	3.6 ± 0.8	0.69 ± 0.11	192
GrxC5 C29S	ND	ND	ND	ND	ND	ND	ND	ND	ND
GrxC5 C32S	0.31 ± 0.03	3.39 ± 0.14	1.09×10^4	0.26 ± 0.02	0.53 ± 0.02	2.04×10^4	2.4 ± 0.4	1.49 ± 0.16	621
GrxC5 C80S	0.37 ± 0.05	1.43 ± 0.07	3.86×10^3	0.18 ± 0.01	0.23 ± 0.01	1.28×10^3	3.1 ± 0.4	0.61 ± 0.05	197
GrxC5 C87S	0.58 ± 0.07	1.83 ± 0.12	3.16×10^3	0.23 ± 0.03	0.24 ± 0.01	1.04×10^3	2.6 ± 0.4	0.53 ± 0.05	204

DHA and a k_{cat} of 0.23 ± 0.01 s^{-1} (Table 2). These values are in the same order as those obtained for PtGrxS12 and CrGrx1 (6, 27). The apparent K_m value for GSH was determined by varying the amount of GSH in the DHA assay. AtGrxC5 WT possesses an apparent K_m value of 3.6 ± 0.8 mM for GSH similar to the one obtained for PtGrxS12 but also for other plant and non-plant Grxs in particular human Grx2 (5, 27). AtGrxC5 C80S and C87S possess catalytic parameters very similar to those of AtGrxC5 WT with only small variations observed in the affinity for glutathionylated β-mercaptoethanol. On the other hand, the AtGrxC5 C32S mutant displayed a better catalytic efficiency (about 2 times) compared with AtGrxC5 WT both in HED and DHA assays, originating from a better turnover number (Table 2).

In a second series of experiments, we used the classical insulin reduction assay to assess the disulfide reductase activity of AtGrxC5 (47). In the presence of DTT, AtGrxC5 and PtGrxC3, another dithiol Grx used for comparison, were able to reduce insulin but, as expected, with a lower efficiency than poplar Trxh1 (Fig. 5*C*). In alternative experiments, we measured the capacity of Grxs to reduce insulin by using an NADPH/glutathione reductase/GSH regeneration system (Fig. 5*D*). The ability of AtGrxC5 to reduce insulin was not improved compared with the DTT-based assay (Fig. 5*D*). Regarding the mutated proteins, as already observed for DHA and HED assays, AtGrxC5 C80S and AtGrxC5 C87S appeared almost as efficient as the WT protein, and AtGrxC5 C32S and PtGrxS12 S32C enzymatic activities were similar to PtGrxS12 WT and AtGrxC5 WT, respectively (Fig. 5*D*). Although delayed in time, AtGrxC5 C29S also surprisingly exhibited the capacity to slightly reduce insulin compared with the GSH alone control, possibly indicating some reactivity of the remaining cysteines toward insulin (Fig. 5*D*).

Next the capacity of AtGrxC5 to reduce putative physiological target proteins was evaluated by measuring the Grx-mediated recycling of MsrB1 and PrxIIE, two plastidial enzymes, which are efficiently reduced by GrxS12 (14, 48). Hence, as already observed for previous activity tests, AtGrxC5 C80S was as efficient as AtGrxC5 WT for the regeneration of MsrB1, whereas AtGrxC5 C32S mutant was slightly more efficient (Fig. 6*A*). On the contrary, AtGrxC5 C87S mutant was significantly less efficient as already observed for PtGrxS12 C87S mutant (Fig. 6*A*) (14). Moreover, MsrB1 possesses an apparent K_m value of 2.3 ± 0.2 μM for AtGrxC5 WT (Fig. 6*B*), a value comparable with that obtained for PtGrxS12 (14). Strictly similar results were obtained with AtPrxIIE (supplemental Fig. 4). These results are consistent with the previously described

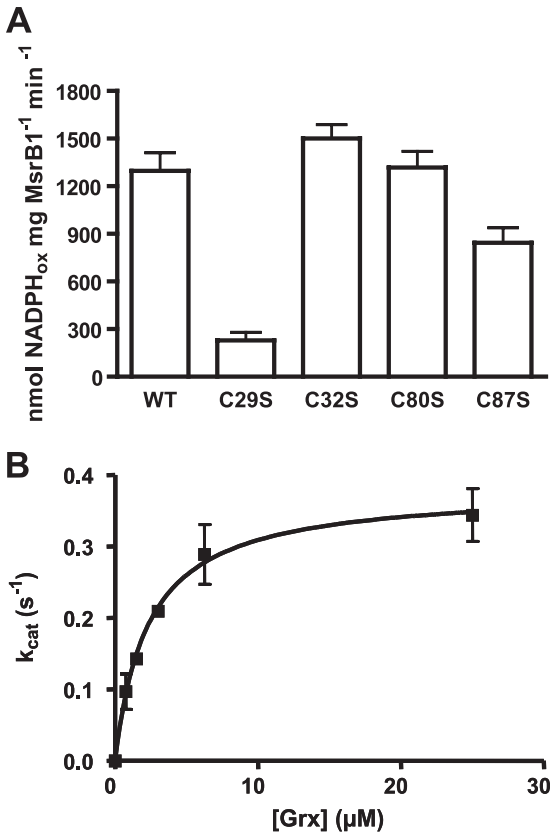

FIGURE 6. **Regeneration of AtMsrB1 by AtGrxC5 variants.** *A*, MsrB1 reduction was achieved using 25 μM GrxC5 variants. The data are represented as mean ± S.D. of three separate experiments. *B*, variation of the apparent turnover during *N*-acetylmethionine sulfoxide reduction catalyzed by 2.5 μM MsrB1 in the presence of GrxC5 WT at concentrations ranging from 0.75 to 25 μM.

regeneration mechanism of these enzymes by class I Grxs (GrxC5 or -S12) through a monothiol mechanism (14), *i.e.* (i) the reduction of the sulfenic acid by GSH followed by (ii) the deglutathionylation of the glutathione adduct by the nucleophilic attack of AtGrxC5 catalytic cysteine and (iii) the glutathione-mediated reduction of glutathionylated AtGrxC5.

Structures of GrxC5 Apo- and Holoforms and Quality of Models—The crystallographic structures of apo- ($GrxC5_{apo}$) and holoforms ($GrxC5_{holo}$) of AtGrxC5 were solved to the resolution limits of 1.2 and 2.4 Å, respectively. AtGrxC5 in the apoform crystallizes in the space group $P2_12_12$ with one glutathionylated polypeptide chain in the asymmetric unit, whereas AtGrxC5 in the holoform crystallizes in the space group *R*3, and the asymmetric unit consists of two monomers and two glutathione molecules ligating one [2Fe-2S] cluster. AtGrxC5 adopts

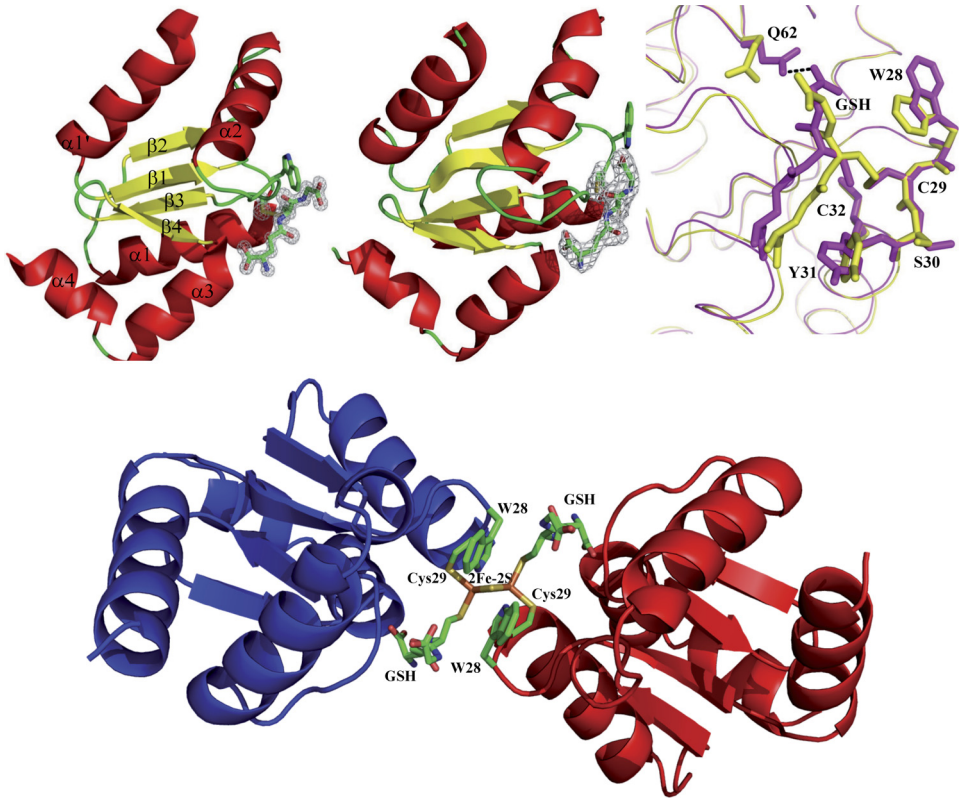

FIGURE 7. **Schematic drawing of apo- and holoform AtGrxC5 structures.** *Upper left* and *middle*, schematic representation of the overall fold of $GrxC5_{apo}$ (*left*) and $GrxC5_{holo}$ (*middle*). All α-helices are shown in *red*, β-strands are in *yellow*, and connecting loops are in *green*. Trp^{28}, Cys^{29}, and the GSH molecule are highlighted in *sticks* with final $2F_o - F_c$ electron densities (1.2σ level) covering chosen residues and ligands for clarity. Secondary structures are labeled in the *left panel*. *Upper right*, superimposition of the structures of the apoform (*yellow*) and holoform (*magenta*). The ^{28}WCSYC^{32} signature, Gln^{62}, and the GSH molecule are highlighted in *sticks*. *Bottom*, α-carbon trace of the dimer of $GrxC5_{holo}$. Monomers A and B are colored *blue* and *red*, respectively. Trp^{28}, Cys^{29}, and the GSH molecules are represented as *sticks*.

TABLE 3

Rotamers of selected side chains in AtGrxC5, poplar GrxS12, poplar GrxC1, and human Grx2 crystal structures

The dashes for the glycinyl residue indicate that no rotamer is defined because its side chain is a hydrogen atom. + represents a trans conformation, p represents a chi angle of +60°, and m a chi angle of −60°. For Trp and Tyr residues, the numeric value corresponds to chi2 angle. For Glu residue, the numeric value corresponds to chi3 angle.

AtGrxC5			PtGrxS12		PtGrxC1			hGrx2		
	apo	holo		apo		apo	holo		apo	holo
W28	p-90	p90	**W28**	p-90	**Y29**	p90	p90	**S36**	p	p
C29	t	t	**C29**	t	**C30**	t	t	**C37**	t	t
S30	p	m	**S30**	p	**G31**	-	-	**S38**	p	m
Y31	m-85	m-30	**Y31**	m-85	**Y32**	m-85	m-85	**Y39**	m-85	m-30
C32	m	m	**C32**	t	**C33**	m	m	**C40**	m	m
Q62	tp60	tt0	**Q62**	tp60	**Q62**	tt0	tt0	**Q69**	tt0	tt0

the classical Grx/Trx fold consisting of a four-stranded mixed β-sheet flanked by five α-helices (see nomenclature in Fig. 7). The crystal structures of AtGrxC5 and poplar GrxS12 are quite similar (root mean square deviation, 0.48 Å). The major difference between the two proteins concerns the presence of two additional cysteines (Cys^{32} and Cys^{80}) in AtGrxC5. The residue Cys^{80}, which is replaced by a Gly in PtGrxS12, is located in the loop between β3 and β4, and its lateral chain does not form any noticeable interaction. Cys^{32} is replaced by a serine in PtGrxS12. Both lateral chains exhibit different rotamers (Table 3). In $GrxC5_{apo}$, the thiol group of Cys^{32} is in the vicinity of the catalytic cysteine (Cys^{29}) and interacts with the backbone NH group of Lys^{26}, whereas in PtGrxS12, the side chain of Ser^{32} points toward the hydroxyl group of Ser^{25}.

In $GrxC5_{apo}$, the glutathione molecule is covalently bound to Cys^{29}, and its binding mode is identical to that of PtGrxS12 and very similar to that of other known glutathionylated Grx structures (25, 49–52). (i) The carboxylate of the glycinyl residue forms a salt bridge with the side chain of His^{72} from the loop α_2-β_3. (ii) The NH and carbonyl groups of the cysteinyl residue are hydrogen-bonded to the main chain of Val^{74}, a generally conserved residue that precedes the *cis*-Pro^{75} found in Trx superfamily members. (iii) The carboxylate of the γ-glutamate interacts with both NH groups of Cys^{87} and Thr^{88} from helix α_3. The high resolution of the electron density maps allowed us to observe two conformations for the lateral chain of Thr^{88}. Only in conformer m ($\chi_1 = -61°$) is the hydroxyl group within hydrogen bond distance from the γ-Glu carboxylate. The other possible hydrogen bond donors and acceptors of the GSH moiety interact with water molecules or symmetry-related molecules.

In the dimeric $GrxC5_{holo}$, each iron atom of the Fe-S cluster is tetracoordinated by sulfur atoms: two from the cluster, one from the catalytic Cys^{29}, and one from glutathione. A comparative structural analysis of $GrxC5_{apo}$ and $GrxC5_{holo}$ illustrates the conformational changes upon Fe-S cluster binding. All the lateral chains of the residues of the ^{28}WCYSC^{32} signature but those of the cysteines adopt different rotamers in the apo- and holoforms with Trp^{28} exhibiting flipped rotamers (Table 3). The side chain is located on the molecular surface, partially buried by a symmetry-related molecule in the apoform. Previ-

ous analyses of the PtGrxS12 crystal structure led to the conclusion that Trp^{28} cannot adopt this p-90 conformation in the dimer because of steric conflicts (27). In $GrxC5_{holo}$, the Trp^{28} rotamer observed is p90 where the NH group of the pyrrole moiety points toward the Fe-S cluster, whereas the phenyl ring is solvent-exposed (Fig. 7). The two residues Tyr^{30} and Ser^{31} also present in the signature of human (hGrx2) undergo the same conformational rearrangement upon Fe-S cluster binding in both enzymes (Table 3) (25). Gln^{62} is the last residue that attracted our attention. Indeed, in $GrxC5_{apo}$, the lateral chain participates in the stabilization of the loop α_2-β_3 containing the $^{73}TVP^{75}$ motif involved in GSH binding, whereas it adopts another rotamer in $GrxC5_{holo}$, interacting with the GSH C-terminal carboxylate group, which also undergoes a conformational change. When $GrxC5_{apo}$ and $GrxC5_{holo}$ are superposed, one noticeable difference is the backward movement of the loops α_2-β_3 and β_4-α_3, of the N-terminal part of the helix α_4, and of the glutathione molecule to accommodate the Fe-S cluster and to preserve their interactions (Fig. 7). In addition to its interaction with the carboxamide of Gln^{62}, the GSH C-terminal group is involved in a salt bridge to Lys^{36}. The rest of the new GSH/protein interactions are quaternary in nature, involving hydrogen bond donors or acceptors of the $^{28}WCSYC^{32}$ signature of monomer B for the GSH molecule of monomer A. These interactions are similar to those observed in the crystal structure of the holoform of hGrx2 (25).

DISCUSSION

GrxC5 Is the Fourth Plastidial Grx in A. thaliana—Trxs and Grxs are key players of the chloroplast redox network. Although considerable knowledge has been accumulated on chloroplastic Trx isoforms (53), the investigation of the roles of chloroplastic Grxs still lags behind. Hence, the characterization of AtGrxC5 is part of a more comprehensive work aimed at deciphering whether Grxs have specialized or redundant functions in plants and particularly in plastids.

The phylogenetic analysis of the GrxC5/S12 subgroup indicates that this subgroup is specific to land plants and that the GrxC5 isoforms are restricted to a specific plant family, the Brassicaceae, likely indicating that a single gene has been duplicated in the last common ancestor of this family. The fact that both genes have been retained suggested that they have developed specialized functions. At the transcript level, although At*GrxS12* shows slightly more expression than At*GrxC5* in rosettes, the expression of these two genes is relatively unaffected in *A. thaliana* leaves subjected to environmental constraints. Thus, despite having similar subcellular localization and transcript expression pattern, the replacement of a single amino acid in the AtGrxC5 active site cysteine conferred it specific properties.

Based on these results and on the previous characterization of GrxS12, GrxS14, and GrxS16, a model summarizing their mode of reduction and possible functions in the chloroplast has been established (Fig. 8). Importantly, GrxC5, GrxS14, and GrxS16 could exist as both apo- and holoforms, which exhibit different functionalities. From the literature on plant Grxs, it is likely that all proteins, except GrxS16, possess the capacity to deglutathionylate protein substrates, making them potential central components regulating many plastidial metabolic pathways as several glutathionylated proteins have been identified in chloroplasts (6, 54, 55). However, this reaction is likely to be preferentially carried out by class I Grxs as only GrxC5 and -S12 have the capacity to efficiently regenerate target proteins, which uses only one cysteine for catalysis, such as PrxIIE and MsrB1 (14, 48).[6] Another major difference is that the reductase activity of GrxC5 and -S12 is dependent on GSH, whereas by analogy to the work achieved with *C. reinhardtii* Grx3, GrxS14 and presumably GrxS16 may be reduced by ferredoxin-thioredoxin reductase but not glutathione (6).

Regarding the role of the holoforms, it has been suggested from experimental data or by analogy to results obtained in yeast that class II Grxs (GrxS14 and -S16), which incorporate air-labile and transferable clusters, play a role in Fe-S cluster assembly machineries or in iron sensing (56). On the contrary, AtGrxC5, which binds a more stable Fe-S cluster that cannot be transferred for example to an apoferredoxin (data not shown), should play a different role. As initially suggested for human Grx2, it could act as a redox sensor, responding to oxidative conditions (23).

Minimum Requirement for Fe-S Cluster Assembly in Grxs—The discovery that AtGrxC5 can assemble an Fe-S cluster was initially unexpected. Our results demonstrate that, among the two additional candidate cysteines present in AtGrxC5 compared with PtGrxS12, Cys^{32} determines the ability of GrxC5 to incorporate an Fe-S cluster and also influences protein activity, whereas Cys^{80} has no impact on both properties. Previous characterization of PtGrxS12 led us to conclude that the presence of a Trp residue in the active site signature prevented the incorporation of an Fe-S cluster as its replacement by a Tyr residue was sufficient to allow Fe-S center assembly (27). The present mutagenesis experiments conducted on both paralogs and their structural interpretation pointed to the importance of Cys^{32}, which is indispensable for AtGrxC5 to integrate a cluster, despite the presence of the *a priori* unfavorable Trp^{28}. Interestingly, the comparison of the crystallographic structures of PtGrxS12 and $GrxC5_{apo}$ with $GrxC5_{holo}$ showed that Trp^{28} adopts a different conformation in $GrxC5_{holo}$ with the hydrophobic part of its side chain being strikingly solvent-exposed. The beneficial effect of Cys^{32} on Fe-S cluster incorporation is likely attributed to its ability to form a hydrogen bond with the main chain of Lys^{26} ($d(S–HN) = 3.46$ Å where d is the bond distance), which would stabilize the loop containing residues 26–32 essential for Fe-S cluster binding. A serine at position 32 adopting the same conformation as Cys^{32} could not stabilize this loop because d(O–HN) would exceed 3.5 Å. This observation is consistent with the results obtained for the PtGrxC1 C34S mutant ($^{30}YCGYS^{34}$ active site) that incorporates a much more labile cluster than the WT. In this case, however, we believe that the mutant kept the ability to integrate a cluster due to the presence of Tyr^{30}, which participates in GSH stabilization.

From all these observations and the work published to date on other Fe-S-containing Grxs, it seems that, in addition to the

[6] J. Couturier and N. Rouhier, unpublished results.

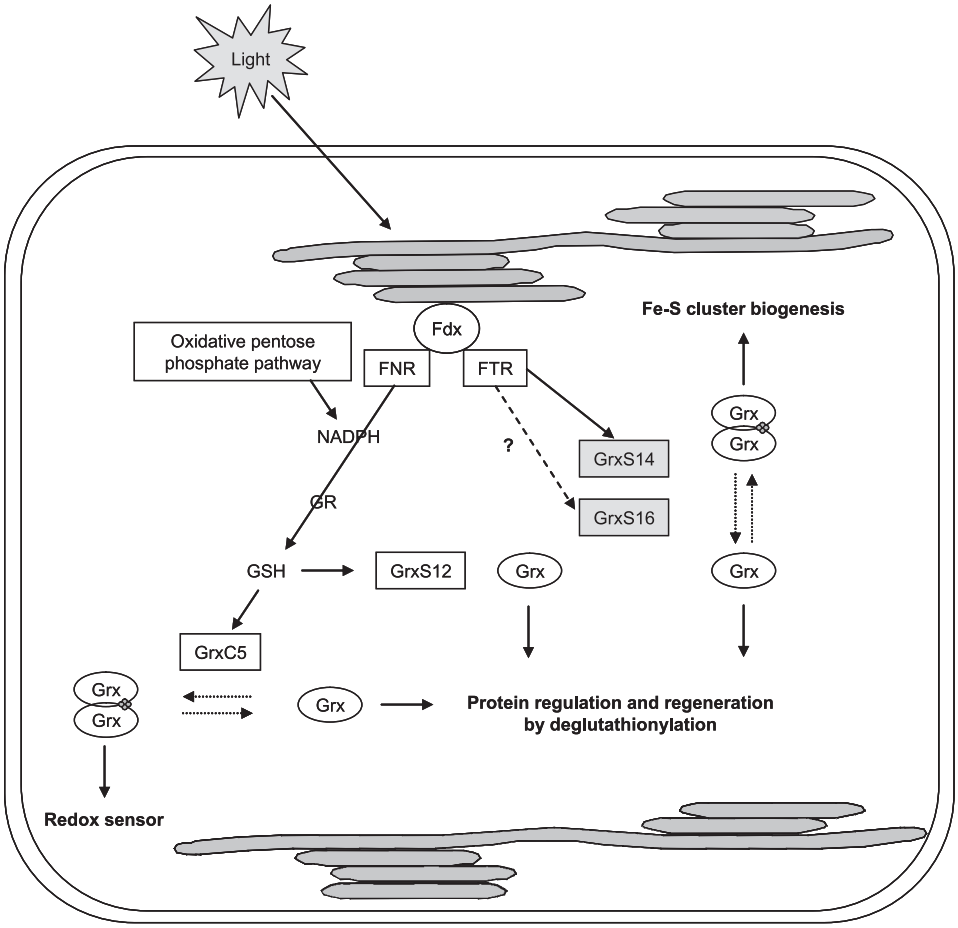

FIGURE 8. **Confirmed or potential roles for plastidial Grxs.** Grxs of class I are depicted in *white*, and those of class II are in *gray*. When the reduction pathway is not clearly demonstrated, *broken lines* are used. GrxC5, GrxS14, and GrxS16 possibly oscillate between an apomonomer and a holodimer state binding an Fe-S cluster. *Fdx*, ferredoxin; *FNR*, ferredoxin:$NADP^+$ reductase; *FTR*, ferredoxin-thioredoxin reductase; *GR*, glutathione reductase.

catalytic cysteine that is absolutely required for the [2Fe-2S] incorporation, there are at least three crucial residues at positions −1, +1, and +3 of the Cys, but they are not necessarily of the same weight (supplemental Table 3). Usually, when two residues at any of these positions have a positive effect, the protein can assemble a cluster. This is exemplified by this study where the stabilizing role of the second active site Cys in AtGrxC5, compared with PtGrxS12, could compensate for the *a priori* unfavorable effect of the Trp, which has to change its conformation without really participating in the cluster or GSH stabilization or in the dimerization.

Nevertheless, the recently identified trypanosome Grx possessing a TCPYC active site is able to incorporate an Fe-S cluster, whereas previous mutagenesis studies had suggested that the presence of the proline prevented Fe-S cluster assembly in plant and human Grxs with a YCPYC active site sequence. This indicates that an additional factor should be considered (8, 57, 58).

Role of Second Active Site Cysteines in Dithiol Grxs—Besides its importance for Fe-S cluster assembly in some Grxs, the role of the second active site Cys residue in the catalytic mechanism of dithiol Grxs remains an important open question. Its mutation affects Grx activity. However, whereas an increase in activity was observed for some yeast and mammalian dithiol Grxs (*e.g.* yeast Grx1, human Grx1 and Grx2, and pig Grx) mutated on this second active site cysteine, other studies revealed a decrease in activity as in the case of yeast Grx2 and *E. coli* Grx1 and Grx3 (5, 18, 19, 50, 52, 59–62). The difference observed between yeast Grx1 and Grx2 has been attributed, at least partially, to the nature of two residues (59). The replacement in yeast Grx2 of Ser by Ala at position 23 and of Gln by Glu at position 52 was proposed to stabilize the glutathionylated form compared with yeast Grx1. However, the absence of conservation of these two residues in other studied proteins prevents the generalization of this hypothesis.

Another recent analysis conducted with several dithiol Grxs has demonstrated that the second active site cysteine determined the glutathione specificity of the second step of peptide deglutathionylation (*i.e.* the reduction of a glutathionylated Grx by a second GSH molecule) in *E. coli* Grx1 but not in human and yeast Grx1 (61). Alternatively, the formation of an intramolecular disulfide bond between the two active site cysteines could constitute a sort of side reaction, which might serve as a protective mechanism for Grx thiol groups in some conditions, although it would certainly at the same time decrease the catalytic efficiency by slowing down Grx regeneration and thus its specific activity. However, this explanation is consistent only for yeast Grx1 and mammalian Grxs but not for yeast Grx2 and *E. coli* Grx1 and Grx3, for which, by extrapolation of the work achieved with *E. coli* Grx1, one can assume that the decrease in

activity observed is correlated to a change in glutathione recognition, binding, or affinity.

Our mutagenesis results and activity measurements clearly demonstrate that AtGrxC5 falls in the same group as mammalian Grxs and yeast Grx1, which might indicate that the second active site cysteine is not involved in the specificity of the second step of the deglutathionylation reaction either (this has yet to be experimentally confirmed) but that an intramolecular disulfide can be formed and can decrease protein reactivity. Contrary to this expectation, we were not able to find conditions allowing the formation of such an intramolecular disulfide. Instead, we found that both Cys^{29} and Cys^{87} can be stably, at least partially, glutathionylated. This is for instance very similar to PtGrxS12, a monothiol Grx, where Cys^{29} was shown to be glutathionylated and Cys^{87} was bound to a β-mercaptoethanol molecule resulting from an HED pretreatment (27). Overall, this indicates that AtGrxC5 likely functions through a monothiol mechanism involving only Cys^{29}, but it does not clarify the role of Cys^{32}.

A comparison between structures of reduced and glutathionylated forms of PtGrxC1 and human Grx2 (although GSH is not covalently linked in this case), which are both dithiol Grxs, shows that thiol groups of the active site cysteines do not adopt the same conformers in both forms (8, 24, 25). Whereas the cysteines are distant and not oriented in the same direction in the reduced forms, the thiol groups of both active site cysteines come closer upon glutathionylation, which might allow formation of an intramolecular bridge if no other unfavorable factor exists. Structural inspection of $GrxC5_{apo}$ revealed that the thiol group of Cys^{32} is present in the direct environment of Cys^{29} (Fig. 7), whereas in PtGrxS12, the side chain of Ser^{32} does not point toward Cys^{29} and would be unchanged between reduced and oxidized forms. This structural characteristic might well be responsible for the difference of a factor 2 in catalytic efficiency observed between AtGrxC5 WT or PtGrxS12 S32C, which possess a Cys, and AtGrxC5 C32S or PtGrxS12, which do not. Hence, although not forming an intramolecular disulfide, it is likely that during the catalytic cycle the proximity of Cys^{32} modifies the chemical environment of Cys^{29}, which might decrease the catalytic efficiency measured under our steady-state conditions.

Acknowledgment—Technical support from Alexandre Kriznik of the Service Commun de Biophysicochimie des Interactions Moléculaires of Nancy University is gratefully acknowledged.

REFERENCES

1. Fernandes, A. P., and Holmgren, A. (2004) *Antioxid. Redox Signal.* **6,** 63–74
2. Rouhier, N., Lemaire, S. D., and Jacquot, J. P. (2008) *Annu. Rev. Plant Biol.* **59,** 143–166
3. Martin, J. L. (1995) *Structure* **3,** 245–250
4. Fernandes, A. P., Fladvad, M., Berndt, C., Andrésen, C., Lillig, C. H., Neubauer, P., Sunnerhagen, M., Holmgren, A., and Vlamis-Gardikas, A. (2005) *J. Biol. Chem.* **280,** 24544–24552
5. Johansson, C., Lillig, C. H., and Holmgren, A. (2004) *J. Biol. Chem.* **279,** 7537–7543
6. Zaffagnini, M., Michelet, L., Massot, V., Trost, P., and Lemaire, S. D. (2008) *J. Biol. Chem.* **283,** 8868–8876
7. Aslund, F., Berndt, K. D., and Holmgren, A. (1997) *J. Biol. Chem.* **272,** 30780–30786
8. Rouhier, N., Unno, H., Bandyopadhyay, S., Masip, L., Kim, S. K., Hirasawa, M., Gualberto, J. M., Lattard, V., Kusunoki, M., Knaff, D. B., Georgiou, G., Hase, T., Johnson, M. K., and Jacquot, J. P. (2007) *Proc. Natl. Acad. Sci. U.S.A.* **104,** 7379–7384
9. Rodríguez-Manzaneque, M. T., Ros, J., Cabiscol, E., Sorribas, A., and Herrero, E. (1999) *Mol. Cell. Biol.* **19,** 8180–8190
10. Rouhier, N., Gelhaye, E., and Jacquot, J. P. (2004) *Cell. Mol. Life Sci.* **61,** 1266–1277
11. Couturier, J., Jacquot, J. P., and Rouhier, N. (2009) *Cell. Mol. Life Sci.* **66,** 2539–2557
12. Rouhier, N., Gelhaye, E., and Jacquot, J. P. (2002) *FEBS Lett.* **511,** 145–149
13. Rouhier, N., Gelhaye, E., Sautiere, P. E., Brun, A., Laurent, P., Tagu, D., Gerard, J., de Faÿ, E., Meyer, Y., and Jacquot, J. P. (2001) *Plant Physiol.* **127,** 1299–1309
14. Tarrago, L., Laugier, E., Zaffagnini, M., Marchand, C., Le Maréchal, P., Rouhier, N., Lemaire, S. D., and Rey, P. (2009) *J. Biol. Chem.* **284,** 18963–18971
15. Vieira Dos Santos, C., Laugier, E., Tarrago, L., Massot, V., Issakidis-Bourguet, E., Rouhier, N., and Rey, P. (2007) *FEBS Lett.* **581,** 4371–4376
16. Greetham, D., Vickerstaff, J., Shenton, D., Perrone, G. G., Dawes, I. W., and Grant, C. M. (2010) *BMC Biochem.* **11,** 3
17. Dalle-Donne, I., Rossi, R., Colombo, G., Giustarini, D., and Milzani, A. (2009) *Trends Biochem. Sci.* **34,** 85–96
18. Bushweller, J. H., Aslund, F., Wüthrich, K., and Holmgren, A. (1992) *Biochemistry* **31,** 9288–9293
19. Peltoniemi, M. J., Karala, A. R., Jurvansuu, J. K., Kinnula, V. L., and Ruddock, L. W. (2006) *J. Biol. Chem.* **281,** 33107–33114
20. Bandyopadhyay, S., Gama, F., Molina-Navarro, M. M., Gualberto, J. M., Claxton, R., Naik, S. G., Huynh, B. H., Herrero, E., Jacquot, J. P., Johnson, M. K., and Rouhier, N. (2008) *EMBO J.* **27,** 1122–1133
21. Molina-Navarro, M. M., Casas, C., Piedrafita, L., Bellí, G., and Herrero, E. (2006) *FEBS Lett.* **580,** 2273–2280
22. Rodríguez-Manzaneque, M. T., Tamarit, J., Bellí, G., Ros, J., and Herrero, E. (2002) *Mol. Biol. Cell* **13,** 1109–1121
23. Lillig, C. H., Berndt, C., Vergnolle, O., Lönn, M. E., Hudemann, C., Bill, E., and Holmgren, A. (2005) *Proc. Natl. Acad. Sci. U.S.A.* **102,** 8168–8173
24. Feng, Y., Zhong, N., Rouhier, N., Hase, T., Kusunoki, M., Jacquot, J. P., Jin, C., and Xia, B. (2006) *Biochemistry* **45,** 7998–8008
25. Johansson, C., Kavanagh, K. L., Gileadi, O., and Oppermann, U. (2007) *J. Biol. Chem.* **282,** 3077–3082
26. Iwema, T., Picciocchi, A., Traore, D. A., Ferrer, J. L., Chauvat, F., and Jacquamet, L. (2009) *Biochemistry* **48,** 6041–6043
27. Couturier, J., Koh, C. S., Zaffagnini, M., Winger, A. M., Gualberto, J. M., Corbier, C., Decottignies, P., Jacquot, J. P., Lemaire, S. D., Didierjean, C., and Rouhier, N. (2009) *J. Biol. Chem.* **284,** 9299–9310
28. Schenk, P. M., Baumann, S., Mattes, R., and Steinbiss, H. H. (1995) *BioTechniques* **19,** 196–198, 200
29. Couturier, J., Didierjean, C., Jacquot, J. P., and Rouhier, N. (2010) *Biochem. Biophys. Res. Commun.* **403,** 435–441
30. Behm, M., and Jacquot, J. P. (2000) *Plant Physiol. Biochem.* **38,** 363–369
31. Horling, F., Lamkemeyer, P., König, J., Finkemeier, I., Kandlbinder, A., Baier, M., and Dietz, K. J. (2003) *Plant Physiol.* **131,** 317–325
32. Wormuth, D., Baier, M., Kandlbinder, A., Scheibe, R., Hartung, W., and Dietz, K. J. (2006) *BMC Plant Biol.* **6,** 15
33. Seidel, T., Golldack, D., and Dietz, K. J. (2005) *FEBS Lett.* **579,** 4374–4382
34. Brown, R. E., Jarvis, K. L., and Hyland, K. J. (1989) *Anal. Biochem.* **180,** 136–139
35. Fish, W. W. (1988) *Methods Enzymol.* **158,** 357–364
36. Crouse, B. R., Sellers, V. M., Finnegan, M. G., Dailey, H. A., and Johnson, M. K. (1996) *Biochemistry* **35,** 16222–16229
37. Kabsch, W. (1993) *J. Appl. Crystallogr.* **26,** 795–800
38. CCP4: Collaborative Computational Project. Number 4 (1994) *Acta Crystallogr. D Biol. Crystallogr.* **50,** 760–763
39. Evans, P. (2006) *Acta Crystallogr. D Biol. Crystallogr.* **62,** 72–82
40. Vagin, A., and Teplyakov, A. (1997) *J. Appl. Crystallogr.* **30,** 1022–1025

41. Murshudov, G. N., Vagin, A. A., and Dodson, E. J. (1997) *Acta Crystallogr. D Biol. Crystallogr.* **53,** 240–255
42. Emsley, P., Lohkamp, B., Scott, W. G., and Cowtan, K. (2010) *Acta Crystallogr. D Biol. Crystallogr.* **66,** 486–501
43. Chen, V. B., Arendall, W. B., 3rd, Headd, J. J., Keedy, D. A., Immormino, R. M., Kapral, G. J., Murray, L. W., Richardson, J. S., and Richardson, D. C. (2010) *Acta Crystallogr. D Biol. Crystallogr.* **66,** 12–21
44. Cheng, N. H., Liu, J. Z., Brock, A., Nelson, R. S., and Hirschi, K. D. (2006) *J. Biol. Chem.* **281,** 26280–26288
45. Ströher, E., Wang, X. J., Roloff, N., Klein, P., Husemann, A., and Dietz, K. J. (2009) *Mol. Plant* **2,** 357–367
46. Luthman, M., and Holmgren, A. (1982) *J. Biol. Chem.* **257,** 6686–6690
47. Holmgren, A. (1979) *J. Biol. Chem.* **254,** 9627–9632
48. Gama, F., Bréhélin, C., Gelhaye, E., Meyer, Y., Jacquot, J. P., Rey, P., and Rouhier, N. (2008) *Physiol. Plant* **133,** 599–610
49. Nikkola, M., Gleason, F. K., Saarinen, M., Joelson, T., Björnberg, O., and Eklund, H. (1991) *J. Biol. Chem.* **266,** 16105–16112
50. Nordstrand, K., slund, F., Holmgren, A., Otting, G., and Berndt, K. D. (1999) *J. Mol. Biol.* **286,** 541–552
51. Xia, T. H., Bushweller, J. H., Sodano, P., Billeter, M., Björnberg, O., Holmgren, A., and Wüthrich, K. (1992) *Protein Sci.* **1,** 310–321
52. Yang, Y., Jao, S., Nanduri, S., Starke, D. W., Mieyal, J. J., and Qin, J. (1998) *Biochemistry* **37,** 17145–17156
53. Meyer, Y., Siala, W., Bashandy, T., Riondet, C., Vignols, F., and Reichheld, J. P. (2008) *Biochim. Biophys. Acta* **1783,** 589–600
54. Gao, X. H., Zaffagnini, M., Bedhomme, M., Michelet, L., Cassier-Chauvat, C., Decottignies, P., and Lemaire, S. D. (2010) *FEBS Lett.* **584,** 2242–2248
55. Michelet, L., Zaffagnini, M., Vanacker, H., Le Maréchal, P., Marchand, C., Schroda, M., Lemaire, S. D., and Decottignies, P. (2008) *J. Biol. Chem.* **283,** 21571–21578
56. Rouhier, N., Couturier, J., Johnson, M. K., and Jacquot, J. P. (2010) *Trends Biochem. Sci.* **35,** 43–52
57. Berndt, C., Hudemann, C., Hanschmann, E. M., Axelsson, R., Holmgren, A., and Lillig, C. H. (2007) *Antioxid. Redox Signal.* **9,** 151–157
58. Ceylan, S., Seidel, V., Ziebart, N., Berndt, C., Dirdjaja, N., and Krauth-Siegel, R. L. (2010) *J. Biol. Chem.* **285,** 35224–35237
59. Discola, K. F., de Oliveira, M. A., Rosa Cussiol, J. R., Monteiro, G., Bárcena, J. A., Porras, P., Padilla, C. A., Guimarães, B. G., and Netto, L. E. (2009) *J. Mol. Biol.* **385,** 889–901
60. Gallogly, M. M., Starke, D. W., Leonberg, A. K., Ospina, S. M., and Mieyal, J. J. (2008) *Biochemistry* **47,** 11144–11157
61. Saaranen, M. J., Salo, K. E., Latva-Ranta, M. K., Kinnula, V. L., and Ruddock, L. W. (2009) *Antioxid. Redox Signal.* **11,** 1819–1828
62. Yang, Y. F., and Wells, W. W. (1991) *J. Biol. Chem.* **266,** 12759–12765

Molecular Plant • Volume 7 • Number 1 • Pages 187–205 • January 2014 RESEARCH ARTICLE

Monothiol Glutaredoxin–BolA Interactions: Redox Control of *Arabidopsis thaliana* BolA2 and SufE1

Jérémy Couturier[a,b,2], Hui-Chen Wu[c,2], Tiphaine Dhalleine[a,b], Henri Pégeot[a,b], Damien Sudre[d], José M. Gualberto[e], Jean-Pierre Jacquot[a,b], Frédéric Gaymard[d], Florence Vignols[c], and Nicolas Rouhier[a,b,1]

a Université de Lorraine, Interactions Arbres–Microorganismes, UMR1136, F-54500 Vandoeuvre-lès-Nancy, France
b INRA, Interactions Arbres–Microorganismes, UMR1136, F-54280 Champenoux, France
c CNRS & UMR186 Résistance des Plantes aux Bio-agresseurs, Institut de Recherche pour le Développement BP 64501, 34394 Montpellier cedex 5, France
d Biochimie et Physiologie Moléculaire des Plantes, CNRS/INRA/Université Montpellier 2, SupAgro. Bat 7, 2 place Viala, 34060 Montpellier cedex 1, France
e Institut de Biologie Moléculaire des Plantes, CNRS UPR2357, F-67084 Strasbourg, France

ABSTRACT A functional relationship between monothiol glutaredoxins and BolAs has been unraveled by genomic analyses and in several high-throughput studies. Phylogenetic analyses coupled to transient expression of green fluorescent protein (GFP) fusions indicated that, in addition to the sulfurtransferase SufE1, which contains a C-terminal BolA domain, three BolA isoforms exist in *Arabidopsis thaliana*, BolA1 being plastidial, BolA2 nucleo-cytoplasmic, and BolA4 dual-targeted to mitochondria and plastids. Binary yeast two-hybrid experiments demonstrated that all BolAs and SufE1, via its BolA domain, can interact with all monothiol glutaredoxins. Most interactions between protein couples of the same subcellular compartment have been confirmed by bimolecular fluorescence complementation. In vitro experiments indicated that monothiol glutaredoxins could regulate the redox state of BolA2 and SufE1, both proteins possessing a single conserved reactive cysteine. Indeed, a glutathionylated form of SufE1 lost its capacity to activate the cysteine desulfurase, Nfs2, but it is reactivated by plastidial glutaredoxins. Besides, a monomeric glutathionylated form and a dimeric disulfide-bridged form of BolA2 can be preferentially reduced by the nucleo-cytoplasmic GrxS17. These results indicate that the glutaredoxin–BolA interaction occurs in several subcellular compartments and suggest that a redox regulation mechanism, disconnected from their capacity to form iron–sulfur cluster-bridged heterodimers, may be physiologically relevant for BolA2 and SufE1.

Key words: BolA; glutaredoxin; interaction; plants; redox control.

INTRODUCTION

BolA proteins have been initially identified in *Escherichia coli* with the observation that their overexpression promoted round cell shape morphology (Aldea et al., 1988). This morphogene effect was shown to be dependent on the presence of FtsZ, a central protein for cell division (Aldea et al., 1988). BolA is also implicated in biofilm formation, likely contributing to the protection of cells from adverse conditions (Vieira et al., 2004). Consistently, BolA gene expression is specifically induced during the transition from exponential to stationary phase and during various stress conditions such as osmotic or oxidative stresses or carbon starvation (Aldea et al., 1989; Santos et al., 1999). The role of *E. coli* BolA seems to rely on the modification of the outer membrane, both by modulating the balance between OmpC and OmpF, two abundant porins, and by regulating the transcript level of three genes, dacA, dacC, and ampC, coding respectively for two D,D-carboxypeptidases (PBP5 and 6) and a β-lactamase, proteins involved in murein metabolism (Santos et al., 2002; Freire et al., 2006). Besides the induction of PBP5 and 6, it was shown recently that BolA can also repress the transcription of the mreBCD operon and thus the transcript and protein levels of mreB, a protein essential for cell elongation, forming filaments upon polymerization (Freire et al., 2009).

[1] To whom correspondence should be addressed. Universite de Lorraine, Interactions Arbres–Microorganismes, UMR1136, F-54500 Vandoeuvre-les-Nancy, France. E-mail nicolas.rouhier@univ-lorraine.fr, tel. + 33 3 83684225

[2] These authors have contributed equally to this work.

doi:10.1093/mp/sst156, Advance Access publication 7 November 2013

Received 17 October 2013; accepted 30 October 2013

This study experimentally confirmed a direct DNA-binding activity of BolA. Indeed, BolA was previously defined as a transcriptional regulator only based on structural evidence indicating the presence of a K-homology domain typical of nucleic acid-binding proteins (Kasai et al., 2004; Chin et al., 2005). This capacity was further addressed by showing that *Ehrlichia chaffeensis* and *E. coli* BolAs bind to some promoters of target genes and that an ortholog from *Chlamydomonas reinhardtii*, uvi31$^+$, exhibits DNA endonuclease activity (Cheng et al., 2011b; Guinote et al., 2011; Shukla et al., 2012). Although most bacteria have two BolA-like proteins, a single study addressed the function of *E. coli* yrbA/ibaG in acid stress resistance (Guinote et al., 2012).

In the yeast species *Schizosaccharomyces pombe*, a BolA ortholog referred to as uvi31$^+$, is rapidly induced by UV radiation (Lee et al., 1994). Its expression is growth phase-dependent and is also regulated during the cell cycle (Kim et al., 1997). A mutant for this gene shows delayed spore germination, modified cell proliferation during vegetative growth, and is indeed more sensitive to UV-light compared to wild-type cells (Kim et al., 1997). As most eukaryotes, *Saccharomyces cerevisiae* possesses three BolA orthologs. In addition to uvi31$^+$, this organism contains two other gene products, named Aim1 and Aim15 (Altered Inheritance of Mitochondria), identified as proteins whose deficiency alters mitochondrial biogenesis and inheritance (Hess et al., 2009). In fact, Aim15 is the same protein as FRA2 (Fe Repressor of Activation) which was characterized as a member of a complex also composed of an aminopeptidase-like protein (FRA1) and two monothiol class II glutaredoxins (Grx3 and 4, CGFS active sites) (Kumanovics et al., 2008). This complex likely constitutes an intermediate linking the status of the mitochondrial Fe–S cluster machinery to the transcriptional control of the iron regulon by regulating the major iron-responsive factor Aft1. Accordingly, a yeast deletion mutant of Fra2 exhibited phenotypes indicative of some defects in the regulation of iron homeostasis (Lesuisse et al., 2005).

The functional relationship between class II glutaredoxins and BolA proteins was initially predicted by genomic analyses which indicated that the two genes are adjacent in many prokaryotic genomes and that there is a strong co-occurrence between these genes (Huynen et al., 2005; Couturier et al., 2009a). Moreover, a physical interaction was described between some CGFS Grxs and BolA-like proteins in *S. cerevisiae*, *Drosophila melanogaster*, and *Arabidopsis thaliana* by genome-wide yeast two-hybrid assays (Ito et al., 2001; Giot et al., 2003; Arabidopsis Interactome Mapping Consortium, 2011). This was confirmed by the co-purification of these proteins in proteome-wide FLAG- and TAP-tag affinity purification studies in yeast and *E. coli* and by immunoprecipitation in yeast (Ho et al., 2002; Butland et al., 2005; Krogan et al., 2006; Kumanovics et al., 2008). Taken together, these data demonstrate a strong phylogenetic and functional connection between the two protein families. However, the nature of the interaction remained unclear until it was shown that both proteins can form [2Fe–2S] cluster-bridged heterodimers (Li et al., 2009; Yeung et al., 2011; Li et al., 2012). This property is consistent with the observation that several CGFS Grxs, including yeast Grx3 and Grx4, can form [2Fe–2S]-bridged homodimers possibly serving as carrier proteins involved in the trafficking of iron–sulfur (Fe–S) clusters (Rodriguez-Manzaneque et al., 2002; Mühlenhoff et al., 2003; Bandyopadhyay et al., 2008; Iwema et al., 2009; Li et al., 2009). Interestingly, a BolA3 mutation in a human patient showed that this mitochondrial protein plays an essential role in the maturation of Fe–S centers contained in lipoate-containing 2-oxoacid dehydrogenases and in the respiratory chain complexes (Cameron et al., 2011).

In this paper, we have performed a phylogenetic analysis of BolAs in photosynthetic organisms and compared them to the gene distribution in all other kingdoms. Indeed, little is known about BolAs in plant species except that it constitutes the C-terminal domain of SufE1, a protein participating to the Fe–S cluster assembly machinery in plastids, and which serves to liberate sulfur atoms from the cysteine desulfurase for a transfer to scaffold proteins (Xu and Moller, 2006; Ye et al., 2006). After investigating their subcellular localizations, we have explored the capacity of all *Arabidopsis* BolAs to interact with the four monothiol Grxs using yeast two-hybrid and bimolecular fluorescence complementation (BiFC) experiments. Moreover, by producing the recombinant proteins, we investigated the possibility of a glutaredoxin-dependent redox regulation of SufE1 and of the BolA2 isoform possessing a single conserved cysteine.

RESULTS

Identification and Classification of BolA Proteins in Photosynthetic Organisms

In order to establish an accurate classification of BolA proteins that can be used in all organisms, a total of 281 sequences, most of them complete, have been retrieved from prokaryotes (eubacteria, archaea of the halobacteriales, and cyanobacteria) but also from eukaryotes, either photosynthetic (green algae and land plants) or non-photosynthetic (fungi, insects, and mammals). Archaea and cyanobacteria analyzed possess only one BolA isoform whereas other organisms analyzed generally have an expanded family comprising two to four BolA isoforms distributed in three major clades representing three monophyletic groups as revealed by phylogenetic analyses (Figure 1 and Supplemental Table 1). However, the careful analysis of the protein sequences and properties led us to propose four different classes named BolA1, BolA2, BolA3, and BolA4, based on the classification used for mammalian BolAs (Kasai et al., 2004; Zhou et al., 2008).

All organisms analyzed, except archaea and cyanobacteria, possess at least one BolA1 member. Sequences from related genera cluster together, the algal and fungal members forming a single group. The ancestor is likely

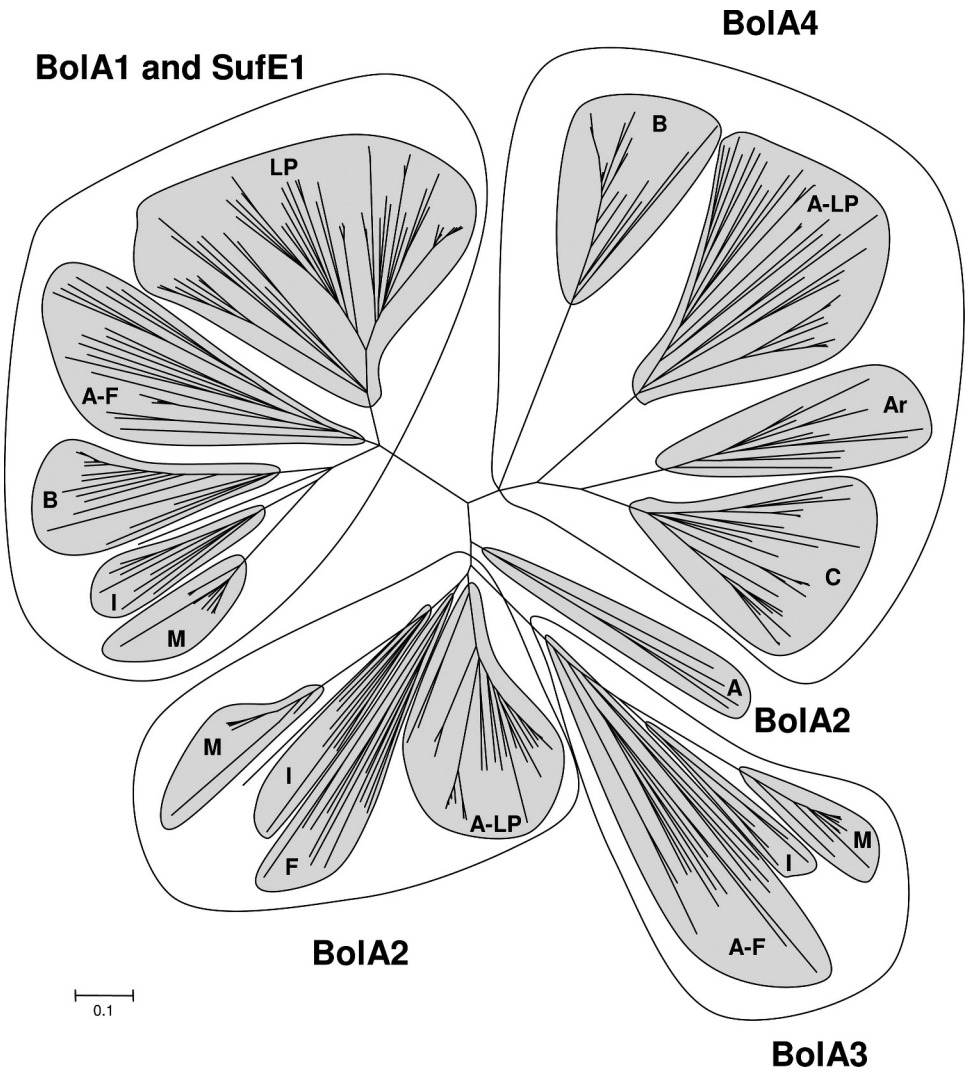

Figure 1. Unrooted, Neighbor-Joining (NJ)-Based Phylogenetic Tree of BolA Family.

The analysis was performed using MEGA4 with the set-up described in the 'Methods' section. Branch lengths are proportional to phylogenetic distances. For clarity, protein names have been removed and only phyla (A, algae; Ar, archaea; B, bacteria; C, cyanobacteria; F, fungi; LP, land plants; I, insects; M, mammals) have been indicated. An isolated branch contains some algal sequences belonging to the BolA2 subgroup. The sequences used are provided as Supplementary material.

the bacterial BolA version and some duplication or gene fusion occurred in the green lineage. Duplication apparently occurred independently in *Micromonas pusilla*, *Oryza sativa*, and *Glycine max*, as these are the only organisms analyzed possessing more than one BolA1 isoform. Moreover, fusion proteins between an N-terminal SufE domain and a C-terminal BolA domain named SufE1 and exclusively restricted to some algae and land plants cluster with BolA1 members. This chimeric protein is absent in cyanobacteria and in Prasinophyceae (*Ostreococcus tauri* and *lucimarinus*, *M. pusilla CCMP1545*) but present in Chlorophyceae (*C. reinhardtii*, *Volvox carteri*, *Chlorella variabilis* NC64A). This suggests that the gene fusion event occurred after the split between Prasinophyceae, an early-diverging class within the green lineage, and Chlorophyceae.

BolA2 and BolA3 classes are specific to eukaryote organisms since no ortholog was found in prokaryotes and they likely derive from a single ancestral gene. The BolA2 class is found in all eukaryotes analyzed (algae, fungi, insects, mammals, and land plants) and contains orthologs of the functionally characterized yeast FRA2 protein. They all possess one BolA2 isoform except *Arabidopsis lyrata*, which has two BolA2 isoforms probably due to a specific and very recent duplication event as *A. thaliana* possesses only one member. Chlorella and Ostreococcus BolA2 isoforms form an isolated branch in the phylogenetic tree, being more distantly related to other BolA2 members. The BolA3 class is restricted to non-photosynthetic eukaryotes with the exceptions of the two algae: *C. reinhardtii* and *V. carteri*. This is not that surprising, as some genes deriving from

the last plant–animal common ancestor have been retained in *Chlamydomonas* and animals but lost in angiosperms (Merchant et al., 2007). Interestingly, in addition to a strictly conserved C-terminal histidine (His66, *A. thaliana* BolA2 numbering) present in all BolAs, proteins of these two classes possess a conserved cysteine in position 29 (*A. thaliana* BolA2 numbering), which might have a structurally or catalytically important function. Nevertheless, two major differences in the primary sequence allow distinguishing BolA2 and BolA3 isoforms. In BolA3 sequences, the cysteine is included in a very conserved SGGCG motif and the His is systematically followed by a Gly, whereas, in BolA2, the cysteine-containing motif is more variable and the HG motif is replaced by an HA motif as in BolA1 and BolA4 isoforms.

The last class, not defined before, has been called BolA4 and it contains orthologs of *E. coli* YrbA. BolA4 proteins are only present in archaea (halobacteriales), bacteria, cyanobacteria, and photosynthetic eukaryotes but are absent in all other eukaryotes. The simplest evolutionary hypothesis would be that the *YrbA* ancestor gene has been conserved in cyanobacteria and then in the whole green lineage and that it has been specifically acquired in halobacteriales. Interestingly, this is the unique BolA present in cyanobacteria and archaea.

Subcellular Localization of *A. thaliana* BolAs

Among the four proteins containing a BolA domain in *A. thaliana*, a dual targeting in chloroplasts and mitochondria has been experimentally determined for AtSufE1 (Xu and Moller, 2006; Ye et al., 2006). In order to determine the subcellular localization of other *Arabidopsis* BolAs, chimeric proteins obtained by fusing the whole sequence of *Arabidopsis* BolA1, BolA2, and BolA4 to green fluorescent protein (GFP) have been used for transient expression experiments using tobacco leaves (Figure 2). A clear fluorescence signal for AtBolA2 was detected both in the cytosol and in the nucleus. Concerning AtBolA1, the reporter protein is directed to the chloroplast as indicated by the superimposition of the GFP signal with the chlorophyll auto-fluorescence in merged images. For AtBolA4, two distinct fluorescence signals consistent with a plastidial and mitochondrial dual targeting have been obtained. It is worth mentioning that similar results have been obtained after expression in tobacco mesophyll, epidermal, and guard cells. Though we

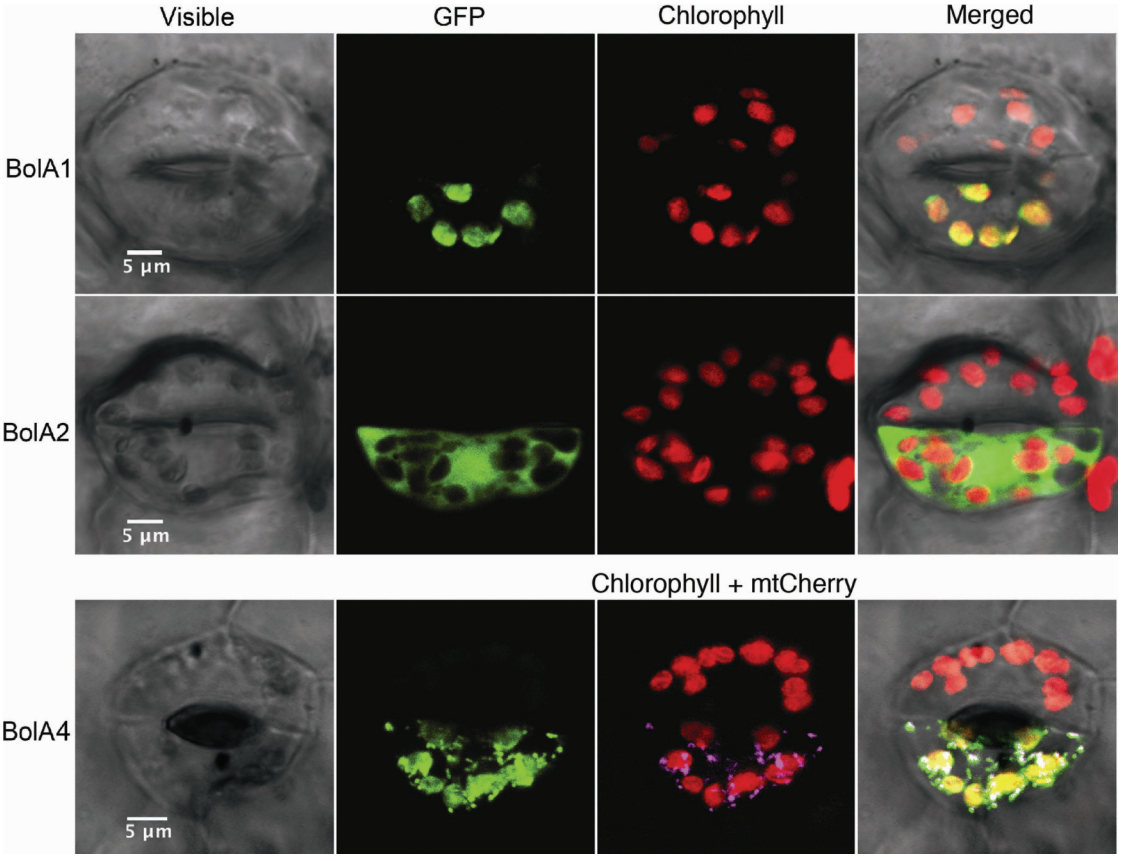

Figure 2. Subcellular Localization of *Arabidopsis thaliana* BolA1, BolA2, and BolA4.

Tobacco cells were transiently transformed with BolA–GFP fusions. From left to right: visible light, fluorescence of the constructions, auto-fluorescence of chlorophyll (red) or fluorescence of a mitochondria targeted mCherry, and merged images. Only one of the guard cells shows GFP signal, because only a small number of cells are transfected in each transformation event.

have to be cautious because overexpression might sometimes lead to mistargeting and BolA2 is a small protein (~10 kDa), the nucleo-cytoplasmic localization of AtBolA2 is consistent with the observation that GFP fusions involving the yeast FRA2/BolA2 and human BolA2 orthologs are also found in both compartments (Kumanovics et al., 2008; Willems et al., 2013).

BolA Proteins Physically Interact with CGFS Grxs

We next assessed the ability of BolA proteins to interact with Grxs, first using a binary Gal4-based yeast two-hybrid approach (Figure 3). By comparison with two representatives of class I Grxs, GrxC5, and GrxS12, we found that only class II/CGFS Grxs were able to physically interact with mono-domain BolAs (Figure 3B). Except for the GrxS14/BolA2 couple, all other co-transformed yeast cells were able to grow in the presence of the HIS3 enzyme inhibitor 3-aminotriazol (3AT) up to a concentration of 5 mM (Figure 3C and 3D), indicating that corresponding interactions are strong. Moreover, it indicates that all CGFS Grxs and BolAs contain the motifs and/or structural arrangement necessary for a physical interaction, regardless of their subcellular compartmentalization or of their domain architecture. As GrxS17 is an atypical protein composed of four different modules, an N-terminal thioredoxin-like domain followed by three CGFS domains, we next analyzed the capacity of each module to interact with BolAs. Whereas the N-terminal Trx domain does not interact by itself with any BolA, we found that the second module of GrxS17 was sufficient to allow interaction with all BolAs (Supplemental Figure 1). This suggests that this domain is

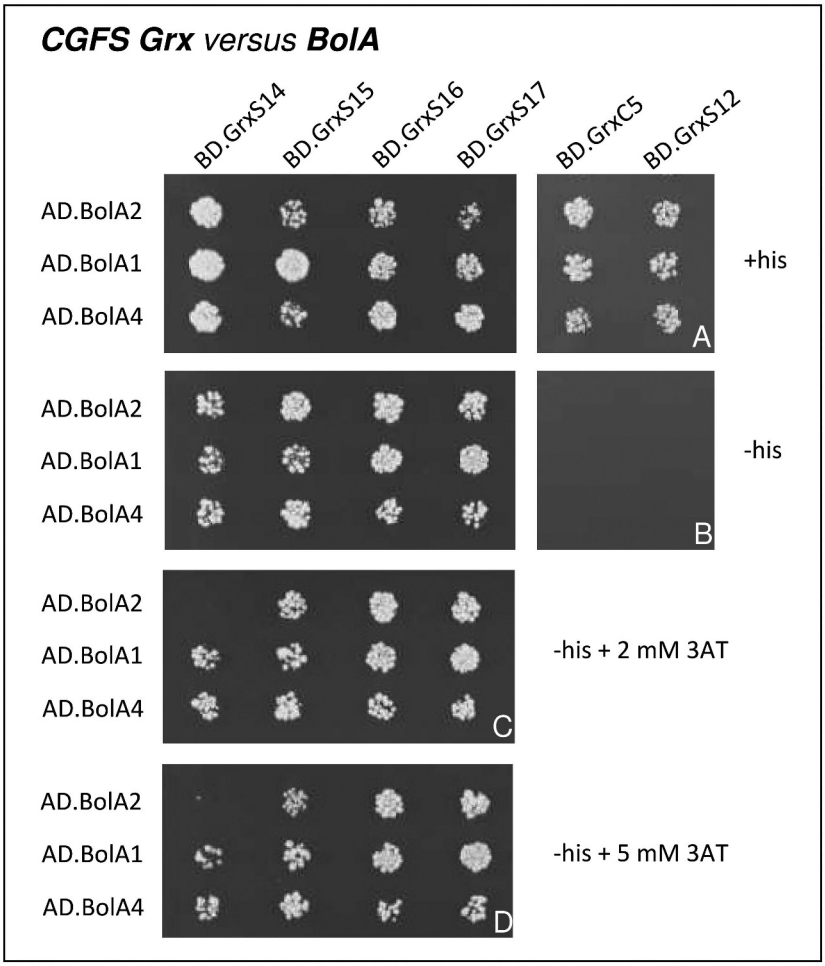

Figure 3. Binary Y2H Interaction of Canonical *Arabidopsis* BolAs with CGFS Grxs.

The yeast strain CY306 was co-transformed with BolA and Grx couples and plated at an optical density of 5.10^{-2} at 600 nm on a control plate containing histidine (+his **(A)**) and on test plates without histidine (-his, **(B–D)**) in the presence of 2 mM (panel C) or 5 mM 3-amino triazol (3AT) (D). Yeast cells were grown at 30°C for 4 d. The results shown have been obtained using BolA proteins expressed as fusion proteins with the Gal4 activator domain (AD) and class II/CGFS Grxs (GrxS14 to S17) or class I Grxs (GrxC5 and S12) expressed as fusion proteins with the Gal4 DNA-binding domain (BD). Similar results were obtained when BolA and Grx were expressed as fusion proteins with BD and AD Gal4 domains, respectively. Neither BolA nor Grx co-transformed with empty vectors allowed yeast growth. Results shown here are representative of four independent experiments.

the one primarily responsible for the observed interactions with BolAs.

Then, the interaction of the multi-domain SufE1 protein with class I and II Grxs was explored using a similar approach. Interestingly, an interaction of SufE1 was also observed with all CGFS Grxs (Figure 4A, middle panel), but with a higher specificity than that observed with canonical BolAs (Figure 4A, right panel). Indeed, when stringency using 3AT was increased, only the interactions with GrxS14 and GrxS17 were maintained. Testing the isolated domains of SufE1, with their putative plastidial and mitochondrial Grx partners, GrxS14, S15 and S16, we observed that only the ^{SufE1}BolA domain of SufE1 was involved in the interaction (Figure 4B, right panel). The fact that the ^{SufE1}BolA domain but not the whole SufE1 protein could interact with GrxS15 and GrxS16 at high stringency (5 mM 3AT) indicates that the ^{SufE1}SufE domain limited the interaction with the full-length SufE1.

Finally, in order to determine whether the active site cysteine of these Grxs is required for the interaction, we tested Grx mutants, namely GrxS14^{C35S} and GrxS16^{C158S}. We found that replacing the CGFS redox center by SGFS in GrxS16 weakened Grx/BolA interaction as yeast growth decreased and was even abolished in the presence of 5 mM 3AT (Figure 5, upper panels). This indicates that, although the GrxS16 catalytic cysteine is dispensable, its presence reinforces the interaction strength with partner proteins. Conversely, a SGFS mutation in GrxS14 does not seem to affect its interaction with canonical BolA proteins, suggesting that other types of interactions (electrostatic, hydrophobic) might be primarily responsible for GrxS14 interactions with partner proteins. A different situation was observed for interactions involving SufE1 (Figure 5, lower panels). The mutation of the active site cysteine in both GrxS14 and GrxS16 drastically reduced the strength of the interactions, as the yeast cells exhibited a highly reduced (GrxS14/SufE1) or null growth (GrxS16/SufE1) even in the absence of 3AT. Overall, this reveals different behaviors or pattern of interactions of CGFS Grxs towards the different classes of BolAs.

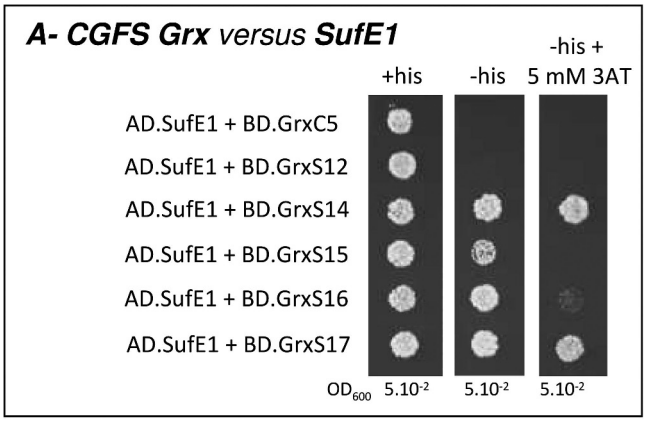

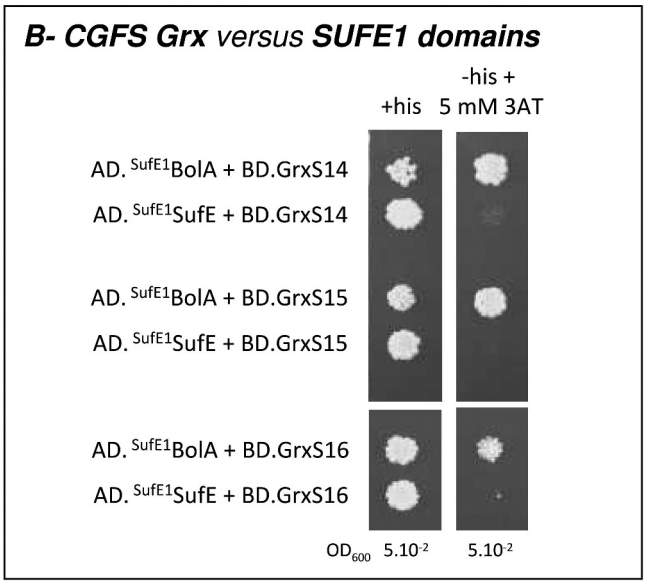

Figure 4. Binary Y2H Interaction of *Arabidopsis* SufE1 with CGFS Grxs.
(A) Interaction of the whole SufE1 protein with class II/CGFS Grxs (GrxS14 to S17) and class I Grxs (GrxC5 and S12).
(B) Interaction of the isolated SufE and BolA domains of SufE1 with plastidial and mitochondrial CGFS Grxs. The yeast strain CY306 was co-transformed, plated, and analyzed as indicated in Figure 3.

Interactions between BolAs and CGFS Grxs Occur *In Planta*

The CGFS Grx–BolA interactions were also assayed in *Arabidopsis* protoplasts by BiFC experiments. For this purpose, pair combinations of constructs producing BolA and Grx proteins fused to half parts of yellow fluorescent protein (YFP) were tested regardless of their previously determined subcellular localization (chloroplastic for GrxS14 and S16, nucleo-cytoplasmic for GrxS17, mitochondrial and chloroplastic for GrxS15) or of previous yeast two-hybrid results. A reconstitution of YFP fluorescence, reporting interactions between the fused partners and co-localizing with the chloroplast compartment, was observed when BolA1, BolA4, and SufE1 constructs were independently co-transformed with either GrxS14 (Figure 6A–6C) or S16 (Figure 6E–6G) constructs.

All these results were confirmed using constructs expressing proteins fused to the other half YFP (Supplemental Figures 2–7). Co-transfection of *Arabidopsis* protoplasts with GrxS15 and BolA4 also led to BiFC and was the only one exhibiting a dual plastidial and mitochondrial pattern (Figure 6D and Supplemental Figure 8). On the other hand, GrxS15/SufE1 co-transfection did not promote fluorescence reconstitution (not shown) whereas GrxS15/BolA1 co-transfection led to very few cells exhibiting fluorescence reconstitution in the chloroplast only (Supplemental Figure 9)—a pattern that we were unable to confirm with fusion proteins cloned in the alternative orientation, except in one cell (Supplemental Figure 9). Hence, we did not consider this interaction as positive. None of the plastidial Grx could reconstitute BiFC when

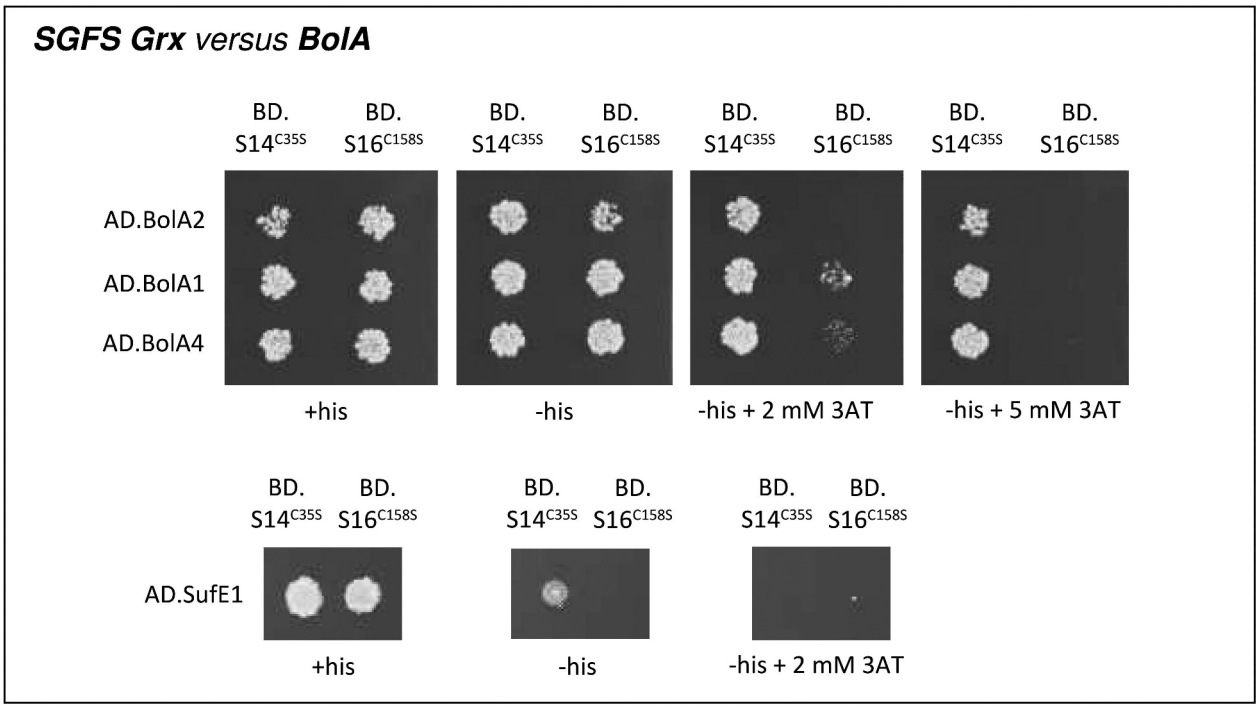

Figure 5. Binary Y2H Interaction of *Arabidopsis* BolAs and SufE1 with Cysteinic Variants of Plastidial Grxs.

Versions of GrxS14 and GrxS16 mutated for the active site cysteine, GrxS14^{C35S} and GrxS16^{C158S}, were co-transformed with BolAs- (upper panels) and SufE1- (lower panels) expressing constructs in the yeast strain CY306. The yeast strain CY306 was co-transformed, plated, and analyzed as indicated in Figure 3.

co-expressed with BolA2. GrxS17 was the only Grx allowing the reconstitution of the fluorescence when co-transfected with BolA2, giving rise to a BiFC in the cytosol and in the nucleus (Figure 6H). A similar result was obtained with the alternative cloning orientation (Supplemental Figure 10). No fluorescence was obtained when BolA1, BolA4, and SufE1 were assayed with this Grx isoform (not shown). These results confirmed that most of the Grx/BolA and Grx/SufE1 BiFC complexes are formed in vivo, with fluorescent patterns compatible with the subcellular localization of the concerned proteins.

AtBolA2 and AtSufE1 Are Sensitive to Oxidizing Treatments

The mature form of all BolA proteins, devoid of N-terminal targeting sequences in the case of BolA1, SufE1, and BolA4, have been expressed as recombinant proteins in *E. coli*. The separation of 'as purified' proteins in reducing or non-reducing SDS–PAGE indicated that a significant amount of BolA2 can form a dimer and that the proportion of dimeric protein gradually increased upon storage. Accordingly, mass spectrometry analyses revealed the presence of two protein peaks with molecular masses of 10 314.6 and 20 627.2 Da (Supplemental Figure 11). The first peak is consistent with a monomeric protein where the first methionine is cleaved whereas the second peak corresponds to a size compatible with a dimeric BolA2. Upon reduction, a single peak with a molecular mass of 10 314.3 Da was detected indicating that the dimeric protein contains an intermolecular disulfide bond. Considering that BolA2 possesses a single conserved cysteine residue (Cys29) which seems to be reactive, we analyzed its sensitivity to oxidative conditions. Oxidative treatments of 2 h with glutathione disulfide (GSSG) or nitrosoglutathione (GSNO) have been performed on a pre-reduced protein using optimal ratios between protein and oxidizing agent of 1/10 and 1/5, respectively, as determined by dose-dependent response curves (not shown). For each experiment, the BolA2 redox state was analyzed both by mass spectrometry and after thiol alkylation. Indeed, reduced and oxidized forms of BolA2 can be distinguished after alkylation by 2 kDa mPEG maleimide and migration on non-reducing SDS–PAGE. As shown in Figure 7A, both treatments led to BolA2 oxidation. In the presence of GSNO, BolA2 is exclusively detected as a monomeric oxidized form. Accordingly, a single peak of 10 619.8 Da was obtained (Supplemental Figure 11). The mass increment of 305.5 Da compared to the molecular mass of the reduced form is consistent with a protein having one glutathione adduct. For GSSG-treated BolA2, two protein peaks, a major one of 10 619.7 Da and a minor one of 20 627.3 Da, have been detected, which correspond respectively to a glutathionylated monomer and to a disulfide-bridged dimer (Figure 7B). The formation of dimeric forms only with GSSG might be related to

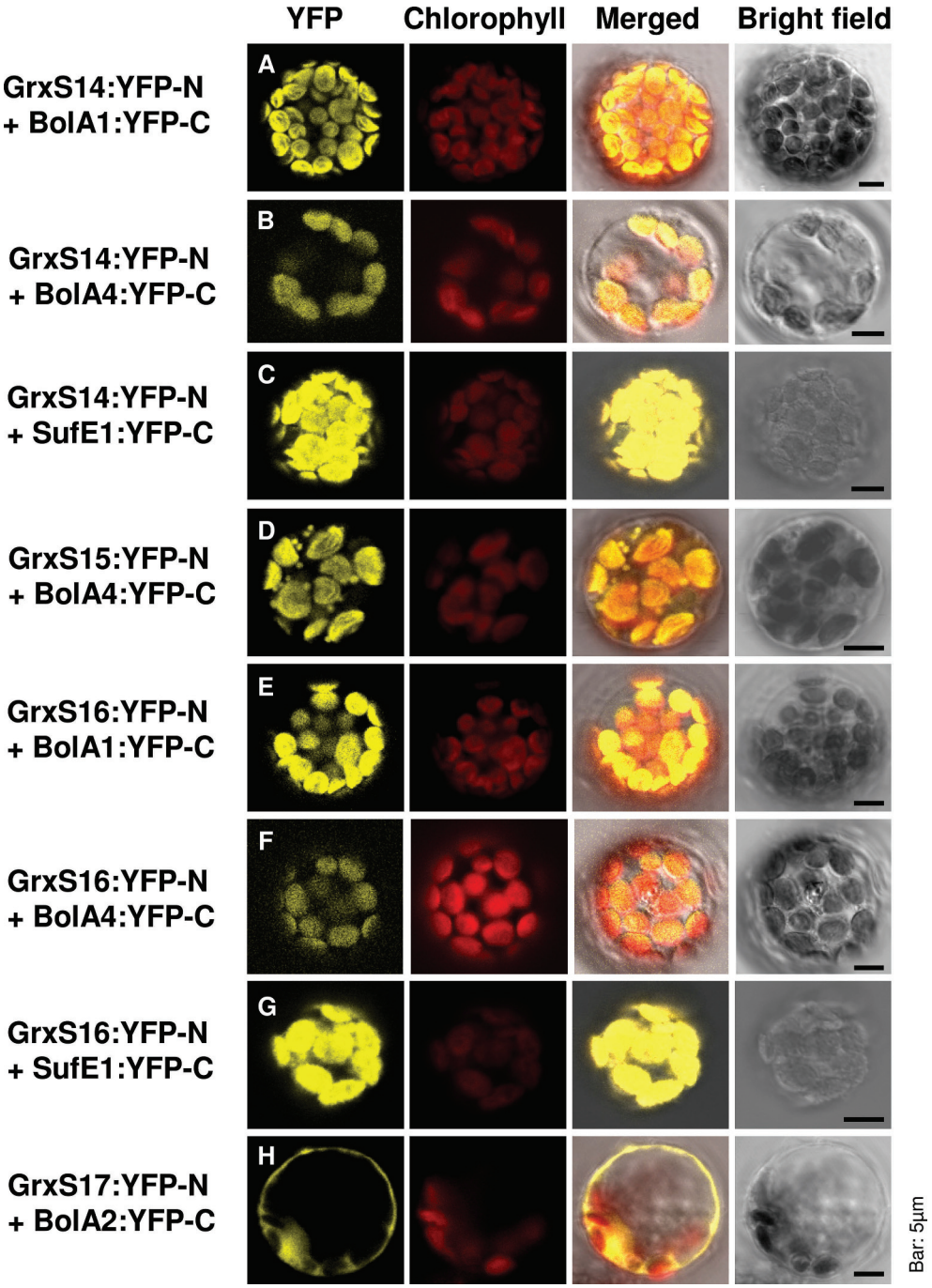

Figure 6. BiFC-Labeled BolA–CGFS Grx Complexes in *Arabidopsis* Protoplasts.

Combinations of N- and C-terminal YFP fragments (*YFP-N* and *YFP-C*, respectively) were transfected as fused downstream from the C-terminus of CGFS Grx and BolA isoforms as follows:

(A) GrxS14:YFP-N and BolA1:YFP-C;
(B) GrxS14:YFP-N and BolA4:YFP-C;
(C) GrxS14:YFP-N and SufE1:YFP-C;
(D) GrxS15:YFP-N and BolA4:YFP-C;
(E) GrxS16:YFP-N and BolA1:YFP-C;
(F) GrxS16:YFP-N and BolA4:YFP-C;
(G) GrxS16:YFP-N and SufE1:YFP-C;
(H) GrxS17:YFP-N and BolA2:YFP-C.

Scale bar: 5 µm. Images are representative of three independent bombardment experiments. Combinations involving Grx or BolA constructs with empty vector controls did not produce BiFC (Supplemental Figures 2–10).

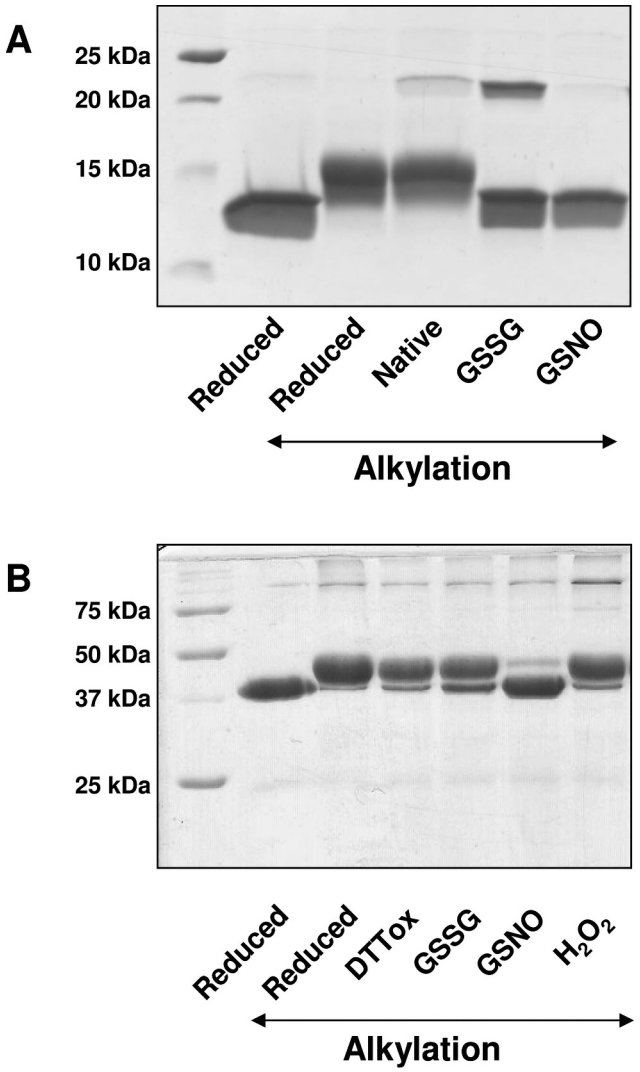

Figure 7. Sensitivity of BolA2 and SufE1 to Oxidative Treatments.

(A) Around 5 µg of pre-reduced, native, and oxidized BolA2 obtained after 2 h oxidative treatments with GSSG or GSNO as described in the 'Methods' section were alkylated or not with 2 kDa mPEG maleimide prior to separation on SDS–PAGE gels in non-reducing conditions.

(B) Pre-reduced SufE1 (5 µM) was subjected to a 1-h oxidative treatment with oxidized DTT (10 mM), H_2O_2 (200 µM), GSSG (1 mM), or GSNO (100 µM). Prior to separation on SDS–PAGE gels in non-reducing conditions, proteins were alkylated or not with 2 kDa mPEG maleimide.

the difference of reactivity compared to GSNO. Indeed, since the reaction with GSSG is slower, some reduced BolA monomers are likely available during the time course of the reaction to react with glutathionylated BolA, promoting the formation of this disulfide-bridged dimer. Among other BolAs, only SufE1 also contains a single conserved cysteine. However, it is located in the ^{SufE1}SufE domain and it is indispensable for the SufE1-dependent activation of Nfs2 activity (Ye et al., 2006). In order to determine whether this observation could prefigure a redox regulation mechanism, the possibility that the cysteine of SufE1 is sensitive to oxidative conditions was also investigated. Whereas an H_2O_2 treatment has no effect on the protein, an oxidative treatment with a 10-fold excess of GSNO, the best glutathionylation agent in this case, prevented alkylation by mPEG maleimide, indicating that the cysteine is indeed oxidized (Figure 7B). Mass spectrometry analysis revealed the presence of a major protein peak corresponding to a molecular mass of 36 070.9 Da (Supplemental Figure 12). Comparing this molecular mass to that of the untreated recombinant protein (35 765.6 Da) pointed to a mass increment of 305.3 Da for one of the peaks, indicating that the protein is glutathionylated.

Altogether, these in vitro experiments demonstrated that BolA2 can undergo different oxidation states being either glutathionylated or forming covalent homodimers, depending on the conditions used and that SufE1 can be glutathionylated.

Deglutathionylation and Reactivation of SufE1 by Glutaredoxins

We then investigated the influence of SufE1 glutathionylation on its ability to stimulate Nfs2 activity and its possible regulation by glutaredoxins. Cysteine desulfurase activity is usually assessed by measuring sulfur released from cysteine in the presence of DTT. While DTT is essential for reducing the persulfide formed on the catalytic cysteine of Nfs2, its presence would prevent evaluating the impact of Grxs on a glutathionylated SufE1. Hence, we have established an activity assay where DTT is replaced by the physiological GSH-reducing system composed of NADPH, GR, and GSH. The amount of sulfur released is decreased nearly two-fold compared to the DTT assay (Figure 8A) and we confirmed that SufE1 still stimulates Nfs2 activity in these conditions. We have also determined, by testing isolated SufE1 domains, that this activation is dependent on the ^{SufE1}SufE domain but not the ^{SufE1}BolA domain (Figure 8B). The difference observed between SufE1 and the ^{SufE1}SufE domain may eventually indicate that ^{SufE1}BolA can contribute to protein–protein interactions. However, the difference might simply reflect the instability of the ^{SufE1}SufE domain compared to full-length SufE1. Indeed, the expression and purification of ^{SufE1}SufE were complicated by the fact that the protein was produced in majority in the insoluble fraction and was prone to precipitation upon storage and to aggregation. As expected, the stimulation of Nfs2 activity is strongly reduced, though not completely, in the presence of glutathionylated SufE1 (Figure 8C). The residual activity is assumed to originate from the capacity of GSH alone (i.e. in the absence of Grxs) to slightly deglutathionylate SufE1 over the time-course experiment as shown by the alkylation assay (Figure 8C). Next, we tested the capacity of all known plastidial *A. thaliana* Grxs to deglutathionylate AtSufE1 by pre-incubating a fully glutathionylated SufE1 with a NADPH/GR/GSH/Grx system (Figure 8C). The measurement of sulfur

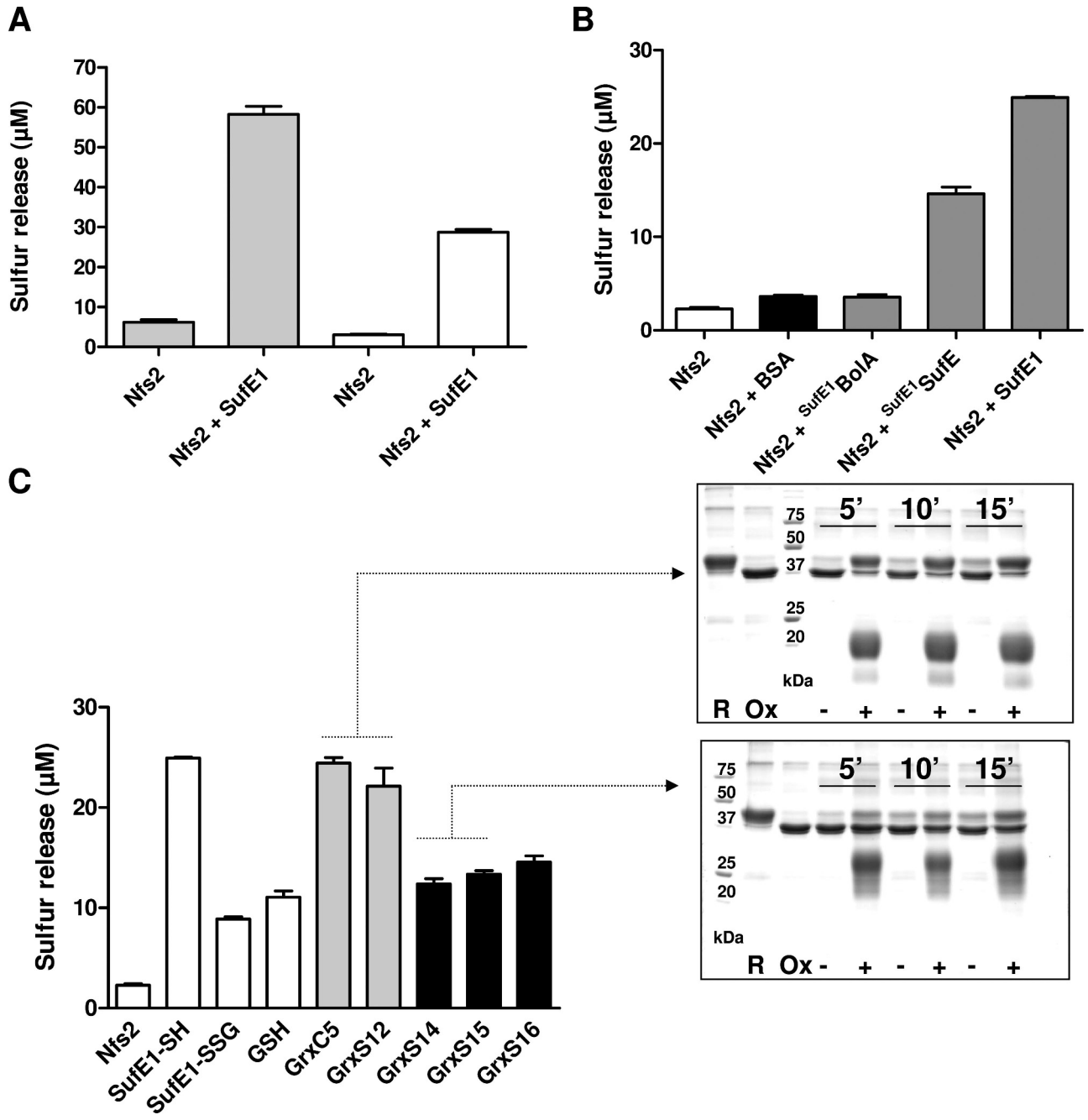

Figure 8. SufE1 Stimulation of Nfs2 Cysteine Desulfurase Activity.

(A) Nfs2 activity is expressed as the amount of liberated sulfur over 30 min in the presence of 2 µM of all proteins, of 500 µM cysteine and with DTT (gray bars), or a glutathione-reducing system (NAPDH/GR/GSH) (white bars).

(B) Influence of isolated ^{SufE1}BolA and ^{SufE1}SufE domains of SufE1. Activities are expressed as the amounts of liberated sulfur over 15 min using a glutathione-reducing system.

(C) Regeneration of glutathionylated SufE1 by plastidial Grxs.

Activities are expressed as the amounts of liberated sulfur over 15 min using a glutathione-reducing system alone or after pre-incubation of glutathionylated SufE1 with Grxs from class I (GrxC5 and S12) or from class II (GrxS14, S15, and S16). The corresponding SDS–PAGE gels compare the reduction of glutathionylated SufE1 after 5, 10, and 15 min of reaction by the NADPH/GR/GSH coupled system alone (–) or with Grx (+). All proteins are alkylated. Reduced (R) or oxidized (Ox) proteins serve as controls.

released and of the SufE1 redox state indicates that GrxC5 and S12 are more efficient than GrxS14, S15, and S16 that only partially reduced and reactivated SufE1. This may be due to the generally lower oxidoreductase activity recorded for monothiol Grxs, at least in the presence of an in vitro GSH-reducing system (Gao et al., 2010).

Redox Properties and Grx-Mediated Regeneration of Oxidized BolA2

Using the same alkylation procedure, the ability of three cytoplasmic disulfide reductases, GrxC1, GrxS17, and Trxh1, to reduce the glutathionylated or dimeric forms of BolA2 was assessed (Figure 9). The glutathionylated protein was obtained after a GSNO treatment and the dimeric form was obtained from the 'as isolated' protein after separation from the monomer by size-exclusion chromatography. After 15-min reaction, DTT was able to completely reduce the glutathionylated monomeric form but only partially the disulfide bond present in the dimeric form. A NADPH/NTR/Trxh1 system was clearly inefficient for the reduction of any oxidized BolA2 form, since only a negligible fraction of glutathionylated BolA2 was reduced (Figure 9A). GSH alone or in combination with NADPH and GR used to mimic the physiological conditions and to maintain a fully reduced GSH pool can only partially reduce the glutathionylated monomeric form but not at all the dimeric form. Adding either GrxC1 or GrxS17 allowed a full reduction of glutathionylated BolA2. Interestingly, GrxS17 was more efficient than GrxC1 for the reduction of the disulfide-bridged dimer.

In order to investigate BolA2 redox properties, the pK_a of Cys29 and the midpoint redox potential (E_m) of both oxidized forms were determined. Using the thiol-cleavable fluorophore PDT-bimane, we have obtained a pK_a value of 7.7 ± 0.2 (Figure 10A), indicating that the thiolate ion will be the dominant species at higher pH values, whereas the protonated thiol will be dominant at lower pH values. Besides, the regeneration of oxidized proteins is also driven by thermodynamic properties such as the E_m values for disulfide/dithiol couples. An E_m value of 287 ± 1 mV was obtained for the dimeric form and a value of 242 ± 1 mV for the glutathionylated form (Figure 10B). The more electronegative redox potential of the intermolecular disulfide bond in the dimer might partly explain why it is less efficiently reduced compared to the glutathione adduct, but other factors as steric hindrance or

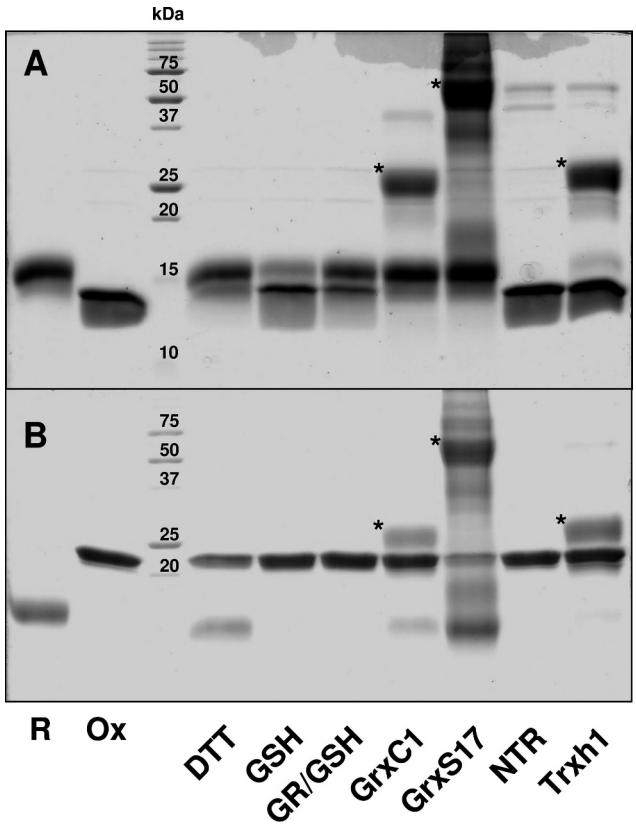

Figure 9. Grx-Dependent Reduction of Oxidized BolA2.

The ability of poplar GrxC1, Trxh1, and *Arabidopsis* GrxS17 to reduce glutathionylated **(A)** and disulfide-bridged dimer **(B)** forms of BolA2 was evaluated in the presence of their corresponding regeneration systems, NADPH/GR/GSH for Grx and NADPH/NTR for Trx. DTT was used as a positive control. Proteins were separated on SDS–PAGE gels in non-reducing conditions after protein alkylation with 2 kDa mPEG maleimide. Reduced (R) or oxidized (Ox) proteins serve as controls. The stars indicate the alkylated forms of the reductants (GrxC1, GrxS17, and Trx h1).

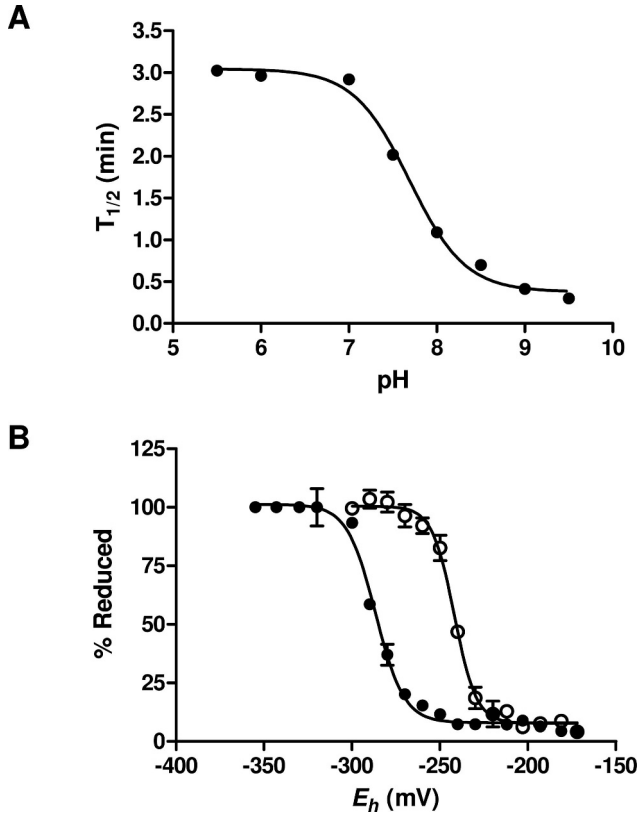

Figure 10. Redox Properties of BolA2.

(A) p*Ka* determination of Cys29 sulfhydryl group. The *t1/2* for the reactions of PDT-bimane with reduced BolA2 were plotted as a function of pH, and the results were fitted to a sigmoidal curve for p*Ka* value determination.

(B) Representative curve of oxidation–reduction titration of glutathionylated (white circles) and disulfide-bridged dimer (black circles) forms of AtBolA2 at pH 7.0. The titration was carried out using a total DTT or GSH concentration of 2 mM for 2 h and resulting free thiol groups were labeled by mBBr. Values in the text are the means ± SD of three replicates.

electrostatic interactions may also play a role as the tested Trx was inefficient in reducing the disulfide bond.

DISCUSSION

Including SufE1 hybrid proteins, the BolA family in *A. thaliana* is composed of four members, but none of the mono-domain BolA proteins has been characterized so far. By transient overexpression of GFP fusions, we observed that BolA1 is plastidial, BolA2 is nucleo-cytoplasmic, and BolA4 is dual-targeted to both plastids and mitochondria. Hence, at least one isoform is expressed in each plant subcellular compartment possessing DNA and/or Fe–S cluster biogenesis systems, which may be consistent with the existence of a DNA-binding domain (Kasai et al., 2004) and with the demonstrated implication of human mitochondrial BolA3 for the maturation of some Fe–S proteins, 2-oxo-dehydrogenases, and complex I subunits (Cameron et al., 2011).

As physical interactions and functional relationships between Grx and BolA proteins are conserved across kingdoms, it is noticeable that at least one CGFS Grx is also expressed in all these subcellular compartments. Indeed, poplar and *A. thaliana* GrxS14 and S16 are located in plastids, whereas *Arabidopsis* GrxS17 is located in the cytoplasm and in the nucleus at least in response to temperature stress conditions (Cheng et al., 2006; Bandyopadhyay et al., 2008; Cheng et al., 2011a; Couturier et al., 2011; Liu et al., 2013). For GrxS15 isoforms, the situation is more uncertain. Transient expression of GFP fusion in tobacco cells indicated an exclusive mitochondrial location for poplar GrxS15 (Bandyopadhyay et al., 2008). On the other hand, overexpressed GFP fusion for *A. thaliana* GrxS15 indicated a chloroplastic localization in tobacco cells (Cheng, 2008) and a mitochondrial localization in soybean suspension cells (Chew et al., 2003). This possible dual targeting for the *A. thaliana* isoform is in line with our BiFC observations that it can interact with BolA4 in both compartments (Figure 6). However, although the maize ortholog was recently found in chloroplasts (Huang et al., 2013), GrxS15 may reside predominantly in mitochondria in *Arabidopsis*, as it was only identified in proteome studies performed with isolated mitochondria, and not in plastid proteomes (Herald et al., 2003; Klodmann et al., 2011). Overall, except for the absence of interaction by BiFC between SufE1 or BolA1 and GrxS15, an interaction between *Arabidopsis* Grxs and BolAs from the same subcellular compartment has been confirmed both by yeast two-hybrid and BiFC approaches. This is for instance consistent with the reported interaction of BolA2 with GrxS17, but also GrxS14 and GrxS15 (Arabidopsis Interactome Mapping Consortium, 2011). Interestingly, among about 6000 studied proteins, these are the only interactants found with BolA2, whereas no partner was reported for BolA1 and BolA4 was not tested.

Whereas the physical interaction between CGFS Grx and BolA from several model organisms including plants seems clear, the function of such complexes in plant is totally unknown. The CGFS Grxs are involved in the maturation of Fe–S proteins, very likely in cellular Fe–S cluster trafficking through their capacity to bind Fe–S clusters into homodimers and to transfer it to acceptor proteins (Rodriguez-Manzaneque et al., 2002; Mühlenhoff et al., 2003; Picciocchi et al., 2007; Bandyopadhyay et al., 2008; Iwema et al., 2009; Rouhier et al., 2010). Besides, genetic analyses in *S. cerevisiae* indicated that a complex, including Grx3 and/or Grx4, BolA2/Fra2, and an aminopeptidase-like protein, serves as a sensor of the mitochondrial Fe and/or Fe–S status and regulates the nuclear translocation of the Aft1 transcription factor (Kumanovics et al., 2008). This role is likely related to the capacity of Grx and BolA to bind an Fe–S cluster into a heterodimer, the cysteine of the CGFS active site motif of these monothiol Grxs serving as one ligand (Li et al., 2009). Because the cluster is more labile in Grx homodimers than in Grx–BolA heterodimers and because adding BolA to Grx homodimers displaces the equilibrium in favor of Grx–BolA heterodimers, it was proposed that BolAs could act as an adapter protein that converts Grxs from a carrier protein to a cellular Fe sensor (Li et al., 2009). While the capacity to form these holo-heterodimers seems universally conserved (Yeung et al., 2011; Li and Outten, 2012; Li et al., 2012), Aft1 orthologs are restricted to a few yeast species, and there is no evidence for another similarly regulated transcription factor in other plants or mammals. Interestingly, in the course of the biochemical characterization of these complexes, it was noticed that both proteins can also interact in their apo-form—that is, without the Fe–S cluster, but the functional relevance of this observation was not clear (Kumanovics et al., 2008; Li et al., 2009). This opens the reverse possibility that Grx may act as a regulator of BolA or SufE1 functions and possibly in an Fe–S cluster-independent manner. The fact that the mutation of the active site cysteine in GrxS14 and S16 does not abolish their interaction with mono-domain BolAs, except in the case of the SufE1/GrxS16 couple, also supports this possibility since the cysteine is absolutely required for Fe–S cluster formation.

Concerning SufE1, it is an essential sulfurtransferase involved in the maturation of Fe–S proteins belonging to the so-called plastidial sulfur mobilization (SUF) machinery and possibly to the mitochondrial iron–sulfur cluster (ISC) machinery (Xu and Moller, 2006; Ye et al., 2006; Couturier et al., 2013). It stimulates the activity of Nfs1 and Nfs2, the mitochondrial and plastidial cysteine desulfurases, respectively, initially mobilizing sulfur atoms necessary for the building of Fe–S clusters from cysteine (Xu and Moller, 2006; Ye et al., 2006). A conserved cysteine residue is crucial for SufE1 activity as it transiently accepts sulfur from the desulfurase in the form of a persulfide before distributing it to scaffold proteins (Ollagnier-de-Choudens et al., 2003; Ye et al., 2006). Besides, two studies, which aimed at identifying partners of *E. coli* SufE and CsdE, revealed that an intermolecular disulfide bond can be formed between these proteins

and Grxs suggesting a possible redox regulation of SufE by Grxs (Bolstad and Wood, 2010; Bolstad et al., 2010). Whereas an interaction of SufE1 was visible with purely plastidial CGFS Grxs, GrxS14 and S16, both by Y2H and BiFC, the strength of the SufE1/GrxS15 interaction observed by Y2H was the lowest among CGFS Grxs and accordingly we did not detect an interaction with GrxS15 by BiFC. The discrepancy between Y2H and BiFC observed for two Grx/BolA couples is puzzling. It might come from the fact that the protein domains fused to the proteins are different, eventually masking some interaction area in one of the methods. Interestingly, the interaction of the multi-domain SufE1 with GrxS14 and S16 is strongly decreased (GrxS14) or abolished (GrxS16) using Grxs mutated for the active site cysteine. Investigating in more detail the reactivity of the SufE1 cysteine residue, we found that it is prone to oxidation in the presence of GSNO, leading to a glutathionylated form but not in response to an H_2O_2 treatment. This result corroborates recent experiments revealing that the *E. coli* SufS–SufE system is relatively resistant to oxidative conditions (Dai and Outten, 2012). Interestingly, this glutathionylated form, which is unable to stimulate Nfs2 activity by accepting sulfur, can be reduced by plastidial Grx isoforms, but more efficiently by class I Grxs (GrxC5 and S12) than by class II Grxs (GrxS14 and S16). As CGFS Grxs usually exhibit a low activity using a GSH-reducing system (Gao et al., 2010), they might require an alternative regeneration system. The fact that no interaction between SufE1 and GrxC5 or S12 was detected by Y2H suggests either that only a glutathionylated form is recognized or that the interaction is too transient to be detected, even in a thioredoxin-minus strain, or that the reduction of an exposed glutathione adduct does not require a strong interaction. Besides this redox level, the presence of the ^{SufE1}BolA domain in SufE1, which is specific to photosynthetic eukaryotes, and its requirement for the observed interactions with CGFS Grxs suggest other possible regulation levels (Figure 11A). Indeed, the formation of a hetero-complex between SufE1 and CGFS Grxs, with or without a Fe–S cluster, could inhibit SufE1 function, simply by promoting particular conformational changes or by masking its cysteine residue. Solving the 3D structure of SufE1 alone or in complex would help in elucidating this point. Overall, as SufE1 is an essential protein for Fe–S cluster biogenesis, controlling its activity via redox or non-redox posttranslational modifications may represent a fundamental regulation point for Fe–S cluster biogenesis, especially in response to oxidative conditions.

Concerning Fe–S cluster-independent functions, a link with redox or stress-response mechanisms has been proposed for BolA proteins from various sources. In *S. pombe*, *E. coli*, and *C. reinhardtii*, the expression of BolA homologs is induced by stress (Aldea et al., 1989; Lee et al., 1994; Shukla et al., 2012) and human BOLA1 prevents mitochondrial morphology aberrations induced by GSH depletion by reducing the associated oxidative shift of the thiol redox potential (Willems et al., 2013). These functions may be related to the DNA-binding activity of BolA proteins which could act as transcriptional regulators (Freire et al., 2009; Cheng et al., 2011b; Guinote et al., 2011) or endonucleases (Shukla et al., 2012). Interestingly, the DNA-binding activity of several transcription factors of bacteria and fungi is controlled by redox posttranslational modifications (D'Autreaux and Toledano, 2007). For example, the formation of an intramolecular disulfide bond activates the DNA-binding activity of OxyR, whereas the reversible reduction by Grx1 deactivates OxyR (Zheng et al., 1998; Choi et al., 2001). The activity of CrtJ, a regulator controlling the biosynthesis of haem, bacteriochlorophyll, and carotenoids in *Rhodobacter capsulatus*, is regulated by the oxidation into sulfenic acid of a cysteine residue located in the HTH (helix-turn-helix) domain responsible of the DNA-binding activity (Cheng et al., 2012). Considering its nucleocytoplasmic localization and the presence of a conserved cysteine (Cys29), BolA2 was the best candidate protein for such a redox control. Although we have not demonstrated the capacity of BolA2 to bind DNA, the oxidative-induced dimerization or glutathionylation forms observed in our in vitro experiments resemble those of redox-regulated transcription factors. By analogy, we hypothesize that GrxS17 might regulate the redox state of BolA2, serving as a redox switch for the activation or inactivation of BolA DNA-binding activity in response to stress conditions (Figure 11). The modeling of BolA2 3D structure based on the solved structure of mammalian BolA (Kasai et al., 2004) indicates that Cys29 is not in the HTH motif as observed in CrtJ, but is situated in a loop containing the conserved histidine involved in the ligation of the Fe–S cluster in the heterodimer (Li et al., 2009). Hence, changes in the DNA-binding capacity, if any, might be influenced, not only by glutathionylation or dimerization, but also by the formation of apo- or holo- Grx–BolA hetero-complexes (Figure 11B). When an activity test becomes available for BolA2, it will be interesting to compare the efficiency of these four conformations. It does not necessarily mean that organellar BolAs without cysteine cannot bind DNA (e.g. the chloroplastic *C. reinhardtii* uvi31+ exhibits DNA endonuclease activity (Shukla et al., 2012)). Their binding could also be regulated by Grxs through the formation of apo- and holo-complexes. Overall, the model of redox regulation only applies to BolA2, but *a priori* not to other BolAs which do not have this conserved cysteine, whereas the model of non-redox regulation could apply to all BolAs.

Our current working model indicates that BolAs alone or in interaction with CGFS Grxs could be (1) redox-regulated transcriptional regulators, (2) factors regulating Fe–S cluster biogenesis either by modulating the Fe–S carrier function of Grx holodimers or as a domain of SufE1; (3) factors contributing to iron sensing as demonstrated in the case of *S. cerevisiae* Aft1 regulation. A single BolA may not have all these functions, and it could depend on the isoform considered and its subcellular compartmentalization.

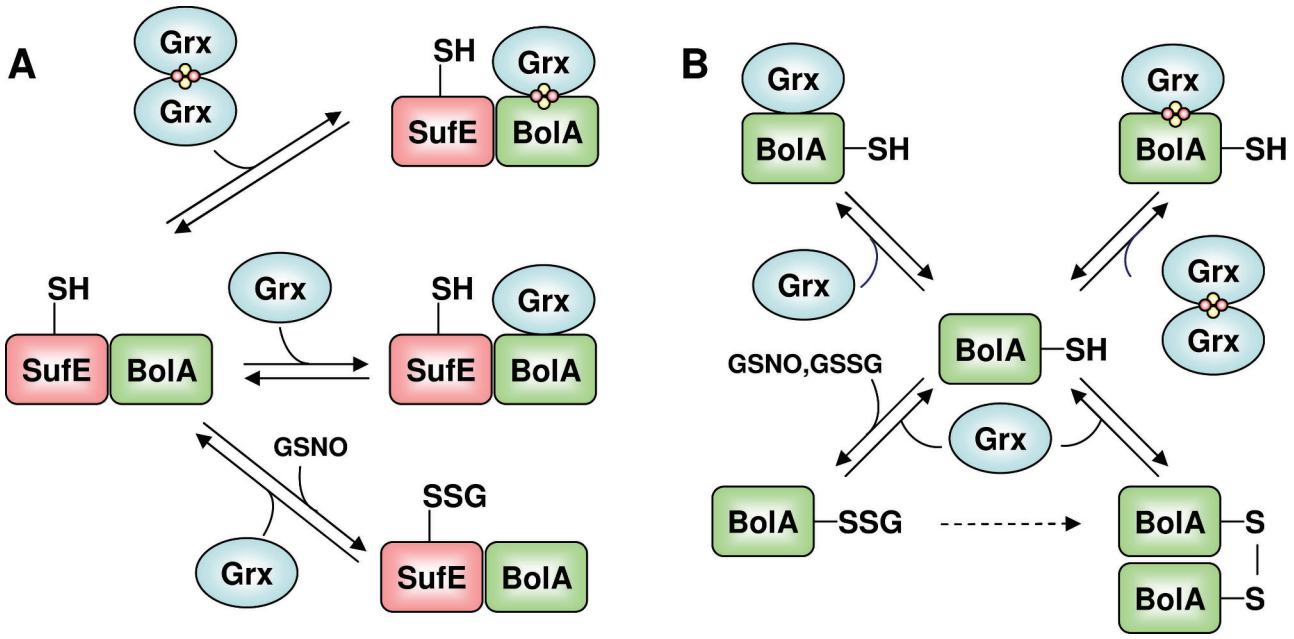

Figure 11. Possible Functions of BolA Proteins in Plants and Regulation by Glutaredoxins.

(A) Regulatory roles of Grxs for SufE1 function.

SufE1 is an essential protein involved in sulfur transfer between the cysteine desulfurase Nfs2 and scaffold proteins using a reactive cysteine. We have obtained evidence that SufE1 interacts with CGFS Grxs, in particular the plastidial GrxS14 and S16, via its BolA domain and that a glutathionylated inactive form of SufE1 can be regenerated by Grxs. This can be viewed as a regulatory mechanism that allows switching on or off the whole biogenesis machinery in some oxidative conditions. The formation of apo or holo-heterodimer could have a similar effect. Another possibility not represented here is that Grxs may receive sulfide from SufE1, functioning either directly as scaffold proteins or constituting sulfur storage forms or intermediates between SufE1 and scaffold proteins.

(B) Regulatory roles of Grxs for mono-domain BolA function. We have obtained evidence that BolA2 interacts in particular with GrxS17, its cytoplasmic counterpart, and that both a glutathionylated and a disulfide-bridged form of BolA2 can be reduced by GrxS17. The functional interpretation might be that the DNA-binding activity or any other function of BolA2 is redox-regulated, in particular in response to oxidative conditions. More generally, and as for SufE1, the formation of apo or holo-heterodimer between Grx and BolA could have similar regulatory effects.

For clarity, the hypothesis that BolA converts monothiol Grxs from carrier proteins to Fe or Fe–S sensors by forming Fe–S cluster-bridged heterodimers instead of Fe–S cluster-bridged homodimers has not been illustrated.

METHODS

Phylogenetic Analyses

Using BLASTP or TBLASTN, *Arabidopsis* BolA sequences were used to search against 18 other genomes from photosynthetic organisms available at the Phytozome database (www.phytozome.net/) and at the following websites, for the 26 cyanobacterial genomes (http://bacteria.kazusa.or.jp/cyanobase/), for *Ostreococcus lucimarinus* (version 2.0) (http://frylock.jgi-psf.org/Ost9901_3/Ost9901_3.home.html), *Ostreococcus RCC809* (version 2.0) (http://frylock.jgi-psf.org/OstRCC809_2/OstRCC809_2.home.html), *O. tauri* (version 2.0) (http://frylock.jgi-psf.org/Ostta4/Ostta4.home.html), *C. variabilis* NC64A (version 1.0) (http://frylock.jgi-psf.org/ChlNC64A_1/ChlNC64A_1.home.html), *V. carteri* (version 1.0), *M. pusilla* CCMP1545 (http://genome.jgi-psf.org/MicpuC2/MicpuC2.home.html) and against EST databases (http://blast.ncbi.nlm.nih.gov/Blast.cgi) for *Hordeum vulgare*, *Panicum virgatum*, *Picea glauca*, *Picea sitchensis*, *Pinus taeda*, *Saccharum hybrid*, *Solanum lycopersicum*, and *Triticum aestivum*. Whenever possible, incomplete sequences have been correctly annotated based on available ESTs and manual inspection of the genomic sequences. For non-photosynthetic prokaryote and eukaryote organisms, sequences were retrieved similarly from Genbank at NCBI but using also *E. coli* YrbA and *E. coli* and yeast BolA sequences, which are more divergent. All protein sequences and corresponding accession numbers used can be found in the supplementary material. The amino acid sequence alignments were done using CLUSTALW and imported into the Molecular Evolutionary Genetics Analysis (MEGA) package version 4.1 (Tamura et al., 2007). Phylogenetic analyses were conducted using the neighbor-joining (NJ) method implemented in MEGA, with the pairwise deletion option for handling alignment gaps, and with the Poisson correction model for distance computation. Bootstrap tests were conducted using 1000 replicates. Branch lengths are proportional to phylogenetic distances.

In Vivo Subcellular Localization by GFP Fusions

The full-length open reading frames including N-terminal extensions were cloned in frame in 5′ of the GFP coding

sequence under the control of a double 35S promoter into the *Nco*I and *Bam*HI restriction sites of pCK S65C for BolA1 and BolA2 or into the *Kpn*I and *Bam*HI restriction sites of pUCAP for BolA4 using primers described in Supplemental Table 2. *Nicotiana benthamiana* cells were transfected by bombardment of leaves with tungsten particles coated with plasmid DNA and images were obtained with a Zeiss LSM510 confocal microscope. For BolA4, co-localization was performed using a pBIN20 plasmid where mCherry is targeted to mitochondria using the yeast CoxIV targeting sequence (Nelson et al., 2007).

Bimolecular Fluorescence Complementation Assay

Full-length open reading frames coding for all Grx, BolA, and SufE1 proteins were cloned into both pUC-SPYCE and pUC-SPYNE (Walter et al., 2004) upstream of the C-terminal and N-terminal regions of YFP, respectively, to preserve N-terminal targeting sequences when present. For nucleo-cytoplasmic proteins, GrxS17 and BolA2 were also fused downstream of the C-terminal and N-terminal regions of YFP using pEZS–CL–NY and pEZS–CL–YC BiFC vectors (Carles and Fletcher, 2009), in order to test a different cloning orientation. All constructs producing fusion proteins were also assayed in control BiFC experiments after co-transformation with either YFP-N or YFP-C empty vectors. Primers are listed in Supplemental Table 2. Isolation and PEG-calcium-mediated transfection of *Arabidopsis* protoplasts by the constructs were as described (Yoo et al., 2007). After incubation for 16–24 h, YFP fluorescence in *Arabidopsis* protoplast cells was detected by laser scanning confocal microscopy using a Zeiss LSM510 META. YFP was excited with an argon laser at 514 nm and detected at 514–550 nm, whereas chlorophyll auto-fluorescence was monitored at 650 nm. Zeiss Zen™ 2009 software was used to obtain images with maximum Z-stack intensity projection. Results are representative of three independent bombardment experiments including the analysis of 10–20 cells per transformation event. For each experiment, we checked that the YFP fluorescence restored by Grx/BolA interactions was not overlapping chlorophyll auto-fluorescence (Supplemental Figure 13).

Yeast Two-Hybrid Binary Assays

All experiments were performed in the Gal4-based yeast two-hybrid reporter strain CY306 (*MAT*α, *ura*3-52, *his*3-200, *ade*2-101, *lys*2-801, *leu*2-3, 112, *trp*1-901, *gal*4-542, *gal*80-538, *lys2::UAS*$_{GAL1}$*-TATA*$_{GAL1}$*-HIS3*, *URA3::UAS*$_{GAL4\ 17MERS(x3)}$*-TATA*$_{CYC1}$*-LacZ*, *trx*1::KanMX4, *trx*2::KanMX4), carrying complete deletions of endogenous *TRX1*- and *TRX2*-encoding genes (Vignols et al., 2005). All open reading frames were cloned in both pGADT7 and pGBKT7 vectors (Clontech) using *Nco*I-, *Nde*I-, and *Bam*HI-containing primers (Supplemental Table 2) in order to test binary interactions in both cloning orientations. CY306 cells co-transformed by pGAD and pGBK constructs were grown on minimal YNB medium (0.7% yeast extract w/o amino acids, 2% glucose, 2% agar) with required amino acids (His, Ade, Lys, Ura, Met). Interactions were visualized as cells growing on YNB medium in the absence of histidine. The strength of the interactions was evaluated by challenging growth in the presence of 2 or 5 mM 3AT. Images were taken 4 d post-dotting (7 µl per dot at an optical density of 5.10^{-2} at 600 nm). Three independent transformations per binary assay were performed, of which two to four colonies were assayed.

Heterologous Expression and Purification of Recombinant Proteins in *E. coli*

The sequences coding for the presumed mature forms (i.e. devoid of N-terminal targeting sequences) of *A. thaliana* GrxS14 to S17, BolA1, BolA2, BolA4, SufE1, and Nfs2 were amplified from *A. thaliana* leaf cDNAs. The sequences coding for BolA and SufE domains of SufE1 (^{SufE1}BolA and ^{SufE1}SufE) were also cloned separately. GrxS14, GrxS15, GrxS16, GrxS17, BolA4, and Nfs2 and ^{SufE1}SufE were cloned into the *Nde*I and *Bam*HI restriction sites of pET15b, BolA1, and BolA2 into the *Nco*I and *Bam*HI restriction sites of pET3d, ^{SufE1}BolA into the *Nde*I and *Bam*HI restriction sites of pET12a, and AtSufE1 into the *Nde*I and *Xho*I restriction sites of pET28a. Details of primers and N- and C-terminal sequences of each expressed recombinant protein are provided in Supplemental Table 2.

For protein expression, the *E. coli* BL21(DE3) strain, containing the pSBET plasmid, was co-transformed with the different recombinant pET3d, pET12a, and pET15b plasmids, but pSBET was omitted for expression of pET28a–SufE1. Cultures were successively amplified up to 2.4 L in LB medium at 37°C supplemented with the adequate antibiotics at 50 µg ml^{-1} (ampicillin is required for pET3d, pET12a, and pET15b, kanamycin for pET28a and pSBET). Protein expression was induced at exponential phase by adding 100 µM isopropyl β-D-thiogalactopyranoside for 4 h at 37°C. The cultures were then centrifuged for 15 min at 4400 *g*. The cell pellets were re-suspended in about 20 ml of 50 mM phosphate pH 8.0, 300 mM NaCl, 10 mM imidazole for his-tagged proteins, or in TE NaCl buffer (30 mM Tris–HCl pH 8.0, 1 mM EDTA, 200 mM NaCl) for untagged proteins and the cells were conserved at –20°C. Cell lysis was performed by sonication and the soluble and insoluble fractions were separated by centrifugation for 30 min at 27 000 *g*.

For his-tagged proteins (BolA4, SufE1, Nfs2, GrxS14, GrxS15, GrxS16, GrxS17, ^{SufE1}SufE), the soluble part was loaded on Ni^{2+} affinity columns (Sigma-Aldrich). After extensive washing, the proteins were eluted using a 50 mM phosphate pH 8.0, 300 mM NaCl, 250 mM imidazole buffer. The recombinant proteins were concentrated by ultrafiltration under nitrogen pressure and dialyzed (Amicon, YM10 membrane) and stored in a TE (30 mM Tris–HCl pH8, 1 mM EDTA) buffer at –20°C.

Aerobic purification of untagged proteins (BolA1, BolA2, ^{SufE1}BolA) was carried out in three steps. The soluble fraction was first precipitated by ammonium sulfate from 0% to 40%

and then to 80% of the saturation. The 40%–80% ammonium sulfate-precipitated fraction was subjected to gel filtration chromatography (ACA44 gel) equilibrated with TE NaCl buffer. After dialysis of the fractions of interest against TE buffer and concentration, the sample was applied to a DEAE sepharose column equilibrated with TE buffer. Proteins were eluted with a NaCl gradient between 0 and 0.4 M. The purest fractions, as judged by SDS–PAGE analysis, were pooled and NaCl was removed by ultrafiltration dialysis using a YM10 membrane and TE buffer. Untagged *Arabidopsis* GrxC5 and poplar GrxC1 and S12 were purified as previously described (Rouhier et al., 2007; Couturier et al., 2009b, 2011).

Oxidizing and Reducing Treatments of BolA2 and SufE1

Around 10 mg of protein were reduced using 40 mM DTT for 2 h at 25°C followed by desalting on G25 column pre-equilibrated with 30 mM Tris–HCl pH 8.0 buffer. Oxidized proteins were prepared by incubating a pre-reduced AtBolA2 with a 10-fold excess GSSG or five-fold excess GSNO and a pre-reduced SufE1 with a 10-fold excess of GSNO for 2 h at 25°C before desalting on G25 columns. The protein oxidation state was then analyzed by electrospray ionization mass spectrometry analysis as described previously (Couturier et al., 2011).

For midpoint redox potential and Trx- or Grx-dependent reduction measurements, the glutathionylated form was obtained by the above-described GSNO treatment whereas the disulfide-bridged dimer of BolA2 was obtained from the as purified protein after separation from the monomer by size-exclusion chromatography onto a Superdex S75 10/300 column equilibrated in 30 mM Tris–HCl pH 8.0, 200 mM NaCl and connected to an Akta purifier system (GE Healthcare).

Cysteine Desulfurase Activity Measurements

The protocol was adapted from a procedure employed previously (Xu and Moller, 2006). Cysteine desulfurase activity was assayed at 25°C in a final volume of 400 µl. Reactions were carried out in 50 mM Tris–HCl pH 7.5, 5 mM $MgCl_2$ 100 mM NaCl, and 10 µM pyridoxal 5′-phosphate using 2 µM Nfs2 in presence or not of 2 µM SufE1, ^{SufE1}BolA, ^{SufE1}SufE, or BSA used as control. Contrary to previous studies, DTT was replaced by a physiological NADPH/GR/GSH system consisting of 200 µM NADPH, 0.1 units of glutathione reductase from bakers' yeast (Sigma), and 500 µM GSH. The reactions were initiated by adding 500 µM L-cysteine and stopped after 30 min by adding 50 µl of 20 mM *N,N*-dimethyl-*p*-phenylenediamine dihydrochloride (prepared in 7.2 M HCl). The addition of 50 µl of 30 mM $FeCl_3$ (prepared in 1.2 M HCl), followed by a 20-min incubation led to formation of methylene blue, which was then measured at 670 nm. Na_2S (1–100 µM) was used for standard curve calibration.

For the regeneration of glutathionylated SufE1, 2 µM was pre-incubated with the NADPH/GR/GSH coupling system with or without 10 µM Grx for 15 min at 25°C prior to adding other reaction components.

Alkylation Assays Assessing the Grx- and Trx-Mediated Reduction of BolA2 and SufE1

For assessing the Grx- and Trx-dependent reduction of oxidized BolA2, around 10 µM of oxidized BolA2 protein was incubated in 50 µl of 30 mM Tris–HCl pH 8.0 buffer for 15 min at 25°C either with 100 µM NADPH, 100 nM of recombinant *A. thaliana* NTRB and 10 µM of poplar Trxh1 isoform, or with 100 µM NADPH, 0.1 units GR, 1 mM GSH, and 10 µM poplar GrxC1 or *Arabidopsis* GrxS17. The 50-µl reaction was then precipitated on ice for 30 min with one volume of 20% trichloroacetic acid (TCA). After centrifugation (10 min at 13 000 *g*) and washing with 100% acetone, the pellet was re-suspended into 10 µl of 100 mM Tris–HCl, pH 8.0, 1% SDS containing 2 mM of methoxyl-PEG maleimide of 2 kDa (mPEG maleimide) which alkylates free thiol groups. The protein mixture was then separated on non-reducing 15% SDS–PAGE.

In the case of the Grx-dependent reduction of glutathionylated SufE1, around 5 µM of oxidized SufE1 protein was incubated in 50 µl of 30 mM Tris–HCl pH 8.0 buffer for 5, 10, and 15 min at 25°C with 100 µM NADPH, 0.1 units GR, 1 mM GSH, and 20 µM poplar GrxS12, *Arabidopsis* GrxC5, GrxS14, or GrxS16. The reaction mixture was then precipitated with TCA and washed with acetone prior to alkylating free thiol groups with mPEG maleimide.

pK_a Determination of Cys29

The p*Ka* measurement of BolA2 Cys29 was performed using (2-pyridyl)-dithiobimane at 25°C as described previously (Couturier et al., 2009b). Reactions were started by the addition of PDT-bimane to a final concentration of 25 µM to 10 µM pre-reduced protein in 500 µl of sodium citrate or phosphate or borate buffers ranging from pH 5.5 to 9.5.

Midpoint Redox Potential Determination

Oxidation-reduction titrations using the fluorescence of the adduct formed between protein free thiols and monobromobimane (mBBr) were carried out at ambient temperature in 200 µl HEPES pH 7.0 buffer containing 10 µM of oxidized proteins, either glutathionylated or disulfide-bridged, and defined mixtures of oxidized and reduced DTT or GSH for more positive values to set the ambient potential (E_h). Total concentration of DTT or GSH was 2 mM. After 2-h incubation, mBBr was added and the reaction was carried out in the dark for 20 min. The reaction mixture was then precipitated on ice for 30 min with one volume of 20% TCA. After centrifugation (10 min at 13 000 *g*) and washing with 100% acetone, the pellet was re-suspended into 400 µl of 100 mM Tris–HCl, pH 8.0, 1% SDS. Fluorescence emission of the resulting solution was measured at 472 nm after excitation at 380 nm.

Accession Numbers

Sequence data from this article can be found using the following AGI locus identifiers for poplar GrxS12 (Potri.002G254100)

and for *A. thaliana* GrxS14 (At3g54900), GrxS15 (At3g15660), GrxS16 (At2g38270), GrxS17 (At4g04950), BolA1 (At1g55805), BolA2 (At5g09830), BolA4 (At5g17560), SufE1 (At4g26500), Nfs2 (At1g08490), and GrxC5 (At4g28730).

FUNDING

This work was supported by the Agence Nationale de la Recherche (grant number: 2010BLAN1616). The UMR 1136 is supported by the French National Research Agency through the Laboratory of Excellence ARBRE (ANR-12-LABXARBRE-01).

ACKNOWLEDGMENTS

The authors would like to thank Drs. Fletcher and Harter for the gift of the BiFC vectors and Dr. Marinus Pilon for the initial gift of an expression plasmid for *Arabidopsis* SufE1. No conflict of interest declared.

REFERENCES

Aldea, M., Garrido, T., Hernandez-Chico, C., Vicente, M., and Kushner, S.R. (1989). Induction of a growth-phase-dependent promoter triggers transcription of bolA, an *Escherichia coli* morphogene. EMBO J. **8**, 3923–3931.

Aldea, M., Hernandez-Chico, C., de la Campa, A.G., Kushner, S.R., and Vicente, M. (1988). Identification, cloning, and expression of bolA, an ftsZ-dependent morphogene of *Escherichia coli*. J. Bacteriol. **170**, 5169–5176.

Arabidopsis Interaction Mapping Consortium (2011). Evidence for network evolution in an *Arabidopsis* interactome map. Science. **333**, 601–607.

Bandyopadhyay, S., Gama, F., Molina-Navarro, M.M., Gualberto, J.M., Claxton, R., Naik, S.G., Huynh, B.H., Herrero, E., Jacquot, J.P., Johnson, M.K., et al. (2008). Chloroplast monothiol glutaredoxins as scaffold proteins for the assembly and delivery of [2Fe–2S] clusters. EMBO J. **27**, 1122–1133.

Bolstad, H.M., and Wood, M.J. (2010). An in vivo method for characterization of protein interactions within sulfur trafficking systems of *E. coli*. J. Proteome Res. **9**, 6740–6751.

Bolstad, H.M., Botelho, D.J., and Wood, M.J. (2010). Proteomic analysis of protein–protein interactions within the cysteine sulfinate desulfinase Fe–S cluster biogenesis system. J. Proteome Res. **9**, 5358–5369.

Butland, G., Peregrin-Alvarez, J.M., Li, J., Yang, W., Yang, X., Canadien, V., Starostine, A., Richards, D., Beattie, B., Krogan, N., et al. (2005). Interaction network containing conserved and essential protein complexes in *Escherichia coli*. Nature. **433**, 531–537.

Cameron, J.M., Janer, A., Levandovskiy, V., Mackay, N., Rouault, T.A., Tong, W.H., Ogilvie, I., Shoubridge, E.A., and Robinson, B.H. (2011). Mutations in iron–sulfur cluster scaffold genes NFU1 and BOLA3 cause a fatal deficiency of multiple respiratory chain and 2-oxoacid dehydrogenase enzymes. Am. J. Hum. Genet. **89**, 486–495.

Carles, C.C., and Fletcher, J.C. (2009). The SAND domain protein ULTRAPETALA1 acts as a trithorax group factor to regulate cell fate in plants. Genes Dev. **23**, 2723–2728.

Cheng, N.H. (2008). AtGRX4, an *Arabidopsis* chloroplastic monothiol glutaredoxin, is able to suppress yeast grx5 mutant phenotypes and respond to oxidative stress. FEBS Lett. **582**, 848–854.

Cheng, N.H., Liu, J.Z., Liu, X., Wu, Q., Thompson, S.M., Lin, J., Chang, J., Whitham, S.A., Park, S., Cohen, J.D., et al.. (2011a). *Arabidopsis* monothiol glutaredoxin, AtGRXS17, is critical for temperature-dependent postembryonic growth and development via modulating auxin response. J. Biol. Chem. **286**, 20398–20406.

Cheng, N.H., Liu, J.Z., Brock, A., Nelson, R.S., and Hirschi, K.D. (2006). AtGRXcp, an *Arabidopsis* chloroplastic glutaredoxin, is critical for protection against protein oxidative damage. J. Biol. Chem. **281**, 26280–26288.

Cheng, Z., Miura, K., Popov, V.L., Kumagai, Y., and Rikihisa, Y. (2011b). Insights into the CtrA regulon in development of stress resistance in obligatory intracellular pathogen *Ehrlichia chaffeensis*. Mol. Microbiol. **82**, 1217–1234.

Cheng, Z., Wu, J., Setterdahl, A., Reddie, K., Carroll, K., Hammad, L.A., Karty, J.A., and Bauer, C.E. (2012). Activity of the tetrapyrrole regulator CrtJ is controlled by oxidation of a redox active cysteine located in the DNA binding domain. Mol. Microbiol. **85**, 734–746.

Chew, O., Whelan, J., and Millar, A.H. (2003). Molecular definition of the ascorbate-glutathione cycle in *Arabidopsis* mitochondria reveals dual targeting of antioxidant defenses in plants. J. Biol. Chem. **278**, 46869–46877.

Chin, K.H., Lin, F.Y., Hu, Y.C., Sze, K.H., Lyu, P.C., and Chou, S.H. (2005). NMR structure note–solution structure of a bacterial BolA-like protein XC975 from a plant pathogen *Xanthomonas campestris* pv. campestris. J. Biomol. NMR. **31**, 167–172.

Choi, H., Kim, S., Mukhopadhyay, P., Cho, S., Woo, J., Storz, G., and Ryu, S.E. (2001). Structural basis of the redox switch in the OxyR transcription factor. Cell. **105**, 103–113.

Couturier, J., Jacquot, J.P., and Rouhier, N. (2009a). Evolution and diversity of glutaredoxins in photosynthetic organisms. Cell Mol. Life Sci. **66**, 2539–2557.

Couturier, J., Koh, C.S., Zaffagnini, M., Winger, A.M., Gualberto, J.M., Corbier, C., Decottignies, P., Jacquot, J.P., Lemaire, S.D., Didierjean, C., et al.. (2009b). Structure–function relationship of the chloroplastic glutaredoxin S12 with an atypical WCSYS active site. J. Biol. Chem. **284**, 9299–9310.

Couturier, J., Stroher, E., Albetel, A.N., Roret, T., Muthuramalingam, M., Tarrago, L., Seidel, T., Tsan, P., Jacquot, J.P., Johnson, M.K., et al. (2011). *Arabidopsis* chloroplastic glutaredoxin C5 as a model to explore molecular determinants for iron–sulfur cluster binding into glutaredoxins. J. Biol. Chem. **286**, 27515–27527.

Couturier, J., Touraine, B., Briat, J.F., Gaymard, F., and Rouhier, N. (2013). The iron–sulfur cluster assembly machineries in plants: current knowledge and open questions. Front Plant Sci. **4**, 259.

D'Autreaux, B., and Toledano, M.B. (2007). ROS as signalling molecules: mechanisms that generate specificity in ROS homeostasis. Nat. Rev. Mol. Cell Biol. **8**, 813–824.

Dai, Y., and Outten, F.W. (2012). The *E. coli* SufS–SufE sulfur transfer system is more resistant to oxidative stress than IscS–IscU. FEBS Lett. **586**, 4016–4022.

Freire, P., Moreira, R.N., and Arraiano, C.M. (2009). BolA inhibits cell elongation and regulates MreB expression levels. J. Mol. Biol. **385**, 1345–1351.

Freire, P., Vieira, H.L., Furtado, A.R., de Pedro, M.A., and Arraiano, C.M. (2006). Effect of the morphogene bolA on the permeability of the *Escherichia coli* outer membrane. FEMS Lett. **260**, 106–111.

Gao, X.H., Zaffagnini, M., Bedhomme, M., Michelet, L., Cassier-Chauvat, C., Decottignies, P., and Lemaire, S.D. (2010). Biochemical characterization of glutaredoxins from *Chlamydomonas reinhardtii*: kinetics and specificity in deglutathionylation reactions. FEBS Lett. **584**, 2242–2248.

Giot, L., Bader, J.S., Brouwer, C., Chaudhuri, A., Kuang, B., Li, Y., Hao, Y.L., Ooi, C.E., Godwin, B., Vitols, E., et al. (2003). A protein interaction map of *Drosophila melanogaster*. Science. **302**, 1727–1736.

Guinote, I.B., Matos, R.G., Freire, P., and Arraiano, C.M. (2011). BolA affects cell growth, and binds to the promoters of penicillin-binding proteins 5 and 6 and regulates their expression. J. Microbiol. Biotechnol. **21**, 243–251.

Guinote, I.B., Moreira, R.N., Freire, P., and Arraiano, C.M. (2012). Characterization of the BolA homolog IbaG: a new gene involved in acid resistance. J. Microbiol. Biotechnol. **22**, 484–493.

Herald, V.L., Heazlewood, J.L., Day, D.A., and Millar, A.H. (2003). Proteomic identification of divalent metal cation binding proteins in plant mitochondria. FEBS Lett. **537**, 96–100.

Hess, D.C., Myers, C.L., Huttenhower, C., Hibbs, M.A., Hayes, A.P., Paw, J., Clore, J.J., Mendoza, R.M., Luis, B.S., Nislow, C., et al. (2009). Computationally driven, quantitative experiments discover genes required for mitochondrial biogenesis. PLoS Genet. **5**, e1000407.

Ho, Y., Gruhler, A., Heilbut, A., Bader, G.D., Moore, L., Adams, S.L., Millar, A., Taylor, P., Bennett, K., Boutilier, K., et al. (2002). Systematic identification of protein complexes in *Saccharomyces cerevisiae* by mass spectrometry. Nature. **415**, 180–183.

Huang, M., Friso, G., Nishimura, K., Qu, X., Olinares, P.D., Majeran, W., Sun, Q., and van Wijk, K.J. (2013). Construction of plastid reference proteomes for maize and *Arabidopsis* and evaluation of their orthologous relationships; the concept of orthoproteomics. J. Proteome Res. **12**, 491–504.

Huynen, M.A., Spronk, C.A., Gabaldon, T., and Snel, B. (2005). Combining data from genomes, Y2H and 3D structure indicates that BolA is a reductase interacting with a glutaredoxin. FEBS Lett. **579**, 591–596.

Ito, T., Chiba, T., Ozawa, R., Yoshida, M., Hattori, M., and Sakaki, Y. (2001). A comprehensive two-hybrid analysis to explore the yeast protein interactome. Proc. Natl Acad. Sci. U S A. **98**, 4569–4574.

Iwema, T., Picciocchi, A., Traore, D.A., Ferrer, J.L., Chauvat, F., and Jacquamet, L. (2009). Structural basis for delivery of the intact [Fe2S2] cluster by monothiol glutaredoxin. Biochemistry. **48**, 6041–6043.

Kasai, T., Inoue, M., Koshiba, S., Yabuki, T., Aoki, M., Nunokawa, E., Seki, E., Matsuda, T., Matsuda, N., Tomo, Y., et al. (2004). Solution structure of a BolA-like protein from Mus musculus. Protein Sci. **13**, 545–548.

Kim, S.H., Kim, M., Lee, J.K., Kim, M.J., Jin, Y.H., Seong, R.H., Hong, S.H., Joe, C.O., and Park, S.D. (1997). Identification and expression of uvi31+, a UV-inducible gene from *Schizosaccharomyces pombe*. Environ. Mol. Mutagen. **30**, 72–81.

Klodmann, J., Senkler, M., Rode, C., and Braun, H.P. (2011). Defining the protein complex proteome of plant mitochondria. Plant Physiol. **157**, 587–598.

Krogan, N.J., Cagney, G., Yu, H., Zhong, G., Guo, X., Ignatchenko, A., Li, J., Pu, S., Datta, N., Tikuisis, A.P., et al. (2006). Global landscape of protein complexes in the yeast *Saccharomyces cerevisiae*. Nature. **440**, 637–643.

Kumanovics, A., Chen, O.S., Li, L., Bagley, D., Adkins, E.M., Lin, H., Dingra, N.N., Outten, C.E., Keller, G., Winge, D., et al. (2008). Identification of FRA1 and FRA2 as genes involved in regulating the yeast iron regulon in response to decreased mitochondrial iron–sulfur cluster synthesis. J. Biol. Chem. **283**, 10276–10286.

Lee, J.K., Park, E.J., Chung, H.K., Hong, S.H., Joe, C.O., and Park, S.D. (1994). Isolation of UV-inducible transcripts from *Schizosaccharomyces pombe*. Biochem. Biophys. Res. Commun. **202**, 1113–1119.

Lesuisse, E., Knight, S.A., Courel, M., Santos, R., Camadro, J.M., and Dancis, A. (2005). Genome-wide screen for genes with effects on distinct iron uptake activities in *Saccharomyces cerevisiae*. Genetics. **169**, 107–122.

Li, H., and Outten, C.E. (2012). Monothiol CGFS glutaredoxins and BolA-like proteins: [2Fe–2S] binding partners in iron homeostasis. Biochemistry. **51**, 4377–4389.

Li, H., Mapolelo, D.T., Dingra, N.N., Naik, S.G., Lees, N.S., Hoffman, B.M., Riggs-Gelasco, P.J., Huynh, B.H., Johnson, M.K., and Outten, C.E. (2009). The yeast iron regulatory proteins Grx3/4 and Fra2 form heterodimeric complexes containing a [2Fe–2S] cluster with cysteinyl and histidyl ligation. Biochemistry. **48**, 9569–9581.

Li, H., Mapolelo, D.T., Randeniya, S., Johnson, M.K., and Outten, C.E. (2012). Human glutaredoxin 3 forms [2Fe–2S]-bridged complexes with human BolA2. Biochemistry. **51**, 1687–1696.

Liu, X., Liu, S., Feng, Y., Liu, J.Z., Chen, Y., Pham, K., Deng, H., Hirschi, K.D., Wang, X., and Cheng, N. (2013). Structural insights into the N-terminal GIY-YIG endonuclease activity of *Arabidopsis* glutaredoxin AtGRXS16 in chloroplasts. Proc. Natl Acad. Sci. U S A. **110**, 9565–9570.

Merchant, S.S., Prochnik, S.E., Vallon, O., Harris, E.H., Karpowicz, S.J., Witman, G.B., Terry, A., Salamov, A., Fritz-Laylin, L.K., Marechal-Drouard, L., et al. (2007). The Chlamydomonas genome reveals the evolution of key animal and plant functions. Science. **318**, 245–250.

Mühlenhoff, U., Gerber, J., Richhardt, N., and Lill, R. (2003). Components involved in assembly and dislocation of iron–sulfur clusters on the scaffold protein Isu1p. EMBO J. **22**, 4815–4825.

Nelson, B.K., Cai, X., and Nebenfuhr, A. (2007). A multicolored set of in vivo organelle markers for co-localization studies in *Arabidopsis* and other plants. Plant J. **51**, 1126–1136.

Ollagnier-de-Choudens, S., Lascoux, D., Loiseau, L., Barras, F., Forest, E., and Fontecave, M. (2003). Mechanistic studies of the SufS–SufE cysteine desulfurase: evidence for sulfur transfer from SufS to SufE. FEBS Lett. **555**, 263–267.

Picciocchi, A., Saguez, C., Boussac, A., Cassier-Chauvat, C., and Chauvat, F. (2007). CGFS-type monothiol glutaredoxins from

the cyanobacterium Synechocystis PCC6803 and other evolutionary distant model organisms possess a glutathione-ligated [2Fe–2S] cluster. Biochemistry. **46**, 15018–15026.

Rodriguez-Manzaneque, M.T., Tamarit, J., Belli, G., Ros, J., and Herrero, E. (2002). Grx5 is a mitochondrial glutaredoxin required for the activity of iron/sulfur enzymes. Mol. Biol. Cell. **13**, 1109–1121.

Rouhier, N., Couturier, J., Johnson, M.K., and Jacquot, J.P. (2010). Glutaredoxins: roles in iron homeostasis. Trends Biochem. Sci. **35**, 43–52.

Rouhier, N., Unno, H., Bandyopadhyay, S., Masip, L., Kim, S.K., Hirasawa, M., Gualberto, J.M., Lattard, V., Kusunoki, M., Knaff, D.B., et al. (2007). Functional, structural, and spectroscopic characterization of a glutathione-ligated [2Fe–2S] cluster in poplar glutaredoxin C1. Proc. Natl Acad. Sci. U S A. **104**, 7379–7384.

Santos, J.M., Freire, P., Vicente, M., and Arraiano, C.M. (1999). The stationary-phase morphogene bolA from *Escherichia coli* is induced by stress during early stages of growth. Mol. Microbiol. **32**, 789–798.

Santos, J.M., Lobo, M., Matos, A.P., De Pedro, M.A., and Arraiano, C.M. (2002). The gene bolA regulates dacA (PBP5), dacC (PBP6) and ampC (AmpC), promoting normal morphology in *Escherichia coli*. Mol. Microbiol. **45**, 1729–1740.

Shukla, M., Minda, R., Singh, H., Tirumani, S., Chary, K.V., and Rao, B.J. (2012). UVI31+ is a DNA endonuclease that dynamically localizes to chloroplast pyrenoids in *C. reinhardtii*. PLoS One. **7**, e51913.

Tamura, K., Dudley, J., Nei, M., and Kumar, S. (2007). MEGA4: Molecular Evolutionary Genetics Analysis (MEGA) software version 4.0. Mol. Biol. Evol. **24**, 1596–1599.

Vieira, H.L., Freire, P., and Arraiano, C.M. (2004). Effect of *Escherichia coli* morphogene bolA on biofilms. Appl. Environ. Microbiol. **70**, 5682–5684.

Vignols, F., Brehelin, C., Surdin-Kerjan, Y., Thomas, D., and Meyer, Y. (2005). A yeast two-hybrid knockout strain to explore thioredoxin-interacting proteins in vivo. Proc. Natl Acad. Sci. U S A. **102**, 16729–16734.

Walter, M., Chaban, C., Schutze, K., Batistic, O., Weckermann, K., Nake, C., Blazevic, D., Grefen, C., Schumacher, K., Oecking, C., et al. (2004). Visualization of protein interactions in living plant cells using bimolecular fluorescence complementation. Plant J. **40**, 428–438.

Willems, P., Wanschers, B.F., Esseling, J., Szklarczyk, R., Kudla, U., Duarte, I., Forkink, M., Nooteboom, M., Swarts, H., Gloerich, J., et al. (2013). BOLA1 is an aerobic protein that prevents mitochondrial morphology changes induced by glutathione depletion. Antioxid. Redox Signal. **18**, 129–138.

Xu, X.M., and Moller, S.G. (2006). AtSufE is an essential activator of plastidic and mitochondrial desulfurases in *Arabidopsis*. EMBO J. **25**, 900–909.

Ye, H., Abdel-Ghany, S.E., Anderson, T.D., Pilon-Smits, E.A., and Pilon, M. (2006). CpSufE activates the cysteine desulfurase CpNifS for chloroplastic Fe–S cluster formation. J. Biol. Chem. **281**, 8958–8969.

Yeung, N., Gold, B., Liu, N.L., Prathapam, R., Sterling, H.J., Willams, E.R., and Butland, G. (2011). The *E. coli* monothiol glutaredoxin GrxD forms homodimeric and heterodimeric FeS cluster containing complexes. Biochemistry. **50**, 8957–8969.

Yoo, S.D., Cho, Y.H., and Sheen, J. (2007). *Arabidopsis* mesophyll protoplasts: a versatile cell system for transient gene expression analysis. Nat. Protoc. **2**, 1565–1572.

Zheng, M., Aslund, F., and Storz, G. (1998). Activation of the OxyR transcription factor by reversible disulfide bond formation. Science. **279**, 1718–1721.

Zhou, Y.B., Cao, J.B., Wan, B.B., Wang, X.R., Ding, G.H., Zhu, H., Yang, H.M., Wang, K.S., Zhang, X., and Han, Z.G. (2008). hBolA, novel non-classical secreted proteins, belonging to different BolA family with functional divergence. Mol. Cell Biochem. **317**, 61–68.

Biochimica et Biophysica Acta 1853 (2015) 1513–1527

Contents lists available at ScienceDirect

Biochimica et Biophysica Acta

journal homepage: www.elsevier.com/locate/bbamcr

Review

The roles of glutaredoxins ligating Fe–S clusters: Sensing, transfer or repair functions?☆

Jérémy Couturier [a,b], Jonathan Przybyla-Toscano [a,b], Thomas Roret [c,d], Claude Didierjean [c,d], Nicolas Rouhier [a,b,*]

[a] Université de Lorraine, UMR 1136 Interactions Arbres Microorganismes, F-54500 Vandœuvre-lès-Nancy, France
[b] INRA, UMR 1136 Interactions Arbres Microorganismes, F-54280 Champenoux, France
[c] Université de Lorraine, UMR 7036 CRM2, BioMod group, 54506 Vandœuvre-lès-Nancy, France
[d] CNRS, UMR 7036 CRM2, BioMod group, 54506 Vandœuvre-lès-Nancy, France

ARTICLE INFO

Article history:
Received 7 July 2014
Received in revised form 17 September 2014
Accepted 18 September 2014
Available online 28 September 2014

Keywords:
Glutaredoxins
Iron–sulfur center
Reductases
Iron sensing

ABSTRACT

Glutaredoxins (Grxs) are major oxidoreductases involved in the reduction of glutathionylated proteins. Owing to the capacity of several class I Grxs and likely all class II Grxs to incorporate iron–sulfur (Fe–S) clusters, they are also linked to iron metabolism. Most Grxs bind [2Fe–2S] clusters which are oxidatively- and reductively-labile and have identical ligation, involving notably external glutathione. However, subtle differences in the structural organization explain that class II Fe–S Grxs, having more labile and solvent-exposed clusters, can accept Fe–S clusters and transfer them to client proteins, whereas class I Fe–S Grxs usually do not. From the observed glutathione disulfide-mediated Fe–S cluster degradation, the current view is that the more stable Fe–S clusters found in class I Fe–S Grxs might constitute a sensor of oxidative stress conditions by modulating their activity. Indeed, in response to an oxidative signal, inactive holoforms i.e., without disulfide reductase activity, should be converted to active apoforms. Among class II Fe–S Grxs, monodomain Grxs likely serve as carrier proteins for the delivery of preassembled Fe–S clusters to acceptor proteins in organelles. Another proposed function is the repair of Fe–S clusters. From their cytoplasmic and/or nuclear localization, multidomain Grxs function in signalling pathways. In particular, they regulate iron homeostasis in yeast species by modulating the activity of transcription factors and eventually forming heterocomplexes with BolA-like proteins in response to the cellular iron status. We provide an overview of the biochemical and structural properties of Fe–S cluster-loaded Grxs in relation to their hypothetical or confirmed associated functions. This article is part of a Special Issue entitled: Fe/S proteins: Analysis, structure, function, biogenesis and diseases.

1. Introduction

Glutaredoxins (Grxs) represent a widespread family of thiol oxidoreductases controlling notably the cellular redox state of a myriad of proteins together with thioredoxins (Trxs). However, for a specific subset of Grxs that bind iron–sulfur clusters, the disulfide reductase activity might have been lost during evolution or became secondary/unnecessary. Both Grxs and Trxs were first identified in the bacterium *Escherichia coli* as electron donors for the ribonucleotide reductase (RNR) [1,2]. However, their reduction system is different. Trxs are usually dependent on NADPH- or ferredoxin-Trx reductases whereas Grxs are dependent on glutathione and its associated NADPH-dependent glutathione reductase. A few studies highlighted that some Grxs can be recycled by Trx reductases [3–5] and some Trxs by GSH and/or Grx [6–8]. From this initial discovery that both systems may have somehow redundant functions, Grxs and Trxs have been extensively studied in both prokaryotes and eukaryotes to understand the differences when existing. Both proteins share a similar 3D structure, but the current view, which suffers of course some exceptions, is that, owing to their capacities to interact and recognize glutathione, Grxs are more particularly involved in the reduction of glutathionylated proteins, whereas Trxs are rather implicated in the reduction of disulfide bonds involving two protein cysteinyl residues. Indeed, glutathionylation is a post-translational modification which corresponds to the formation of specific disulfide bond between the cysteine of glutathione and a single protein cysteinyl residue. This modification occurs as an intermediate of some catalytic mechanisms, especially in enzymes using a sulfenic acid chemistry, but it is also viewed as a regulatory mechanism modulating protein function for signaling purposes or as a protective mechanism of cysteine residues from irreversible oxidation [9–11].

In principle, the reduction of glutathionylated proteins requires a single catalytic cysteine residue, but many Grxs have a dithiol CxxC active site motif. It served initially as a basis to distinguish dithiol (CPY/FC motif) and monothiol (CGFS motif) Grxs [12]. However, from

☆ This article is part of a Special Issue entitled: Fe/S proteins: Analysis, structure, function, biogenesis and diseases.

* Corresponding author at: Université de Lorraine, UMR 1136 Interactions Arbres Microorganismes, F-54500 Vandœuvre-lès-Nancy, France. Tel.: +33 3 83 68 42 25.
E-mail address: Nicolas.Rouhier@univ-lorraine.fr (N. Rouhier).

http://dx.doi.org/10.1016/j.bbamcr.2014.09.018
0167-4889/

deeper comparative genomics and phylogenetic analyses, the classification was later refined especially for photosynthetic organisms, as an important variability in the active site sequences exists and for instance many Grxs with monothiol active sites (CSYS or CPYS) form a clade with CPYC prototypes. Hence, Grxs with CPY/FC or close active sites belong to the class I, whereas Grxs with CGFS active sites belong to the class II [13]. Except some bacterial and archaeal phyla, at least one representative of these two Grx classes is present in most living organisms [14,15]. Note that the class II Grx isoforms are split into single domain and multidomain Grxs. The CGFS-type Grxs with a single domain are present in both eukaryotes and prokaryotes, whereas multidomain monothiol Grxs, which consist of a conserved N-terminal Trx-like domain fused to 1 to 3 Grx domains at the C-terminus, are restricted to eukaryotes [13,16]. At this point, it can be noticed that all class II Grxs should have the capacity to bind Fe–S clusters owing in particular to their extremely conserved CGFS active site sequence. Among class I Grxs, the situation is more complex. The current view is that the "ancestor" Grxs containing CPYC active site motifs were unable to ligate Fe–S clusters and that during evolution the lost of the active site proline notably allowed some members to acquire the capacity to bind Fe–S clusters and possibly new functions. However, the demonstration that certain Grxs with a CPYC motif have a similar ability raises new evolutionary questions. Several additional classes contain proteins with a domain architecture including a Grx module but they are usually present only in specific kingdoms, the active site signatures are quite variable and they have often not yet been characterized [13,14].

Concerning the catalytic mechanism employed by Grxs, the number of cysteines in the active site motif and the type of disulfide bond in the target proteins will be important factors [15]. In any case, the N-terminal active site cysteine constitutes the catalytic residue and is indispensable for the reductase activity. In the so-called monothiol mechanism which applies mostly for the reduction of glutathionylated proteins, this cysteine becomes glutathionylated and it is regenerated by a GSH molecule. On the other hand, the reduction of disulfide bonds involving protein cysteinyl residues requires a dithiol mechanism and thus an additional recycling residue that can be either the second active site cysteine residue or an additional extra active site cysteine. The latter mechanism is similar to the one used by Trxs. In this case, oxidized Grxs can be regenerated either by two GSH molecules or by dithiol–disulfide exchange with Trx reductase as mentioned above. Thus, it is important to mention that Grxs with dithiol active sites can potentially use both a monothiol and a dithiol mechanism [17].

Concerning the physiological roles, Grxs are associated to a large number of cellular processes. Reverse genetic analyses indicated they were primarily connected to oxidative stress response mechanisms including regulation of apoptosis, tolerance to heavy metals but also that some Grxs are important for developmental processes (see recent reviews) [16,18–22]. Considering the increasing number of identified glutathionylated proteins, which all constitute potential Grx substrates, we anticipate that the cellular processes implicating Grxs will continue to expand in the coming years.

Beyond the functions connected to the Grx oxidoreductase activity, several studies conducted since 2002 pointed to the capacity of both class I and II Grxs to bind iron–sulfur (Fe–S) clusters and to the importance of class II Fe–S Grxs for different iron-regulated processes. These Grxs will be referred thereafter to as class I Fe–S Grxs and class II Fe–S Grxs. Grxs from class II are particular since their function(s) could rely uniquely on their capacity to bind an Fe–S cluster not on a potential reductase activity which still has to be demonstrated in several cases. In any case, considering the fact that human Grx2 holoform, a class I Grx, has no significant disulfide reductase activity [23], none of the Fe–S ligating Grxs, do they belong to class I or II, should exhibit reductase activity under their holoforms. In this review, we discuss the recent genetic, biochemical, structural and molecular studies that contributed to improve our understanding about the physiological roles of Fe–S containing Grxs. A wealth of information is available from studies conducted in yeast and human models, whereas it lags behind in bacteria and plants. After illustrating the types of Fe–S clusters bound by Grxs and the structural bases explaining the differences between class I and class II Fe–S Grxs, we will focus our attention on the role of class II Fe–S Grxs in the maturation or repair of Fe–S clusters and in the regulation of iron homeostasis.

2. Structural and spectroscopic insights into the Fe–S cluster binding capacity of glutaredoxins

2.1. Class I Fe–S glutaredoxins usually bind stable [2Fe–2S] clusters into homodimers

Human Grx2 was the first member characterized as an Fe–S cluster-binding protein [23]. The biochemical characterization of the recombinant protein demonstrated that it can bind a [2Fe–2S] cluster into a homodimer, a property which was then confirmed for poplar GrxC1. Moreover, analytical GSH measurements coupled to the resolution of the three dimensional structure of the GrxC1 holoform showed that the Fe–S cluster is in fact coordinated by the N-terminal active site cysteine of both monomers and by the cysteines of two GSH molecules [24,25]. A similar ligation mode was observed in human Grx2 [26,27], *A. thaliana* GrxC5 [28] and very likely *S. cerevisiae* Grx6 [29] (Table 1). In the case of ScGrx6, the form binding Fe–S clusters is a tetramer but it is likely related to the existence of an N-terminal extension that promotes noncovalent dimerization [29,30]. Note that an extra beta-sheet is found in the Grx domain of ScGrx6 [30]. However, since this addition is likely present in yeast Grx7, a protein that does not incorporate an Fe–S cluster, it should not be crucial for cofactor ligation. Although the cluster of poplar GrxC1 is reductively labile [25], the Fe–S clusters assembled onto class I Fe–S Grxs are much more stable compared to those assembled onto class II Fe–S Grxs. Indeed, the proteins, at least the plant isoforms, can generally be homogeneously purified under aerobic conditions without loosing much Fe–S cluster. Compared to conventional class I Grxs with CPYC and CPFC active site sequences, all these proteins have the peculiarity not to have the active site proline, but instead a glycine (poplar GrxC1) or a serine (HsGrx2, AtGrxC5 and ScGrx6). Consistently, site-directed mutagenesis studies performed on poplar GrxC1 and HsGrx2 as well as on Grxs with a CPxx active site signature (poplar GrxC2, C3, and C4 and human Grx1) that do not visibly assemble such an Fe–S cluster showed that, in all these proteins, the proline prevents the assembly of an Fe–S cluster, whereas the presence of a glycine or a serine was sufficient for Fe–S cluster incorporation (Fig. 1) [25,26].

However, depending on the Grxs considered, other factors are clearly important. Indeed, *Trypanosoma brucei* 2-C-Grx1 and zebrafish Grx2 are able to bind an Fe–S cluster despite having a CPYC active site [31,32]. In the case of zebrafish Grx2, the Fe–S cluster binding is unusual since it is bound within a monomer and the coordination could involve four cysteines present outside the active site and specific to teleosts [31]. Other information came from the biochemical and structural comparison of two plant chloroplastic isoforms, PtGrxS12 (^{28}WCSYS^{32} active site) and AtGrxC5 (^{28}WCSYC^{32}). Indeed, despite having a strong sequence identity, only GrxC5 can form a [2Fe–2S] cluster-bridging homodimer [28]. Site-directed mutagenesis performed on GrxS12 indicated that the simple substitution of Trp28 by a tyrosine or of Ser32 by a cysteine enabled the incorporation of an Fe–S cluster, meaning that these two positions (−1 and +3 compared to the ligand cysteine) are also crucial for Fe–S cluster binding [28,33]. Accordingly, the opposite Cys32 to serine mutation in GrxC5 prevents Fe–S cluster binding [28]. The observed stabilizing effect of Cys32 was attributed to the formation of a hydrogen bond between Cys32 and a lysine residue preceding the active site (Lys26) which helps stabilizing the loop containing the active site residues essential for Fe–S cluster coordination [28].

All these biochemical, spectroscopic and structural studies have been performed with recombinant proteins. An important aspect to

Table 1
Mutant phenotypes and associated functions of Fe–S cluster-binding glutaredoxins.

Class I				
Organism	Protein names	Active site signatures	Mutant phenotype(s)	References
Saccharomyces cerevisiae	Grx6	CSYS	Increased sensitivity toward oxidizing agents, reduced sensitivity to the glycosylation inhibitor, tunicamycin.	[143,144]
Danio rerio	Grx2	CPYC	Impaired angiogenesis and brain and heart development	[145–147]
Homo sapiens	Grx2	CSYC	Increased sensitivity toward cell death inducers	[148]
Mus musculus	Grx2	CSYC	Increased sensitivity to oxidative stress, decreased mitochondrial complex I activity	[149]
Rattus norvegicus	Grx2	CSYC	Impaired mitochondrial Fe–S cluster assembly and IRP1 regulation	[38]
Trypanosoma brucei	2-C-Grx1	CPYC	No growth phenotype	[32]
Arabidopsis thaliana	GrxC1	CGYC	No visible phenotype in standard growth conditions	[150]
Arabidopsis thaliana	GrxC5	CSYC	None yet described	
Sinorhizobium meliloti	Grx1	CGYC	Decreased growth, increased sensitivity to H_2O_2, impaired nodule formation and nitrogen fixation capacity	[108]
Class II				
Organism	Protein names	Active site signatures	Mutant phenotype(s)	References
Single domain				
Saccharomyces cerevisiae	Grx5	CGFS	Increased sensitivity to oxidative stress and defaults in Fe–S cluster assembly	[12,48,49,51]
Schizosaccharomyces pombe	Grx5	CGFS	Defaults in Fe–S cluster assembly, decreased amount of mitochondrial DNA, reduced growth and sensitivity toward oxidants	[65,128]
Danio rerio	Grx5	CGFS	Embryo lethal	[53]
Homo sapiens	Grx5	CGFS	Defaults in Fe–S cluster assembly, sideroblastic anemia, nonketotic hyperglycemia, increased apoptosis in osteoblasts	[52,54,55,151]
Trypanosoma brucei	1-C-Grx1	CAYS	Lethal	[39]
Trypanosoma brucei	1-C-Grx2	CGFT	None yet described	
Trypanosoma brucei	1-C-Grx3	CGFT	None yet described	
Sinorhizobium meliloti	Grx2	CGFS	Defaults in Fe–S cluster assembly, deregulation of RirA transcriptional activity, increased intracellular iron content, modified nodule development	[108]
Escherichia coli	Grx4	CGFS	Sensitivity to iron depletion	[80]
Azotobacter vinelandii	Grx5	CGFS	None yet described	
Azotobacter vinelandii	Grx-nif	CGFS	None yet described	
Gloeobacter Violaceus	GvGrx3	CGFS	None yet described	
Thermosynechococcus elongatus	TeGrx3	CGFS	None yet described	
Synechocystis PCC6803	SyGrx3	CGFS	Hypersensitivity to metals and oxidative stress (H_2O_2, heat, high light) treatments	[152]
Arabidopsis thaliana	GrxS14	CGFS	Sensitivity of root growth to H_2O_2	[77]
Arabidopsis thaliana	GrxS15	CGFS	Sensitivity of root growth to H_2O_2	[153]
Arabidopsis thaliana	GrxS16	CGFS	None yet described	
Multidomain				
Saccharomyces cerevisiae	Grx3	CGFS	Impaired regulation of Aft1/iron homeostasis	[112,113]
Saccharomyces cerevisiae	Grx4	CGFS	Impaired regulation of Aft1/iron homeostasis	[112,113]
Schizosaccharomyces pombe	Grx4	CGFS	Lethal	[128]
Saccharomyces cerevisiae	Grx3/4	CGFS	Impaired iron trafficking and assembly of Fe-S proteins, heme, and iron-containing proteins, reduced growth and sensitivity to oxidizing agents	[104,113]
Danio rerio	Grx3	CGFS	Impaired heme synthesis and Fe–S protein maturation	[107]
Homo sapiens	Grx3/Picot	CGFS	Decreased activities of cytosolic Fe–S proteins	[107]
Mus musculus	Grx3	CGFS	Embryonic lethality, cardiac hypertrophy in heterozygous mice	[154]
Arabidopsis thaliana	GrxS17	CGFS	Hypersensitivity to elevated temperature and altered auxin perception	[91]

consider is the *in cellulo* existence and proportion of Fe–S bound Grx forms. The presence of an Fe–S cluster was in fact rarely unambiguously demonstrated and the relative abundance compared to apo-proteins never assessed. Grx2 immunoprecipitation from human cell lines cultivated with ^{55}Fe isotope indicated the presence of radiolabelled iron which suggested that an Fe–S cluster is assembled *in vivo* [23]. Another confirmation of the capacity of human Grx2 to bind an Fe–S cluster *in vivo* came from the genetic engineering of a Grx2 fusion with Venus fluorescent protein fragments and its expression in the cytosol of bacterial and mammalian cells [34]. The detection of fluorescence in these cells which resulted from reassembly of the split Venus was indicative of the building of a [2Fe–2S] cluster onto a dimeric Grx2. In mammalian cells, it was shown to require the iron–sulfur cluster assembly proteins, ISCU and NFS1.

Another crucial question is the function of these Fe–S bound Grx forms. Indeed, contrary to the apoform, the holoform of human Grx2 has no reductase activity [23]. Moreover, in recombinant human Grx2, the Fe–S cluster is stabilized in the presence of GSH, whereas GSSG but also dithionite and ascorbate promoted Fe–S cluster degradation [23]. From this observation, the authors proposed that the Fe–S cluster serves as redox sensor, by modulating Grx2 activity in response to changing conditions. Indeed, they proposed that Grx2 could exist mostly under an inactive holoform under non-stress conditions, whereas the disruption of the Fe–S cluster upon oxidative stress conditions would result in the formation of catalytically active monomers. A similar GSH or glutathionyl-spermidine (Gsp) stabilization effect was also observed for example for poplar GrxC1 and *T. brucei* 2-C-Grx1 respectively [25,32]. Indeed, in the parasite, specific thiols such as Gsp and trypanothione ($T(SH)_2$) can replace GSH as non-protein Fe–S cluster ligands. The observed GSH stabilizing effect might be related to the constant exchange observed between the GSH involved in Fe–S ligation and the free GSH pool as observed for human Grx2 and poplar GrxC1 [26,35] but also for poplar GrxS14, a class II Fe–S Grx [35]. Accordingly, it was shown also that GSH prevents the Fe–S cluster transfer from plant holo Grxs to an apo-ferredoxin, the effect being more marked with class I compared to class II Fe–S Grxs. For instance, according to its inability to complement the yeast *grx5* mutant, it was initially shown that GrxC1 is unable to transfer its Fe–S cluster to an apo-ferredoxin in

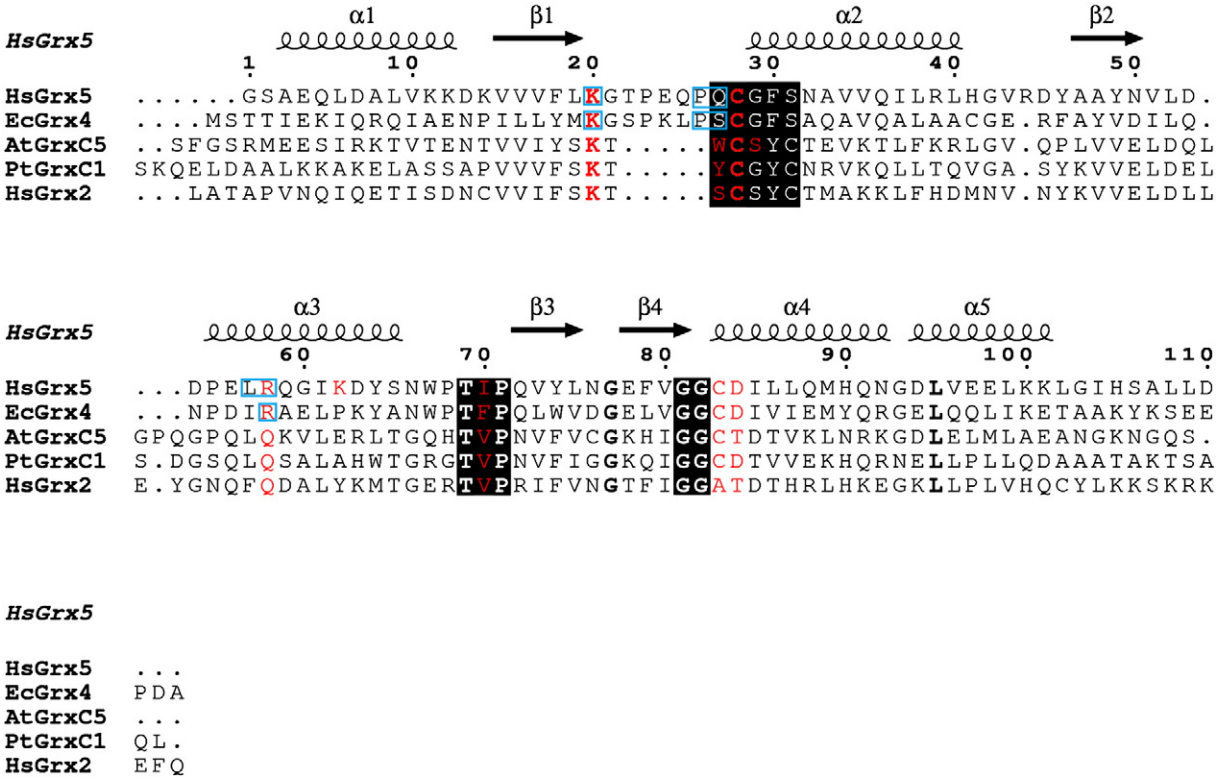

Fig. 1. Structural alignment of [2Fe–2S]-cluster bridged glutaredoxins. Sequences from Fe–S containing Grxs whose structures are solved were aligned using Strap (http://www.bioinformatics.org/strap/) based on all available X-ray structures. The secondary-structure elements of human Grx5 are indicated on top of the figure, with arrows representing β-sheets and cylinders α-helices. The active site Grx signature and the TVP and GG motifs are in black rectangles. Residues interacting with GSH molecules are colored in red. Residues involved in the monomer–monomer interface in class II Grx holoforms are highlighted with blue rectangles.

the presence of GSH [36] A transfer occurs in fact in the absence of GSH albeit with a relatively weak rate constant compared to class II Fe–S Grxs [35]. A bidirectional Fe–S cluster transfer between human Grx2 and the scaffold protein ISU was also evident from *in vitro* experiments [37]. All these Fe–S cluster transfer results have to be interpreted with caution since GSH likely shifts the thermodynamic equilibrium of the reaction. Additionally, other parameters such as the GSH/GSSG ratio and total glutathione concentration which are varying in a cellular context are important to consider when thinking to the *in vivo* Fe–S cluster delivery steps involving Grxs. Since the GSSG destabilizing effect on poplar GrxC1 was very weak and since Fe–S clusters are also known to be sensitive to reactive oxygen species, it might be that the oxidative sensing mechanism relies on superoxide ion (O_2^-)or on H_2O_2 instead of GSSG. Indeed, as assessed with redox sensitive GFP (roGFP) probes, the GSSG levels, which are very low compared to GSH levels in cells under normal conditions, would remain far below GSH levels under stress conditions and may not be sufficient to promote Fe–S cluster disassembly. The phenotypic and molecular analyses of cells or organisms depleted for these Fe–S cluster containing class I Grxs are scarce (Table 1). In most examples, the observed defects were either developmental as in the case of zebrafish Grx2 or consisted in a decreased tolerance to oxidative stress conditions. The only study that pointed to a clear relationship with iron homeostasis was performed with rat cell lines, showing that the extinction of mitochondrial Grx2 led to the impaired assembly of several mitochondrial Fe–S proteins and to IRP1 deregulation [38]. However, there was no evidence that it was linked to the capacity of Grxs to assemble Fe–S clusters.

2.2. Fe–S clusters ligated by class II Fe–S glutaredoxins are more labile and their nature and binding mode is more variable

Following the identification of Fe–S clusters in class I Fe–S Grxs, several studies reported that CGFS Grxs also formed holo-homodimers incorporating a [2Fe–2S] cluster with a ligation similar to class I Fe–S Grxs [36,39–41]. Interestingly, human Grx5 might incorporate two [2Fe–2S] clusters into a tetramer, but the existence of such oligomeric form is debated [42,43]. The analysis of human Grx3 and Arabidopsis GrxS17, multidomain CGFS Grxs possessing two and three Grx domains, indicates that the holoproteins also form dimers but that they contain two or three Fe–S clusters respectively according to the number of Grx domains (our unpublished result, [44]). In the case of the mitochondrial 1-C-Grx1 isoform of *T. brucei* and as reported for Tb2-C-Grx1, Gsp and $T(SH)_2$ can serve as ligands instead of GSH [45]. While class I Fe–S Grxs were shown to bind uniquely [2Fe–2S] clusters, the recent spectroscopic characterization of a recombinant ScGrx5 demonstrated its ability to incorporate linear [3Fe–4S] and [4Fe–4S] clusters [46]. Strikingly, there was no sign of Fe–S cluster when purification is achieved immediately after cell lysis and regardless of the use of aerobic or anaerobic conditions, whereas exposure of cell-free extracts to aerobic conditions allowed purifying linear [3Fe–4S] cluster-bound forms. Accordingly, *in vitro* anaerobic reconstitution experiments showed that, in the presence of GSH, a linear [3Fe–4S] cluster is predominantly reconstituted. On the other hand, in the presence of DTT but in the absence of GSH, a [4Fe–4S] cluster is the only Fe–S cluster bound form into a dimer. These results also prompted the authors to reinterpret previous UV/visible spectra obtained for several recombinant class II Fe–S Grxs initially attributed as [2Fe–2S] cluster [41], as containing linear [3Fe–4S] clusters or a mixture between linear [3Fe–4S] and [2Fe–2S] clusters. Such a variation has also been observed for *A. thaliana* GrxS16 which binds a [2Fe–2S] cluster into a dimer upon reconstitution experiments in the presence of GSH, but a [4Fe–4S] cluster into a tetramer when GSH is replaced by DTT (our unpublished result).

Besides the active site cysteine, the contribution of other active site residues including the CGFS signature and the GSH binding residues has been examined by site-directed mutagenesis on a few isoforms. Using *Synechocystis* Grx3 and yeast Grx4 as models, it was shown that

mutating residues involved in GSH recognition abolished or decreased Fe–S cluster formation respectively [41,47]. This is explained by the fact that GSH position in apo- and holo-Grxs does not vary much (see Section 2.3). From most of the mutagenesis work performed with class I Grxs, it was initially thought that the presence of a glycine or a small residue after the catalytic cysteine (at position +1) is required. However, a mutational analysis achieved by Hoffmann and co-workers revealed that the requirements for Fe–S cluster stabilization, at least in yeast Grx4, are different, not to say opposite [47]. Indeed, they showed that substituting the glycine by a proline does not prevent cofactor assembly, whereas replacing the serine (position +3) by a cysteine, forming a dithiol active site as in human Grx2, poplar GrxC1 or Arabidopsis GrxC5, resulted in its destabilization. Importantly all tested variants were able to bind iron and most likely Fe–S clusters and restored the growth of a *S. cerevisiae* strain where Grx3 is deleted and Grx4 is expressed under the control of the glucose-repressible GAL-L promoter. However, most of these variants were unable to completely compensate Aft1 deregulation (see explanation about the connexion in Section 4) indicating that these changes somehow disturbed the cofactor environment, preventing interaction or cofactor transfer with Aft1.

2.3. Structural properties and comparison of Fe–S cluster binding Grxs

Only five crystal structures of Fe–S cluster-bridged Grxs have been solved to date, three from class I (PtGrxC1, AtGrxC5, HsGrx2) and two from class II (HsGrx5, EcGrx4) and they are all with [2Fe–2S] clusters [25,27,28,40,43]. In all these structures, the [2Fe–2S] cluster is at the interface of two Grx chains and each iron atom is coordinated by four sulfur atoms, two inorganic from the cluster, one from the N-terminal active site cysteine of Grx chain and one from the cysteine moiety of GSH. However, not all Grx holoforms are dimeric. Indeed, crystallographic studies showed a higher oligomerization in the solid state for PtGrxC1 and HsGrx5. Both crystal forms contained four protein molecules in the asymmetric unit. For poplar GrxC1, the tetramer contains only one [2Fe–2S] cluster and owing to the use of aerobic conditions, it likely resulted from co-crystallization of one holodimer and of two monomers coming from the disruption of another holodimer [25]. On the other hand, the tetrameric organization of HsGrx5 which contains two [2Fe–2S] clusters, forming a dimer of holodimer, may be biologically relevant (Fig. 2a). However, while the oligomerization state was initially confirmed by gel-filtration chromatography experiments and sedimentation velocity analytical ultracentrifugation [43], NMR and analytical gel filtration analyses performed in another study provided evidence for the presence of a single Fe–S cluster into a dimer [42]. Interestingly, crystal packing analysis of the X-ray structure of EcGrx4 revealed a tetramer similar to HsGrx5, but there has been no experimental confirmation about the formation of such oligomers in solution. Among these contacts, there are only few polar interactions which might explain the observed discrepancy in the oligomerization state depending on the conditions and concentrations used. Only the *S. cerevisiae* Grx6 [29] and a specific *A. thaliana* [4Fe–4S]-loaded GrxS16 holoform (our unpublished results) proved to exist as tetramers in solution. However, compared to HsGrx5, the tetramer formation in ScGrx6 is different as it involves a specific N-terminal domain.

Before comparing in more details apo- and holoforms in each class and class I *vs* class II holoforms, it is important to describe the organization of a Grx monomer. All Grx monomers exhibit a thioredoxin fold made of a central four-stranded mixed β-sheet flanked by five α-helices with an α1β1α2β2α3β3β4α4α5 topology. At the primary sequence level, typical motifs, containing residues forming the active site, are conserved in most Grxs. The Cxx[C/S] signature is invariably positioned at the N-terminus of α2, the TVP sequence is situated in the loop between β3 and α3 and the GG sequence is found at the N-terminal end of α4. In apoforms of both class I and class II Grxs, the GSH binding site is conserved and involves four anchor points. The first crucial amino acid is the N-terminal active site cysteine since it is involved in the formation of a mixed disulfide with glutathione during the catalytic cycle. The second region involves two residues interacting with the carboxyl group of glycine. It is composed of a well-conserved lysine found in the loop between β1 and α2 and of another residue found in α3, predominantly a glutamine or an arginine in class I or class II Grx isoforms respectively. The third key position is occupied by the residue preceding the *cis*-proline of the consensus TVP motif (in general a valine) that interacts with the GSH cysteinyl moiety via main chain-main chain hydrogen bonds. The last GSH anchor point is formed by the interaction of the γ-glutamyl group of GSH with two residues located in α4 and immediately following the characteristic GG motif.

Surprisingly, despite having a similar Fe–S cluster coordination, the orientation of the two Grx monomers in class I and class II Grx holodimers is different (Fig. 2b). In both cases, the monomers are related by a 2-fold axis. In class I Fe–S Grxs, the mean β-sheet planes of both monomers are quasi perpendicular, while in class II Fe–S Grxs they are quasi coplanar in a head-to-head fashion [25,27,40,43]. The presence of a 5 residue insertion prior to the active site cysteine in class II Fe–S Grxs seems to determine the type of assembled dimer (Fig. 1). There is no contact between the two monomers in class I Grx holodimers, except via the glutathione molecules (see below), whereas conserved hydrogen bonds between monomers stabilize the dimers in *E. coli* Grx4 and human Grx5 (Lys22, Pro28, Ser29 and Arg59 in *E. coli* Grx4 and equivalent residues in human Grx5) (Fig. 3a). Nevertheless, the Fe–S cluster is more solvent-exposed in class II Fe–S Grxs compared to class I Fe–S Grxs.

Upon Fe–S cluster incorporation, the GSH position only slightly varies. Nevertheless, additional residues from the active site participates to GSH stabilization in class I Fe–S Grxs but not class II Fe–S Grxs. In poplar GrxC1 (YCGYC signature), the Tyr at position −1 compared to the ligand cysteine interacts with the GSH of the same monomer, whereas in human Grx2 (SCSYC signature), the serine (position −1) interacts with the GSH of the other monomer. In AtGrxC5 (WCSYC signature), the Trp and Ser residues interact with GSH of the other monomer (Fig. 3b). On the other hand, more drastic changes occur to the residues forming the active site during the transition from apo-monomer to holo-dimer, since Fe–S cluster incorporation causes steric constraints. Confirming the site-directed mutagenesis experiments, an in-depth analysis of class I Fe–S Grx structures indicated that, except the catalytic/ligand cysteine, most residues adopt different rotamers in the apo- *vs* holo-form (Fig. 3c & d). In human Grx2, it concerns essentially the lateral chains of serine and tyrosine at position +1 and +2 respectively [27]. In Arabidopsis GrxC5, the lateral chains of residues at position −1, +1 and +2 also adopt different rotamers in both forms [28]. Moreover, as already mentioned, the cysteine at position +3 forms a hydrogen bond with the main chain of the conserved lysine preceding the active site motif in Grxs, which stabilizes the loop containing other residues essential for Fe–S cluster binding [28]. Interestingly, most of these changes help protecting the cluster from solvent and from oxidative degradation. The residue at position +3 is also important for Fe–S cluster incorporation into class II Fe–S Grxs. Indeed, in *E. coli* Grx4 apoform, this Ser residue interacts with another serine, at position −1, whereas it interacts with the conserved lysine preceeding the active site in holodimers [40].

Overall, these structural analyses revealed that the formation of Grx holodimers necessitates local conformational rearrangements, affecting notably most residues of the active site signature. Indeed these residues provide the required protein backbone flexibility for Fe–S cluster binding and also allow the formation of favorable interactions with the neighboring GSH. Finally, these changes and the differences in subunit orientation between class I and II Grx holoforms confer different Fe–S cluster stabilities which could explain the distinct functions attributed to these proteins, Fe–S cluster transfer for class II Fe–S Grxs and oxidative signaling via Fe–S cluster degradation for class I Fe–S Grxs.

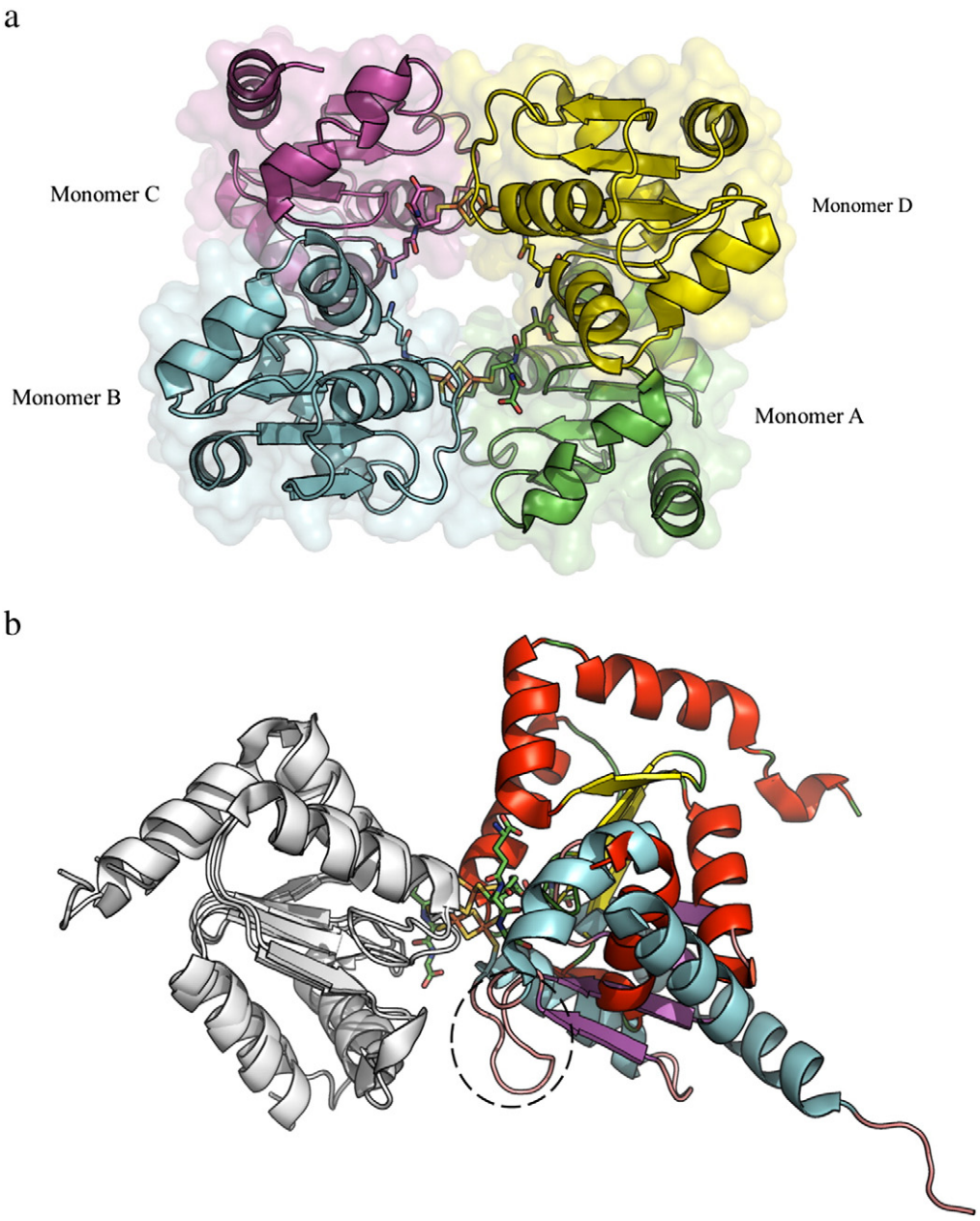

Fig. 2. Oligomerization states of Grxs. (a) Tetrameric organization of human Grx5 which contains two [2Fe–2S] clusters and four GSH molecules (in sticks), forming a dimer of holodimer (holodimer 1: A–B and holodimer 2: C–D). (b) Superposition of the X-ray structures of HsGrx2 (class I) and EcGrx4 (class II) holoforms. Monomers A (colored in white) of both structures were superposed to highlight differences in monomer B orientation. For monomer B, secondary structures (helices, strands and loops) are colored respectively in red, yellow and green for HsGrx2 and in cyan, purple and pink for EcGrx4. The 5 residue insertion before the active site of class II Grxs is circled.

3. Involvement of organellar class II Fe–S Grxs in the maturation of Fe–S proteins

3.1. Mitochondrial monodomain class II Fe–S Grxs mediate the transfer of Fe–S clusters by linking early and late-acting components of the ISC machinery

3.1.1. Phenotypic analyses of mutants

The implication of class II Fe–S Grxs in Fe–S cluster biogenesis was initially demonstrated by the phenotypic characterization of a *S. cerevisiae* null strain for the mitochondrial Grx5 [12,48]. It was first shown that the *grx5* mutant displays a high sensitivity to hydrogen peroxide and menadione resulting in growth defects in minimal medium, a decreased tolerance to an osmotic stress and it is unable to grow on respiratory media [12]. Accordingly, higher levels of glutathionylated and carbonylated proteins have been detected in this mutant [12,49]. These observations together with the *in vitro* demonstrated reductase activity of Grx5 towards a glutathionylated carbonic anhydrase from rat suggested that Grx5 primarily acted as an oxidoreductase playing a central role in the protection of proteins against oxidative damage under normal growth conditions and stress conditions [50]. However, an experiment aiming at isolating genes/proteins that suppress *grx5* mutant phenotypes led to the isolation of proteins involved in the maturation of Fe–S clusters, including the chaperone Ssq1 and the carrier protein Isa2 [48]. Interestingly, the Isa1 paralog was unable to suppress the phenotypes. Hence, the refined analysis of *grx5* mutant phenotypes indicated that iron accumulated in the cells and that the activities of two mitochondrial Fe–S proteins, aconitase and succinate dehydrogenase, were impaired [48,51].

In vertebrates, the mutation of *grx5* leads to severe diseases and is embryo-lethal in zebrafish [52–54]. In all analyzed mutants or patients,

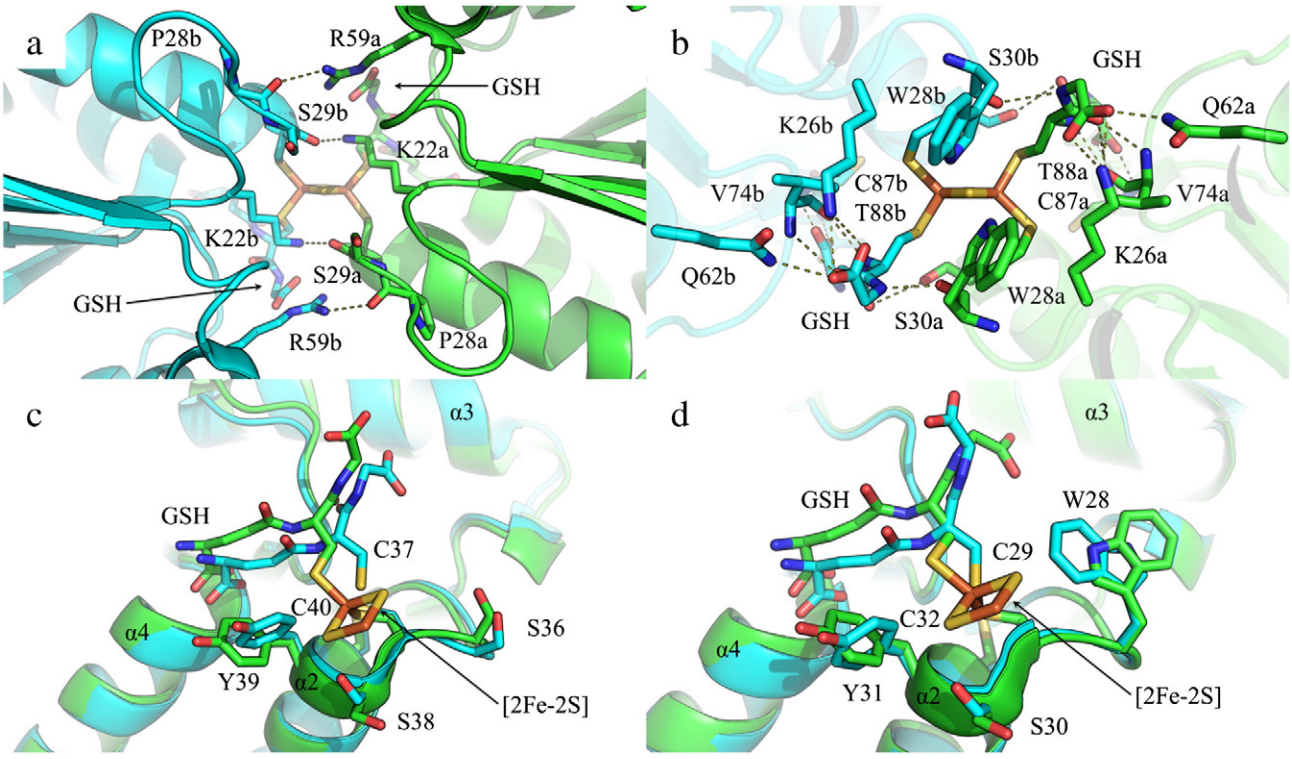

Fig. 3. Intermolecular interactions and structural rearrangements upon [2Fe–2S] cluster ligation. (a) [2Fe–2S] cluster coordination in EcGrx4 (class II) with contacting residues at the dimer interface. Monomer A is colored in green and monomer B in cyan. (b) [2Fe–2S] cluster coordination of AtGrxC5 (class I) with GSH intermolecular bonds. (c) and (d) Conformational rearrangements in HsGrx2 and AtGrxC5 upon [2Fe–2S]-cluster ligation, respectively. Apoforms and holoforms are colored in cyan and green, respectively.

a heme synthesis defect was observed explaining that the zebrafish *shiraz* mutant developed an hypochromic anemia which corresponds to a defect in hemoglobin production [53] and that a human patient with a mutation in *grx5* developed a sideroblastic-like microcytic anemia [52]. The functional and molecular characterization of these mutants indicated that the mitochondrial Fe–S cluster assembly is indeed impaired [54]. Consequently, the major regulator of iron homeostasis, the iron-regulatory protein 1 (IRP1), which is connected to the mitochondrial Fe–S cluster biosynthesis, is also affected. IRP1 is a cytosolic protein that acts as an aconitase when binding a [4Fe–4S] cluster but as a post-transcriptional regulator under apoform, recognizing iron responsive elements (IRE) of target genes for their regulation. The defect in heme synthesis is thus explained by the deregulation of the aminolaevulinate synthase (ALAS2) which codes for the enzyme involved in the first step of heme biosynthesis and the expression of which is usually repressed by IRP1. More recently, another mutation in the human *Grx5* gene has been associated to nonketotic hyperglycemia [55]. This patient harbors a deficient lipoylation, suggesting that Grx5 is required for the maturation of the mitochondrial Fe–S containing lipoate synthase [55].

3.1.2. Molecular mechanisms

At the molecular level, the question was to delineate the precise function of these Grx5 orthologs in this multistep Fe–S cluster maturation process. Indeed, there is a plethora of proteins involved and although their position in the sequence of events is often clearly established, their exact function(s) are sometimes less clear. The current knowledges are that the cysteine desulfurase Nfs1 is responsible of sulfur mobilization from cysteine and is stabilized by Isd11 [56]. They form ternary complexes with Isu/IscU scaffold proteins and quaternary complexes upon frataxin arrival (Fig. 4). The frataxin would regulate the entry of iron into the complex [57], but it is likely not the iron donor or storage protein, meaning that another iron chaperone/delivery system should exist. The electrons required to reduce sulfane sulfur into sulfide would be provided by a NADH/ferredoxin reductase (FdxR)/ferredoxin (Fdx) system. From studies performed with the bacterial IscS, it is interesting to note that ferredoxin and frataxin were found to compete for IscS binding, suggesting that there might be a continuous exchange between both proteins in this complex [58,59]. What is pretty clear is that the Ssq1 (HSP70 type) and Jac1 (J-type) chaperone proteins as well as the nucleotide exchange factor Mge1 participate in the early steps of the Fe–S cluster transfer but whether they are essential for all reactions is unclear. Additional carrier proteins, namely Ind1, Isa1/Isa2 and Nfu1, are required for the maturation of specific clusters [56]. Isa1/Isa2 are acting in conjunction with Iba57 proteins [60]. While it is not clear how Ind1 gets its Fe–S cluster, Nfu and Isa/IscA are likely supplied by Grx5 [60,61].

In order to assign a precise function to Grx5, Mühlenhoff and collaborators initially analyzed the *in vivo* incorporation of radiolabelled ^{55}Fe into some target proteins after feeding the yeast *grx5* mutant by this element [51]. Using this approach, they observed an accumulation of iron and possibly of Fe–S cluster on Isu1 as for *ssq1* or *jac1* mutants which suggested that they are all acting after Isu1, having either redundant or eventually complementary functions [51]. It is noteworthy that this observation was consistent with the complementation of the *grx5* mutant by Ssq1 overexpression [48]. At this point, the question was to know whether Grx5 was involved in the reduction of some specific ISC components or acceptor proteins or whether it incorporated itself an Fe–S cluster for its subsequent delivery to final acceptors or to ISC partner proteins. Whereas the first point is difficult to assess, it was shown that a recombinant ScGrx5 did bind a [2Fe–2S] cluster *in vitro* [62]. Moreover, it also very likely binds an Fe–S cluster *in vivo* since radiolabelled ^{55}Fe protein can be immunoprecipitated from cells overproducing ScGrx5 [62]. However, the nature of the incorporated Fe–S cluster is not yet completely clear since in another study, an in depth spectroscopic characterization of ScGrx5 demonstrated the ability of the recombinant protein to incorporate linear [3Fe–4S] clusters and [4Fe–4S] clusters in addition to [2Fe–2S] cluster [46]. Moreover,

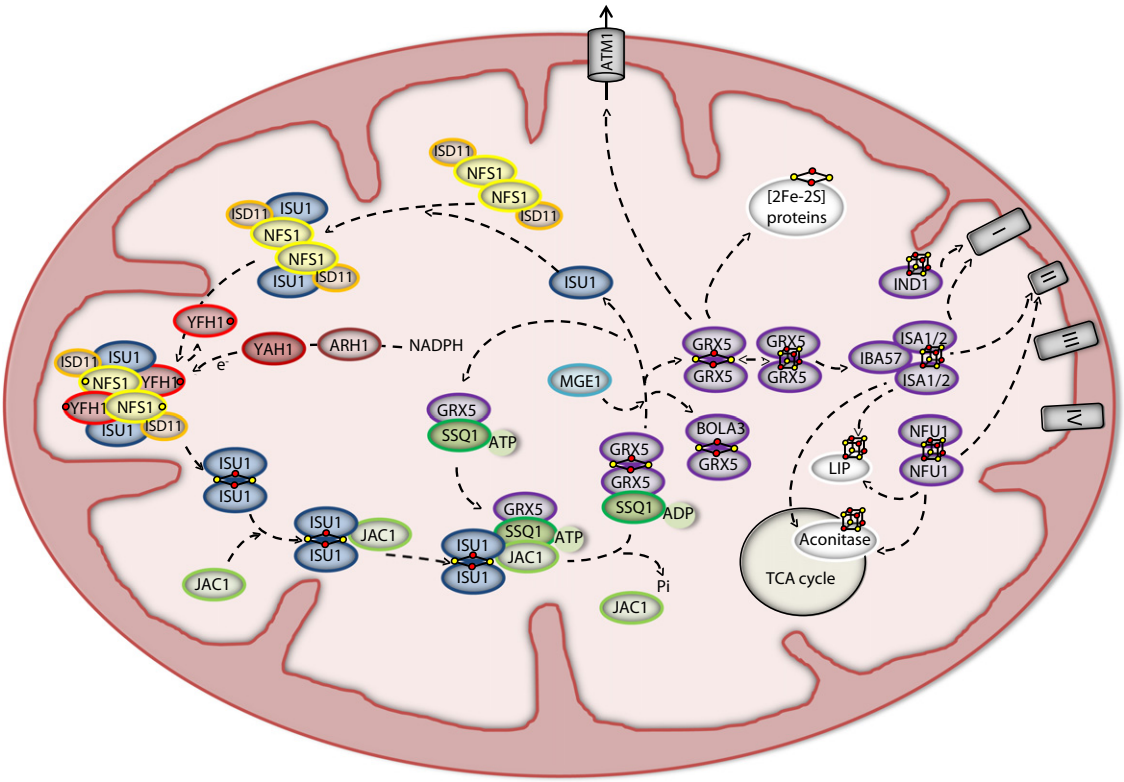

Fig. 4. Working model of the mitochondrial Fe–S cluster biogenesis with emphasis on the central role of Grx5. As discussed in the text, Grx5 is the last acting protein among the core components of the ISC machinery. From genetic studies performed essentially in yeast and mammals, it receives Fe–S clusters from Isu/IscU scaffolds, in a process requiring the Ssq1/Jac1 chaperones. The type of received Fe–S cluster is not clear since both Grx5 and IscU are able to integrate [2Fe–2S] and [4Fe–4S] clusters and are required for the assembly of proteins containing both cluster types, contrary to other carrier proteins (Isa1/2, Nfu1, Ind1/H) which are only required for the maturation of [4Fe–4S] cluster-containing proteins. Among carrier proteins, a physical interaction involving Grx5 has only been characterized with Isa proteins. The pathways for supplying Fe–S clusters to Ind1 and Nfu1 are not yet clear. Another major function of Grx5 could also be to supply a substrate to the ATM1 transporter, would it be GSH derivatives or GSH complexed Fe–S clusters. Protein names mostly correspond to yeast protein nomenclature. Human and plant protein names have been used respectively for BolA3 and Ind1/H that only exists in organisms having complex I. Note that in plants additional proteins may be required since SufE1 is found in mitochondria and interact with Nfs1 and some families are expanded. For instance, there are likely 2 Nfu and 3 IscA-like proteins in this organelle. When documented, the stoichiometries of each component in protein complexes, the protein oligomerization states and the Fe–S cluster types have been indicated. LIP is for lipoate synthase, sulfur atoms are represented in yellow and iron atoms in red.

in vitro Fe–S cluster transfer experiments showed the capacity of [4Fe–4S] cluster-bridged ScGrx5 to transfer its cluster to an apo-aconitase [46]. These results were particularly interesting considering that aconitase activity is affected in the *grx5* mutant and that Grx5 is involved in the maturation of both [2Fe–2S] and [4Fe–4S] clusters as shown by examining the Fe–S cluster binding of two reporter Fe–S proteins bearing both types of clusters in *Δgrx5* cells [62].

Recently, Uzarska and collaborators deciphered the molecular determinants controlling the interactions between Isu1, Grx5, Ssq1 and Jac1 [62]. Since Fe–S cluster incorporation into a *S. pombe* Grx5 expressed in *isu1*, *jac1* or *ssq1* mutant backgrounds is decreased, it was concluded that all three proteins are required for the maturation of Grx5 holoform. Then, by coupling *in vitro* and *in vivo* approaches, they have demonstrated that an apoform of Grx5 interacted with Ssq1, preferentially when the latter is in an ADP rather than in an ATP state. The fact that it did not prevent Isu1–Ssq1 interaction indicated that Grx5 and Isu1 can bind Ssq1 simultaneously at independent sites. Hence, the current view is that a Jac1–holoIsu1 complex is recruited by Ssq1, already in complex or not with Grx5, thus facilitating the Fe–S cluster transfer from Isu1 to Grx5 (Fig. 4). Then, by exchanging ADP to ATP onto Ssq1, Mge1 would promote the disassembly of the Ssq1–Grx5 complex. Consistent with this model, the *in vitro* [2Fe–2S] cluster transfer between Isu and Grx5 from *Azotobacter vinelandii* is strongly stimulated by the presence of HscA and HscB, the bacterial chaperones orthologous to yeast Ssq1 and Jac1 respectively [63].

At this point, the question was to determine what the physiological Fe–S acceptors of Grx5 were. Among the known components of the ISC machinery, this could be Ind1, Nfu1, Isa1/2 or eventually Iba57, although there is no evidence that the latter protein can incorporate an Fe–S cluster. Whereas there is no direct evidence for an interaction with Ind1, Nfu1 or Iba57, several evidences link Grx5 with Isa proteins. First, an interaction between *S. cerevisiae* Grx5 and Isa1 was demonstrated by binary yeast two-hybrid [64]. Using bimolecular fluorescence complementation, an interaction between Grx5 and Isa1 and Isa2 was also observed for *S. pombe* proteins [65]. More recently, it was demonstrated by nuclear magnetic resonance (NMR) experiments that human Grx5 is able to transfer its [2Fe–2S] cluster to human Isa orthologs, IscA1 and IscA2 [42]. This transfer seems unidirectional as no Fe–S cluster transfer was observed when IscA1 under holoform and Grx5 under apoform were incubated together [42]. These NMR experiments also revealed that, in solution, Grx5 holoform would exist as a mixture of two species and that one of these species preferentially transfers its Fe–S cluster to IscA1. Moreover, according to previous reports pointing to the stabilizing effect of GSH [35], increasing GSH concentration does not favor Fe–S cluster release revealing that it is stably bound in Grx5 and that its transfer requires specific protein–protein interactions between Grx5 and acceptor protein. Finally, as no interaction was visible between both proteins under apoform, the [2Fe–2S] cluster seems indispensable to promote the interaction between Grx5 and IscA1/2 as already observed for other metal transfer reactions [42]. From the documented existence of Grx–BolA interaction in numerous species, another likely partner of Grx5 is BolA3. The study of a human patient presenting a mutation in the *bolA3* gene demonstrated that this protein is required for the normal maturation of Fe–S enzymes in

the respiratory chain complexes and for lipoate-containing 2-oxoacid dehydrogenases [55,66,67]. As BolAs cannot incorporate an Fe–S cluster by itself, this suggests that BolA3 function would be linked either to its capacity to form holo-heterodimer with Grx5 or to an inhibitory effect of some Grx5 homodimer functions. However, the latter effect is unlikely since the defects in the *bolA3* mutant do not exactly match those in the *grx5* mutant.

Overall, these results indicate that mitochondrial Grx5 members belong to the core mitochondrial ISC assembly machinery. Indeed, several target proteins of the mitochondrial ISC machinery are affected in *grx5* mutants (aconitase, succinate dehydrogenase, lipoate synthase) but, more importantly, *grx5* mutants are the only one described so far among carrier proteins where the cytosolic CIA machinery and the Aft1 or IRP1 regulation are also impaired [54,62,68]. Hence, by facilitating the transfer of Fe–S clusters preformed on Isu scaffold proteins to more specific ISC targeting factors such as IscA1/2, Grx5 seems to be the first acting protein among all carrier proteins. Moreover, to date, this is the only carrier protein which proved to be required for the assembly of both [2Fe–2S] and [4Fe–4S], whereas Nfu, IscA, Iba57, Ind1 seem devoted to the maturation of proteins containing [4Fe–4S] clusters. For this reason, it is assumed that it could also provide Fe–S clusters to mitochondrial [2Fe–2S] binding proteins such as ferrochelatase or ferredoxin [69]. Concerning its contribution to the ISC export machinery, an attractive hypothesis would be that it provides glutathione-complexed Fe–S clusters or other glutathione persulfide forms to the ATM transporters. Indeed, GSH is clearly required for this process [70], and GSH, GSH derivatives and glutathione-complexed Fe–S clusters proved to significantly stimulate the ATPase activity of ATM transporters [71–73].

While the role of the mitochondrial Grx5 seems conserved across kingdoms, it is important to mention that the poplar GrxS15 ortholog does not complement the *grx5* mutant phenotypes [36]. In *Trypanosoma brucei*, there are 2 class II Grxs in mitochondria, namely 1-C-Grx1 and 1-C-Grx2, While 1-C-Grx1 possesses an N-terminal extension unrelated to the Trx domain found in multidomain CGFS Grxs and a slightly different CAYS active site signature, it binds an Fe–S cluster and based on its capacity to complement the yeast *grx5* mutant, it might be the one participating to the Fe–S cluster biogenesis [39]. The protein seems indispensable for the parasite life, since gene silencing or deletion is impossible [45]. In summary, it is puzzling that the deletion of *Grx5* in yeast species only leads to relatively mild phenotypes whereas it is lethal in some other organisms and the deletion of *Isu*/*IscU*, the Fe–S cluster donor recurrently leads to strong phenotype defects. Possible interpretations are that Grx5 only assists cofactor assembly for a specific subset of non-essential Fe–S proteins or that it is an accessory protein in yeast, i.e. Fe–S clusters can still be transferred from Isu to acceptor proteins possibly through the chaperone system. We have mentioned already above that overexpression of Ssq1 but also Isa2 can suppress Grx5 defects. On the other hand, the observed synthetic lethality when *Grx5* mutation is combined to *Grx2* deletion or to *Grx3/4* deletion in *S. cerevisiae* is another point to integrate in this scheme [12]. Indeed, this indicates that these Grxs can somehow substitute to Grx5 function. Since *S. cerevisiae* Grx2 does not likely incorporate an Fe–S cluster, this could imply that at least part of the Grx5 function relies on a reductase activity.

3.2. Undefined roles of chloroplastic class II Fe–S glutaredoxins in the SUF machinery

In photosynthetic organisms, many Fe–S proteins are also present in chloroplasts and they are essential for photosynthesis, some proteins being present in the cytochrome b6/f and photosystem I complexes and involved in chlorophyll metabolism. They are also required for example for nitrogen or sulfur metabolism, an Fe–S cofactor being found in GOGAT and nitrite reductase or in APS reductase and sulfite reductase respectively [74–76]. Hence, plants possess an additional Fe–S cluster assembly machinery specifically devoted to the maturation of chloroplastic Fe–S proteins [76]. This SUF machinery, derived from a bacterial system, is present along the green lineage (cyanobacteria, algae, terrestrial plants). While the role of many actors has been precisely determined, the one of plant class II Fe–S Grxs in this process, if any, is not yet elucidated (reviewed in [76]).

The hypothesis that GrxS14 and GrxS16 participate to the maturation of Fe–S clusters in the chloroplast in association with the SUF machinery was built on the observation that poplar and Arabidopsis proteins were able to complement the yeast *grx5* mutant defects when targeted into mitochondria [36,77]. Moreover, poplar and Arabidopsis recombinant proteins can incorporate labile [2Fe–2S] clusters that can be rapidly and quantitatively transferred to the apoform of *Synechocystis* ferredoxin [35,36]. Altogether, these data suggested a role of carrier proteins similar to the one attributed to mitochondrial Grx5. For this reason, the relationship with other known SUF components was investigated. For example, *in vitro* transfer experiments between [2Fe–2S]-bridged monothiol Grxs and potential acceptor apoproteins have revealed a rapid, unidirectional and quantitative transfer from AtGrxS14 to AtSufA1, a chloroplastic A-type protein [78] or to the sirohydrochlorin ferrochelatase SirB (Albetel, Couturier, Rouhier, Johnson, unpublished results). On the other hand, using the same approach, it was shown that GrxS16 but not to GrxS14 can receive a [2Fe–2S] cluster from AtNfu2 [79]. These different results confirmed that, depending on the partners, chloroplastic class II Fe–S Grxs can either receive or transfer Fe–S clusters but their exact role and position in the whole process remain undetermined. Indeed, genetic evidences are still lacking maybe because of a redundancy between these proteins. The phenotypic analysis of a GrxS14 knock-out mutant showed that the root development of Murashige and Skoog medium grown plants was slightly altered in response to H_2O_2 treatment [77] but it did not reveal any link to a deregulation of the SUF machinery or of iron homeostasis.

Some more evidence came from the study of Grx4, the only class II Fe–S Grx from *E. coli*. Albeit its role(s) is not yet elucidated, a link with the SUF machinery was done from some genetic analyses. It was observed that a *grx4*/*grxD* mutant is sensitive to iron depletion [80] and that the mutation of the *grx4* gene is synthetic lethal when combined to any mutation of genes of the *isc* operon [81]. Given that mutants for genes of the *suf* operon display the same characteristics [82], it was concluded that Grx4 is functionally linked to the SUF system. Also, it was shown that the activity of MiaB, a radical SAM enzyme involved in tRNA methylation, is impaired in a *grx4* mutant [83]. Besides, the description of a covalent interaction of Grx4 with the SufE sulfurtransferase via their respective cysteine residues pointed to a possible role of Grx4 in regulating sulfur release from SufE or to the direct assembly of an Fe–S cluster onto Grx4 without the involvement of the identified SUFBCD scaffold complex [84]. This interaction may also make echo to the existence of SufE1 proteins in plants, hybrid proteins formed by a SufE domain fused to a BolA domain [85,86]. SufE1 is essential for the Fe–S cluster biogenesis in chloroplasts and possibly in mitochondria, acting as a sulfur-transferase in conjunction to the cysteine desulfurase Nfs2 and possibly Nfs1 [85,86]. Using binary yeast two-hybrid and bimolecular fluorescence complementation assays in *A. thaliana* protoplasts, an interaction of both plastidial GrxS14 and GrxS16 with SufE1 has been demonstrated and this interaction seems to depend on the presence of the BolA domain of SufE1 [87]. Besides a possible regulation of the redox state of SufE1 was suggested by the observation that these Grxs can reduce an inactive SufE1 glutathionylated form [87]. Hence, the question of a possible regulatory role of plastidial CGFS Grxs is raised. Since SufE1 activity is crucial for activation of Nfs2, the interaction with Grxs might allow the fine tuning of the whole chloroplastic Fe–S cluster assembly system. This could be achieved via a redox control, via a simple non Fe–S dependent interaction or eventually via the formation of Grx–SufE1 holo-heterodimers since the formation of Fe–S bridged BolA–Grx dimers seems universal.

3.3. Putative roles of class II Fe–S glutaredoxins in Fe–S cluster repair/regeneration

Beyond the *de novo* assembly of Fe–S clusters, other evidences suggest that monodomain class II Fe–S Grxs could play a role in the repair of Fe–S clusters. This role has been notably proposed following the demonstration that ScGrx5 has the ability to incorporate linear [3Fe–4S] clusters [46]. The observation that these linear [3Fe–4S] cluster-loaded Grx5 forms were only isolated after exposure of cell-free extracts to aerobic conditions, whereas it was devoid of Fe–S clusters when purification was achieved directly after bacterial cell lysis, suggested that ScGrx5 could recycle released Fe–S clusters from damaged proteins. Incidentally, this might also prevent the harmful effects due to the iron accumulation observed in *grx5* mutant cells. Another result consistent with a role in Fe–S repair or regeneration comes from the observed impaired MiaB activity in an *E. coli grx4* mutant [83]. Indeed, MiaB is a radical SAM enzyme which binds two [4Fe–4S] clusters, one of them is an auxiliary cluster which serves for sulfur donation [88]. This implies that an Fe–S cluster regeneration or repair mechanism should exist to keep MiaB functional. Although the existence of a [4Fe–3S] cluster on MiaB after turnover activity still has to be proved, the fact that Grx4 interacts with MiaB under both apo-and holoforms but, contrary to NfuA, is unable to transfer an Fe–S cluster led the authors to hypothesize that Grx4 might participate to the regeneration of an active MiaB either by providing the missing sulfur atom under holoforms or by scavenging the partially degraded [4Fe–3S] cluster under apoforms [83]. Further experiments are urgently needed to substantiate this point.

4. Regulatory functions of nucleo-cytoplasmic multidomain class II Fe–S Grxs in iron metabolism

4.1. General overview

Among multidomain Grxs, only higher plants possess class II Grxs with three Grx domains, referred to as GrxS17, whereas other photosynthetic and non-photosynthetic eukaryotes have isoforms formed by one Grx domain such as in *S. cerevisiae* Grx3 and Grx4 or two Grx domains such as in mammalian Grx3 also called PICOT (protein kinase C interacting cousin of thioredoxin) [89]. Most multidomain class II Grxs are localized in the cytosol and/or in the nucleus [90–93]. Although not involved in Fe–S cluster binding, the N-terminal Trx-domain found in these proteins proved to have important contributions. Despite the lack of specific NLS signature, the Trx-domain is responsible for the nuclear localization of yeast Grx3/4 [93]. Moreover, it is essential for their roles in iron trafficking and Aft1 regulation *in vivo*, possibly functioning as a docking site facilitating the interaction with partner proteins [47,94]. Accordingly, its importance was also confirmed for the interactions of Grx4 with Fep1 and Php4, two transcriptional regulators of iron homeostasis in *S. pombe* (see Section 4.3) [95,96] and for the demonstrated role in actin cytoskeleton organization [97]. Interestingly, all these functions do not require the remnant cysteine of the Trx-like active site signature [47,97].

From their specific subcellular localization and their specific properties, multidomain class II Fe–S Grxs represents a distinct functional group [47]. Previous studies assigned numerous functions to these eukaryote specific proteins (Table 1). For example, yeast Grx3 and Grx4 are involved in the polarization of actin cytoskeleton, thus contributing to oxidative stress resistance [97]. Human Grx3, which was originally identified as interacting with the protein kinase C-θ [98], is involved in various signalling pathways [99–101]. In *A. thaliana*, GrxS17 is associated to the temperature-dependent post-embryonic development through the modulation of auxin response [91]. While these functions do not necessarily link them to iron metabolism, other studies have reported that, at least in some organisms, multidomains Grxs are in fact directly or indirectly involved in the sensing of iron status and in the cellular distribution of iron.

Most multidomain Grxs tested so far (ScGrx3, ScGrx4, poplar and Arabidopsis GrxS17 and human Grx3) are able to restore the deficiency of yeast *grx5* mutant when they are expressed in mitochondria [36,93,102]. These data suggested that these Grxs could fulfill a carrier function similar to Grx5 isoforms, i.e., to accept an Fe–S cluster from a donor and to transfer it to an acceptor. Strikingly, the maturation of holo-Grx3 is only dependent on the mitochondrial ISC assembly machinery but not on the cytosolic CIA machinery system [103]. Indeed, in the absence of two early-acting CIA components, Nbp35 and Dre2, iron binding to Grx3/4 unexpectedly increased rather than decreased [104]. By analogy to the Fe–S cluster accumulation on the mitochondrial Isu1 in the absence of Grx5, the absence of recipient proteins as Nbp35 might have led to the accumulation of Fe–S loaded Grx3/4 forms. These obsevations clearly make these Grxs as ideal candidates linking the ISC and CIA machineries by receiving the mitochondrial signal exported from mitochondria by ATM transporters. Whether mitoNEET, an Fe–S protein present in the outer membrane of mitochondria is also involved remains to be determined.

Because of this central position, diverse phenotypes have been described for yeast *grx3* and *grx4* mutant strains (Table 1). Besides their involvement in Aft1/2-dependent iron sensing (detailed below), an independent function in the regulation of intracellular Fe trafficking was suggested. Indeed, the deletion of both Grx3 and 4 in the W303 genetic background is lethal [104]. Using a conditional mutant strain, it was shown that all iron-requiring reactions in cytosol, mitochondria and nucleus are affected. Despite the induction of Aft1-dependent iron uptake, the Grx3 and 4 depletion also leads to the impairment of several mitochondrial iron-dependent proteins such as complexes II and III, the mitochondrial Fe–S protein aconitase, but also of cytosolic proteins such as the heme-containing catalase [104]. In addition, the activity of several proteins containing di-iron centers such as the cytosolic ribonucleotide reductase (RNR), the mitochondrial mono-oxygenase Coq7 are also strongly decreased [104,105]. These Grx3/4 depleted cells also displayed a decreased iron level in mitochondria and an increased iron level in the cytosol respectively. The lower iron level in mitochondria is quite surprising since previous studies reported that defects in mitochondrial Fe–S cluster biogenesis were rather associated to higher iron levels [106]. Altogether, these data indicate that, in *S. cerevisiae*, Grx3 and 4 facilitate the correct assembly of several types of iron containing centers in various proteins. The exact biochemical role of these Grxs is however unclear. Since the mutation of the active site cysteine abolished the ability of these Grxs to function in iron regulation and trafficking, the role might be either related to their ability to bind an Fe–S cluster, which was proved to occur *in vivo* or to its inability to mediate GSH-dependent reactions [47,104]. Measuring the GSH levels and its redox state in the various subcellular compartments would be very informative.

In vertebrates, a crucial role of the cytosolic Grx3 in cellular iron homeostasis was also observed [107]. The silencing of Grx3 in human HELA cells decreased the activity of several cytosolic Fe–S proteins and these Grx3-deficient cells displayed features characteristic of iron starvation. Moreover, the deletion of Grx3 in zebrafish impaired heme biosynthesis as exemplified by the observed defects in the maturation of hemoglobin during embryonic development. All these results suggest that the function of cytosolic multidomain class II Fe–S Grxs in iron homeostasis could be conserved between yeast and vertebrates despite human Grx3 is unable to functionally complement the corresponding yeast mutant [47].

The absence of multidomain Grxs in prokaryotes raises the question of whether a similar Grx controlled Fe regulation system exists and whether this role is played by monodomain class II Fe–S Grxs. As mentioned above, the role of *E. coli* Grx4 is rather associated to the maturation of Fe–S clusters in connexion with the SUF machinery. However, the described interaction of *E. coli* Grx4 with BolA [80], which rather suggests sensing or regulatory roles, may complicate a bit the picture. Nevertheless, there is no evidence to date for a direct relationship

with Fur, the major iron regulator in *E. coli*. In *Sinorhizobium meliloti*, deletion of *grx2* coding for the only class II Fe–S Grx leads to defects in the maturation of Fe–S proteins and to an increase in the intracellular iron content, but also to the deregulation of RirA, which has analogous roles to Aft1, regulating notably genes involved in iron uptake [108]. This suggests dual functions in the sensing of the cellular iron status and in the maturation of Fe–S proteins.

4.2. Implication of BolA in the Grx-mediated Aft1/2 regulation in *S. cerevisiae*

In *S. cerevisiae*, the iron metabolism is controlled at the transcriptional level by two major transcription factors, Aft1/2 constituting the sensing system under low-iron conditions and Yap5 representing the sensing system in response to high-iron conditions (reviewed in [109]). Aft1 and its paralog Aft2 are involved in the response to iron deficiency by activating the iron regulon i.e., genes coding for proteins involved in iron uptake and intracellular sequestration and in mitochondrial iron metabolism, whereas Yap5 only regulates the expression of four genes, one of which is *grx4*, suggesting a cross-link between both systems [110]. However, the activation mechanisms seem different since both Grx3 and Grx4 are required to control the Aft1/2 activity [104,111–113], whereas they are apparently not implicated in the regulation of Yap5 activity [114].

The interaction between Aft1 and Grx3 was initially discovered via a high-throughput yeast two-hybrid approach [115]. Then, the study of simple *grx3* or *grx4* mutants revealed an overloading of intracellular iron and the constitutive activation of iron regulon [112,113] and this was confirmed for a *grx3grx4* double mutant [104]. As already mentioned, cells defective for core components of the mitochondrial ISC machinery or mutated for *atm1* also exhibited a constitutive expression of the iron regulon [70,111,116]. Thus, it suggested that the inhibition of Aft1/2 necessitates the transmission of signal dependent on the ISC and ISC export machineries and that is relayed by Grxs [117]. A more complete picture of the molecular mechanism responsible for this regulation has been obtained recently and is detailed below.

Under low-iron conditions, Aft1 is localized in the nucleus where it is able to promote gene transcription, whereas under iron-sufficient conditions, Aft1 is inactive being exported to the cytoplasm by interaction with the nuclear exporter Msn5 [118,119]. Nevertheless although Aft1 remained in the nucleus in a yeast *msn5* mutant, its activity was still suppressed in iron-replete conditions which suggested that Aft1 dissociation from DNA requires an additional step [117]. In fact, using a genetic screen designed to identify genes that regulate the iron regulon, it has been shown that Grx3 and Grx4 were involved in a protein complex also comprising two cytosolic proteins named Fra1 (Fe repressor of activation 1), an aminopeptidase P-like and Fra2 (Fe repressor of activation 2), a BolA-like protein, the depletion of which also led to an increased transcription of the iron regulon [111]. The isolation of Fra2 was consistent with the iron homeostasis defects previously observed for a *fra2* mutant [120].

Subsequently, several studies have reported that, besides the capacity of Grx3/4 to bind an Fe–S cluster into homodimers, they can also form [2Fe–2S] cluster-bridging heterodimeric complexes with Fra2 [94]. Interestingly, Fra2 converted the [2Fe–2S] Grx3 homodimer to [2Fe–2S] Grx3–Fra2 heterodimer, this conversion being thermodynamically and kinetically favored [121]. From the biochemical and spectroscopic characterizations of these clusters, it was concluded that the ligation involved the cysteinyl residues of the CGFS active site signature and of one glutathione molecule and a histidyl residue from Fra2, whereas the nature of the fourth ligand was unknown [94,121]. Recent spectroscopic and structural characterization of a GrxS14–BolA1 heterocomplex involving Arabidopsis proteins indicated that an additional histidyl residue from BolA1 is the fourth ligand, forming a Rieske-type Fe–S cluster [122]. However, BolA1 and Fra2 do not belong to the same phylogenetic clade and Fra2 does not possess the equivalent His residue. Instead, it was proposed that a cysteine residue found in the same loop could constitute the fourth ligand for members of the Fra2 clade.

The *in vivo* validation that the mutation of the conserved C-terminal His103 destabilized the Fe–S cluster and prevented the iron-dependent inhibition of Aft1 [121], confirmed that the [2Fe–2S] Grx3/4–Fra2 heterodimer is indispensable for Aft1 inhibition. The understanding of the precise molecular mechanism involved in the regulation of Aft1/2 came from the report that Aft2 can bind a [2Fe–2S] cluster into a dimer and that it only interacts with and accepts an Fe–S cluster from a [2Fe–2S] loaded Fra2–Grx3 complex but not from a [2Fe–2S] cluster bound form of a Grx3–Grx3 homodimer [123]. Overall, it was concluded that the DNA affinity of the [2Fe–2S] loaded Aft2 is decreased, which promotes its nuclear export, preventing as explained above its ability to activate the iron regulon. The fact that Aft1/2 is only partially repressed in the *fra2* mutant under iron-replete conditions suggests that a Grx3/4 holo-homodimer may be able to transfer Fe–S cluster to Aft1/2 *in vivo* although less efficiently [111]. Recently, structural and spectroscopic data on Grx–BolA complexes showed that the apo- and holo-heterodimers formed between both proteins involved different protein regions [122]. This evidence may help in refining the model of Aft1/2 regulation by Grx–BolA heterodimers. Under iron-replete conditions, favoring the formation of holo-heterodimers, the Grx C-terminal region, which was shown to be involved in Aft1 recognition [47], is accessible. Hence, this might allow the recruitement of Aft1/2 and thus the Fe–S cluster transfer to Aft1/2 and its subsequent export from the nucleus. On the contrary, under iron-depleted conditions, the formation of Grx–BolA apo-heterodimers should be favored. In this complex, the Grx C-terminal tail is part of the interaction area with BolA. Thus, the masking of this region likely prevents the interaction with Aft1/2 which promotes its accumulation in nucleus where it can activate the iron regulon [122]. For more complete information on all the Aft1 regulation aspects, we invite the reader to refer to a recent review [109].

To conclude on the role of yeast cytosolic class II Fe–S Grxs in iron metabolism, it is noteworthy that the Fe trafficking and Aft1/2 regulation functions are independent although both require Fe–S cluster binding. Indeed, mutagenesis studies aiming at deciphering the specificity of interaction between Grx4 and Aft1 demonstrated that the replacement of the C-terminal part of *S. cerevisiae* Grx4 by the corresponding region of *Schizosaccharomyces pombe* Grx4 abolished the interaction between Grx4 and Aft1 but did not impair Fe trafficking functions [47].

4.3. Glutaredoxins also control iron homeostasis in *Schizosaccharomyces pombe*

In *S. pombe*, iron homeostasis is essentially regulated by two transcription factors Fep1 and Php4 [124,125]. Under iron-replete conditions, Fep1 represses the expression of iron uptake and transport genes to avoid iron overload. On the contrary, under low-iron conditions, Php4 represses the expression of genes involved in iron-dependent metabolic pathways [126]. In addition, the expression of these two transcription factors is reciprocally controlled allowing a direct cross-talk between iron uptake and iron utilization [126,127]. Interestingly, both repressors are controlled at the post-translational level by Grx4, the only cytosolic class II Fe–S Grx in *S. pombe* [128]. Indeed, genetic studies of the *grx4* mutant revealed that Php4- and Fep1-regulated genes are constitutively repressed and that Php4 was constantly localized in the nucleus [95,96,129,130]. Similarly, it was shown that Fep1 is also constitutively active and bound to its target gene promoters in a *fra2 S. pombe* mutant [131].

The physical interaction of Grx4 with Fep1 and Php4 was confirmed by yeast two hybrid assays, bimolecular fluorescence complementation and co-immunoprecipitation studies and it was shown by mutagenesis to depend on the cysteine of the Grx domain [95,96,129,130]. Hence, these results suggest that the presence of an Fe–S cluster on Grx4 is indispensable for its ability to interact with Fep1 and Php4. However,

the physiological and likely molecular mechanisms involving the Fe–S binding Grx4 homodimer in the regulation of Fep1 and Php4 should be different, since Grx4 inhibits Fep1 under low-iron conditions and Php4 under iron-replete conditions [124]. In the case of the Fep1 interaction with Grx4 and Fra2, it was shown that the Trx domain of Grx4 strongly interacts with the C-terminal part of Fep1 and that Fra2 interacts with Fep1 independently of the cellular iron status [95,131]. On the contrary, the Grx domain of Grx4 interacts with the N-terminal part of Fep1 only under iron-limiting conditions [95,129]. Finally, it was demonstrated that the Fep1–Fra2 interaction occurs in nuclei and that both proteins form a complex with Grx4 [131]. Hence, all these results seem to indicate that the regulation of Fep1 by both Grx4 and Fra2 in *S. pombe* resembles the regulation of Aft1/2 by the Grx3/4–Fra2 complex in *S. cerevisiae*. However, considering that iron binding is not necessary for Fep1 DNA binding and that there is no demonstration of an Fe–S cluster bound to Fep1 [95,129], the requirement of an holo-Grx4 for regulating Fep1 activity implies that it does not involve an Fe–S cluster transfer between both proteins but that the interaction of Fep1 with Fra2 and/or holoGrx4 would trigger conformational changes on Fep1, favoring its DNA binding and thus its repressive activity [124].

In contrast to Fep1, the regulation of Php4 activity by monothiol Grx4 might be different from the Grx3/Grx4 regulation of Aft1/Aft2 in *S. cerevisiae*. As in the case of Fep1–Grx4 interaction, the Trx domain of Grx4 is constitutively associated with Php4 whatever the cellular iron status [96]. On the contrary, the interaction between the Grx domain of Grx4 and Php4 occurs under high-iron conditions. This Php4–Grx4 interaction is abolished when the cysteine of the CGFS signature or when two conserved cysteine residues in Php4 are mutated [96]. Hence, it has been proposed that under high-iron conditions, Grx4 and Php4 may form an holoheterodimer preventing the binding of Php4 to the Php2/Php3/Php5 complex and favoring its export from the nucleus by the Crm1 exportin [96]. From all these data, a model for the iron-dependent control of gene expression in *S. pombe* involving notably Fep1, Php4 and Grx4 but not Fra2 has been proposed recently. We invite the reader to refer to this review for more exhaustive details about these molecular mechanisms [124].

4.4. Evolutive conservation of the Grx–BolA interaction and possible additional roles

There is a plethora of evidence that the class II Fe–S Grx–BolA functional relationship is conserved in both prokaryotes and eukaryotes. Indeed, both genes are found in adjacent position in several prokaryote genomes and a strong co-occurrence exists between both genes [13,132]. Moreover, hybrid proteins where a BolA domain is fused to a Grx domain are present in some proteobacteria of the Methylococcale order. Besides these genomic evidences, high-throughput approaches experimentally confirmed a physical interaction for *S. cerevisiae*, *Drosophila melanogaster*, *E. coli* and *A. thaliana* proteins [133–138]. During the last five years, the Grx–BolA interaction has been more extensively studied using targeted biochemical and cellular approaches, focusing in particular on the molecular and structural determinants involved in the formation of Grx–BolA holo-heterodimer [87,94,111]. However, despite the demonstration that proteins from *E. coli*, human and *A. thaliana* can form [2Fe–2S] cluster-bridged heterodimer [80,139,140], their involvement in the regulation of iron homeostasis has been demonstrated only in *S. cerevisiae* whereas it awaits a firm confirmation in *S. pombe* and in other organisms.

On the other hand, several reports suggest that the interaction between some Grx and BolA, essentially the protein couples present in organelles (mitochondria and chloroplasts), could fulfill other functions notably related to the maturation of Fe–S clusters and its regulation. Indeed, there are 3 BolA isoforms in *S. cerevisiae* 4 in *S. pombe*, 2 in *Homo sapiens* and 3 in plants (4 by including the BolA domain of SufE1 protein) [87,141]. In *S. pombe*, it seems that they are not interchangeable since, among the four BolA-like proteins, only *fra2* deletion caused defects in the transcriptional response to iron starvation [131]. In human, BolA1 and BolA3 are found in mitochondria together with Grx5 [66,142]. While the role of BolA1 seems associated to the control of the mitochondrial thiol redox potential, BolA3 would participate to the maturation of Fe–S proteins. The demonstration that Grx–BolA heterodimers can give or receive Fe–S clusters supports a widespread distribution of the latter role. Indeed, *in vitro* transfer experiments showed an efficient [2Fe–2S] cluster transfer from an *A. vinelandii* A-type protein (^{NIF}IscA) to a *S. cerevisiae* Fra2–Grx3 apo heterodimer [78]. On the other hand, although the Fe–S cluster transfer occurs for regulatory purposes, a *S. cerevisiae* Fra2–Grx3 heterodimer is able to transfer its Fe–S cluster to an apoAft2 [123]. Finally, as explained in the Section 3.2, the presence of a BolA domain in plant SufE1 proteins raises the possibility that it contributes to a Grx-controlled regulation mechanism allowing to modulate SUF functioning.

5. Conclusions and perspectives

Considering the variability found in the domain organization of Grxs, the existence of numerous Fe–S bound Grxs and BolAs in different subcellular compartments, and the capacity of Grxs to integrate various types of Fe–S clusters alone or with BolA, the roles associated to these Grxs are very diverse. *In vitro* analyses dealing in particular with the spectroscopic and structural characterization of recombinant proteins are still required since mutational analyses indicated that it is fairly impossible to predict from the primary sequence, which Grxs can assemble Fe–S clusters. However, an important aspect in the future will be to validate these *in vitro* observations by demonstrating the physiological relevance of these forms. In this respect, the observation that Grx functions are impaired when the cysteine of the active site signature is mutated is insufficient as it affects both the oxidoreductase and Fe–S cluster binding properties. In addition, although showing the presence of Fe–S clusters bound to Grxs *in vivo* is already a good start, evaluating the relative proportion of apo *vs* holoforms would be more valuable. However, this aspect currently encounters major technical problems.

Acknowledgements

The UMR1136 is supported by a grant overseen by the French National Research Agency (ANR) as part of the "Investissements d'Avenir" program (ANR-11-LABX-0002-01, Lab of Excellence ARBRE).

References

[1] A. Holmgren, Hydrogen donor system for Escherichia coli ribonucleoside-diphosphate reductase dependent upon glutathione, Proc. Natl. Acad. Sci. U. S. A. 73 (1976) 2275–2279.
[2] T.C. Laurent, E.C. Moore, P. Reichard, Enzymatic synthesis of deoxyribonucleotides. IV. Isolation and characterization of thioredoxin, the hydrogen donor from *Escherichia coli* B, J. Biol. Chem. 239 (1964) 3436–3444.
[3] A.P. Fernandes, M. Fladvad, C. Berndt, C. Andresen, C.H. Lillig, P. Neubauer, M. Sunnerhagen, A. Holmgren, A. Vlamis-Gardikas, A novel monothiol glutaredoxin (Grx4) from Escherichia coli can serve as a substrate for thioredoxin reductase, J. Biol. Chem. 280 (2005) 24544–24552.
[4] C. Johansson, C.H. Lillig, A. Holmgren, Human mitochondrial glutaredoxin reduces S-glutathionylated proteins with high affinity accepting electrons from either glutathione or thioredoxin reductase, J. Biol. Chem. 279 (2004) 7537–7543.
[5] M. Zaffagnini, L. Michelet, V. Massot, P. Trost, S.D. Lemaire, Biochemical characterization of glutaredoxins from Chlamydomonas reinhardtii reveals the unique properties of a chloroplastic CGFS-type glutaredoxin, J. Biol. Chem. 283 (2008) 8868–8876.
[6] E. Gelhaye, N. Rouhier, J.P. Jacquot, Evidence for a subgroup of thioredoxin h that requires GSH/Grx for its reduction, FEBS Lett. 555 (2003) 443–448.
[7] C.S. Koh, N. Navrot, C. Didierjean, N. Rouhier, M. Hirasawa, D.B. Knaff, G. Wingsle, R. Samian, J.P. Jacquot, C. Corbier, E. Gelhaye, An atypical catalytic mechanism involving three cysteines of thioredoxin, J. Biol. Chem. 283 (2008) 23062–23072.
[8] H. Zhang, Y. Du, X. Zhang, J. Lu, A. Holmgren, Glutaredoxin 2 reduces both thioredoxin 2 and thioredoxin 1 and protects cells from apoptosis induced by auranofin and 4-hydroxynonenal, Antioxid. Redox Signal. 21 (2014) 669–681.
[9] I. Dalle-Donne, R. Rossi, G. Colombo, D. Giustarini, A. Milzani, Protein S-glutathionylation: a regulatory device from bacteria to humans, Trends Biochem. Sci. 34 (2009) 85–96.

[10] J.J. Mieyal, M.M. Gallogly, S. Qanungo, E.A. Sabens, M.D. Shelton, Molecular mechanisms and clinical implications of reversible protein S-glutathionylation, Antioxid. Redox Signal. 10 (2008) 1941–1988.
[11] M. Zaffagnini, M. Bedhomme, C.H. Marchand, S. Morisse, P. Trost, S.D. Lemaire, Redox regulation in photosynthetic organisms: focus on glutathionylation, Antioxid. Redox Signal. 16 (2012) 567–586.
[12] M.T. Rodriguez-Manzaneque, J. Ros, E. Cabiscol, A. Sorribas, E. Herrero, Grx5 glutaredoxin plays a central role in protection against protein oxidative damage in Saccharomyces cerevisiae, Mol. Cell. Biol. 19 (1999) 8180–8190.
[13] J. Couturier, J.P. Jacquot, N. Rouhier, Evolution and diversity of glutaredoxins in photosynthetic organisms, Cell. Mol. Life Sci. 66 (2009) 2539–2557.
[14] R. Alves, E. Vilaprinyo, A. Sorribas, E. Herrero, Evolution based on domain combinations: the case of glutaredoxins, BMC Evol. Biol. 9 (2009) 66.
[15] N. Rouhier, S.D. Lemaire, J.P. Jacquot, The role of glutathione in photosynthetic organisms: emerging functions for glutaredoxins and glutathionylation, Annu. Rev. Plant Biol. 59 (2008) 143–166.
[16] E. Herrero, M.A. de la Torre-Ruiz, Monothiol glutaredoxins: a common domain for multiple functions, Cell. Mol. Life Sci. 64 (2007) 1518–1530.
[17] J. Couturier, J.P. Jacquot, N. Rouhier, Toward a refined classification of class I dithiol glutaredoxins from poplar: biochemical basis for the definition of two subclasses, Front. Plant Sci. 4 (2013) 518.
[18] E.M. Allen, J.J. Mieyal, Protein-thiol oxidation and cell death: regulatory role of glutaredoxins, Antioxid. Redox Signal. 17 (2012) 1748–1763.
[19] M.A. Comini, R.L. Krauth-Siegel, M. Bellanda, Mono- and dithiol glutaredoxins in the trypanothione-based redox metabolism of pathogenic trypanosomes, Antioxid. Redox Signal. 19 (2013) 708–722.
[20] E.M. Hanschmann, J.R. Godoy, C. Berndt, C. Hudemann, C.H. Lillig, Thioredoxins, glutaredoxins, and peroxiredoxins—molecular mechanisms and health significance: from cofactors to antioxidants to redox signaling, Antioxid. Redox Signal. 19 (2013) 1539–1605.
[21] Y. Meyer, C. Belin, V. Delorme-Hinoux, J.P. Reichheld, C. Riondet, Thioredoxin and glutaredoxin systems in plants: molecular mechanisms, crosstalks, and functional significance, Antioxid. Redox Signal. 17 (2012) 1124–1160.
[22] N. Rouhier, Plant glutaredoxins: pivotal players in redox biology and iron–sulphur centre assembly, New Phytol. 186 (2010) 365–372.
[23] C.H. Lillig, C. Berndt, O. Vergnolle, M.E. Lonn, C. Hudemann, E. Bill, A. Holmgren, Characterization of human glutaredoxin 2 as iron–sulfur protein: a possible role as redox sensor, Proc. Natl. Acad. Sci. U. S. A. 102 (2005) 8168–8173.
[24] Y. Feng, N. Zhong, N. Rouhier, T. Hase, M. Kusunoki, J.P. Jacquot, C. Jin, B. Xia, Structural insight into poplar glutaredoxin C1 with a bridging iron–sulfur cluster at the active site, Biochemistry 45 (2006) 7998–8008.
[25] N. Rouhier, H. Unno, S. Bandyopadhyay, L. Masip, S.K. Kim, M. Hirasawa, J.M. Gualberto, V. Lattard, M. Kusunoki, D.B. Knaff, G. Georgiou, T. Hase, M.K. Johnson, J.P. Jacquot, Functional, structural, and spectroscopic characterization of a glutathione-ligated [2Fe–2S] cluster in poplar glutaredoxin C1, Proc. Natl. Acad. Sci. U. S. A. 104 (2007) 7379–7384.
[26] C. Berndt, C. Hudemann, E.M. Hanschmann, R. Axelsson, A. Holmgren, C.H. Lillig, How does iron–sulfur cluster coordination regulate the activity of human glutaredoxin 2? Antioxid. Redox Signal. 9 (2007) 151–157.
[27] C. Johansson, K.L. Kavanagh, O. Gileadi, U. Oppermann, Reversible sequestration of active site cysteines in a 2Fe–2S-bridged dimer provides a mechanism for glutaredoxin 2 regulation in human mitochondria, J. Biol. Chem. 282 (2007) 3077–3082.
[28] J. Couturier, E. Stroher, A.N. Albetel, T. Roret, M. Muthuramalingam, L. Tarrago, T. Seidel, P. Tsan, J.P. Jacquot, M.K. Johnson, K.J. Dietz, C. Didierjean, N. Rouhier, Arabidopsis chloroplastic glutaredoxin C5 as a model to explore molecular determinants for iron–sulfur cluster binding into glutaredoxins, J. Biol. Chem. 286 (2011) 27515–27527.
[29] N. Mesecke, S. Mittler, E. Eckers, J.M. Herrmann, M. Deponte, Two novel monothiol glutaredoxins from Saccharomyces cerevisiae provide further insight into iron–sulfur cluster binding, oligomerization, and enzymatic activity of glutaredoxins, Biochemistry 47 (2008) 1452–1463.
[30] M. Luo, Y.L. Jiang, X.X. Ma, Y.J. Tang, Y.X. He, J. Yu, R.G. Zhang, Y. Chen, C.Z. Zhou, Structural and biochemical characterization of yeast monothiol glutaredoxin Grx6, J. Mol. Biol. 398 (2010) 614–622.
[31] L. Brautigam, C. Johansson, B. Kubsch, M.A. McDonough, E. Bill, A. Holmgren, C. Berndt, An unusual mode of iron–sulfur-cluster coordination in a teleost glutaredoxin, Biochem. Biophys. Res. Commun. 436 (2013) 491–496.
[32] S. Ceylan, V. Seidel, N. Ziebart, C. Berndt, N. Dirdjaja, R.L. Krauth-Siegel, The dithiol glutaredoxins of African trypanosomes have distinct roles and are closely linked to the unique trypanothione metabolism, J. Biol. Chem. 285 (2010) 35224–35237.
[33] J. Couturier, C.S. Koh, M. Zaffagnini, A.M. Winger, J.M. Gualberto, C. Corbier, P. Decottignies, J.P. Jacquot, S.D. Lemaire, C. Didierjean, N. Rouhier, Structure–function relationship of the chloroplastic glutaredoxin S12 with an atypical WCSYS active site, J. Biol. Chem. 284 (2009) 9299–9310.
[34] K.G. Hoff, S.J. Culler, P.Q. Nguyen, R.M. McGuire, J.J. Silberg, C.D. Smolke, In vivo fluorescent detection of Fe–S clusters coordinated by human GRX2, Chem. Biol. 16 (2009) 1299–1308.
[35] L. Wang, B. Ouyang, Y. Li, Y. Feng, J.P. Jacquot, N. Rouhier, B. Xia, Glutathione regulates the transfer of iron–sulfur cluster from monothiol and dithiol glutaredoxins to apo ferredoxin, Protein Cell 3 (2012) 714–721.
[36] S. Bandyopadhyay, F. Gama, M.M. Molina-Navarro, J.M. Gualberto, R. Claxton, S.G. Naik, B.H. Huynh, E. Herrero, J.P. Jacquot, M.K. Johnson, N. Rouhier, Chloroplast monothiol glutaredoxins as scaffold proteins for the assembly and delivery of [2Fe–2S] clusters, EMBO J. 27 (2008) 1122–1133.
[37] W. Qi, J.A. Cowan, Mechanism of glutaredoxin-ISU [2Fe–2S] cluster exchange, Chem. Commun. (Camb.) 47 (2011) 4989–4991.
[38] D.W. Lee, D. Kaur, S.J. Chinta, S. Rajagopalan, J.K. Andersen, A disruption in iron–sulfur center biogenesis via inhibition of mitochondrial dithiol glutaredoxin 2 may contribute to mitochondrial and cellular iron dysregulation in mammalian glutathione-depleted dopaminergic cells: implications for Parkinson's disease, Antioxid. Redox Signal. 11 (2009) 2083–2094.
[39] M.A. Comini, J. Rettig, N. Dirdjaja, E.M. Hanschmann, C. Berndt, R.L. Krauth-Siegel, Monothiol glutaredoxin-1 is an essential iron–sulfur protein in the mitochondrion of African trypanosomes, J. Biol. Chem. 283 (2008) 27785–27798.
[40] T. Iwema, A. Picciocchi, D.A. Traore, J.L. Ferrer, F. Chauvat, L. Jacquamet, Structural basis for delivery of the intact [Fe2S2] cluster by monothiol glutaredoxin, Biochemistry 48 (2009) 6041–6043.
[41] A. Picciocchi, C. Saguez, A. Boussac, C. Cassier-Chauvat, F. Chauvat, CGFS-type monothiol glutaredoxins from the cyanobacterium Synechocystis PCC6803 and other evolutionary distant model organisms possess a glutathione-ligated [2Fe–2S] cluster, Biochemistry 46 (2007) 15018–15026.
[42] L. Banci, D. Brancaccio, S. Ciofi-Baffoni, R. Del Conte, R. Gadepalli, M. Mikolajczyk, S. Neri, M. Piccioli, J. Winkelmann, [2Fe–2S] cluster transfer in iron–sulfur protein biogenesis, Proc. Natl. Acad. Sci. U. S. A. 111 (2014) 6203–6208.
[43] C. Johansson, A.K. Roos, S.J. Montano, R. Sengupta, P. Filippakopoulos, K. Guo, F. von Delft, A. Holmgren, U. Oppermann, K.L. Kavanagh, The crystal structure of human GLRX5: iron–sulfur cluster co-ordination, tetrameric assembly and monomer activity, Biochem. J. 433 (2011) 303–311.
[44] P. Haunhorst, C. Berndt, S. Eitner, J.R. Godoy, C.H. Lillig, Characterization of the human monothiol glutaredoxin 3 (PICOT) as iron–sulfur protein, Biochem. Biophys. Res. Commun. 394 (2010) 372–376.
[45] B. Manta, C. Pavan, M. Sturlese, A. Medeiros, M. Crispo, C. Berndt, R.L. Krauth-Siegel, M. Bellanda, M.A. Comini, Iron–sulfur cluster binding by mitochondrial monothiol glutaredoxin-1 of Trypanosoma brucei: molecular basis of iron–sulfur cluster coordination and relevance for parasite infectivity, Antioxid. Redox Signal. 19 (2013) 665–682.
[46] B. Zhang, S. Bandyopadhyay, P. Shakamuri, S.G. Naik, B.H. Huynh, J. Couturier, N. Rouhier, M.K. Johnson, Monothiol glutaredoxins can bind linear [Fe3S4] + and [Fe4S4]2+ clusters in addition to [Fe2S2]2+ clusters: spectroscopic characterization and functional implications, J. Am. Chem. Soc. 135 (2013) 15153–15164.
[47] B. Hoffmann, M.A. Uzarska, C. Berndt, J.R. Godoy, P. Haunhorst, C.H. Lillig, R. Lill, U. Muhlenhoff, The multidomain thioredoxin-monothiol glutaredoxins represent a distinct functional group, Antioxid. Redox Signal. 15 (2011) 19–30.
[48] M.T. Rodriguez-Manzaneque, J. Tamarit, G. Belli, J. Ros, E. Herrero, Grx5 is a mitochondrial glutaredoxin required for the activity of iron/sulfur enzymes, Mol. Biol. Cell 13 (2002) 1109–1121.
[49] D. Shenton, G. Perrone, K.A. Quinn, I.W. Dawes, C.M. Grant, Regulation of protein S-thiolation by glutaredoxin 5 in the yeast Saccharomyces cerevisiae, J. Biol. Chem. 277 (2002) 16853–16859.
[50] J. Tamarit, G. Belli, E. Cabiscol, E. Herrero, J. Ros, Biochemical characterization of yeast mitochondrial Grx5 monothiol glutaredoxin, J. Biol. Chem. 278 (2003) 25745–25751.
[51] U. Mühlenhoff, J. Gerber, N. Richhardt, R. Lill, Components involved in assembly and dislocation of iron–sulfur clusters on the scaffold protein Isu1p, EMBO J. 22 (2003) 4815–4825.
[52] C. Camaschella, A. Campanella, L. De Falco, L. Boschetto, R. Merlini, L. Silvestri, S. Levi, A. Iolascon, The human counterpart of zebrafish shiraz shows sideroblastic-like microcytic anemia and iron overload, Blood 110 (2007) 1353–1358.
[53] R.A. Wingert, J.L. Galloway, B. Barut, H. Foott, P. Fraenkel, J.L. Axe, G.J. Weber, K. Dooley, A.J. Davidson, B. Schmid, B.H. Paw, G.C. Shaw, P. Kingsley, J. Palis, H. Schubert, O. Chen, J. Kaplan, L.I. Zon, Deficiency of glutaredoxin 5 reveals Fe–S clusters are required for vertebrate haem synthesis, Nature 436 (2005) 1035–1039.
[54] H. Ye, S.Y. Jeong, M.C. Ghosh, G. Kovtunovych, L. Silvestri, D. Ortillo, N. Uchida, J. Tisdale, C. Camaschella, T.A. Rouault, Glutaredoxin 5 deficiency causes sideroblastic anemia by specifically impairing heme biosynthesis and depleting cytosolic iron in human erythroblasts, J. Clin. Invest. 120 (2010) 1749–1761.
[55] P.R. Baker II, M.W. Friederich, M.A. Swanson, T. Shaikh, K. Bhattacharya, G.H. Scharer, J. Aicher, G. Creadon-Swindell, E. Geiger, K.N. MacLean, W.T. Lee, C. Deshpande, M.L. Freckmann, L.Y. Shih, M. Wasserstein, M.B. Rasmussen, A.M. Lund, P. Procopis, J.M. Cameron, B.H. Robinson, G.K. Brown, R.M. Brown, A.G. Compton, C.L. Dieckmann, R. Collard, C.R. Coughlin II, E. Spector, M.F. Wempe, J.L. Van Hove, Variant non ketotic hyperglycinemia is caused by mutations in LIAS, BOLA3 and the novel gene GLRX5, Brain 137 (2014) 366–379.
[56] R. Lill, B. Hoffmann, S. Molik, A.J. Pierik, N. Rietzschel, O. Stehling, M.A. Uzarska, H. Webert, C. Wilbrecht, U. Muhlenhoff, The role of mitochondria in cellular iron–sulfur protein biogenesis and iron metabolism, Biochim. Biophys. Acta 1823 (2012) 1491–1508.
[57] F. Colin, A. Martelli, M. Clemancey, J.M. Latour, S. Gambarelli, L. Zeppieri, C. Birck, A. Page, H. Puccio, S. Ollagnier de Choudens, Mammalian frataxin controls sulfur production and iron entry during de novo Fe4S4 cluster assembly, J. Am. Chem. Soc. 135 (2013) 733–740.
[58] J.H. Kim, R.O. Frederick, N.M. Reinen, A.T. Troupis, J.L. Markley, [2Fe–2S]-ferredoxin binds directly to cysteine desulfurase and supplies an electron for iron–sulfur cluster assembly but is displaced by the scaffold protein or bacterial frataxin, J. Am. Chem. Soc. 135 (2013) 8117–8120.
[59] R. Yan, P.V. Konarev, C. Iannuzzi, S. Adinolfi, B. Roche, G. Kelly, L. Simon, S.R. Martin, B. Py, F. Barras, D.I. Svergun, A. Pastore, Ferredoxin competes with bacterial frataxin in binding to the desulfurase IscS, J. Biol. Chem. 288 (2013) 24777–24787.

[60] U. Mühlenhoff, N. Richter, O. Pines, A.J. Pierik, R. Lill, Specialized function of yeast Isa1 and Isa2 proteins in the maturation of mitochondrial [4Fe–4S] proteins, J. Biol. Chem. 286 (2011) 41205–41216.
[61] A. Navarro-Sastre, F. Tort, O. Stehling, M.A. Uzarska, J.A. Arranz, M. Del Toro, M.T. Labayru, J. Landa, A. Font, J. Garcia-Villoria, B. Merinero, M. Ugarte, L.G. Gutierrez-Solana, J. Campistol, A. Garcia-Cazorla, J. Vaquerizo, E. Riudor, P. Briones, O. Elpeleg, A. Ribes, R. Lill, A fatal mitochondrial disease is associated with defective NFU1 function in the maturation of a subset of mitochondrial Fe–S proteins, Am. J. Hum. Genet. 89 (2011) 656–667.
[62] M.A. Uzarska, R. Dutkiewicz, S.A. Freibert, R. Lill, U. Muhlenhoff, The mitochondrial Hsp70 chaperone Ssq1 facilitates Fe/S cluster transfer from Isu1 to Grx5 by complex formation, Mol. Biol. Cell 24 (2013) 1830–1841.
[63] P. Shakamuri, B. Zhang, M.K. Johnson, Monothiol glutaredoxins function in storing and transporting [Fe2S2] clusters assembled on IscU scaffold proteins, J. Am. Chem. Soc. 134 (2012) 15213–15216.
[64] F. Vilella, R. Alves, M.T. Rodriguez-Manzaneque, G. Belli, S. Swaminathan, P. Sunnerhagen, E. Herrero, Evolution and cellular function of monothiol glutaredoxins: involvement in iron–sulphur cluster assembly, Comp. Funct. Genomics 5 (2004) 328–341.
[65] K.D. Kim, W.H. Chung, H.J. Kim, K.C. Lee, J.H. Roe, Monothiol glutaredoxin Grx5 interacts with Fe–S scaffold proteins Isa1 and Isa2 and supports Fe–S assembly and DNA integrity in mitochondria of fission yeast, Biochem. Biophys. Res. Commun. 392 (2010) 467–472.
[66] J.M. Cameron, A. Janer, V. Levandovskiy, N. Mackay, T.A. Rouault, W.H. Tong, I. Ogilvie, E.A. Shoubridge, B.H. Robinson, Mutations in iron–sulfur cluster scaffold genes NFU1 and BOLA3 cause a fatal deficiency of multiple respiratory chain and 2-oxoacid dehydrogenase enzymes, Am. J. Hum. Genet. 89 (2011) 486–495.
[67] T.B. Haack, B. Rolinski, B. Haberberger, F. Zimmermann, J. Schum, V. Strecker, E. Graf, U. Athing, T. Hoppen, I. Wittig, W. Sperl, P. Freisinger, J.A. Mayr, T.M. Strom, T. Meitinger, H. Prokisch, Homozygous missense mutation in BOLA3 causes multiple mitochondrial dysfunctions syndrome in two siblings, J. Inherit. Metab. Dis. 36 (2013) 55–62.
[68] C. Gelling, I.W. Dawes, N. Richhardt, R. Lill, U. Muhlenhoff, Mitochondrial Iba57p is required for Fe/S cluster formation on aconitase and activation of radical SAM enzymes, Mol. Cell. Biol. 28 (2008) 1851–1861.
[69] L.K. Beilschmidt, H.M. Puccio, Mammalian Fe–S cluster biogenesis and its implication in disease, Biochimie 100 (2014) 48–60.
[70] J.C. Rutherford, L. Ojeda, J. Balk, U. Muhlenhoff, R. Lill, D.R. Winge, Activation of the iron regulon by the yeast Aft1/Aft2 transcription factors depends on mitochondrial but not cytosolic iron–sulfur protein biogenesis, J. Biol. Chem. 280 (2005) 10135–10140.
[71] J.Y. Lee, J.G. Yang, D. Zhitnitsky, O. Lewinson, D.C. Rees, Structural basis for heavy metal detoxification by an Atm1-type ABC exporter, Science 343 (2014) 1133–1136.
[72] W. Qi, J. Li, J.A. Cowan, A structural model for glutathione-complexed iron–sulfur cluster as a substrate for ABCB7-type transporters, Chem. Commun. (Camb.) 50 (2014) 3795–3798.
[73] V. Srinivasan, A.J. Pierik, R. Lill, Crystal structures of nucleotide-free and glutathione-bound mitochondrial ABC transporter Atm1, Science 343 (2014) 1137–1140.
[74] J. Balk, M. Pilon, Ancient and essential: the assembly of iron–sulfur clusters in plants, Trends Plant Sci. 16 (2011) 218–226.
[75] J. Balk, T.A. Schaedler, Iron cofactor assembly in plants, Annu. Rev. Plant Biol. 65 (2014) 125–153.
[76] J. Couturier, B. Touraine, J.F. Briat, F. Gaymard, N. Rouhier, The iron–sulfur cluster assembly machineries in plants: current knowledge and open questions, Front. Plant Sci. 4 (2013) 259.
[77] N.H. Cheng, J.Z. Liu, A. Brock, R.S. Nelson, K.D. Hirschi, AtGRXcp, an Arabidopsis chloroplastic glutaredoxin, is critical for protection against protein oxidative damage, J. Biol. Chem. 281 (2006) 26280–26288.
[78] D.T. Mapolelo, B. Zhang, S. Randeniya, A.N. Albetel, H. Li, J. Couturier, C.E. Outten, N. Rouhier, M.K. Johnson, Monothiol glutaredoxins and A-type proteins: partners in Fe–S cluster trafficking, Dalton Trans. 42 (2013) 3107–3115.
[79] H. Gao, S. Subramanian, J. Couturier, S.G. Naik, S.K. Kim, T. Leustek, D.B. Knaff, H.C. Wu, F. Vignols, B.H. Huynh, N. Rouhier, M.K. Johnson, Arabidopsis thaliana Nfu2 accommodates [2Fe–2S] or [4Fe–4S] clusters and is competent for in vitro maturation of chloroplast [2Fe–2S] and [4Fe–4S] cluster-containing proteins, Biochemistry 52 (2013) 6633–6645.
[80] N. Yeung, B. Gold, N.L. Liu, R. Prathapam, H.J. Sterling, E.R. Willams, G. Butland, The E. coli monothiol glutaredoxin GrxD forms homodimeric and heterodimeric FeS cluster containing complexes, Biochemistry 50 (2011) 8957–8969.
[81] G. Butland, J.M. Peregrin-Alvarez, J. Li, W. Yang, X. Yang, V. Canadien, A. Starostine, D. Richards, B. Beattie, N. Krogan, M. Davey, J. Parkinson, J. Greenblatt, A. Emili, Interaction network containing conserved and essential protein complexes in Escherichia coli, Nature 433 (2005) 531–537.
[82] F.W. Outten, O. Djaman, G. Storz, A suf operon requirement for Fe–S cluster assembly during iron starvation in Escherichia coli, Mol. Microbiol. 52 (2004) 861–872.
[83] S. Boutigny, A. Saini, E.E. Baidoo, N. Yeung, J.D. Keasling, G. Butland, Physical and functional interactions of a monothiol glutaredoxin and an iron sulfur cluster carrier protein with the sulfur-donating radical S-adenosyl-L-methionine enzyme MiaB, J. Biol. Chem. 288 (2013) 14200–14211.
[84] H.M. Bolstad, M.J. Wood, An in vivo method for characterization of protein interactions within sulfur trafficking systems of E. coli, J. Proteome Res. 9 (2010) 6740–6751.
[85] X.M. Xu, S.G. Moller, AtSufE is an essential activator of plastidic and mitochondrial desulfurases in Arabidopsis, EMBO J. 25 (2006) 900–909.
[86] H. Ye, S.E. Abdel-Ghany, T.D. Anderson, E.A. Pilon-Smits, M. Pilon, CpSufE activates the cysteine desulfurase CpNifS for chloroplastic Fe–S cluster formation, J. Biol. Chem. 281 (2006) 8958–8969.
[87] J. Couturier, H.C. Wu, T. Dhalleine, H. Pegeot, D. Sudre, J.M. Gualberto, J.P. Jacquot, F. Gaymard, F. Vignols, N. Rouhier, Monothiol glutaredoxin-BolA interactions: redox control of Arabidopsis thaliana BolA2 and SufE1, Mol. Plant 7 (2014) 187–205.
[88] N.D. Lanz, S.J. Booker, Identification and function of auxiliary iron–sulfur clusters in radical SAM enzymes, Biochim. Biophys. Acta 1824 (2012) 1196–1212.
[89] N. Isakov, S. Witte, A. Altman, PICOT-HD: a highly conserved protein domain that is often associated with thioredoxin and glutaredoxin modules, Trends Biochem. Sci. 25 (2000) 537–539.
[90] Y. Babichev, N. Isakov, Tyrosine phosphorylation of PICOT and its translocation to the nucleus in response of human T cells to oxidative stress, Adv. Exp. Med. Biol. 495 (2001) 41–45.
[91] N.H. Cheng, J.Z. Liu, X. Liu, Q. Wu, S.M. Thompson, J. Lin, J. Chang, S.A. Whitham, S. Park, J.D. Cohen, K.D. Hirschi, Arabidopsis monothiol glutaredoxin, AtGRXS17, is critical for temperature-dependent postembryonic growth and development via modulating auxin response, J. Biol. Chem. 286 (2011) 20398–20406.
[92] R. Lopreiato, S. Facchin, G. Sartori, G. Arrigoni, S. Casonato, M. Ruzzene, L.A. Pinna, G. Carignani, Analysis of the interaction between piD261/Bud32, an evolutionarily conserved protein kinase of Saccharomyces cerevisiae, and the Grx4 glutaredoxin, Biochem. J. 377 (2004) 395–405.
[93] M.M. Molina, G. Belli, M.A. de la Torre, M.T. Rodriguez-Manzaneque, E. Herrero, Nuclear monothiol glutaredoxins of Saccharomyces cerevisiae can function as mitochondrial glutaredoxins, J. Biol. Chem. 279 (2004) 51923–51930.
[94] H. Li, D.T. Mapolelo, N.N. Dingra, S.G. Naik, N.S. Lees, B.M. Hoffman, P.J. Riggs-Gelasco, B.H. Huynh, M.K. Johnson, C.E. Outten, The yeast iron regulatory proteins Grx3/4 and Fra2 form heterodimeric complexes containing a [2Fe–2S] cluster with cysteinyl and histidyl ligation, Biochemistry 48 (2009) 9569–9581.
[95] M. Jbel, A. Mercier, S. Labbe, Grx4 monothiol glutaredoxin is required for iron limitation-dependent inhibition of Fep1, Eukaryot. Cell 10 (2011) 629–645.
[96] P. Vachon, A. Mercier, M. Jbel, S. Labbe, The monothiol glutaredoxin Grx4 exerts an iron-dependent inhibitory effect on Php4 function, Eukaryot. Cell 11 (2012) 806–819.
[97] N. Pujol-Carrion, M.A. de la Torre-Ruiz, Glutaredoxins Grx4 and Grx3 of Saccharomyces cerevisiae play a role in actin dynamics through their Trx domains, which contributes to oxidative stress resistance, Appl. Environ. Microbiol. 76 (2010) 7826–7835.
[98] S. Witte, M. Villalba, K. Bi, Y. Liu, N. Isakov, A. Altman, Inhibition of the c-Jun N-terminal kinase/AP-1 and NF-kappaB pathways by PICOT, a novel protein kinase C-interacting protein with a thioredoxin homology domain, J. Biol. Chem. 275 (2000) 1902–1909.
[99] C. Brynczka, P. Labhart, B.A. Merrick, NGF-mediated transcriptional targets of p53 in PC12 neuronal differentiation, BMC Genomics 8 (2007) 139.
[100] D. Jeong, H. Cha, E. Kim, M. Kang, D.K. Yang, J.M. Kim, P.O. Yoon, J.G. Oh, O.Y. Bernecker, S. Sakata, T.T. Le, L. Cui, Y.H. Lee, H. Kim do, S.H. Woo, R. Liao, R.J. Hajjar, W.J. Park, PICOT inhibits cardiac hypertrophy and enhances ventricular function and cardiomyocyte contractility, Circ. Res. 99 (2006) 307–314.
[101] D. Jeong, J.M. Kim, H. Cha, J.G. Oh, J. Park, S.H. Yun, E.S. Ju, E.S. Jeon, R.J. Hajjar, W.J. Park, PICOT attenuates cardiac hypertrophy by disrupting calcineurin-NFAT signaling, Circ. Res. 102 (2008) 711–719.
[102] N.H. Cheng, W. Zhang, W.Q. Chen, J. Jin, X. Cui, N.F. Butte, L. Chan, K.D. Hirschi, A mammalian monothiol glutaredoxin, Grx3, is critical for cell cycle progression during embryogenesis, FEBS J. 278 (2011) 2525–2539.
[103] D.J. Netz, J. Mascarenhas, O. Stehling, A.J. Pierik, R. Lill, Maturation of cytosolic and nuclear iron–sulfur proteins, Trends Cell Biol. 24 (2014) 303–312.
[104] U. Mühlenhoff, S. Molik, J.R. Godoy, M.A. Uzarska, N. Richter, A. Seubert, Y. Zhang, J. Stubbe, F. Pierrel, E. Herrero, C.H. Lillig, R. Lill, Cytosolic monothiol glutaredoxins function in intracellular iron sensing and trafficking via their bound iron–sulfur cluster, Cell Metab. 12 (2010) 373–385.
[105] Y. Zhang, L. Liu, X. Wu, X. An, J. Stubbe, M. Huang, Investigation of in vivo diferric tyrosyl radical formation in Saccharomyces cerevisiae Rnr2 protein: requirement of Rnr4 and contribution of Grx3/4 AND Dre2 proteins, J. Biol. Chem. 286 (2011) 41499–41509.
[106] R. Lill, U. Muhlenhoff, Maturation of iron–sulfur proteins in eukaryotes: mechanisms, connected processes, and diseases, Annu. Rev. Biochem. 77 (2008) 669–700.
[107] P. Haunhorst, E.M. Hanschmann, L. Brautigam, O. Stehling, B. Hoffmann, U. Muhlenhoff, R. Lill, C. Berndt, C.H. Lillig, Crucial function of vertebrate glutaredoxin 3 (PICOT) in iron homeostasis and hemoglobin maturation, Mol. Biol. Cell 24 (2013) 1895–1903.
[108] S.M. Benyamina, F. Baldacci-Cresp, J. Couturier, K. Chibani, J. Hopkins, A. Bekki, P. de Lajudie, N. Rouhier, J.P. Jacquot, G. Alloing, A. Puppo, P. Frendo, Two Sinorhizobium meliloti glutaredoxins regulate iron metabolism and symbiotic bacteroid differentiation, Environ. Microbiol. 15 (2013) 795–810.
[109] C.E. Outten, A.N. Albetel, Iron sensing and regulation in Saccharomyces cerevisiae: Ironing out the mechanistic details, Curr. Opin. Microbiol. 16 (2013) 662–668.
[110] C. Pimentel, C. Vicente, R.A. Menezes, S. Caetano, L. Carreto, C. Rodrigues-Pousada, The role of the Yap5 transcription factor in remodeling gene expression in response to Fe bioavailability, PLoS One 7 (2012) e37434.
[111] A. Kumanovics, O.S. Chen, L. Li, D. Bagley, E.M. Adkins, H. Lin, N.N. Dingra, C.E. Outten, G. Keller, D. Winge, D.M. Ward, J. Kaplan, Identification of FRA1 and FRA2 as genes involved in regulating the yeast iron regulon in response to decreased mitochondrial iron–sulfur cluster synthesis, J. Biol. Chem. 283 (2008) 10276–10286.
[112] L. Ojeda, G. Keller, U. Muhlenhoff, J.C. Rutherford, R. Lill, D.R. Winge, Role of glutaredoxin-3 and glutaredoxin-4 in the iron regulation of the Aft1 transcriptional activator in Saccharomyces cerevisiae, J. Biol. Chem. 281 (2006) 17661–17669.

[113] N. Pujol-Carrion, G. Belli, E. Herrero, A. Nogues, M.A. de la Torre-Ruiz, Glutaredoxins Grx3 and Grx4 regulate nuclear localisation of Aft1 and the oxidative stress response in Saccharomyces cerevisiae, J. Cell Sci. 119 (2006) 4554–4564.
[114] L. Li, R. Miao, S. Bertram, X. Jia, D.M. Ward, J. Kaplan, A role for iron–sulfur clusters in the regulation of transcription factor Yap5-dependent high iron transcriptional responses in yeast, J. Biol. Chem. 287 (2012) 35709–35721.
[115] P. Uetz, L. Giot, G. Cagney, T.A. Mansfield, R.S. Judson, J.R. Knight, D. Lockshon, V. Narayan, M. Srinivasan, P. Pochart, A. Qureshi-Emili, Y. Li, B. Godwin, D. Conover, T. Kalbfleisch, G. Vijayadamodar, M. Yang, M. Johnston, S. Fields, J.M. Rothberg, A comprehensive analysis of protein–protein interactions in Saccharomyces cerevisiae, Nature 403 (2000) 623–627.
[116] O.S. Chen, S. Hemenway, J. Kaplan, Inhibition of Fe–S cluster biosynthesis decreases mitochondrial iron export: evidence that Yfh1p affects Fe–S cluster synthesis, Proc. Natl. Acad. Sci. U. S. A. 99 (2002) 12321–12326.
[117] R. Ueta, N. Fujiwara, K. Iwai, Y. Yamaguchi-Iwai, Iron-induced dissociation of the Aft1p transcriptional regulator from target gene promoters is an initial event in iron-dependent gene suppression, Mol. Cell. Biol. 32 (2012) 4998–5008.
[118] R. Ueta, N. Fujiwara, K. Iwai, Y. Yamaguchi-Iwai, Mechanism underlying the iron-dependent nuclear export of the iron-responsive transcription factor Aft1p in Saccharomyces cerevisiae, Mol. Biol. Cell 18 (2007) 2980–2990.
[119] Y. Yamaguchi-Iwai, R. Ueta, A. Fukunaka, R. Sasaki, Subcellular localization of Aft1 transcription factor responds to iron status in Saccharomyces cerevisiae, J. Biol. Chem. 277 (2002) 18914–18918.
[120] E. Lesuisse, S.A. Knight, M. Courel, R. Santos, J.M. Camadro, A. Dancis, Genome-wide screen for genes with effects on distinct iron uptake activities in Saccharomyces cerevisiae, Genetics 169 (2005) 107–122.
[121] H. Li, D.T. Mapolelo, N.N. Dingra, G. Keller, P.J. Riggs-Gelasco, D.R. Winge, M.K. Johnson, C.E. Outten, Histidine 103 in Fra2 is an iron–sulfur cluster ligand in the [2Fe–2S] Fra2–Grx3 complex and is required for in vivo iron signaling in yeast, J. Biol. Chem. 286 (2011) 867–876.
[122] T. Roret, P. Tsan, J. Couturier, B. Zhang, M.K. Johnson, N. Rouhier, C. Didierjean, Structural and spectroscopic insights into BolA–glutaredoxin complexes, J. Biol. Chem. 289 (2014) 24588–24598.
[123] C.B. Poor, S.V. Wegner, H. Li, A.C. Dlouhy, J.P. Schuermann, R. Sanishvili, J.R. Hinshaw, P.J. Riggs-Gelasco, C.E. Outten, C. He, Molecular mechanism and structure of the Saccharomyces cerevisiae iron regulator Aft2, Proc. Natl. Acad. Sci. U. S. A. 111 (2014) 4043–4048.
[124] S. Labbe, M.G. Khan, J.F. Jacques, Iron uptake and regulation in Schizosaccharomyces pombe, Curr. Opin. Microbiol. 16 (2013) 669–676.
[125] S. Labbe, B. Pelletier, A. Mercier, Iron homeostasis in the fission yeast Schizosaccharomyces pombe, Biometals 20 (2007) 523–537.
[126] A. Mercier, B. Pelletier, S. Labbe, A transcription factor cascade involving Fep1 and the CCAAT-binding factor Php4 regulates gene expression in response to iron deficiency in the fission yeast Schizosaccharomyces pombe, Eukaryot. Cell 5 (2006) 1866–1881.
[127] A. Mercier, S. Watt, J. Bahler, S. Labbe, Key function for the CCAAT-binding factor Php4 to regulate gene expression in response to iron deficiency in fission yeast, Eukaryot. Cell 7 (2008) 493–508.
[128] W.H. Chung, K.D. Kim, J.H. Roe, Localization and function of three monothiol glutaredoxins in Schizosaccharomyces pombe, Biochem. Biophys. Res. Commun. 330 (2005) 604–610.
[129] K.D. Kim, H.J. Kim, K.C. Lee, J.H. Roe, Multi-domain CGFS-type glutaredoxin Grx4 regulates iron homeostasis via direct interaction with a repressor Fep1 in fission yeast, Biochem. Biophys. Res. Commun. 408 (2011) 609–614.
[130] A. Mercier, S. Labbe, Both Php4 function and subcellular localization are regulated by iron via a multistep mechanism involving the glutaredoxin Grx4 and the exportin Crm1, J. Biol. Chem. 284 (2009) 20249–20262.
[131] J.F. Jacques, A. Mercier, A. Brault, T. Mourer, S. Labbe, Fra2 is a co-regulator of fep1 inhibition in response to iron starvation, PLoS One 9 (2014) e98959.
[132] M.A. Huynen, C.A. Spronk, T. Gabaldon, B. Snel, Combining data from genomes, Y2H and 3D structure indicates that BolA is a reductase interacting with a glutaredoxin, FEBS Lett. 579 (2005) 591–596.
[133] A.I.M. Consortium, Evidence for network evolution in an Arabidopsis interactome map, Science 333 (2011) 601–607.
[134] G. Butland, M. Babu, J.J. Diaz-Mejia, F. Bohdana, S. Phanse, B. Gold, W. Yang, J. Li, A. G. Gagarinova, O. Pogoutse, H. Mori, B.L. Wanner, H. Lo, J. Wasniewski, C. Christopolous, M. Ali, P. Venn, A. Safavi-Naini, N. Sourour, S. Caron, J.Y. Choi, L. Laigle, A. Nazarians-Armavil, A. Deshpande, S. Joe, K.A. Datsenko, N. Yamamoto, B.J. Andrews, C. Boone, H. Ding, B. Sheikh, G. Moreno-Hagelseib, J.F. Greenblatt, A. Emili, eSGA: E. coli synthetic genetic array analysis, Nat. Methods 5 (2008) 789–795.
[135] L. Giot, J.S. Bader, C. Brouwer, A. Chaudhuri, B. Kuang, Y. Li, Y.L. Hao, C.E. Ooi, B. Godwin, E. Vitols, G. Vijayadamodar, P. Pochart, H. Machineni, M. Welsh, Y. Kong, B. Zerhusen, R. Malcolm, Z. Varrone, A. Collis, M. Minto, S. Burgess, L. McDaniel, E. Stimpson, F. Spriggs, J. Williams, K. Neurath, N. Ioime, M. Agee, E. Voss, K. Furtak, R. Renzulli, N. Aanensen, S. Carrolla, E. Bickelhaupt, Y. Lazovatsky, A. DaSilva, J. Zhong, C.A. Stanyon, R.L. Finley Jr., K.P. White, M. Braverman, T. Jarvie, S. Gold, M. Leach, J. Knight, R.A. Shimkets, M.P. McKenna, J. Chant, J.M. Rothberg, A protein interaction map of Drosophila melanogaster, Science 302 (2003) 1727–1736.
[136] Y. Ho, A. Gruhler, A. Heilbut, G.D. Bader, L. Moore, S.L. Adams, A. Millar, P. Taylor, K. Bennett, K. Boutilier, L. Yang, C. Wolting, I. Donaldson, S. Schandorff, J. Shewnarane, M. Vo, J. Taggart, M. Goudreault, B. Muskat, C. Alfarano, D. Dewar, Z. Lin, K. Michalickova, A.R. Willems, H. Sassi, P.A. Nielsen, K.J. Rasmussen, J.R. Andersen, L.E. Johansen, L.H. Hansen, H. Jespersen, A. Podtelejnikov, E. Nielsen, J. Crawford, V. Poulsen, B.D. Sorensen, J. Matthiesen, R.C. Hendrickson, F. Gleeson, T. Pawson, M.F. Moran, D. Durocher, M. Mann, C.W. Hogue, D. Figeys, M. Tyers, Systematic identification of protein complexes in Saccharomyces cerevisiae by mass spectrometry, Nature 415 (2002) 180–183.
[137] T. Ito, K. Tashiro, S. Muta, R. Ozawa, T. Chiba, M. Nishizawa, K. Yamamoto, S. Kuhara, Y. Sakaki, Toward a protein-protein interaction map of the budding yeast: A comprehensive system to examine two-hybrid interactions in all possible combinations between the yeast proteins, Proc. Natl. Acad. Sci. U. S. A. 97 (2000) 1143–1147.
[138] N.J. Krogan, G. Cagney, H. Yu, G. Zhong, X. Guo, A. Ignatchenko, J. Li, S. Pu, N. Datta, A.P. Tikuisis, T. Punna, J.M. Peregrin-Alvarez, M. Shales, X. Zhang, M. Davey, M.D. Robinson, A. Paccanaro, J.E. Bray, A. Sheung, B. Beattie, D.P. Richards, V. Canadien, A. Lalev, F. Mena, P. Wong, A. Starostine, M.M. Canete, J. Vlasblom, S. Wu, C. Orsi, S.R. Collins, S. Chandran, R. Haw, J.J. Rilstone, K. Gandi, N.J. Thompson, G. Musso, P. St Onge, S. Ghanny, M.H. Lam, G. Butland, A.M. Altaf-Ul, S. Kanaya, A. Shilatifard, E. O'Shea, J.S. Weissman, C.J. Ingles, T.R. Hughes, J. Parkinson, M. Gerstein, S.J. Wodak, A. Emili, J.F. Greenblatt, Global landscape of protein complexes in the yeast Saccharomyces cerevisiae, Nature 440 (2006) 637–643.
[139] T. Dhalleine, N. Rouhier, J. Couturier, Putative roles of glutaredoxin-BolA holo-heterodimers in plants, Plant Signal. Behav. 9 (2014).
[140] H. Li, D.T. Mapolelo, S. Randeniya, M.K. Johnson, C.E. Outten, Human glutaredoxin 3 forms [2Fe–2S]-bridged complexes with human BolA2, Biochemistry 51 (2012) 1687–1696.
[141] H. Li, C.E. Outten, Monothiol CGFS glutaredoxins and BolA-like proteins: [2Fe–2S] binding partners in iron homeostasis, Biochemistry 51 (2012) 4377–4389.
[142] P. Willems, B.F. Wanschers, J. Esseling, R. Szklarczyk, U. Kudla, I. Duarte, M. Forkink, M. Nooteboom, H. Swarts, J. Gloerich, L. Nijtmans, W. Koopman, M.A. Huynen, BOLA1 is an aerobic protein that prevents mitochondrial morphology changes induced by glutathione depletion, Antioxid. Redox Signal. 18 (2013) 129–138.
[143] A. Izquierdo, C. Casas, U. Muhlenhoff, C.H. Lillig, E. Herrero, Saccharomyces cerevisiae Grx6 and Grx7 are monothiol glutaredoxins associated with the early secretory pathway, Eukaryot. Cell 7 (2008) 1415–1426.
[144] N. Mesecke, A. Spang, M. Deponte, J.M. Herrmann, A novel group of glutaredoxins in the cis-Golgi critical for oxidative stress resistance, Mol. Biol. Cell 19 (2008) 2673–2680.
[145] C. Berndt, G. Poschmann, K. Stuhler, A. Holmgren, L. Brautigam, Zebrafish heart development is regulated via glutaredoxin 2 dependent migration and survival of neural crest cells, Redox Biol. 2 (2014) 673–678.
[146] L. Brautigam, L.D. Jensen, G. Poschmann, S. Nystrom, S. Bannenberg, K. Dreij, K. Lepka, T. Prozorovski, S.J. Montano, O. Aktas, P. Uhlen, K. Stuhler, Y. Cao, A. Holmgren, C. Berndt, Glutaredoxin regulates vascular development by reversible glutathionylation of sirtuin 1, Proc. Natl. Acad. Sci. U. S. A. 110 (2013) 20057–20062.
[147] L. Brautigam, L.D. Schutte, J.R. Godoy, T. Prozorovski, M. Gellert, G. Hauptmann, A. Holmgren, C.H. Lillig, C. Berndt, Vertebrate-specific glutaredoxin is essential for brain development, Proc. Natl. Acad. Sci. U. S. A. 108 (2011) 20532–20537.
[148] C.H. Lillig, M.E. Lonn, M. Enoksson, A.P. Fernandes, A. Holmgren, Short interfering RNA-mediated silencing of glutaredoxin 2 increases the sensitivity of HeLa cells toward doxorubicin and phenylarsine oxide, Proc. Natl. Acad. Sci. U. S. A. 101 (2004) 13227–13232.
[149] H. Wu, L. Lin, F. Giblin, Y.S. Ho, M.F. Lou, Glutaredoxin 2 knockout increases sensitivity to oxidative stress in mouse lens epithelial cells, Free Radic. Biol. Med. 51 (2011) 2108–2117.
[150] C. Riondet, J.P. Desouris, J.G. Montoya, Y. Chartier, Y. Meyer, J.P. Reichheld, A dicotyledon-specific glutaredoxin GRXC1 family with dimer-dependent redox regulation is functionally redundant with GRXC2, Plant Cell Environ. 35 (2012) 360–373.
[151] G.R. Linares, W. Xing, K.E. Govoni, S.T. Chen, S. Mohan, Glutaredoxin 5 regulates osteoblast apoptosis by protecting against oxidative stress, Bone 44 (2009) 795–804.
[152] A.M. Sanchez-Riego, L. Lopez-Maury, F.J. Florencio, Glutaredoxins are essential for stress adaptation in the cyanobacterium Synechocystis sp. PCC 6803, Front. Plant Sci. 4 (2013) 428.
[153] N.H. Cheng, AtGRX4, an Arabidopsis chloroplastic monothiol glutaredoxin, is able to suppress yeast grx5 mutant phenotypes and respond to oxidative stress, FEBS Lett. 582 (2008) 848–854.
[154] H. Cha, J.M. Kim, J.G. Oh, M.H. Jeong, C.S. Park, J. Park, H.J. Jeong, B.K. Park, Y.H. Lee, D. Jeong, D.K. Yang, O.Y. Bernecker, H. Kim do, R.J. Hajjar, W.J. Park, PICOT is a critical regulator of cardiac hypertrophy and cardiomyocyte contractility, J. Mol. Cell. Cardiol. 45 (2008) 796–803.

Journal of Experimental Botany
doi:10.1093/jxb/erz213 Advance Access Publication 4 May 2019

REVIEW PAPER

Rhodanese domain-containing sulfurtransferases: multifaceted proteins involved in sulfur trafficking in plants

Benjamin Selles, Anna Moseler, Nicolas Rouhier and Jérémy Couturier*

Université de Lorraine, Inra, IAM, F-54000 Nancy, France

* Correspondence: jeremy.couturier@univ-lorraine.fr

Received 17 April 2019; Editorial decision 29 April 2019; Accepted 29 April 2019

Editor: Stanislav Kopriva, University of Cologne, Germany

Abstract

Sulfur is an essential element for the growth and development of plants, which synthesize cysteine and methionine from the reductive assimilation of sulfate. Besides its incorporation into proteins, cysteine is the building block for the biosynthesis of numerous sulfur-containing molecules and cofactors. The required sulfur atoms are extracted either directly from cysteine by cysteine desulfurases or indirectly after its catabolic transformation to 3-mercaptopyruvate, a substrate for sulfurtransferases (STRs). Both enzymes are transiently persulfidated in their reaction cycle, i.e. the abstracted sulfur atom is bound to a reactive cysteine residue in the form of a persulfide group. Trans-persulfidation reactions occur when sulfur atoms are transferred to nucleophilic acceptors such as glutathione, proteins, or small metabolites. STRs form a ubiquitous, multigenic protein family. They are characterized by the presence of at least one rhodanese homology domain (Rhd), which usually contains the catalytic, persulfidated cysteine. In this review, we focus on Arabidopsis STRs, presenting the sequence characteristics of all family members as well as their biochemical and structural features. The physiological functions of particular STRs in the biosynthesis of molybdenum cofactor, thio-modification of cytosolic tRNAs, arsenate tolerance, cysteine catabolism, and hydrogen sulfide formation are also discussed.

Keywords: Cysteine, hydrogen sulfide signaling, persulfide group, rhodanese, sulfur trafficking, sulfurtransferase.

Introduction

Unlike animals, which cannot assimilate inorganic sulfur and thus need to absorb cysteine or methionine, plants achieve the reductive assimilation of sulfate to synthesize cysteine, forming sulfite and sulfide as plastidial intermediates, and subsequently methionine and glutathione (GSH) (Takahashi *et al.*, 2011). Other key cellular components, such as vitamins (biotin, thiamine, lipoic acid), tRNAs containing thionucleosides, or cofactors such as iron–sulfur (Fe–S) clusters and molybdenum cofactor (Moco), contain sulfur atoms coming from various origins. In the case of vitamin or camalexin biosynthesis, sulfur is respectively provided by the degradation of Fe–S clusters (Lanz and Booker, 2015) or by a GSH molecule via the action of glutathione transferase (Su *et al.*, 2011). In the case of thionucleoside formation or Fe–S cluster and Moco synthesis, other sulfur sources are used (Mueller, 2006). For instance, the pyridoxal 5′-phosphate-dependent cysteine desulfurases (CDs) catalyse the desulfuration of cysteine (Zheng *et al.*, 1993), leading to the formation of a persulfide enzyme intermediate and the concomitant release of alanine (Behshad and Bollinger, 2009). The efficiency and specificity of sulfur transfer to acceptor molecules vary according to the subclass of CDs and the type of sulfur acceptors, the nature of which dictates the direction and flow of the sulfur transfer reaction. Whereas glutathione persulfide (GSSH) may represent a relatively stable

and specific transport form of sulfur atoms (Hildebrandt and Grieshaber, 2008; Ida *et al.*, 2014), carrier proteins ensure the specific transfer of sulfur to acceptors. This function is primarily achieved by sulfurtransferases (STRs; E.C.2.8.1.x). They possess one or several rhodanese (Rhd) domains usually including a reactive catalytic cysteine (Hatzfeld and Saito, 2000; Bordo and Bork, 2002; Cipollone *et al.*, 2007; Guretzki and Papenbrock, 2011). Hence, most STRs catalyse the transfer of a sulfur atom from donors to nucleophilic acceptors by forming intermediate protein persulfides on a reactive catalytic cysteine. When two polypeptides are involved, the transfer of persulfide groups is referred to as a trans-persulfidation reaction. Although STRs are ubiquitously distributed, they differ quite considerably in terms of primary sequences, protein domain architecture, and structure/length of the active site loop (Bordo and Bork, 2002). Nonetheless, three major groups can be differentiated (Bordo and Bork, 2002; Cipollone *et al.*, 2007; Bartels *et al.*, 2007). The first one comprises STRs formed by a single Rhd domain that include so-called CDC25 phosphatases and thiosulfate sulfurtransferases (TSTs; EC.2.8.1.1) according to their ability to use thiosulfate as a sulfur donor *in vitro*. The presence of an additional residue in the active-site loop of CDC25 phosphatases (seven residues compared with six in TSTs) constitutes an important difference involved in the capacity of CDC25 to dephosphorylate tyrosine residues (Bordo and Bork, 2002). The second major group is formed by STRs containing two Rhd domains but only the C-terminal one possesses the catalytic cysteine. They are present in most organisms. According to their ability to use 3-mercaptopyruvate (3-MP) as a substrate *in vitro*, they are referred to as 3-MP-STRs or mercaptopyruvate sulfurtransferases (MSTs; EC.2.8.1.2) (Nakamura *et al.*, 2000; Papenbrock and Schmidt, 2000; Colnaghi *et al.*, 2001; Yadav *et al.*, 2013). It is worth mentioning that bacteria and mammals possess additional STR isoforms with two Rhod domains (Bordo and Bork, 2002; Nambi *et al.*, 2015), such as the bovine rhodanese protein named Rhobov, which display TST activity (Blumenthal and Heinrikson, 1971). The mammalian rhodanese isoforms have a CRXGX[R/T] active site signature instead of the characteristic CG[S/T]GVT motif found in MSTs (Bordo and Bork, 2002; Cipollone *et al.*, 2007). In fact, interchanging the two residues following the catalytic cysteine of rat rhodanese and MST by site-directed mutagenesis was sufficient to change the activity profile from one to the other (Nagahara *et al.*, 1995; Nagahara and Nishino, 1996). Finally, the third main group is formed by STRs containing a Rhd domain possessing the catalytic cysteine fused to a domain having another function conferring them specific roles (Bordo and Bork, 2002; Cipollone *et al.*, 2007).

The recent comparative analysis of 25 genomes of photosynthetic organisms has provided a detailed classification and information about evolutionary features of STRs pointing to the expansion of this family in higher plants. Hence, in photosynthetic organisms, the STR family comprises 5–35 genes, and was divided into nine clusters according to the STR primary sequences and domain arrangements (Moseler *et al.*, 2019). Plant STR isoforms of clusters I (MSTs), VII (multidomain STRs), VIII (TSTs) and IX (TSTs) possess orthologs in most organisms whereas other clusters are specific (clusters III and V) or contain an increased number of representatives in plants (clusters II, IV and VI). In the context of this review on the involvement of plant STRs in sulfur transfer reactions, those that belong to cluster II and do not possess the conserved catalytic cysteine in the Rhd domain will not be described in detail. Hence, we discuss the recent genetic, biochemical, structural, and molecular studies that have contributed to improving our understanding of the physiological roles of STRs in plants. After illustrating the diversity of plant STRs in terms of primary sequences, protein domain architecture, subcellular localization and gene expression using Arabidopsis isoforms as representatives, we focus our attention on the documented roles of STRs in molybdopterin synthesis, thionucleoside modification, arsenate tolerance, cysteine catabolism, and the biosynthesis of hydrogen sulfide (H_2S), a signaling molecule promoting protein persulfidation.

Diversity of plant STR isoforms: focus on Arabidopsis

The Arabidopsis nuclear genome was initially reported to encode 20 STR sequences (Papenbrock *et al.*, 2011). However, a recent careful analysis led us to include an additional protein containing a Rhd domain, which was numbered consecutively as AtSTR19 (At3g59780), even though it does not have the conserved cysteine residue (Moseler *et al.*, 2019).

Domain organization, expression, and subcellular localization

According to the variability observed among STRs in terms of primary sequence and domain organization (including potential transmembrane spans), the Arabidopsis STR equipment forms nine different clusters (Table 1; Moseler *et al.*, 2019). STRs composed of two Rhd domains form the first group comprising so-called MSTs, i.e. STR1 and STR2, which are 379 and 342 residues long, respectively (Table 1). STR3 (387 residues), STR4 (466 residues), STR4a (264 residues), and STR19 (686 residues) form cluster II as they contain a single Rhd domain associated with one, two, one, and three predicted transmembrane regions, respectively (Table 1). Note that STR3, STR4, and STR19 are considered as inactive STRs because the catalytic cysteine is replaced by an aspartate. Cluster III contains the sole STR5 isoform. It possesses a single Rhd domain exhibiting the catalytic cysteine but in a quite divergent HCALSQVR signature typical of the general HCX_5R signature of CDC25 phosphatases. STR6, STR7, and STR8 belong to cluster IV. They have also a single Rhd domain with a strictly conserved CTGGIR signature, but they are elongated (581, 474, and 448 residues respectively) on both sides of the Rhd domain. The next group (cluster V) comprises STR9, STR10, and STR11 isoforms (214–292 residues) corresponding to proteins with a single Rhd domain exhibiting a catalytic cysteine and a predicted C-terminal transmembrane segment (Table 1). STR12 (299 residues) and STR13 (464 residues) form two additional groups (clusters VI and VII), having

Table 1. *Subcellular localization and domain organization of the STR/rhodanese family members from Arabidopsis*

Name (accession no.)	Cluster	Length (aa)	Active site motif	Domain arrangement	Subcellular localization
STR1 (At1g79230)	I	379	**C**GTGVT		**Mitochondrion** GFP fusion (Hatzfeld and Saito, 2000; Nakamura *et al.*, 2000; Bauer *et al.*, 2004) and immunoblot analysis (Nakamura *et al.*, 2000; Bauer *et al.*, 2004)
STR2 (At1g16460)	I	342	**C**GTGVT		**Cytosol** GFP fusion (Hatzfeld and Saito, 2000; Nakamura *et al.*, 2000; Bauer *et al.*, 2004) and immunoblot analysis (Nakamura *et al.*, 2000; Bauer *et al.*, 2004)
STR3 (At5g23060)	II	387	DSYTDS		**Chloroplast (thylakoid membrane)** GFP/YFP fusion (Weinl *et al.*, 2008; Nomura *et al.*, 2008; Vainonen *et al.*, 2008), immunoblot analysis (Weinl *et al.*, 2008; Vainonen *et al.*, 2008) and proteomics (Peltier *et al.*, 2004)
STR4/TROL (At4g01050)	II	466	DKFDGN		**Chloroplast (inner membrane envelope and thylakoid)** YFP fusion (Jurić *et al.*, 2009) and proteomics (Friso *et al.*, 2004; Peltier *et al.*, 2004)
STR4a (At3g25480)	II	264	**C**VLDNF		**Chloroplast (thylakoid)** Proteomics (Peltier *et al.*, 2004; Tomizioli *et al.*, 2014)
STR5/ CDC25/ACR2 (At5g03455)	III	146	**C**ALSQVR		**Mitochondrion** GFP fusion (Narsai *et al.*, 2011)
STR6 (At1g09280)	IV	581	**C**TGGIR	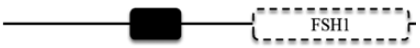	Unknown
STR7 (At2g40760)	IV	474	**C**TGGIR		Unknown
STR8 (At1g17850)	IV	448	**C**TGGIR		**Chloroplast (thylakoid membrane)** Proteomics (Tomizioli *et al.*, 2014)
STR9 (At2g42220)	V	234	**C**QEGLR		**Chloroplast (thylakoid membrane)** Proteomics (Tomizioli *et al.*, 2014)
STR10 (At3g08920)	V	214	**C**GEGLR		**Mitochondrion** GFP fusion (Bartels, 2006)
STR11 (At4g24750)	V	292	**C**QKGLR		**Chloroplast (thylakoid membrane)** GFP fusion (Bartels, 2006) and proteomics (Tomizioli *et al.*, 2014)
STR12 (At5g19370)	VI	299	**C**KVGGR		**Chloroplast (stroma)** Proteomics (Tomizioli *et al.*, 2014)
STR13/CNX5 (At5g55130)	VII	464	**C**RRGND	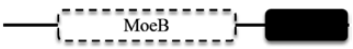	**Cytosol** Bimolecular fluorescence complementation (Kaufholdt *et al.*, 2013)
STR14 (At4g27700)	VIII	224	**C**SSAGT		**Chloroplast (envelope, thylakoid)** GFP fusion (Bauer *et al.*, 2004)
STR15/Sen1 (At4g35770)	IX	182	**C**ESGQM	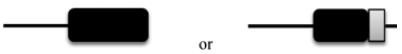	**Chloroplast (thylakoid membrane)** GFP fusion (Bauer *et al.*, 2004) and electronic microscopy (Bauer *et al.*, 2004)
STR16 (At5g66040)	IX	120	**C**QSGGR		**Chloroplast** GFP fusion (Bauer *et al.*, 2004)
STR17 (At2g17850)	IX	156	**C**KSGVR		Unknown
STR17a/ ARQ1/HAC1 (At2g21045)	IX	169	**C**NAGGR		**Cytosol/nucleus** GFP fusion (Sánchez-Bermejo *et al.*, 2014)
STR18 (At5g66170)	IX	136	**C**QSGAR		**Cytosol** GFP fusion (Bauer *et al.*, 2004)
STR19 (At3g59780)	II	686	DADGTR		**Chloroplast** Proteomics (Peltier *et al.*, 2004; Tomizioli *et al.*, 2014)

The catalytic cysteine is indicated in bold. Domain prediction is based on Pfam (http://pfam.xfam.org/) and Interpro (http://www.ebi.ac.uk/interpro/). FSH1, serine hydrolase; MoeB, molybdopterin biosynthesis; Rota, rotamase.

an N-terminal rotamase and MoeB domain, respectively, in addition to the active Rhd domain (Table 1). Cluster VIII contains only AtSTR14 because the Rhd domain has a specific CSSAGT signature and it displays a short N-terminal extension forming a protein of 224 residues. Finally, cluster IX comprises STR15–STR18. They are all short STR versions of less than 182 amino acids, the difference residing in the active site signature and in the presence of N-terminal targeting sequences, but none has additional recognizable domains, except a predicted C-terminal transmembrane segment in STR15 likely promoting its localization to thylakoids (Bauer *et al.*, 2004).

As an additional criterion to understand the diversity and evolution of the STR family in plants, the gene expression pattern and protein subcellular localization of Arabidopsis STRs was analysed. A recent, high resolution developmental transcript profile was analysed (Winter *et al.*, 2007; Klepikova *et al.*, 2016) and selected tissues and stages were represented as a heat map (Fig. 1). Three main clusters are distinguished. A first cluster regroups *STR2*, *STR5*, *STR15*, and *STR16* representatives. They are mostly expressed in leaves and hypocotyl/stems (Fig. 1). *STRs* present in the second cluster (*STR3*, *STR4*, *STR4a*, *STR7*, *STR8*, *STR9*, *STR10*, *STR11*, *STR12*, and *STR14*) have in common a higher expression level in cotyledons, mature leaves (8–12) and vegetative rosette before or after the transition to flowering (Fig. 1). Two sub-clusters can be distinguished mainly based on their differential expression in seeds. Consistently, all STRs that have been demonstrated or predicted as targeted to the chloroplasts/plastids (Bauer *et al.*, 2004; Friso *et al.*, 2004; Peltier *et al.*, 2004; Bartels, 2006; Nomura *et al.*, 2008; Vainonen *et al.*, 2008; Weinl *et al.*, 2008; Jurić *et al.*, 2009; Tomizioli *et al.*, 2014) are encoded by genes present in these two clusters (Table 1; Fig. 1). With regards to genes present in the third cluster (*STR1*, *STR6*, *STR13*, *STR17*, *STR17a*, and *STR18*), their expression does not vary much among organs but they have in common a highest transcript level in dry and imbibed seeds and in roots. Note that AtSTR17a is specifically more expressed in roots. The proteins encoded by these genes are expressed in the cytosol (STR13, STR17a, and STR18) (Bauer *et al.*, 2004), in mitochondria (STR1) (Hatzfeld and Saito, 2000; Nakamura *et al.*, 2000; Bauer *et al.*, 2004), or have unknown localizations (STR6 and STR17) having no typical targeting sequences. These diverse subcellular localizations and gene expression patterns are understandable considering the existence of numerous sulfur-containing compounds in the different subcellular compartments of plant cells and thus the need of specific systems to mobilize and transfer sulfur for their biosynthesis or modification.

Biochemical and structural properties

Despite the described diversity of STR primary sequences, the fold adopted by the Rhd domain consists of a $\beta_1\alpha_1\beta_2\alpha_2\beta_3\alpha_3\beta_4\alpha_4\beta_5\alpha_5$ topology organizing into a

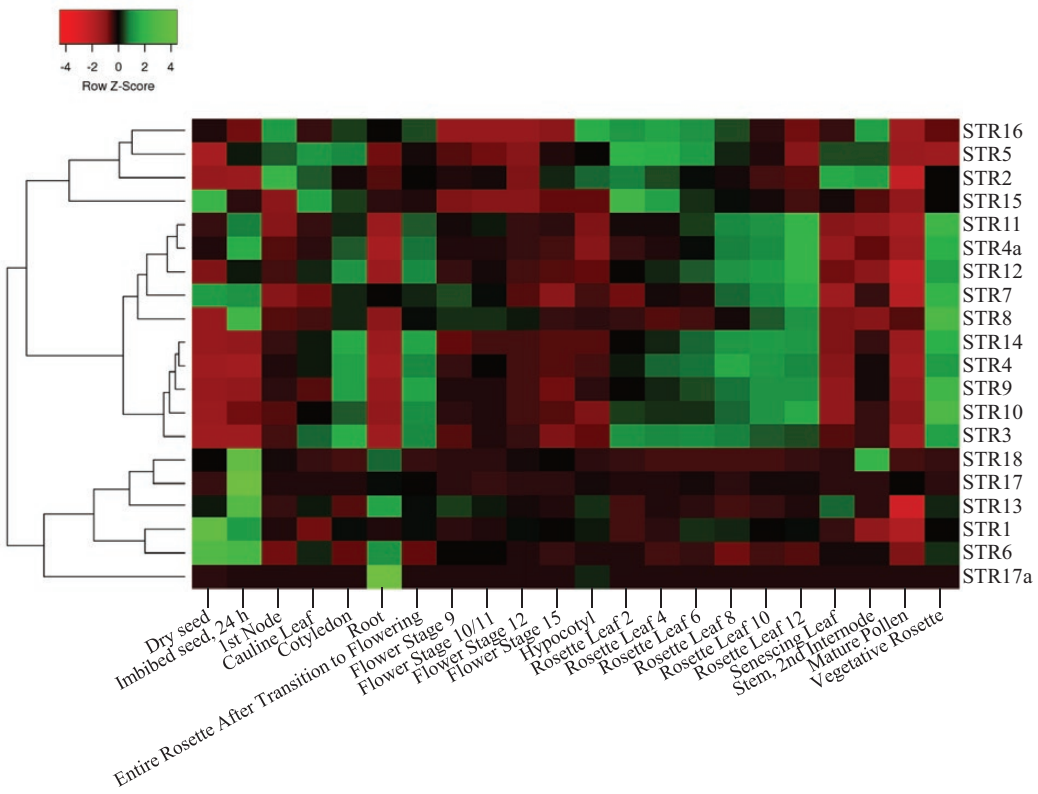

Fig. 1. Heatmap representation of STR transcript profiles at selected developmental stages and tissues of Arabidopsis. Gene expression data for each Arabidopsis STR were retrieved from the 'Developmental Map' tab of the Arabidopsis eFP Browser database (http://bar.utoronto.ca/efp/cgi-bin/efpWeb.cgi) (Winter *et al.*, 2007; Klepikova *et al.*, 2016). No data were available for STR19. Numerical data were extracted and represented as a heatmap using the expression tool of Heatmapper software (http://www2.heatmapper.ca/expression/) (Babicki *et al.*, 2016). The parameters applied are score representation by row, clustering method by average linkage, and Pearson distance measurement.

well-conserved central β-sheet composed of five strands surrounded by four to five α-helices (Ploegman *et al.*, 1978). Up to now, three-dimensional structures have been solved for AtSTR5/CDC25, AtSTR16, and the inactive Rhd domain of AtSTR4/TROL (Landrieu *et al.*, 2004*a*; Pantoja-Uceda *et al.*, 2005; Cornilescu *et al.*, 2006). A structure-based amino acid alignment of Arabidopsis STRs possessing the catalytic cysteine, using AtSTR16 NMR structure (PDB 1TQ1) as a template, indicates that only a few residues are strictly conserved (Fig. 2A). In the N-terminal part of the Rhd domain, a three residue motif, D^{28}[V/A]$^{29}R^{30}$ (AtSTR16 numbering unless otherwise indicated), is highly conserved in Arabidopsis paralogs (Fig. 2A). It is also conserved in representatives of the STR5/CDC25 family and more generally in the Rhd domains of all plant STRs (Moseler *et al.*, 2019). The residues are located at the end of β2 (Fig. 2B) and were proposed to participate in AtSTR16 stability (Cornilescu *et al.*, 2006). The catalytic cysteine (Cys^{80}) is strictly conserved and is present in the loop between β_4 and α_4 secondary structures and forms with the five or six (in the case of CDC25) following amino acids the so-called active site loop of Rhd domain (Figs 2B, 3). The residues forming the active site are quite variable.

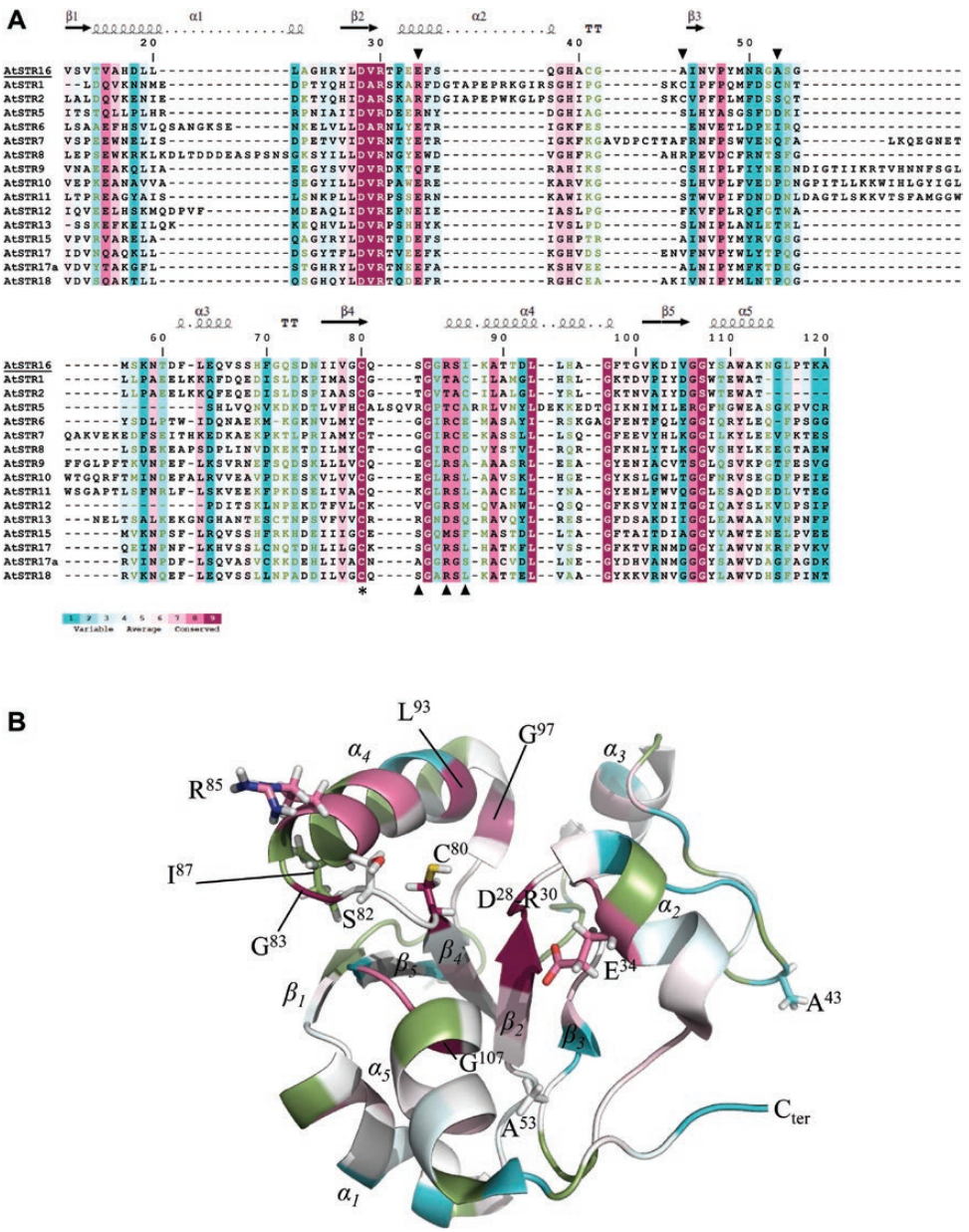

Fig. 2. Structure-based sequence alignment of Rhd domains of Arabidopsis STR isoforms. The sequences corresponding to the Rhd domain of Arabidopsis STRs possessing a cysteine residue were aligned with MUSCLE (https://www.ebi.ac.uk/Tools/msa/muscle/). Colored alignment (A) and the corresponding structure representing the structural conservation level at each amino acid position (B) were generated by CONSURF (http://consurf.tau.ac.il/2016/) using the PDB file of the AtSTR16 NMR structure (PDB 1TQ1). The sequence numbering and secondary structures correspond to AtSTR16. In (A) the catalytic cysteine residue is marked by an asterisk and amino acids studied by mutagenesis indicated by triangles. In (B) the residues studied by mutagenesis in various selected STR representatives are shown with their lateral chains as stick and labeled. The most conserved structural positions (D^{28}[V/A]$^{29}R^{30}$, C^{80}, G^{82}, L^{93}, G^{97}, and G^{107}) are also labeled whereas green parts correspond to regions with insufficient data to represent a conservation.

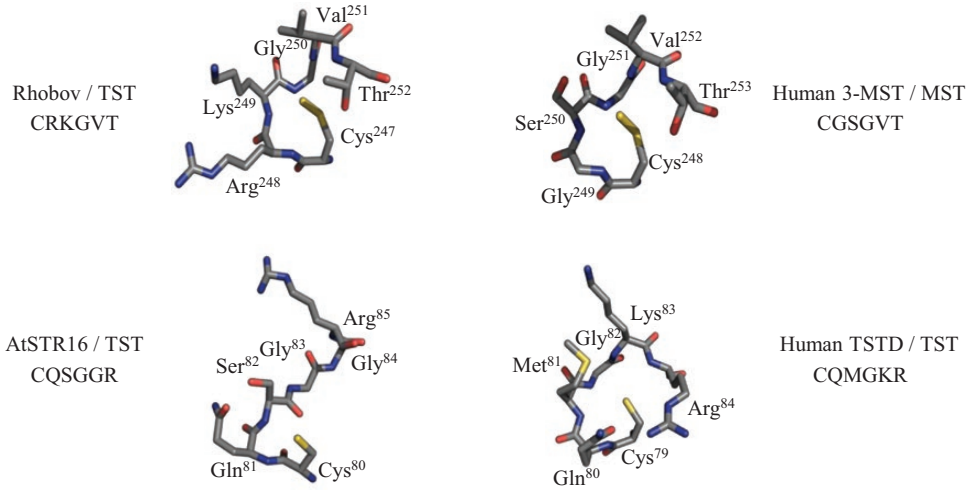

Fig. 3. Structural comparison of the active site loops of TST-type and MST-type STRs. The representation of the six amino acids forming the so-called active site loop from bovine Rhobov (PDB 1RHD), human 3-MST (PDB 4JGT), Arabidopsis STR16 (PDB 1TQ1), and human TSTD (PDB 6BEV) was generated using PyMOL.

A characteristic signature was defined for MSTs (CGSGVT) and TSTs (CRKGVT) and it is likely that this relates at least in part to electrostatic differences of their substrates, as exemplified by 3-MP and thiosulfate, respectively (Bordo and Bork, 2002). At positions +1 and +2 after the catalytic cysteine, bulky and charged residues (Arg/Lys) are found in TSTs whereas smaller and uncharged residues (Gly/Ser) are present in MSTs (Fig. 3). The Gly residue usually at position +3 of the catalytic cysteine and the Leu residue at position 93 (Fig. 2A) are conserved in all Arabidopsis STRs even though the AtSTR5 signature containing the catalytic cysteine does not align at all. Two other Gly residues at positions 97 and 107 are present in all plant STR isoforms except in STR1/2 orthologs in which Gly^{107} is replaced by a serine. These three Gly residues are located just before and at the end of α4, and at the initiation of α5, respectively (Fig. 2B). Despite the high conservation of these four residues (Gly^{83}, Leu^{93}, Gly^{97}, Gly^{107}), their roles in STR structure/function are unknown. On the contrary, the importance of other residues was investigated more deeply using both plant and non-plant STRs (Table 2). Hence, besides the mandatory catalytic cysteine (Cys^{80} in Fig. 2), other residues are important for the catalytic activity of the Rhd domain. For example, the change of the cysteine residue close to the active site in AtSTR1 (Cys^{339}, position 87) to a valine residue led to a 4-fold decrease of the TST activity whereas the MST activity was slightly reduced (Burow *et al.*, 2002). However, although highly conserved in MSTs from terrestrial plants, this cysteine is not present in other STRs. For instance, it corresponds to Ile^{87} of AtSTR16, a position presenting a weak conservation score (Fig. 2A). Substitutions of the two other Cys residues, Cys^{294} to Asn and Cys^{304} to Asp, found in the active C-terminal Rhd domain of AtSTR1 had minor effects with a slight decrease of both K_m and k_{cat} towards thiosulfate (Burow *et al.*, 2002). According to the alignment, the corresponding amino acids in AtSTR16 (positions 43 and 53) are found respectively in the α2–β3 and β3–α3 loops and exhibit a low conservation score (Fig. 2B).

As the biochemical data concerning plant STRs are relatively scarce, we consider here mutagenesis studies conducted on non-plant STR orthologs such as bovine rhodanese (Rhobov), the *Escherichia coli* MST ortholog SseA, the *Azotobacter vinelandii* RhdA protein and the Rhd domain of human MOCS3 to identify other residues potentially important for the structure and activity of plant STRs (Table 2). Structural analysis of human MST and biochemical characterization of *E. coli* SseA indicated that two arginine residues, Arg^{178} and Arg^{187} (position 34 and insertion between positions 36 and 37, respectively), play a role in substrate recognition, being involved in the proper positioning of the substrate relative to the catalytic Cys^{237} (Figs 2A, 3) (Yadav *et al.*, 2013; Lec *et al.*, 2018). Hence in EcSseA, the change of Arg^{178} to Leu leads to a decrease of protein affinity towards 3-MP (Lec *et al.*, 2018). Both AtSTR1 and AtSTR2 (and AtSTR5) possess this Arg residue whereas most other STRs possess a Glu residue (Fig. 2A). On the contrary, Arg^{187} is only present in AtSTR1 and is located into an insertion sequence specific to MST orthologs (Fig. 2). Interestingly, the mutation of Arg^{187}, which is part of the hydrophobic pocket of the active site (Ploegman *et al.*, 1978), into a Leu in bovine Rhobov, a TST-type STR, leads to a 20-fold decrease of affinity towards thiosulfate (K_m shifted from 3.7 to 73.2 mM in the R187L variant) (Luo and Horowitz, 1994). Hence, this residue may also be important for thiosulfate accommodation in the active site.

It is expected that other residues found in the active site loops of MST, TST, or CDC25 generate the necessary selectivity of these proteins towards their respective substrates (Bordo and Bork, 2002; Cipollone *et al.*, 2007; Lec *et al.*, 2018; Libiad *et al.*, 2018). Thus, apart from the Arg residues described above, the importance of the residues present at positions +2 and +5 of the catalytic Cys in regular STRs was investigated.

For MST-type STR proteins, studies performed using EcSseA, human and *Leishmania major* MST variants initially suggested that the +2 residue (Ser^{82} in Figs 2A, 3) is involved in the deprotonation of 3-MP and in the stabilization of the pyruvate enolate (Colnaghi *et al.*, 2001; Alphey *et al.*, 2003; Huang

Table 2. *Mutagenesis studies performed using STR isoforms*

Protein name	Uniprot Ref	Type	Position in the original sequence	Corresponding position in AtSTR16	Substitution	Catalytic effect	Reference
Rhobov	P00586	TST	187	34	R→L	Decreased reactivity towards thiosulfate	Luo and Horowitz (1994)
SseA	P31142	MST	178	34	R→L	Decreased reactivity towards 3-MP	Lec *et al.* (2018)
STR1	O64530	MST	294	43	C→N	Slightly reduced TST activity, no impact on MST activity	Burow *et al.* (2002)
STR1	O64530	MST	304	53	C→E	Slightly reduced TST activity, no impact on MST activity	Burow *et al.* (2002)
STR1	O64530	MST	333	**80**	C→S	Abolished TST and MST activities	Burow *et al.* (2002)
MOCS3	O95396	—	412	**80**	C→A	Abolished STR activity	Matthies *et al.* (2004)
RhdA	P52197	TST	232	82	T→K	Increased TST activity	Pagani *et al.* (2000)
RhdA	P52198	TST	232	82	T→A	Increased TST activity	Pagani *et al.* (2000)
Rhobov	P00586	TST	250	82	K→A	Abolished TST activity	Luo and Horowitz (1994)
SseA	P31142	MST	239	82	S→A	Decreased affinity for 3-MP; abolished thiosulfate binding	Colnaghi *et al.* (2001), Lec *et al.* (2018)
SseA	P31142	MST	239	82	S→K	Decreased MST activity; increased affinity for thiosulfate	Colnaghi *et al.* (2001)
MOCS3	O95396	—	417	85	D→R	470-fold increased activity	Krepinsky and Leimkühler (2007)
MOCS3	O95396	—	417	85	D→T	90-fold increased activity	Krepinsky and Leimkühler (2007)
STR1	O64530	MST	339	87	C→V	4-fold decreased TST activity; slightly reduced MST activity	Burow *et al.* (2002)

Summary table describing the catalytic effects of STR residue mutations. The nature and position of the mutations are indicated as well as the corresponding AtSTR16 numbering used in Fig. 2. The catalytic cysteine is indicated in bold.

and Yu, 2016). However, another study, focusing on catalytic cysteine persulfide formation and regeneration by thioredoxin (TRX) of EcSseA and human MST, reported different results. In this work, it was found that the step of sulfur transfer between 3-MP and the thiol group of the catalytic cysteine, and the protonation state of 3-MP at various pH values is not affected in the corresponding S239A variant (Lec *et al.*, 2018). These contradictory results raise questions about the importance of the residue found at the +2 position within the active site loop of MST-type STRs.

Regarding TST-type proteins, the residue at this position is important for their activity but again effects in protein variants are variable and sometimes opposite. The change of Lys^{250} to Ala in bovine Rhobov abolishes its activity towards thiosulfate whereas it does not affect activity towards more complex substrates such as thiosulfonate (Table 2; Luo and Horowitz, 1994), pointing to substrate-dependent effects. A mutational analysis was also performed using *A. vinelandii* RhdA, an atypical enzyme that uses only thiosulfate as a sulfur donor *in vitro*. Contrary to expectation, the change of Thr^{232} to Lys or Ala leads in fact to an increase of TST activity (Pagani *et al.*, 2000).

Finally, the importance of the residue at position +5 (Arg^{85} in Fig. 2) for protein activity was also investigated. Most STRs have an Arg or sometimes a Thr but AtSTR13 and human MOCS3 have an Asp, which makes a considerable difference. In human MOCS3, the change of this Asp^{417} to an Arg or a Thr results in a strong increase of protein activity towards thiosulfate (Table 2; Krepinsky and Leimkühler, 2007). Hence, the fact that AtSTR13 and MOCS3 possess an N-terminal MoeB domain required for Moco synthesis and thus have particular substrates/partners may explain why the basic residue usually found at this position and which seems important for the protein activity with thiosulfate has been replaced by an acidic residue.

Dual functions of STR13 in the delivery of sulfur atoms

Implication in Moco synthesis

Moco consists of a molybdenum atom covalently bound to two sulfur atoms of a tricyclic pterin moiety referred to

as molybdopterin (MPT). Moco is found at the active site of molybdenum enzymes. In plants, the Moco-dependent enzymes nitrate reductase (NR), aldehyde oxidase (AO), xanthine dehydrogenase (XDH), and sulfite oxidase (SO) function respectively in nitrogen assimilation, abscisic acid synthesis, purine catabolism, and sulfite detoxification (Schwarz and Mendel, 2006). Moco biosynthesis is therefore crucial and is now well understood (Fig. 4A). The first step, consisting of the condensation of GTP into cyclic pyranopterin monophosphate (cPMP), is catalysed by the Fe–S protein CNX2 and by CNX3 and takes place in the mitochondrial matrix. cPMP is then exported to the cytosol. Initially it was suggested that the ABC transporter ATM3 transports cPMP, as the corresponding mutants show a strong phenotype for Moco-containing proteins such as NR (Bernard *et al.*, 2009; Teschner *et al.*, 2010). Nevertheless, it was shown that *atm3* mutants contain a lower content of cPMP but a more oxidized mitochondrial matrix, suggesting that the role of ATM3 in the Moco biosynthesis pathway may be indirect (Kruse *et al.*, 2018). In the cytosol, two sulfur atoms are inserted into cPMP by the concerted action of CNX5, CNX6, and CNX7, resulting in the formation of MPT (Kaufholdt *et al.*, 2013). Thereafter, CNX1 inserts the molybdenum atom, which is coordinated by a dithiolene group, leading to the formation of Moco (Fig. 4A). Finally, additional modifications occur before the final insertion of Moco into apoproteins. In NR and SO, a sulfur atom of a conserved protein cysteine residue covalently binds the Mo atom. On the contrary in XDH and AO, the Moco sulfuration is independent of protein cysteine residues and depends on the activity of the cytosolic cysteine desulfurase ABA3 (Bittner *et al.*, 2001). This CD is relatively atypical as it consists of two domains, an N-terminal CD domain that transfers the sulfur atom to a Moco bound to the C-terminal domain, prior to the transfer and insertion of this sulfurated Moco into AO and XDH (Wollers *et al.*, 2008). A functional characterization demonstrated that an Arabidopsis *cnx5/str13* mutant containing a change of the conserved Ser^{149} residue to Phe accumulates high levels of cPMP, whereas *cnx5* null mutants have a strong growth defect and are sterile (Nakai *et al.*, 2012; Kruse *et al.*, 2018). STR13, also named CNX5/MOCS3, has the particularity of containing a MoeB-like domain necessary for MPT biosynthesis in the N-terminal region associated to a Rhd domain with a CRRGND active site motif. *In vitro* assays performed with the human ortholog, MOCS3, revealed that the persulfidated Rhd domain of MOCS3 is able to provide sulfur to MOCS2A, the human ortholog of CNX7, enabling the synthesis of MPT (Matthies *et al.*, 2004). Moreover, mutating the catalytic cysteine of the Rhd domain prevents the formation of MPT revealing the importance of this residue for STR13/CNX5/MOCS3 function (Matthies *et al.*, 2004).

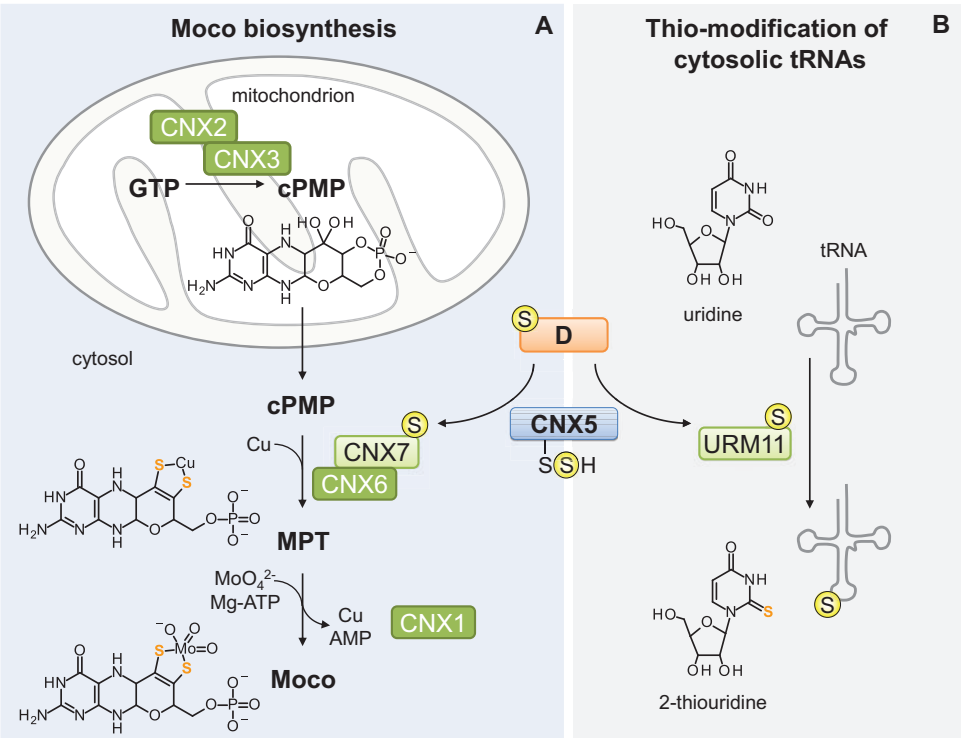

Fig. 4. Role of STR13/CNX5 in molybdenum cofactor biosynthesis and thio-modification of cytosolic tRNAs. (A) Simplified representation of molybdenum cofactor (Moco) biosynthesis in Arabidopsis modified from Kaufholdt *et al.* (2013). The biosynthesis of Moco starts in the mitochondrial matrix where guanosine-5′-triphosphate (GTP) is converted to cyclic pyranopterin monophosphate (cPMP) by CNX2 (cofactor for nitrate reductase and xanthine dehydrogenase 2) and CNX3. The cPMP is then exported to the cytosol and a heteromeric complex, consisting of CNX6 and CNX7, inserts two sulfur atoms into cPMP and converts it to molybdopterin (MPT). CNX7 receives the sulfur atoms from STR13/CNX5 but the primary sulfur donor of CNX5 (X-S) is yet unknown. During the last step, one molybdenum atom is inserted via the activity of CNX1, finally leading to the mature Moco. (B) Synthesis of thiolated nucleoside in tRNAs. STR13/CNX5 provides sulfur to its partner, URM11 (ubiquitin-related modifier 11) and possibly URM12 (not represented), which is essential for the thio-modification (such as s^2U34) of cytosolic tRNAs (Nakai *et al.*, 2012).

Implication in thio-modification of tRNAs

In addition to its role in Moco biosynthesis, STR13 is also involved in the thio-modification of cytosolic tRNAs (Fig. 4B; Nakai *et al.*, 2012). The thio-modification of tRNAs is one out of *ca* a hundred possible post-transcriptional modifications that can influence tRNA folding or stability that would consequently affect translation and ultimately growth (Phizicky and Hopper, 2010). The 2-thiouridine s^2U corresponds to the 2-thio modification that is universally found at U_{34} of tRNA species. In yeast and higher eukaryotes, U_{34} in $tRNA^{Lys}$ (anticodon UUU), $tRNA^{Gln}$ (anticodon UUG) and $tRNA^{Glu}$ (anticodon UUC) are modified and sulfurated to form 5-methyl-2-thiouridine derivatives (xm^5s^2U), the most important being the 5-methoxycarbonylmethyl-2-thiouridine (mcm^5s^2U) modification in eukaryotic cytosolic tRNAs (Ranjan and Rodnina, 2017). In eukaryotes, the biosynthesis of s^2U in cytosolic tRNAs involves a protein thiocarboxylate as intermediate sulfur donor that is functionally and evolutionarily related to the ubiquitin-like post-translational modification system as demonstrated notably in yeast (Nakai *et al.*, 2008). Hence, in yeast, both Urm1 and the yeast STR13 ortholog Uba4 are involved in the thio-modification of cytosolic tRNAs. Consistently, cytosolic tRNAs from *Δurm1* and *Δuba4* cells are not thiolated (Leidel *et al.*, 2009). Arabidopsis STR13/CNX5 can fully complement the yeast *Δuba4* mutant. Both *cnx5-1* and *cnx5-2* mutants exhibit a dwarf phenotype with slightly green and morphologically aberrant leaves and in addition, the thio-modification of cytosolic tRNAs is impaired (Nakai *et al.*, 2012). Interestingly, Arabidopsis possesses two orthologs of ScUrm1, URM11 and URM12, both of them capable of complementing the yeast *Δurm1* mutant (Nakai *et al.*, 2012). As URM11 is the predominantly expressed isoform, it was suggested that this protein is primarily responsible for the thio-modification of cytosolic tRNAs. Nevertheless, an Arabidopsis *urm11-1* null mutant did not exhibit any visible phenotypic changes, although the mutant lacked thio-modified cytosolic tRNAs. Hence, the strong/lethal phenotype observed for *str13/cnx5* mutants should be related to a defect in Moco biosynthesis, not in cytosolic tRNA modifications (Nakai *et al.*, 2012). Altogether, these data reveal that STR13 represents an essential link between these two sulfur-dependent biosynthetic pathways but its sulfur donor is yet unidentified (Fig. 4). In human cells, a cytosolic form of the cysteine desulfurase NFS1 is proposed to provide sulfur to the MOCS3 ortholog (Marelja *et al.*, 2008, 2013). In plants, the sole CD isoform in the cytosol is ABA3. However, *aba3* mutants (*aba3-1*, *aba3-2*, *los5-1*, *los5-2*) have less severe phenotypes (Xiong *et al.*, 2001; Zhong *et al.*, 2010) than *cnx5/str13* mutants indicating that it should not provide sulfur to STR13, leaving the question of the sulfur source open.

Roles of STR5 and STR17a in arsenate tolerance

The presence of inorganic arsenic in soils and fresh water is a widely recognized problem. Some plant species, such as the ferns *Pteris vittata* and *Pityrogamma calomelanos*, are known to accumulate arsenic, and thus represent good candidates for arsenic phytoremediation approaches (Peer *et al.*, 2006). Meanwhile, arsenic accumulation in crops is a challenging issue and particularly in rice, which is the staple diet for more than half of the world's population (Williams *et al.*, 2006). Hence, the investigation of how plants cope with this useless metal is a decisive research area and recent advances have been made in Arabidopsis, implicating two STR isoforms, AtSTR5 and AtSTR17a.

According to the involvement of dual-specificity CDC25 phosphatases in cell cycle regulation, AtSTR5 exhibits phosphatase activity *in vitro* and enhances cyclin-dependent serine/threonine kinase activity of purified CDK complexes via tyrosine dephosphorylation (Landrieu *et al.*, 2004*a*,b). Also, the heterologous expression of *AtSTR5* in fission yeast reduces the size of mitotic cells and Arabidopsis *str5* mutants are hypersensitive to a replication blocking agent (Sorrell *et al.*, 2005; Spadafora *et al.*, 2011). In parallel, other studies have suggested the involvement of AtSTR5 in arsenate reduction. Interestingly, both tyrosine phosphatase and arsenate reductase activities depend on the presence of the catalytic cysteine present in the active site motif (HCX_5R) of the Rhd domain (Landrieu *et al.*, 2004*a*). Plant *STR5* genes complement the arsenate-sensitive phenotype of the *E. coli arsC* and yeast *acr2* mutants and recombinant proteins display arsenate reductase activity *in vitro* (Dhankher *et al.*, 2006; Ellis *et al.*, 2006). Accordingly, Arabidopsis *STR5* down-regulated lines are sensitive to arsenate treatments and present a hyperaccumulation of arsenic when they are cultured *in vitro* for 3 weeks (Dhankher *et al.*, 2006). Moreover, a 2-fold higher arsenate reductase activity was observed in *AtSTR5*-overexpressing lines in comparison with wild-type plants (Dissmeyer *et al.*, 2009). Puzzlingly, in another study the content of arsenic species was not modified in both Arabidopsis *STR5* knockout or overexpression lines exposed to arsenate for 0.5, 2, 6 or 24 h as compared with wild-type plants (Liu *et al.*, 2012). Another piece of positive evidence is, however, that transgenic tobacco plants expressing *AtSTR5* are more tolerant to arsenic than wild-type plants (Nahar *et al.*, 2017). The subcellular localization of AtSTR5 is also subject to some uncertainty. An experiment using the first 100 amino acids of AtSTR5 fused to green fluorescent protein (GFP) demonstrated a mitochondrial localization (Narsai *et al.*, 2011). This might correlate with the N-terminal truncation at the position of the Ser^{20} reported in an N-terminal proteome study performed with Arabidopsis seedlings (Venne *et al.*, 2015). Nonetheless, this mitochondrial localization of AtSTR5 would not be compatible with its described function in cell cycle regulation, which would require a nuclear localization. More experimental evidence is required here to validate whether AtSTR5 is indeed expressed in multiple subcellular compartments.

The involvement of AtSTR17a in arsenate resistance/accumulation has been independently identified by two groups performing genome-wide association studies focusing either on root growth recovery after arsenate exposure in a collection of 82 Arabidopsis accessions (Sánchez-Bermejo *et al.*, 2014) or on arsenate accumulation in leaves of 349 Arabidopsis accessions (Chao *et al.*, 2014). Based on expression profile analysis,

AtSTR17a is highly expressed in roots (Fig. 1). Experiments using AtSTR17a–GFP fusion reporter revealed a nucleocytosolic localization (Sánchez-Bermejo *et al.*, 2014) and an accumulation in root hairs, epidermis, and pericycle cells (Chao *et al.*, 2014). As AtSTR17a displays an arsenate reductase activity and Arabidopsis *str17a* mutants significantly accumulate arsenic in leaves, Chao and co-workers proposed that arsenate reduction by AtSTR17a in roots and notably in the pericycle may limit arsenic loading into the xylem, avoiding its transfer to the shoots. The difference in the V[G/A]CXXGXR active site motif found in AtSTR17a compared with the canonical HCX_5R active site encountered in yeast and Arabidopsis ACR2 led to naming AtSTR17a as ARQ1 (arsenate reductase QTL1) or HAC1 (high arsenic content 1) (Chao *et al.*, 2014; Sánchez-Bermejo *et al.*, 2014). Both groups also sought to establish a link between *AtSTR5* and *AtSTR17a* in arsenate tolerance by investigating the impact of *AtSTR5/ACR2* mutation on their respective experimental schemes. No significant changes of the root growth recovery or of arsenate leaf content were observed in a *str5* knockout mutant and the analysis of a double *str17a str5* mutant did not highlight an epistasic interaction between the two genes (Chao *et al.*, 2014; Sánchez-Bermejo *et al.*, 2014). Altogether, these observations support a role of both proteins in arsenate tolerance but raise some questions about their respective roles, possibly pointing to their involvement in distinct mechanisms/pathways.

From a molecular point of view, it is informative to correlate the polymorphism present in naturally variable sequences to some phenotypes, as was done for AtSTR17a between the Col-0 ecotype and two arsenate hypersensitive ecotypes, Kas-1 and Kr-0. In Kr-0, the *AtSTR17a* gene exhibits a premature stop codon leading to the synthesis of an inactive protein devoid of the Rhd domain (Chao *et al.*, 2014). In Kas-1, the AtSTR17a protein has differences in the N-terminal part but also four internal substitutions in the Rhd domain. A chimeric AtSTR17a Kas-1 protein bearing the N-terminal extension and the internal substitutions found in the Col-0 allele is able to complement the *arsC* mutant. Concomitantly, mutagenesis analysis of the AtSTR17a Col-0 protein bearing a combination of three substitutions from the AtSTR17a Kas-1 protein demonstrates a non-additive effect of these mutations, but specific substitution pairs needed for loss of activity (Sánchez-Bermejo *et al.*, 2014). Altogether, these data illustrate the natural variability in the AtSTR17a-related arsenate resistance/accumulation encountered in different Arabidopsis accessions and the complexity of structural features that can promote or destabilize enzymatic reactions catalysed by STR members.

Multiple roles for the mitochondrial STR1

In plants, three pathways for cysteine degradation have been described (for a detailed review see Hildebrandt *et al.*, 2015), the mitochondrial STR1 contributing to one of these. This pathway starts with the transamination of cysteine to 3-MP, a reaction catalysed by a so far unknown aminotransferase (Fig. 5A). STR1 forms pyruvate from 3-MP, the persulfide group concomitantly formed on the catalytic cysteine being eventually transferred to GSH. The resulting GSSH could then be oxidized to sulfite (SO_3^{2-}) by the sulfur dioxygenase ethylmalonic encephalopathy protein 1 (ETHE1) (Krüßel *et al.*, 2014). Sulfite is likely preferentially transferred to peroxisomes and oxidized to sulfate by SO (Brychkova *et al.*, 2007, 2013; Lang *et al.*, 2007), but it could eventually be further converted to thiosulfate ($S_2O_3^{2-}$) via a persulfidated STR1 (Fig. 5B; Krüßel *et al.*, 2014; Höfler *et al.*, 2016). A role of STR1 in sulfite detoxification was suggested by the observation of a higher thiosulfate level and STR-dependent sulfite-consuming activity in RNAi-silenced plants for SO in comparison with wild-type plants (Brychkova *et al.*, 2013). Instead of being transferred to GSH, the persulfide group formed on the catalytic Cys of STR1 could be transmitted to other sulfur acceptor molecules or could lead to the production of hydrogen sulfide (H_2S) by reaction with mitochondrial disulfide reductases, notably TRXo1 and TRXo2 (Fig. 5B). This aspect is further discussed in the next section. An alternative route by which STR1 could obtain sulfur atoms and deliver them to target compounds/proteins without relying on 3-MP (Fig. 5) is via the mitochondrial cysteine desulfurase NFS1 because an interaction with the MST TUM1 has been reported in human and yeast (Noma *et al.*, 2009; Fräsdorf *et al.*, 2014). This enzyme catalyses cysteine desulfuration into alanine, providing the sulfur required for *de novo* Fe–S cluster biogenesis (Couturier *et al.*, 2013). In this pathway, NFS1 forms an assembly complex with several other proteins and the persulfide group formed on its active site cysteine residue provides the sulfur atoms used for building Fe–S clusters. It is worth noting that a similar reaction is catalysed by NFS2 in chloroplasts (Couturier *et al.*, 2013). Whether plant NFS1 and NFS2 do interact with some STRs is not known.

So far, STR1 is the sole MST identified in Arabidopsis mitochondria (Nakamura *et al.*, 2000; Papenbrock and Schmidt, 2000; Senkler *et al.*, 2016). The second MST isoform, named STR2 and displaying a high sequence identity with STR1 (79%), was shown to be localized in the cytosol using immunoblots on fractionated cellular extracts and GFP fusion (Nakamura *et al.*, 2000; Papenbrock and Schmidt, 2000). However, a longer STR2 transcript (At1g16460.2) is also expressed and encodes a protein with an N-terminal extension of 24 residues that is predicted to constitute a mitochondrial targeting sequence. Hence, this will have to be experimentally addressed even though STR2 was not detected in a recent mitochondrial proteome analysis, unlike STR1 (Senkler *et al.*, 2016). The study of *str* mutants indicates that STR1 accounts for 50–80% of the MST activity whereas *str2* mutant seedlings have a wild-type MST activity level (Mao *et al.*, 2011; Höfler *et al.*, 2016). However, their physiological and molecular roles *in planta* have not been elucidated because *str2* null mutants do not have any phenotype and *str1* null mutants show a shrunken seed phenotype with ~87.5% of the embryos arrested at the heart stage (Mao *et al.*, 2011). The residual 12.5% can develop further and show a normal development of vegetative tissue. Importantly, the double *str1 str2* mutant is not viable indicating that both STRs ensure an essential function at least for embryo development, but that STR1 likely has a predominant role (Mao *et al.*, 2011). Similar to *STR1*, *ETHE1* null mutants show an embryo-lethal phenotype (Krüßel *et al.*, 2014). Whereas this

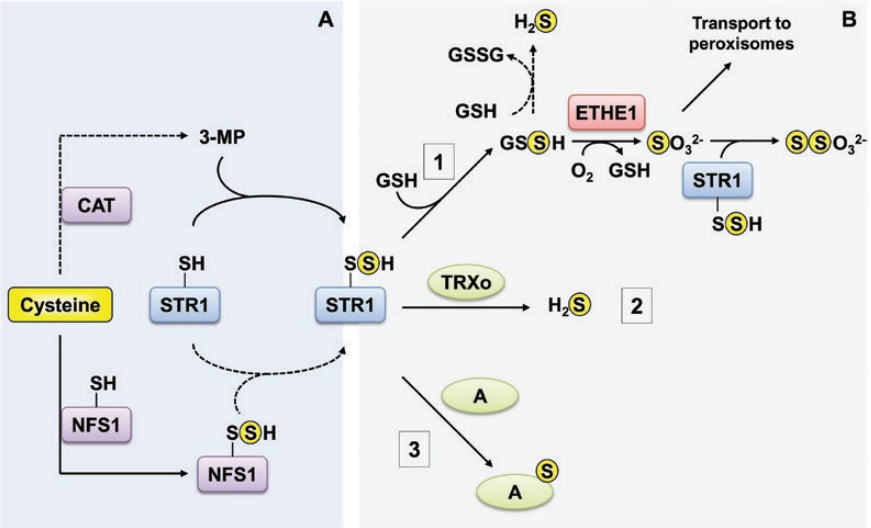

Fig. 5. Confirmed or hypothetical roles of STR1 in sulfur trafficking in mitochondria. (A) Persulfidation of mitochondrial STR1. This might occur upon reaction with 3-mercaptopyruvate (3MP) formed from cysteine by a so far unknown cysteine aminotransferase (CAT) or via the transfer of a persulfide formed on the NFS1 cysteine desulfurase. Whether the latter pathway operates in plants in unknown but the human and yeast STR and NFS orthologs were shown to interact. (B) Putative reaction pathways of persulfidated STR1. (1) A reaction with reduced glutathione (GSH) generates glutathione persulfide (GSSH) that can then either react with another GSH molecule leading to the release of hydrogen sulfide (H_2S) and oxidized glutathione (GSSG) or be used as substrate by the sulfur dioxygenase ethylmalonic encephalopathy protein 1 (ETHE1) to form sulfite (SO_3^{2-}). Sulfite is either detoxified in sulfate by sulfite oxidase after its transport in peroxisomes, or converted to thiosulfate in mitochondria by persulfidated STR1. (2) A reaction with thioredoxin o (TRXo) isoforms would lead to H_2S formation. (3) In addition to the already described reaction with GSH, TRXo, or sulfite, a reaction with mitochondrial protein or non-protein acceptors such as cysteine results in the formation persulfidated proteins or of low molecular mass per/polysulfides, respectively.

would fit with their functional association described in animals (Kabil and Banerjee, 2014) and with the existence of naturally occurring chimeric proteins containing a sulfur dioxygenase domain fused to one or several Rhd domains (Shen *et al.*, 2015; Motl *et al.*, 2017), the mutants have substantial differences. A knockdown mutant of *ETHE1* (*ethe1-1* line) with 1% of wild-type sulfur dioxygenase activity produces seeds morphologically indistinguishable from the wild-type although with a delayed embryo development. Moreover, germination, vegetative growth under short day conditions, and senescence are differentially impacted in the e*the1-1* and *str1-1* mutants (Krüßel *et al.*, 2014; Höfler *et al.*, 2016).

Hence, it might be that STR1/2 possess additional physiological functions in this compartment. Mao and colleagues speculated about a role of both STRs in the protection of developing embryos by converting cyanide, a co-product of ethylene biosynthesis, to the less toxic thiocyanate (Mao *et al.*, 2011) as proposed previously for the mitochondrial MST from rat to protect cytochrome *c* oxidase against cyanide (Nagahara *et al.*, 1999). However, a direct role in cyanide detoxification seems unlikely because enzymes catalysing this reaction use thiosulfate, which is not a good substrate for STR1/2, that rather produce thiosulfate (Höfler *et al.*, 2016). Hence, an indirect contribution is possible if STR1/2 produce thiosulfate that is used by other mitochondrial STRs, such as STR10. Still, mitochondria already contain the β-cyanoalanine synthase CAS-C1 that is involved in the detoxification of cyanide through the formation of β-cyanoalanine (García *et al.*, 2010). For comparison purpose, it is worth noting that the *cas-c1* mutant accumulates cyanide notably in roots, strongly inhibiting root hair elongation and altering the plant response to pathogens (García *et al.*, 2013). In the absence of additional data, for instance about cyanide, sulfite, and thiosulfate levels in both *str1* and *str2* mutants, a contribution of STR1/2 in cyanide detoxification remains uncertain.

Production of hydrogen sulfide by STRs

The study of H_2S production and its associated physiological and signaling roles in plants but also in other organisms is a recently emerging area, many aspects remaining mysterious, notably in plants (Mustafa *et al.*, 2009; Paul and Snyder, 2012; Greiner *et al.*, 2013; Longen *et al.*, 2016; Aroca *et al.*, 2017). In plants, H_2S is linked to the regulation of many developmental stages and to stress response mechanisms, being possibly produced in several subcellular compartments (Hancock and Whiteman, 2014). Noticeably, it is produced in chloroplasts in the frame of the reductive assimilation of sulfate (Takahashi *et al.*, 2011), in mitochondria through the synthesis of β-cyanoalanine by CAS-C1 (Álvarez *et al.*, 2012) and in the cytosol through cysteine degradation by L-cysteine desulfhydrase 1 (DES1) (Álvarez *et al.*, 2010). In mammals, H_2S is produced by the side-reactions of cystathionine β-synthase and cystathionine γ-lyase, two enzymes of the trans-sulfuration pathway that normally convert cysteine to homocysteine (reviewed in Kabil and Banerjee, 2014). In a third pathway, H_2S is released when persulfide-bound forms of the mitochondrial MST interact with a reductant such as TRX or dihydrolipoic acid as shown in mice (Shibuya *et al.*, 2009; Mikami *et al.*, 2011; Yadav *et al.*, 2013). The released H_2S may serve for modifying specific proteins (see below). Interestingly, in mouse

hepatocytes lacking both TRX reductase and glutathione reductase the level of persulfidated proteins is markedly elevated (Dóka *et al.*, 2016). Although this underlines the importance of both reducing systems for protein persulfidation, their exact contribution remains unclear. It may simply be that they serve for the reduction of persulfidated proteins.

A connection between STR1 and the reducing systems seems true in plants as well given that STR1 has been repeatedly isolated by pull-down approaches as a partner of TRX including the mitochondrial TRXo1 isoform from Arabidopsis (Balmer *et al.*, 2004; Yoshida *et al.*, 2013; Pérez-Pérez *et al.*, 2017). In this species, the STR1–TRXo1 interaction has been confirmed *in vivo* using bimolecular fluorescence complementation experiments (Henne *et al.*, 2015). Interestingly, *in vivo* interactions between TSTs, such as STR14, STR15, and STR16, and chloroplastic TRXs have been reported suggesting that the STR–TRX interaction is not restricted to MSTs. These STRs may be also involved in H_2S biogenesis in addition to their capacity to perform trans-persulfidation reactions. An STR–GRX interaction has not been reported so far but natural fusion proteins containing both protein domains exist in some prokaryotes. If such an interaction is confirmed, it will be important to make a distinction between the TRX and GSH/GRX reducing systems (Fig. 6). Indeed, the majority of plant TRXs employ two cysteines to reduce disulfide substrates whereas GRXs mostly use a single cysteine (even though there is another cysteine in the active site signature). Hence, the presence of a persulfide group on a catalytic cysteine of a TRX should be short-lived because of the presence of a resolving cysteine and should lead to the release of H_2S. On the contrary, a persulfide group formed on the catalytic cysteine of a GRX may be more stable and allow trans-persulfidation reactions with some partner proteins (Mishanina *et al.*, 2015). Accordingly, seven GRX isoforms and 16 TRX isoforms were retrieved as persulfidated proteins in Arabidopsis (Aroca *et al.*, 2017). Such a relay with TRX or GRX may be convenient to achieve an additional degree of specificity towards target proteins (Fig. 6).

The signaling functions of H_2S likely rely on the reactions with specific proteins leading to their persulfidation. It is important to mention that H_2S will react only with oxidized cysteines, possibly sulfenylated, nitrosylated, glutathionylated, or forming a disulfide bond. Hence, a complex interplay exists between all these redox post-translational modifications. Alternatively, H_2S-mediated protein persulfidation occurs when polysulfides ($RS(S)_nH$ and $RS(S)_nSR$) derived from H_2S react with cysteine thiol or thiolate (Greiner *et al.*, 2013). Remarkable amounts of these polysulfides have been detected *in vivo* in mammalian cells in addition to cysteine-persulfide (Cys-SSH) and glutathione-persulfide (GSSH) (Ida *et al.*, 2014). All persulfide species present in cells, i.e. polysulfides (notably H_2S_2 and H_2S_3), low molecular mass persulfides (Cys-SSH and GSSH) and persulfidated protein cysteine residues, have been designated as forming the bound sulfane sulfur forms. The levels of total persulfidated species in the brain of MST-KO mice are less than 50% of that in the brain of wild-type mice indicating that mitochondrial MST is indeed an important actor (Kimura *et al.*, 2015, 2017). Similarly, *E. coli* SseA is involved in the production of reactive sulfane sulfur and notably GSSH and GSSSH (Li *et al.*, 2019).

Whether plant MST orthologs, STR1 and STR2, participate in the production of such molecules in plants is poorly documented. Nevertheless, in addition to its interaction with TRXo1 leading to H_2S release, Arabidopsis STR1 is able to

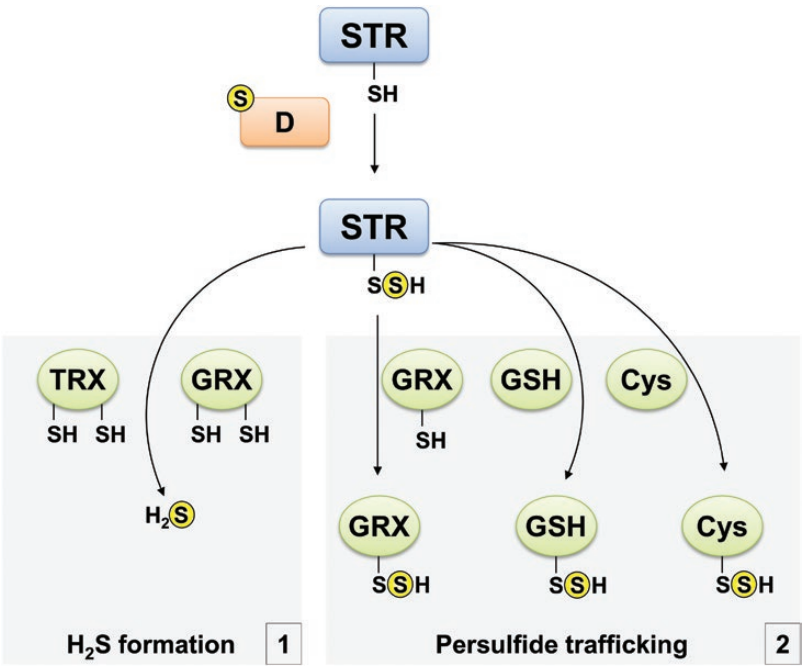

Fig. 6. Possible interaction of STRs with the cellular reducing components. The reaction of persulfidated STRs with dithiol thioredoxin (TRX) or glutaredoxin (GRX) isoforms generates H_2S (1) whereas reaction with monothiol proteins/molecules (monothiol GRX, GSH, cysteine) generates persulfidated molecules that could participate to subsequent trans-persulfidation reactions (2).

produce GSSH (Höfler *et al.*, 2016). Moreover, a proteomic analysis identified 2015 persulfidated proteins from leaves of wild-type Arabidopsis plants (Aroca *et al.*, 2017). A similar number (2130 persulfidated proteins) and almost the same proteins (85% of concordance) were identified in the *des1* mutant, which is defective for a cytosolic protein generating H_2S (Aroca *et al.*, 2017). This suggests that the major factors promoting protein persulfidation may indeed be STR1 and STR2 but also other STRs or yet uncharacterized proteins. In mammals, the ubiquitous mitochondrial cysteinyl-tRNA synthetase has been characterized as the major Cys-SSH synthase *in vivo*, playing an important role in the formation of both low molecular mass polysulfides and persulfidated proteins (Akaike *et al.*, 2017). To conclude, elucidating the molecular mechanisms underlying H_2S-mediated protein persulfidation and its regulation in plants should become a priority and more intense investigations are necessary to understand the effect of these modifications on protein activity and function.

Conclusions

Despite the physiological importance of many sulfur-containing molecules, the molecular mechanisms associated with the trafficking and specific delivery of sulfur atoms to their acceptors remain unclear in a number of pathways. Through their ability to act as sulfur carrier proteins, STRs fulfill important and diverse roles in these reactions in all organisms and more particularly in plants. Accordingly, the STR family in higher plants is composed on average of 20 members that are quite divergent considering their primary sequence, protein domain organization, and subcellular localization. The best documented functions for STR members include roles of STR5 and STR17a in arsenate tolerance, of STR13/CNX5 in Moco biosynthesis and thio-modification of cytosolic tRNAs, and of STR1 in cysteine degradation and H_2S formation.

Surprisingly, the exact roles of other STRs and more particularly those localized in chloroplasts are yet to be explored. This is all the more important as these isoforms represent nearly half of all STRs and sulfide and sulfite are produced in plastids during sulfate reduction. STR4/thylakoid rhodanese-like protein (TROL), which is inactive as STR, is required for tethering ferredoxin-NADP oxidoreductase to the thylakoid membrane (Jurić *et al.*, 2009). This interaction is proposed to control the flow of photosynthetic electrons prior to activation of pseudo-cyclic electron flow (Vojta *et al.*, 2015).

In addition to genetic and physiological studies, experiments aiming at identifying STR partners are required and should help in defining their precise roles and eventually lead to the identification of new STR-dependent pathways. *In vitro* analyses of the interactions between STRs and sulfur donors/acceptors appear crucial and this necessitates more systematic exploration of the biochemical and structural properties of STR isoforms alone or upon interaction.

Whether and how STR activity is regulated is another aspect to investigate in the future. As the role of STRs in sulfur exchange reactions relies on the presence of a catalytic cysteine in their Rhd domain, any modifications of this mandatory residue will represent a way for their post-translational regulation. Although limited evidence exist so far, several Arabidopsis STR isoforms were identified as possessing reversibly oxidized cysteines (Slade *et al.*, 2015) and STR1 was identified as sulfenylated in plants treated with H_2O_2 (Akter *et al.*, 2015; De Smet *et al.*, 2019). This may further link STRs with the TRX and GRX reducing systems besides their connection for the formation of H_2S and for protein (trans)-persulfidation.

Acknowledgements

The salary of AM was funded by grants of the French National Research Agency (ANR) as part of the 'Investissements d'Avenir' program (ANR-11-LABX-0002-01, Lab of Excellence ARBRE) and of the SULPAR (17_GE2_016) GrandEst region contract. AM also greatly appreciates a postdoc fellowship from the Alexander von Humboldt Foundation. The salary of BS and the work on plant sulfurtransferases are supported by grant of the ANR-16-CE20-0012 contract.

References

Akaike T, Ida T, Wei FY, *et al.* 2017. Cysteinyl-tRNA synthetase governs cysteine polysulfidation and mitochondrial bioenergetics. Nature Communications **8**, 1177.

Akter S, Huang J, Bodra N, *et al.* 2015. DYn-2 based identification of *Arabidopsis* sulfenomes. Molecular & Cellular Proteomics **14**, 1183–1200.

Alphey MS, Williams RA, Mottram JC, Coombs GH, Hunter WN. 2003. The crystal structure of *Leishmania* major 3-mercaptopyruvate sulfurtransferase. A three-domain architecture with a serine protease-like triad at the active site. The Journal of Biological Chemistry **278**, 48219–48227.

Álvarez C, Calo L, Romero LC, García I, Gotor C. 2010. An *O*-acetylserine(thiol)lyase homolog with L-cysteine desulfhydrase activity regulates cysteine homeostasis in Arabidopsis. Plant Physiology **152**, 656–669.

Álvarez C, García I, Romero LC, Gotor C. 2012. Mitochondrial sulfide detoxification requires a functional isoform *O*-acetylserine(thiol)lyase C in *Arabidopsis thaliana*. Molecular Plant **5**, 1217–1226.

Aroca A, Benito JM, Gotor C, Romero LC. 2017. Persulfidation proteome reveals the regulation of protein function by hydrogen sulfide in diverse biological processes in Arabidopsis. Journal of Experimental Botany **68**, 4915–4927.

Babicki S, Arndt D, Marcu A, Liang Y, Grant JR, Maciejewski A, Wishart DS. 2016. Heatmapper: web-enabled heat mapping for all. Nucleic Acids Research **44**, W147–W153.

Balmer Y, Vensel WH, Tanaka CK, *et al.* 2004. Thioredoxin links redox to the regulation of fundamental processes of plant mitochondria. Proceedings of the National Academy of Sciences, USA **101**, 2642–2647.

Bartels A. 2006. Functional characterisation of sulfurtransferase proteins in higher plants. PhD thesis, Leibniz Universität Hannover.

Bartels A, Mock HP, Papenbrock J. 2007. Differential expression of *Arabidopsis* sulfurtransferases under various growth conditions. Plant Physiology and Biochemistry **45**, 178–187.

Bauer M, Dietrich C, Nowak K, Sierralta WD, Papenbrock J. 2004. Intracellular localization of Arabidopsis sulfurtransferases. Plant Physiology **135**, 916–926.

Behshad E, Bollinger JM Jr. 2009. Kinetic analysis of cysteine desulfurase CD0387 from *Synechocystis* sp. PCC 6803: formation of the persulfide intermediate. Biochemistry **48**, 12014–12023.

Bernard DG, Cheng Y, Zhao Y, Balk J. 2009. An allelic mutant series of ATM3 reveals its key role in the biogenesis of cytosolic iron-sulfur proteins in Arabidopsis. Plant Physiology **151**, 590–602.

Bittner F, Oreb M, Mendel RR. 2001. ABA3 is a molybdenum cofactor sulfurase required for activation of aldehyde oxidase and xanthine dehydrogenase in *Arabidopsis thaliana*. The Journal of Biological Chemistry **276**, 40381–40384.

Blumenthal KM, Heinrikson RL. 1971. Structural studies of bovine liver rhodanese. I. Isolation and characterization of two active forms of the enzyme. The Journal of Biological Chemistry **246**, 2430–2437.

Bordo D, Bork P. 2002. The rhodanese/Cdc25 phosphatase superfamily. Sequence-structure-function relations. EMBO Reports **3**, 741–746.

Brychkova G, Grishkevich V, Fluhr R, Sagi M. 2013. An essential role for tomato sulfite oxidase and enzymes of the sulfite network in maintaining leaf sulfite homeostasis. Plant Physiology **161**, 148–164.

Brychkova G, Xia Z, Yang G, Yesbergenova Z, Zhang Z, Davydov O, Fluhr R, Sagi M. 2007. Sulfite oxidase protects plants against sulfur dioxide toxicity. The Plant Journal **50**, 696–709.

Burow M, Kessler D, Papenbrock J. 2002. Enzymatic activity of the *Arabidopsis* sulfurtransferase resides in the C-terminal domain but is boosted by the N-terminal domain and the linker peptide in the full-length enzyme. Biological Chemistry **383**, 1363–1372.

Chao DY, Chen Y, Chen J, Shi S, Chen Z, Wang C, Danku JM, Zhao FJ, Salt DE. 2014. Genome-wide association mapping identifies a new arsenate reductase enzyme critical for limiting arsenic accumulation in plants. PLoS Biology **12**, e1002009.

Cipollone R, Ascenzi P, Visca P. 2007. Common themes and variations in the rhodanese superfamily. IUBMB Life **59**, 51–59.

Colnaghi R, Cassinelli G, Drummond M, Forlani F, Pagani S. 2001. Properties of the *Escherichia coli* rhodanese-like protein SseA: contribution of the active-site residue Ser240 to sulfur donor recognition. FEBS Letters **500**, 153–156.

Cornilescu G, Vinarov DA, Tyler EM, Markley JL, Cornilescu CC. 2006. Solution structure of a single-domain thiosulfate sulfurtransferase from *Arabidopsis thaliana*. Protein Science **15**, 2836–2841.

Couturier J, Jacquot JP, Rouhier N. 2013. Toward a refined classification of class I dithiol glutaredoxins from poplar: biochemical basis for the definition of two subclasses. Frontiers in Plant Science **4**, 518.

De Smet B, Willems P, Fernandez-Fernandez AD, Alseekh S, Fernie AR, Messens J, Van Breusegem F. 2019. In vivo detection of protein cysteine sulfenylation in plastids. The Plant Journal **97**, 765–778.

Dhankher OP, Rosen BP, McKinney EC, Meagher RB. 2006. Hyperaccumulation of arsenic in the shoots of *Arabidopsis* silenced for arsenate reductase (ACR2). Proceedings of the National Academy of Sciences, USA **103**, 5413–5418.

Dissmeyer N, Weimer AK, Pusch S, *et al.* 2009. Control of cell proliferation, organ growth, and DNA damage response operate independently of dephosphorylation of the *Arabidopsis* Cdk1 homolog CDKA;1. The Plant Cell **21**, 3641–3654.

Dóka É, Pader I, Bíró A, *et al.* 2016. A novel persulfide detection method reveals protein persulfide- and polysulfide-reducing functions of thioredoxin and glutathione systems. Science Advances **2**, e1500968.

Ellis DR, Gumaelius L, Indriolo E, Pickering IJ, Banks JA, Salt DE. 2006. A novel arsenate reductase from the arsenic hyperaccumulating fern *Pteris vittata*. Plant Physiology **141**, 1544–1554.

Fräsdorf B, Radon C, Leimkühler S. 2014. Characterization and interaction studies of two isoforms of the dual localized 3-mercaptopyruvate sulfurtransferase TUM1 from humans. The Journal of Biological Chemistry **289**, 34543–34556.

Friso G, Giacomelli L, Ytterberg AJ, Peltier JB, Rudella A, Sun Q, Wijk KJ. 2004. In-depth analysis of the thylakoid membrane proteome of *Arabidopsis thaliana* chloroplasts: new proteins, new functions, and a plastid proteome database. The Plant Cell **16**, 478–499.

García I, Castellano JM, Vioque B, Solano R, Gotor C, Romero LC. 2010. Mitochondrial β-cyanoalanine synthase is essential for root hair formation in *Arabidopsis thaliana*. The Plant Cell **22**, 3268–3279.

García I, Rosas T, Bejarano ER, Gotor C, Romero LC. 2013. Transient transcriptional regulation of the *CYS-C1* gene and cyanide accumulation upon pathogen infection in the plant immune response. Plant Physiology **162**, 2015–2027.

Greiner R, Pálinkás Z, Bäsell K, Becher D, Antelmann H, Nagy P, Dick TP. 2013. Polysulfides link H_2S to protein thiol oxidation. Antioxidants & Redox Signaling **19**, 1749–1765.

Guretzki S, Papenbrock J. 2011. Characterization of the sulfurtransferase family from *Oryza sativa* L. Plant Physiology and Biochemistry **49**, 1064–1070.

Hancock JT, Whiteman M. 2014. Hydrogen sulfide and cell signaling: team player or referee? Plant Physiology and Biochemistry **78**, 37–42.

Hatzfeld Y, Saito K. 2000. Evidence for the existence of rhodanese (thiosulfate:cyanide sulfurtransferase) in plants: preliminary characterization of two rhodanese cDNAs from *Arabidopsis thaliana*. FEBS Letters **470**, 147–150.

Henne M, König N, Triulzi T, Baroni S, Forlani F, Scheibe R, Papenbrock J. 2015. Sulfurtransferase and thioredoxin specifically interact as demonstrated by bimolecular fluorescence complementation analysis and biochemical tests. FEBS Open Bio **5**, 832–843.

Hildebrandt TM, Grieshaber MK. 2008. Redox regulation of mitochondrial sulfide oxidation in the lugworm, *Arenicola marina*. The Journal of Experimental Biology **211**, 2617–2623.

Hildebrandt TM, Nunes Nesi A, Araújo WL, Braun HP. 2015. Amino acid catabolism in plants. Molecular Plant **8**, 1563–1579.

Höfler S, Lorenz C, Busch T, Brinkkötter M, Tohge T, Fernie AR, Braun HP, Hildebrandt TM. 2016. Dealing with the sulfur part of cysteine: four enzymatic steps degrade L-cysteine to pyruvate and thiosulfate in *Arabidopsis mitochondria*. Physiologia Plantarum **157**, 352–366.

Huang GT, Yu JS. 2016. Enzyme catalysis that paves the way for S-sulfhydration via sulfur atom transfer. The Journal of Physical Chemistry. B **120**, 4608–4615.

Ida T, Sawa T, Ihara H, *et al.* 2014. Reactive cysteine persulfides and S-polythiolation regulate oxidative stress and redox signaling. Proceedings of the National Academy of Sciences, USA **111**, 7606–7611.

Jurić S, Hazler-Pilepić K, Tomasić A, *et al.* 2009. Tethering of ferredoxin:$NADP^+$ oxidoreductase to thylakoid membranes is mediated by novel chloroplast protein TROL. The Plant Journal **60**, 783–794.

Kabil O, Banerjee R. 2014. Enzymology of H_2S biogenesis, decay and signaling. Antioxidants & Redox Signaling **20**, 770–782.

Kaufholdt D, Gehl C, Geisler M, Jeske O, Voedisch S, Ratke C, Bollhöner B, Mendel RR, Hänsch R. 2013. Visualization and quantification of protein interactions in the biosynthetic pathway of molybdenum cofactor in *Arabidopsis thaliana*. Journal of Experimental Botany **64**, 2005–2016.

Kimura Y, Koike S, Shibuya N, Lefer D, Ogasawara Y, Kimura H. 2017. 3-Mercaptopyruvate sulfurtransferase produces potential redox regulators cysteine- and glutathione-persulfide (Cys-SSH and GSSH) together with signaling molecules H_2S_2, H_2S_3 and H_2S. Scientific Reports **7**, 10459.

Kimura Y, Toyofuku Y, Koike S, Shibuya N, Nagahara N, Lefer D, Ogasawara Y, Kimura H. 2015. Identification of H_2S_3 and H_2S produced by 3-mercaptopyruvate sulfurtransferase in the brain. Scientific Reports **5**, 14774.

Klepikova AV, Kasianov AS, Gerasimov ES, Logacheva MD, Penin AA. 2016. A high resolution map of the *Arabidopsis thaliana* developmental transcriptome based on RNA-seq profiling. The Plant Journal **88**, 1058–1070.

Krepinsky K, Leimkühler S. 2007. Site-directed mutagenesis of the active site loop of the rhodanese-like domain of the human molybdopterin synthase sulfurase MOCS3. Major differences in substrate specificity between eukaryotic and bacterial homologs. The FEBS Journal **274**, 2778–2787.

Kruse I, Maclean AE, Hill L, Balk J. 2018. Genetic dissection of cyclic pyranopterin monophosphate biosynthesis in plant mitochondria. The Biochemical Journal **475**, 495–509.

Krüßel L, Junemann J, Wirtz M, *et al.* 2014. The mitochondrial sulfur dioxygenase ETHYLMALONIC ENCEPHALOPATHY PROTEIN1 is required for amino acid catabolism during carbohydrate starvation and embryo development in Arabidopsis. Plant Physiology **165**, 92–104.

Landrieu I, da Costa M, De Veylder L, *et al.* 2004*a*. A small CDC25 dual-specificity tyrosine-phosphatase isoform in *Arabidopsis thaliana*. Proceedings of the National Academy of Sciences, USA **101**, 13380–13385.

Landrieu I, Hassan S, Sauty M, Dewitte F, Wieruszeski JM, Inzé D, De Veylder L, Lippens G. 2004*b*. Characterization of the *Arabidopsis thaliana* Arath;CDC25 dual-specificity tyrosine phosphatase. Biochemical and Biophysical Research Communications **322**, 734–739.

Lang C, Popko J, Wirtz M, Hell R, Herschbach C, Kreuzwieser J, Rennenberg H, Mendel RR, Hänsch R. 2007. Sulphite oxidase as key enzyme for protecting plants against sulphur dioxide. Plant, Cell & Environment **30**, 447–455.

Lanz ND, Booker SJ. 2015. Auxiliary iron-sulfur cofactors in radical SAM enzymes. Biochimica et Biophysica Acta **1853**, 1316–1334.

Lec J-C, Boutserin S, Mazon H, Mulliert G, Boschi-Muller S, Talfournier F. 2018. Unraveling the mechanism of cysteine persulfide formation catalyzed by 3-mercaptopyruvate sulfurtransferases. ACS Catalysis **8**, 2049–2059.

Leidel S, Pedrioli PG, Bucher T, Brost R, Costanzo M, Schmidt A, Aebersold R, Boone C, Hofmann K, Peter M. 2009. Ubiquitin-related modifier Urm1 acts as a sulphur carrier in thiolation of eukaryotic transfer RNA. Nature **458**, 228–232.

Li K, Xin Y, Xuan G, Zhao R, Liu H, Xia Y, Xun L. 2019. *Escherichia coli* uses separate enzymes to produce H_2S and reactive sulfane sulfur from L-cysteine. Frontiers in Microbiology **10**, 298.

Libiad M, Motl N, Akey DL, Sakamoto N, Fearon ER, Smith JL, Banerjee R. 2018. Thiosulfate sulfurtransferase-like domain-containing 1 protein interacts with thioredoxin. The Journal of Biological Chemistry **293**, 2675–2686.

Liu W, Schat H, Bliek M, Chen Y, McGrath SP, George G, Salt DE, Zhao FJ. 2012. Knocking out ACR2 does not affect arsenic redox status in *Arabidopsis thaliana*: implications for as detoxification and accumulation in plants. PLoS ONE **7**, e42408.

Longen S, Richter F, Köhler Y, Wittig I, Beck KF, Pfeilschifter J. 2016. Quantitative persulfide site identification (qPerS-SID) reveals protein targets of H_2S releasing donors in mammalian cells. Scientific Reports **6**, 29808.

Luo GX, Horowitz PM. 1994. The sulfurtransferase activity and structure of rhodanese are affected by site-directed replacement of Arg-186 or Lys-249. The Journal of Biological Chemistry **269**, 8220–8225.

Mao G, Wang R, Guan Y, Liu Y, Zhang S. 2011. Sulfurtransferases 1 and 2 play essential roles in embryo and seed development in *Arabidopsis thaliana*. The Journal of Biological Chemistry **286**, 7548–7557.

Marelja Z, Mullick Chowdhury M, Dosche C, Hille C, Baumann O, Löhmannsröben HG, Leimkühler S. 2013. The L-cysteine desulfurase NFS1 is localized in the cytosol where it provides the sulfur for molybdenum cofactor biosynthesis in humans. PLoS ONE **8**, e60869.

Marelja Z, Stöcklein W, Nimtz M, Leimkühler S. 2008. A novel role for human Nfs1 in the cytoplasm: Nfs1 acts as a sulfur donor for MOCS3, a protein involved in molybdenum cofactor biosynthesis. The Journal of Biological Chemistry **283**, 25178–25185.

Matthies A, Rajagopalan KV, Mendel RR, Leimkühler S. 2004. Evidence for the physiological role of a rhodanese-like protein for the biosynthesis of the molybdenum cofactor in humans. Proceedings of the National Academy of Sciences, USA **101**, 5946–5951.

Mikami Y, Shibuya N, Kimura Y, Nagahara N, Ogasawara Y, Kimura H. 2011. Thioredoxin and dihydrolipoic acid are required for 3-mercaptopyruvate sulfurtransferase to produce hydrogen sulfide. The Biochemical Journal **439**, 479–485.

Mishanina TV, Libiad M, Banerjee R. 2015. Biogenesis of reactive sulfur species for signaling by hydrogen sulfide oxidation pathways. Nature Chemical Biology **11**, 457–464.

Moseler A, Selles B, Rouhier N, Couturier J. 2019. Novel insights into the diversity of the sulfurtransferase family in photosynthetic organisms with emphasis on oak. New Phytologist, doi: 10.1111/nph.15870.

Motl N, Skiba MA, Kabil O, Smith JL, Banerjee R. 2017. Structural and biochemical analyses indicate that a bacterial persulfide dioxygenase-rhodanese fusion protein functions in sulfur assimilation. The Journal of Biological Chemistry **292**, 14026–14038.

Mueller EG. 2006. Trafficking in persulfides: delivering sulfur in biosynthetic pathways. Nature Chemical Biology **2**, 185–194.

Mustafa AK, Gadalla MM, Sen N, Kim S, Mu W, Gazi SK, Barrow RK, Yang G, Wang R, Snyder SH. 2009. H_2S signals through protein S-sulfhydration. Science Signaling **2**, ra72.

Nagahara N, Ito T, Minami M. 1999. Mercaptopyruvate sulfurtransferase as a defense against cyanide toxication: molecular properties and mode of detoxification. Histology and Histopathology **14**, 1277–1286.

Nagahara N, Nishino T. 1996. Role of amino acid residues in the active site of rat liver mercaptopyruvate sulfurtransferase. CDNA cloning, overexpression, and site-directed mutagenesis. The Journal of Biological Chemistry **271**, 27395–27401.

Nagahara N, Okazaki T, Nishino T. 1995. Cytosolic mercaptopyruvate sulfurtransferase is evolutionarily related to mitochondrial rhodanese. Striking similarity in active site amino acid sequence and the increase in the mercaptopyruvate sulfurtransferase activity of rhodanese by site-directed mutagenesis. The Journal of Biological Chemistry **270**, 16230–16235.

Nahar N, Rahman A, Ghosh S, Nawani N, Mandal A. 2017. Functional studies of *AtACR2* gene putatively involved in accumulation, reduction and/or sequestration of arsenic species in plants. Biologia **72**, 520–526.

Nakai Y, Harada A, Hashiguchi Y, Nakai M, Hayashi H. 2012. Arabidopsis molybdopterin biosynthesis protein Cnx5 collaborates with the ubiquitin-like protein Urm11 in the thio-modification of tRNA. The Journal of Biological Chemistry **287**, 30874–30884.

Nakai Y, Nakai M, Hayashi H. 2008. Thio-modification of yeast cytosolic tRNA requires a ubiquitin-related system that resembles bacterial sulfur transfer systems. The Journal of Biological Chemistry **283**, 27469–27476.

Nakamura T, Yamaguchi Y, Sano H. 2000. Plant mercaptopyruvate sulfurtransferases: molecular cloning, subcellular localization and enzymatic activities. European Journal of Biochemistry **267**, 5621–5630.

Nambi S, Long JE, Mishra BB, Baker R, Murphy KC, Olive AJ, Nguyen HP, Shaffer SA, Sassetti CM. 2015. The oxidative stress network of *Mycobacterium tuberculosis* reveals coordination between radical detoxification systems. Cell Host & Microbe **17**, 829–837.

Narsai R, Law SR, Carrie C, Xu L, Whelan J. 2011. In-depth temporal transcriptome profiling reveals a crucial developmental switch with roles for RNA processing and organelle metabolism that are essential for germination in Arabidopsis. Plant Physiology **157**, 1342–1362.

Noma A, Sakaguchi Y, Suzuki T. 2009. Mechanistic characterization of the sulfur-relay system for eukaryotic 2-thiouridine biogenesis at tRNA wobble positions. Nucleic Acids Research **37**, 1335–1352.

Nomura H, Komori T, Kobori M, Nakahira Y, Shiina T. 2008. Evidence for chloroplast control of external Ca^{2+}-induced cytosolic Ca^{2+} transients and stomatal closure. The Plant Journal **53**, 988–998.

Pagani S, Forlani F, Carpen A, Bordo D, Colnaghi R. 2000. Mutagenic analysis of Thr-232 in rhodanese from *Azotobacter vinelandii* highlighted the differences of this prokaryotic enzyme from the known sulfurtransferases. FEBS Letters **472**, 307–311.

Pantoja-Uceda D, López-Méndez B, Koshiba S, *et al.* 2005. Solution structure of the rhodanese homology domain At4g01050(175-295) from *Arabidopsis thaliana*. Protein Science **14**, 224–230.

Papenbrock J, Guretzki S, Henne M. 2011. Latest news about the sulfurtransferase protein family of higher plants. Amino Acids **41**, 43–57.

Papenbrock J, Schmidt A. 2000. Characterization of two sulfurtransferase isozymes from *Arabidopsis thaliana*. European Journal of Biochemistry **267**, 5571–5579.

Paul BD, Snyder SH. 2012. H_2S signalling through protein sulfhydration and beyond. Nature Reviews. Molecular Cell Biology **13**, 499–507.

Peer WA, Baxter IR, Richards EL, Freeman JL, Murphy AS. 2006. Phytoremediation and hyperaccumulator plants. In: Tamas MJ, Martinoia E, eds. Topics in current genetics. Molecular biology of metal homeostasis and detoxification: from microbes to man. Berlin, Heidelberg: Springer, 299–340.

Peltier JB, Ytterberg AJ, Sun Q, van Wijk KJ. 2004. New functions of the thylakoid membrane proteome of *Arabidopsis thaliana* revealed by a simple, fast, and versatile fractionation strategy. The Journal of Biological Chemistry **279**, 49367–49383.

Pérez-Pérez ME, Mauriès A, Maes A, Tourasse NJ, Hamon M, Lemaire SD, Marchand CH. 2017. The deep thioredoxome in *Chlamydomonas reinhardtii*: new insights into redox regulation. Molecular Plant **10**, 1107–1125.

Phizicky EM, Hopper AK. 2010. tRNA biology charges to the front. Genes & Development **24**, 1832–1860.

Ploegman JH, Drent G, Kalk KH, Hol WG. 1978. Structure of bovine liver rhodanese. I. Structure determination at 2.5 Å resolution and a comparison of the conformation and sequence of its two domains. Journal of Molecular Biology **123**, 557–594.

Ranjan N, Rodnina MV. 2017. Thio-modification of tRNA at the Wobble position as regulator of the kinetics of decoding and translocation on the ribosome. Journal of the American Chemical Society **139**, 5857–5864.

Sánchez-Bermejo E, Castrillo G, del Llano B, *et al.* 2014. Natural variation in arsenate tolerance identifies an arsenate reductase in *Arabidopsis thaliana*. Nature Communications **5**, 4617.

Schwarz G, Mendel RR. 2006. Molybdenum cofactor biosynthesis and molybdenum enzymes. Annual Review of Plant Biology **57**, 623–647.

Senkler J, Senkler M, Eubel H, Hildebrandt T, Lengwenus C, Schertl P, Schwarzländer M, Wagner S, Wittig I, Braun H-P. 2016. The

mitochondrial complexome of *Arabidopsis thaliana*. The Plant Journal **89**, 1079–1092.

Shen J, Keithly ME, Armstrong RN, Higgins KA, Edmonds KA, Giedroc DP. 2015. *Staphylococcus aureus* CstB is a novel multidomain persulfide dioxygenase-sulfurtransferase involved in hydrogen sulfide detoxification. Biochemistry **54**, 4542–4554.

Shibuya N, Tanaka M, Yoshida M, Ogasawara Y, Togawa T, Ishii K, Kimura H. 2009. 3-Mercaptopyruvate sulfurtransferase produces hydrogen sulfide and bound sulfane sulfur in the brain. Antioxidants & Redox Signaling **11**, 703–714.

Slade WO, Werth EG, McConnell EW, Alvarez S, Hicks LM. 2015. Quantifying reversible oxidation of protein thiols in photosynthetic organisms. Journal of the American Society for Mass Spectrometry **26**, 631–640.

Sorrell DA, Chrimes D, Dickinson JR, Rogers HJ, Francis D. 2005. The Arabidopsis CDC25 induces a short cell length when overexpressed in fission yeast: evidence for cell cycle function. New Phytologist **165**, 425–428.

Spadafora ND, Doonan JH, Herbert RJ, Bitonti MB, Wallace E, Rogers HJ, Francis D. 2011. Arabidopsis T-DNA insertional lines for *CDC25* are hypersensitive to hydroxyurea but not to zeocin or salt stress. Annals of Botany **107**, 1183–1192.

Su T, Xu J, Li Y, Lei L, Zhao L, Yang H, Feng J, Liu G, Ren D. 2011. Glutathione-indole-3-acetonitrile is required for camalexin biosynthesis in *Arabidopsis thaliana*. The Plant Cell **23**, 364–380.

Takahashi H, Kopriva S, Giordano M, Saito K, Hell R. 2011. Sulfur assimilation in photosynthetic organisms: molecular functions and regulations of transporters and assimilatory enzymes. Annual Review of Plant Biology **62**, 157–184.

Teschner J, Lachmann N, Schulze J, Geisler M, Selbach K, Santamaria-Araujo J, Balk J, Mendel RR, Bittner F. 2010. A novel role for *Arabidopsis* mitochondrial ABC transporter ATM3 in molybdenum cofactor biosynthesis. The Plant Cell **22**, 468–480.

Tomizioli M, Lazar C, Brugière S, *et al.* 2014. Deciphering thylakoid subcompartments using a mass spectrometry-based approach. Molecular & Cellular Proteomics **13**, 2147–2167.

Vainonen JP, Sakuragi Y, Stael S, *et al.* 2008. Light regulation of CaS, a novel phosphoprotein in the thylakoid membrane of *Arabidopsis thaliana*. The FEBS Journal **275**, 1767–1777.

Venne AS, Solari FA, Faden F, Paretti T, Dissmeyer N, Zahedi RP. 2015. An improved workflow for quantitative N-terminal charge-based fractional diagonal chromatography (ChaFRADIC) to study proteolytic events in *Arabidopsis thaliana*. Proteomics **15**, 2458–2469.

Vojta L, Carić D, Cesar V, Antunović Dunić J, Lepeduš H, Kveder M, Fulgosi H. 2015. TROL-FNR interaction reveals alternative pathways of electron partitioning in photosynthesis. Scientific Reports **5**, 10085.

Weinl S, Held K, Schlücking K, Steinhorst L, Kuhlgert S, Hippler M, Kudla J. 2008. A plastid protein crucial for Ca^{2+}-regulated stomatal responses. New Phytologist **179**, 675–686.

Williams PN, Islam MR, Adomako EE, Raab A, Hossain SA, Zhu YG, Feldmann J, Meharg AA. 2006. Increase in rice grain arsenic for regions of Bangladesh irrigating paddies with elevated arsenic in groundwaters. Environmental Science & Technology **40**, 4903–4908.

Winter D, Vinegar B, Nahal H, Ammar R, Wilson GV, Provart NJ. 2007. An "Electronic Fluorescent Pictograph" browser for exploring and analyzing large-scale biological data sets. PLoS ONE **2**, e718.

Wollers S, Heidenreich T, Zarepour M, Zachmann D, Kraft C, Zhao Y, Mendel RR, Bittner F. 2008. Binding of sulfurated molybdenum cofactor to the C-terminal domain of ABA3 from *Arabidopsis thaliana* provides insight into the mechanism of molybdenum cofactor sulfuration. The Journal of Biological Chemistry **283**, 9642–9650.

Xiong L, Ishitani M, Lee H, Zhu JK. 2001. The Arabidopsis *LOS5/ABA3* locus encodes a molybdenum cofactor sulfurase and modulates cold stress- and osmotic stress-responsive gene expression. The Plant Cell **13**, 2063–2083.

Yadav PK, Yamada K, Chiku T, Koutmos M, Banerjee R. 2013. Structure and kinetic analysis of H_2S production by human mercaptopyruvate sulfurtransferase. The Journal of Biological Chemistry **288**, 20002–20013.

Yoshida K, Noguchi K, Motohashi K, Hisabori T. 2013. Systematic exploration of thioredoxin target proteins in plant mitochondria. Plant & Cell Physiology **54**, 875–892.

Zheng L, White RH, Cash VL, Jack RF, Dean DR. 1993. Cysteine desulfurase activity indicates a role for NIFS in metallocluster biosynthesis. Proceedings of the National Academy of Sciences, USA **90**, 2754–2758.

Zhong R, Thompson J, Ottesen E, Lamppa GK. 2010. A forward genetic screen to explore chloroplast protein import in vivo identifies Moco sulfurase, pivotal for ABA and IAA biosynthesis and purine turnover. The Plant Journal **63**, 44–59.

Résumé

Le soufre est un élément indispensable au développement et à la croissance des plantes qui sont capables d'assimiler le soufre inorganique présent au niveau du sol pour former de la cystéine. Donneur majeur de soufre, cet acide aminé est un métabolite clé pour la biosynthèse de méthionine et de glutathion mais également de nombreux composés/cofacteurs soufrés comme les centres fer-soufre, la biotine, la thiamine, l'acide lipoïque, le cofacteur à molybdène et les bases soufrées des ARNt. Ces voies de biosynthèse reposent notamment sur des réactions de transfert de soufre impliquant la formation de groupements persulfures sur des cystéines réactives des protéines au travers de réactions de trans-persulfuration. En dépit de son importance dans la physiologie des plantes, l'étude du métabolisme soufré reste en retrait comparée à celle des métabolismes de l'azote et du phosphore et les mécanismes moléculaires impliqués dans le transfert du soufre restent majoritairement peu décrits. Au cours de ces dernières années, mes recherches ont principalement porté sur l'identification et la caractérisation des acteurs moléculaires impliqués dans la biogenèse des centres Fe-S et le transfert de soufre chez les plantes au travers de l'étude de deux familles de protéines, les cystéine désulfurases et les sulfurtransférases.

Summary

Sulfur represents an essential element for the growth and development of plants that are able to assimilate inorganic sulfur present in the soil to synthesize cysteine. As a major sulfur donor molecule, this amino acid is a key metabolite for methionine and glutathione biosynthesis but also many sulfur containing compounds/cofactors such as iron-sulfur centers, biotin, thiamine, lipoic acid, molybdenum cofactor and sulfur-containing bases in tRNAs. The related biosynthetic pathways rely on sulfur transfer reactions involving notably the formation of persulfide groups on reactive cysteine residues through trans-persulfidation reactions. Despite its importance for plant physiology, the molecular mechanisms of sulfur trafficking remain mostly undescribed. During the last years, my research activity has mainly focused on the identification and characterization of the molecular actors involved in the biogenesis of Fe-S clusters and sulfur trafficking in plants through the study of two protein families, cysteine desulfurases and sulfurtransferases.